Loughborough University

This item was submitted to Loughborough University as a PhD thesis by the author and is made available in the Institutional Repository (https://dspace.lboro.ac.uk/) under the following Creative Commons Licence conditions.

creative commons

COMMONS DEED

Attribution-NonCommercial-NoDerivs 2.5

You are free:

- to copy, distribute, display, and perform the work

Under the following conditions:

BY: **Attribution**. You must attribute the work in the manner specified by the author or licensor.

Noncommercial. You may not use this work for commercial purposes.

No Derivative Works. You may not alter, transform, or build upon this work.

- For any reuse or distribution, you must make clear to others the license terms of this work.
- Any of these conditions can be waived if you get permission from the copyright holder.

Your fair use and other rights are in no way affected by the above.

This is a human-readable summary of the Legal Code (the full license).

Disclaimer

For the full text of this licence, please go to:
http://creativecommons.org/licenses/by-nc-nd/2.5/

BLDSC no :- DX 91955

LOUGHBOROUGH
UNIVERSITY OF TECHNOLOGY
LIBRARY

AUTHOR/FILING TITLE
DEMIR, A

ACCESSION/COPY NO.
015049/02

VOL. NO. | CLASS MARK

LOAN COPY

~~20 MAR 1992~~
12 JUN 1992
-2 JUL 1993
-8 NOV 1993
14 NOV 1994
-6 OCT 1995
21 MAR 1997
20 MAR 1998
12 JUN 1998
-2 OCT 1998

LB 0015049027

THE AIR-JET YARN TEXTURING PROCESS WITH PARTICULAR REFERENCE TO NOZZLE DESIGN AND IMPROVED YARN TEST METHODS

By

ALI DEMIR

BSc (ITU, Istanbul), MSc (ITU, Istanbul)

A DOCTORAL THESIS

Submitted in Partial Fulfilment of the Requirements

For the Award of

DOCTOR OF PHILOSOPHY

of the

LOUGHBOROUGH UNIVERSITY OF TECHNOLOGY

October 1987

© By A. DEMIR, 1987

Loughborough University
of Technology Library
Date Jan '88
Class
Acc. No. 015049/02
W7212254

SUMMARY

The air-jet yarn texturing process has made enormous progress since its industrial introduction some 30 years ago. However, major drawbacks such as high compressed air consumption and the low process speeds still hinder the long predicted breakthrough.

This work deals with the problems of the texturing nozzles predominantly from an experimental view point and an improved description of the air flow through such nozzles is given. Several nozzles which provide better texturing conditions at lower air pressures, i.e. lower air consumption, have been designed by the author. Preliminary investigations have utilised scaled-up models and prototypes manufactured by Heberlein Maschinenfabrik A.G. of Switzerland. These novel nozzles have successfully produced textured yarns with great reductions in compressed air consumption.

An improved understanding of the wetting mechanism on the process has been established and it is concluded that the wetting of the supply yarn merely reduces the interfilament friction thereby resulting in an enhanced separation of the filaments.

Yarn tests are reviewed. Special emphasis is given to instability and a standard test method is suggested. All 'off-line' test methods are shown to be time consuming and not to provide immediate feed back to the process. The possibility of an 'on-line' instability measuring technique is demonstrated via a microcomputer controlled unit.

The effects of the process parameters and the properties of supply yarns on the air-jet textured yarns are ascertained to provide a reference information to current air-jet texturisers and other researchers.

The thesis claims originality for the nozzles designed, and for the 'on-line' instability concept and relevant system.

ACKNOWLEDGEMENTS

The author would like to acknowledge Professor Gordon R Wray, Head of Department and Director of Research, Dr Memiş Acar and Mr R Keith Turton, Research Supervisiors for their joint supervision, continuous support and encouragement. The author is particularly indebted to Dr M Acar for his invaluable, constructive and unlimited advice, criticism and discussions which made possible to complete this work on time.

The author also would like to acknowledge Turkish Government, Ministry of Education for the financial support and Heberlein Machine Works of Switzerland for their help in making the prototype nozzles to required tolerances.

Sincere thanks are due to Mr P Norton, the laboratory superintendant, Mr R S Ludlam, the chief technician, Mr J Guy, the chief electronic technician, and all other departmental technicians who showed tremendous patience with the author during the course of this work.

LIST OF CONTENTS

4. INVESTIGATION OF RECENT TEXTURING NOZZLES

5. EFFECTS OF NOZZLE GEOMETRY ON THE AIR FLOW

6. THE DESIGN OF MORE EFFECTIVE NOZZLES

7. EFFECTS OF WETTING ON THE AIR-JET TEXTURING PROCESS

8. INSTABILITY TESTS FOR AIR-JET TEXTURED YARNS

9. ON-LINE QUALITY CONTROL OF AIR-JET TEXTURED YARNS

10. EFFECTS OF PROCESS AND SUPPLY YARN PARAMETERS ON THE QUALITY OF AIR-JET TEXTURED YARNS

11. GENERAL CONCLUSIONS AND SUGGESTIONS FOR FURTHER WORK

LIST OF TABLES

LIST OF FIGURES

1. INTRODUCTION

2. LITERATURE SURVEY

3. DESCRIPTION OF THE AIR FLOW THROUGH CYLINDRICAL NOZZLES

4. INVESTIGATION OF RECENT TEXTURING NOZZLES

5. EFFECTS OF NOZZLE GEOMETRY ON THE AIR FLOW

6. THE DESIGN OF MORE EFFECTIVE NOZZLES

8. INSTABILITY TESTS FOR AIR-JET TEXTURED YARNS

9. ON-LINE QUALITY CONTROL OF AIR-JET TEXTURED YARNS

10. EFFECTS OF PROCESS PARAMETERS AND SUPPLY YARN PROPERTIES ON THE PROPERTIES OF AIR-JET TEXTURED YARNS

APPENDICES

LIST OF SYMBOLS

A Cross-sectional area

C_p Specific heat capasity at constant pressure

D Nozzle main duct area

M Mach number

P Pressure

R Universal gas constant

T Temperature

V Velocity

W Weight

a Speed of sound

d Diameter of the inlet hole, main duct diameter after modification

p Static pressure

x Axial coordinate

y Radial coordinate

α Inclination angle of the inlet holes

δ Total deflection angle of the incoming jet

γ Gas constant (γ =1.4 for air)

ψ Area ratio across an abrupt enlargement

ρ Density

Superscripts

$*$ Critical values (Values at sonic conditions)

$'$ Isentropic values

Subscripts

atm Atmospheric values (Ambient conditions)

e Values at the exit section

o Stagnation values

p Primary flow conditions

s Secondary flow conditions

t Values at the throat

NOTES ON UNITS

SI units are generally used throughout the thesis. Nevertheless the units related to pressure and tension are allowed to form an exception due to the measuring equipment available. The following table gives necessary conversion factors.

	Unit Used	SI Unit	Conversion Factor
Pressure*	bar	N/m^2	1 bar=10^5 N/m^2
Tension	gf	cN	1 gf=0.981 cN

* Pressures are gauge pressures unless otherwise stated

CHAPTER 1

INTRODUCTION

Air-jet texturing is one of several processes used to convert synthetic filament yarns to textured yarns and is the most versatile of all known texturing methods. Yarns produced by this technique resemble the natural fibre spun yarns both in appearance and physical characteristics. The process is therefore becoming important in the textile industry where the usage of synthetic and man-made fibres is approaching 50% of the market share. However, it is quite complicated and not without problems and drawbacks, among these being a lack of understanding of the process, a high compressed air consumption and low production rates compared with other texturing techniques, in particular false-twist texturing.

This thesis aims to investigate the technique of air-jet texturing so as to make contributions and improvements to the process, particularly nozzle design, and to suggest improvements to yarn test techniques which are known to be unsatisfactory.

1.1 Texturing

Warmth, handle, natural texture and appearance are considered to be desirable properties of most textile yarns. Flat, continuous synthetic filament yarns do not possess such qualities, but they are more often stronger and much more uniform than the natural fibre yarns. When producing textile yarns from synthetic filaments the ideal objective would be to combine the desired properties of both natural and synthetic fibres but this is an impossible task to achieve. Therefore the primary objective of all synthetic filament yarn conversion processes is to imitate the features of the natural fibre yarns whilst maintaining the desirable properties of synthetic fibres.

One method of achieving this is to cut the continuous filaments into staple fibres and then process them into yarn form using conventional spinning methods as for cotton and wool; however, this is a time consuming and therefore a wasteful process although it is useful for blends of man-made fibres with the natural fibres. Alternatively, continuous filaments can be converted into yarns by various texturing methods at lower costs but often these inadequately simulate spun yarns.

Texturing in general can be described as a technique by which closely packed parallel arrangements of continuous synthetic filaments are changed into more open, voluminous structures. Most of the texturing methods involve simple mechanical distortion during heat treatment of thermoplastic yarns. In contrast, the air-jet texturing process is a purely mechanical texturing method which uses a cold air stream to produce bulked yarns of low extensibility; these more closely resemble spun natural fibre yarns in their appearance and physical characteristics (See Fig. 1.1) and they can be made from man-made filaments which are not thermoplastic, e.g. cellulosic filaments, such as acetate and viscose rayon, and glass filament yarns.

Yarns textured by the methods based on heat setting during mechanical distortion (Fig. 1.1b) have a common characteristic of high extensibility under quite low loads. This extreme extensibility arises from the very open structures which result in such 'stretch' yarns. On the other hand, yarns produced by the air-jet technique (Fig. 1.1a) are of totally different structures in that they much more closely simulate spun yarn structures (Fig. 1.1c). Whereas the bulkiness of the stretch yarns decreases with the degree of tension imposed on them, the form of air-jet textured yarns can be made to remain virtually unchanged at loads corresponding to those normally imposed in fabric production and during wear. This is due to the 'locked-in' entangled loop structure attributed to air-jet textured yarns, as shown in Fig. 1.2. Air-jet textured yarns again more closely resemble conventionally spun yarns in that the yarn surface is covered with fixed resilient loops, and these serve the same purpose as the protruding hairs in spun yarns by forming an insulating layer of entrapped still air between neighbouring garments.

The air-jet texturing process is by far the most versatile of all the yarn texturing methods in that it can 'blend' filaments together during processing and it therefore simulate a desirable attribute of spun fibre yarns. This greater versatility offers the texturiser far greater scope than other types of textured yarns. Moreover, the feed yarns need not be restricted to the synthetic filament yarns with their good thermoplastic properties. Although polyester and polyamide multi-filament types have so far been mainly used for the air-jet yarn products to date, other filament types such as polypropylene, glass, and viscose and acetate rayons are also being used for certain speciality end-uses.

1.2 The Air-jet Texturing Process

The air-jet texturing process converts flat, continuous synthetic yarns into entangled, convoluted, bulky, spun-like structured yarns (See Fig. 1.3).

Fig. 1.4 schematically illustrates the basic requirements of the air-jet texturing process. The process involves the 'overfeed' principle where the multifilament supply yarn, as supplied 'over-end' from a creel, is fed into the nozzle at a greater rate than it is taken away. To achieve this degree of overfeed the yarn passes through feed roller systems FR1 and/or FR2 faster than it does through the delivery roller systems DR2. The overfed filaments enter the nozzle and are blown out from the exit end; they are formed into textured yarn under the turbulent effects of the supersonic air stream provided from a suitable compressed air supply.

The zone between the feed rollers and the nozzle is termed the feed zone, and that between the nozzle and the delivery rollers is termed the delivery zone. The supply yarn is normally wetted just before it is fed into the texturing nozzle by passing it through a water bath or through a wetting unit which can either be separate from or integrated with the nozzle assembly. Wet texturing apparently improves the quality of the yarn produced. It is also believed that an impact element such as a small sphere (See item 3 in Fig. 1.5) at the nozzle exit enhances the quality of the yarn. Texturing nozzles are usually enclosed in a chamber, not only to reduce the noise created by the air-jet, but also to collect the used water and the spin finish that is washed away from the filaments during the process.

Three main types of operations are established to produce a range of yarns. These are; (i) single-end texturing, (ii) parallel texturing, and (iii) core-and-effect texturing.

Single-end texturing denotes the situation whereby a single end is overfed to the texturing nozzle and the resultant textured yarn is withdrawn. In the case of parallel texturing, two or more ends are fed at the same overfeed into the nozzle so as to facilitate a blend of different types of supply material, or of the same material but with different filament linear densities or number of filaments, or different cross-sectional shapes. Yarns produced by the parallel texturing have a reasonably uniform bulk as the overfeeds of all the component yarns are equal. The versatility of the air-jet texturing process is best observed by the core-and-effect operation in which one or more ends of yarns are fed into the nozzle at a low overfeed to form the core, whilst a second group of yarns is simultaneously fed to the same nozzle at a higher overfeed to create the desired bulk. By changing the overfeeds, a wide range of such yarns can be produced. Any of these three main yarn types can be modified by intermittently varying the overfeed conditions so as to cause periodic longitudinal variations in the bulking effect to create fancy effect yarns.

1.3 Air-jet Textured Yarns

The combined effects of surface loops with a well entangled core enable the air-jet textured yarns to simulate the appearance and feel of spun staple yarns. They are certainly more spun-like than the other types of textured yarns, and consequently find similar application fields to spun yarns, ranging from woven apparel fabrics to heavy 'technical' yarns.

When air-jet textured yarns are woven or knitted into fabrics, they offer an excellent performance with air permeability approaching that of worsted fabrics, better covering power and no snagging due to the locked-in yarn structure. Since the texturing process does not affect the individual filament cross-section, the fabrics do not glitter in the brightest sunshine. Furthermore, air-jet textured yarns offer superior abrasion resistance, dimensional stability and crease resistance than worsted fabrics.

1.4 Scope of the Work

Although the air-jet texturing process has been available to the textile industry for nearly three decades, due to certain drawbacks it has not yet seen wide utilisation. High conversion costs due to expensive compressed air consumption is the first problem. Low production speed when compared with other texturing processes, is also another factor leading to high costs. Nevertheless, during this current decade, the air-jet texturing process has been revived and interest in it is growing. This is perhaps because of the relatively reduced conversion costs due to the technological advancements such as improved nozzles, more suitable supply yarns, and also the long delayed recognition of the versatility of the air-jet textured yarns to produce a wide variety of end products by blending different filaments at different rates which can compete with the spun yarns.

However the air-jet texturing process still suffers from higher air consumptions and lower production speeds. Despite recent research investigations, it can not yet be claimed that a thorough understanding of the process has been achieved. Therefore, it is the aim of this present work to research into the process in general and into the flow through the texturing nozzles in particular to achieve a better understanding of the process and its mechanism of loop formation. The flow through the texturing nozzle has been investigated experimentally by means of flow measurement and flow visualisation techniques. Full size texturing nozzles have been used in experimental work wherever possible and scaled-up nozzles used when necessary. The outcome of the work is intended to lead to the design of more effective nozzles which could reduce the compressed air consumption and consequently reduce the conversion costs of the textured yarns.

Water application to the filaments prior to their entry to the nozzle is now a well recognised requirement for improved texturing but the mechanism of this improvement is imperfectly understood. An approach towards better understanding of this phenomenon has been made together with an investigation of possible ways of enhancing the wetting qualities of water.

Quality assessment of air-jet textured yarns is made in the same way as for other textile yarns by measurements of linear density and strength related properties. However the air-jet textured yarns possess some other unique properties such as increased bulk, the size and frequency of the surface loops and texture stability. The assessment of yarn bulk, and size and frequency of the loops can simply be made by visual or microscopic inspection of typical yarn samples. The lack of a consistent method for measuring the instability of air-jet textured yarns warrants a detailed study. An improved instability test method will be proposed. 'Off-line' test methods currently used fail to provide rapid information and feedback to correct the faults in the process or to set-up the process parameters to the required conditions. Therefore, an 'on-line' quality control system which will assess the instability of the yarn and provide feed back to the texturing machine will be described.

In order to provide a reference for current air-jet texturisers regarding the effects of process and supply yarn parameters on the properties of textured yarns, an extensive study of these parameters concludes this thesis.

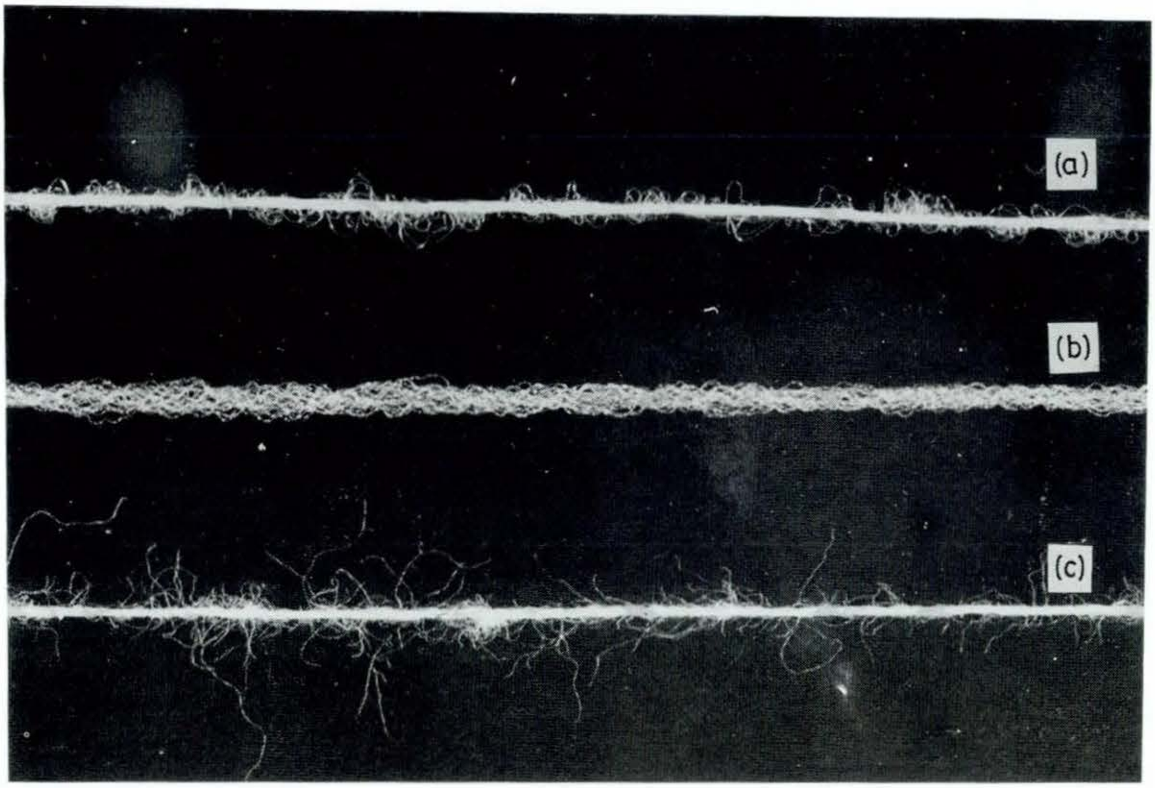

Figure 1.1 The visual comparison of: (a) air-jet textured yarn; (b) stretch yarn produced by false-twist texturing process; and (c) conventional spun fibre yarn made by cotton spinning process

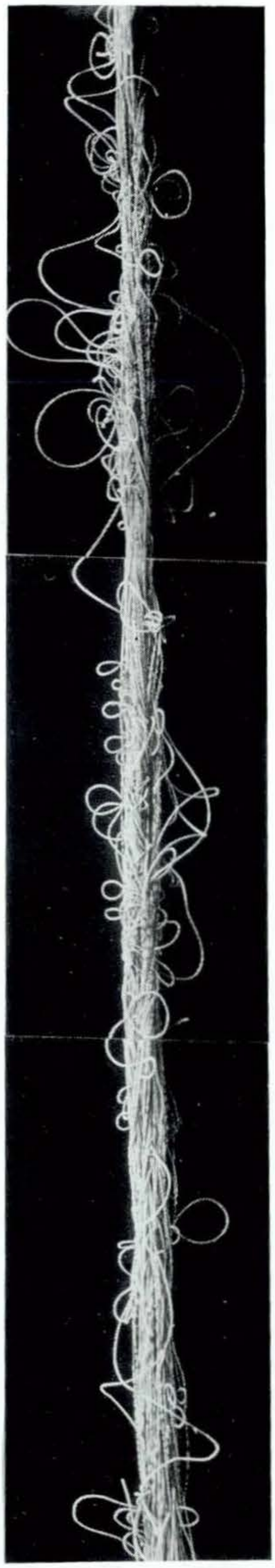

Figure 1.2

Air-jet textured yarn showing the 'locked-in' entangled loop structure

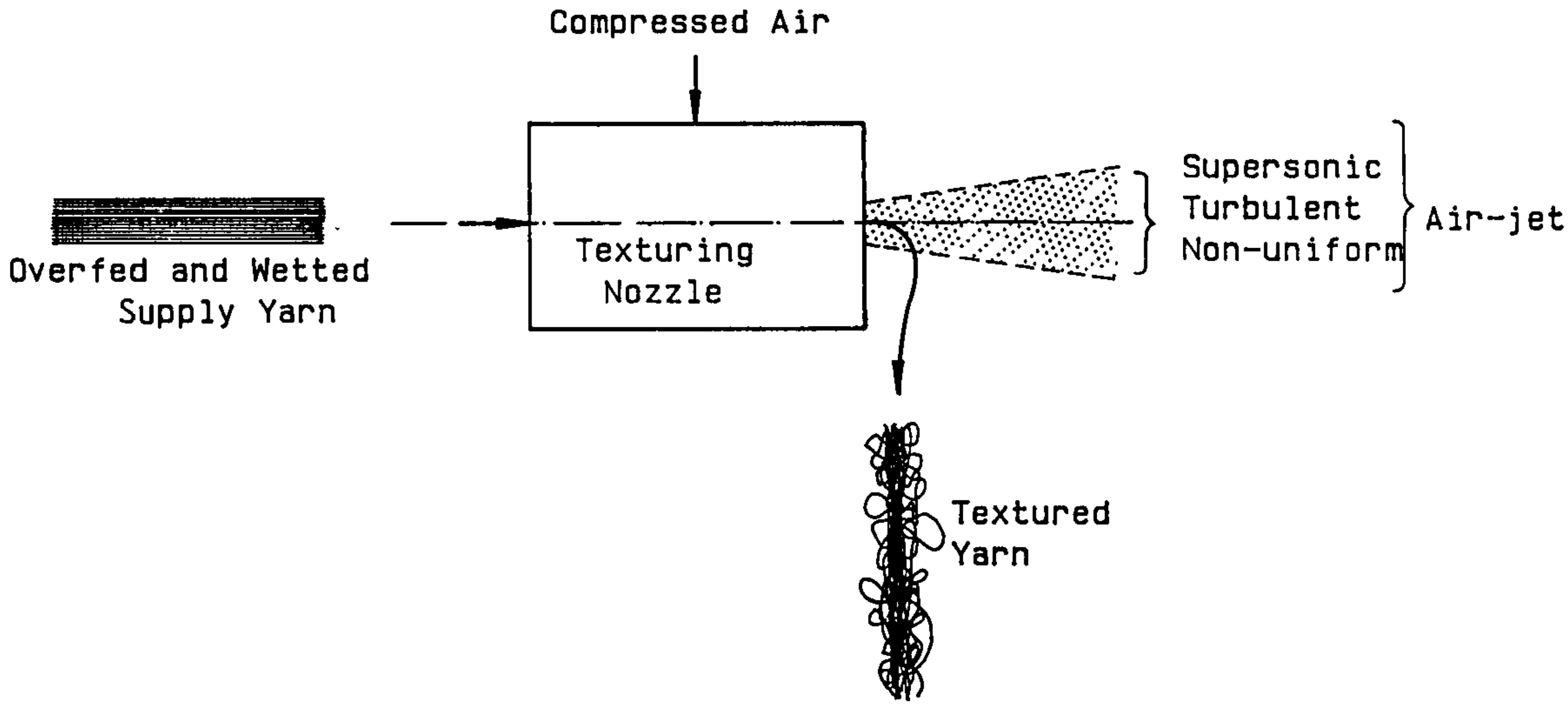

Figure 1.3 Block diagram of the air-jet texturing process

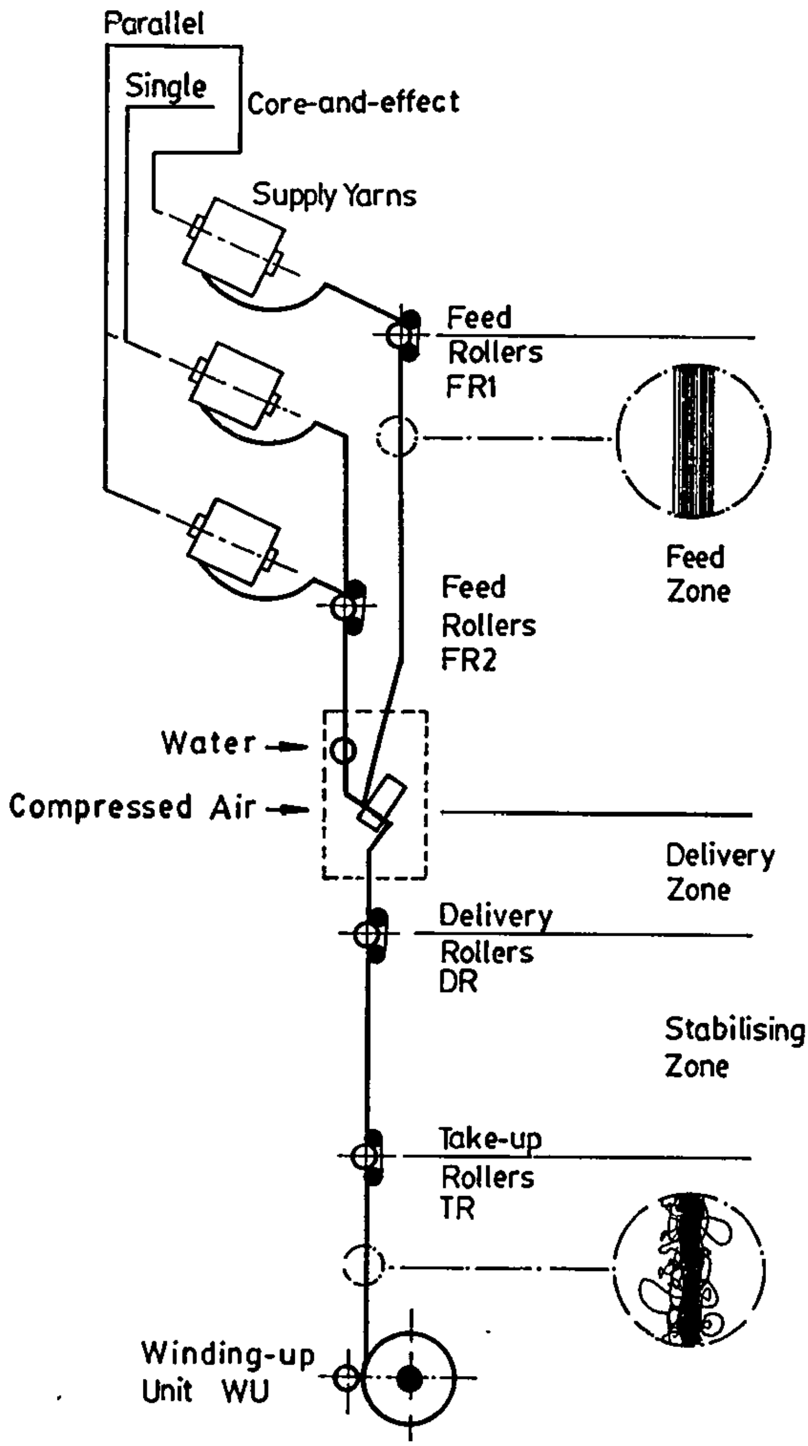

Figure 1.4 Schematic illustration of the basic requirements of the air-jet texturing process

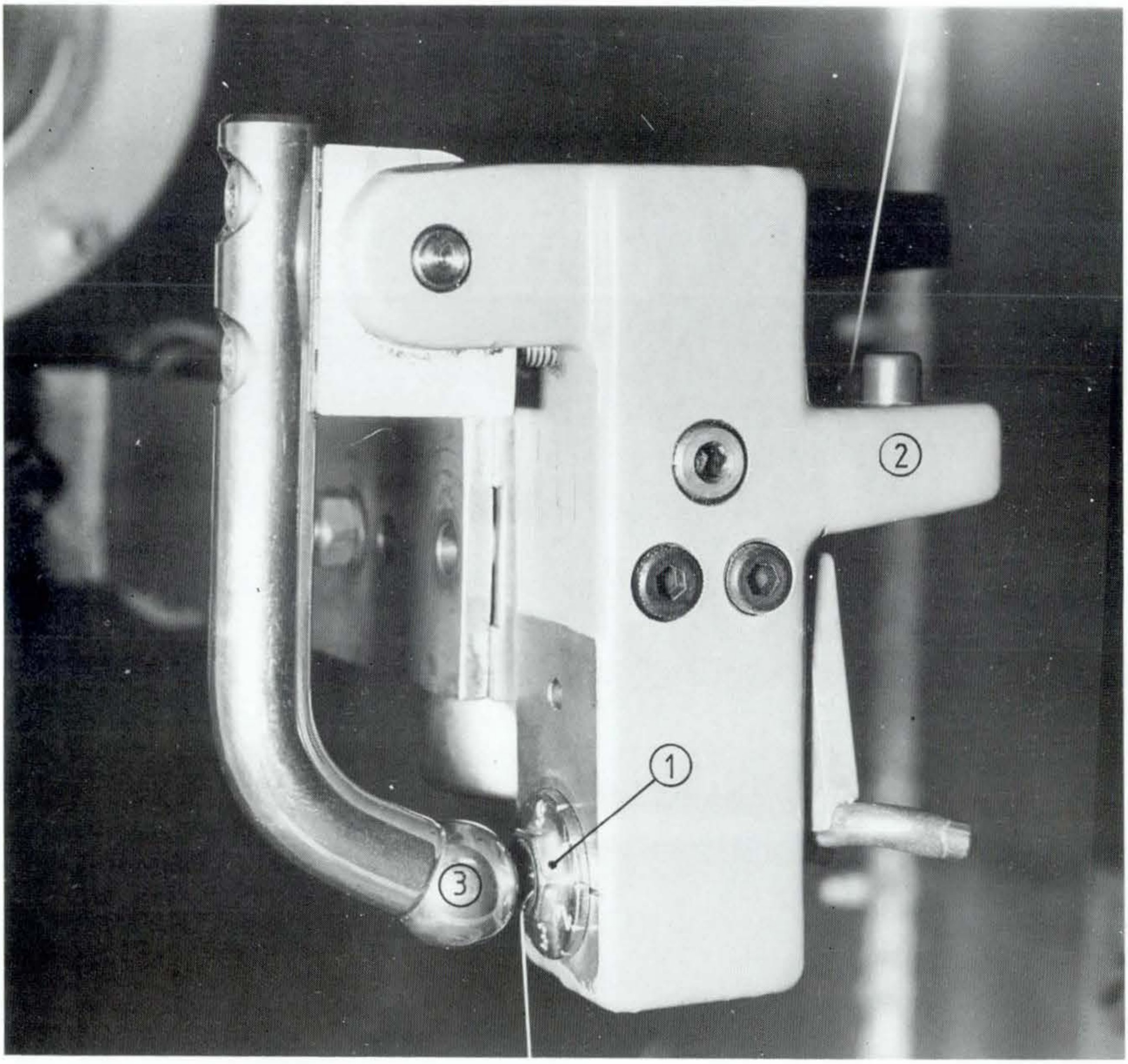

Figure 1.5 Hemajet nozzle housing: (1) texturing nozzle; (2) integrated wetting unit; and (3) baffle ball

CHAPTER 2

LITERATURE SURVEY

2.1 State of the Air-jet Texturing Process

From the announcement of the first nozzle patent in 1952 to the present day, the air-jet texturing process has experienced many developments and improvements. Although texturing speeds have been increased from 10 m/min up to 600 m/min and the compressed air consumption has been reduced from about 22 m^3/h to about 6 m^3/h per nozzle, whilst the yarn properties have been considerably improved, the process can still hardly be regarded as fully established. High energy demand due to high compressed air consumption has been one of the initial reasons for the slow development of the air-jet texturing process. The lack of a thorough understanding of the basics of the process has also handicapped improvements such as improved nozzle design and systematic provisions of current process parameters. One of the major obstacles to such improvements from the outset has been the 'cloak of secrecy' placed over the strictly licenced Taslan texturing process by the Du Pont company; this has mitigated against objective investigations by impartial 'non-licenced' researchers and has thus impeded the progress of the air-jet texturing progress whilst the unlicenced false-twist texturing techniques have rapidly made ground and established themselves in new markets.

Today's air-jet texturing technology requires no pretwisted supply yarns to produce a wide range of textured yarns ranging from very fine polyester and polyamide yarns for apparel fabrics[1] to heavy carbon filaments for aerospace technology[2] and glass fibres. In contrast with early texturing machines equipped with only one type of nozzle, i.e. Taslan IX, a number of texturing nozzles[3] are available for modern purpose built texturing machines. Such machines also facilitate many other new features such as drawing POY (partially oriented yarns) yarns, to provide process economics, and heat setting after texturing, to satisfy growing market demands.

2.2 Reviews of the Air-jet Texturing Technology

The first review of the air-jet texturing process was made by Wray[4] in 1965 more than a decade after the strictly licenced Du Pont Taslan process became known to outsiders. Wray mainly reviewed the patent literature relating to the Taslan IX jet, then the only known industrial nozzle. Since then several others[5-14], both from industry and the universities, have reviewed the development of the air-jet texturing process. Among these, a Textile Progress review by Wilson[9] covers the period up to 1977 including a large list of references and patents published. A future edition of this review, which will cover the period up to 1985 has also been mentioned by Kollu[13], though it has not yet been published.

Whilst industrialists[5,6,8] have reviewed the process in general terms, university researchers have preferred to study the relevant aspects of air-jet texturing. Sivakumar[7], Wray and Acar[10], and Acar and Wray[14] mainly reviewed nozzle developments and suggested texturing mechanisms, whereas Kollu[11,13] and Gülal[12] surveyed the literature regarding the structure, properties and blending of the air-jet textured yarns.

2.3 Economic Aspects of the Process

In the early days of the strictly licenced, and therefore highly secret, Taslan texturing process, the conversion costs were thought to be so unfavourable that no attempts at comparison with the other yarn texturing techniques appeared in the literature. The licence fee was, of course, additional to those costs. As air-jet processing gradually improved, with the introduction of more efficient nozzles, the conversion costs decreased to such a level that some comparisons with both false-twist textured and spun staple yarns started to be made. By comparing the costs of per kilo of 100% wool, 40/60 Polyester/wool, 50/50 Polyester/wool, and 100% Polyester worsted yarns with false-twist textured yarns of approximately the same linear density, Brehm[15], in 1978, concluded that the energy consumption of air-jet texturing needs to be reduced in order for the air-jet textured yarns to compete with false-twist textured yarns. Since air-jet textured yarns closely resemble spun staple yarns and are of completely different characteristics than false-twist textured yarns, a competition between the two texturing processes is reported to be unjustifiable[1].

The energy requirements of the air-jet texturing process have been compared with other conventional spinning processes by many researchers[16-21]. The most recent report by Wilson[21] has illustrated that the energy requirement for 167 dtex ringspun 67/33 cotton/Polyester yarn is 4.41 kWh/kg, whilst the same linear density POY polyester yarn can be air-jet textured at 600 m/min with an energy consumption of only 3.1 kWh/kg. The paper also reported that this amount could even be reduced to as little as 1.8 kWh/kg if a 2 fold 167 dtex yarn is used.

With such economic advantages, the air-jet textured yarns are predicted to have an opportunity of competing for 54% of home furnishings, 15% of industrial fabrics and 53% of apparel fabrics in the USA[22]. Similarly the air-jet textured yarns are also occupying a considerable slice of textile yarn application in Western Europe. Despite the estimated total of 24500 tons of air-jet textured yarns in 1984[23], the approximate production, however, was reported[24] to be 63% more at 40000 tons.

2.4 The Future

The predictions by Wilson[17,18,25] that the air-jet textured yarns will replace 20% of the present spun yarn market by the year 2000 and furthermore that they have the potential to replace another 20% of polyester filament yarns which are textured today by the false-twist method are considered by Wray and Acar[26] to be over-optimistic. Nevertheless, they also admit that the air-jet texturing is steadily increasing its market share owing to: (i) the developments in nozzle design; (ii) the provision of wider ranges of suitable supply yarns; and (iii) increased awareness of its unique capabilities to adequately simulate spun yarns cheaply and to blend different types of yarns during processing.

2.5 Nozzle Development

Being at the heart of the entire air-jet texturing process, the various industrially used texturing nozzles have been developed through practical experience rather than by informed theoretical considerations. Their continuous evolution may be divided into the following four major groupings[27]: (i) early stages and 'false start' with the Taslan IX nozzle; (ii) upsurge of improved nozzles, i.e. Taslan X and XI; (iii) further improvements to the Taslan nozzles (Taslan XIV and XV) with impact elements, and interest from textile companies besides other than Du Pont; and (iv) the contemporary stage with the Taslan XX and cylindrical type nozzles, e.g. HemaJets.

At the first stage of the development, nozzles[28] utilised the compressed air so inefficiently and unreliably[29] that they not only created a negative public image of the process by being energy intensive, but they also diverted the attention of nozzle designers to inadequate designs which occupied the first ten years of development. Therefore the hesitant beginnings of the process was perhaps rightly termed as a 'false start' by Phillips[30] and Isaacs[31]. However, when the very first patented nozzle[28], shown in Fig. 2.1, is studied, it is interesting to note that this apparently little used nozzle design covered almost all the features of the modern Taslan nozzles. It had an axial yarn feed while the compressed air was admitted to the nozzle body through a side entry. It also had an impact element of a flat plate type. Nevertheless, the lack of aerodynamic design of the inner configuration caused tremendous losses to the air flow resulting in inefficient texturing. Another early design reported by Piller[6] also suffered from similar deficiencies.

Following the failure of this nozzle, the nozzle designers were forced to change the basic configuration and introduced a completely different design[32]. The Taslan IX nozzle shown in Fig. 2.2 had an axial air flow which was accelerated by well established converging-diverging geometry, while the highly pretwisted overfed yarn was admitted to the main channel through a stepped hollow needle inclined at 45^{o} to the nozzle axis. This nozzle had serious wear problems and was very difficult for an inexperienced operator to set and operate[27] due to the crucial importance of the needle setting. Nevertheless, it was used by licencees of the Taslan process for well over a decade.

Du Pont's nozzle designers, dissatisfied with the poor performance of the Taslan IX nozzle, had to resort to the basic features of their earlier design (Fig. 2.1). With improved aerodynamic design of the inner surfaces of the nozzle as well as the implimentation of the converging-diverging nozzle geometry, a long lasting breakthrough began and the Taslan X nozzle[33] gradually emerged, from behind all the closed doors of the Du Pont laboratories, as the most acceptable nozzle for the Taslan licencees. Over this period, Wray and Entwistle[34], working as impartial researchers and having been consistently denied the opportunity of becoming experimental licencees of the Du Pont Taslan texturing process, had thoroughly investigated the Type IX nozzle, as revealed in the patent literature, and had publically revealed many drawbacks of its design. They, furthermore, suggested a modification which improved the performance by reducing the air consumption up to 65%. This modification was also reported to be eliminating the sensitive needle setting of the original Taslan IX nozzle whilst making little negative effect to the yarn quality. The Taslan XI[35] and other nozzles[36] then followed by improving performance by creating asymmetric flows in the nozzle venturis. The asymmetry in the flow is created by one sided air entry to the so called turbulence chamber in the Taslan XI and the eccentric fitting of the needle in the Taslan XII. Through these developments in the nozzle design, the texturing speeds have been increased in the order of 10 times, i.e. to 600 m/min from the earlier 50 m/min[27].

The introduction of external impact elements such as plates, bars and spheres immediately after the nozzle exit was another development stage. The Taslan XIV[37] and XV[38] jets with impact plate and bar respectively have been introduced which have allowed the use of twist free supply yarns. In 1985, Du Pont patented[39] its Taslan XX nozzle which possesses an easy string-up facility with no needle or venturi adjustment. Nevertheless Acar[40] argued that this jet might require more frequent cleaning and servicing due to the contamination of the moving venturi and it has apparently proved to be an industrial failure.

Despite the continuous development and improvement attempts, certain drawbacks such as high compressed air consumption, nozzle to nozzle inconsistency due to the need for precise adjustment of both the needle and the venturi, and the frequent contamination of the venturi with spin finish material washed away from the yarn surface, thereby requiring regular cleaning and servicing[27], still needed to be solved. Such factors have induced some other manufacturers to take an interest, particularly after the expiration of the main Du Pont patents which formed the basis of the Taslan process. They are too numerous to mention them all, but two, namely Enterprise Machine and Development Co. (EMAD) of the USA and Heberlein Maschinenfabrik A.G. of Switzerland, stand out. The latter has recently made even more contributions to the air-jet texturing process than Du Pont. Although the nozzles[27] developed by EMAD have also followed the similar configuration to the Taslan nozzles, having converging-diverging geometry, the Heberlein nozzles are of completely different geometry.

The most significant developments in the nozzle design have therefore taken place in the last decade. Heberlein took over the air-jet technology developed by Berliner Maschinenbau A.G. of Switzerland in 1977 and introduced its first HemaJet nozzle called the Standard-core HemaJet shown in Fig. 2.3 in 1978[41]. This nozzle is reported to be similar to an earlier design, i.e. the Mirlan nozzle from

Czechoslovakia[6]. In this design, the air is fed into the main duct of the nozzle through three small inlet holes, where it impinges upon the overfed supply yarn which follows a straight axial path in the nozzle. Since the Standard-core HemaJet had no adjustable parts, the need for a skilled operator for manning the Taslan nozzles has been eliminated. Better nozzle-to-nozzle consistency is obtained by keeping the machining tolerances very tight. The design has a self cleaning facility, as spin finish constituents are washed away from the yarn surface because of the straight geometry of the main duct which is constantly in contact with the moving yarn[20]. Heberlein[3] later introduced six other nozzles designated as T100, T311, T341, T110, T140 and T350 with the first digit indicating the provision of either one or three inlet holes. Some of these nozzles for the apparel range have reduced the air consumption drastically.

It appears that the majority of the nozzles to date have been developed by the industry through practical experience. Acar[42], utilising the results of his theoretical and experimental investigation with the Standard-core HemaJet designed novel nozzles. The prototypes of these nozzles were manufactured by Heberlein and were reported to yield satisfactory texturing. The present work has also covered these nozzles (See Chapter 4).

2.6 Aerodynamics of the Nozzles

Since the actual texturing process, i.e. loop and entanglement of the overfed supply yarn, is carried out by the air flow in the nozzle and the air-jet created by this flow, a detailed study of the aerodynamics of the nozzles is of paramount significance for the improvement of the nozzle performance. Therefore, in parallel to the nozzle development the flow properties have been studied. While Wray and Entwistle[43] studied the air flow in the Taslan IX nozzle, Şen[44] extended his research to investigate the air-jet created by that nozzle. Later on, Sivakumar[7] applied the theory for converging-diverging nozzles to both the Taslan IX and X nozzles. However, the more recent Taslan nozzles (Taslan XIV and XV) have been examined by the researchers from Aachen, Germany[45-49]. Finally Acar et al[50] have studied the air flow through the Standard-core HemaJet, and also built a mathematical model for the flow[51].

In the 1960's, Wray[4], and Wray and Entwistle[43], concentrated their flow studies on the wake flow created by the tilted needle of the Taslan IX. By extending the turbulent flow theory of flow passing over a cylinder, they envisaged the vortices created in the wake of the needle. They also concluded that the overfed and pretwisted yarn is untwisted by the effect of such rotational flow resulting in a loop and entanglement formation. Such an explanation of the flow, led Wray and Entwistle[34] to modify the Taslan IX nozzle and achieve up to 65% compressed air savings. Şen[44], working under Wray's supervision, proved this theory to be incorrect. He used scaled-up transparent versions of the Taslan IX nozzle to verify that the actual texturing takes place outside the nozzle and that the Reynolds Number, based on the nozzle throat diameter, is well above the range at which such vortices at the wake of a cylinder could exist. Şen furthermore visualised the air-jet by means of the Schlieren technique and showed the formation of oblique shock waves. Şen's flow velocity and turbulence measurements by means of Hot Wire Anemometry also showed that the air-jet created by the Taslan IX nozzle was supersonic, and highly turbulent. The asymmetry in the velocity profile was attributed to the presence and setting of the feed needle.

Sivakumar[7], on the other hand, studied the air-flow through the Taslan IX nozzle without the needle by theoretical means and thereby predicted the formation of shock waves at the throat. By making a nozzle similar to the Taslan X patents, with his theoretically predicted dimensions, Sivakumar carried out some experimental research and concluded that the loop formation and the formation of the shock waves at the exit of the nozzle are closely related. He also surmised that pretwisted overfed yarn collapses when it reaches the shock wave (i.e. a pressure barrier) and that this creates the entanglement.

Bock and Lünenschloss[45-47] reconstructed the flow path in the Taslan XIV nozzle by observations of the surface structure of the deposits within the nozzle venturi resulting from the spin finish washed away from the yarn inside the turbulence chamber. Utilising this technique, they studied the effects of supply pressure and nozzle geometry and concluded that the air flow is affected by both.

When the feed needle channel is blocked, Taslan nozzles behave closely similar to the classic converging-diverging nozzle for which the flow of compressible fluids such as air and steam is well established by experimental and theoretical means. Therefore Bock and Lünenschloss made use of such established theory for their study and extended their work into the air-jet created by the Taslan XIV nozzle; using the Schlieren technique, like Şen earlier, they visualised the jet flow and measured the total pressure distribution in the jet. Together with the theoretical study, they constructed a picture of the jet consisting of high and low pressure zones.

The most recent work of Bock and Lünenschloss[48,49] examined a flat, transparent version of the Taslan XIV nozzle. The Schlieren technique enabled them to observe the turbulence chamber and the formation of oblique shock waves in and out of this nozzle. The turbulent nature of the air-jet was also verified by both the instantaneous flow visualisation and pressure measurements with a high frequency (100 kHz) transducer.

A scaled-up model of the Standard-core HemaJet was used by Acar et al[50]. Through velocity measurements at the exit plane of the nozzle, it was concluded that the Standard-core HemaJet nozzle also creates supersonic, turbulent, slightly asymmetric jets with a non-uniform velocity profile. The result is apparently in agreement with previous researchers conclusions. The air-jet was also visualised by means of interferometric and shadowgraphic techniques. Acar et al, measuring the static pressures in the main channel of the scaled-up nozzle through wall static pressure tappings, reached the conclusion that the flow in the nozzle near the air-inlet bores is very complex and contributes to the asymmetry and non-uniformity of the jet.

In order to predict the flow properties created by a converging-diverging type nozzle, the steady one-dimensional isentropic flow equations as described in standard texts[52,53] can be utilised. Nevertheless, the cylindrical geometry of all HemaJets precludes the use of such equations. Therefore Acar et al[51] attempted to develop a mathematical model for such nozzles, and claimed that the developed theoretical model provided reasonably close predictions of the flow properties at the exit plane of the Standard-core HemaJet.

2.7 Loop Formation Mechanism

The two essentials of the air-jet texturing process as stated by Wray[54] are firstly overfeed, so that an excess length of filaments is available for forming into loops and convolutions, and secondly turbulent air-flow, sufficient to disarrange and entangle the filament bundle so that the looped filaments possess sufficient inter-filament friction to be stable at working loads. These basic requirements are also valid for the most modern air-jet texturing technology. However, the hypotheses of the bulking mechanism, i.e. loop formation mechanism, has been changed.

Since pre-twisted yarns were required for effective texturing at the time of Wray[54] and Sivakumar[7], both of these researchers have based their different hypotheses on the presence of twist. Having done a number of experiments with the Taslan IX, including observation of the longitudinal filament displacement in the yarn, yarn structure investigation by means of tracer filaments, and observation of the yarn leaving the venturi by means of high speed cine-photography, Wray postulated the loop formation mechanism as:

> "the pre-twisted yarn is overfed into the venturi, where it is temporarily untwisted by a complex wortex-action, and consequently individual filaments buckle and snarl into loops due to the filament torsional energy." (Wray[54])

Although Şen[44] verified that no vortex shedding occurs in the venturi, he postulated that the untwisting of pre-twisted yarn occurs just outside the nozzle thus leading to the formation of loops and arcs.

Sivakumar[7] in 1975, having theoretically predicted the formation of shock waves in and out of the nozzles (Taslan IX and X), postulated another loop formation mechanism. He surmised that:

> "as the overfed yarn comes under the influence of the air flow in the nozzle, it is suddenly retarded by the pressure barrier created by the formation of the compression shock waves. As the tension suddenly reduces, the twist lively filaments in the yarn tend to develop snarls, which are entangled by the turbulence of the jet." (Sivakumar[7])

The introduction of more effective nozzles has eliminated the need for pretwisted yarns discrediting the above postulated loop formation mechanisms. However, two conflicting hypotheses on the formation of the loop and entanglement on the twist free supply yarns have been suggested by Bock and Lünenschloss[45-49] and Acar et al[10,55-57].

Bock and Lünenschloss are of the opinion that

> "overfed, twist free filament yarn is opened in the nozzle by the turbulence and/or gradients of the flow velocity, and places itself in a stream of high kinetic energy. With right-angled draw-off after the nozzle, an interlacing point forms above the axis (in the case of upwards yarn delivery), at the interface between two zones of different flow states. The filaments blown through below this interlacing point pass through a zone of high air turbulence, and are decelerated by the subsequent drop of dynamic pressure due to the formation of shock waves. When the filaments interlace, loops projecting from the yarn are formed by the differently sized filament bends." (Bock and Lünenschloss[46])

This loop formation mechanism, which is based mainly on the formation of the shock waves and in turn high and low energy zones in the air-jet, has been said to be invalid by Acar et al[56]. They argue that the shock waves are destroyed when a bundle of filaments are introduced into the jet. Consequently, Acar et al postulated another mechanism on the basis of their observations and investigations on the Standard-core HemaJet nozzle. The postulated loop formation mechanism is stated to be as follows:

> "When a bundle of filaments are introduced into the air-jet, some of these filaments will be moving at faster speeds than others owing to the relatively greater fluid forces acting on them. The free excess lengths provided by overfeeding the filaments enable the faster moving-filaments to slip and be displaced longitudinally with respect to the slower-moving filaments. The degree of these longitudinal displacements is affected by local drag and frictional forces instantaneously acting on the filaments and also by the overfeed.
>
> The textured yarn is withdrawn from the nozzle at right angles to the nozzle axis at the texturing speed. Since the filaments are entangled and formed into loops, the resultant textured yarn is shortened, and a tension is created of a magnitude determined by the effectiveness of the texturing. Thus, on the one hand, the emerging filaments are blown out of the nozzle along the direction of the air stream at much greater speeds than the yarn-texturing speed; on the other hand, the tension created in the yarn pulls the 'leading ends' of the emerging filaments in the direction of the yarn delivery. Whereas the 'trailing ends' of the filaments in the nozzle are blown out at very high speeds, the 'leading ends' of the filaments are held within the core of the much more slowly moving textured yarn and are pulled downward while being kept fairly close to the nozzle exit plane. The emerging filaments are therefore forcibly bent into bows and arcs by the fluid forces acting on them. These are then entangled with other emerging filaments, which are formed into fixed stable loops within the textured yarn." (Acar et al[57])

Acar et al furthermore claimed that the above stated mechanism of the loop and entanglement formation could be valid for all types of texturing nozzles, despite detailed differences in their design, because the underlying requirement to create a supersonic, turbulent, asymmetric, and non-uniform flow and a substantial change of the direction of the yarn path at the nozzle exit is common to all satisfactory air-jet texturing processes. Nevertheless, Bock and Lüneneschloss[48,49], disclosing the results of their research with a flat, transparent version of the Taslan XIV nozzle, have insisted, though admitting that the presence of the filaments partly obscure the air flow, that the shock waves created in the free flow at the exit of the nozzle evidently exert a force on the filaments making them to follow an ondulating path in the venturi and to deflect at the exit. They also claimed that this deflection causes an arching of the filaments which is responsible for taking up the extra length of the overfed yarn.

2.8 Wetting of the Supply Yarn

Wetting or moistening of the supply yarn prior to its entry to the nozzle is an integral and indispensible part of the air-jet texturing process today, because it highly improves the texturing conditions, thereby resulting in a more uniform and stable yarn. Nevertheless, the mechanism of the improvement caused by the addition of water is not yet understood. However, as with the above mentioned two different loop formation mechanism hypotheses, two widely differing explanations of the effects of yarn wetting were given by Bock and Lünenschloss[47] and Acar et al[58]. The former suggested that the water entrained into the air flow alters the flow characteristics and causes the formation of condensation shock waves, whilst the latter, having theoretically verified that water droplets adversely affect the air flow, postulated that the water applied to the yarn acts as a lubricant and reduces the yarn-to-nozzle friction as well as the interfilament friction. Acar et al have supported their claim by tension measurements in the feed and delivery zones where a great increase in the tension in the feed zone is observed with the wet supply yarns indicating increased forces applied to the yarn as a consequence of reduced friction.

Two different means of water application are possible. While the earlier texturing machines[59,60] had a water bath through which the immersed supply yarns passed, modern machines utilise a wetting unit[61] by which the amount of water applied can be more accurately controlled. The amount of water necessary to impart the desired improved texturing effects was found to be very little[47,58,62].

2.9 Properties of Air-jet Textured Yarns

The air-jet textured yarns are of different characteristics to their parent yarns, in that they are of higher bulk, exhibit increased covering power, have a more subdued lustre, and are warmer in hand. Therefore they possess some unique properties which require investigation.

The work on the properties of air-jet textured yarns starts with Wray's[4] well known pioneering research. He defined some of these unique properties such as increase in linear density due to texturing, loop size and frequency, physical bulk and instability and the suggested improvements in their measurement techniques.

The Du Pont Company has suggested a microscopical test method[63] by which the over-all diameter, core diameter, the loop size and the loop frequency of a Taslan air-jet textured yarn can be assessed. Wray[64], criticizing this method as being tedious and inaccurate, devised a quicker and yet more accurate graphical method[65] for measuring the yarn diameter and average loop size. Ten years later, Fischer[66] reported that a more elaborate system which uses photodiode cells to detect the loops and arcs around the core and sorts out the loop size and frequency of the yarn had been developed in Aachen, West Germany. Bock[45] made use of such a system for his investigations. Here in Britain, however, Wilson[18] reported that a fray counter developed by Toray Co. offered possibilities of counting the loops and evaluating their sizes. Also Kollu[11] described another system which makes use of a microdensiometer and ancilliary equipment. Using such a system in a graphical way, Kollu obtained an estimate of the loop size and number. Very recently, Acar et al[67] developed a highly sophisticated device with a line of 256 monolithic Charge Coupled Devices (CCD) as the image recognition element. They claim that this device, together with a microcomputer and suitable software, will enable the user to measure the mean yarn diameter, loop size and frequency at test speeds up to 10 m/min.

Depending on the amount of overfeed and the effectiveness of the texturing conditions viz. nozzle type, air pressure, texturing speed, the physical bulk of the textured yarn is increased. In order to quantify physical bulk, Du Pont[63] recommended a test which compared the package densities of the yarn before and after texturing. In addition to this, Wray[69] utilised another method in which he compared the specific volumes of fabrics woven from both textured and supply yarns. A specially designed device was used by Rozmarynowska and Godek[68] in 1966 to measure the apparent volume of the air-jet textured yarns. This bulkiness test consisted in gauging a skein of yarn subjected to a known initial tension. Şen and Wray[69] have refined the Du Pont's physical bulk test by weighing and accurately measuring the outside diameters of the two packages of supply and textured yarns. They also devised a water absorption technique to evaluate the bulkiness of the textured yarn, and concluded that the water absorption test was much quicker and simpler to use than the package density tests.

The stability of an air-jet textured yarn is its resistance to having the loops pulled out by tension. This unique property is tested by means of instability measurements. Both Du Pont[63] and Heberlein[70] have suggested their own instability measuring techniques. On the other hand, three more instability measuring techniques have also been proposed by Wray[54], and Acar et al[56]. Therefore, it is the common concern of many[62,70,71] that a standard, objective instability measuring technique should be developed.

In an attempt to establish a quality control criterion, Piller[71] defined an SVS (Stabilitat, Voluminositat, Schligenhaufigkeit) Value which is an aggregate total of Instability, bulkiness, and loop frequency, but this value does not seem to have attracted any interest to date. Piller and Lesykova[19], using idealised models, also attempted to build up a mathematical model for the structure of the air-jet textured yarns, but they came to the conclusion that the structure of an actual yarn differs considerably from that of an idealised model, thereby confirming the view that determining the characteristics of the yarn seems to be very complex if not impossible. Another mathematical approach to the mechanics of the air-jet textured yarns was intended by Kollu[72] but this has yet to emerge significantly in the literature.

The over-all quality assessment of air-jet textured yarns is made to limited extent by means of some of the above discussed test techniques together with simple visual inspection and tensile tests. The majority of these tests leave much to be desired in that these are laborious, time consuming and largely subjective. In contrast, the modern textile industry requires fast and objective on-line quality control[73,74] whenever possible.

2.10 Effects of Process and Supply Yarn Parameters on the Properties of Air-jet Textured Yarns

The effects of process parameters and supply yarn properties on the properties of air-jet textured yarns (which include: the final linear density or linear density increase; strength related properties such as breaking elongation, load-elongation characteristics, and tenacity; instability; loop size and frequency; bulk; boiling water shrinkage; unwinding performance from a package; and cover features in a woven or knitted fabric) are probably the most investigated aspect of the air-jet texturing process. Starting with Price[75] in 1960 to the present author, many researchers both from industry and universities have ascertained the effects of various parameters on the yarn quality. Since they are too numerous to detail here, lists of the process parameters and supply yarn properties together with the reference numbers indicating the publications in which the various investigations have appeared are offered in Table 2.1.

2.11 Texturing Machines

In parallel with developments in the process, several texturing machines have also been developed by various textile machinery companies. Most of the machines used in the early days were either spinning or winding machines retrofitted with the texturing nozzles or in-house built machines. In more recent years false-twist texturing machines were retrofitted for air-jet texturing. Today, most air-jet texturing machines are specifically designed and built for the purpose and therefore provide optimum working conditions for yarn processing.

In Europe, the first purpose built machine was introduced in early 70's by the Eltex Company of West Germany. In 1975 and 1978, two other companies, namely Berliner Machinenbau A.G.[59] of Switzerland and Barmag Company[65] of West Germany, respectively introduced their machines. While these existing companies were improving their machines, several new ones also appeared in the market and Enterprise, Murata, Toray, Theiler are a few worthy of mention in this respect. The most recent versions of texturing machines have been reviewed by Kollu[13] and Acar[40].

With these modern types of machines, speeds up to 1000 m/min can be reached. Most of them also facilitate the drawing of POY yarns and provide heaters for heat setting after texturing. The choice of the nozzle type is generally left to the operator.

2.12 Miscellaneous other Aspects of Air-jet Texturing

The basic types of operation are single, parallel and core-and-effect texturing[75]. With these basic operations, an almost infinite number of types of yarns with linear densities ranging from 50 to 20,000 dtex in materials ranging from acrylic and acetate to glass and carbon, are said to be textured[25].

Since heat setting is not an essential part of the process, any types of supply yarn can be blended so intimately that it is reported to be an ideal process for heather blend yarns[30]. Blending properties of the air-jet textured yarns have been investigated in detail by Gülal[12] and Kollu[13].

The application and end-uses for the various types of air-jet textured yarns are normally determined by their properties. However, due to the above mentioned versatility of the process and yarns, air-jet textured yarns find application in almost every corner of the textile industry such as shoe inseaming thread, men's shirting, shoe laces, sheeting, tent fabrics, upholstery, drapery, neckties, women's sweaters[75], men's jacket, women's blouses, dresses, sewing threads, automobile upholstery, towels, blankets, swimsuits[5], tapes, embroidery articles, certain medical fabrics[71], anoraks, structural and coated applications[1], chaffer fabrics, luggage, rainwear, sportswear[30], canvas type fabrics for luggage, glass fibres in printed circuit boards and automobile body parts[84].

Despite the extremely wide variety of these claimed applications, more and more extensions and modifications to the air-jet texturing process have been innovated. Şen and Wray[85,86] endeavoured to create yarns similar to the air-jet textured yarns, but without using compressed air. Kollu[13] claims that if the supply yarn is directly fed from the package to the texturing nozzle without any mechanical drive, texturing speeds could be improved. With the alteration of core or effect yarn overfeed by means of devices called Zutex[87] and Fatex[88] varieties of other yarns such as slub, nub, fancy and flake yarns can be produced. Air-jet textured yarns comprising a well defined core and surrounding loops and arcs already closely resemble spun staple yarns, however, by breaking some of the surface loops, this resemblance can be improved. A device to do this known as Texspun is reported[13,40] to be available for most existing machines. If false-twisted yarns are sequentially air textured, a worsted look and handle is said to be achieved. This process is patented under the trade name of Tusma[25] and Milpa[89] by the Teijin Co. of Japan.

Since the whole process is carried out by a jet of compressed air, the air supply should be the highest quality, i.e. oil, moisture and dust free[73]. Correct selection of the compressor is therefore vital from both process and ecomomic viewpoints[84,90].

When highly compressed air is released from a nozzle. it naturally creates noise. The noise level created by the air-jet texturing compressors and nozzles is reported[15,91,92] to be in the range of 90-100 dB(a). Rilling[91] also foresees the possibility of reducing this noise level, which is already within the likely acceptable limits, by using special sound boxes and he reports that they are already being used for yarns over 6000 dtex when working with air pressures up to 15 bar.

TABLE 2.1

List of investigations carried out on the effects of process parameters and supply yarn properties on the properties of air-jet textured yarns

Process Parameters	Reference Number
Needle Setting	54,7
Air Pressure	75,64,76,7,73,10,77,1,47 81,13
Overfeed	75,68,64,76,7,15,71,10,13
Texturing Speed	75,68,64,77,7,15,70,10,1,13
Nozzle Setting	47,45
Wetting	76,45,10,47,58
Stabilising Extension	47
Heater Type	78,80
Heat Setting	73,62,47,80
Overfeed to the Heater	62,78,80
POY effect	62
Impact Element	45,10,47
Supply Yarn Properties	
Pretwist	75,68,64,76,7,77
Steam Setting	7
Material	76,77,79
Filament Linear Density	75,64,13
Number of Filaments	68,47,13
Total Linear Density	1,79
Filament Cross Section	47,13,82
Filament Density	13

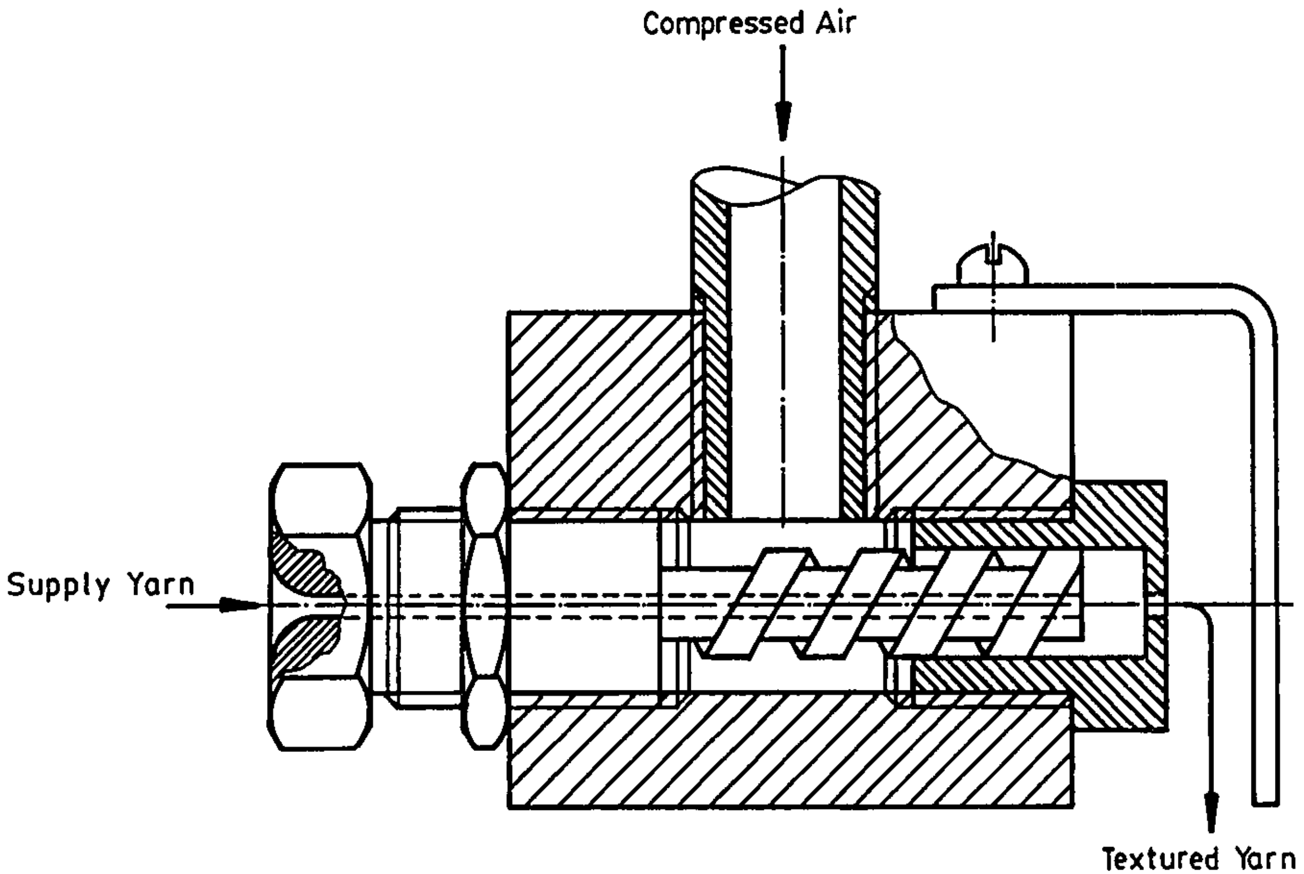

Figure 2.1 An early Taslan texturing nozzle

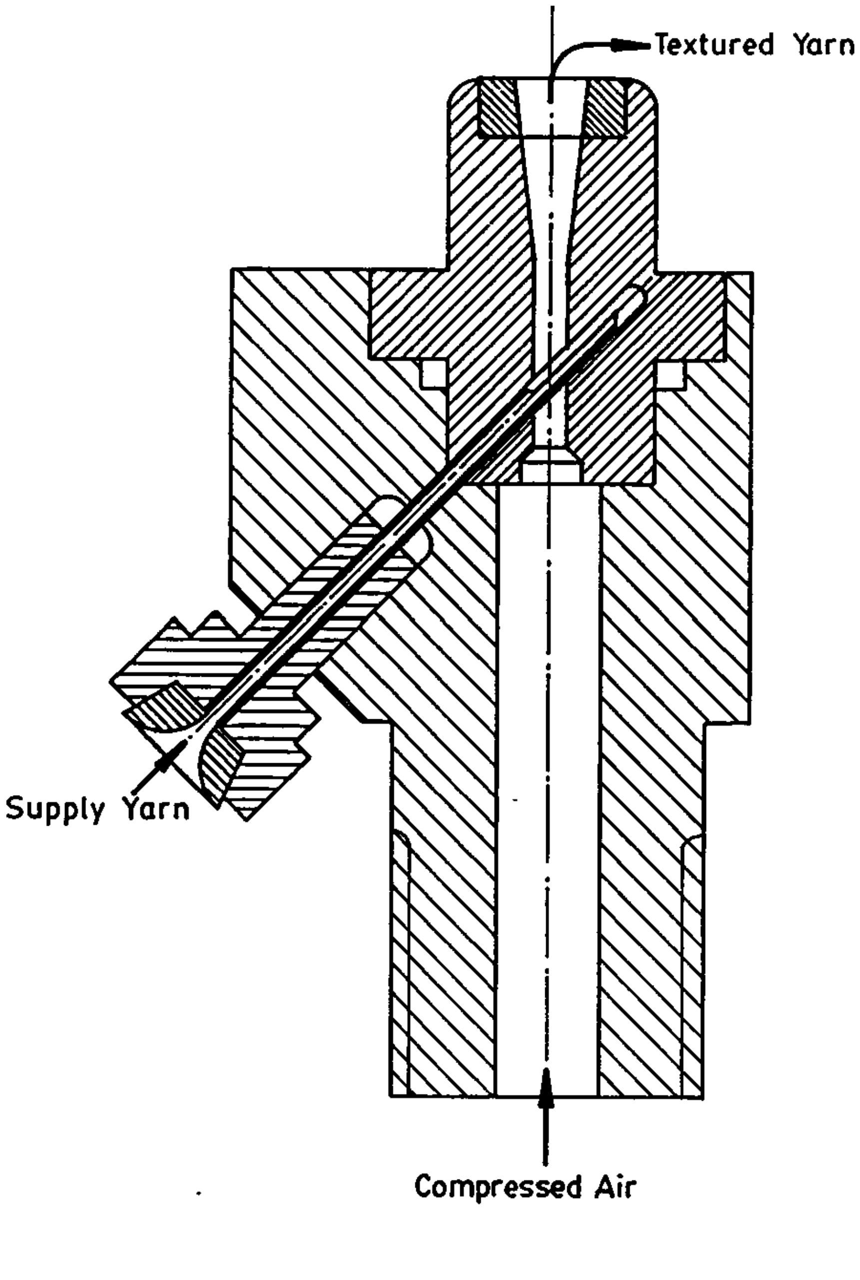

Figure 2.2 Taslan Type IX texturing nozzle

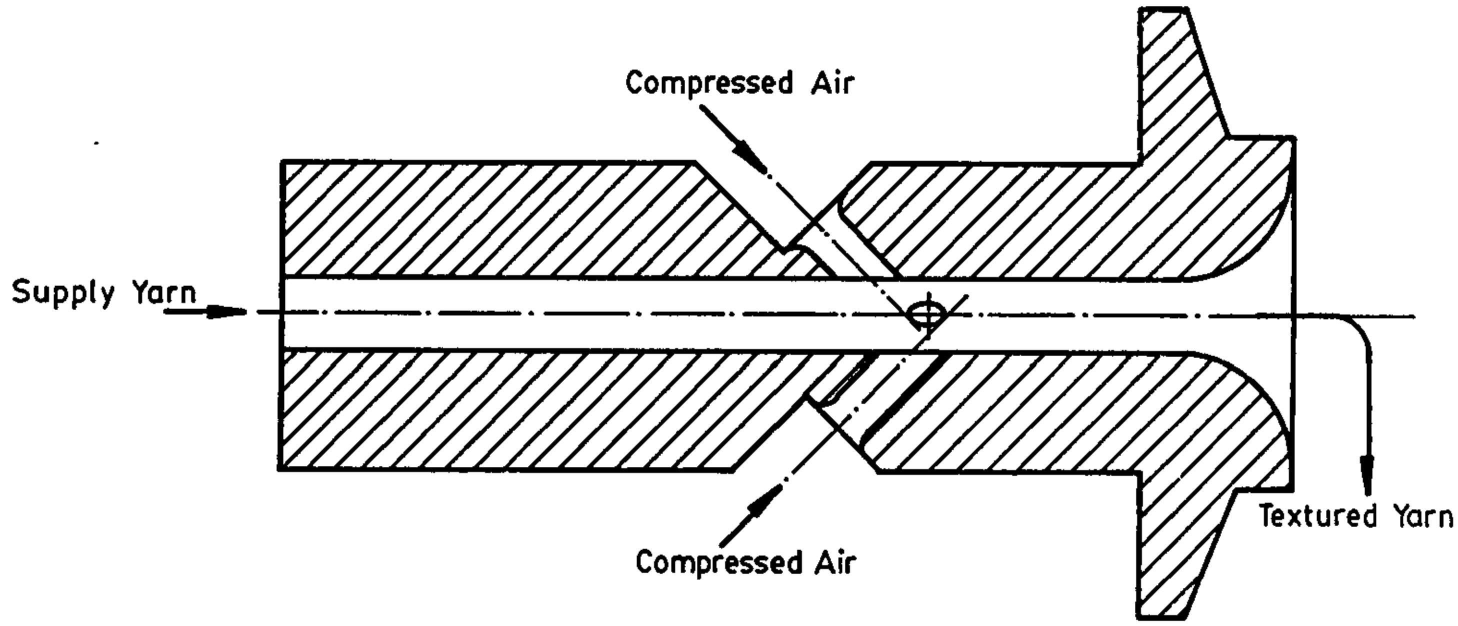

Figure 2.3 Standard-core HemaJet texturing nozzle

CHAPTER 3

DESCRIPTION OF THE AIR FLOW THROUGH CYLINDRICAL NOZZLES

Du Pont Company of USA who pioneered the air-jet texturing process from the early 1950's, supplies 'Taslan' texturing nozzles to licenced users. These are of the converging-diverging type i.e. de Laval type nozzles. There are also other manufacturers who produce texturing nozzles very similar to the Taslan nozzles, but these share only a small fraction of the market.

Although the Heberlein Company of Switzerland is comparatively new in the market, it became a major texturing nozzle manufacturer in the mid 1980's. Heberlein's nozzles are of cylindrical type and are known by the trade name 'HemaJet'. Du Pont and Heberlein have each been producing different variations of their nozzle types, while keeping the main features of them unchanged. For example, Du Pont's range includes Taslan IX[33], X[35], XI[36], XIV[37], XV[38] and most recently XX[39], Heberlein started with its 'Standard-core' HemaJet[41] and continued with other types such as T100, T300, T341 etc[43]. The main structural features of the HemaJet and Taslan nozzles are compared in Fig. 3.1. The compressed air is admitted to the straight main channel of the HemaJet nozzle, where it is divided into primary and secondary flows, whereas in a Taslan nozzle air flows into the venturi through a circumferential gap and is then divided into primary and secondary flows. The choked flow in the throat of the Taslan nozzles is subsequently accelerated by the diverging section of the venturi, but no such controlled acceleration takes place in the HemaJets.

Investigation of the air flow in the Taslan nozzles was left outside the scope of this research mainly for two reasons; the Taslan nozzles utilise a very common supersonic nozzle configuration, i.e. converging-diverging nozzle, to which a well established and proven flow theory is applicable, and many research workers[4,7,44-49] have already investigated this type of texturing nozzle in detail. HemaJet nozzles, however, are relatively recent and have not been investigated thoroughly. Apart from Acar's prominent work[42] on these nozzles, very little published work exists. However, these nozzles are increasingly being used in today's textile industry. Therefore, this chapter is devoted to a detailed and more thorough investigation of the cylindrical type, i.e. HemaJet nozzles. In this research, primarily the T100 type HemaJet with one inlet hole has been studied, since it typifies the whole range of HemaJet nozzles and the same principles of investigation apply to all cylindrical nozzles whether they have a single hole or three inlet holes.

In this chapter, only the undisturbed air flow flowing through the mentioned nozzle is studied. Although it has been proven by Acar et al[56] that the presence of the filaments affects the flow to a large extent, a comprehensive understanding of air flow in the absence of filaments is first required. This investigation has led to the design of more efficient texturing nozzles, as discussed in Chapter 6.

3.1 Description of Cylindrical Texturing Nozzles

The commercial texturing nozzles in this category consist of a cylindrical main duct into which one inlet hole or three inlet holes of smaller diameter are obliquely opened. The compressed air is admitted into the main duct through this inlet hole(s), while the yarn follows a straight path in the nozzle as shown in Fig. 3.2. The yarn inlet section of the cylindrical duct is called the secondary flow section and the other end of the duct is the primary flow section usually with a trumpet shaped divergent exit. In the early types of the HemaJets (e.g. the obsolete 'Standard-core'), this divergent exit had a smaller radius (small trumpet). However, all the recent HemaJets have trumpet shaped exits with larger radii. A comparison of exit shapes of early and recent HemaJets is also seen in Fig. 3.2.

The major difference between various different HemaJets is the number of inlet holes and, with the exception of 'Standard-core', these are designated according to the number of inlet holes they possess[43]. The three inlet holes of the Standard-core HemaJet are not only radially equispaced but are also longitudinally slightly staggered. This configuration is said to impart a swirl to the air flow[55]. However, the recent HemaJets with three inlet holes, e.g. T341, appear to have inlet holes on the same circumferential line, i.e. the staggered configuration has been eliminated.

The two most common features of all cylindrical nozzles are that the ratio of the sum of inlet hole areas to the main duct area is always less than unity and the inclination of the inlet hole(s) to the main duct is at the same angle. These two features of HemaJet nozzles, together with other geometrical parameters, are broadly studied in Chapter 5. Through this investigation their optimum values (from the air flow standpoint) are sought.

3.2 Means of Investigation

The investigation has been mostly undertaken experimentally, e.g. velocity measurement by use of pitot tubes, visualisation of flow by means of laser shadowgraphy and air mass flow rate measurement by rotameter. A theoretical approach, however, has been made by utilising the well established isentropic compressible flow equations.

Full-size texturing nozzles have been used where possible. However, scaled-up nozzles have also been used to justify the experimental results obtained from the full-size nozzles.

A pitot tube has been used in velocity measurements because it was shown by previous researchers[42,44] that other methods, such as hot-wire, hot-film or laser doppler anemometry, presented difficulties when measuring the very high speeds encountered in texturing nozzles.

The essential features of the experimental rig for flow measurement are shown diagramatically in Fig. 3.3. Total (stagnation) pressures were recorded by means of a fine pitot tube of 0.4 mm inner diameter and 0.7 mm outer diameter. The size of pitot tube used, although the smallest practicable, is comparatively large with respect to the full-size nozzles, but this problem was much reduced when the scaled up models were used. A standard pressure test gauge of an accuracy of 0.25% of the full gauge scale was used to record the pressure. The pitot tube was mounted on a three-dimensional manually operated traversing system (Fig. 3.4) facilitating the displacement measurements in the x, y and z planes to an accuracy of 0.01 of a millimetre, measurements being taken at 0.2 mm intervals in all three coordinate directions. The static pressure was assumed to be atmospheric since the flow in question is a free jet. The axial flow velocities may then be calculated using the established formulae.

When a pitot tube is placed in a supersonic flow, a normal shock wave is formed just ahead of the pitot tube. Since the pitot tube measures the total pressures downstream of the shock wave, normal shock wave theory may be used to calculate the upstream flow conditions, as summarised in Appendix A.

It is shown in Chapter 5 that in a supersonic jet the static pressure may be slightly different from the ambient (atmospheric) pressure. Despite this fact, the assumption that the static pressure in a free supersonic jet is equal to the ambient pressure does not make a significant difference in the velocity calculations. In Fig. 3.5, on the one hand, the curve (a) represents the centre line axial velocities calculated by assuming atmospheric pressure for the static pressure in the jet. On the other hand, curve (b) shows the centre line axial velocities calculated by using measured static pressures in the jet. It is evident that the difference between these two calculations is more pronounced in the vicinity of the nozzle exit plane where the highest static pressure difference exists. However, in the further downstream part of the jet, the difference is less substantial (below 10%).

The only relevant work available in the literature for air velocity measurements of the texturing nozzles is that of Acar et al[50] obtained from a four-times linearly scaled-up model of the Standard-core nozzle. These measurements have been repeated and the results are compared in Fig. 3.6 with the results of air velocity measurements obtained from a full-size Standard-core nozzle. The discrepancy between these two measurements is in the range of 5% maximum at about the centre line. Additionally, similar comparisons have been made by using a scaled-up version and a full-size T100 nozzle (Fig. 3.7). This also shows that these two measurements are in reasonable agreement, thereby justifying the use of full size nozzles rather than scaled-up versions in the experimentation.

The air jets emerging from texturing nozzles were visualised by using the shadowgraph technique. In order to do this the shadowgraph unit shown in Fig. 3.8 was deployed. In this apparatus a coherent light beam from a 5 mW Helium-Neon laser was first filtered and passed through a pin-hole. This diffused light then passed through the jet. Since the shock waves cause density variations in the flow, the second derivative of the density[93] is thus recorded directly on to 35 mm film as dark bands.

For the qualitative investigation of the turbulence characteristics of the jets, a high speed shadowgraphy technique was deployed. An Argon spark-gap flash unit made by Pulse Photonics Ltd., which has an exposure time of 200 ns, was used as the light source. The light emiting from the spark was first condensed and then a parallel beam was produced by means of a condenser lens and a slit assembly. This parallel light beam was later passed through the jet at right angles to its axis and an instantaneous shadow of the jet was cast on to 35 mm. film.

3.3 Air Flow Through Cylindrical Nozzles

Fig. 3.9 shows a HemaJet nozzle mounted in a nozzle housing. It can be said that the compressed air that flows through the inlet holes is divided into two streams in the main duct. The primary flow, which has the largest momentum due to the inclination of the inlet hole, flows vigorously and creates a supersonic, asymmetric, non-uniform and turbulent air jet, as claimed by Acar et al[50]. The secondary flow having smaller momentum, flows in the opposite direction to the primary flow and is always subsonic and uniform. This description of the flow is insufficient, however correct, for the objectives of this study. Therefore, the flow field will be divided into sub-sections and investigated in detail. This subdivision, as dictated by the geometry of the nozzle, can be defined as follows:

a. The inlet hole;
   i. convergent section,
   ii. sonic section,
   iii. abrupt enlargement and backward deflection.
b. The main duct;
   i. oblique impingement and division of the flow,
   ii. primary flow,
   iii. secondary flow.
c. The jets;
   i. primary jet (supersonic jet),
   ii. secondary jet (subsonic jet).

3.4 The Inlet Hole

The experimental investigation of the air flow through the inlet hole has been done on a simplified scaled-up model as shown in Fig. 3.10. The first simplification is that the jet created by this model is assumed to expand into an infinitely large area at atmospheric conditions, although the cross-sectional area of the main duct of the texturing nozzles is finite and pressure builds up due to the static pressure recovery in the main duct (See Section 5.2). As the second simplification, the originally circular main duct is assumed to be rectangular. This facilitates visualisation of the flow at the very intersection of the inlet hole with the main duct. Furthermore, in order to facilitate the explanations which follows, the inlet hole is divided into three subsections as seen in Fig. 3.10.

3.4.1 Convergent section

The theory for compressed air flow in converging channels can be applied to the converging section of the inlet hole. Appendix B outlines the theory of isentropic flow through converging nozzles. It will be seen from the theory that if the reservoir pressure is above the critical value, the flow chokes at the throat of the converging section and delivers only the critical mass flow rate, the flow velocity being sonic. Since the working pressures of the texturing process are well above the critical value, texturing nozzles operate under choking conditions. Hence, at a given pressure, a nozzle delivers only the critical mass flow rate. Fig. 3.11 shows the theoretically predicted and measured mass flow rates for the T100 HemaJet. The observed slight discrepancy is due to both the 'vena contracta' phenomenon and the pressure build up in the main channel of the nozzle which causes the flow rate to decrease.

3.4.2 Sonic section

The sonic section (Fig. 3.10) is a cylindrical channel which continues from the throat of the convergent section. Since the length of this channel is short and no area change is observed, the flow conditions are assumed to remain constant throughout this section.

3.4.3 Abrupt enlargement and backward flow deflection

The total area of the inlet holes is always less than the cross-sectional area of the main duct. An abrupt enlargement of the sonic flow is, therefore, inevitable. Pressure losses occur there due to the abrupt enlargement of the flow, as explained in Appendix C, and therefore pressure energy is not fully converted into kinetic energy. Flow velocity reaches supersonic levels, but some energy is wasted due to the pressure loss.

When a sonic flow passes over a sharp convex corner, the flow accelerates and turns through large angles without separating; such deflection of a flow is termed 'Prandtl-Meyer deflection' and is described in most text books[52,53,95]. A Prandtl-Meyer deflection occurs at the intersection of the inlet hole and the main duct of the nozzle. The simplified and scaled-up model of the inlet hole, as shown in Fig. 3.10, is used to visualise this deflection. The shadowgraph of the phenomenon is given in Fig. 3.12a. Since the intersection is oblique, the flow at point A deflects through a series of expansion waves (an expansion 'fan'), whilst the flow at point B is still sonic and parallel to the axis. The flow at point C, however, also observes the Prandtl-Meyer deflection. Nevertheless the whole jet deflects 'backward' at point A (See Fig. 3.12a), because the flow reaches point A well before it reaches point C due to the oblique opening of the inlet hole. Hence the deflection at point A dominates and causes a total 'backward' deflection of the whole jet, whereas a similar model of the inlet hole without any oblique opening creates no flow deflection (See Fig. 3.12b).

Shadowgraphs of the jets created by the simplified and scaled-up model of the inlet hole with the oblique opening have revealed that the total 'backward' deflection of the jet is a function of the driving pressure. The variation in this deflection angle with the driving pressure has been measured from the shadowgraphs and is shown in Fig. 3.13 together with the shadowgraphs of the jets. Fig. 3.13 shows that the higher the pressure, the more the jet is deflected backward. This backward deflection increases the angle of impingement of the incoming jet with the opposite wall. The secondary flow velocities, therefore, increase. Furthermore, these higher angles of impingement cause more flow losses and in turn create primary flow velocities which are lower than expected. Fig. 3.14, illustrating the deflection angle and the ratio of the primary flow rate to the total flow rate with varying air pressures, shows that as the backward flow deflection increases, the primary flow rate decreases.

3.5 The Main Duct

Being a straight cylindrical channel, the main duct is of no aerodynamic significance. However, the impingement and division of the incoming jets occurs in this channel; moreover, the primary jet, which carries out the actual texturing, is formed at the end of the primary flow section of the channel. Although the secondary flow is always seen as a source of energy loss, this flow does contribute to the texturing by blowing off the surplus water and the spin-finish constituents from the surfaces of the filaments. Therefore, the main duct will be investigated by dividing it into three sub-sections.

3.5.1 Oblique impingement and division of the flow

In the case of the T100 HemaJet, only one incoming jet carries the whole mass flow of the air into the main duct. The impingement of this jet on the opposite wall of the main duct, and its division, have been experimentally investigated in this section. In order to be able to visualise this oblique impingement and the reflection of the flow in the main duct, the originally circular duct had to be converted to a square cross-section with transparent walls (Fig. 3.15).

The investigation of this two dimensional flat nozzle was made in three steps. In the first step, the opposite wall to which the incoming jet impinges was removed and the incoming jet was visualised by the shadowgraph method. This is a slightly deflected jet conforming to the preceding study in Section 3.4 (Fig. 3.16a). In the second step, the counter wall was mounted, but no glass walls were used and the shadowgraph of the impingement was taken (Fig. 3.16b). This illustrates that the incoming jet creates a normal shock wave obliquely attached to the opposing wall. The flow naturally disperses in all directions due to the absence of side walls. Lastly, the glass side walls of the nozzle were mounted, thus forming a square main duct. When the flow was visualised (Fig. 3.16c), it was observed that the normal shock wave attached to the wall had become a detached shock wave. The mass of the incoming flow was diverted to the primary flow section of the nozzle after this shock wave. It was also noted that the expansion waves crossed the whole secondary flow section, whereas in the primary flow section they only crossed less than half of the channel. In both directions, after the expansion waves, the pressure became less than the upstream pressure. In the secondary flow section, this corresponds to a pressure equal to or less than the atmospheric pressure.

The entire flow divides into the primary and secondary flows in such a way that the secondary flow momentum flux, (depending on the working pressure), only varies between 15% and 30% of the primary flow momentum flux as seen in Table 3.1.

3.5.2 Primary flow

Due to the inclination of the inlet holes, a greater portion of the incoming flow, despite the backward deflection of the incoming jets, goes to the primary flow section of the nozzle (See Table 3.1). The speed of the flow is supersonic, provided that the reservoir pressure is well above the critical value.

An acceleration or deceleration of a supersonic flow requires an area change. Being a cylindrical channel, the main duct of the nozzle fails to fulfil this requirement. Consequently, no velocity change is observed by the flow, until the divergent section of the duct is reached. As soon as the flow area increases, the speed of the flow increases at the expense of pressure, in other words the flow expands and the flow pressure decreases. The rate of the divergence is so large that the flow cannot follow the full contour of the surface and separates as is seen in Fig. 3.17 which shows the shadowgraph of the primary flow from the transparent walled square nozzle. Thus a free air-jet is created. Fig. 3.17 also shows the expansion waves emanating from where the divergence of the main duct starts.

3.5.3 Secondary flow

The static pressure measurements obtained by Acar et al[50], using wall tappings, and the static pressure measurements which have been carried out by the author, using a centre line static pressure tube (See Chapter 5), both indicate that the secondary flow pressure is atmospheric. Very little momentum occurs in the secondary flow direction as is noted in Table 3.1. Therefore, the secondary flow is almost exclusively subsonic for all the working pressures and appears to have no significance.

3.6 The Jets

Both the primary and the secondary flows create free jets when they leave the nozzle walls. Being supersonic, the primary jet possesses many characteristics whilst the secondary jet is fully subsonic and uniform.

3.6.1 The primary jet (supersonic jet)

A general background study, resorting to the established theory and published works of an axisymmetric supersonic jet is given in Appendix D.

3.6.1.1 Experimental investigation

Since the aim of this research was to investigate industrial texturing nozzles, it was most desirable to conduct experiments using them. However, certain characteristics of these nozzles make it difficult, if not impossible, to conduct satisfactory investigations due to difficulties associated with the geometry of the texturing nozzles. As seen in Fig. 3.18, the jet emerging from the T100 HemaJet can only be visualised much further downstream; however, the most complicated part of the jet is at the very exit of the diverging section of the nozzle as indicated by L_{SC} for the Standard-core and L_{T100} for the T100 nozzles respectively. On the other hand, both the walls of the texturing nozzles' diverging exit interfere with the flow measurement pitot tube and thus a complete velocity trace across the jet cannot be obtained; the presence of the probe is also likely to block the flow.

These shortcomings of the use of texturing nozzle in the supersonic jet investigation suggested another supersonic jet model needed to be devised. The simplest solution to this was thought to be a straight pipe. Although this only produces sonic velocity at the exit, as soon as the sonic flow with a pressure which is higher than the ambient pressure reaches the exit, it suddenly expands and becomes supersonic due to both the pressure difference and the sudden change of area. Such a jet has been utilised in the further experimental research. Fig. 3.18 also shows that, by using such a pipe, the flow velocities even at the very exit section could be measured without any interference with the solid walls of the pipe, and in addition, the flow could be visualised from the exit plane onwards.

For the jet from such a straight pipe, an 'average' shadowgraph, obtained by means of a fairly long light exposure, and an instantaneous shadowgraph, taken by using a high speed flash, are given in Fig. 3.19a and b respectively. These two shadowgraphs clearly delineate the expansion fans as white bands and the shock waves as dark bands where the density gradient changes rapidly[93]. The instantaneous shadowgraph also shows the turbulent nature of the jet. These shadowgraphs are reconstructed in Fig. 3.19c.

By using a fine pitot tube as described in Section 3.2, the total pressures were recorded at 0.2 mm intervals in both the radial and axial directions up to 4 pipe diameters. The measured values are given in Fig. 3.20a in topographic form. Since the total pressure is related to the local kinetic energy (static pressure being constant as atmospheric pressure), the high and low velocity regions are shown in this figure. It was thought to be informative to show the distribution of the centre line total pressure and the total pressure distribution across the jet at different distances downstream from the exit plane. Therefore, these are also included in Fig. 3.20 as b and c respectively.

3.6.1.2 Centre line velocity fluctuations

In order to elaborate further on the behaviour of the supersonic jet emerging from an underexpanded nozzle, the centre line total pressure distribution given in Fig. 3.20b is repeated on a transparent sheet covering Fig. 3.19a, and b. It is seen from this re-presentation that the flow decelerates up to the point where the intersection of the expansion waves occurs. Having passed this intersection point, the flow recovers rapidly (See Fig. 3.19 with transparent sheet), then slows down up to the point where the shock waves have intersected. Further downstream from the jet these rises and falls of the centre line total pressure are repeated and they finally fade out due to the viscous and turbulent mixing of the jet into the surrounding atmosphere.

3.6.1.3 Non-uniform axial velocity distribution

The axial total pressure distribution illustrated in Fig. 3.20c is not of the same pattern at various distances from the exit plane. It is fairly uniform just at the exit plane, whilst a central deficit is observed in the downstream section of the jet. However, further downstream where the viscous mixing through a thick boundary layer dissipates the flow, the traverse velocity distribution across the jet becomes bell-shaped.

Che-Haing[96] has also shown a similar phenomenon in his extensive investigation on underexpanded supersonic jets. He pointed out that the maximum axial velocity does not occur on the centre line of the flow just after the intersection of the expansion waves. However, since Che-Haing has concentrated his work on an investigation of the first barrel, where only expansion waves occur, he assumed the velocity distribution at the downstream of the first barrel as though this was of a gausian shape. Fig. 3.20c clearly illustrates, however, that the non-uniformity exists at the other sections of the jet also.

In order to shed more light on this phenomenon, the plane numbered III in Fig. 2.20c will be considered in conjuction with the corresponding cross-section AA of Fig. 3.19c. When the pitot tube (which is parallel to the flow) is held at the point 1, the lowest total pressure is recorded, because the point 1 is on the boundary line. At the point 2 which is at the outer border of the expansion fan, the flow pressure is atmospheric, and the flow passing through the expansion has been accelerated. Therefore, the highest flow velocity is recorded at the point 2. By advancing in the expansion fan from the points 2 to 3, less accelerated flow is observed due to the smaller number of expansion waves through which the flow has passed. As soon as the point 3 is reached, the least flow velocity is recorded, because the streamline at the point point 3 is not affected by the expansion waves at all. From points 3 to 4, the flow is uniform and parallel to the nozzle axis. A reversed pattern is recorded when the pitot tube is traversed from the points 4 to 7.

Similar axial velocity distributions are observed at different distances from the exit plane, but the level of the central deficit varies from one point to another due to the formation of expansion and/or compression waves which causes acceleration or deceleration of the flow as seen in Fig. 3.20c. Finally, further downstream, the central deficit dissappears because of the dissipation of the density discontinuities i.e. shock or expansion waves. Thus the velocity profile becomes a bell-shaped. For this reason, the axial velocities measured at the exit plane of the T100 nozzle (which is located at 4.5D, D being the nozzle diameter further downstream from the beginning of the diverging section where the flow separates) do not show any central deficit. Neither do the centre-line velocities fluctuate as is seen in Fig. 3.21a and b.

3.6.2 Secondary jet (subsonic jet)

When the secondary flow leaves the nozzle, it creates a secondary jet which is subsonic. The pressure in the jet is atmospheric and no density discontinuities are present. Fig. 3.22a shows the secondary jet axial velocities at various working pressures for the T100 HemaJet nozzle. These are all subsonic and of uniform distribution. In addition to this, the centre-line velocities for this nozzle at various pressures are shown in Fig. 3.22b. The figure shows that the flow velocity remains constant indicating a potential core. According to the established subsonic flow theory[97] the potential core is the central portion of the flow in which the velocity remains constant and equal to the velocity at the nozzle exit. The length of the potential-core is claimed to vary from 4.7D to 7.7D depending on the Reynolds number, D being the nozzle diameter.

3.7 Overall Consideration

This chapter has described the experimentally obtained air flow using a step by step approach. By combining the steps in a sequential manner, the air flow may be better understood. Acar et al[51] used the same step by step approach to build their mathematical model. Appendix E gives a review of their work. The developed mathematical model has been applied to the full size Standard-core and T100 HemaJet nozzles. Figs. 3.23a and b show the comparison of the predicted and experimental flow velocities created by the full-size nozzles. It can be seen that the mathematical model provides a good prediction of the air velocities created by the Standard-core nozzle. Nevertheless, the T100 nozzle creates higher velocities than those predicted. In order to improve the mathematical model, Acar[42] suggested an emprical correction by substituting the measured secondary flow rate and hence calculating of the primary flow velocity. When this correction is made, it has been found that the corrected mathematical model also provides a better prediction for the T100 HemaJet. However, the correction has made little contribution to the Standard-core nozzle prediction, indicating that the collision of a single jet with the nozzle duct creates more backward flow than that of the three incoming jets design studied by Acar[42].

In Section 3.4, it has been demonstrated that the incoming flow deflects backward due to the oblique opening of the inlet holes. It has also been proven that the total backward flow deflection is a function of the supply pressure. As a further correction to the Acar mathematical model, experimentally measured deflection angles are introduced. This correction only improved the secondary flow velocity predictions whilst making insignificant contributions to the primary flow velocity predictions as seen in Fig. 3.23a and b.

3.8 Conclusions

In an attempt to describe the flow through HemaJets, the cylindrical type nozzles, the following conclusions have been achieved:

i. The flow is choked at the throat of the inlet hole and delivers only the critical mass flow determined by the reservoir pressure.

ii. Flow in the inlet hole is only sonic and possesses excess pressure again determined by the resevoir pressure.

iii. Due to the sudden opening of the inlet hole into the main duct, abrupt enlargement losses which create energy loss are inevitable.

iv. The oblique opening of the inlet hole deflects the incoming jet backward, and consequently increases the angle of collision to the opposite wall.

v. The oblique collision of the incoming jet is a paramount source of energy loss.

vi. The primary flow is supersonic in the main duct, whereas the secondary flow remains subsonic both in the main duct and in the jet form.

vii. Further acceleration of the primary flow occurs at a place where the divergence of the main duct starts. However, the flow soon separates from the wall of the nozzle because of the large divergence of the trumpet-shaped exit.

viii. Since the supersonic jet has pressures above atmospheric, it creates an underexpanded supersonic jet. The properties of this jet has been investigated by means of another underexpanded jet created by a straight pipe. The results are applicable to the jets created by all the texturing nozzles under consideration.

ix. The axial velocities from a supersonic jet fluctuate on the centre-line due to the semi-periodic expansion and compression of the flow.

x. The non-uniform distribution of the flow velocities is due to the formation of pressure waves and the viscous and turbulent mixing of the flow on the boundary layer.

xi. Being a subsonic jet, the secondary jet has the characteristics of all well-defined subsonic jets.

xii. The mathematical model developed by Acar et al[51] is shown to yield good predictions even with full-size nozzles.

TABLE 3.1

Momentum flux division for the T100 HemaJet nozzle

Air Pressure bar(gauge)	Primary Flow Momentum Flux kgm/s^2	Secondary Flow Momentum Flux kgm/s^2	(PFMF▲/SFMF■)*100 %
5	0.522	0.078	14.94
6	0.644	0.111	17.23
7	0.713	0.192	26.92
8	0.799	0.223	27.90
9	0.860	0.278	32.23

▲ PFMF : Primary Flow Momentum Flux

■ SFMF : Secondary Flow Momentum Flux

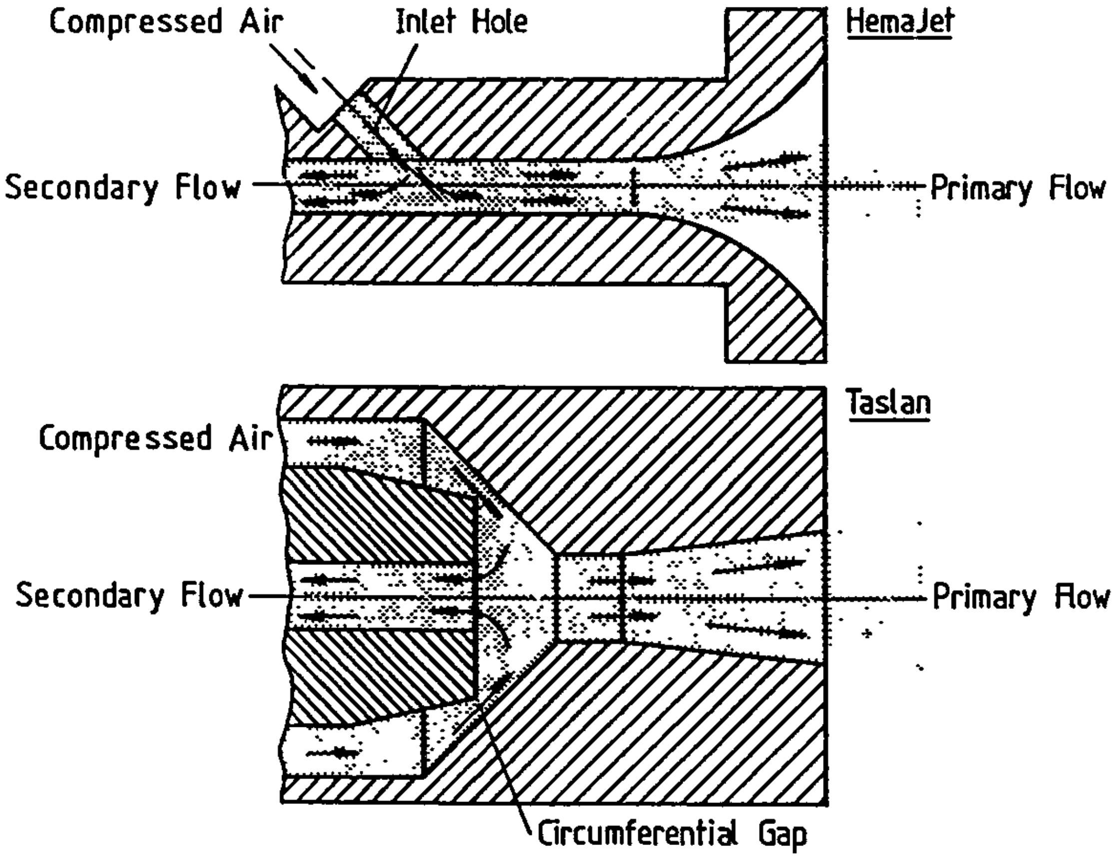

Figure 3.1 Structural comparison of the Taslan and HemaJet nozzles

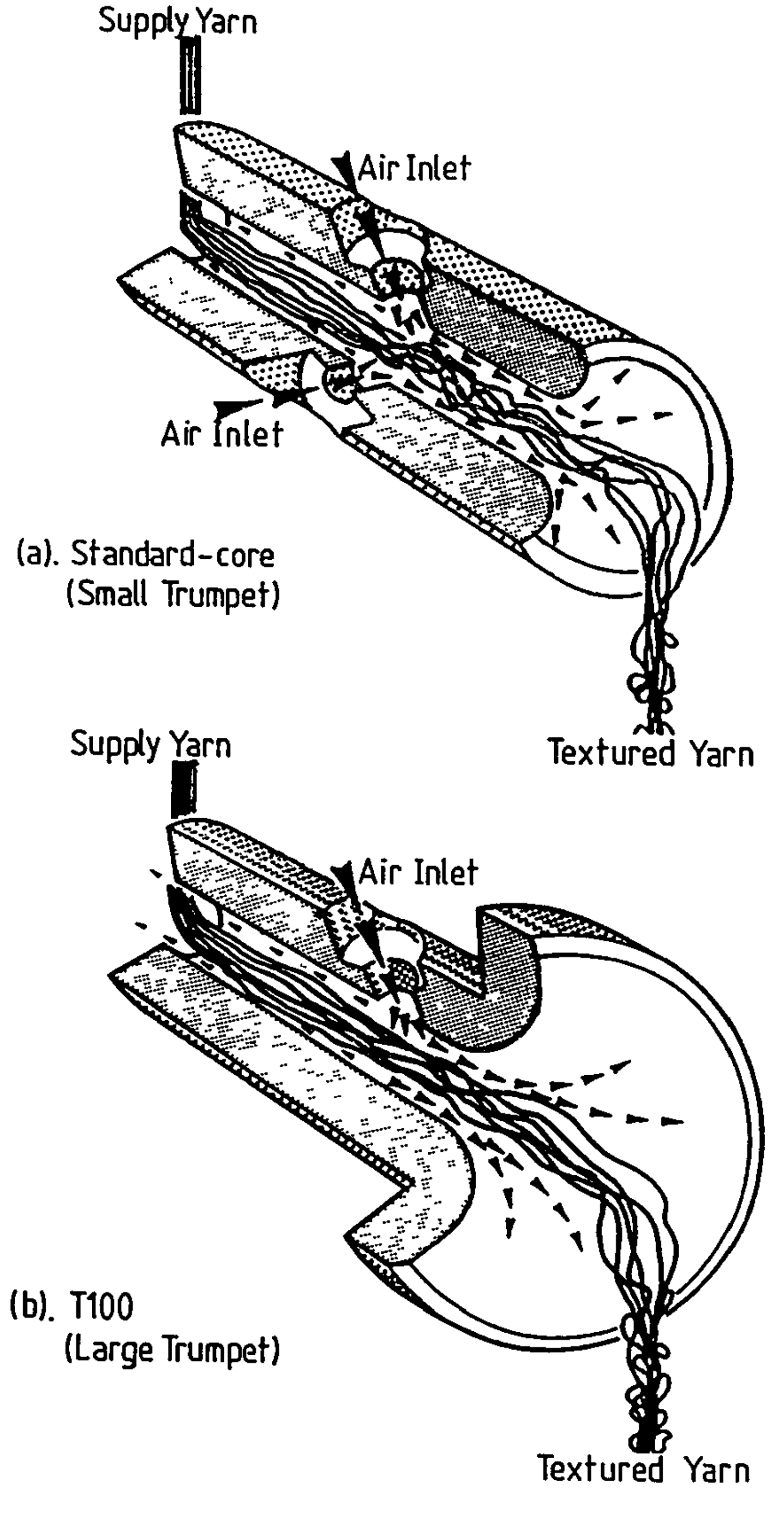

Figure 3.2 The HemaJets (a) Standard-core, (b) T100

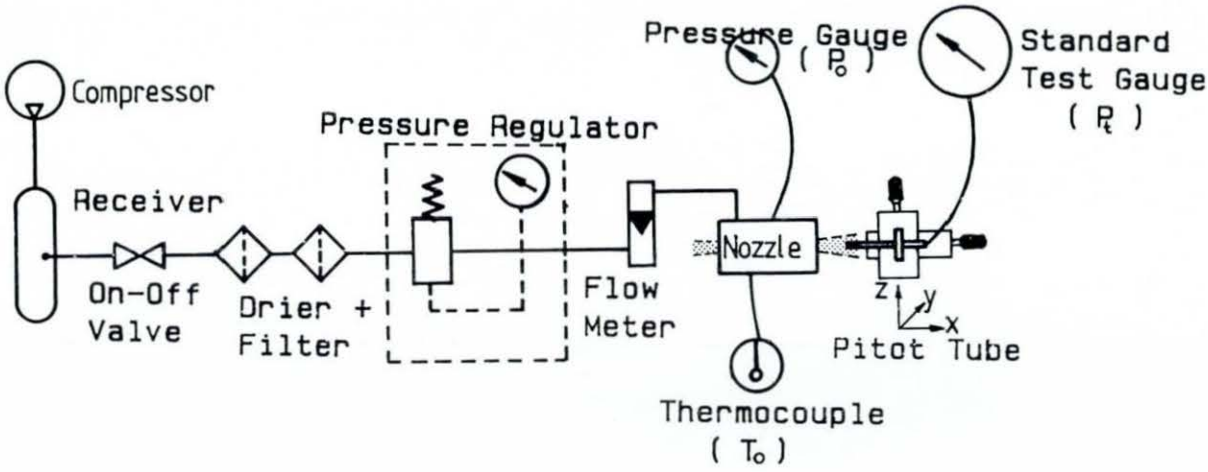

Figure 3.3 The experimental rig for the flow measurements

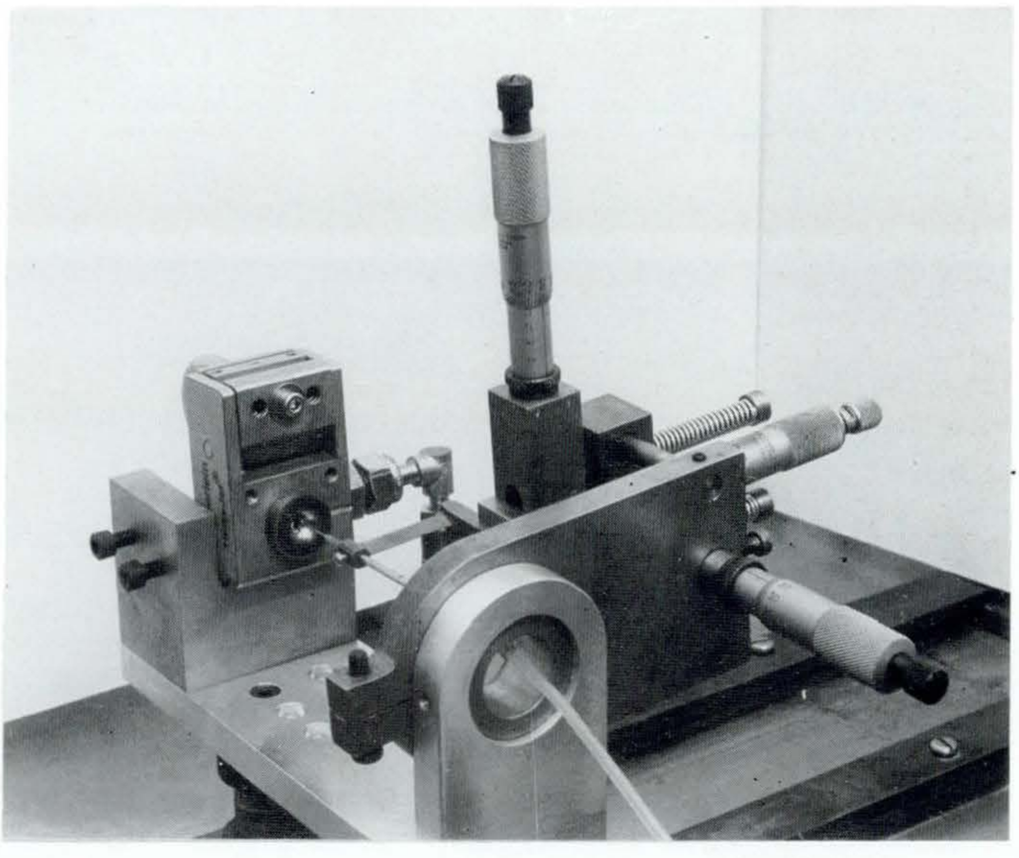

Figure 3.4 3-dimensional pitot tube traverse mechanism

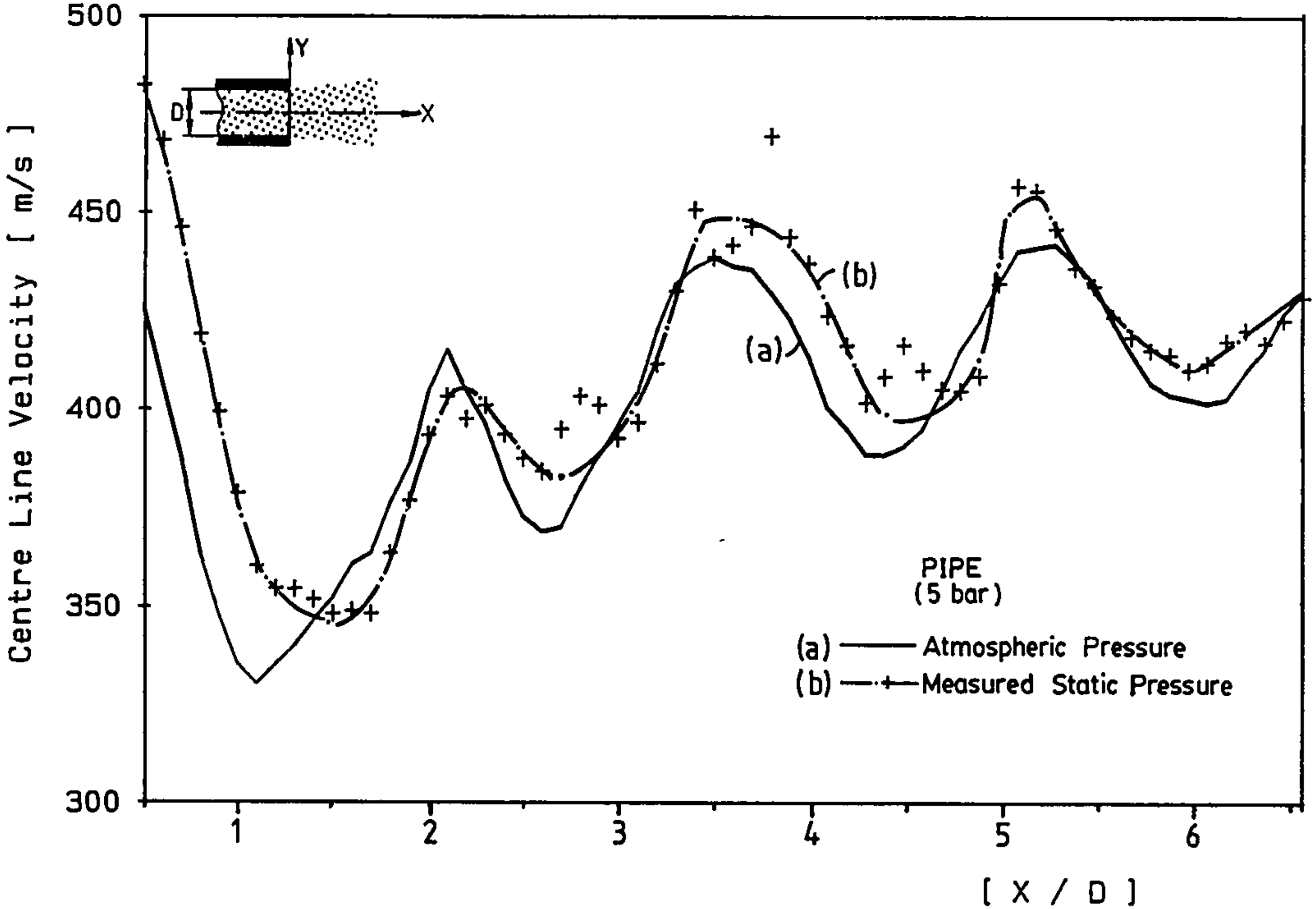

Figure 3.5 Comparison of the velocity calculations: (a) where the static pressure in the jet is assumed to be atmospheric; and (b) where the static pressures are measured

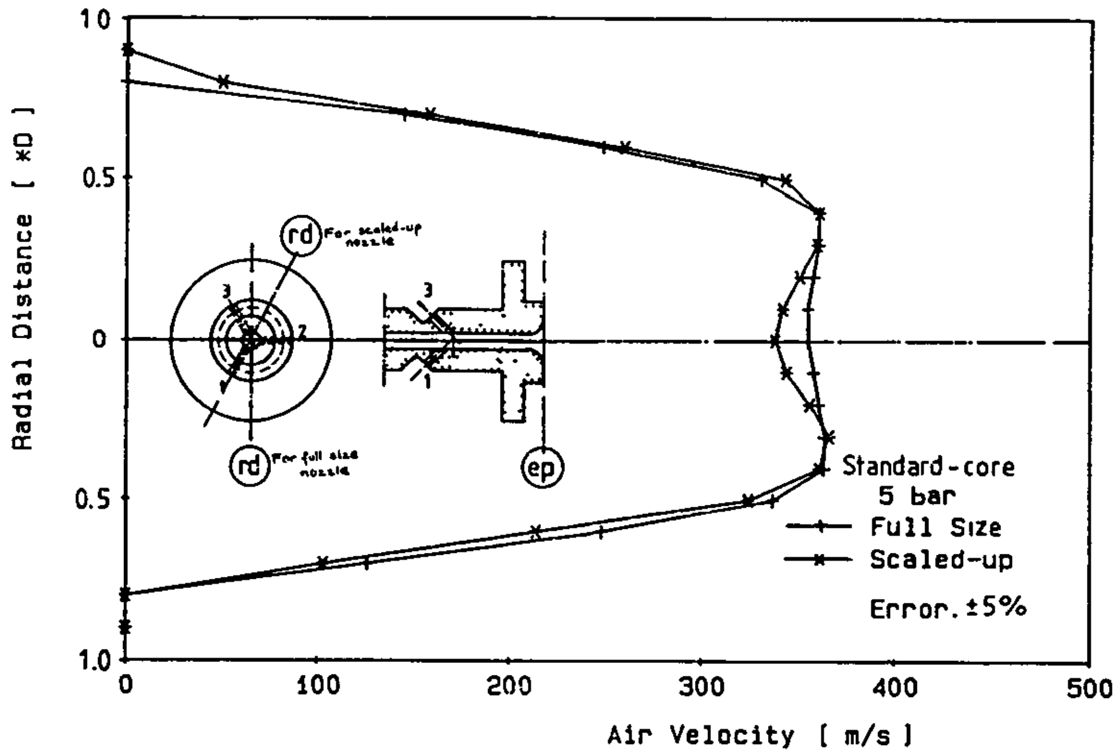

Figure 3.6 Comparison of the results obtained from the full-size Standard-core HemaJet and the four-times scaled-up model of the Standard-core HemaJet as measured by Acar.

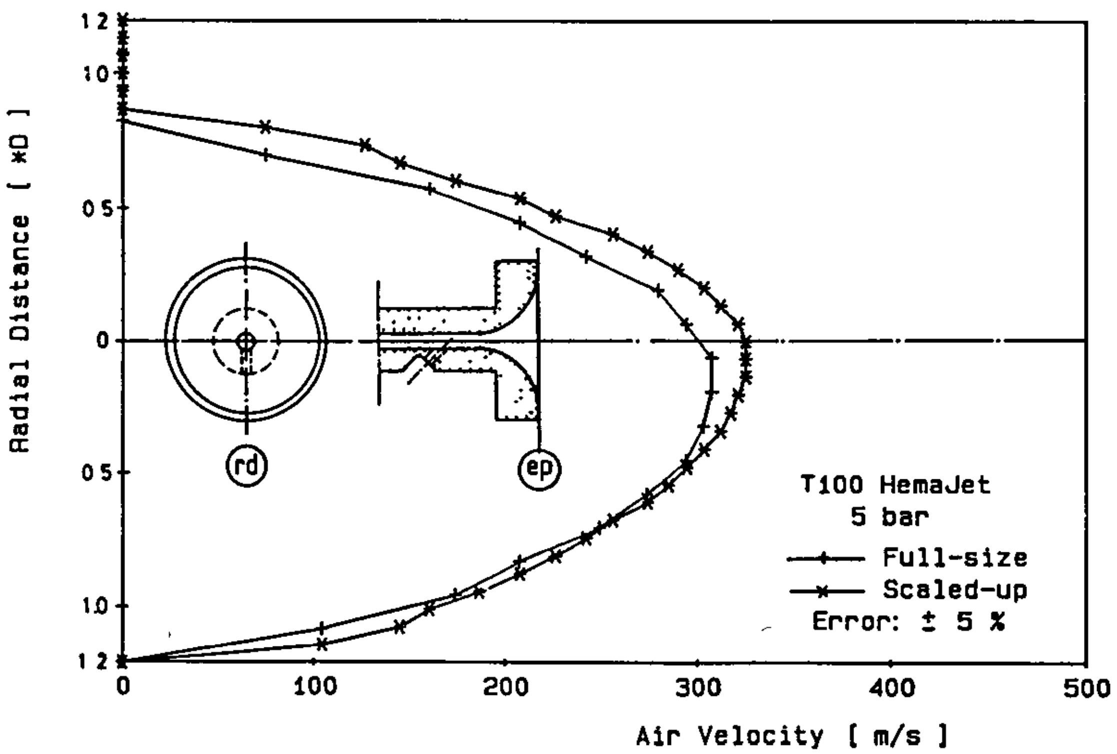

Figure 3.7 Comparison of the results obtained from the full-size T100 HemaJet and the four-times scaled-up T100 HemaJet

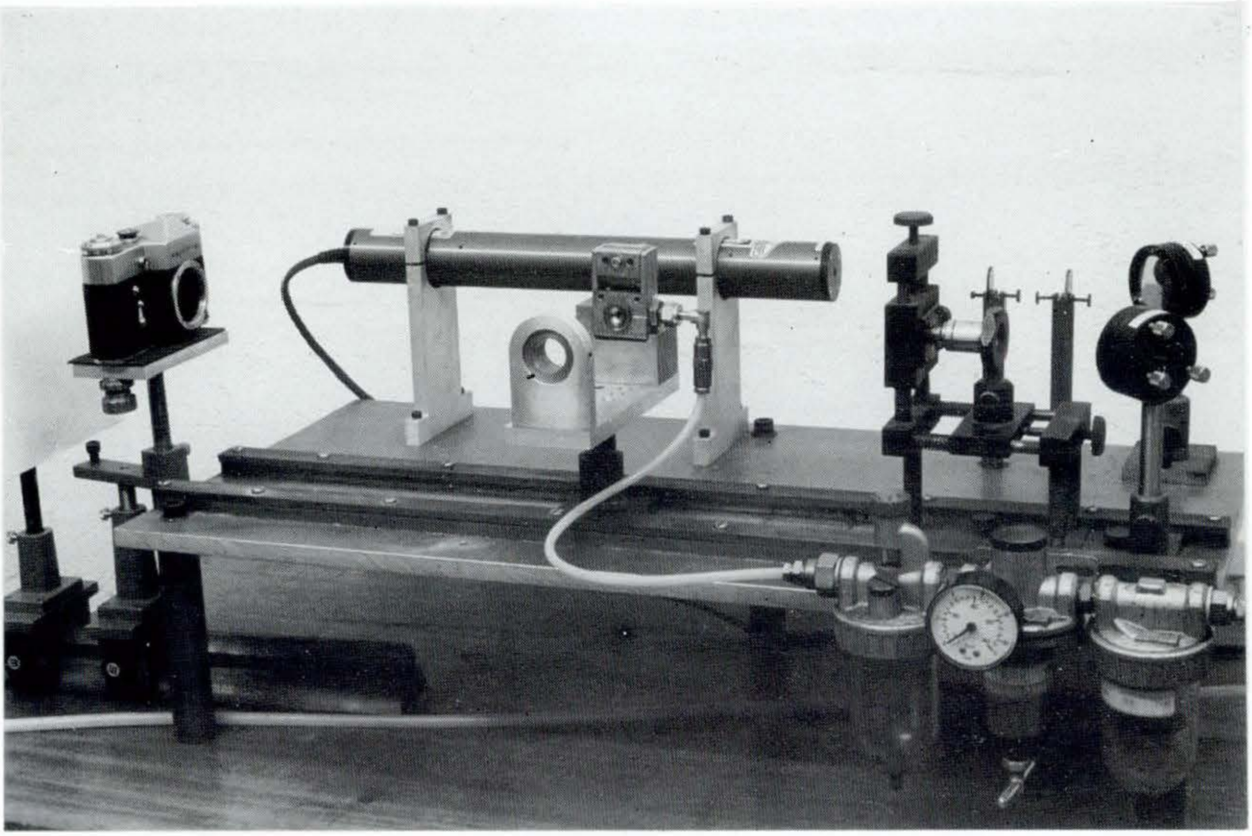

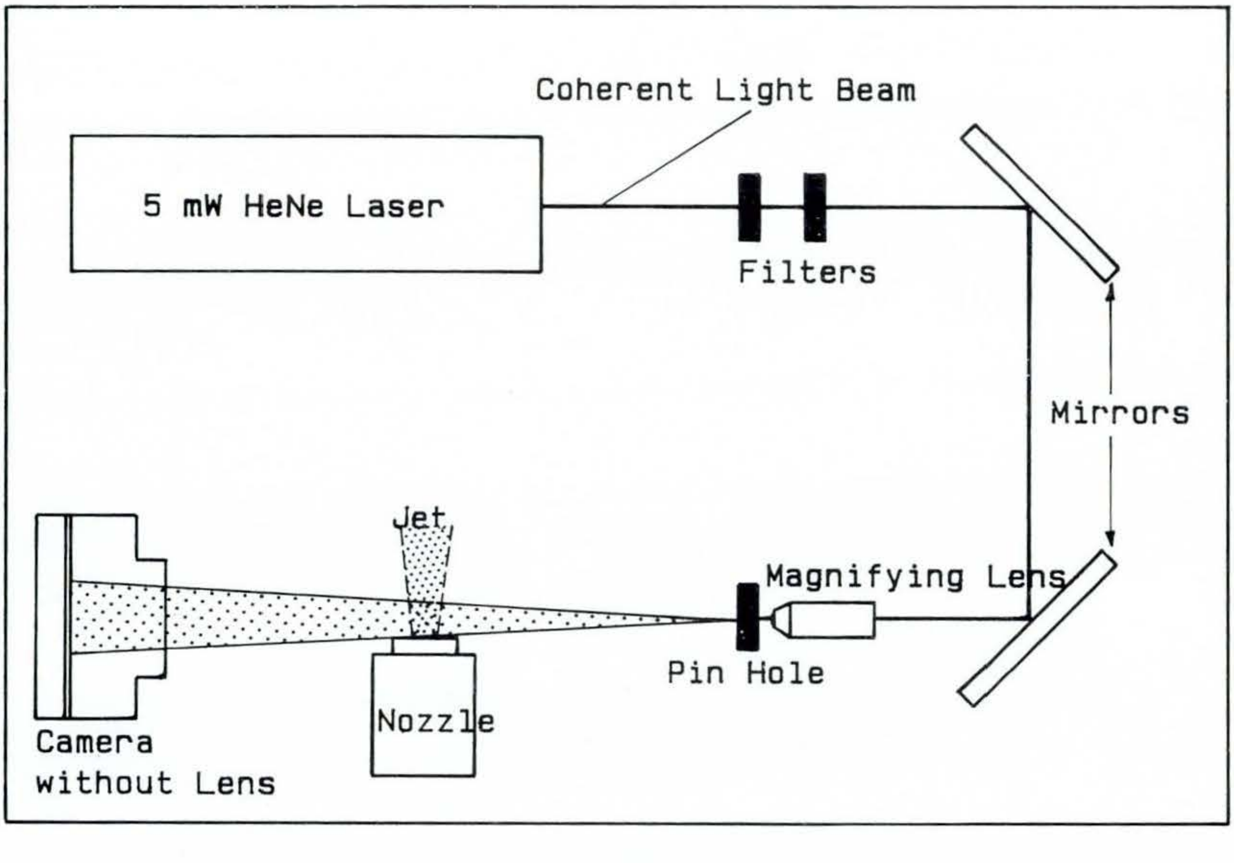

Figure 3.8 The shadowgraph unit

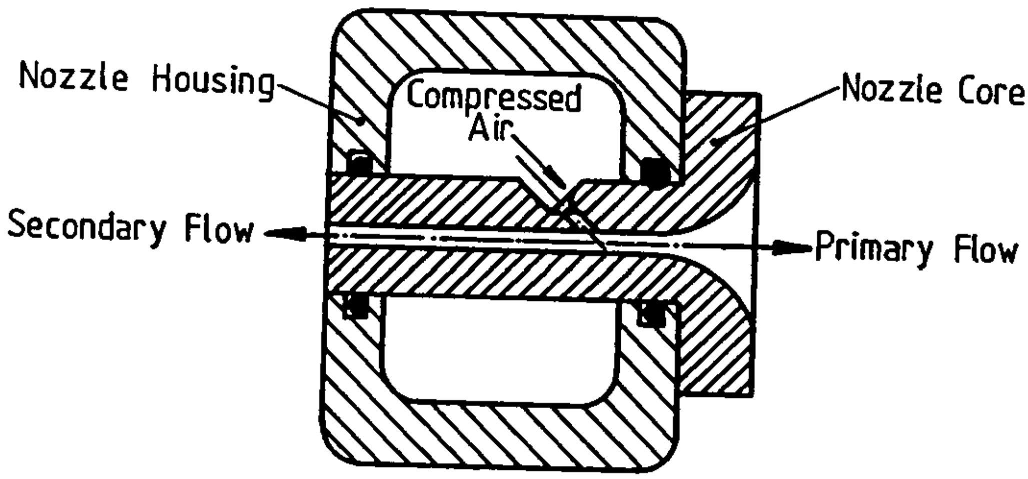

Figure 3.9 A HemaJet nozzle mounted in a nozzle housing

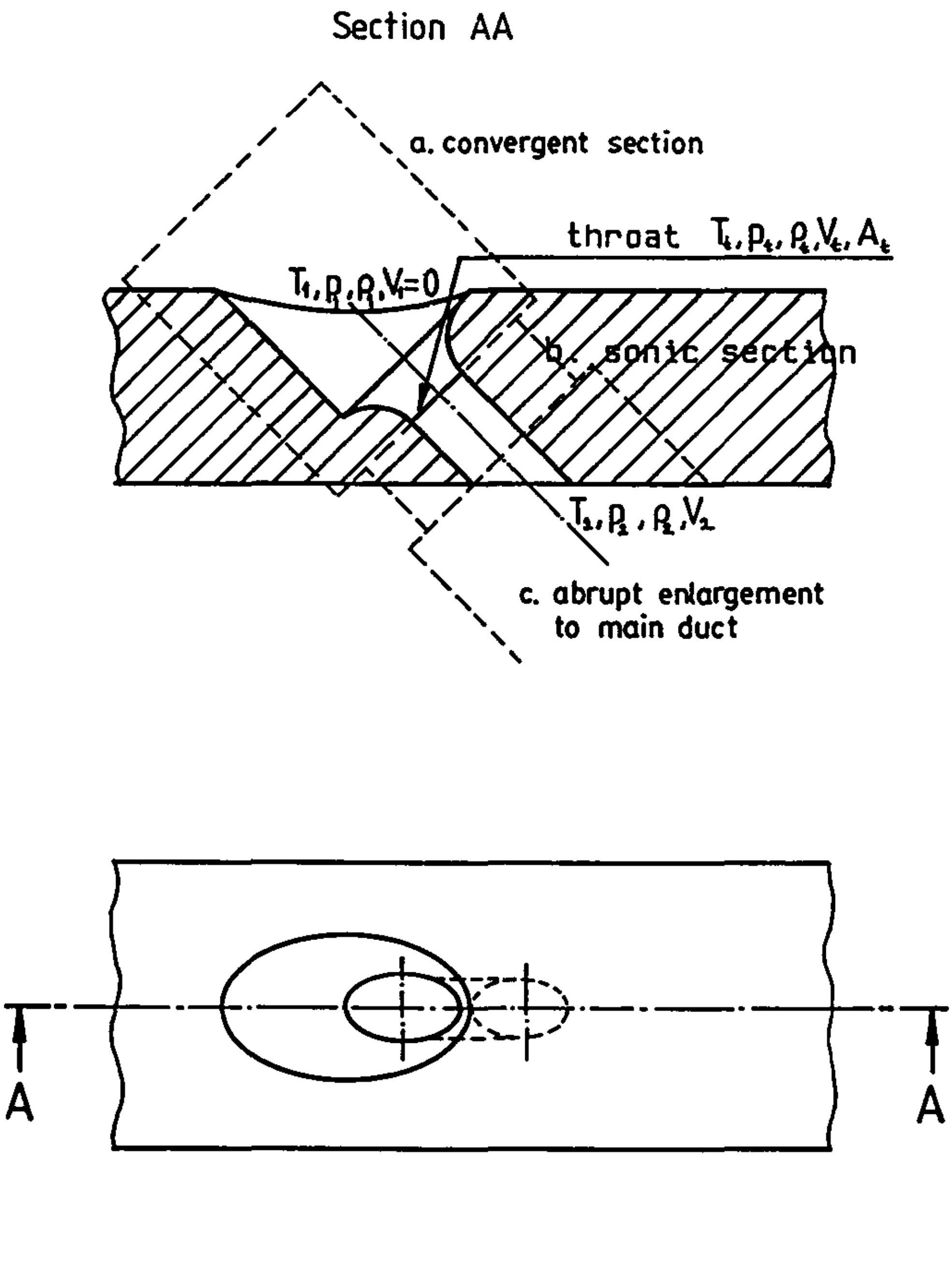

Figure 3.10 The inlet hole (convergent nozzle)

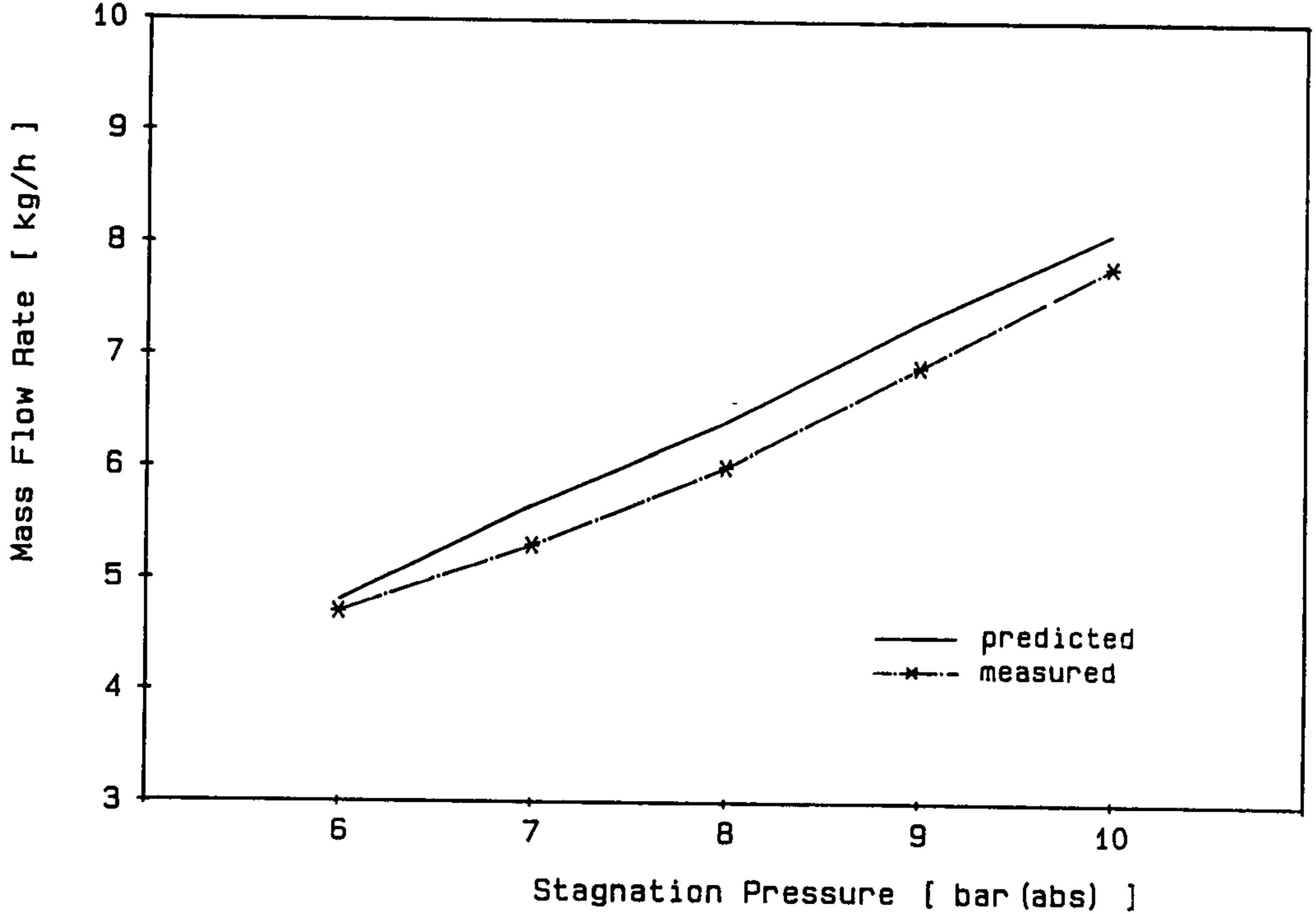

Figure 3.11 Measured and predicted mass flow rates of the T100 HemaJet

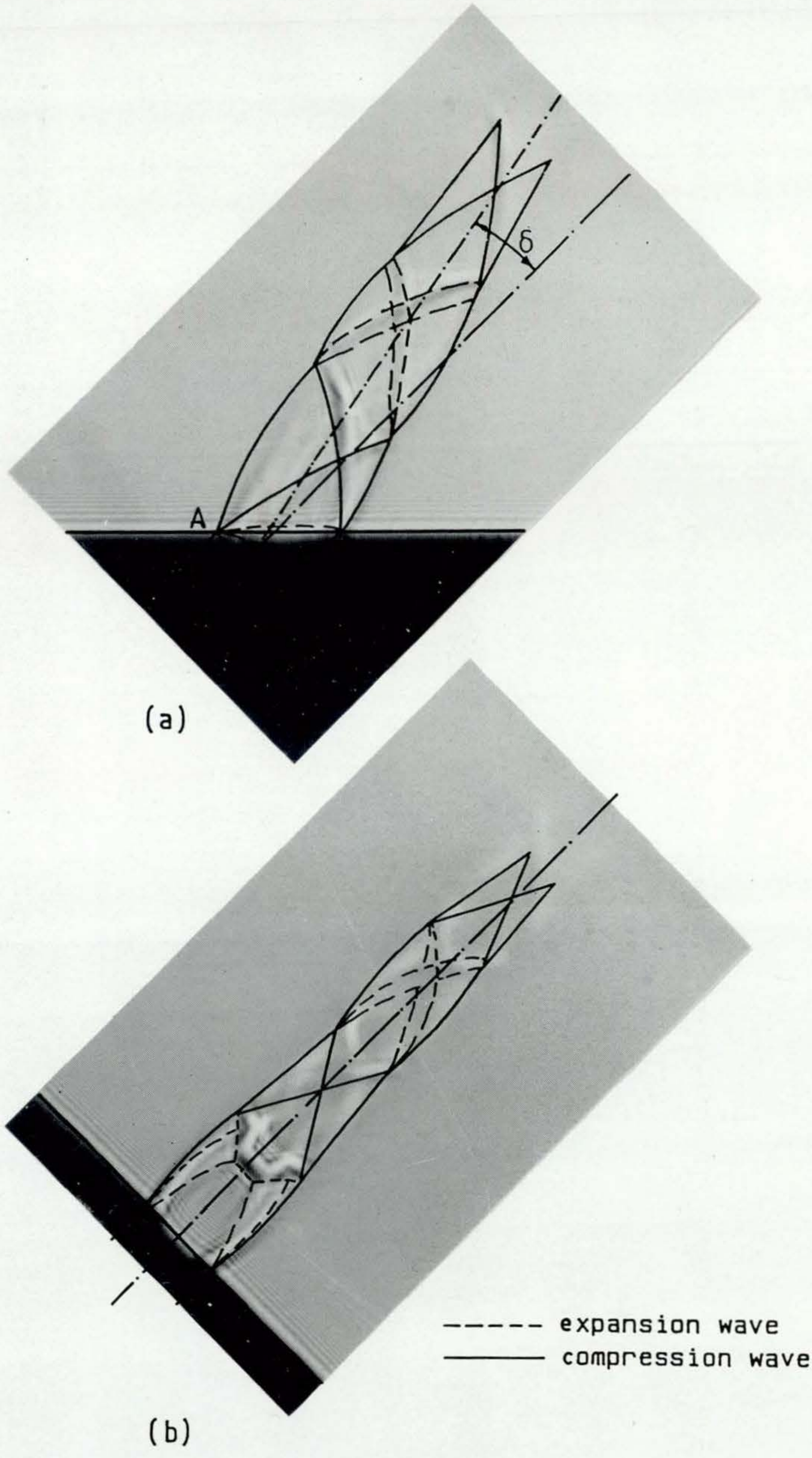

Figure 3.12 Shadowgraphs and line drawings of the jets created by the simplified and scaled-up model of the inlet hole with: (a) oblique opening; and (b) square opening

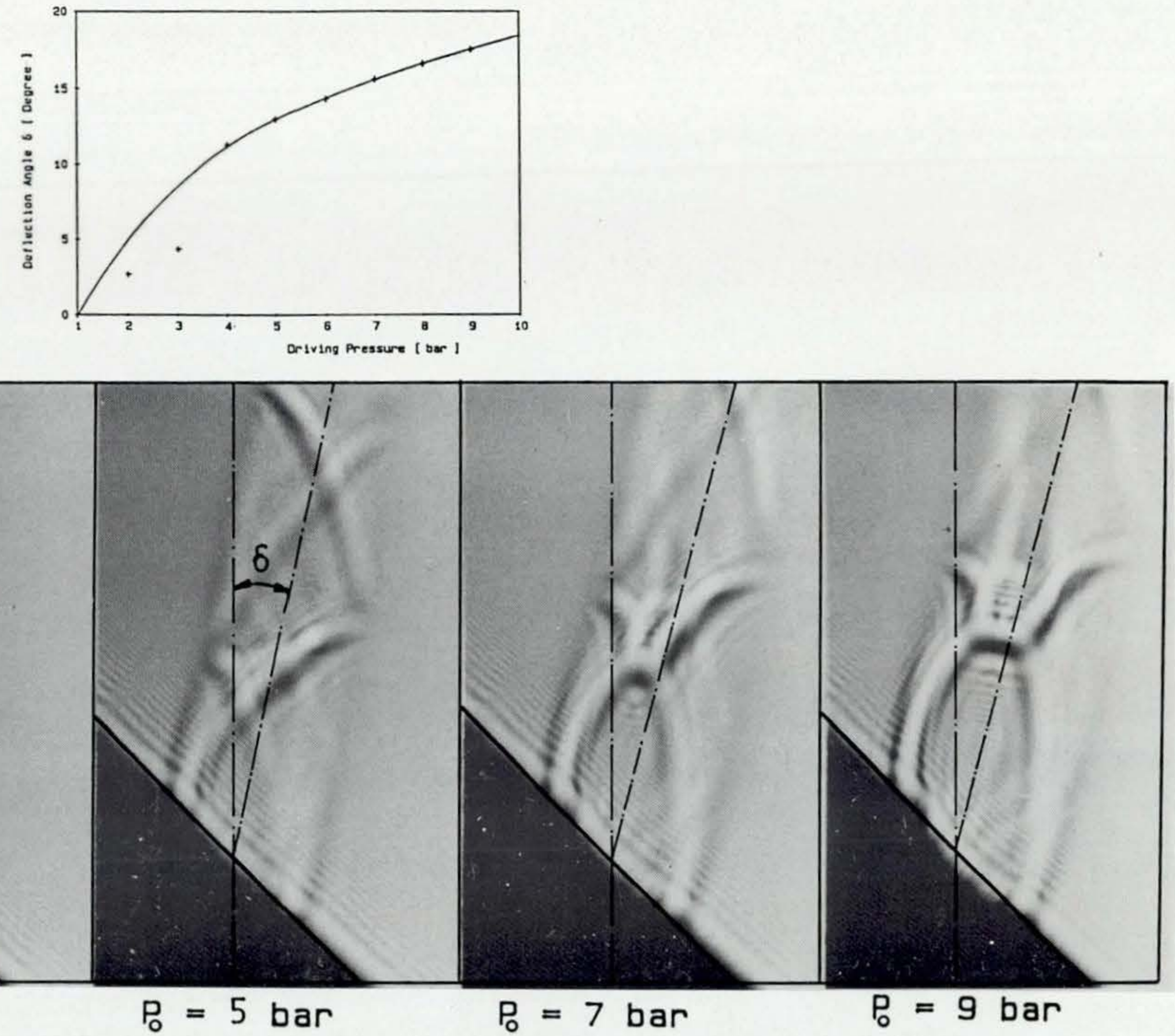

Figure 3.13 Variation of the backward flow deflection with increasing reservoir pressure

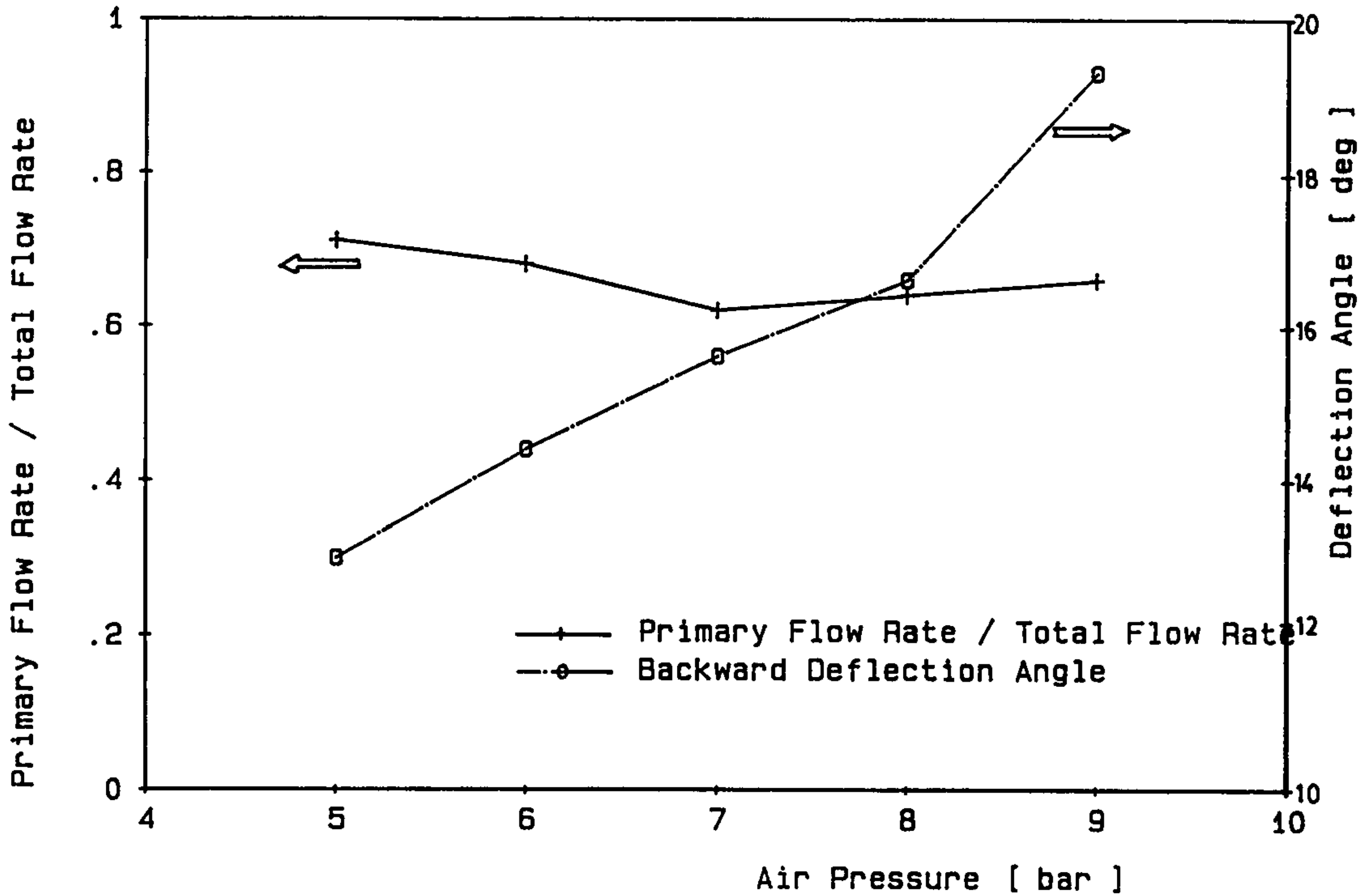

Figure 3.14 Variation of the primary flow rate to total flow rate with the reservoir pressure and its relation to the backward flow deflection

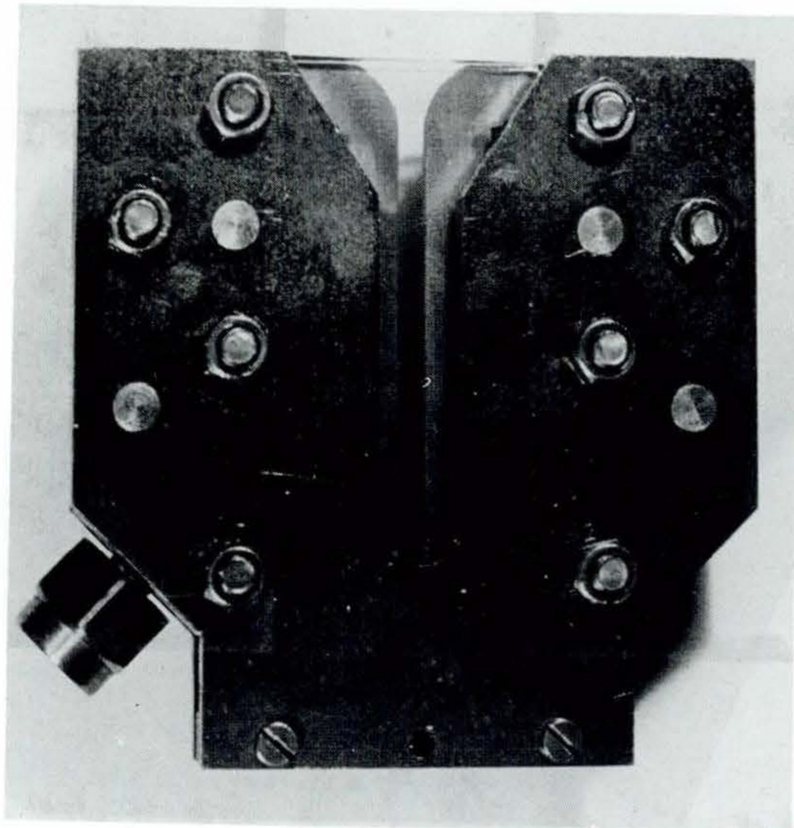

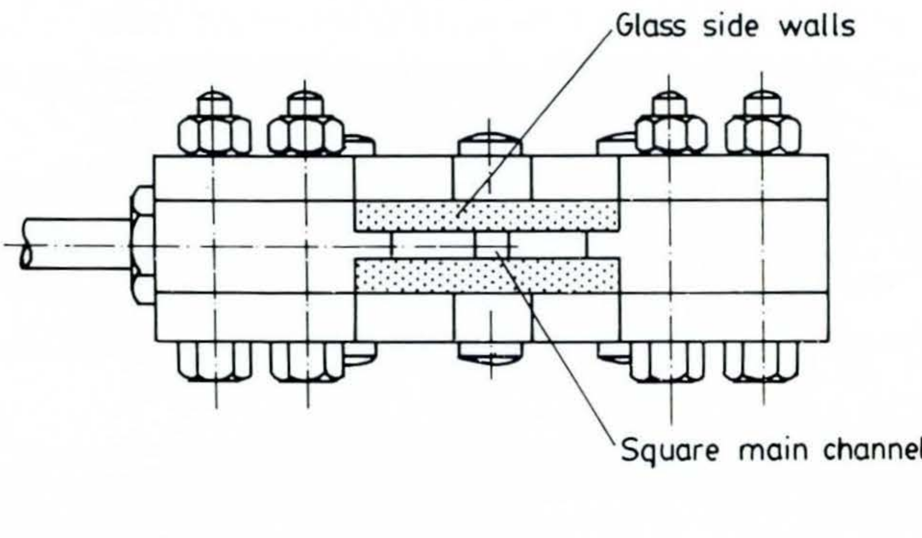

Figure 3.15 2.5-times scaled-up 2-dimensional nozzle with glass walls

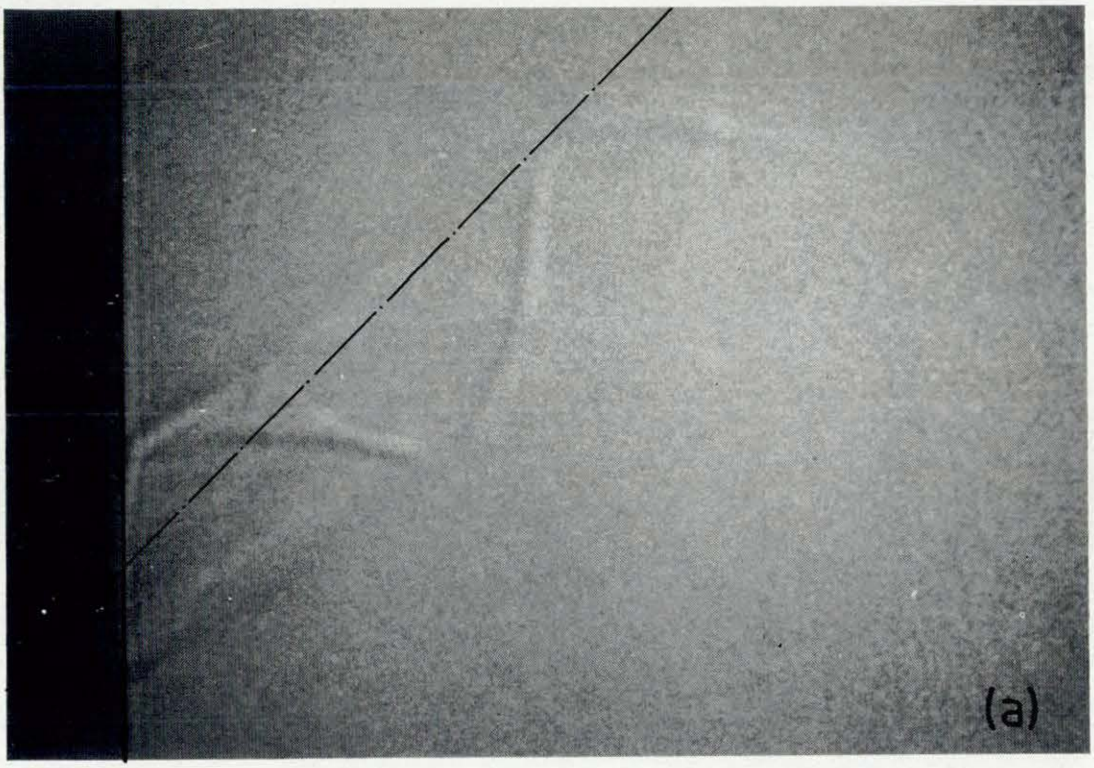

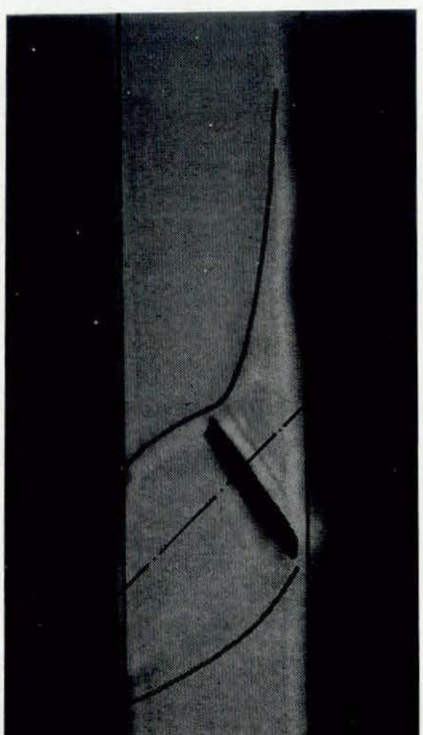

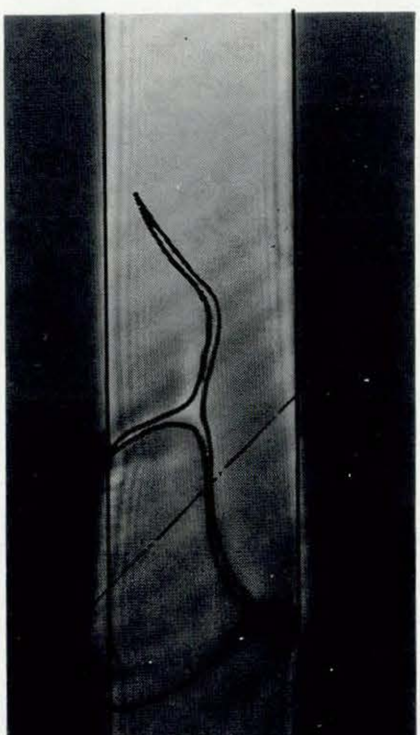

Figure 3.16 Shadowgraph of the jet from the transparent flat nozzle: (a) with no counter wall; (b) with counter wall but without glass side walls; and (c) with both counter wall and glass walls

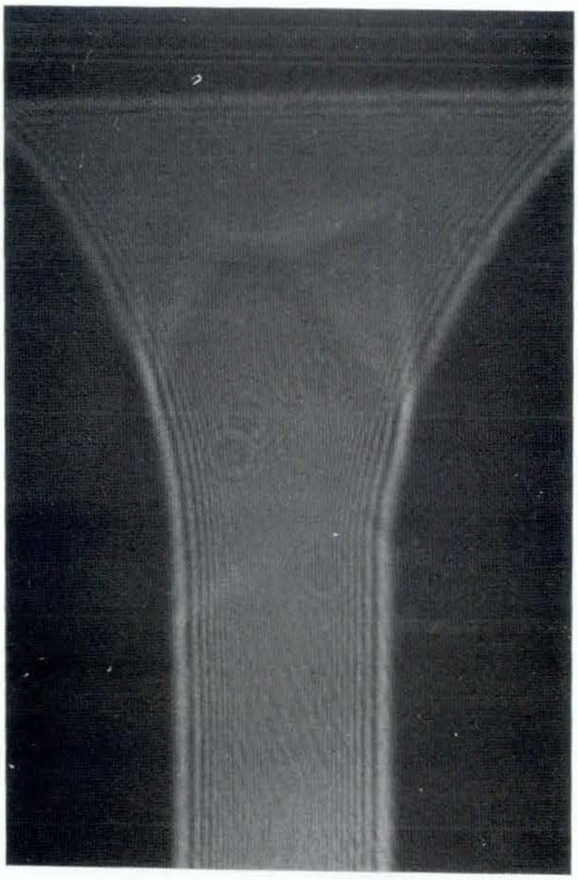

Figure 3.17 Shadowgraph of the primary jet showing the beginning of the divergence and the expansion waves

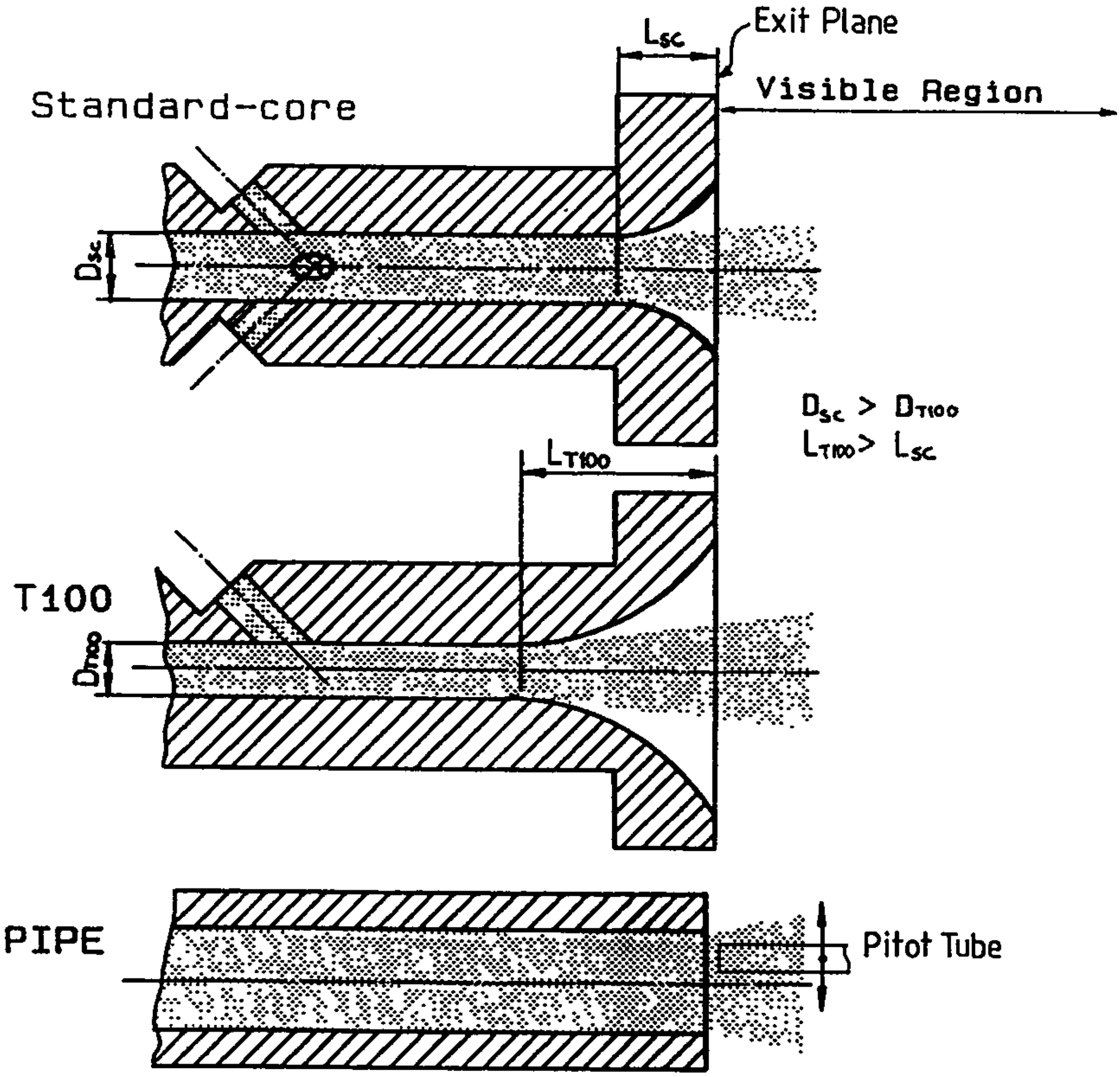

Figure 3.18 Jets emerging from: the Standard-core HemaJet; the T100 HemaJet; and a straight pipe

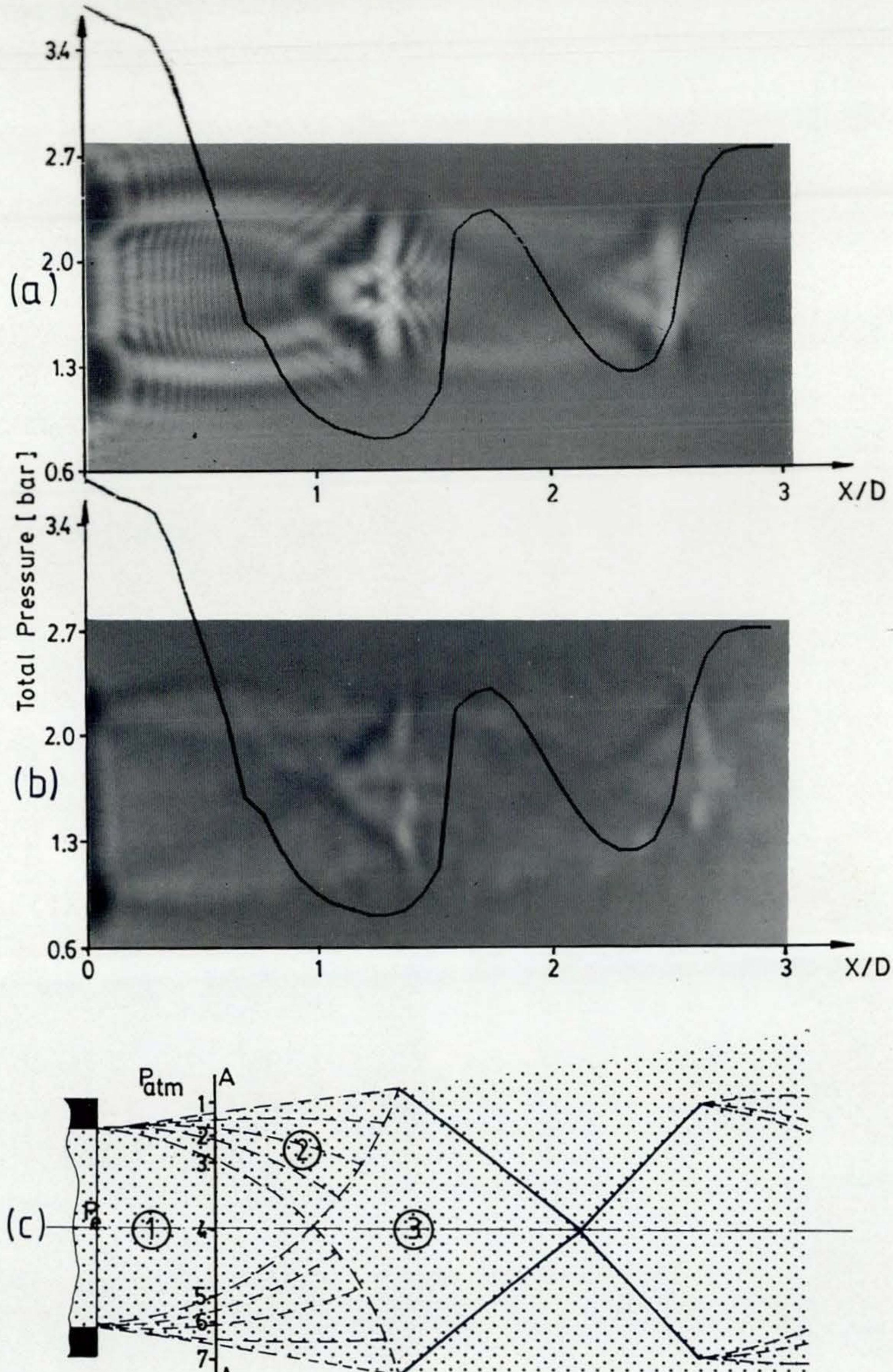

Figure 3.19 Shadowgraphs of a jet from a staight pipe (p_o=5 bar): (a) average shadowgraphy; (b) instantaneous shadowgraphy; and (c) reconstruction of the shadowgraphs

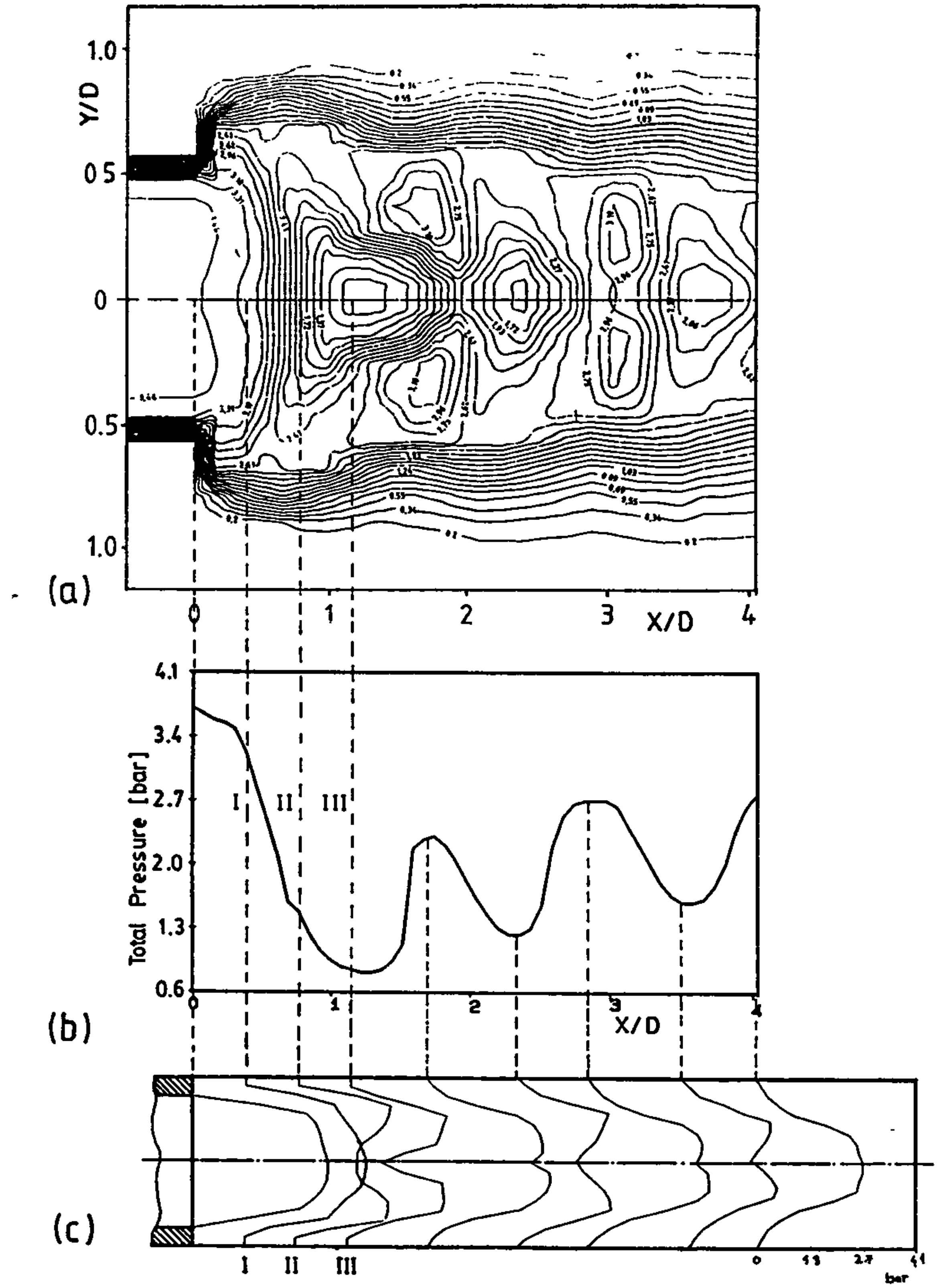

Figure 3.20 Illustrations of total pressure measurement results for the jet from a straight pipe: (a) total pressure distribution in topographic form; (b) total pressure distribution on the centre-line; and (c) traverse total pressure distributions at different locations downstream from the exit plane

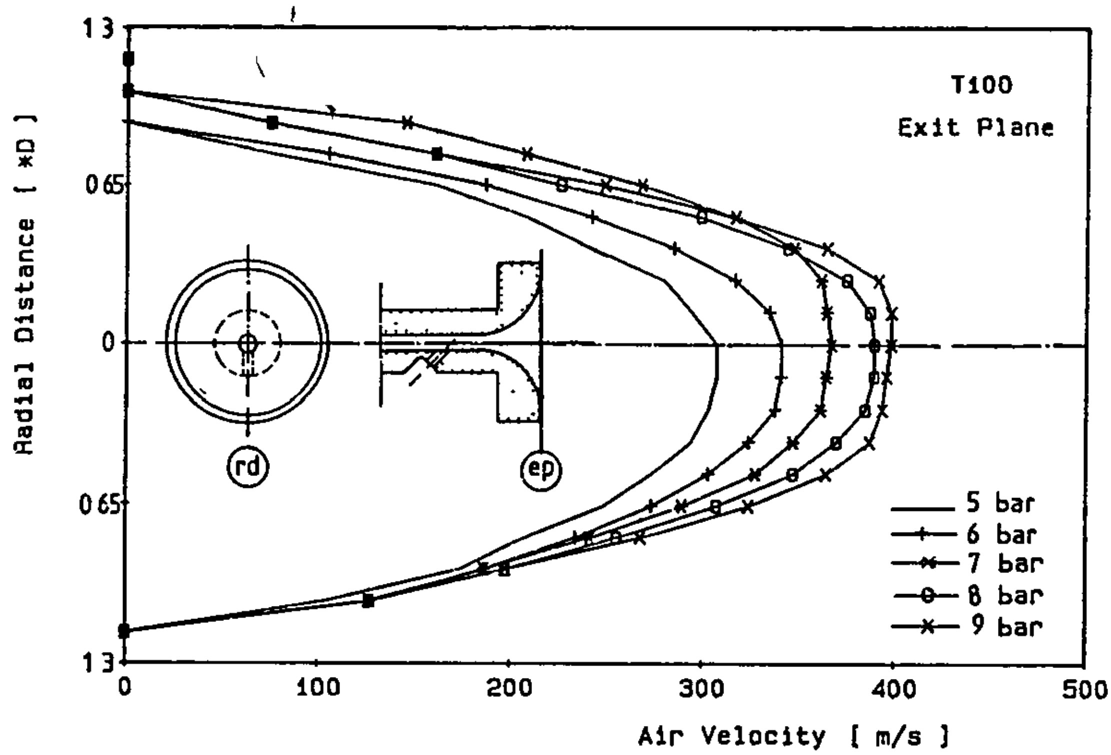

Figure 3.21a The primary jet traverse velocities at the exit plane of the T100 HemaJet at various driving pressures

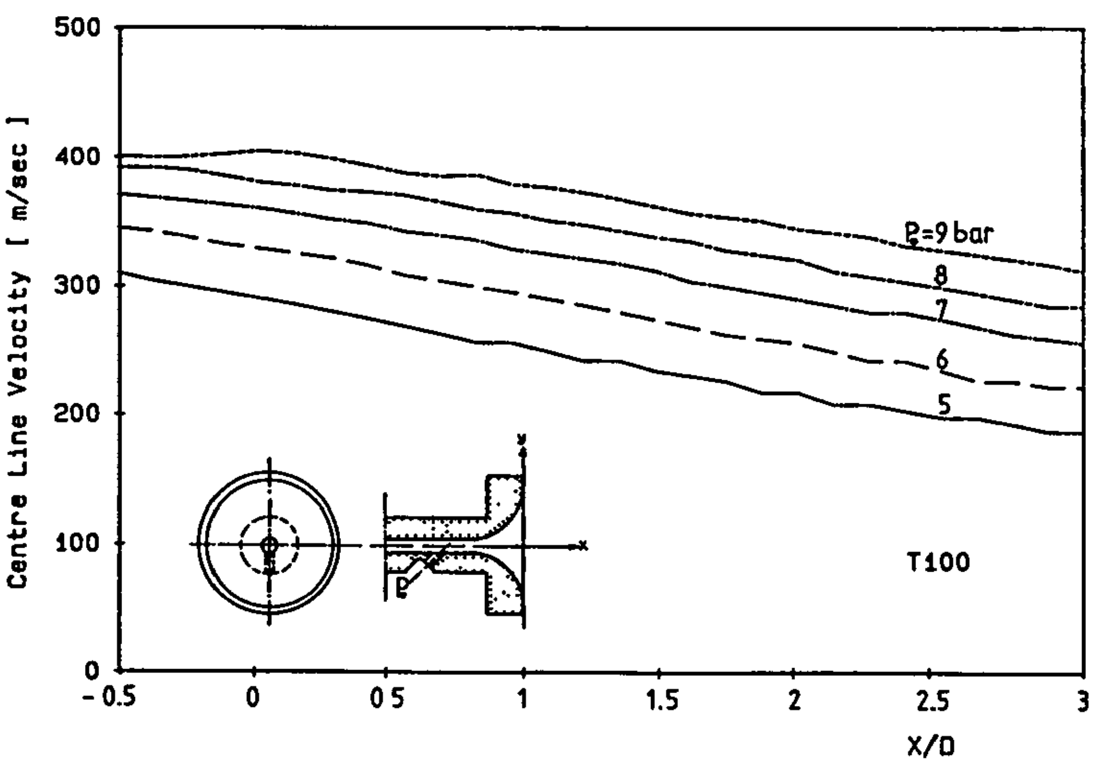

Figure 3.21b The primary jet centre-line velocities of the T100 HemaJet at various driving pressures

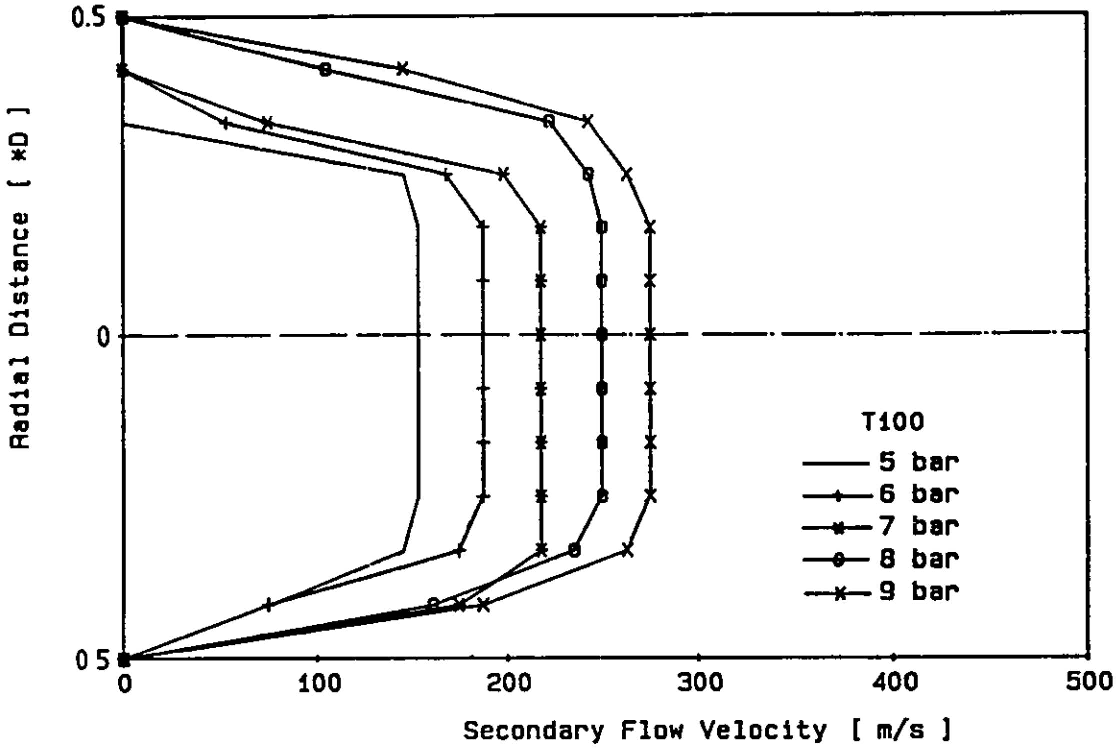

Figure 3.22a The secondary jet traverse velocities from the T100 HemaJet at various driving pressures

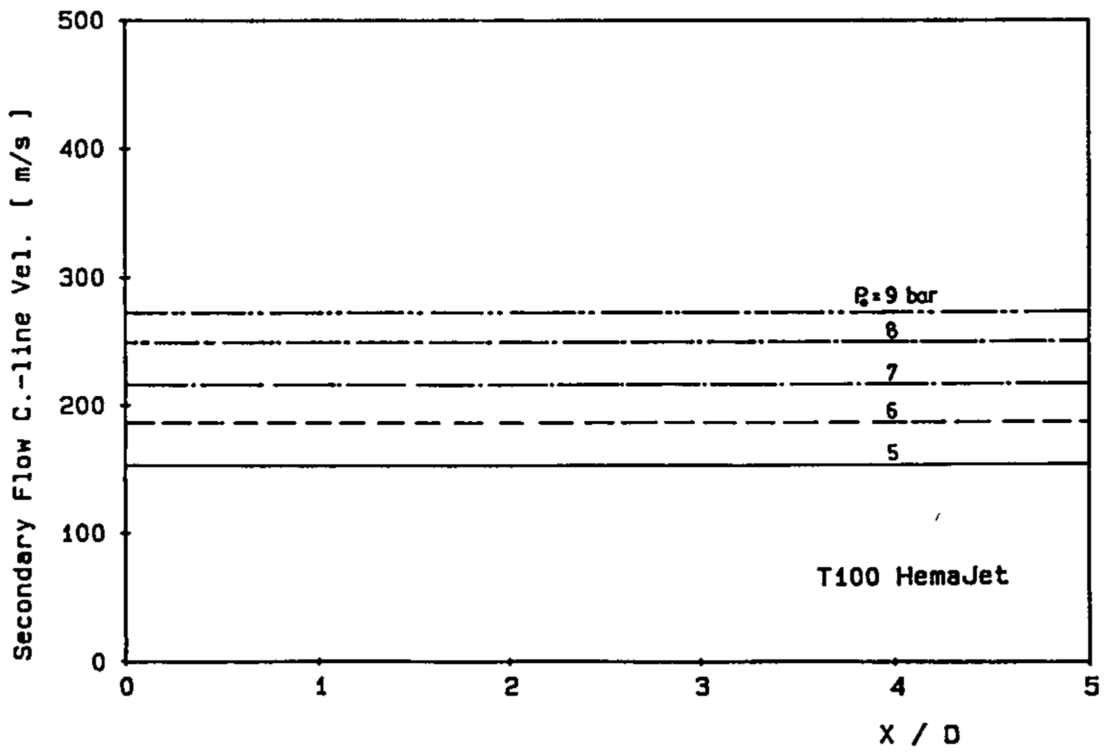

Figure 3.22b The secondary jet centre-line velocities from the T100 HemaJet at various driving pressures

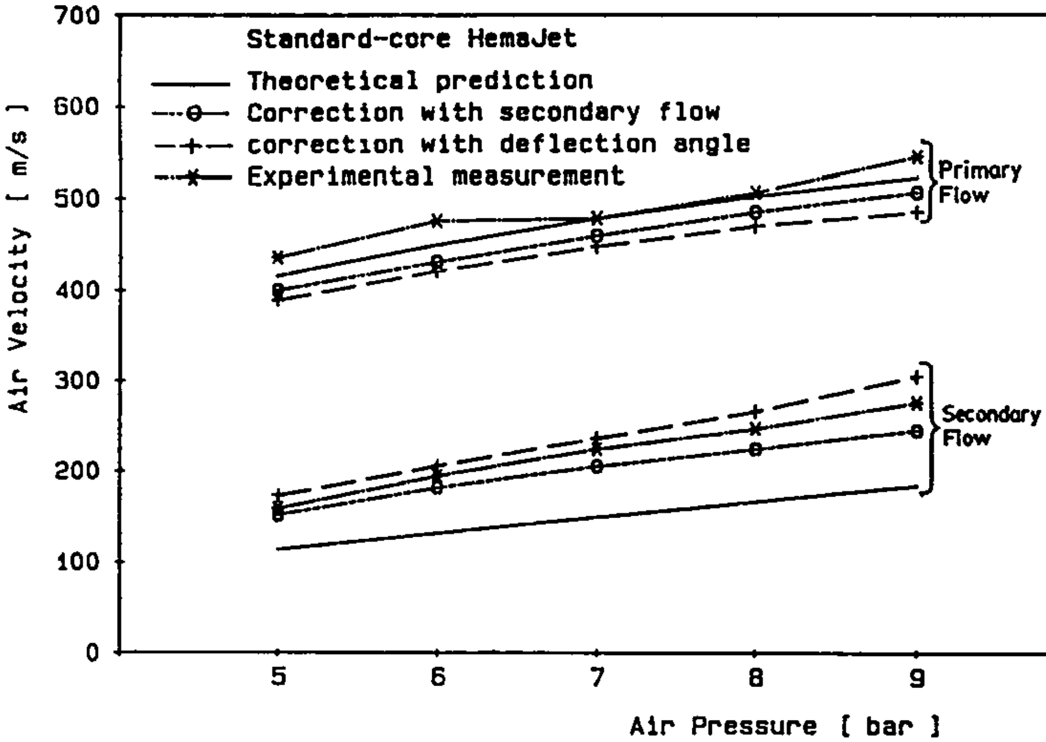

Figure 3.23a Comparisons of the theoretical, corrected theoretical and experimental primary jet velocities from the Standard-core HemaJet

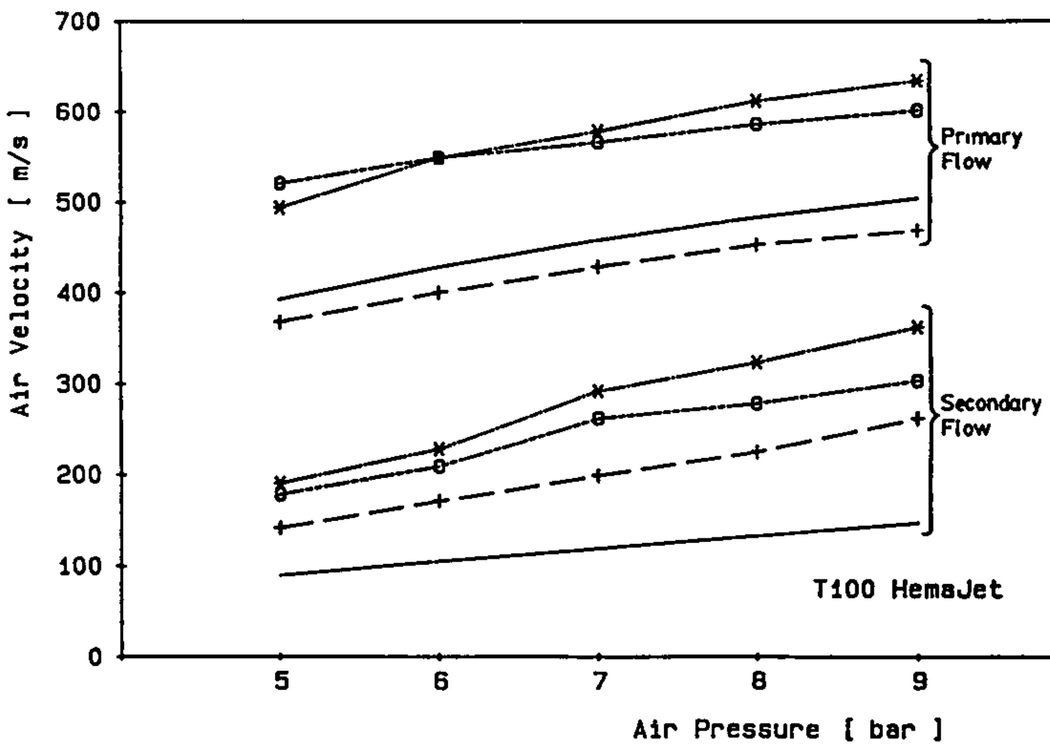

Figure 3.23b Comparison of the theoretical, corrected theoretical and experimental primary jet velocities from the T100 HemaJet

CHAPTER 4

INVESTIGATION OF RECENT TEXTURING NOZZLES

4.1 Nozzles

Four industrial designs, namely the Standard-core, T100 and T341 HemaJets, and the Taslan XIV nozzle, together with two other nozzles (designated as L1 and L2) as designed by Acar[42], are investigated in this chapter. Figs. 4.1a, b, and c illustrate the general features of the three HemaJets, the Taslan XIV, the L1 and L2 nozzles respectively. The figures also show the technical drawings of these nozzles.

A detailed description of the HemaJets, together with a comparison of the nozzles, is made in Chapter 3. Being effectively cylindrical nozzles, both the L1 and L2 nozzles can be included in the same category although they have two inlet holes in comparison to the one inlet hole in the T100 and the three inlet holes in the T341 and Standard-core nozzles. The diameters of the inlet holes are different in the case of the L1, but the inlet holes of the L2 nozzle are of equal diameter. The main channel of the L2 nozzle is slightly tapered towards the exit and in this respect it differs from the HemaJets and the L1 nozzle. Both L1 and L2 nozzles have enlarged trumpet-shaped exits as do the Heberlein T-series HemaJets.

In a Taslan XIV nozzle, as seen in Fig. 4.1b, air is passed through a one-sided hole by which an asymmetry as well as a swirl is said to be imparted to the flow[45]. The flow then is admitted through an annular gap between the needle and the so called 'venturi' to the converging section of the nozzle. The width of this gap is adjusted by moving the converging-diverging nozzle part backwards and forwards via a thumb-screw. The annular gap and the throat area are determining factors for the air consumption of such Taslan nozzles. The optimum working condition is therefore adjusted by this gap during the texturing trials. Under the working conditions, the air flow is choked at the throat of the venturi (reaching the sonic velocity) and is then accelerated in the diverging section which extends up to the exit plane of the nozzle without an exit shape. The amount of secondary flow is determined by the air pressure, the size of the needle hole, and the annular gap. Fig. 4.1b also illustrates that the needle hole of the Taslan XIV nozzle may be restricted by a sapphire insert. The size of this restriction varies according to the supply yarn linear density and therefore, several interchangeable sizes of needles can be used with a single nozzle body[38] for use with different yarns. In this current investigation, only one needle size which has the same linear density range as the other nozzles investigated was studied.

The air consumption levels of these nozzles at 7 bar are given in Fig. 4.2. The figure shows that the T341 HemaJet consumes the highest amount of air compared with the other nozzles and the T100 HemaJet, with only one inlet hole, appears to be the most economical nozzle.

4.2 Experimentation

Many researchers[42,44] preferred to use scaled-up models in experimental studies due to the minute size of the actual texturing nozzles. As a natural consequence of this, these researchers have faced two major problems: (i) manufacturing faults subsequently affecting the geometric similarity which in turn affect the flow characteristics; and (ii) the high volume of compressed air supply requirement for scaled-up nozzles, thereby severely limiting the working pressures to relatively low levels which are hardly representative of today's air-jet texturing process pressures.

In order to eliminate the drawbacks of scaling-up, full-size texturing nozzles were studied, even though it was believed that some additional shortcomings, such as the interaction between the measuring probe and the flow due to the relatively large size of the probe with respect to the nozzle, may have some slight effects on the results. To reduce this effect a very fine pitot tube as detailed in

Section 3.2, was used in the experiments. The flow velocity measurements obtained from full-size nozzles, however, have been proven to be in close agreement with the previous flow measurements from scaled-up models (See Section 3.2).

The turbulent nature of the jets was qualitatively investigated by means of a high speed shadowgraph technique described in Section 3.2. This technique was also utilised to visualise the interactions between the pressure waves and the filament behaviour during the texturing. The experimental rig which facilitated this study is shown in Fig. 4.3.

The mutual interactions between the filaments and the air flow were quantified by measuring the air velocities during the texturing process by using the same rig. The behaviour of the filaments in the jet was also photographed by means of high-speed still photography. In this technique, a spark-gap flash unit with an exposure time of 200 ns. was used. This enabled the motion of the filaments to be seen as 'frozen' as they emerge from the nozzle.

Finally, the performance of the nozzles was investigated through a series of yarn tests. A two-fold 110 dtex 66 filament (220 dtex/132 fil.) (See Table 10.1 for the other properties) polyester yarn was used to produce the textured yarns. While varying the air pressure from 5 to 9 bar, all other process parameters had been kept constant, these being:

Texturing speed	:	400 m/min
Overfeed	:	20 %
Wetting	:	0.2 litre/hour (by means of a wetting unit)

4.3 Results of Flow Measurements

4.3.1 Axial velocity profiles

At varying air pressures, the axial velocity distributions at the exit plane of the Standard-core, T100, T341, Taslan XIV, L1 and L2 nozzles are given in Figs. 4.4a, b, c, d, e and f respectively. These velocity distributions are also presented in 3-dimensional, and topographic form, in Figs. 4.5a, b, c, d, e and f for a typical 7 bar supply pressure.

From these figures, the supersonic and non-uniform nature of the flow can be seen. The asymmetric nature of the flow is obvious in the case of the T100 jet (Fig. 4.4b), whereas the other nozzles more closely approximate to symmetrical air velocity distributions. Some dissimilarities in the axial velocity profile from these three nozzles were observed (See Fig. 4.4).

4.3.2 Shock waves and centre-line velocities

Flows from all these nozzles at different pressures were also studied by using a shadowgraph system in order to obtain a better understanding of them. From the shadowgraphs and the centre-line velocity fluctuations (which are also indicators of the occurrence of shock waves) as shown in Figs. 4.6a, b, c, d, e and f, it can be concluded that the strengths of the shock waves produced by different nozzles are varying. Since the shock waves are known to affect the velocity distribution as discussed in Section 3.6.1, it is not surprising to see different velocity profiles from different nozzles with varying degrees of shock strengths.

Shock waves are surmised initially to occur at the start of the trumpet-shaped exit part where the flow separates from the wall of the nozzle. This point is 2 nozzle diameters to the exit plane in the Standard-core nozzle, is 4.5 nozzle diameters in the T100, L1 and L2 nozzles, and is 3 nozzle diameters in the T341 nozzle. However, it corresponds to the very exit plane in the case of the Taslan XIV nozzle. Since the repetitive shock waves will gradually diminish and expand to the ambient atmospheric conditions, waves of relatively lesser strengths are highly unlikely to be observed in the emerging flows from different nozzles with various diverging shape and sizes. For instance, the T341 nozzle, even at high pressures, produces no clearly visible shock waves outside the nozzle, whilst the Taslan XIV and Standard-core nozzles produce relatively strong shock waves (Fig. 4.6). Since the strong shock waves do not dissipate in very short distances and repeat themselves periodically in the further downstream of the flow as seen in Fig. 4.6d, they are expected to be visible (by a flow visualisation technique) outside the nozzle. Therefore it can be argued that different nozzles produce shock waves of different strengths.

4.3.3 Turbulence

The turbulent nature of the jets created by several nozzles was demonstrated by means of a high speed shadowgraphy technique. Fig. 4.7 shows three such photographs obtained from jets created by: (a) a straight pipe; at 7 bar supply pressure (b) the Standard-core HemaJet; and (c) the Taslan XIV nozzle; at 9 bar supply pressure. It is seen that the instantaneous shadowgraph of the jet from a straight pipe is almost the same as that obtained with long exposure times indicating the less disturbed nature of the flow. However, the other two shadowgraphs of the jets from the Standard-core HemaJet and Taslan XIV nozzles illustrate the local density variations caused by the highly turbulent nature of the flow.

Furthermore, by comparing these shadowgraphs, it could be argued that the Standard-core HemaJet creates jets which are more turbulent than the Taslan nozzles. It could be suggested that this higher turbulence is created by the oblique impingement of the incoming jets of the HemaJet nozzles.

4.4 Interactions Between the Air-jet and the Filaments

In the course of the investigations reported up to this point, all the air jets were free of disturbances from the filaments. During the actual texturing process, however, overfed filaments exist in the nozzle and they are transported through the nozzle and entangled to form a looped structure by the action of the air flow. It is, therefore, certain that a mutual interaction between the filaments and the air flow will take place and in turn the characteristics of the air flow will change as discussed by Acar et al[56] and Bock and Lünenschloss[49]. This interaction has been investigated by means of air velocity measurements, shadowgraph techniques, and high-speed still photography during the actual texturing process.

4.4.1 Velocity measurements during the texturing process

Using the flow measurement techniques described in Section 3.2, the velocities of the air flow during the actual texturing process have been measured. In order to avoid any possible interference with the filaments, the pitot tube has been kept at a distance of 1.5 nozzle diameters from the exit plane. The presence of the water droplets in the flow caused ice formation just at the tip of the measuring probe which consequently made the measurements impossible.

Two different methods were deployed to defrost the probe. The first one involved an external heating of the probe so that the condensed water particles would be evaporated. This was done by focusing an intense light on to the probe and the nozzle. Although the heat released from the light did not affect the texturing process itself, the probe holder expanded due to the intense heat, resulting in the uncontrolled displacement of the probe. This method of defrosting the instrument was, therefore, abandoned.

The second method considered was heating of the water. Before making any attempt to do this, the possible effects of the water temperature on the process itself and the resultant textured yarns needed to be ascertained. As was disclosed in Section 7.4, at the end of that investigation, it was concluded that the effect of water temperature in the range of 15-65°C was negligible. Having obtained this result, the air velocity measurements were carried out at 65°C water temperature. Unfortunately, at high pressures and low texturing speeds, ice formation still hindered the smooth running of the measurements and cast some doubt over the repeatibility and reliablility of the results. Some results, however, were obtained and Figs. 4.8a, b and c show the centre-line velocity fluctuations at 5, 7 and 9 bar pressures respectively. Fig. 4.9 also shows the axial flow velocities at 1.5D distance from the exit plane in the vertical diameter. These figures clearly indicate that the presence of the filaments in the nozzle reduces the flow velocity and makes the shock waves weaker. The degree of the velocity deceleration due to the filaments is almost equal for all the driving pressures used.

4.4.2 Shadowgraphy during the texturing process

By using the experimental rig shown in Fig. 4.3, the instantaneous shadowgraphy of the process was performed at different process conditions with the Standard-core Hemajet and the Taslan XIV nozzles because these two nozzles produce the strongest shock waves. The shadowgraphs given in Fig. 4.10 and Fig. 4.11 illustrate that a substantial change in the characteristics of the jet occurs in that shock waves are partly destroyed and the intensity of turbulence is increased by the presence of the filaments in the flow.

No consistent relation between the shock waves and the turning points of the filaments as claimed by Bock and Lünenschloss[49] could be detected.

4.5 High Speed Still Photography During the Texturing Process

Although numerous instantaneous photographs of the texturing process with all the nozzles were taken under different process conditions, only three such photographs for each nozzle at 5, 7 and 9 bar pressures and under the standard process conditions are presented in Figs. 4.12a, b, c, d, e and f. These photographs demonstrate that the actual texturing, i.e. loop and entanglement formation, takes place in the vicinity of the nozzle exit. In the case of the nozzles with trumpet-shaped exits, the process takes place in the diverging exit section and therefore the still photographs taken from a right-angled position show only the textured yarn emerging from the nozzle, not the loop forming filaments as is the case for the Taslan XIV (Fig. 4.12c).

4.6 Textile Properties of the Yarns

A series of yarns have been produced by using all the mentioned nozzles, and tests of these yarns have been carried out to ascertain their textile properties. The yarn tests are mainly measurements of the linear density and tensile related properties of yarns i.e. tenacity, breaking elongation and instability. The instability of the yarns has been measured according to the recommendations made in Section 8.8. In addition to these yarn tests, the average tensions in the feeding, and stabilising zones were recorded during the texturing process in order to assess the quality of the yarns.

Figs. 4.13a, b, c, and d show the percentage linear density increase, tenacity, breaking elongation, and instability, respectively, of the yarns textured at varying air pressures. Figs. 4.14a, and b show the average yarn tension in the feeding and stabilising zones respectively. These results suggest that the differences between the yarns produced by the Standard-core, T100, L1 and L2 nozzles are not substantial, whereas the T341 HemaJet and Taslan XIV nozzle produce comparatively better yarns. It is believed that this is due to the higher flow velocities and higher compressed air consumptions of these nozzles (Fig. 4.6c).

4.7 Conclusions

The current investigation has shown that the air flows from various texturing nozzles, despite the substantial differences in their geometrical configurations, are supersonic. However, the strength of shock waves created by these supersonic air flows may substantially vary from one nozzle to another. A non-uniform velocity profile, on the other hand, is common to all the texturing nozzles, whereas the axial centre-line velocity fluctuations which are caused by the formation of the shock waves may also vary from one nozzle to another. Turbulence, as visualised by the instantaneous shadowgraph technique, is found to be more intensive in the flows created by the HemaJets than the Taslan XIV nozzle due to the oblique impingement of the incoming jets of the HemaJet nozzles.

The flow investigations carried out during the texturing process illustrated that the flow velocity is decreased and the shock waves are partially destroyed by the presence of the filaments in the flow. Numerous instantaneous shadowgraphs taken at different texturing conditions did not reveal any obvious correlation between the loop and entaglement formation and the occurence and position of the shock waves as argued by Bock and Lünenschloss[47]. Therefore, it can be concluded, as Acar et al[56] claimed, that the shock waves do not appear to contribute to the loop and entanglement formation. Absence of shock waves in certain nozzles is a further evidence that supports this conclusion.

High-speed still photographs of the process with different nozzles pointed out one further difference between the HemaJets and the Taslan nozzles in that the actual entanglement of the separated filaments takes place in the trumpet-shaped exit of the HemaJets whereas it occurs just outside the Taslan XIV nozzle.

When the textile properties of the yarns textured by different nozzles are considered altogether, it could be concluded that all the yarns are quite similar. However the yarns textured by the T341 HemaJet and the Taslan XIV nozzles seem to be somewhat superior to the rest. This could be attributed to the high air velocities and high compressed air consumption of these particular nozzles.

HemaJet Nozzles

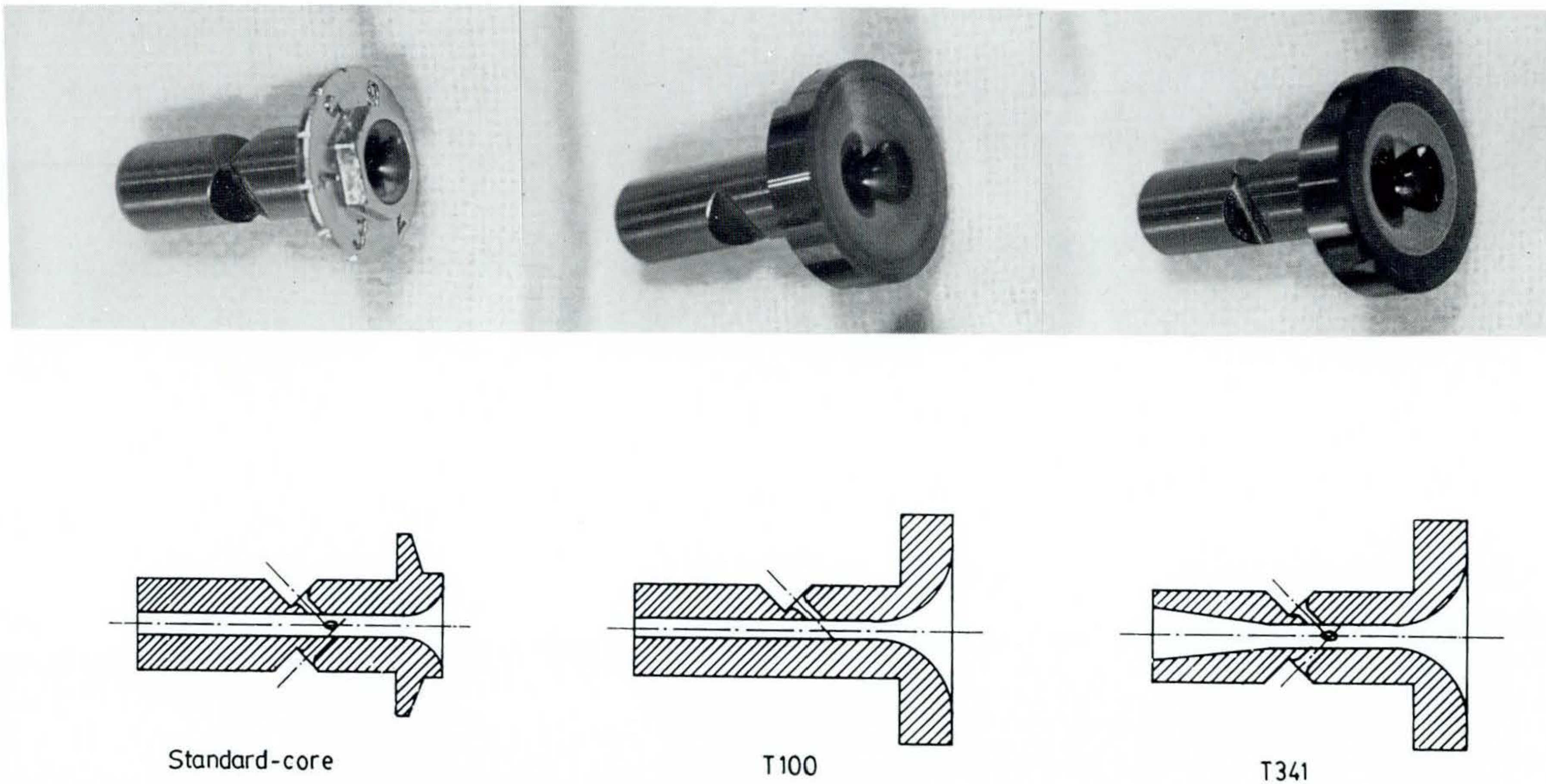

Figure 4.1a Photographs and technical drawings of HemaJet nozzles

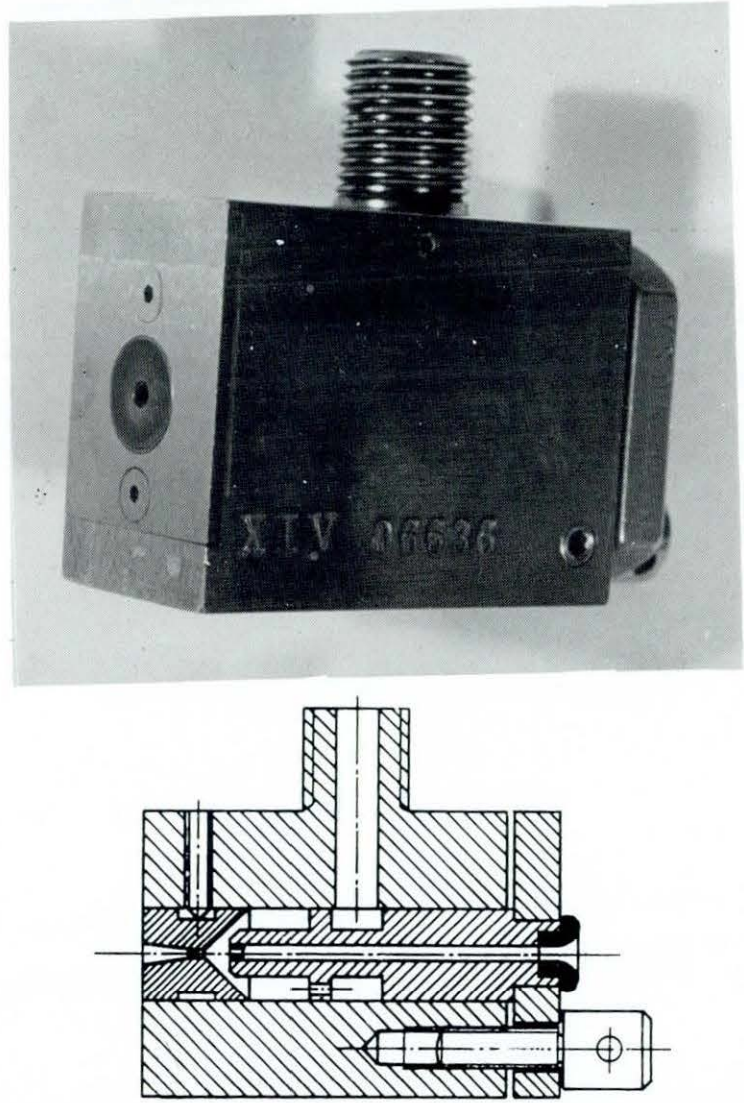

Figure 4.1b Photograph and technical drawing of the Taslan XIV nozzle

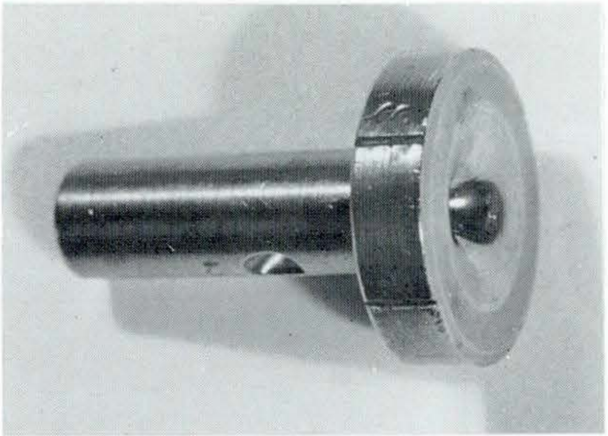

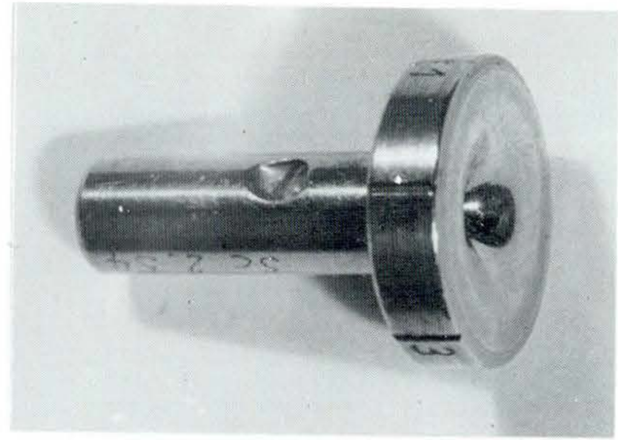

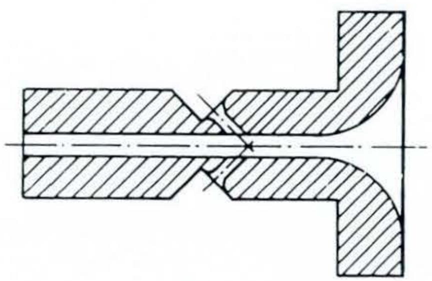

L1

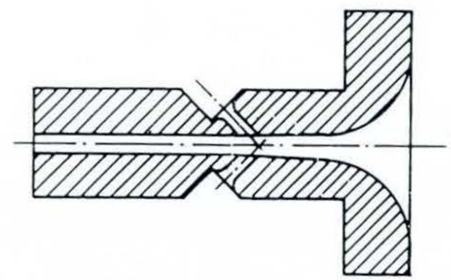

L2

Figure 4.1c Photographs and technical drawings of the texturing nozzles designed by Acar[42]

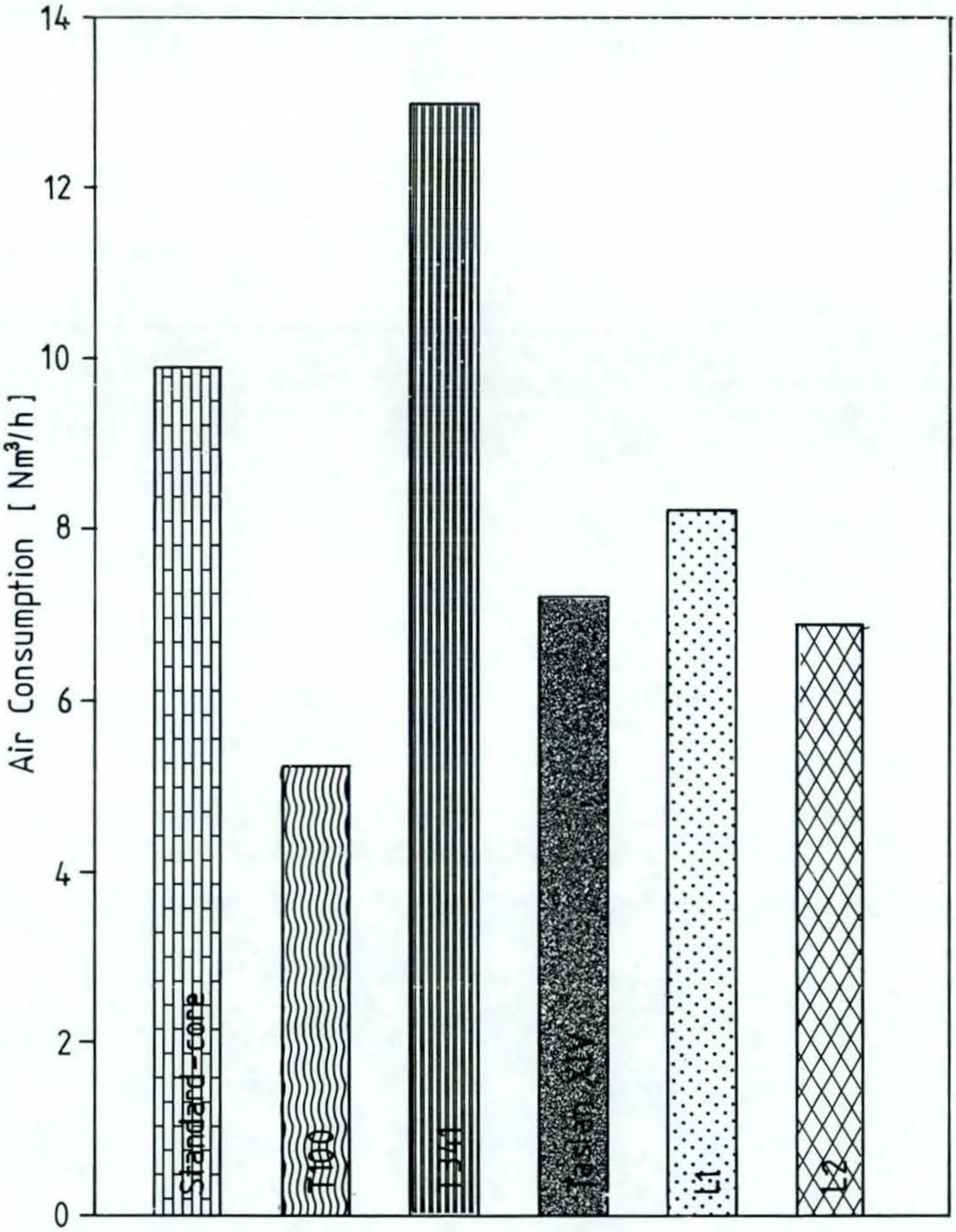

Figure 4.2 Air consumption levels of the nozzles at 7 bar

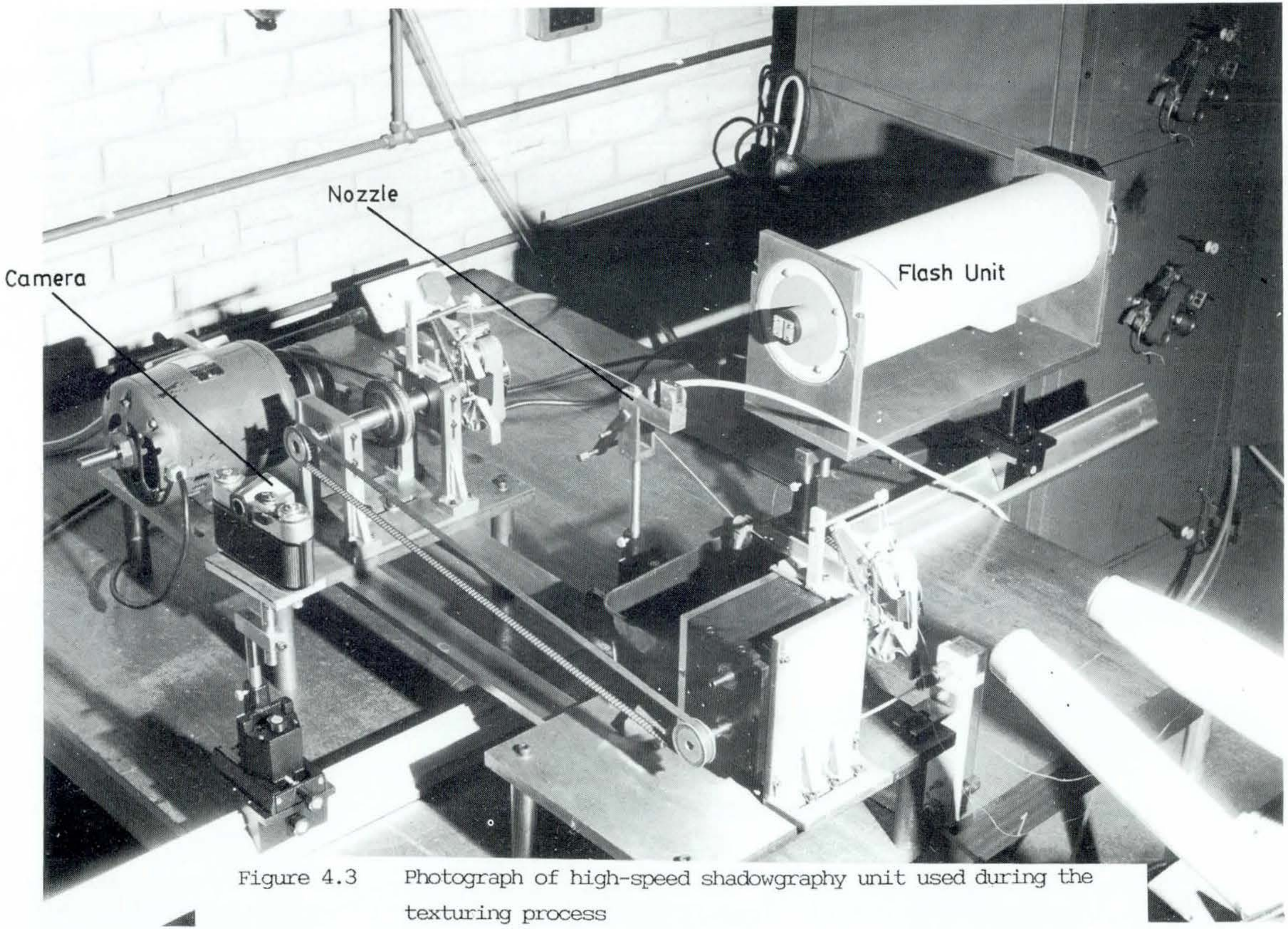

Figure 4.3 Photograph of high-speed shadowgraphy unit used during the texturing process

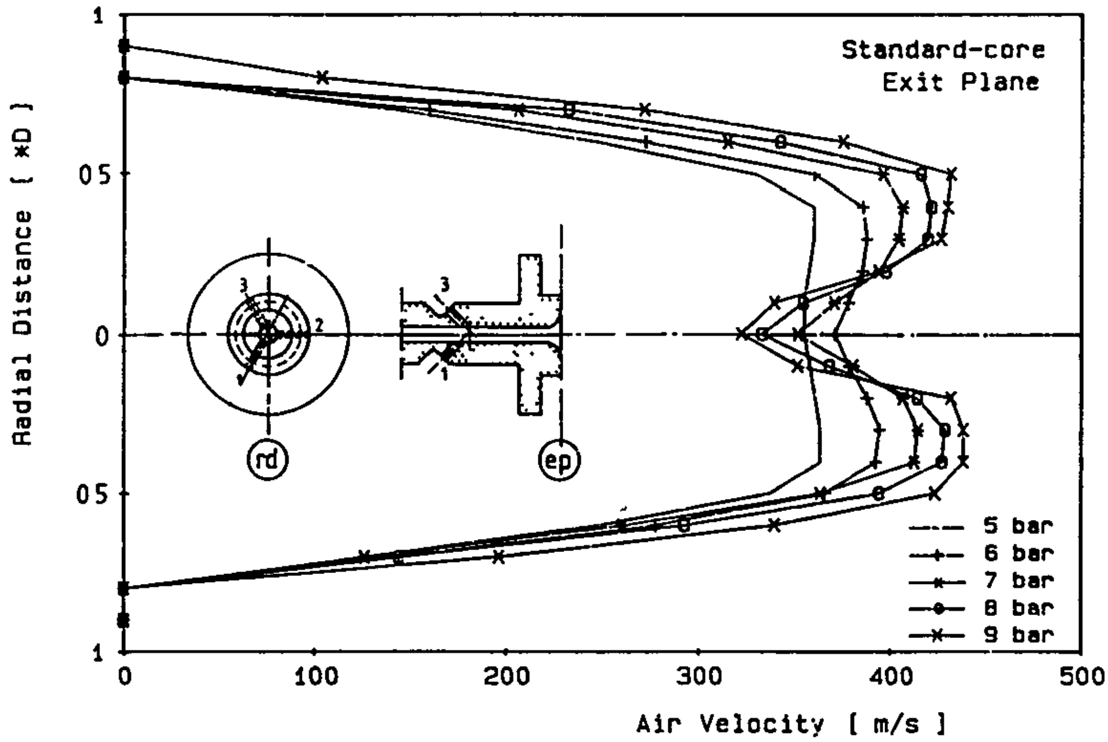

Figure 4.4a The air velocity distribution of the jet produced by the Standard-core HemaJet at varying pressures

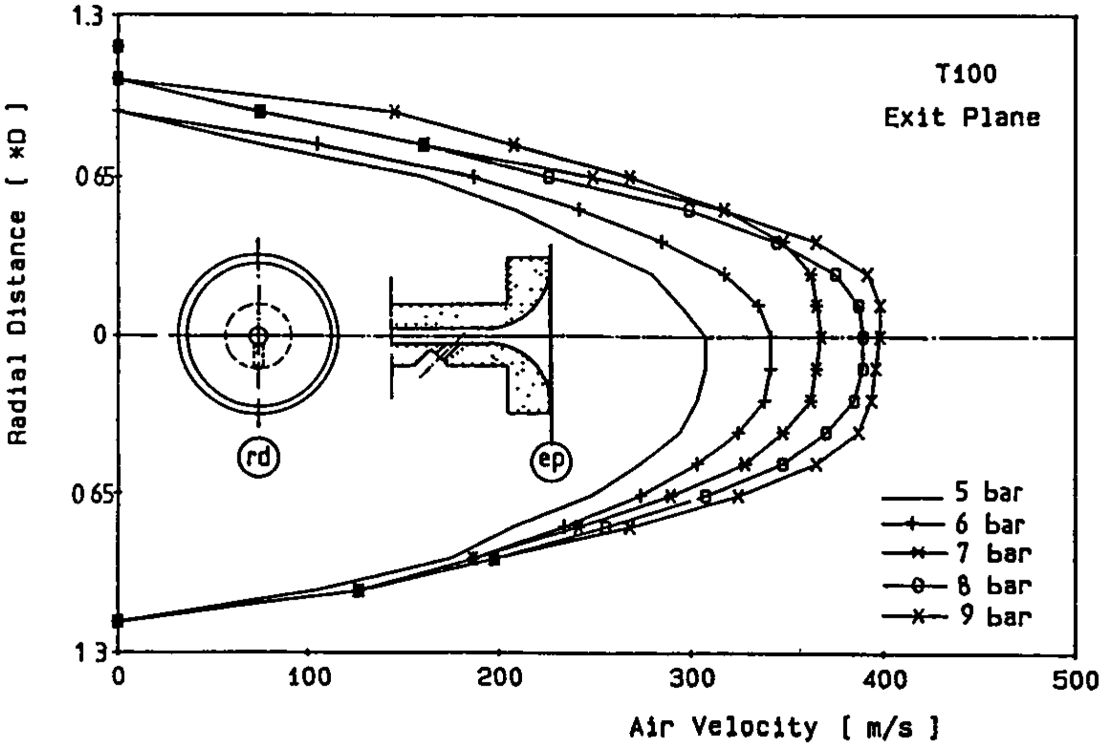

Figure 4.4b The air velocity distribution of of the jet produced by the T100 HemaJet at varying pressures

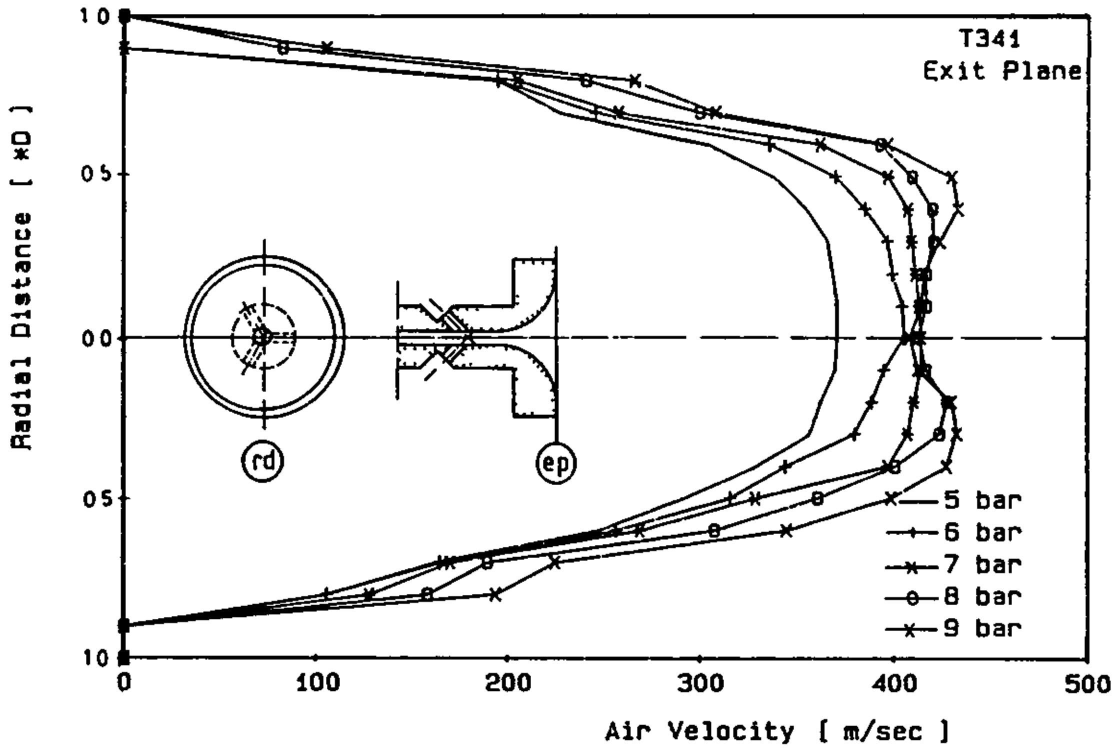

Figure 4.4c The air velocity distribution of the jet produced by the T341 HemaJet at varying pressures

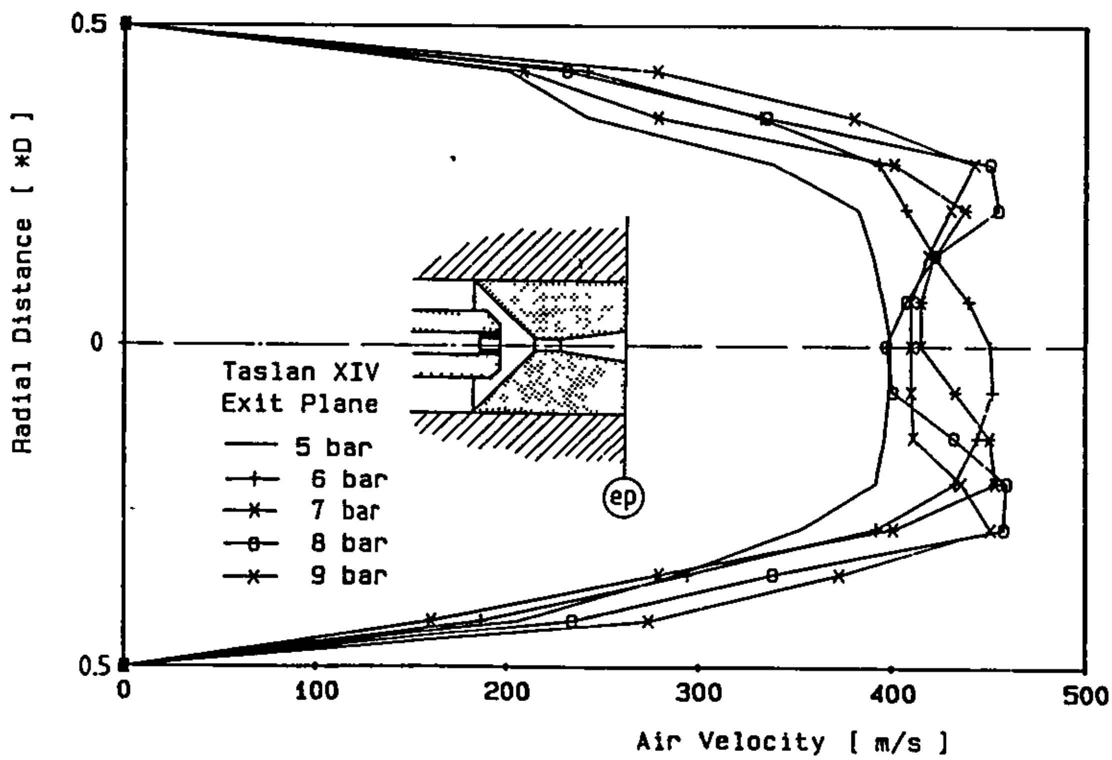

Figure 4.4d The air velocity distribution of the jet produced by the Taslan XIV at varying pressures

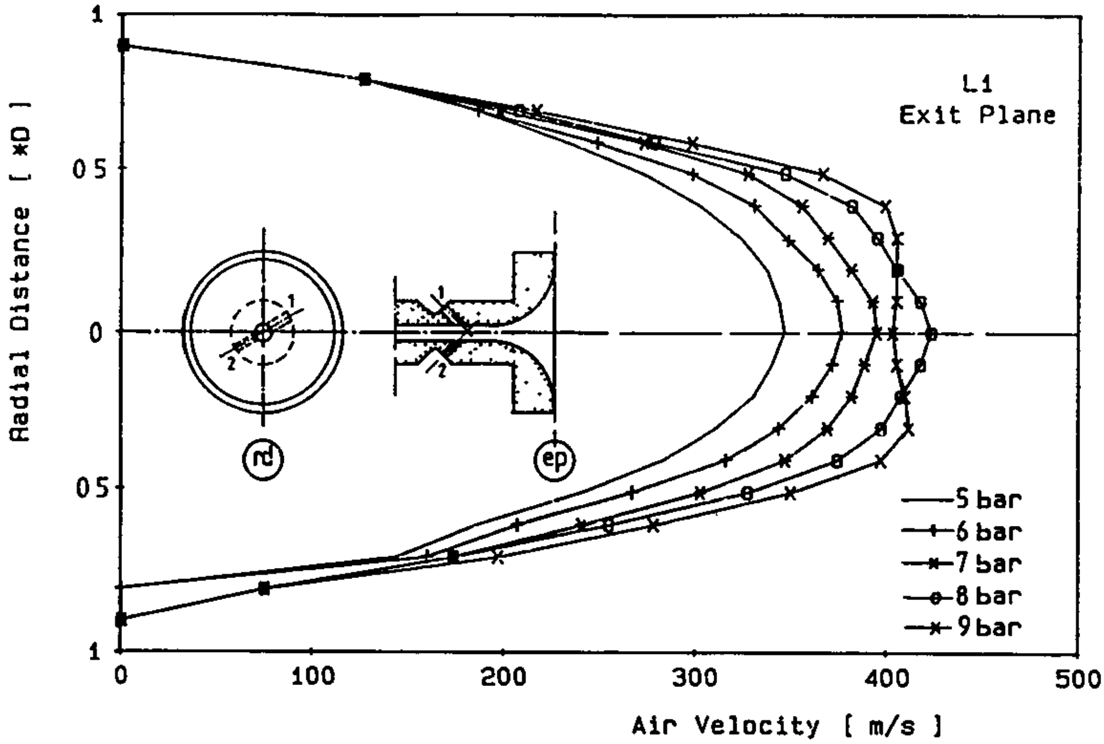

Figure 4.4e The air velocity distribution of the jet produced by the L1 nozzle at varying pressures

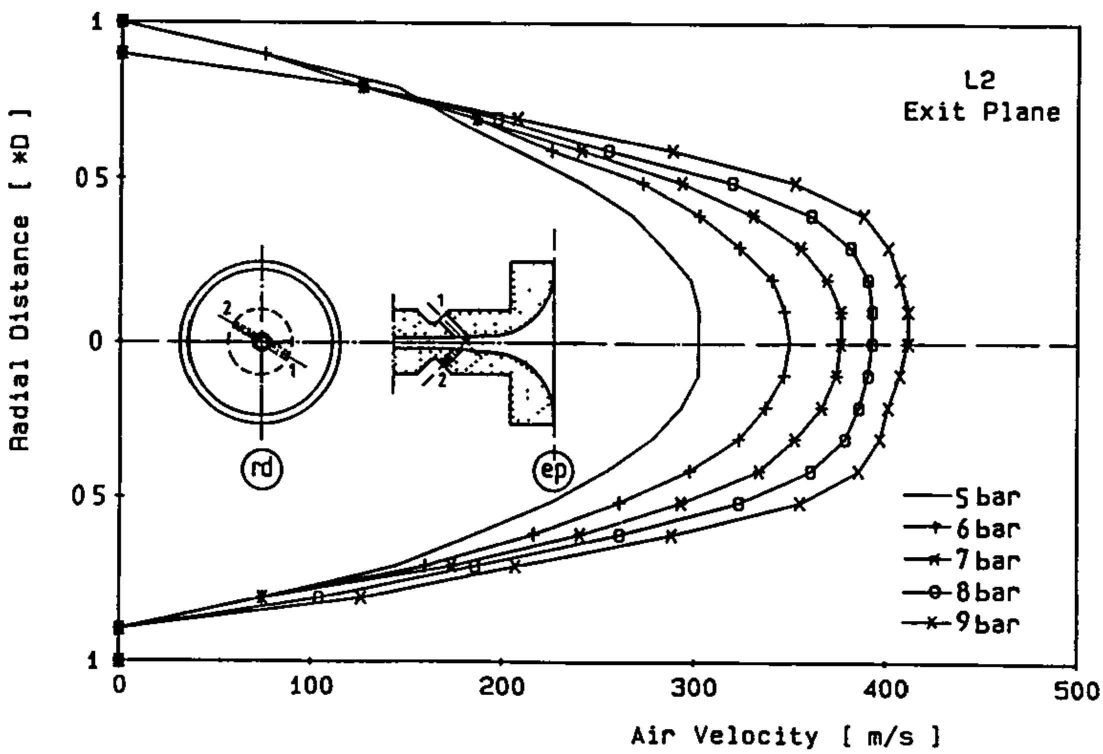

Figure 4.4f The air velocity distribution of the jet produced by the L2 nozzle at varying pressures

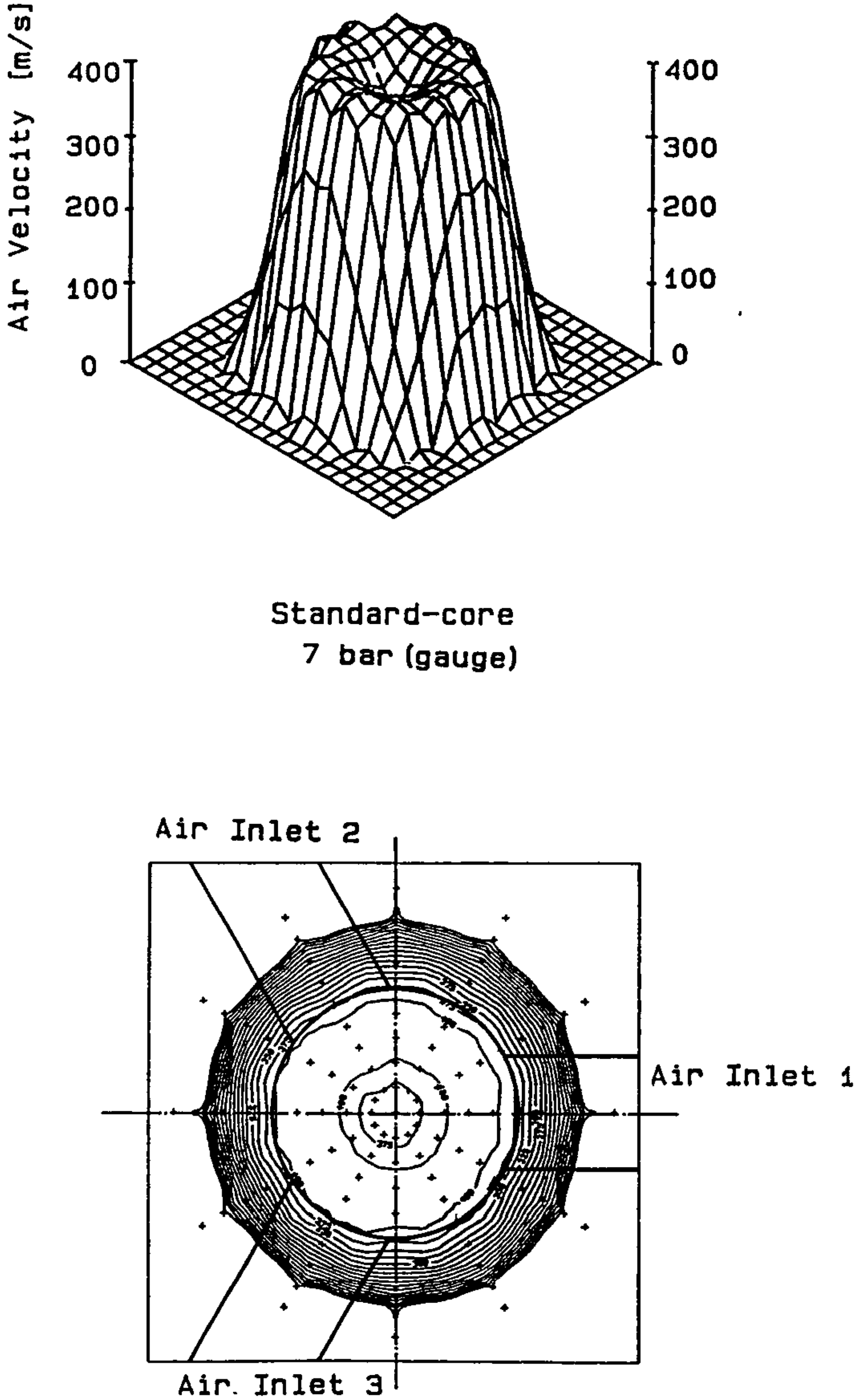

Figure 4.5a 3-Dimensional and topographic representation of the air velocity distribution of the jet produced by the Standard-core HemaJet at 7 bar pressure

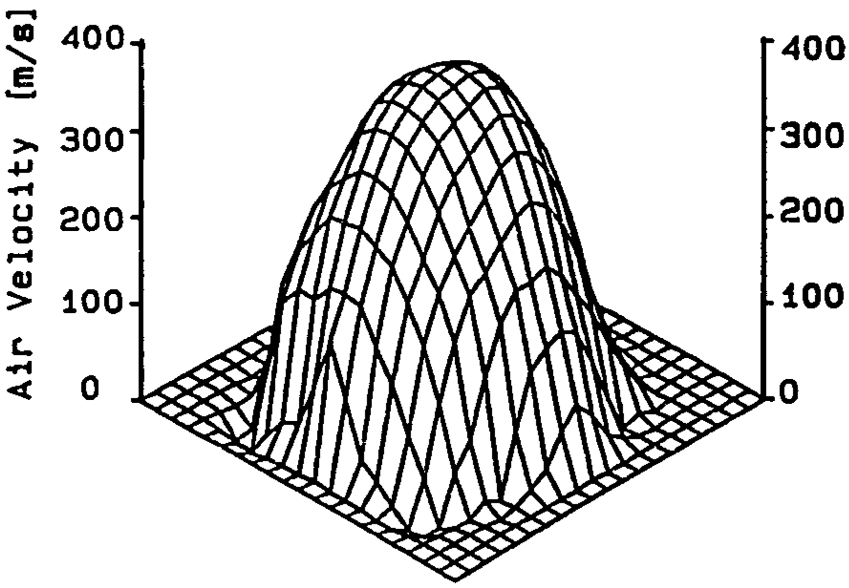

T100
7 bar (gauge)

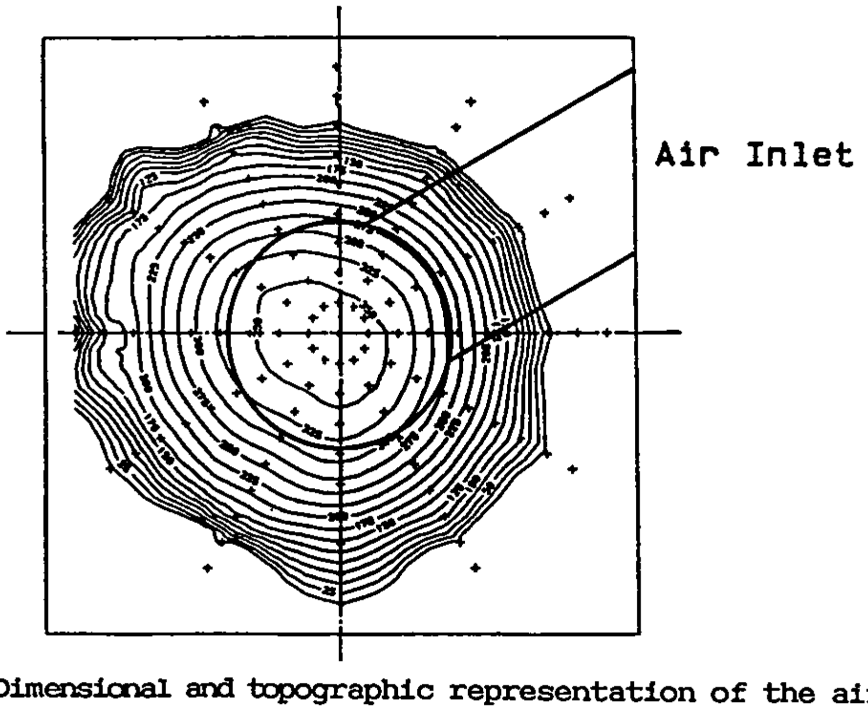

Figure 4.5b 3-Dimensional and topographic representation of the air velocity distribution of the jet produced by the T100 HemaJet at 7 bar pressure

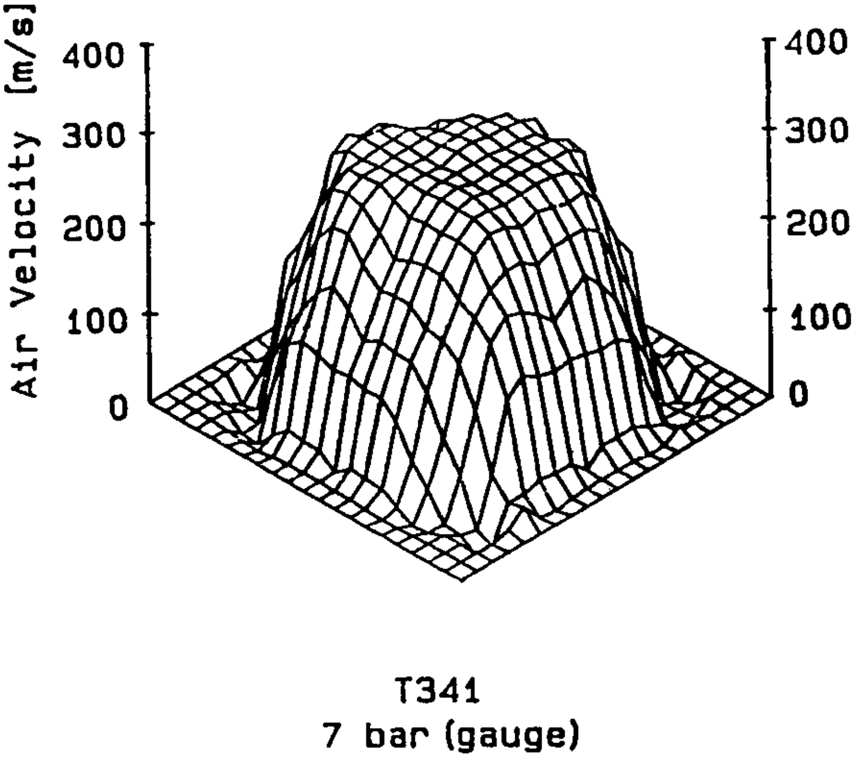

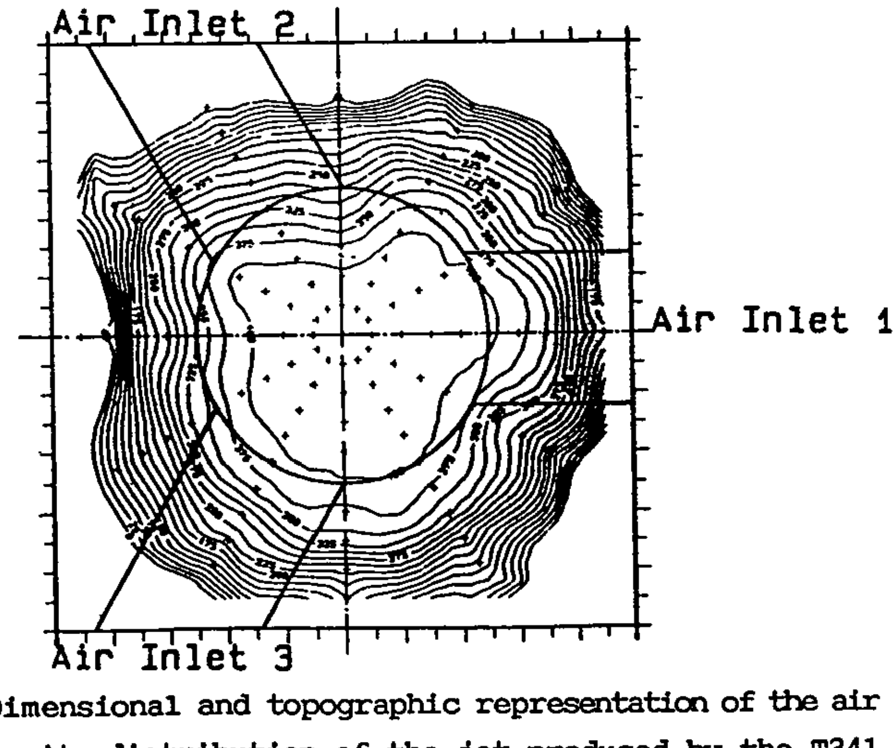

Figure 4.5c 3-Dimensional and topographic representation of the air velocity distribution of the jet produced by the T341 HemaJet at 7 bar pressure

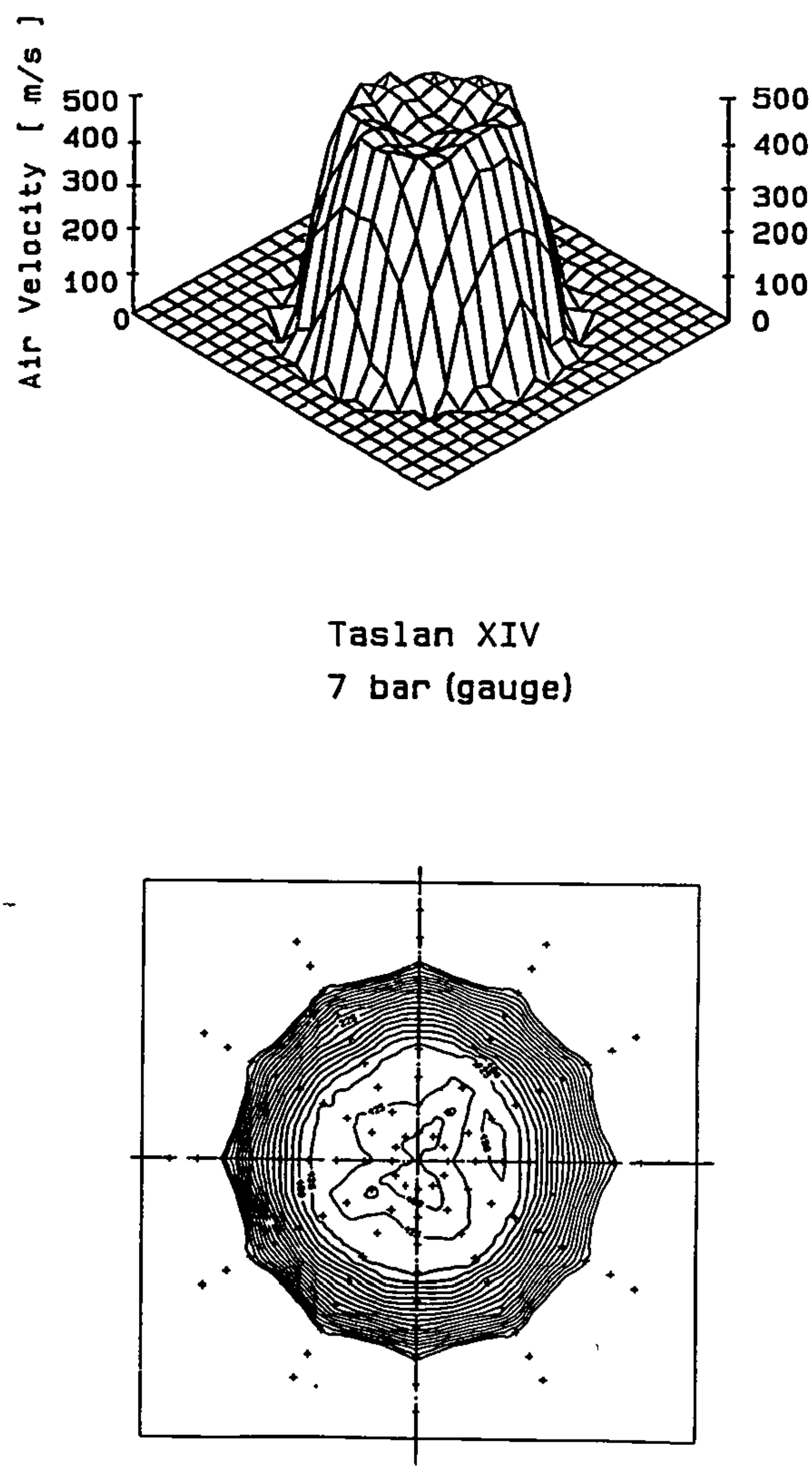

Figure 4.5d 3-Dimensional and topographic representation of the air velocity distribution of the jet produced by the Taslan XIV at 7 bar pressure

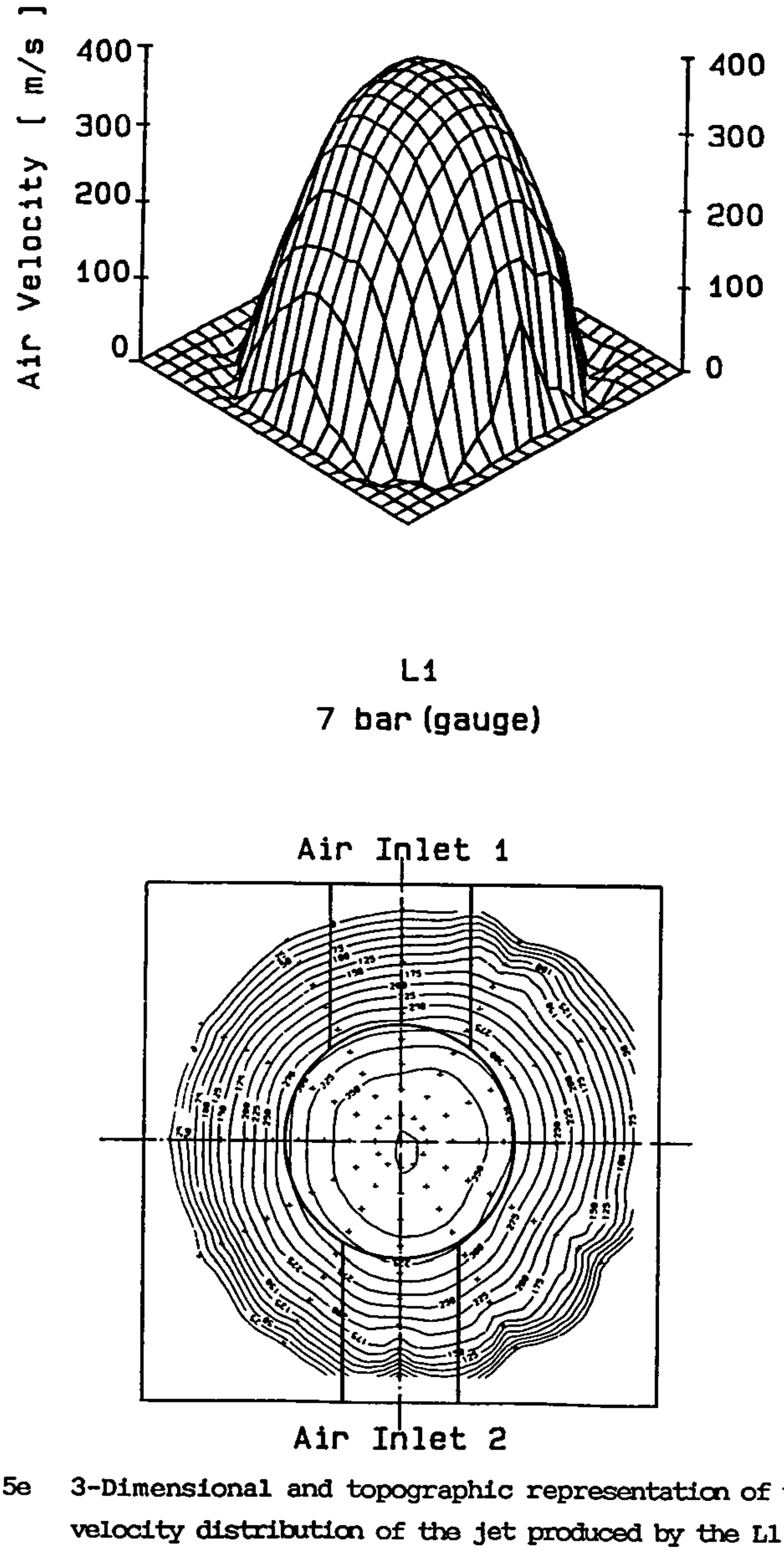

Figure 4.5e 3-Dimensional and topographic representation of the air velocity distribution of the jet produced by the L1 nozzle at 7 bar pressure

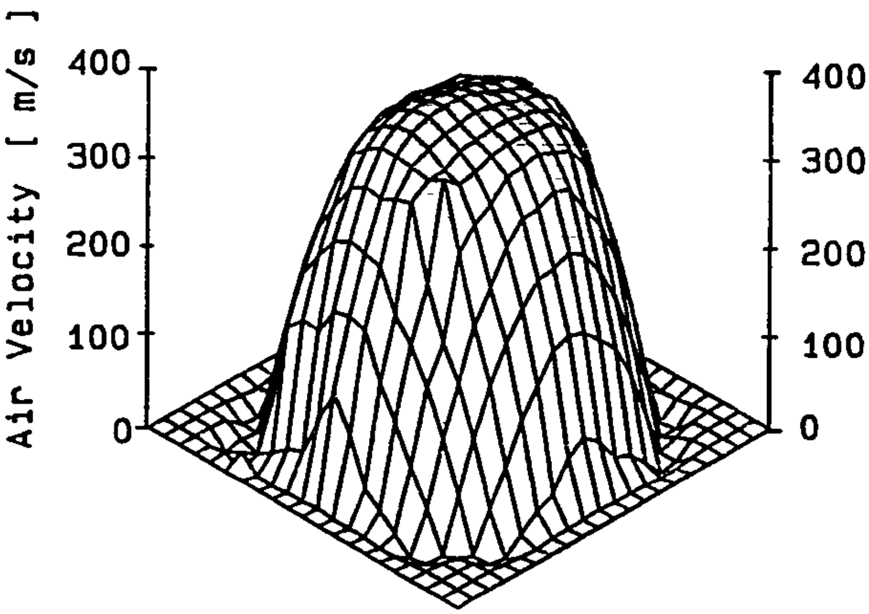

L2
7 bar (gauge)

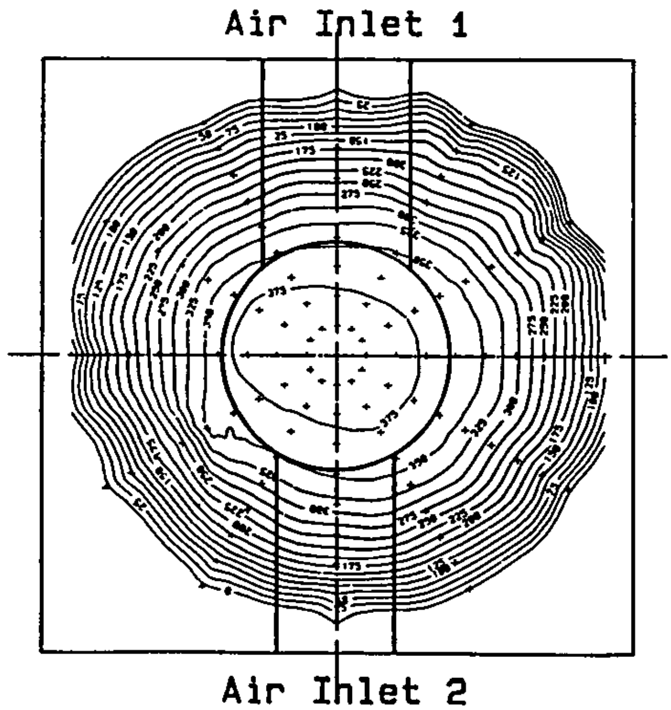

Figure 4.5f 3-Dimensional and topographic representation of the air velocity distribution of the jet produced by the L2 nozzle at 7 bar pressure

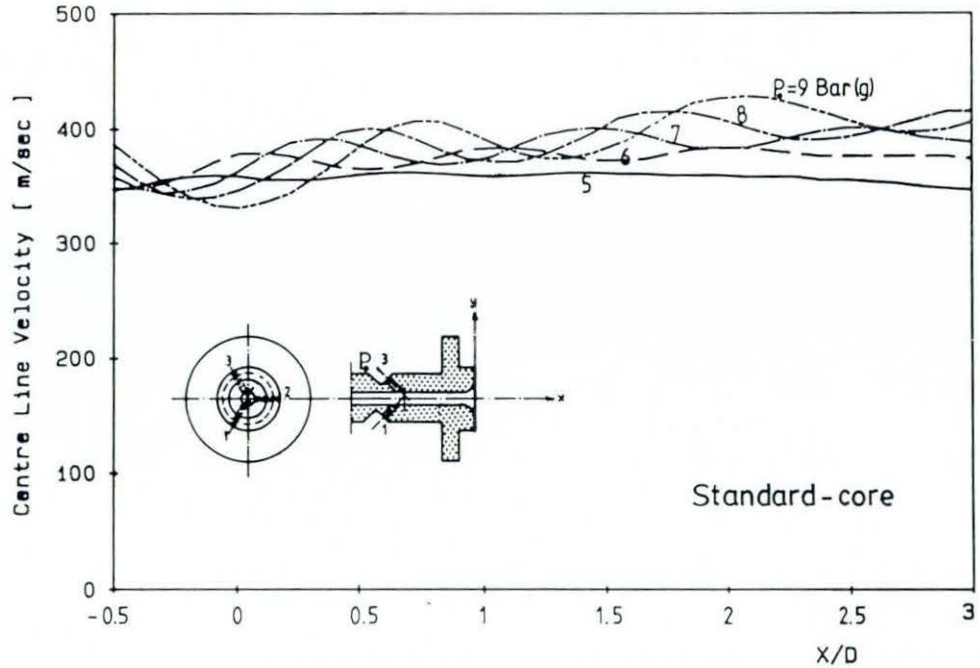

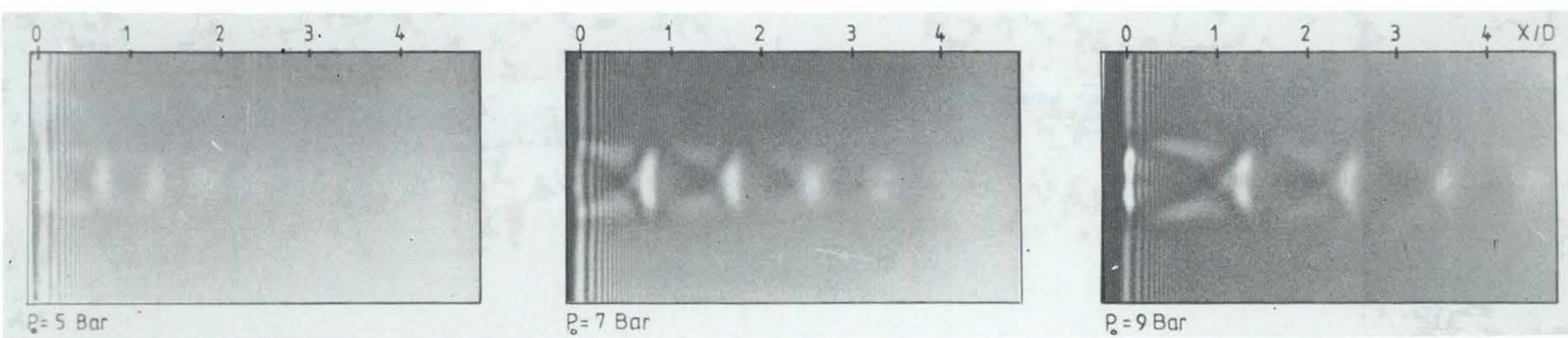

Figure 4.6a Centre-line velocities and shadowgraphs of the flow from the Standard-core HemaJet at varying pressures

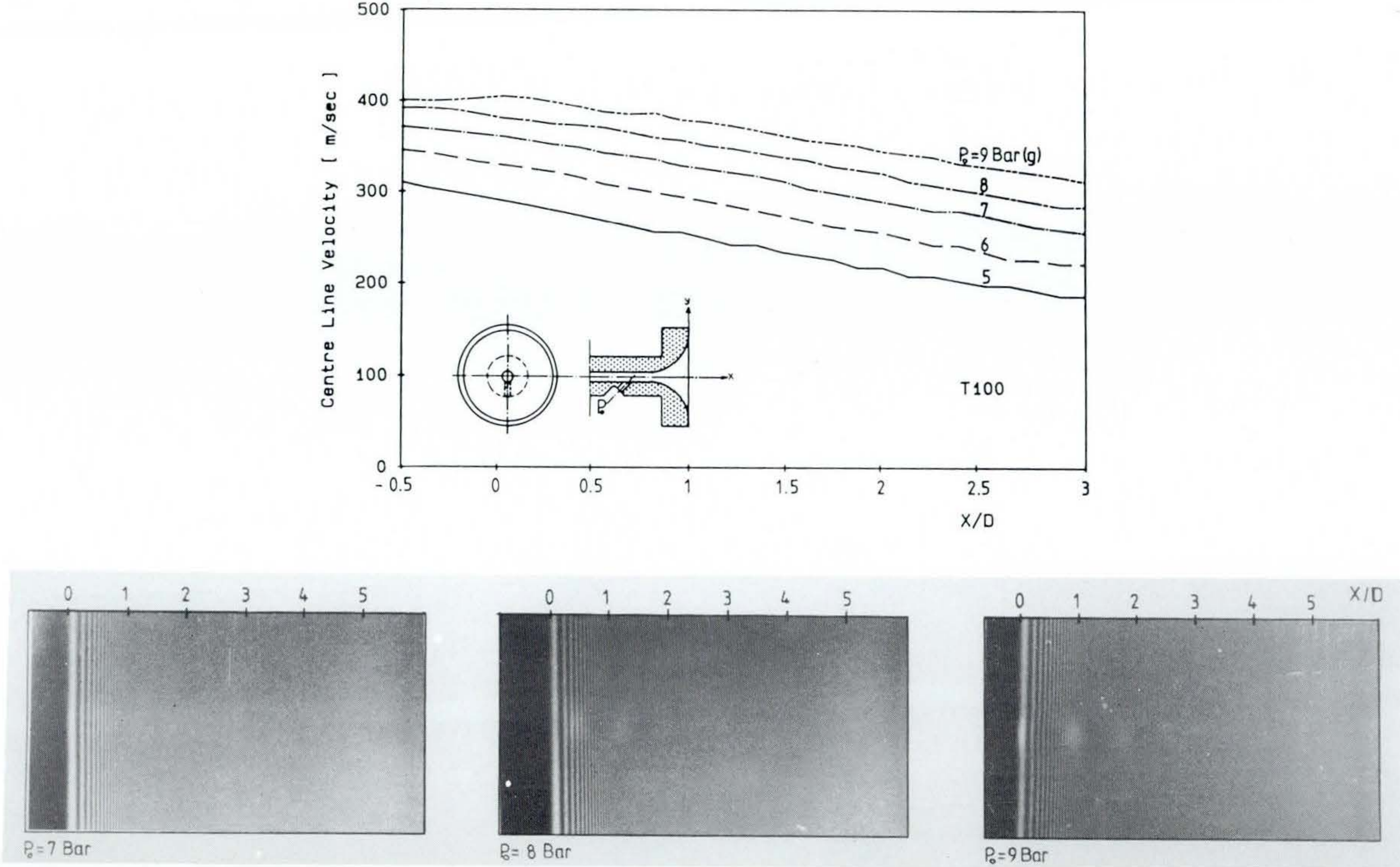

Figure 4.6b Centre-line velocities and shadowgraphs of the flow from the T100 HemaJet at varying pressures

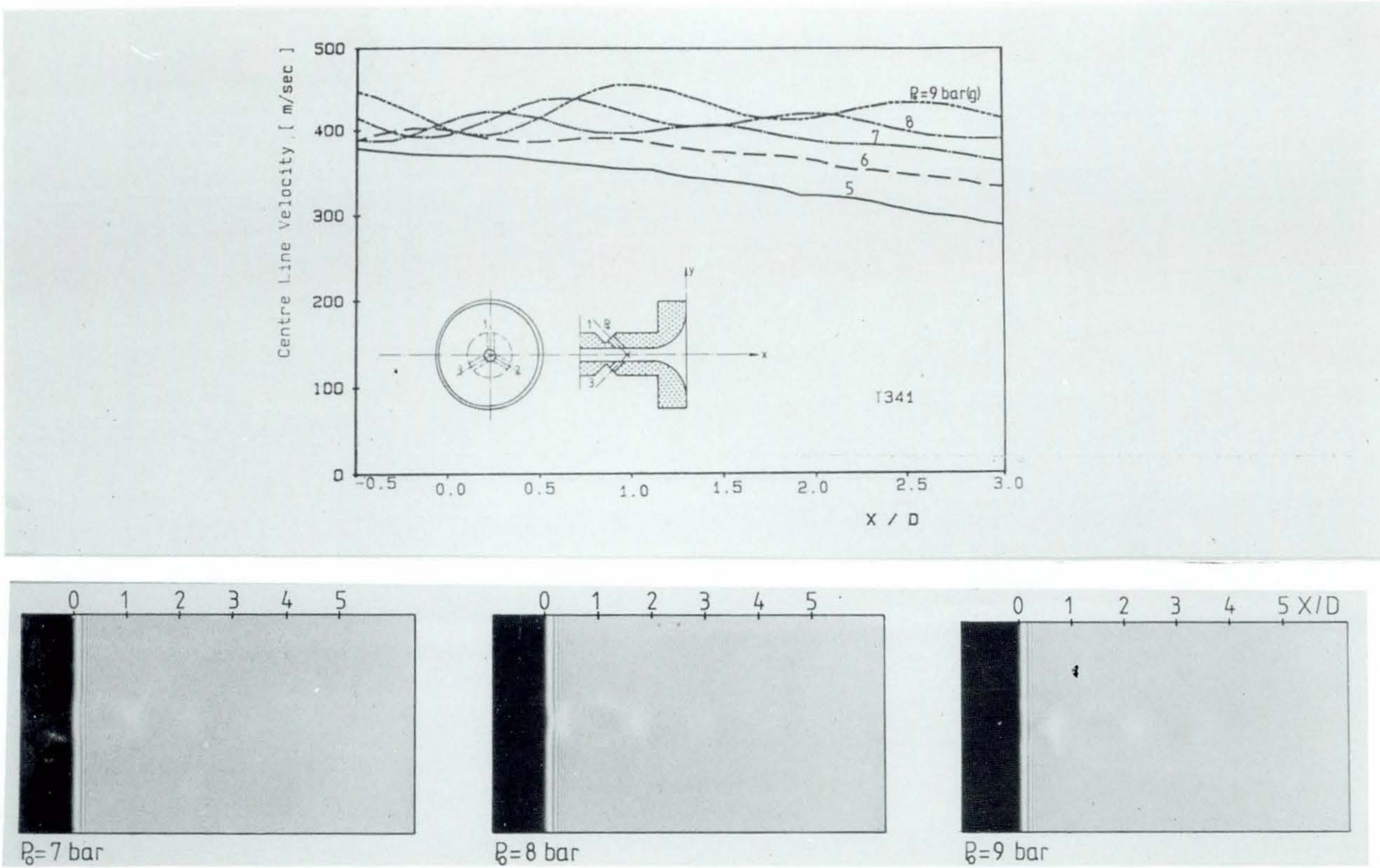

Figure 4.6c Centre-line velocities and shadowgraphs of the flow from the T341 HemaJet at varying pressures

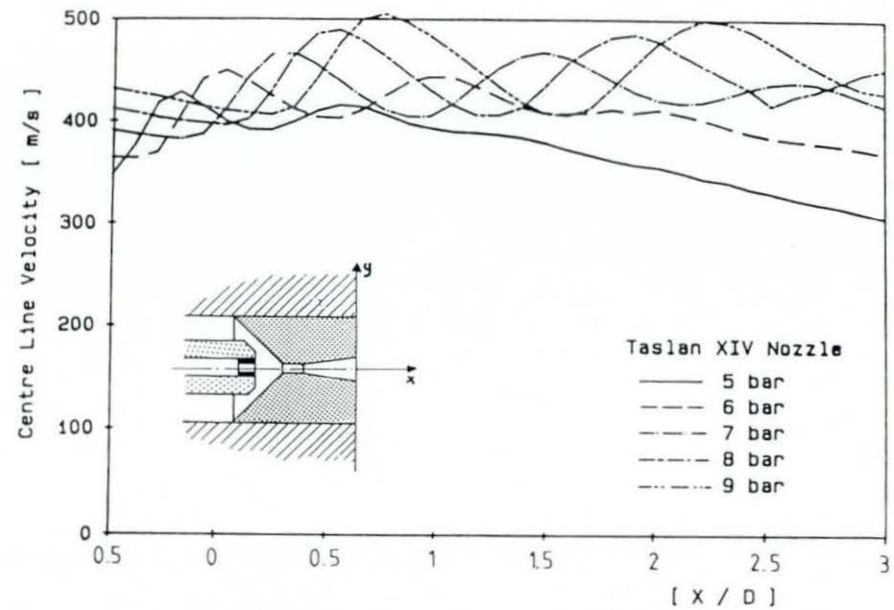

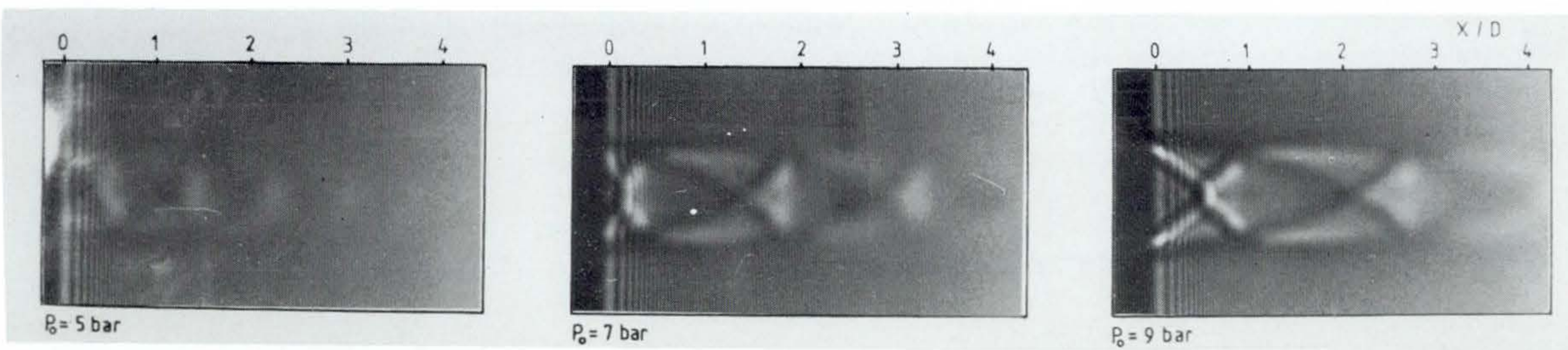

Figure 4.6d Centre-line velocities and shadowgraphs of the flow from the Taslan XIV at varying pressures

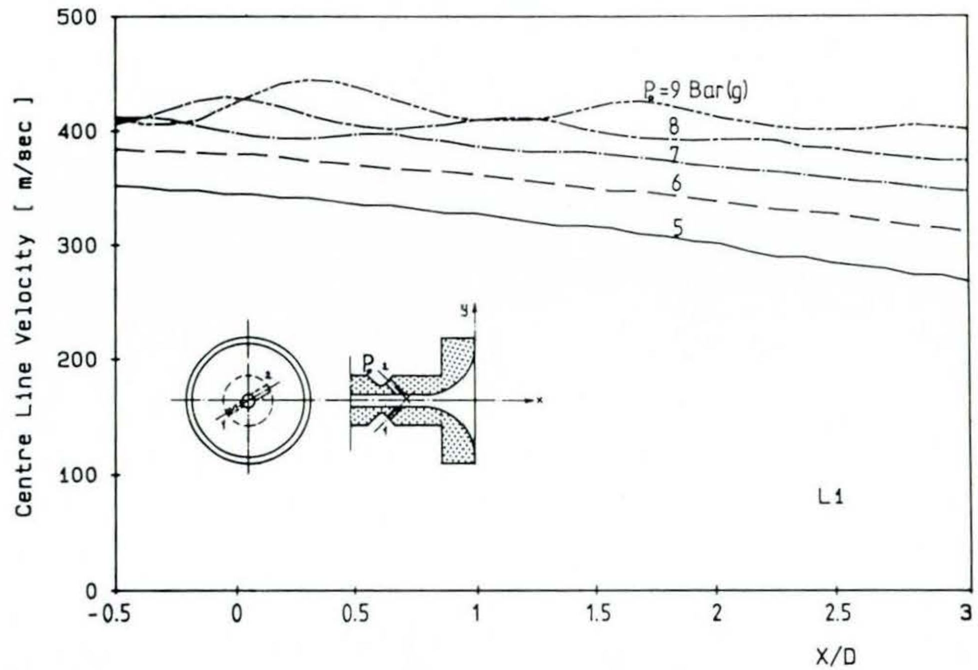

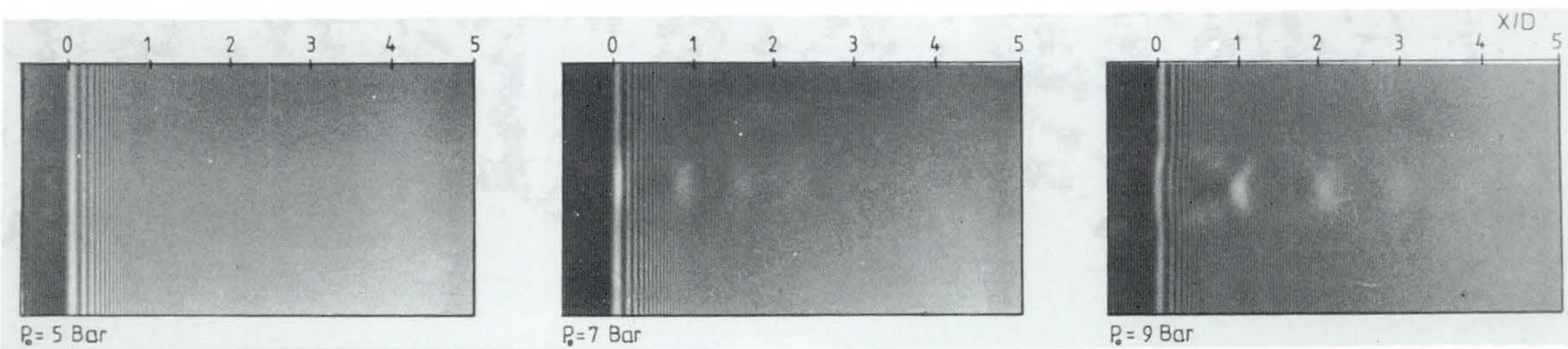

Figure 4.6e Centre-line velocities and shadowgraphs of the flow from the L1 nozzle at varying pressures

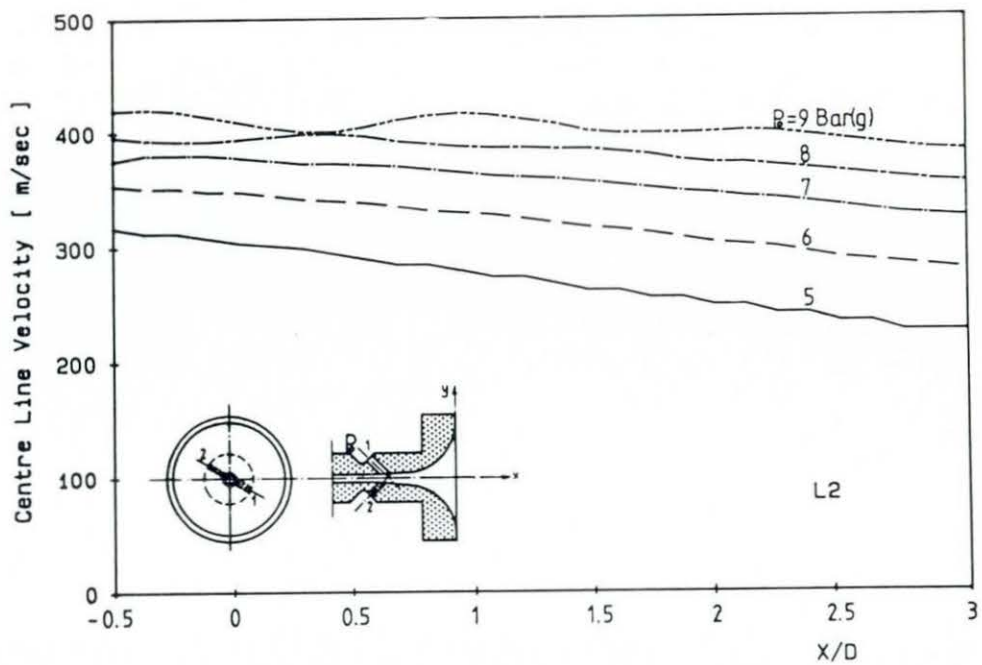

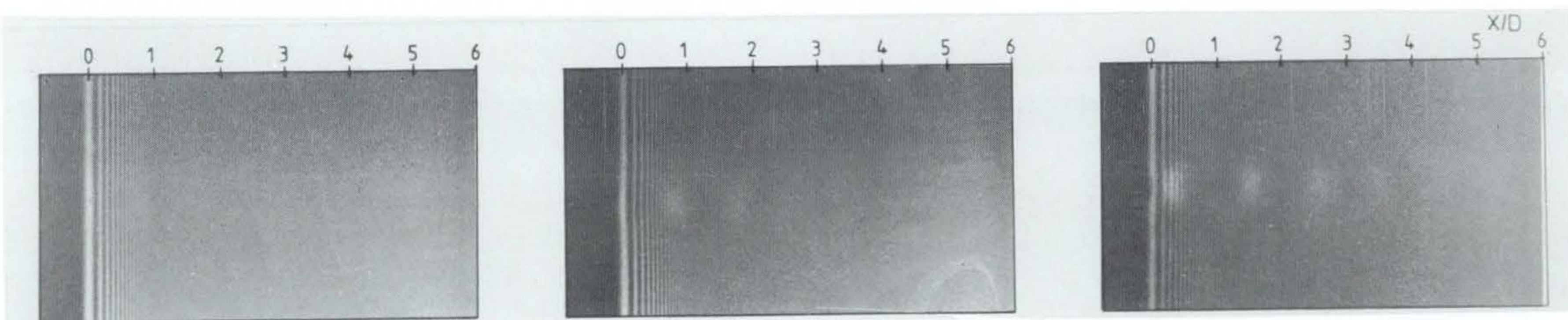

P_o = 7 Bar P_o = 8 Bar P_o = 9 Bar

Figure 4.6f Centre-line velocities and shadowgraphs of the flow from the L2 nozzle at varying pressures

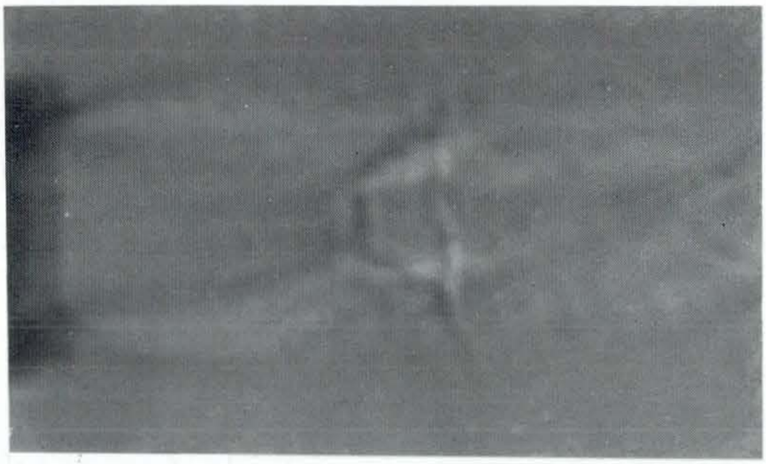

(a) Pipe-7 bar

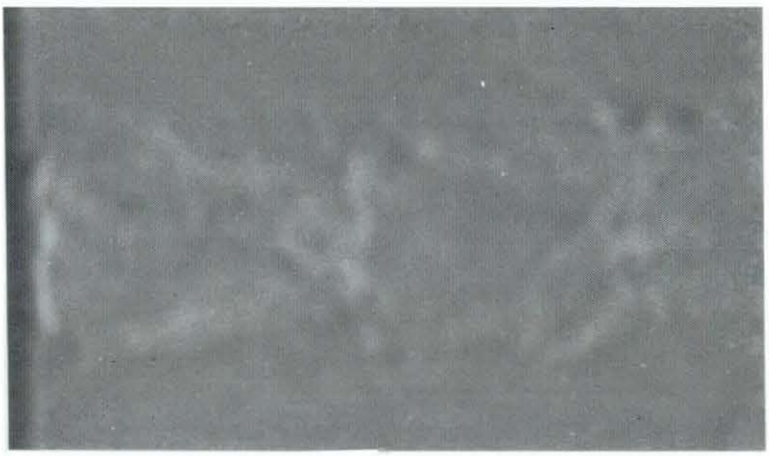

(b) Standard-core - 9 bar

(c) Taslan XIV - 9 bar

Figure 4.7 Instantaneous shadowgraphs of the jets

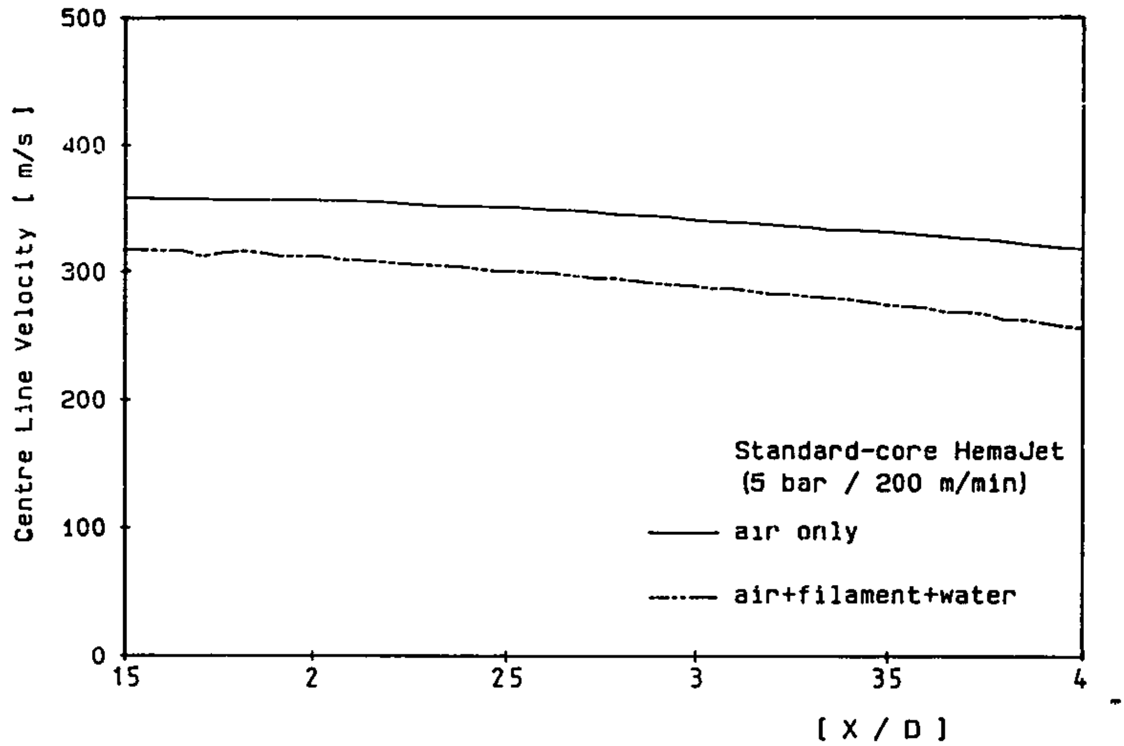

Figure 4.8a Centre-line velocities measured during the texturing process at 5 bar

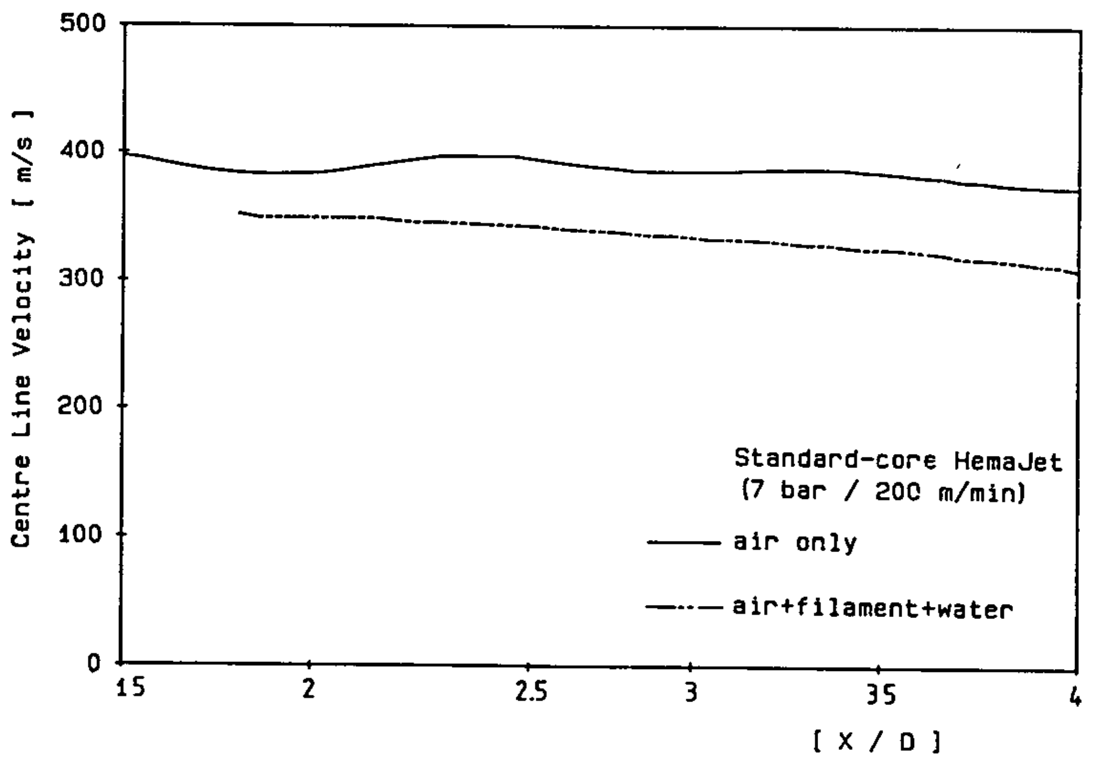

Figure 4.8b Centre-line velocities measured during the texturing process at 7 bar

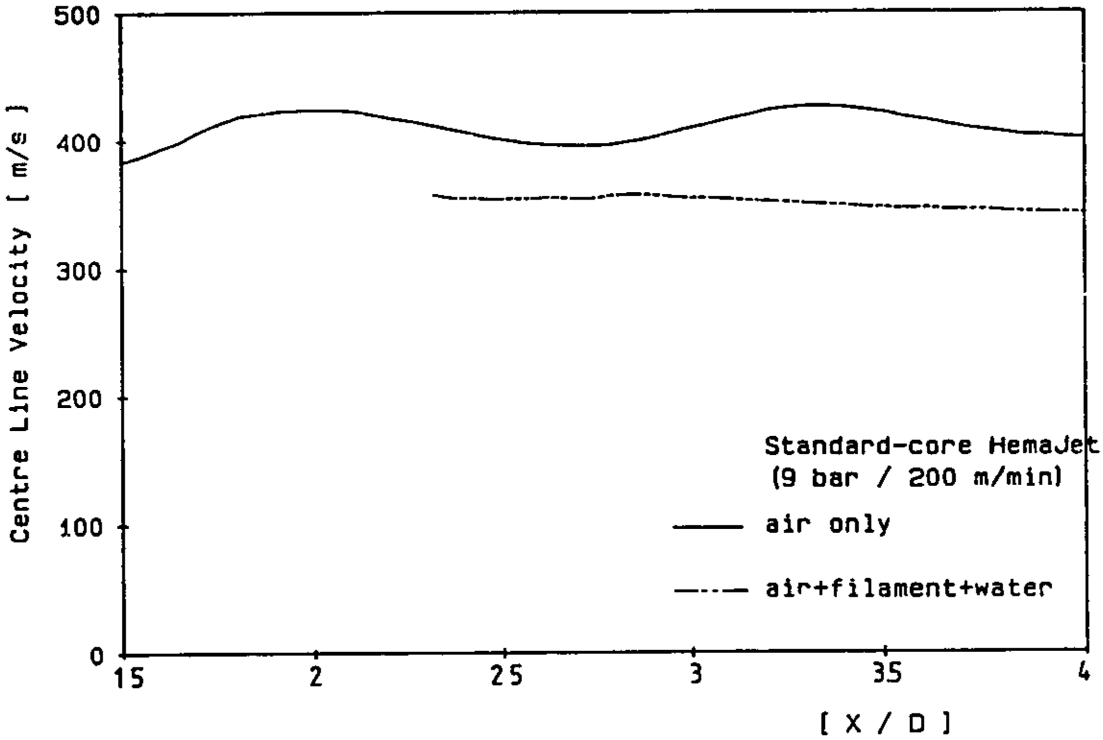

Figure 4.8c Centre-line velocities measured during the texturing process at 9 bar

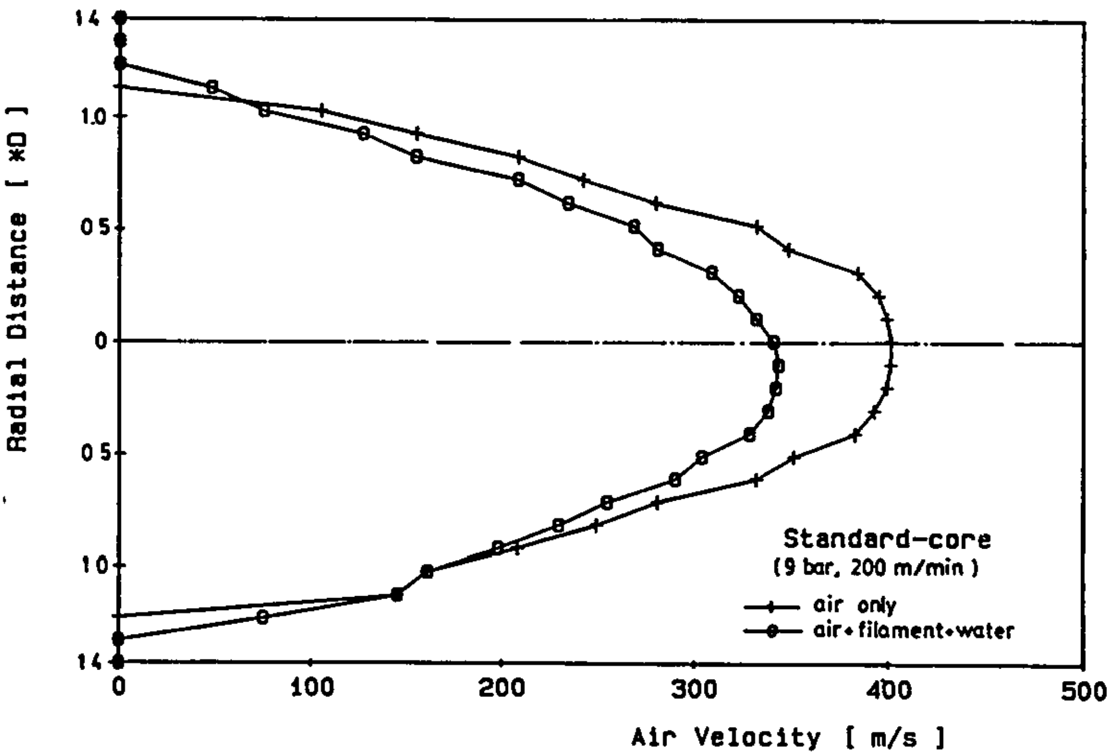

Figure 4.9 Axial velocity profile recorded during texturing process

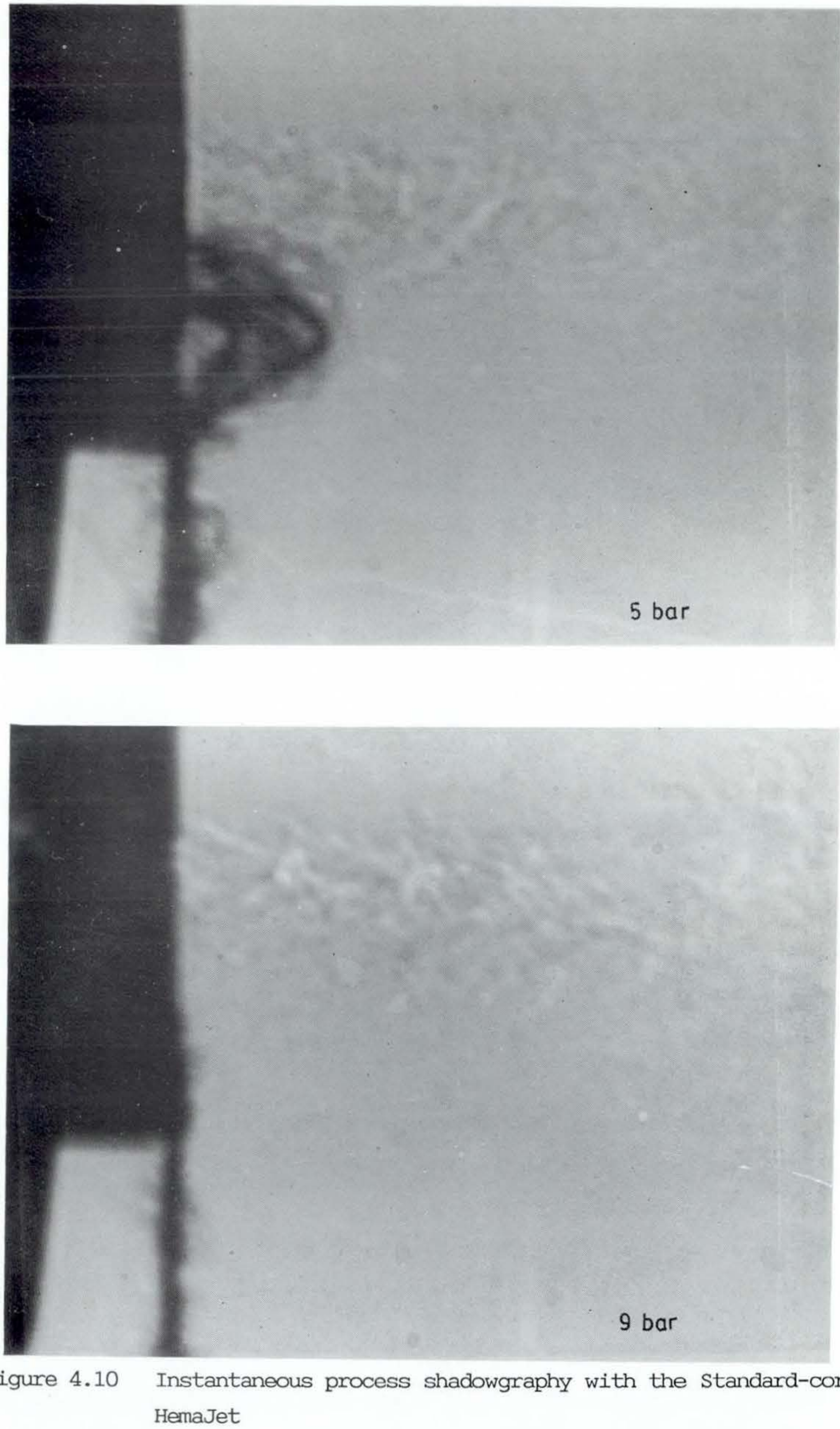

Figure 4.10 Instantaneous process shadowgraphy with the Standard-core HemaJet

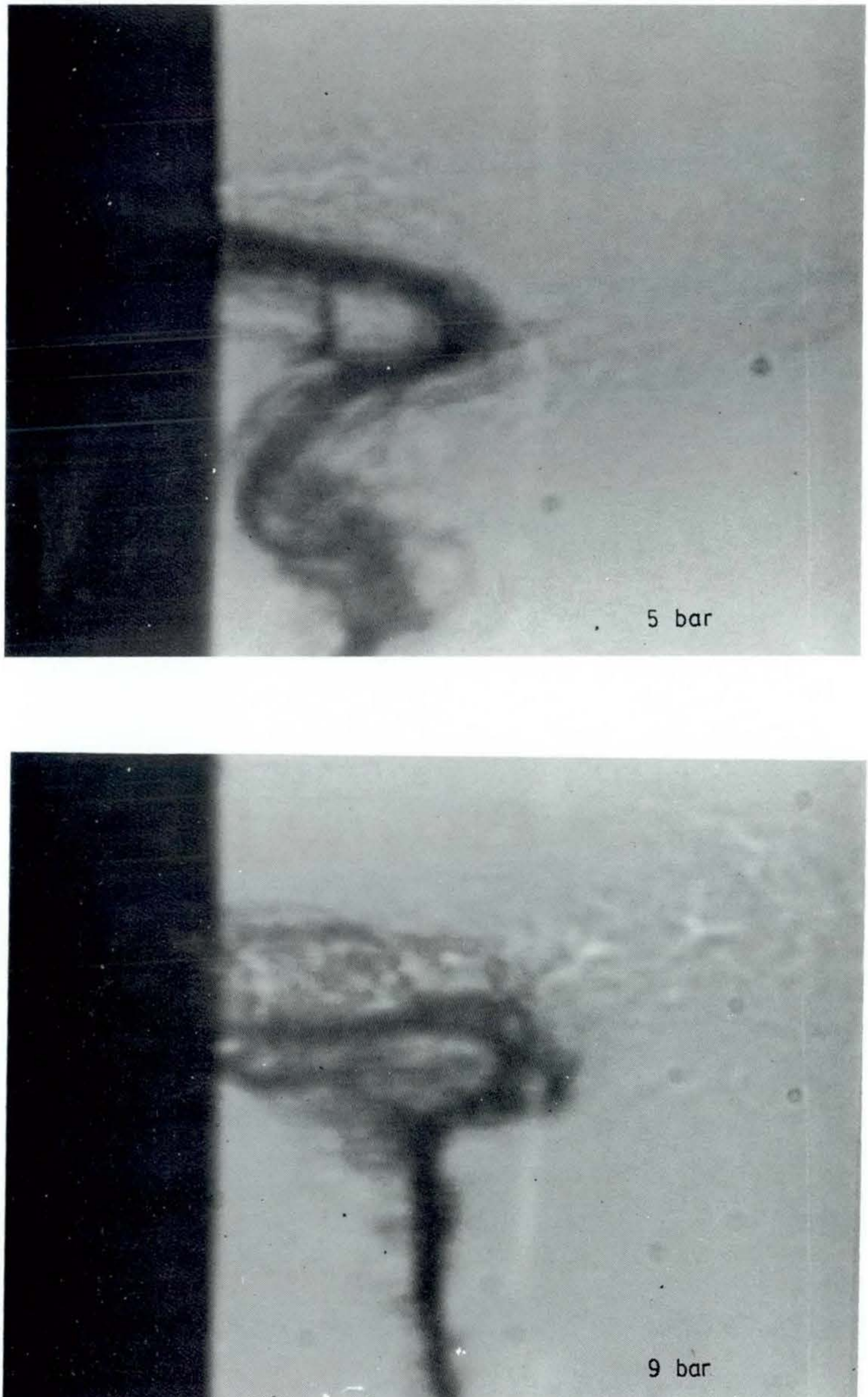

Figure 4.11 Instantaneous process shadowgraphy with the Taslan XIV nozzle

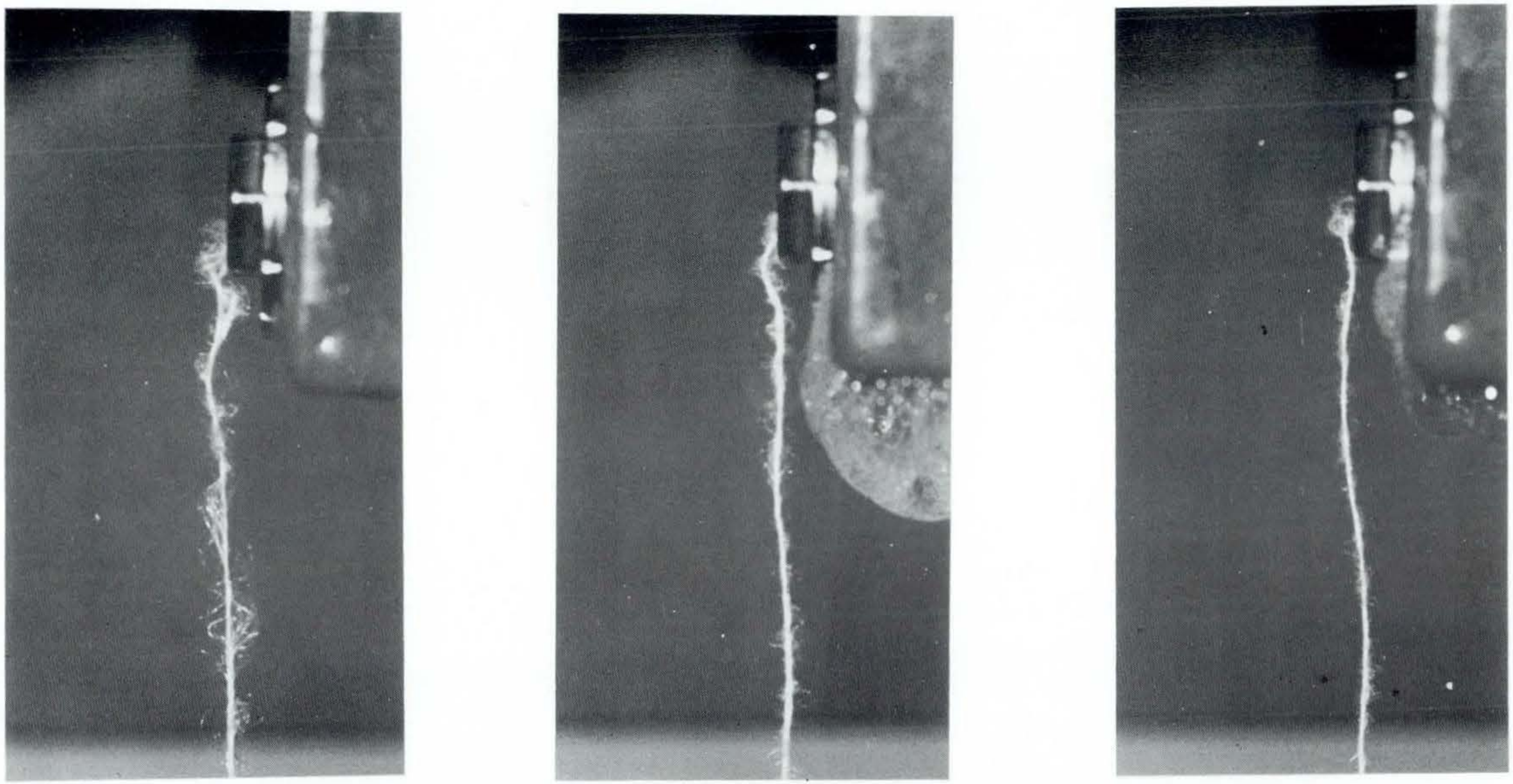

5 bar   7 bar   9 bar

Figure 4.12a High-speed still photographs of the process with the Standard-core HemaJet nozzle at 5, 7 and 9 bar pressures

T100 HemaJet

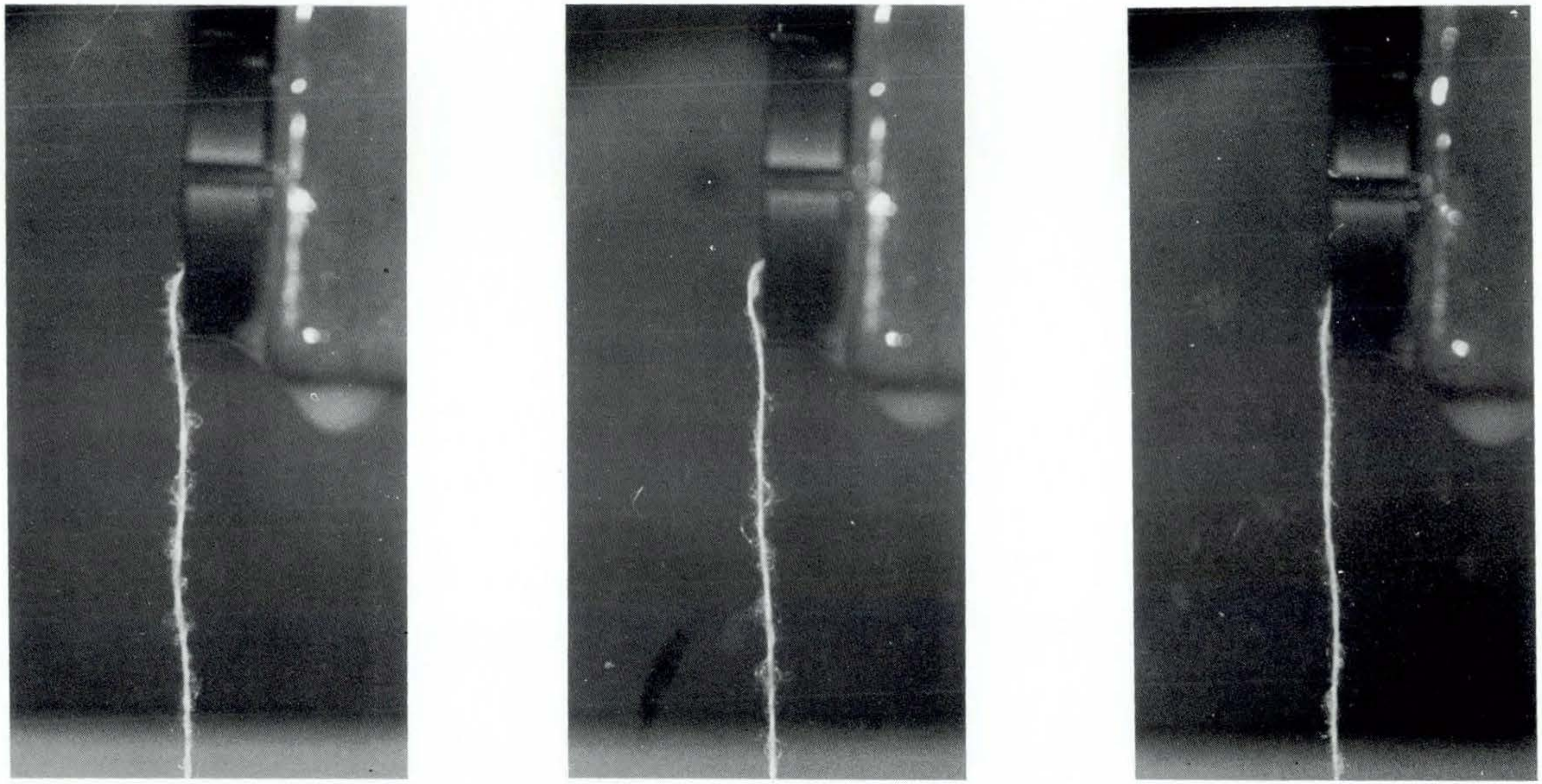

5 bar 7 bar 9 bar

Figure 4.12b High-speed still photographs of the process with the T100 nozzle at 5, 7 and 9 bar pressures

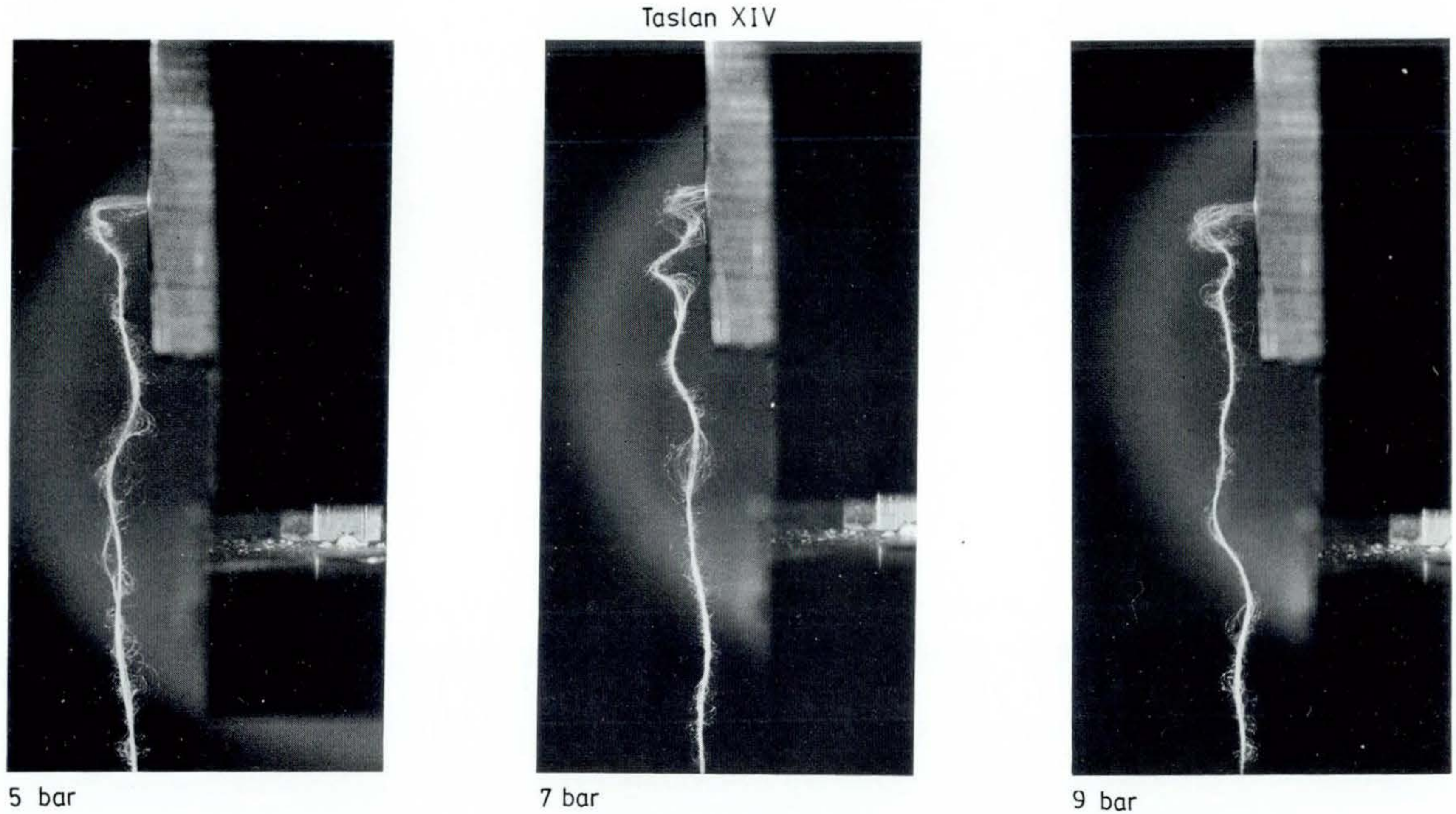

Figure 4.12c High-speed still photographs of the process with the Taslan XIV nozzles at 5, 7 and 9 bar pressures

L1 L2

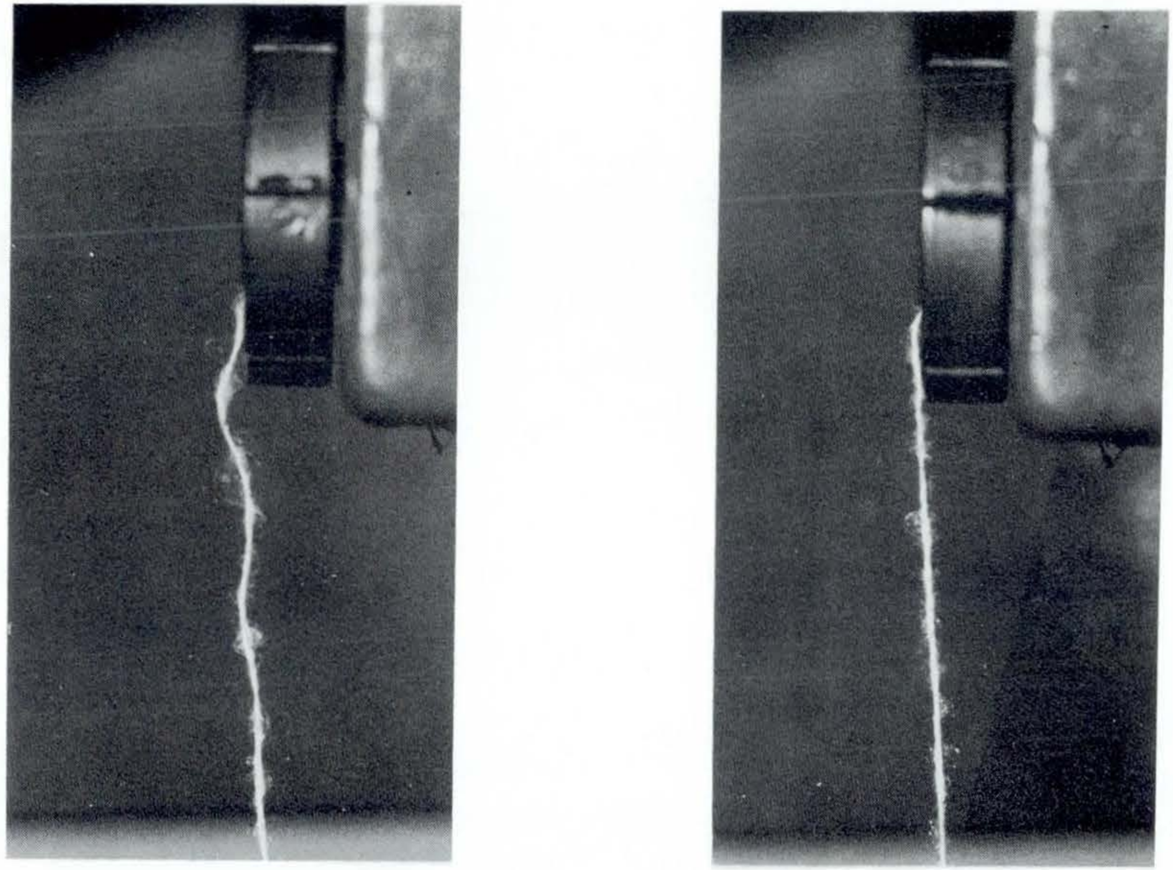

7 bar

Figure 4.12d High-speed still photographs of the process with the L1 and L2 nozzles at 7 bar pressure

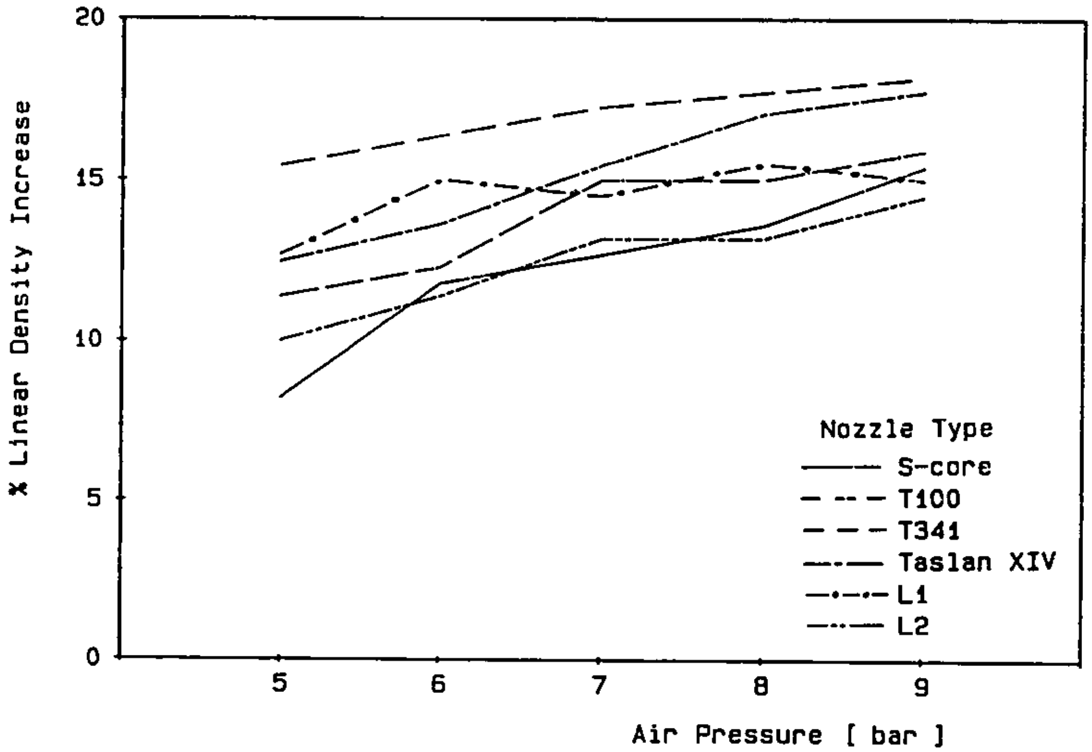

Figure 4.13a Percentage linear density increase of yarns textured by different nozzles

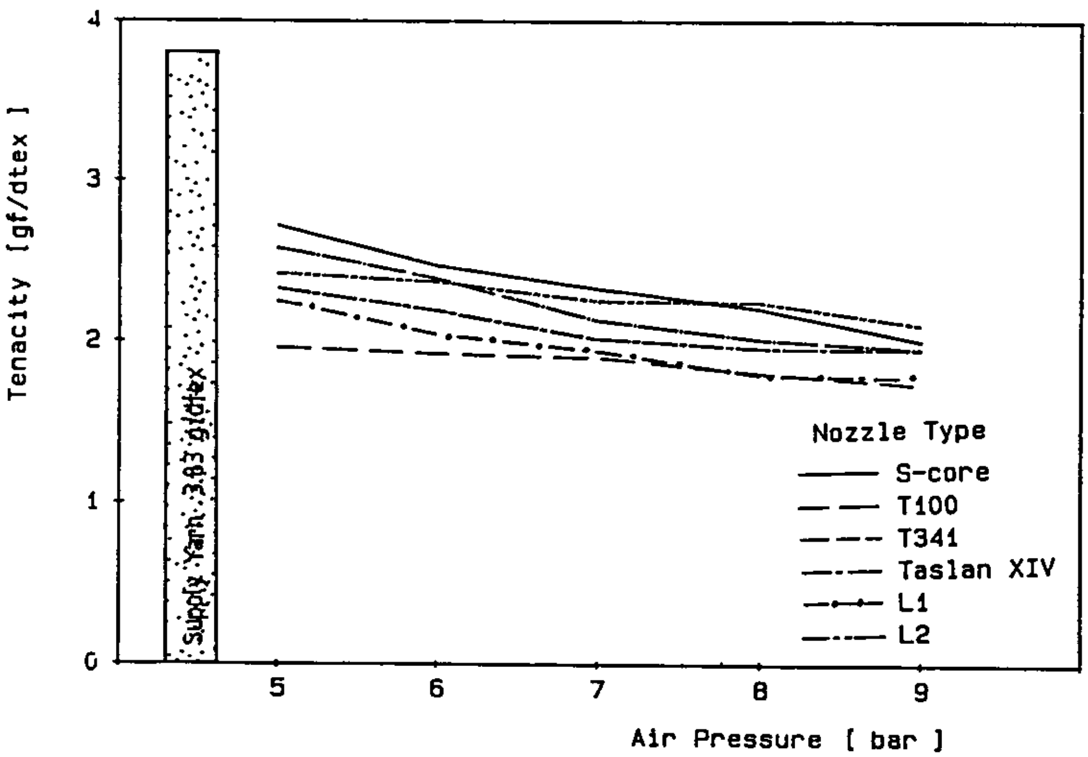

Figure 4.13b Tenacity of yarns textured by different nozzles

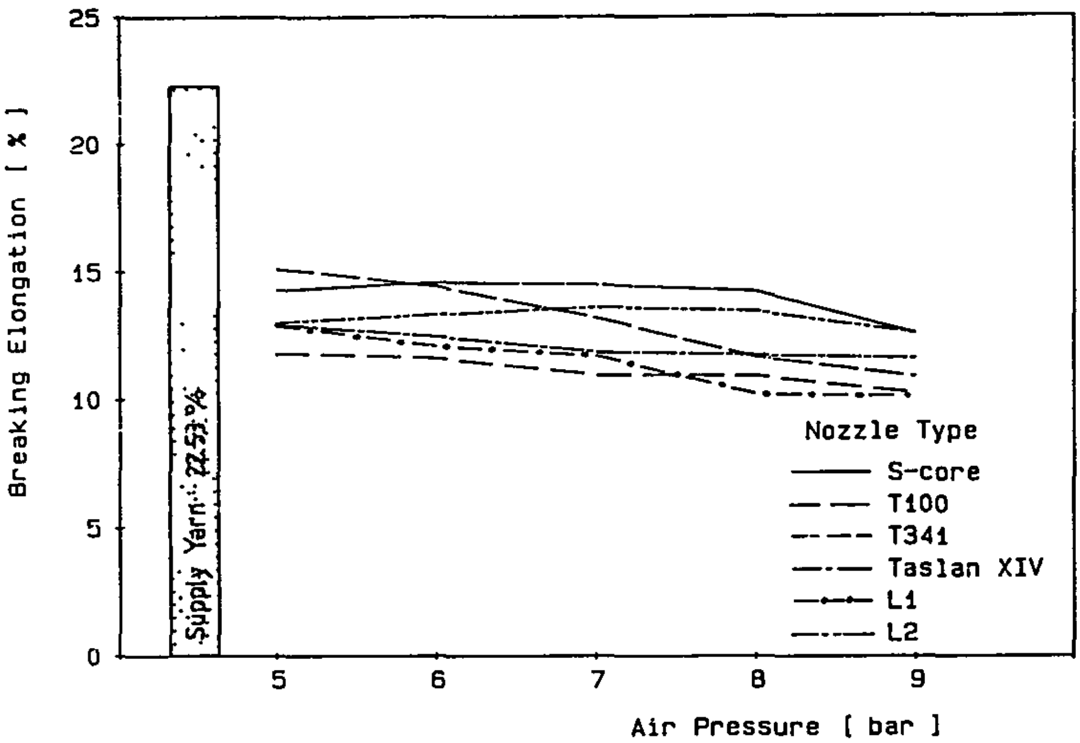

Figure 4.13c Breaking elongation of yarns textured by different nozzles

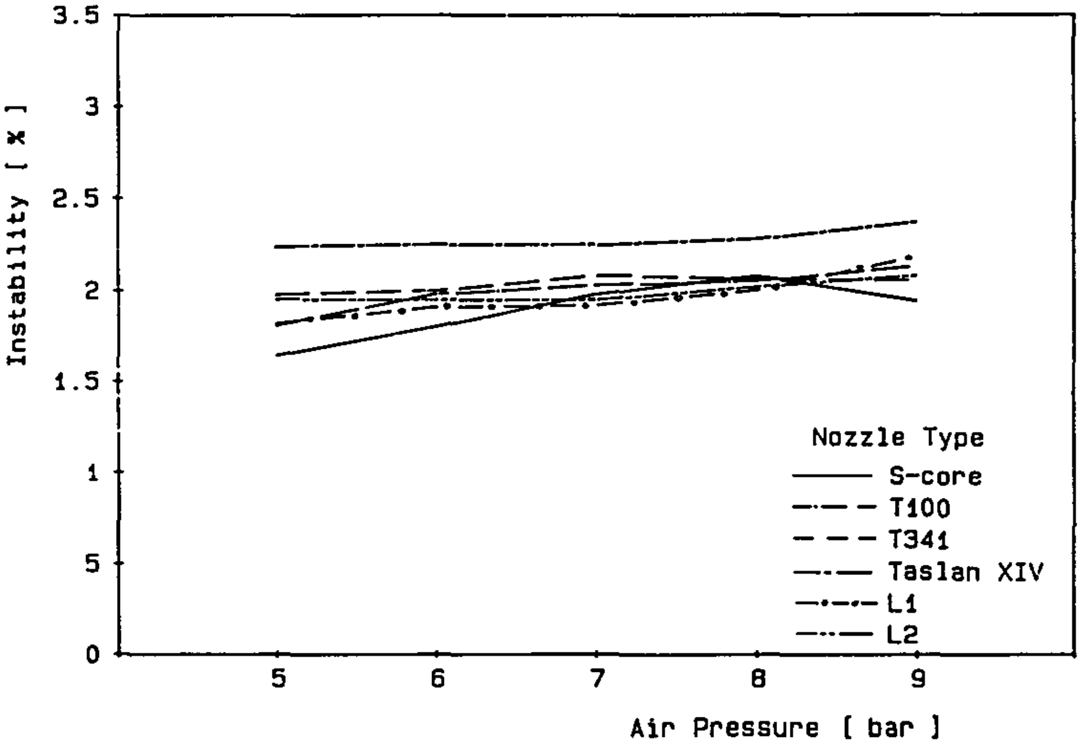

Figure 4.13d Instability of yarns textured by different nozzles

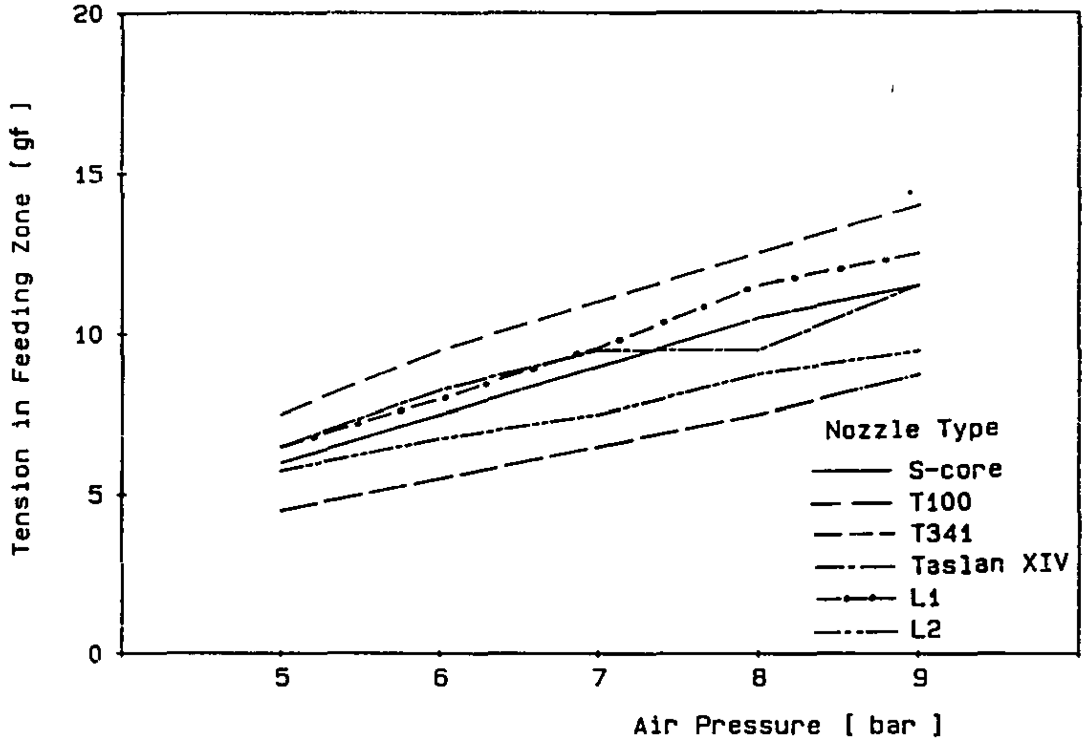

Figure 4.14a Yarn tension in the feeding zone at varying air pressures

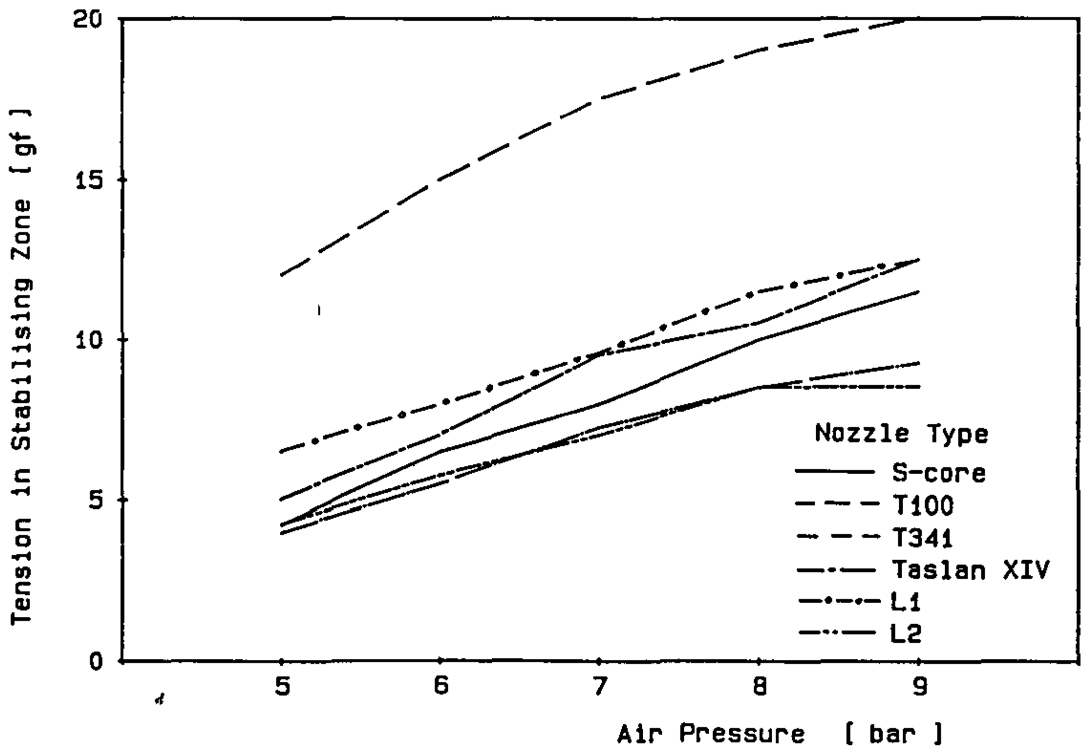

Figure 4.14b Yarn tension in the stabilising zone at varying air pressures

CHAPTER 5

EFFECTS OF NOZZLE GEOMETRY ON THE AIR FLOW

Cylindrical type texturing nozzles have a characteristic geometrical construction of inclined air inlet holes opening to the main duct and a trumpet-shaped diverging exit section. The number of inlet holes may be one, two or three, but the angle of inclination is always in the vicinity of 45° for all three configurations. The ratio of the total air inlet hole area to the main duct area may also be different for various nozzles available in Heberlein's T-series texturing jets. Although a trumpet-shaped exit section is typical of these nozzles, the curvature of the diverging exit in the T-series nozzles is larger than in that the original Standard-core HemaJet.

The underlying principles governing the flow in the cylindrical nozzles with slightly varying geometrical configurations may be the same, but it is certain that the difference in geometrical parameters would affect the air flow in such nozzles. Therefore it is desirable to investigate the effects of various geometrical parameters on the air flow in order to optimise the nozzle design.

Because of the difficulties of manufacturing full-size texturing nozzles, four-times linearly scaled-up models of variations of the T100 HemaJet were used in the investigations. The experiments mainly consisted of measuring both the air velocities of the emerging jet and the static pressure in the nozzle.

5.1 Experimental Apparatus and Nozzles

The apparatus for measuring the flow velocities was the same as the one used to test actual texturing nozzles as described in Section 3.2 (See Fig. 3.4). The compressed air, in this case, was supplied from the departmental compressed air-supply line, because the volume of compressed air required for the scaled-up nozzles was 16 times as much as that of the full-size nozzles. Although the departmental air supply was capable of delivering large volumes of compressed air, it was able to deliver only at a maximum pressure of 6 bar, whereas the actual working pressure for texturing nozzles varies between 5 and 10 bar. However, it was thought that the behaviour of the air flow in these experimental nozzles at higher reservoir pressures could be perceived by investigating the air flow at lower reservoir pressures.

The geometrical parameters investigated were:

(i) the shape of exit section;

(ii) the longitudinal position of the inlet hole along the main duct;

(iii) the inclination angle of the inlet hole with respect to the axis of the main duct; and

(iv) the ratio of inlet hole area to the main duct area.

Seventeen nozzles were made and the flow through these nozzles was ascertained. In order to examine the effect of a certain geometry, all the other geometric parameters were kept unchanged when one of them was altered. The contours of the nozzles are given in Fig. 5.1.

In the first group, Fig. 5.1a, six different exit shapes are shown. These nozzles are identical except the exit sections, i.e. the part of the nozzle up to the start of the diverging section is common in all 6 nozzles, eliminating the effects of any other factor but the exit shapes on the air flow. Nozzle number 1 (which is exactly a 4-times scaled-up model of the T100 HemaJet) has the least divergence in the vicinity of the transition section between the cylindrical main duct and the exit shape. The exit is of trumpet-shape with a large radius, called here a 'large trumpet'. The exit shape of the nozzle number 2 is again of trumpet shape, however, with a small radius which is similar to that of the Standard-core HemaJet. This type of exit shape is called a 'small trumpet'. The nozzles numbered 4 and 5 have conical exit shapes with 60° and 90° (inclusive) angle of divergence respectively starting from the same point where the divergence of the other nozzles starts. The most unusual exit shape is that of the nozzle number 3. This shape is obtained from a polinomial function the coefficient and order of which is taken from the work of Abraham et al[100] on the investigation of divergent supersonic nozzles with small throat areas who showed that this particular exit shape has the characteristic that it creates a high flow velocity. Finally the nozzle number 6 has no diverging exit section, i.e. the flow duct extends uniformly up to the point corresponding to the start of divergent parts in other nozzles (Fig. 5.1). The exit planes of these nozzles are not at the same distance from the start of the diverging section and these distances are shown in Fig. 5.1a in terms of the nozzle diameter.

In the second category, the longitudinal situation of the inlet hole where it opens to the main duct was varied. Four cases were studied (as shown in Fig. 5.1b). The nozzle number 1 represents the T100 HemaJet configuration, the reference nozzle. The situations of the inlet holes of nozzles number 7 to 10 with respect to that of the reference nozzle number 1 are shown in Fig. 5.1b. The distance between the positions of the inlet holes is 10 mm. Hence the nozzle number 7 has the furthest and number 10 has the closest inlet hole to the nozzle exit plane. In fact, the inlet hole of the nozzle number 10 is so positioned that the incoming jet opens to the exit section and thus produces an oblique jet. Therefore, this nozzle had to be abandoned.

Having accepted the nozzle number 1 with an inclination angle of 45^{o}, as the standard nozzle, the inclination angle of the inlet hole was varied about this angle. Thus the inclination angle for the nozzle number 11 and 12 were chosen as 30^{o} and 60^{o} respectively (Fig. 5.1c).

The ratio of the inlet hole area to the main duct area was also varied with respect to the standard nozzle (nozzle 1) area ratio which is 0.537. Two smaller ratios (i.e. 0.302 and 0.444) were chosen for the nozzles number 13 and 14 respectively. Three area ratios larger than that of the nozzle number 1 were also chosen as 0.6, 0.751 and 1.0 for the nozzles 15, 16, and 17 respectively (Fig. 5.1d). It was hoped that the nozzle number 17 having the ratio of unity would give informative results, because no area enlargement occurs in the nozzle when the flow from air inlet hole opens to the main duct.

5.2 Experiments

By using the described experimental rig (See Section 3.2), the axial air velocity distribution across the jet at the exit plane, centre-line velocities from one nozzle diameter upstream of the exit plane to 5 diameters downstream and the secondary flow velocities, were recorded for all the nozzles described. The results are given in Figs. 5.5 to 5.9.

The comparatively large dimensions of the scaled-up nozzles enabled a steel tube of 1 mm diameter with 3 static pressure holes of 0.3 mm on a ring, to be introduced through the nozzles (Fig. 5.2). By traversing this tube along the nozzle centre-line the static pressures both in and outside the nozzle (i.e. in the emerging jet) were measured for all the nozzles investigated. The results of these measurements are also included in Figs. 5.5 to 5.9.

Prior to the utilisation of the centre-line static pressure tube on the nozzles, it was installed in a calibration unit possessing wall pressure tappings. Fig. 5.3 compares the results obtained from centre-line static pressure tubing and wall static pressure tappings. It is seen that the discrepancy between these two readings is less than 5%, hence the effect of the presence of the tube in the channel is proven to be negligible. The obvious advantage of using a centre-line static pressure tubing is that it provides point by point recording of the static pressures in the nozzle.

Fig. 5.4 illustrates a typical static pressure distribution along the tested nozzles. The whole trace could be divided into five sub-sections, as seen in the figure. This offers a useful tool which facilitates a better explanation of the events occuring in the nozzle. The sub-division is mainly dictated by the geometry of the nozzles.

Section 1 is the secondary flow section of the nozzle. Within this channel the flow pressure is atmospheric as argued in Chapters 3 and 4. However, in the vicinity of the inlet holes where the section 1 ends, there is a short section in which the flow pressure is below atmospheric. This is due to the very complex flow movements created by the impingement of the incoming jet.

Section 2 is the impingement section. Since the incoming jet hits both the pressure tube and the opposite wall, it is hardly possible to accept this recorded pressure as fully static. The impingement of the incoming jet makes the pressure readings uncertain. They should not be taken into consideration in the further interpretations of the nozzle effectiveness.

The third section, showing the level and distribution of the flow pressure in the primary flow channel is the most informative portion of the whole trace. Although it is difficult to define a starting point for this section, it ends where flow separation occurs due to the area gradient (i.e. where the diverging exit section starts).

The last two sections actually depict the static pressures in the free air-jet separated from the nozzle walls. Section 4 has many fine details, e.g. fluctuations of the pressure above and below the atmospheric pressure until it eventually settles at atmospheric pressure. These fluctuations are basically due to the formation of pressure waves.

Finally, the fifth section illustrates the pressures in the air jet outside the exit plane. Most of the nozzles tested have shown that the pressures in the free jet at the exit plane and at the further downstream are fully atmospheric.

Although all the measurements have been carried out at varying reservoir pressures from 3 to 6 bar, only the results obtained at 6 bar are given here and will be discussed in the following section. This is due to the fact that the results obtained at 6 bar are not only similar to the results measured at lower pressures but also they are thought to be representative of much the higher pressures used in actual texturing conditions.

5.3 Results and Discussions

5.3.1 The effects of exit shape

Compressed air enters the main duct through the inlet hole. The incoming air impinges on the nozzle wall and at the steady-state conditions, a pressure builds up in the main duct. Since the inlet hole is inclined towards the secondary flow section of the main duct, the primary flow gains more momentum than the secondary flow. Therefore, much of the pressure built up in the duct starts expanding in the primary flow direction because at the end of the duct the pressure is atmospheric. When the flow reaches the transition point where the divergence starts, it possesses a supersonic speed and a pressure higher than atmospheric. Subsequently, any suitable divergence would help the flow to convert its extra pressure energy into velocity so that the natural balance could be maintained; this is where the exit shape plays an important role.

As seen in Fig. 5.1a, the nozzle 1 has the least divergence from the transition point onwards. Therefore, the flow somehow follows the contour and accelerates further. But no sooner has the flow separated from the contour of the nozzle wall, than flow commences a process of adjusting its high pressure to the ambient pressure through expansion waves (Fig. 5.5d) (See also Appendix D).

The procedure is the same with the other exit shapes also. Neverthless, the steeper the divergence, the less the chance for the flow to follow the exit contour and the greater likelihood that it will separate earlier. Consequently the place where the expansion starts moves towards the transition section (in the case of no diverging exit section, the expansion waves start right at the edge of the main duct). Since the flow anticipates its high pressure earlier, i.e. at higher pressures, it takes action to compensate this unbalanced situation earlier and expands through a series of expansion waves but as previously mentioned the overshooting of the pressure occurs and the velocity rises and falls in the jet. Thus, the larger the divergence of the exit shape, the more the fluctuations of the flow occur as seen in Fig. 5.5a.

Regarding the velocity distributions at the exit plane of the nozzles, no substantial difference is observed (See Fig. 5.5b). The velocity profiles are bell-shaped, because the effect of density variations due to the oblique waves do not exist at these sections of the nozzles. Fig. 5.5b shows that the nozzle 1 possesses a more axially asymmetric velocity profile than the other nozzles although no obvious reason can be suggested.

Fig. 5.5c shows the secondary flow velocity profiles from these nozzles and it is observed that the different exit shapes of the nozzles have almost no effect on these.

The static pressure distribution along the centre-line of the nozzles is given in Fig. 5.5d, the pressure rise in the primary flow channel corresponding to the impingement section being shown in this figure. It also indicates the occurence of the shock waves in the vicinity of the transition plane where the diverging exit section starts. It should however be noted that the position of the first expansion wave varies from one nozzle to another due to the respective differences in the positions of separation points for each nozzle caused by the different steepness of the diverging exit sections.

5.3.2 Relative situation of inlet hole

In order to demonstrate the significance of the inlet hole position with respect to the start of the diverging exit section, Fig. 3.16c in Chapter 3 will be resorted to and reproduced here. Fig. 5.6 is a line drawing of Fig. 3.16c which is a shadowgraph of the incoming jet taken from a flat, glass walled nozzle simulating the flow in the cylindrical nozzles. Four different flow conditions are observed from the figure. The impingement section is the part of the nozzle where the incoming jet hits to the opposite wall of the nozzle duct and scatters and eventually becomes divided into primary and secondary flows. The peak of the static pressure occurs in this section. The scattered flow soon settles down and creates a fully axial flow in the primary and secondary flow sections. The secondary flow section is a region where a backward flow occurs. However the events in the primary flow section are divided into two sub sections as settlement and fully axial flow sections.

If the uniform, cylindrical flow duct before the start of the diverging exit section is sufficiently long to develop a fully axial flow, as in the case of Nozzle 7 (as defined in Fig. 5.1b) where higher flow velocities seemed to be obtained (See Fig. 5.7a). As the position of the inlet hole is moved towards the beginning of the exit section, the flow velocities decrease and the asymmetry of the velocity profile becomes enhanced. This is due to the fact that the flow requires some distance to settle in the main duct.

Since the place of the inlet hole does not affect the division of the momentum flux into primary and secondary flows, no substantial change in the secondary flow velocities is observed (Fig. 5.7c).

5.3.3 The angle of inclination of the inlet hole

To date no question has been raised as to whether Heberlein's inclination angle of approximately 45^{o} for the inlet hole(s) is the optimum angle from the dual viewpoints of flow dynamics and effective texturing. An experimental investigation into the aerodynamic effect of the inclination angle of the inlet holes is, therefore, included in this study. From the division of momentum into the primary and secondary flows, it is evident that this angle plays a significant role; the smaller the angle, the more momentum is transferred to the primary flow and in turn this results in higher velocities at the exit of the nozzle.

In order to quantify this effect three nozzles (nozzles 11, 1 and 12) with three different inclination angles (30^o, 45^o and 60^o respectively as shown in Fig. 5.1c) have been experimentally studied. The results are given in Fig. 5.8. The incoming jet of nozzle 12, having the steepest inclination angle, vigorously hits the opposite wall of the duct and the resulting energy of the flow is highly dissipated, the flow velocities being so small that their profile at the exit plane could not be traced by the pitot tube and pressure gauge used. However, the nozzles 11 and 1 give supersonic velocities at the same pressure (See Fig. 5.8b).

The advantage of the lesser inclination angles, i.e. 30^o appears to be in the resultant increased momentum in the primary flow direction due to the reduced momentum flux in the secondary flow. Fig. 5.8c shows that the nozzle 11 has the slowest secondary flow, and in turn has an increased primary flow velocity which is most desirable for effective texturing.

5.3.4 Area ratio

When the compressed air is admitted into the main duct of the nozzle, the flow encounters two kinds of losses due to the sudden enlargement and impingement against the opposite wall. Since the basic geometric details of the nozzles considered are the same, the impingement losses could be assumed to remain the same for each nozzle. For the sudden enlargement losses, however, the major contributing factor is the area ratio of the incoming flow to the outgoing flow, i.e. the main flow duct, as illustrated in Appendix C.

In order to show the effects of this ratio on the primary and secondary flow properties, six nozzles with different area ratios (as defined in Fig. 5.1d) were tested. The results of the flow measurements are given in Fig. 5.9. It should be noted here that the last two nozzles, i.e. Nozzles 16 and 17 with larger inlet holes were tested at 5 bar pressure, because of the increased volume requirement for the compressed air, whereas the rest of the batch were tested at 6 bar.

Fig. 5.9a, illustrating the axial flow velocities along the centre-line of the jet, shows that Nozzle 13 (with the smallest area ratio) fails to create supersonic velocities and the jet expands quickly. However, much higher velocities are recorded from the other nozzles with larger area ratios. The common conclusion of Figs. 5.9a and b is that the greater the area ratio, the higher the flow velocities. The nozzles with greater area ratios also create higher secondary flow velocities which may be troublesome for texturing.

Since the sudden enlargement losses decrease as the area ratio approaches unity, higher flow pressures could be achieved in the main duct which is responsible for the higher flow velocities. This fact was evidenced by the static pressure measurements as shown in Fig. 5.9d.

5.4 Conclusions

When a compressible fluid flowing supersonically through a nozzle possesses a different pressure than the ambient pressure at the exit of the nozzle (the exit is referred to the place where the flow separates from the solid boundary), a series of compression and expansion waves (or vice versa) take place in the jet. These compressions and/or expansions waves cause different density levels in the jet. One further consequence of these expansion and compressions is that the velocity, as well as the direction of the flow, varies from one section of the jet to another.

The free air jets from texturing nozzles, such as the Heberlein Standard-core, the T-series HemaJet and the Taslan nozzles have similar structures to those described above.

The shape of the diverging exit section appears to have no significant role on the flow properties recorded. The cause of the non-uniformity was proven to be the formation of the shock waves (See Section 3.6). This disagrees with the predictions of Acar et al[51], that the nonuniformity is caused by the trumpet-shaped exit section. Nevertheless, the curved exit shape may have some effect on the texturing properties of the nozzles.

The inlet hole should be at a sufficient distance away from the exit such that the flow settles down in the nozzle duct and hence the drag forces exerted on the filaments are enhanced. Additionally, the primary flow momentum flux and consequently the primary flow velocity, could be enhanced by reducing the inclination angle of the inlet hole(s). The ratio of the incoming jet area to the main duct area has a significant role on the sudden enlargement losses. As the ratio approaches unity the losses decrease and in turn the flow velocities increase.

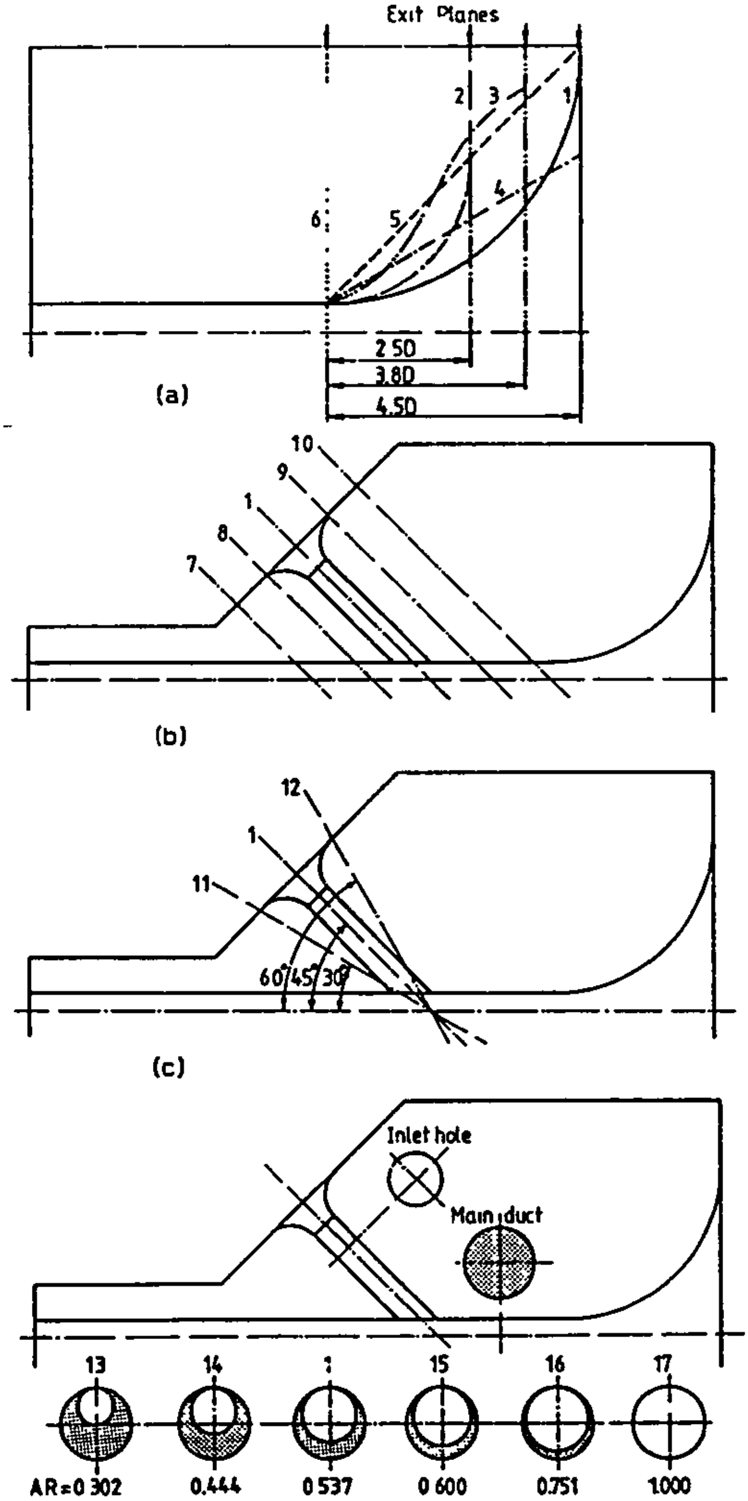

Figure 5.1 Configurations of the nozzles tested: (a) exit shape; (b) situation of the inlet hole; (c) inclination angle of the inlet hole; and (d) area ratio

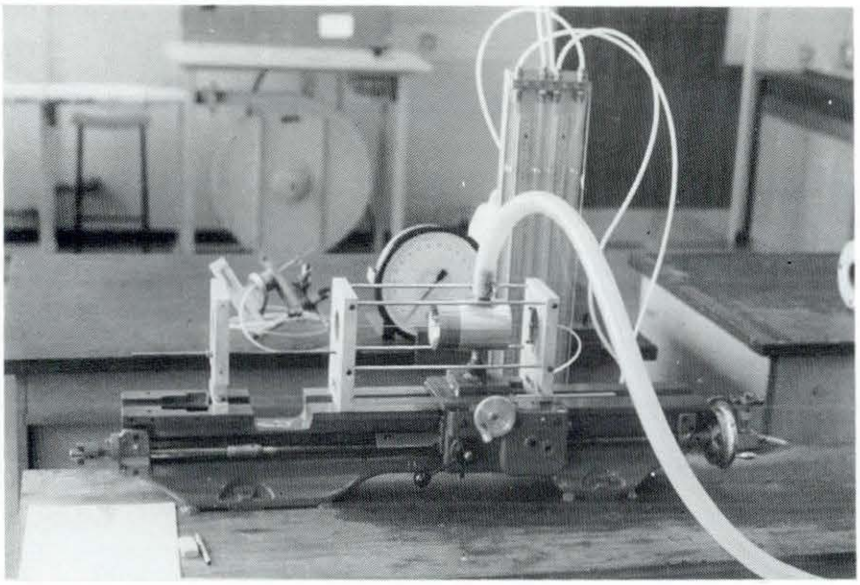

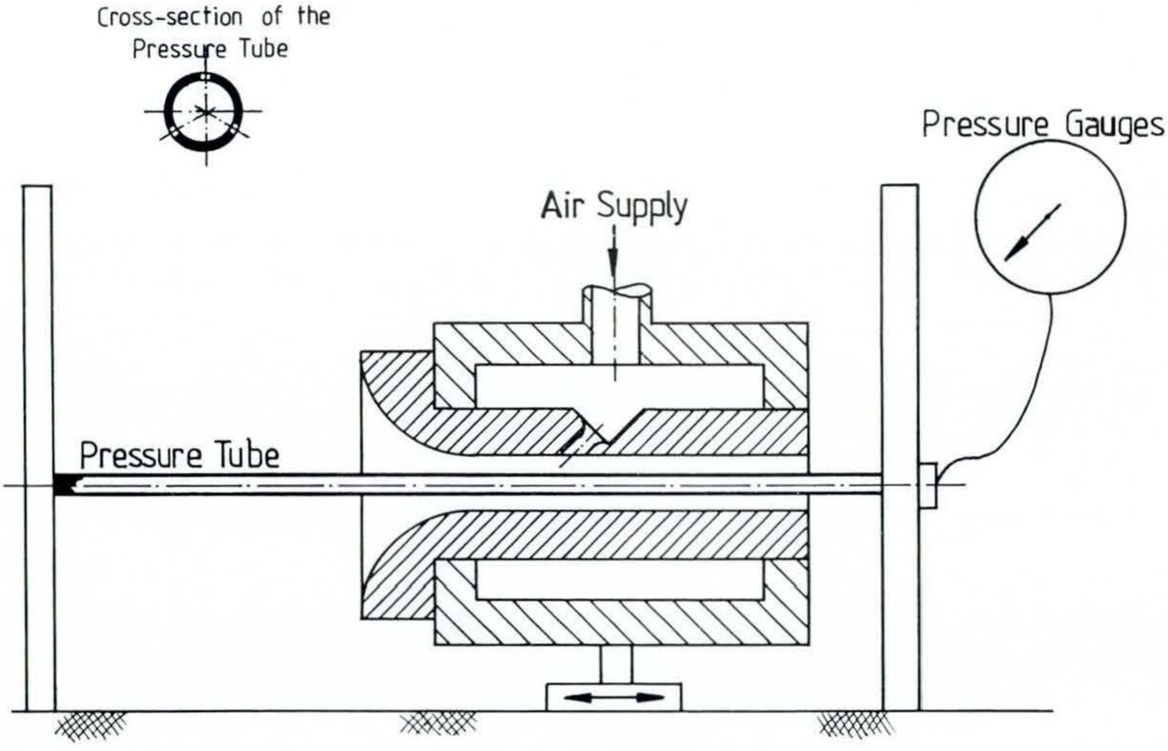

Figure 5.2 The photograph and sketch of the static pressure measurement rig

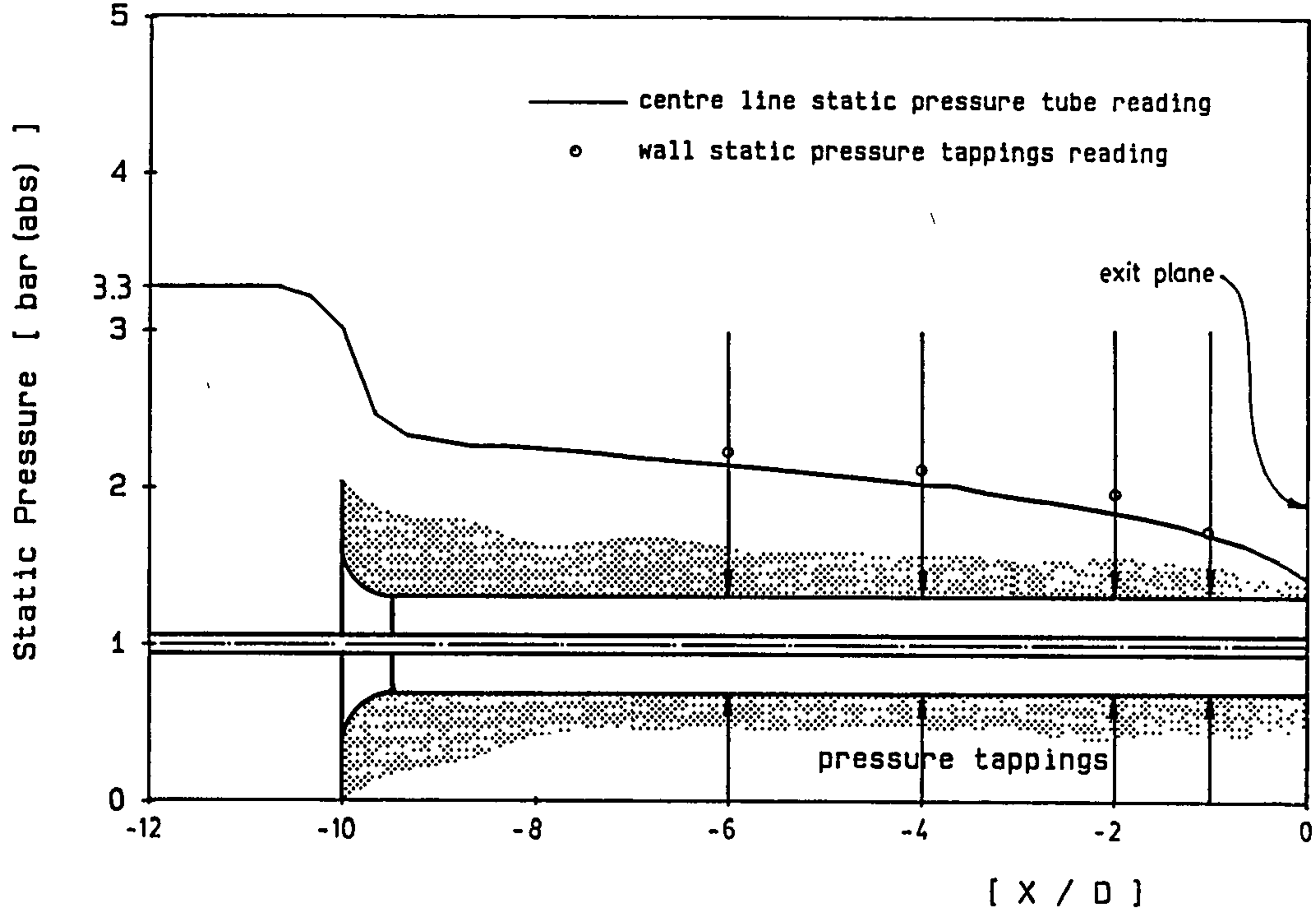

Figure 5.3 Comparison of the static pressure measurement results obtained from the centre-line static pressure tubing with the wall static pressure tappings

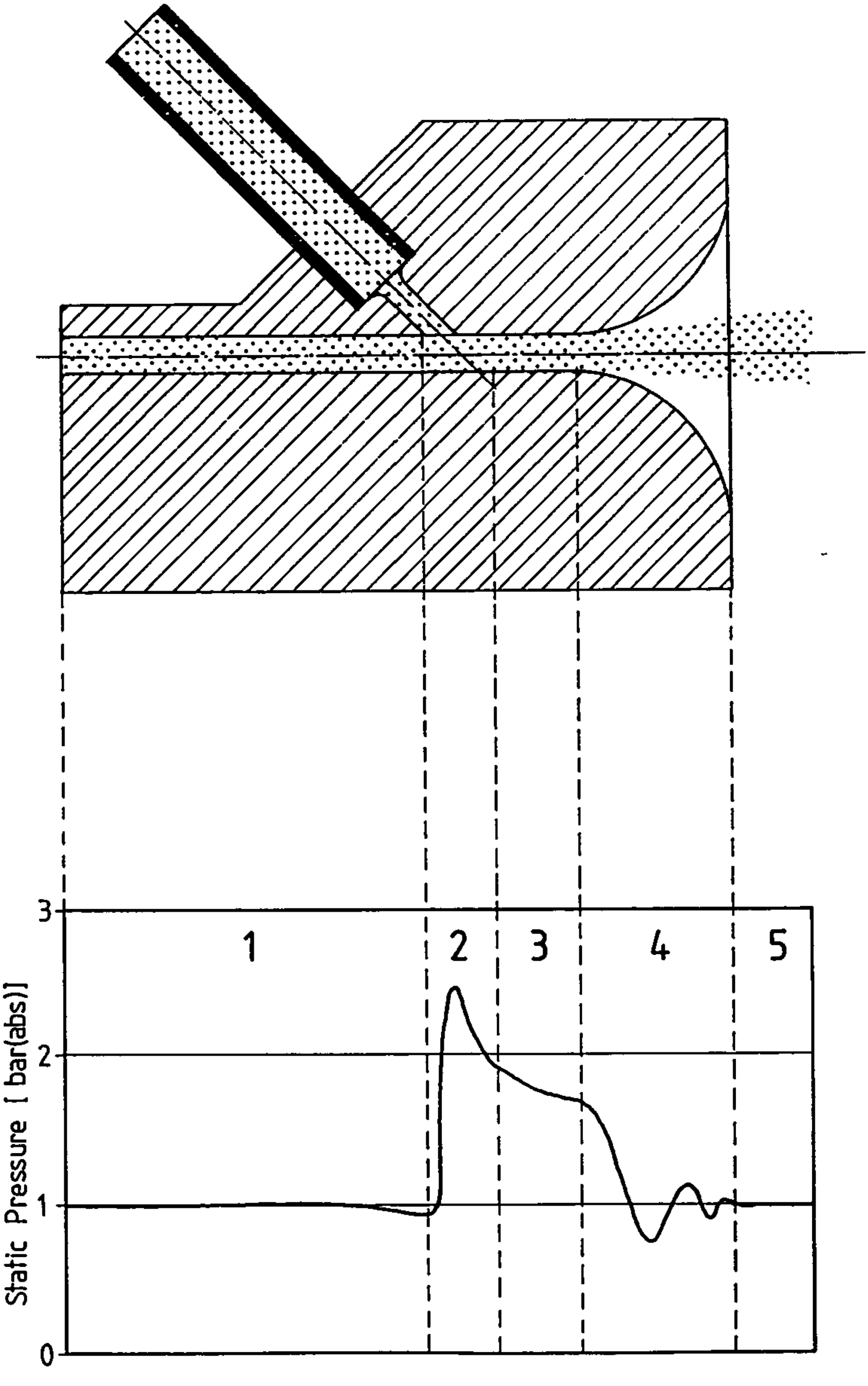

Figure 5.4 Different levels of static pressure in the main duct

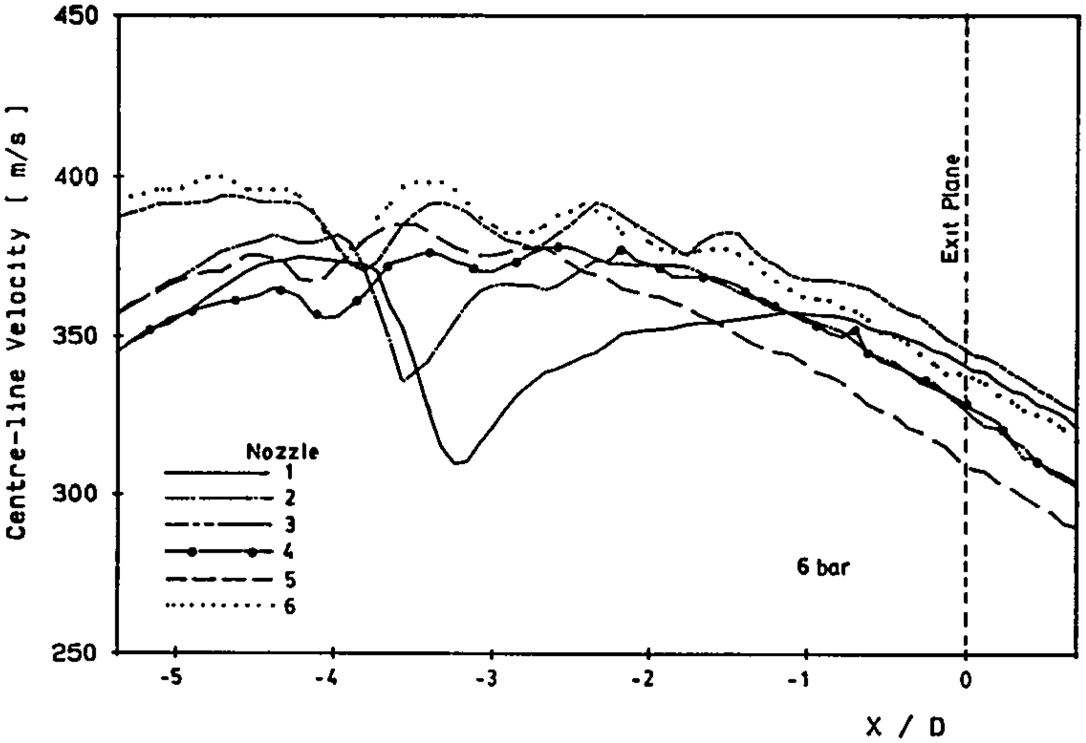

Figure 5.5a The effects of the exit shape on the centre-line velocities

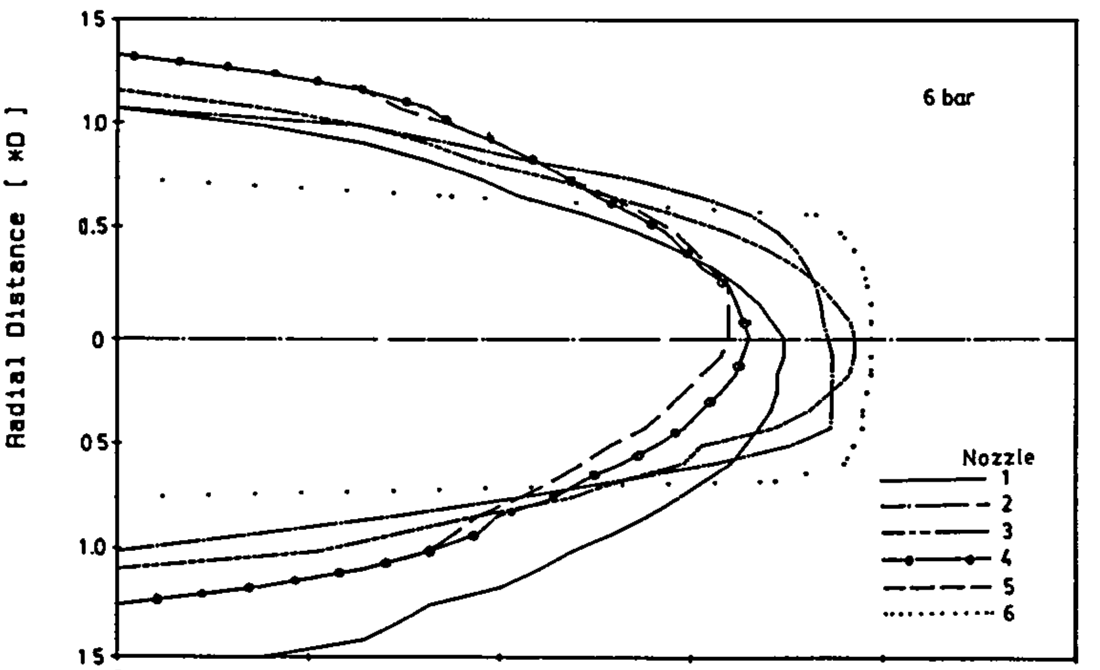

Figure 5.5b The effects of the exit shape on thetraverse velocities at the exit plane of the nozzles

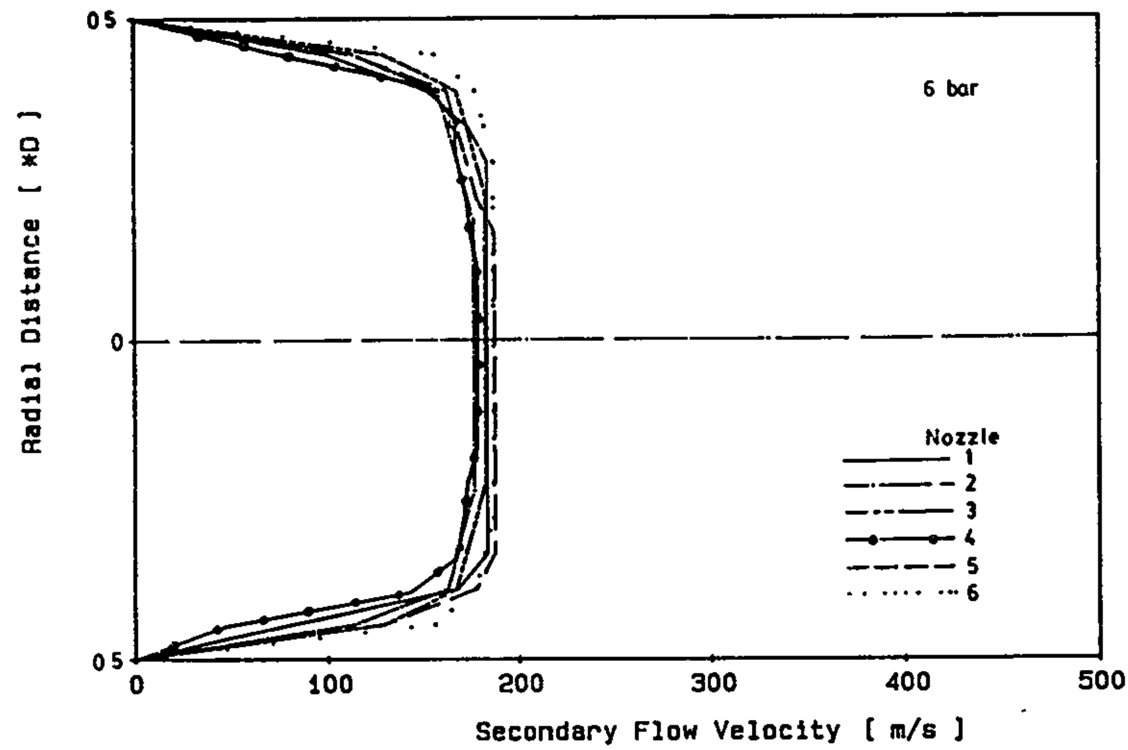

Figure 5.5c The effects of the exit shape on the secondary flow traverse velocities

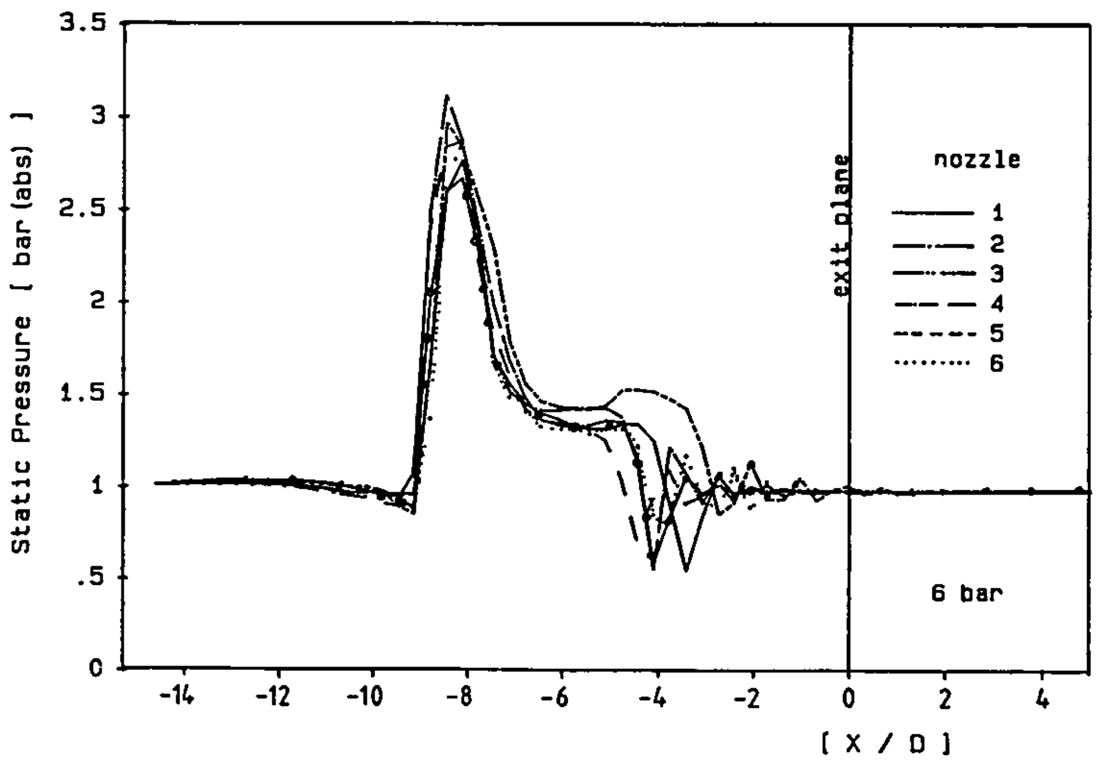

Figure 5.5d The effects of the exit shape on the static pressure distribution in and out of the nozzles

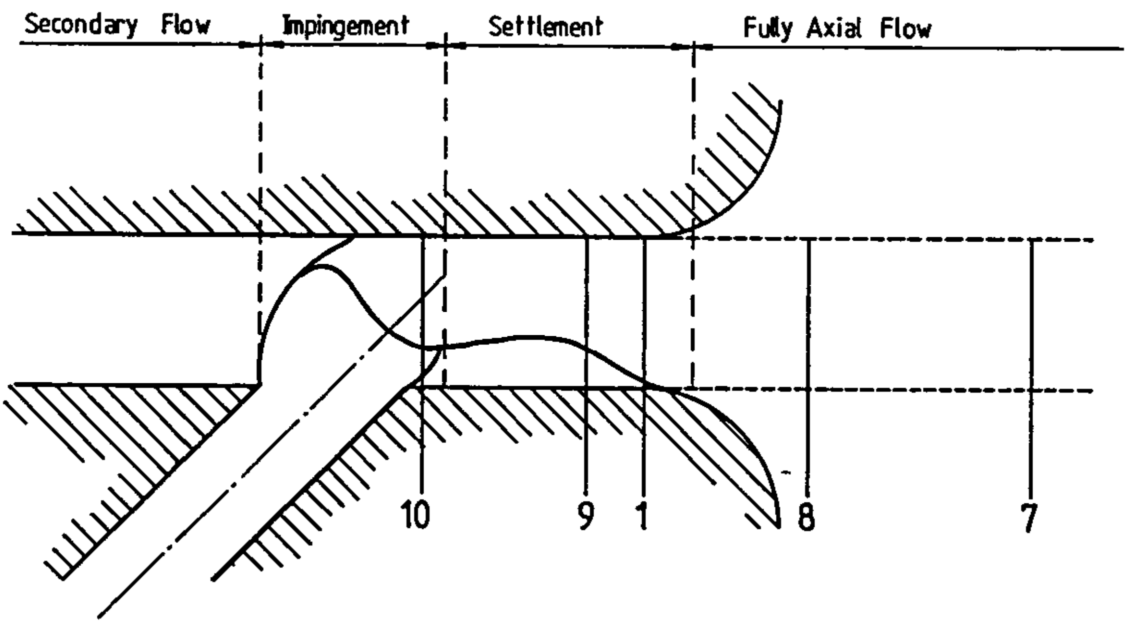

Figure 5.6 Impingement of the incoming jet and formation of shock waves in the main duct

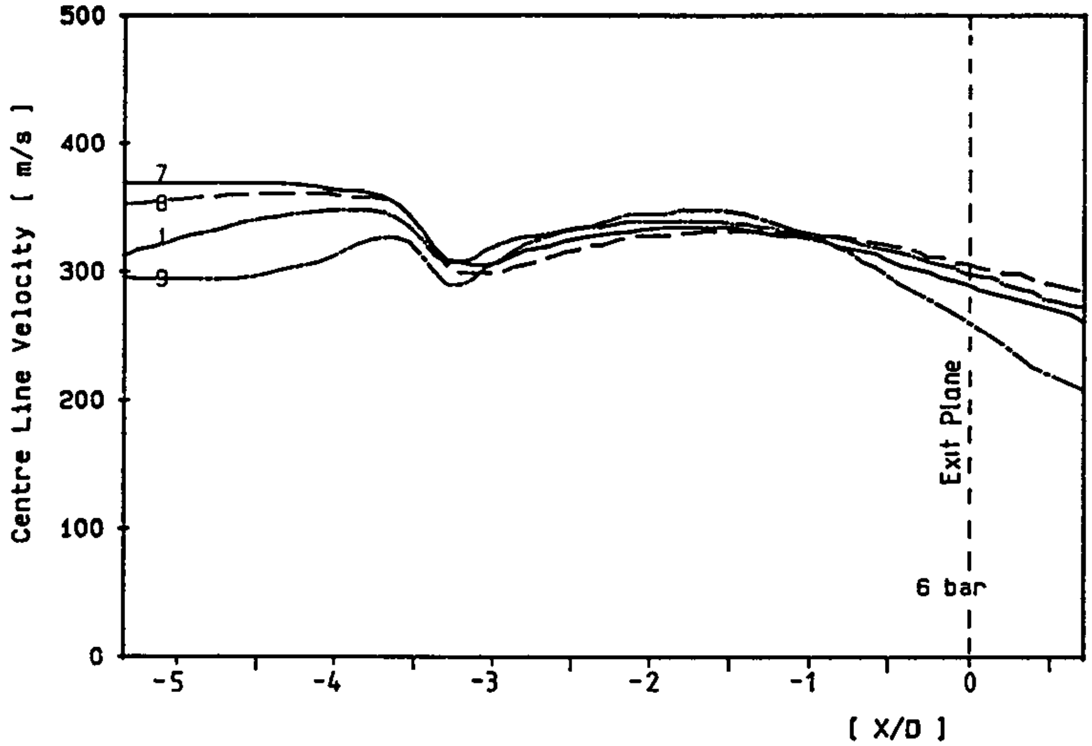

Figure 5.7a The effects of the situation of the inlet hole on the centre-line velocities

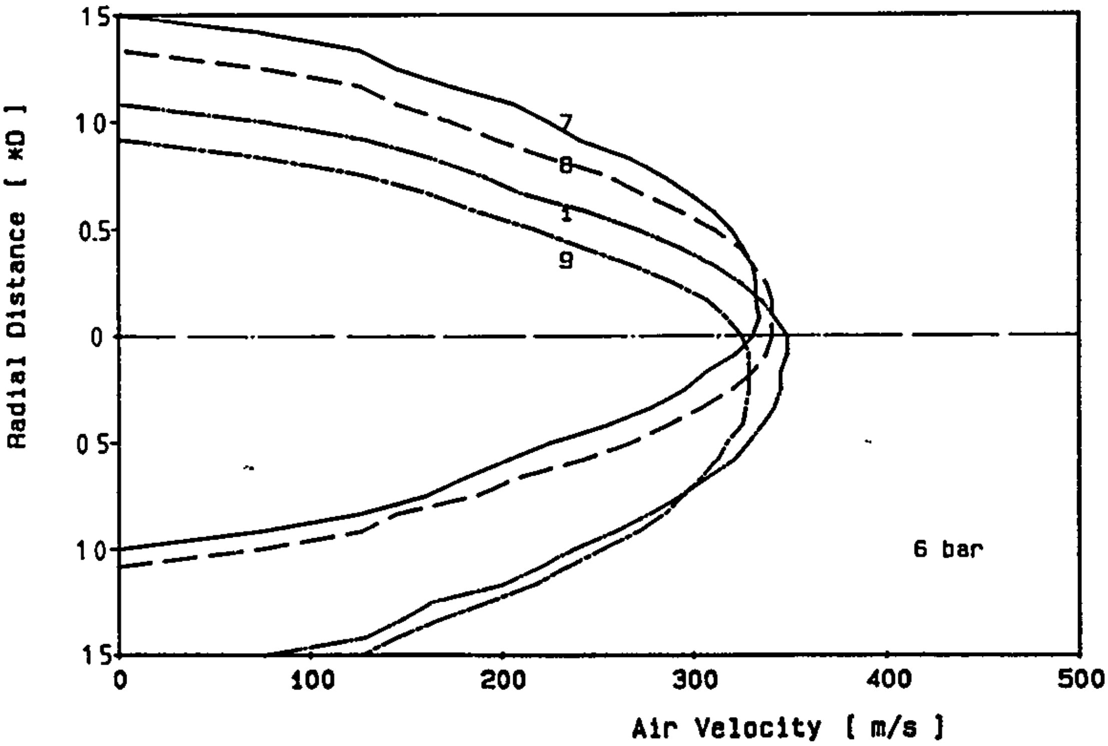

Figure 5.7b The effects of the situation of the inlet hole on the traverse velocities at the exit plane of the nozzles

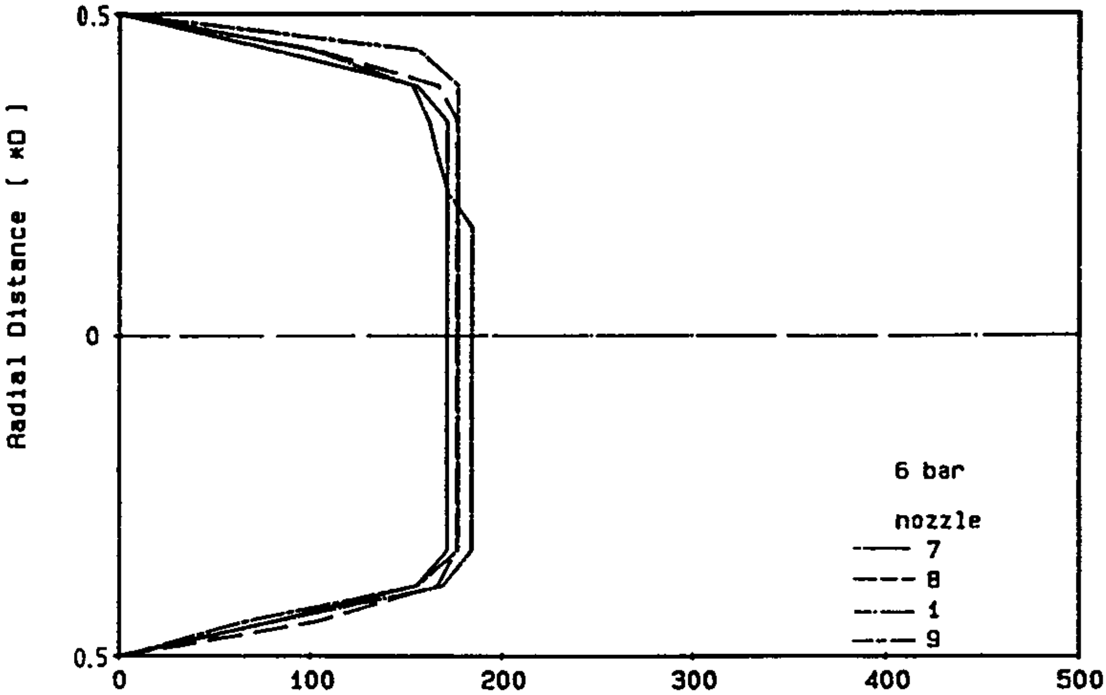

Figure 5.7 c The effects of the situation of the inlet hole on the secondary flow traverse velocities

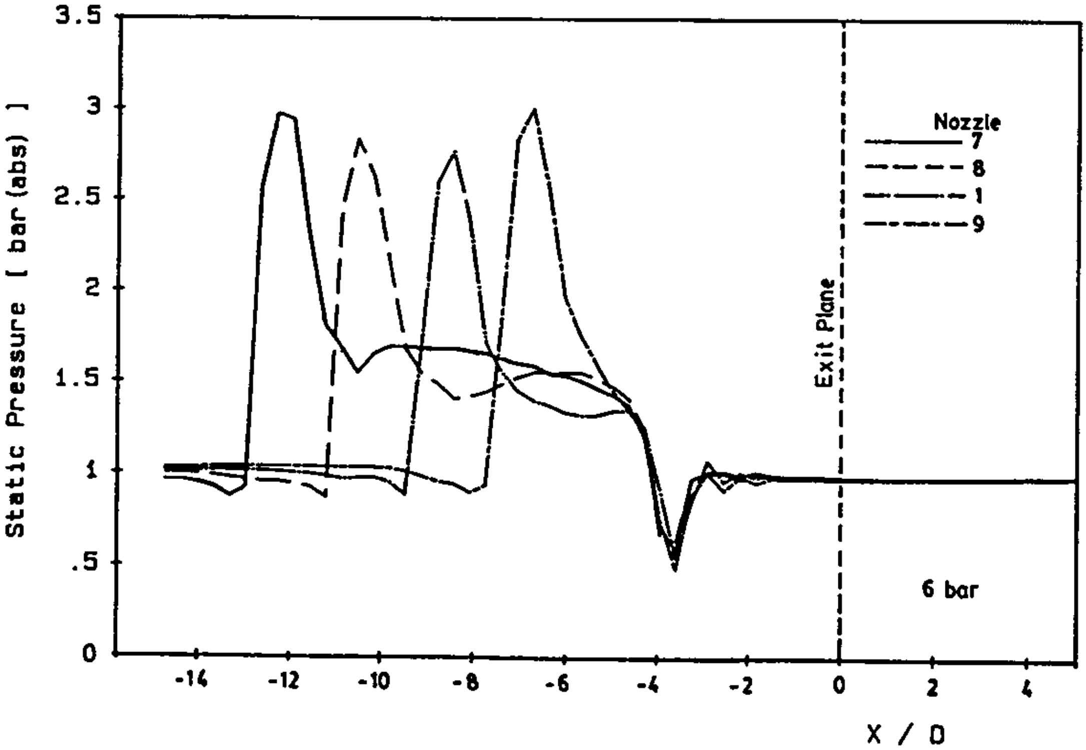

Figure 5.7 d The effects of the situation of the inlet hole on the static pressure distribution in and out of the nozzles

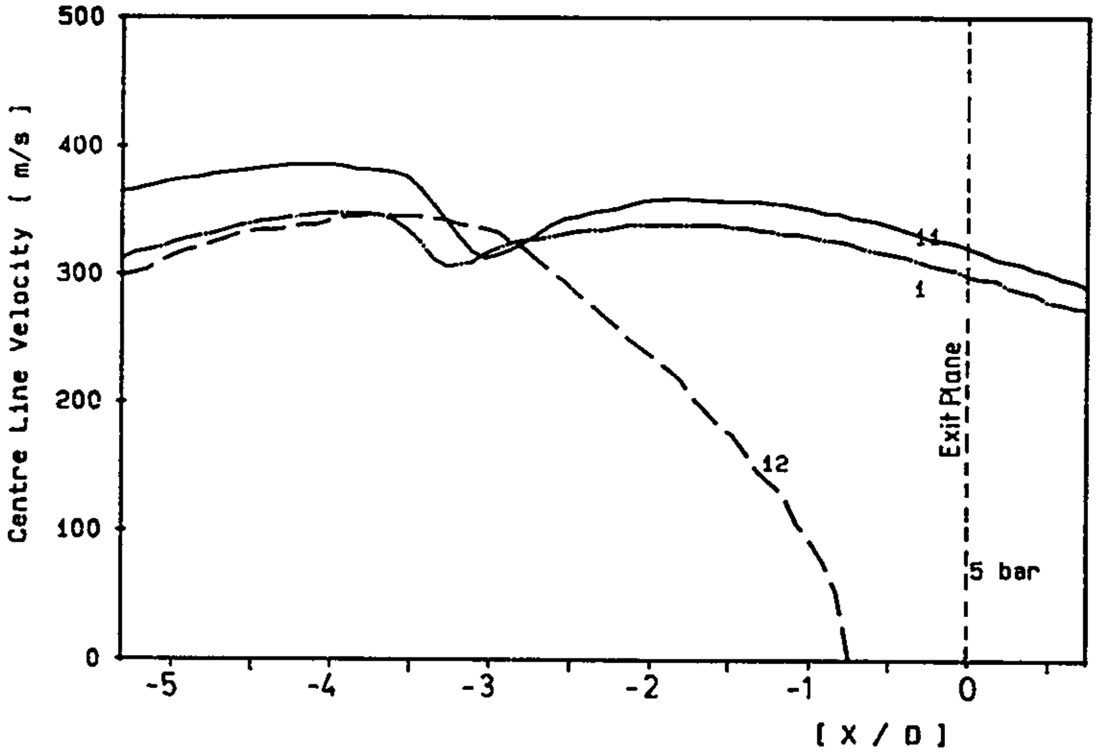

Figure 5.8a The effects of the inclination angle of the inlet hole on the centre-line velocities

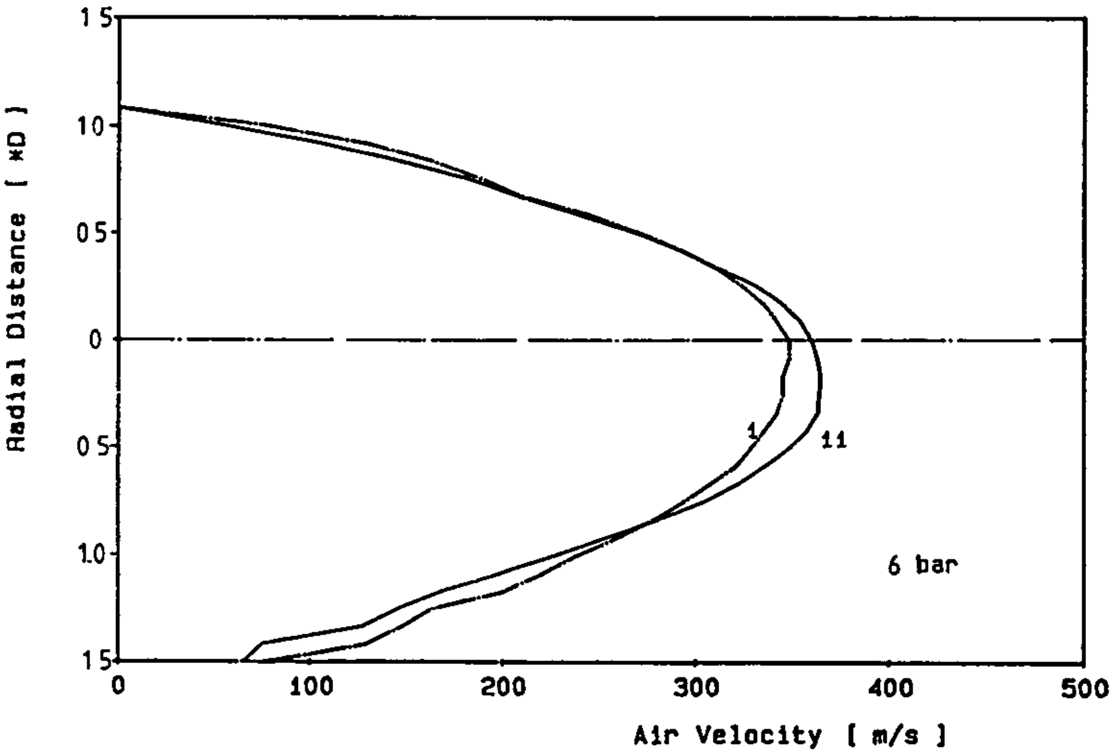

Figure 5.8b The effects of the inclination angle of the inlet hole on the traverse velocities at the exit plane of the nozzles

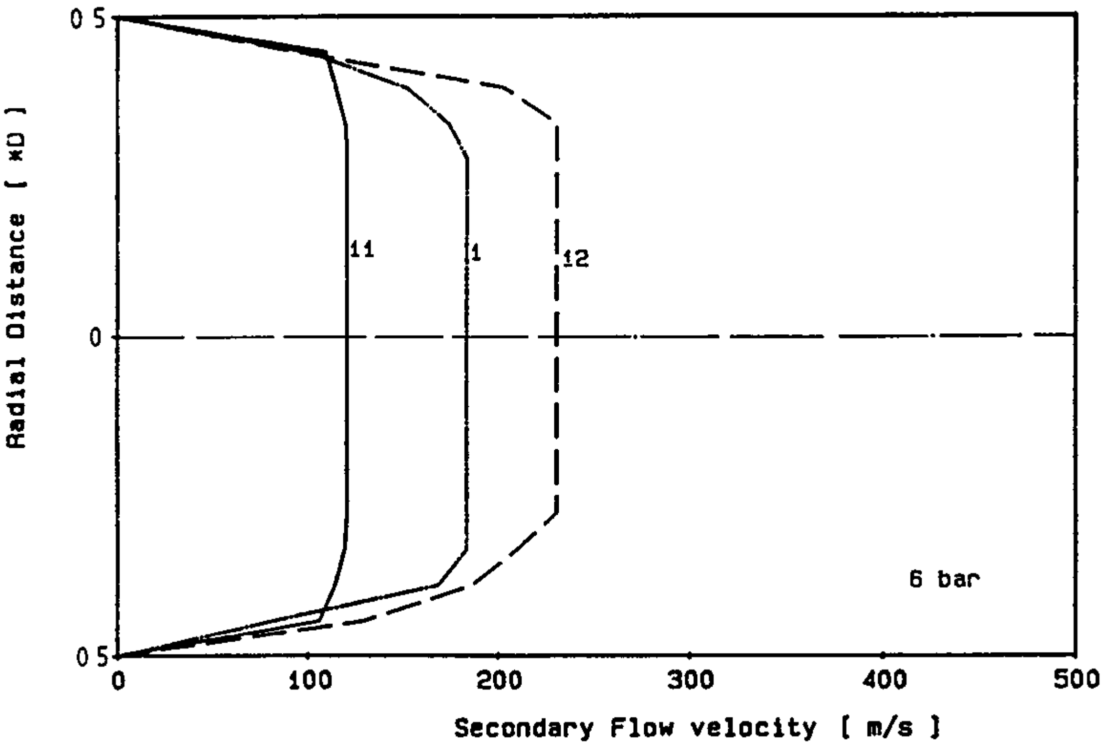

Figure 5.8c The effects of the inclination angle of the inlet hole on thesecondary flow traverse velocities

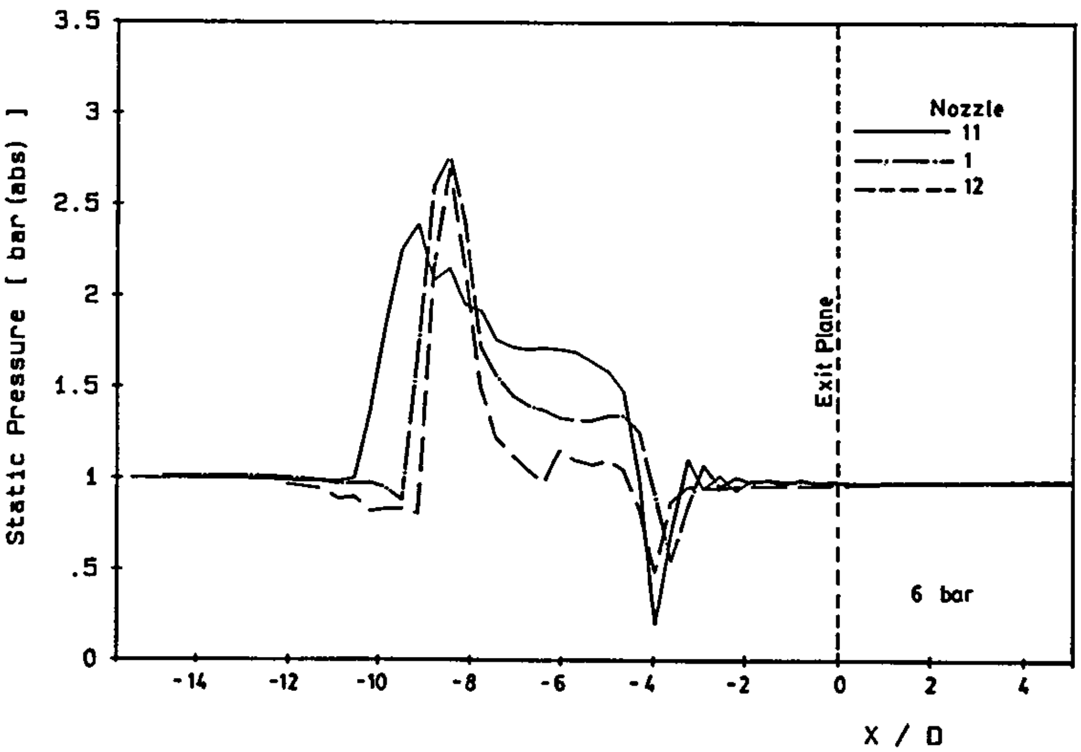

Figure 5.8d The effects of the inclination angle of the inlet hole on the static pressure distribution in and out of the nozzles

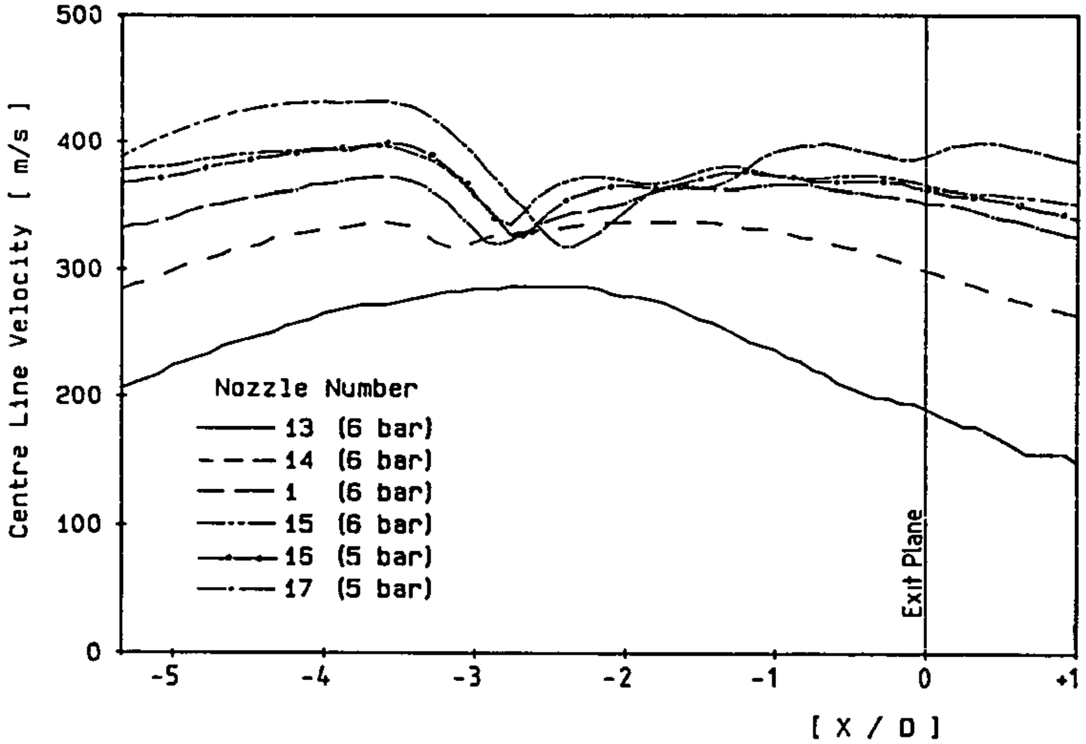

Figure 5.9a The effects of area ratio on the centre-line velocities

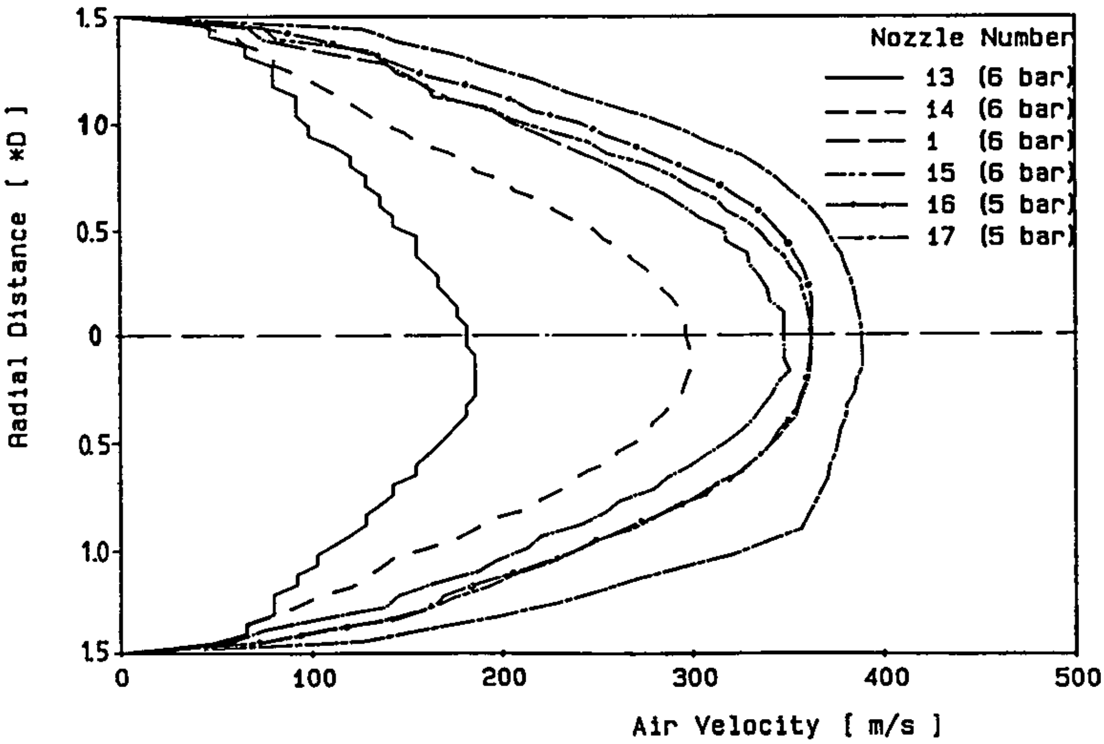

Figure 5.9b The effects of area ratio on the traverse velocities at the exit plane of the nozzle

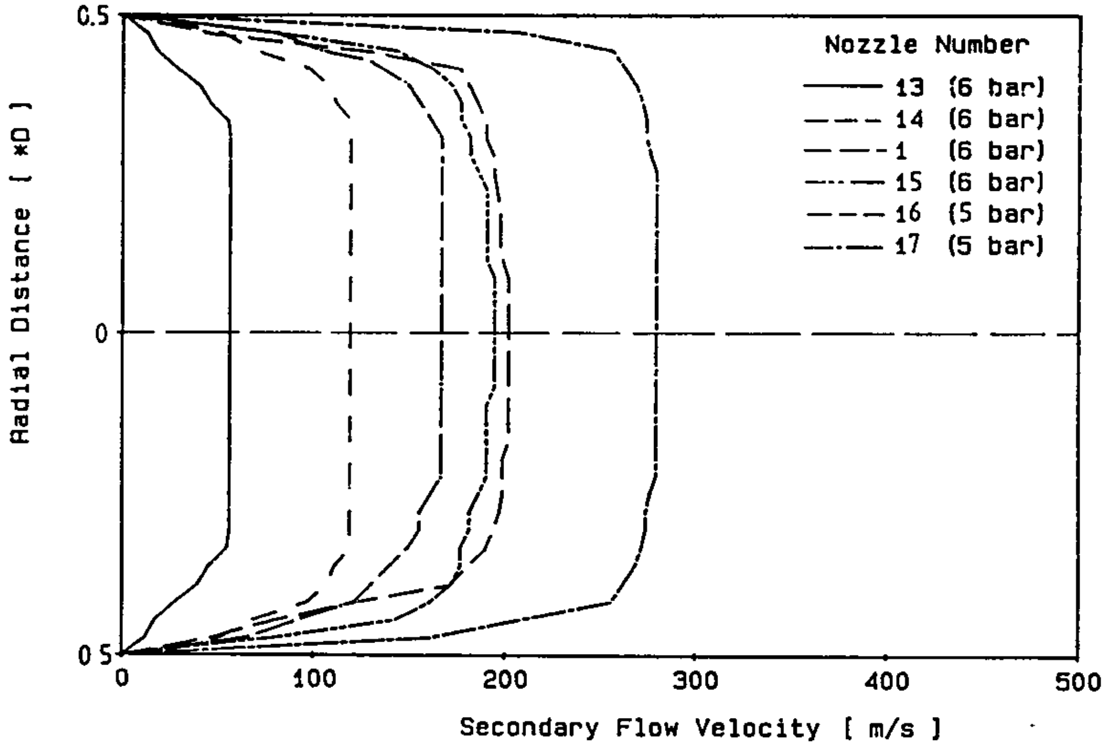

Figure 5.9c The effects of area ratio on the secondary flow traverse velocities

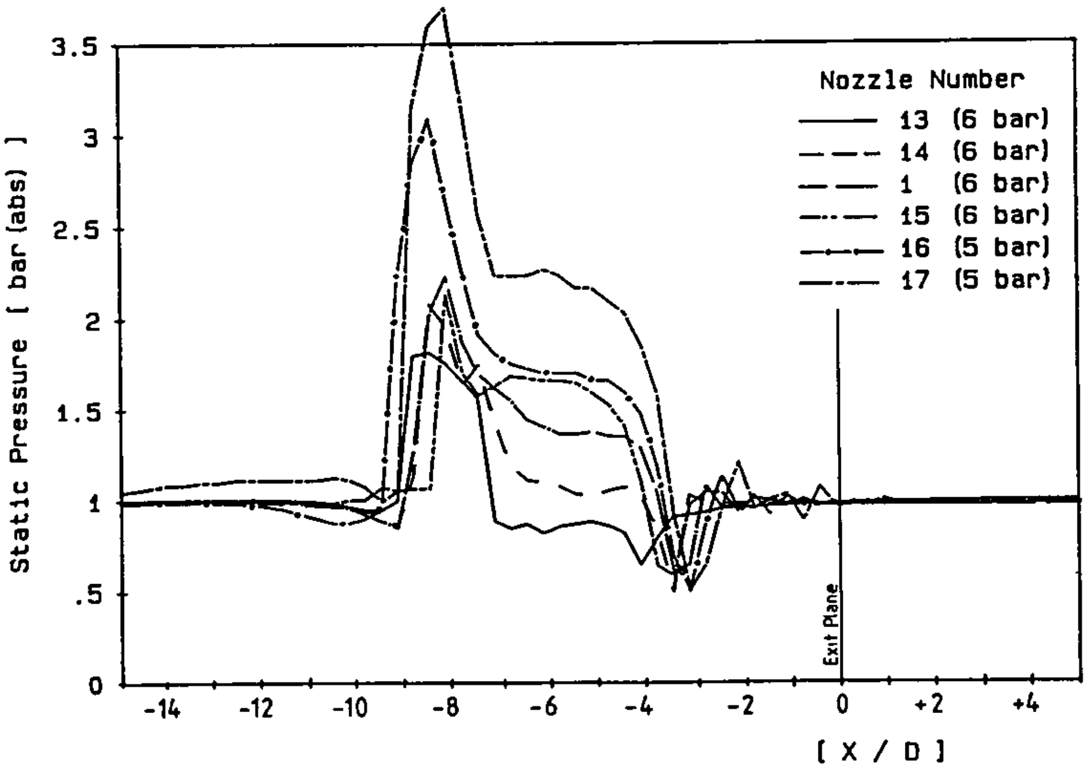

Figure 5.9d The effects of area ratio on the static pressure distribution in and out of the nozzles

CHAPTER 6

THE DESIGN OF MORE EFFECTIVE NOZZLES

In the previous chapters, studies of several industrially used texturing nozzles and the effects of their geometry on the air flow created have been described. In this chapter, through the interpretations of these flow studies, novel and improved designs are suggested.

6.1 Shortcomings of the Existing Nozzles

The high level of air consumption is the major obstacle to the air-jet yarn texturing process. Although air consumption levels have been reduced over the course of the years, it still constitutes more than 40% of the overall costs of the process[17]. It has been reported by some authors[25,31] that as soon as the air consumption of air-jet texturing nozzles is reduced to acceptable levels without causing any deterrioration of the process itself, then air-jet texturing will make its long expected breakthrough.

Benedict et al[94] have shown that an abrupt enlargement of any flow, both in the subsonic and supercritical ranges, causes considerable losses and hence dissipates the flow energy. As reported in Section 3.4.3, all the HemaJets suffer from these abrupt enlargement losses due to the ratio of incoming jet area to the nozzle main duct area being less than unity. A further factor is the fact that, due to the oblique opening of the inlet holes to the main duct, the incoming jets vigorously hit the opposite wall of the duct. Additionally, the backward deflection of the inlet jets (See Section 3.4.3) increases the angle of impingement and therefore makes the losses worse. This oblique impingement therefore forms another source of loss. It is surmised that these losses are more significant in those nozzles with one incoming jet than in nozzles with two or three incoming jets. This is because the collision of the opposing air jets occurs between the jets and on the centre line of the main duct, rather than between a single air-jet and the solid walls of the main duct. A further undesired effect of this oblique impingement of a single incoming jet is that it presses the filament yarn against the opposite wall. Since the filament yarn is in motion, this causes increased friction and hence wear of the nozzle. It has been reported by a major company of the U.K.[101] that they had to renew their nozzles every six months due to this wear problem. Nevertheless, it should be borne in mind that the collision of incoming jet(s) has a useful function for texturing by causing a better separation of the filaments and consequently improving the effectiveness of the loop and entanglement formation.

Static pressure measurements (Section 5.2) have revealed that, after the sudden enlargement of the incoming jets, the flow still possesses pressures much higher than the ambient pressure. Since the area of the main duct is constant up to the point where the trumpet-shaped divergence starts, very little acceleration of the flow is observed thereby resulting in an incomplete expansion within the nozzle. Bearing in mind that the trumpet-shaped exit is not designed for the complete expansion of the flow, the flow with pressures higher than the ambient pressure expands to the atmospheric conditions creating expansion waves which dissipate a great deal of energy (See Section 3.6.3). Therefore it could be said that the flow energy is not fully utilised by the existing nozzles.

Some of the useful energy of the flow is wasted through secondary flow. Since all the HemaJets have cylindrical main ducts, the only factor which affects the division of the flow into primary and secondary flows is the geometry of the nozzle and particularly the oblique opening of the inlet holes as was stated earlier. Furthermore, increasing input pressures increase the rate of secondary flow due to the increased backward deflection of the incoming jets, hence making the nozzles less efficient.

In summary, the high level of air consumption, the sudden enlargement and oblique impingement of the incoming jet(s), the cylindrical geometry of the main duct which does not allow the flow to expand further, and the high level of secondary flow rate are the major shortcomings of the existing cylindrical type nozzles.

6.2 Areas of Improvement

In the light of the investigations reported in Chapters 3, 4 and 5, some improvements for the above shortcomings of the existing nozzles have been sought. The ultimate aim of these changes has been to reduce the compressed air consumption as much as possible without affecting the texturing efficiency of the nozzles.

6.2.1 Air consumption

The texturing trials in Section 4.6 have shown that the effectiveness of texturing with all nozzles increases with increasing input pressures, at the expense of increased air consumption (See Section 4.2), which makes the process expensive, i.e less efficient. On the other hand it is known that the behaviour of compressible fluids varies with the pressure. This indicates that maximum efficiency from a nozzle with a certain geometry can only be achieved at a certain pressure. The same efficiency cannot necessarily be achieved even at higher pressures than for that which it is designed.

Unfortunately none of the texturing nozzle manufacturers has yet specified the pressure at which the nozzle attains maximum efficiency. Therefore it could be suggested that the design of nozzles for a given pressure would be a step forward towards the full utilisation of input energy. Choosing this pressure as low as 5 bar will obviously reduce the air consumption whilst keeping the nozzles as effective as they might be at supply pressures of 8 or 9 bars.

6.2.2 Abrupt enlargement

The effect of the area ratio of the inlet holes to the main duct on the air flow has been discussed in Section 5.3.4. It is concluded that the closer the area ratio is to unity, the higher the velocities at the exit plane of the nozzle are attained. Although this result has been obtained from the velocity and static pressure measurements, the same result could be supported by the texturing trials of the existing nozzles. With the closest area ratio to unity (0.75), the T341 HemaJet is more effective than those which have area ratios of 0.607 and 0.537, i.e. the Standard-core and T100 Hemajets respectively (See Section 4.6).

In conclusion, it could be argued that choosing an area ratio of unity eliminates the drawback of an abrupt enlargement. The consequence is that the sonic flow conditions will be introduced to the main duct of the nozzle.

6.2.3 Impingement

Having more than one incoming jet will reduce the impingement losses. Additionally, as concluded in Section 5.3.3, by reducing the angle of inclination of the inlet holes, the impingement conditions will improve. This also will enhance the momentum flux transferred to the primary flow which is responsible for the texturing effect. Additionally the implementation of the suggestion of choosing an area ratio of unity, will minimise the impingement losses.

However, the desired effects of the impingement of the inlet jets that is to say that their contribution to the better separation of the filaments, should not be forgotten.

6.2.4 Expansion of the primary flow

By making the area ratio unity, sonic conditions will be introduced into the main duct. By increasing the duct area from there onwards, the sonic flow could be accelerated to supersonic velocities. Provided that the area of the exit plane where the atmospheric conditions are present is designed to provide a complete isentropic expansion of the flow[95], the whole pressure could be converted into the kinetic energy which is essential for texturing. Through this design, the energy dissipating pressure waves (both expansion and compression) which have been proved to be of no significance for the actual texturing (See Section 4.7), could be eliminated. The acceleration of the flow in the nozzle will obviously facilitate the better transport of the filaments during the process, because the drag force acting on the filaments will be higher due to the increased air flow velocities.

6.2.5 Exit shape

The investigations in Section 5.3.1 have proved that several exit shapes have little effect on the air flow produced by the experimental nozzles. Therefore, from the aerodynamic point of view, exit shapes could be eliminated. This obviously will reduce the manufacturing costs of the nozzles. However, from the texturing viewpoint, a curved exit shape, i.e. trumpet-shape may facilitate a smooth right-angled turning of the textured yarn, thus contributing to the texturing process.

6.2.6 Secondary flow

It has been observed that the secondary flow plays no positive role in texturing but blows the superfluous water particles from the filaments (See Section 7.2). It further reduces the net momentum in the direction of the primary flow. Therefore the secondary flow is a mere source of energy loss for the primary flow which facilitates the texturing.

It is believed that any restriction on the secondary flow will enhance the effectiveness of the primary flow, and in turn will increase the performance of the nozzle.

Since the filaments occupy only a small fraction of the nozzle duct and only a small amount of air is sufficient to blow off the excess water from the supply yarn, any restriction of secondary flow by reducing its cross-sectional area should not normally affect the performance of the nozzle. A restriction of this wasted secondary flow will enhance the primary flow because the momentum transferred into this direction will be increased.

6.3 A Step Forward: A Modification to the Existing Nozzles

The idea of restricting the secondary flow has been applied to the Standard-core HemaJet by inserting a short tube in the secondary flow section of the nozzle (See Fig. 6.1). By making this modification, the secondary flow area is reduced to 1/4 of its original area. Momentum fluxes of both the primary and secondary flows from both nozzles are plotted against driving pressures in Fig. 6.2. From this, it is seen that the modification enhances the momentum flux of the primary flow, whilst reducing the momentum flux of the secondary flow as was intended.

Fig. 6.3 shows the air velocity distributions from the modified Standard-core HemaJet at different driving pressures. Fig. 6.4 shows a comparison of the Standard-core at 7 bar and the modified Standard-core at 6 bar working pressures. From these figures, it can be concluded that higher velocities of the primary flow can be achieved at lower pressures. Consequently, the texturing pressures can be lowered and hence the compressed air consumption can be reduced.

Centre-line axial velocities and shock waves at various pressures also provide supporting evidence. This fact is shown in Fig. 6.5 which shows shadowgraphs of jets producad by the modified Standard-core HemaJet at different air pressures as well as the centre-line velocity fluctuations with varying distances.

To supplement the investigation, yarns produced by using the modified nozzle were tested. The results are compared with results from the original Standard-core HemaJet as shown in Figs. 6.6a, b, c, d, e, and f. The yarn tests also show that by using 1 bar less air pressure with the modified nozzle, yarns with a similar quality can be obtained.

The investigations have shown that by restricting the secondary flow, the efficiency of texturing nozzles could be improved; subsequently the pressure could be reduced by as much as 1 bar and in turn the compressed air consumption could be lessened.

6.4 Nozzle Design: Preliminary Investigations with Scaled-up Models

In the light of the above considerations, four new nozzles have been designed in order to improve the efficiency of HemaJet-type nozzles.

Nozzle 1 (Fig. 6.7a) is designed to operate at 6 bar pressure to produce the maximum possible air velocity at the exit plane, this being theoretically M=1.828 which is virtually equal to the maximum velocities produced by the HemaJets at 9 bar. It possesses an area ratio of unity (Sections 5.3.4 and 6.2.2). The inlet holes have been placed further back, i.e. closer to the secondary flow exit of the main duct (Section 5.3.2). The inclination angles of the three inlet holes have all been reduced to 30° (Sections 5.3.3 and 6.2.3). The main channel of the nozzle has been so designed that the sonic flow conditions which are achieved in the main channel have been fully expanded when the flow reaches the exit plane (Section 6.2.4). This has been achieved by making the duct conical with an area ratio of 1.47, i.e. the exit to the critical (sonic) flow section area. No exit shape is made at the end of the main duct (Sections 5.3.1 and 6.2.5) and the secondary flow channel area is reduced to 40% of the sonic section (Sections 6.2.6 and 6.3).

Nozzle 3 which is designed to operate at 5 bar pressure is a compromise between nozzle 1 and the existing HemaJets, in that the inlet holes have a 45° inclination and are placed halfway along the duct.

Nozzles 2 and 4 (Figs. 6.7b and 6.7d) have the same geometrical configuration as nozzles 1 and 3 (Figs. 6.7a and 6.7c) respectively.

The only difference between these two sets is in their inlet hole diameters. The inlet hole diameters have been made different, i.e. 3.2, 3.6 and 4.0 mm, keeping the total area equal to the main duct area. By this difference in the diameters, a swirl which has been reported[55] as a contributing factor to the texturing, is expected to be imparted to the flow.

These four times scaled-up nozzles were manufactured and the measurements of the velocity profiles of primary and secondary flows at their respective exit planes, the centre-line velocities, and the static pressures in and out of the nozzles, were carried out at 5 bar pressure. The results are given in Figs. 6.8a, b, c and d. For comparison purposes these graphs also include results obtained from the Standard-core HemaJet at 9 bar. In order to compare the results measured at the same plane, the trumpet-shaped exit of the Standard-core HemaJet was removed. This made possible the measurement of the flow velocities at the very exit plane (where the divergence of the trumpet-shaped exit starts). Unfortunately, the small size of the actual Standard-core HemaJet does not permit measurements of the static pressure in the nozzle. Nevertheless the scaled-up version of it has been utilised and the static pressures in and out of the nozzle have been recorded at 5 bar and the results included in Fig. 6.8d.

The results clearly demonstrate that the previous predictions are valid in that the velocities produced by the designed nozzles at pressures as low as 5 bar were virtually equal to the velocities produced by conventional nozzles at 9 bar at corresponding sections. This indicates that the high air consumption levels could be reduced by such improved designs.

Although the isentropic flow theory predicts that with the designs of the nozzles 3 and 4, a Mach number of 1.708 should be reached at the exit plane, a Mach number of only 1.574 is obtained in practice (7.8% deviation). The reason for this discrepancy is suspected to be the presence of the secondary flow (i.e. losses). When the secondary flow is completely blocked, the primary flow has attained a Mach number of 1.666, thereby reducing the deviation to 2.4%. It is thought that slight manufacturing faults have played some role in this small difference.

Contrary to the expectations of higher velocities from the nozzles 1 and 2 due to the 30^{O} inclination of the inlet holes the experimental results (Fig. 6.8a and b) show no substantial difference from those obtained from nozzles 3 and 4. This may be explained as follows: since the area ratio of the inlet holes to the main duct is unity, the flow observes no expansion up to the point where the conical divergence starts. Therefore, the inclination of the incoming flow has no significant effect on the air flow. The same explanation may be valid for the difference in the diameters of the inlet holes. However both of these geometrical factors may affect the behaviour of the filaments during the texturing, i.e. the 30^{O} inclination of the incoming jets may exert more force on the filaments, whereas the 45^{O} inclination may create a better separation of the filaments. Moreover the difference in the hole diamenters may introduce some desired swirl. Therefore all these factors have been considered in deciding on the final designs.

Fig. 6.8c, depicting the centre-line velocities of the primary flows, shows the formation of strong shock waves in the jet created by the Standard-core HemaJet. This figure also shows that nozzles 1 and 2 create some, albeit weak, shock waves. This is due to the fact that they were operated at a 5 bar pressure for which they are not designed. (This has been done intentionally for the purpose of comparison. Nevertheless, the tests of nozzles 1 and 2 could not be performed because the air supply feeding the scaled-up nozzles was inadequate to give a continuous pressure at 6 bar pressure).

The diverging geometry of the main duct accelerates the sonic flow and converts pressure into kinetic energy. This is illustrated in Fig. 6.8d. While the static pressure in the cylindrical duct of the Standard-core HemaJet is almost constant up to the point of divergence, the static pressure in the conical (diverging) section of the nozzles 1 to 4 continually decreases. Again the large divergence of the trumpet-shaped exit of the Standard-core HemaJet causes a sudden expansion of the flow creating a strong pressure wave which is observed as a sudden change in the static pressure in Fig. 6.8d, whereas the nozzles 1 to 4 create rather gentle fluctuations in the static pressure; this is thought to be due to manufacturing errors in the case of the nozzles 3 and 4, but it is also due to the off-design operation and manufacturing faults in the nozzles 1 and 2.

The secondary flows created by the nozzles 1 to 4 (Fig 6.8b) are higher than those created by all the conventional nozzles. Aerodynamically speaking, this is no problem whatsoever, because the primary flow velocities are sufficiently high for even better texturing. However, it may be a practical problem in the actual texturing operation, as Simmen[102] has stated that the high secondary flow velocities can cause intermingling of supply yarns comprising finer filaments and this results in a deterioration of the texturing quality. Therefore, the secondary flow velocities need to be minimised.

When the secondary flow velocities at the beginning of the secondary flow channel were calculated by using the measured total and local static pressures the subsonic nature of the flow was found, although it became supersonic at the exit plane due to the expansion of the flow. Therefore it was planned to decelerate this flow through a divergent opening of the channel and this idea has been implemented on nozzle 4 as illustrated in Fig. 6.9.

Fig. 6.10a showing the velocity profile of the secondary flow before and after this modification illustrates that the expected reduction in the flow velocity was achieved. The primary flow, however, was not affected by this modification (Fig. 6.10b).

6.5 Final Design and The Prototypes

The above reported preliminary investigations with the scaled-up models led the author to design six novel texturing nozzles. The technical drawings of these improved nozzles are given in Figs. 6.11a, b, c, d, e and f. The prototype nozzles have been manufactured to the required tolerances by Heberlein and tested from both the air flow and texturing viewpoints.

6.5.1 Aerodynamic Properties of the Prototype Nozzles

6.5.1.1 The prototype nozzle 1 (Reference nozzle)

The prototype nozzle 1 is an exact prototype of the scaled-up experimental nozzle 1. However, it is designed to operate at 5 bar air pressure. Furthermore, the prototype nozzle 1 possesses a trumpet-shaped exit to facilitate the easy withdrawal at right angles of the textured yarn. The deceleration of the secondary flow is achieved by a divergent opening of the secondary flow channel which is of smaller cross-sectional area than the primary flow channel cross-sectional area (a direct implementation of the suggestion made in Section 6.3). This particular design feature is repeated on all of the prototype nozzles.

When the axial velocities at the exit plane of the prototype nozzle 1 were recorded, it was found that at 5 bar design pressure the nozzle creates air velocities which are nearly equal to the air velocities created by the Standard-core HemaJet at 9 bar (Fig. 6.12a). As the air pressure is increased even higher, air velocities are created reaching up to 500 m/s at 9 bar. The centre line velocities and the shadowgraphs as shown in Fig 6.12b reveal that the prototype nozzle 1 at the design pressure of 5 bar hardly creates any standing pressure waves even though the flow is highly supersonic (M=1.5). The small and gentle fluctuations in the centre-line velocities and light areas on the shadowgraph of the flow at 5 bar pressure are suspected to be due to the presence of the secondary flow which reduces the effective pressure in the nozzle's main duct. Fig. 6.12b also illustrates that as the air pressure is increased above the design pressure stronger expansion and compression waves are produced.

6.5.1.2 The prototype nozzle 2 (Enhanced swirl)

A swirl in the primary flow is thought to be be created by making the diameters of the three inlet holes different, provided that the total cross-sectional area is equal to the main duct area. Therefore, the three inlet holes of the prototype nozzle 2 are made to the diameters of 0.8, 0.9 and 1 mm, this being the only geometrical difference between this nozzle and the prototype nozzle 1.

As the preliminary investigations with the scaled-up nozzle 2 (Section 6.4) have revealed, the different diameters of the inlet holes do not seem to have an appreciable effect on the flow velocities. Figs. 6.13a and b depict respectively the axial velocities at the exit plane and the centre-line velocities as well as the shadowgraphs of the jet generated at different pressures. The figures also include the flow velocities produced by the Standard-core HemaJet at 9 bar air pressure showing that these velocities are almost equal to the velocities created by the prototype nozzle 2 at 5 bar air pressure.

6.5.1.3 The prototype nozzle 3 (No exit shape)

The only geometrical difference between the prototype nozzles 1 and 3 is in their exit shapes. The prototype nozzle 3 has no trumpet-shaped exit. Therefore, together with its diverging main channel, it may be likened to the Taslan nozzles.

The air velocity profile at the end of the divergent main duct is almost uniform at all pressures as seen in Fig. 6.14a. Fig 6.14b depicting the centre line velocity fluctuations and the shadowgraphs of the jets indicates the formation of strong expansion waves at 9 bar, and an almost shock free jet flow at 5 bar pressure. The level of air velocity created by the prototype nozzle 3 is almost equal to the previous prototype nozzles. Hence it could again be concluded that the exit shapes play an insignificant role in the air flow created by the texturing nozzles.

6.5.1.4 The prototype nozzle 4 (Better filament separation)

A 45^{o} inclination angle of the inlet holes is the only different geometrical feature of the prototype nozzle 4 compared to the previous three prototype nozzles. In Section 6.4, it has been argued that, in this particular design, the acute angle of inlet holes play an insignificant role on the downstream air flow. However, it was then surmised that this acute impingement of the incoming jets may improve the filament separation and hence enhance the texturing effectiveness. These conclusions are once again evidenced by the air velocities created by the prototype nozzle 4 (See Fig. 6.15a and b) which are only slightly less than the air velocities created by the prototype nozzle 1 with a 30^{o} inlet hole inclination angle.

6.5.1.5 The prototype nozzle 5

When manufacturing faults are excluded from the considerations, the only geometrical difference between the prototype nozzles 4 and 5 is in the situation of the inlet holes along the main duct. The inlet holes of the prototype nozzle 5 are closer to the exit plane of the primary flow whilst the inlet holes of the prototype nozzle 4 are further back, i.e. closer to the secondary flow exit plane. As far as the air velocities at the exit plane, as well as on the centre-line, are concerned (See Figs. 6.16a and b), the difference in the situation of the inlet holes seems to have little effect.

6.5.1.6 The prototype nozzle 6 (High secondary flow velocity)

Section 6.4 pointed out a difficulty of the high secondary flow velocity inherent in this present design and offered a possible solution. That section of the thesis also verified the validity of the solution by means of scaled-up nozzles and flow velocity measurements; consequently this solution was implemented on all the above mentioned prototype nozzles. However, it was thought it would be revealing to investigate the effects of high secondary flow velocity from the texturing point of view and hence for this purpose the secondary flow channel of the prototype nozzle 4 was left cylindrical, i.e. no divergence.

It was noted that this nozzle created, as surmised, supersonic secondary flow velocities at the secondary exit plane and furthermore the formation of expansion and compression waves were observed by means of the shadowgraph technique. However, the primary flow velocities of the prototype nozzle 6 were no less than the parent prototype nozzle 4 (See Figs. 6.17a and b).

6.5.2 Textile properties of yarns textured by the prototype nozzles

A preliminary process investigation with the prototype nozzles was performed by measuring the yarn tension in the stabilising zone at reference texturing conditions as described in Section 4.2 with varying air pressures ranging from 4 to 9 bar with increments of 0.5 bar. The results of this investigation is given in Fig. 6.18 for all the novel nozzles. The figure also shows the compressed air savings offered by these prototype nozzles. The figure illustrates that the prototype nozzles 1 and 5 texture better than the Standard-core HemaJet up to 7 bar air pressure. Above this pressure, however, the Standard-core appears to produce better textured yarns. Thus, no further quality investigation of yarns textured with the prototype nozzles 1 and 5 has been carried out as these nozzles are aimed to improve the texturing economics by effectively texturing yarns at all pressures. However, these nozzles have proved to have the potential of reducing the air consumption by about 10% when it is operated at 5 bar design pressure.

Despite the fact that the prototype nozzles 1 and 2 produce similar air velocities, prototype nozzle 2 textures far better yarns than the prototype nozzle 1 as seen in Fig. 6.18 and should therefore provide up to about 20% compressed air saving compared with the Standard-core HemaJet. In order to support this argument, further yarn tests were undertaken for yarns textured with the prototype nozzle 2. As seen in Figs. 6.19a to f, the properties of the yarns textured by the prototype nozzle 2 are similar to the properties of the yarns textured by the Standard-core HemaJet nozzle at higher pressures. The graphs illustrate that the reduction in pressure could be up to 1.6 bar.

Since the only difference between the prototype nozzles 1 and 2 is in the inlet hole diameters of the prototype nozzle 2, the improvements in yarn quality are attributed to the enhanced swirl characteristics of the primary flow.

The preliminary tension measurements in the stabilising zone (Fig. 6.18) have shown that even better texturing conditions are achieved by the prototype nozzle 3. The level of the reduction in air consumption offered by this nozzle could be up to 30%. Further yarn tests as shown in Figs. 6.19a to f also support this conclusion.

It has been observed during the texturing operation with the prototype nozzle 3 that the actual texturing process takes place outside the nozzle's exit plane, whilst it happens in the trumpet-shaped exit of both the HemaJets and the rest of the prototype nozzles. This also constitutes another similarity with the Taslan nozzles. Since the velocity difference between the jet core and just outside the jet boundary is so great, the difference between the forces acting on the leading and trailing ends of the individual overfed filaments are also great. Consequently, the textured yarns constitute fairly large loops around a well entangled core, in turn yielding low tenacities and breaking elongations (Figs. 6.19d and e).

The tests of yarns textured by the prototype nozzle 4 at 5 bar revealed that the yarns have closely similar properties to those textured by the Standard-core HemaJet at 9 bar (Figs. 6.19a to f). Hence it could be said that the prototype nozzle 4 has the potential of reducing the compressed air consumption by as much as 60%.

However, the preliminary texturing trials, as well as the yarn tests, revealed that the superior texturing effectiveness of the prototype nozzle 4 is not achieved by the prototype nozzle 6 indicating the paramount adverse effect of the high secondary flow velocities. Nevertheless the prototype nozzle 6 also offers the possibility of reducing the air consumption by about 25%.

6.6 Conclusion and Discussions

Air velocity measurements of the flow created by the prototype nozzles revealed the expected results in that the air velocities produced at the design pressure, 5 bar, are as high as the air velocities produced by the Standard-core HemaJet at 9 bar. Texturing trials and yarn tests furthermore revealed that all the prototypes successfully texture yarns and offer reductions in compressed air consumption of the order of 10 to 60% of that for the Standard-core HemaJet.

The prototype nozzle 4 appears to be the most effective nozzle and substantiates all the conclusions of Chapter 5, i.e. (a) an area ratio of unity is advantageous; (b) the controlled expansion, through a diverging channel, of the choked flow in the nozzle duct improves the nozzle efficiency; (c) the inlet holes need to be further back in the main duct; (d) the secondary flow needs to be reduced via smaller channel diameters; and (e) this secondary flow needs to be decelerated through a diverging channel. Nevertheless this nozzle showed that a 45^{o} inclination of the inlet holes is superior to a 30^{o} inclination angle from the texturing point of view. This is surmised to be due to the improved filament separation achieved by the acute impingement of the incoming jets to the overfed filaments.

The prototype nozzle 3 has also illustrated the possibility of eliminating the exit shape, hence reducing the manufacturing costs of the jet.

All of these prototype novel nozzles further prove that there is no evident relationship between the strength of the compression and/or expansion waves and the texturing effectiveness, since they produce textured yarns at 5 bar with fairly weak, if at all present, pressure waves; even so these yarns are similar in quality to those produced by the Standard-core HemaJet at higher pressures with much stronger pressure waves.

Since these novel nozzles have been designed to the dimensions of the Standard-core HemaJet and were aimed at reducing the air consumption by reducing the air pressure, the comparisons have been restricted to the Standard-core HemaJet. However, the most effective of these six nozzles, i.e. the prototype nozzle 4, is also compared with the most effective of the HemaJet series, i.e. the T341 HemaJet in Figs. 6.20a to f. These graphs also include the properties of yarns textured by the Standard-core HemaJet. From these, it could be argued that at corresponding air pressures, similar quality yarns are produced. This indicates the potential of replacing the T341 HemaJet with the prototype nozzle 4 since it achieves about 20% reduction in compressed air consumption.

These novel nozzles are characterised by high air velocities at the exit plane and shock-free jets at the design condition. The high air velocities are surmised to provide effective texturing even at high texturing speeds as well as the accommodation of higher overfeed levels, a process limitation from which most of the HemaJets suffer.

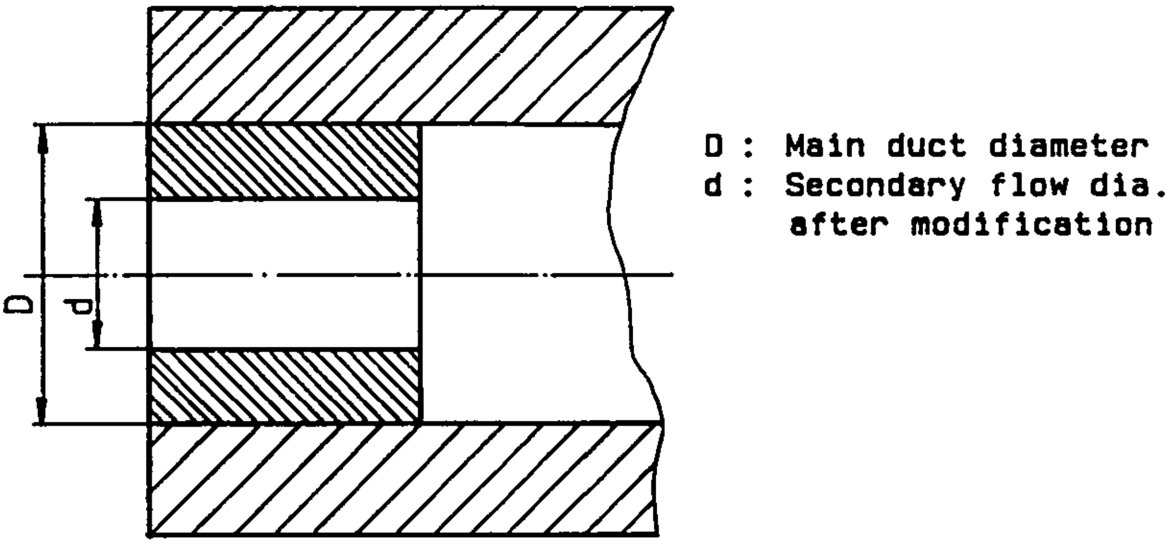

Figure 6.1 A sketch of the suggested nozzle modification

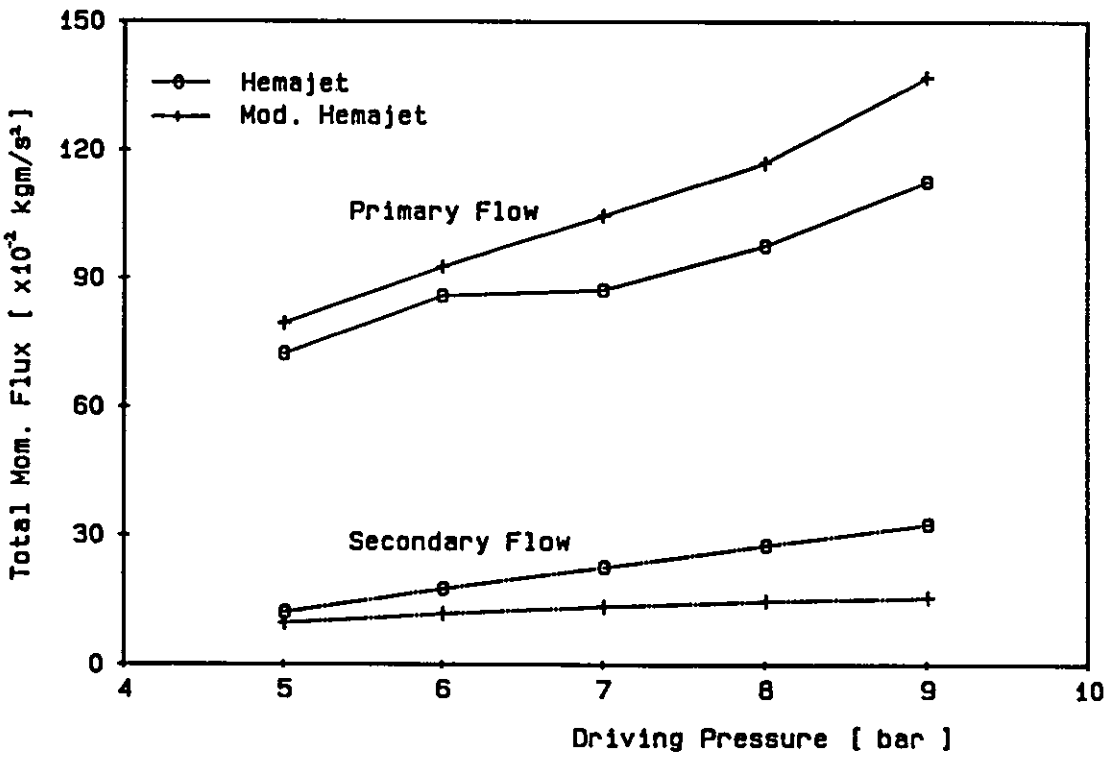

Figure 6.2 Primary and secondary flow momentum fluxes of the Standard-core Hemajet at varying pressures before and after the modification

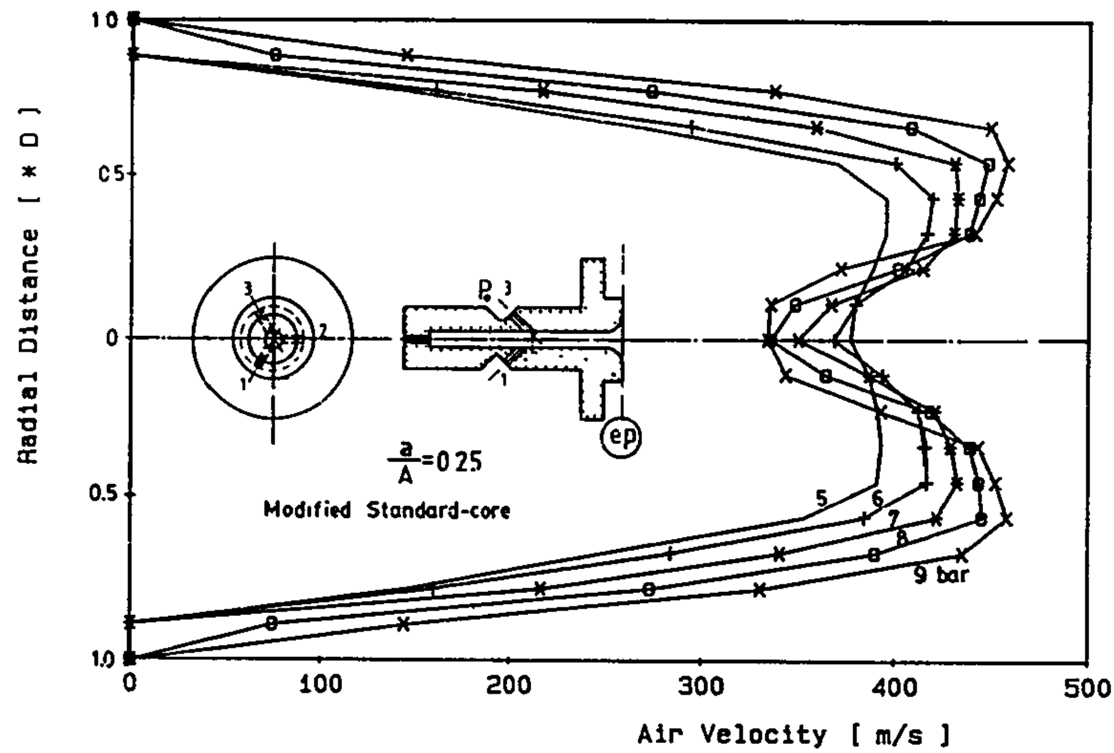

Figure 6.3 Velocity distribution of the flow from the modified Standard-core HemaJet at varying air pressures

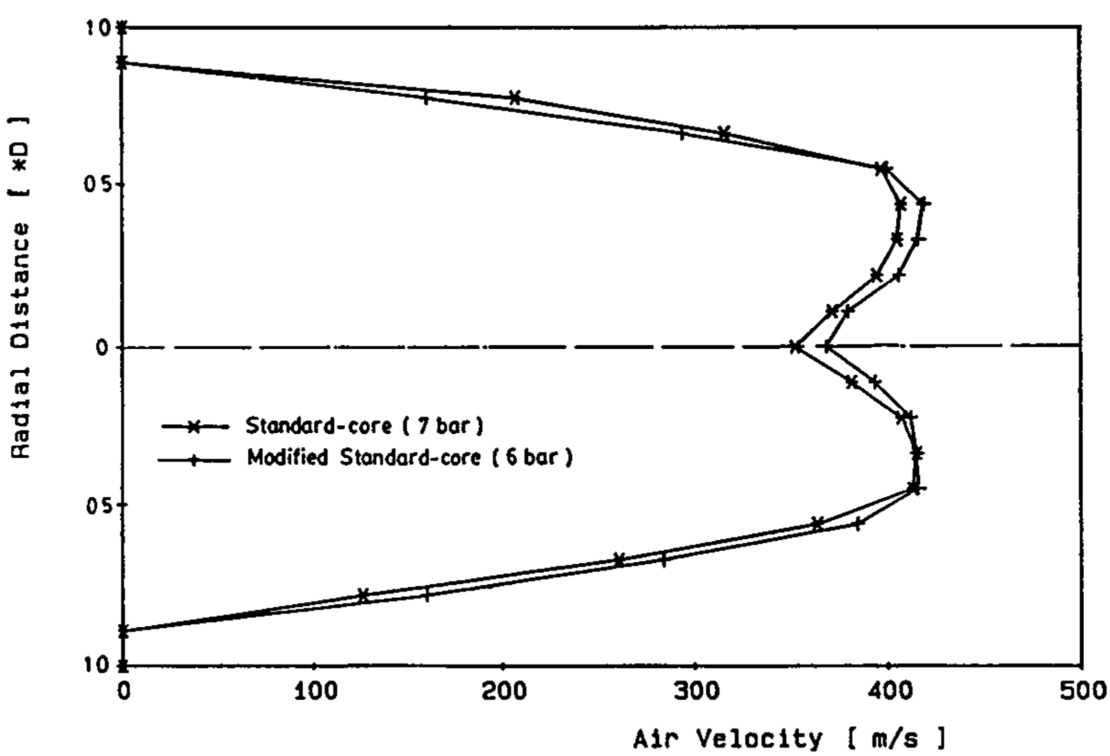

Figure 6.4 Comparison of the velocities at different pressures before and after the modification

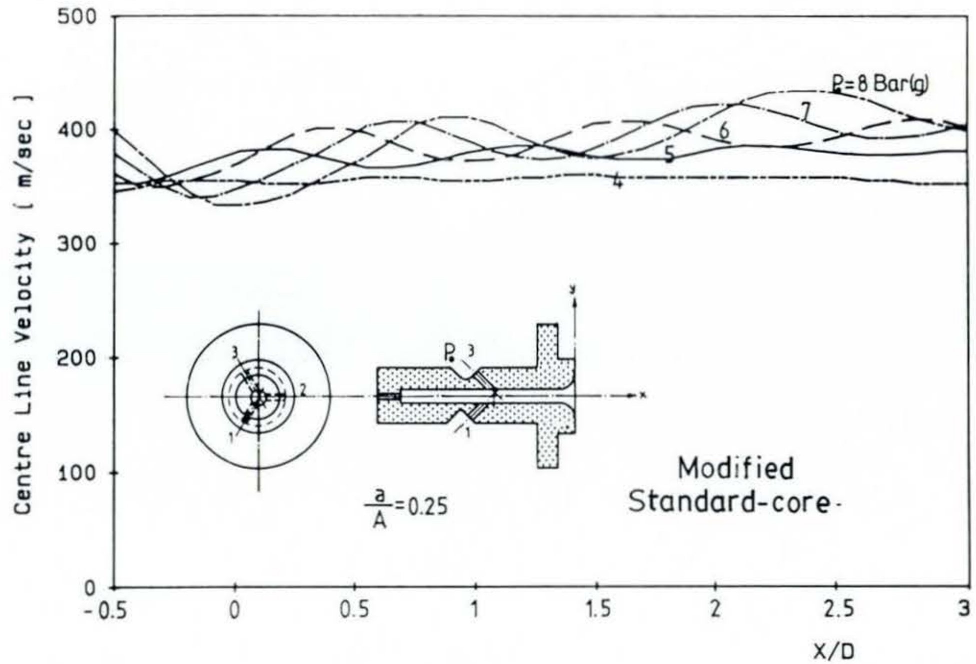

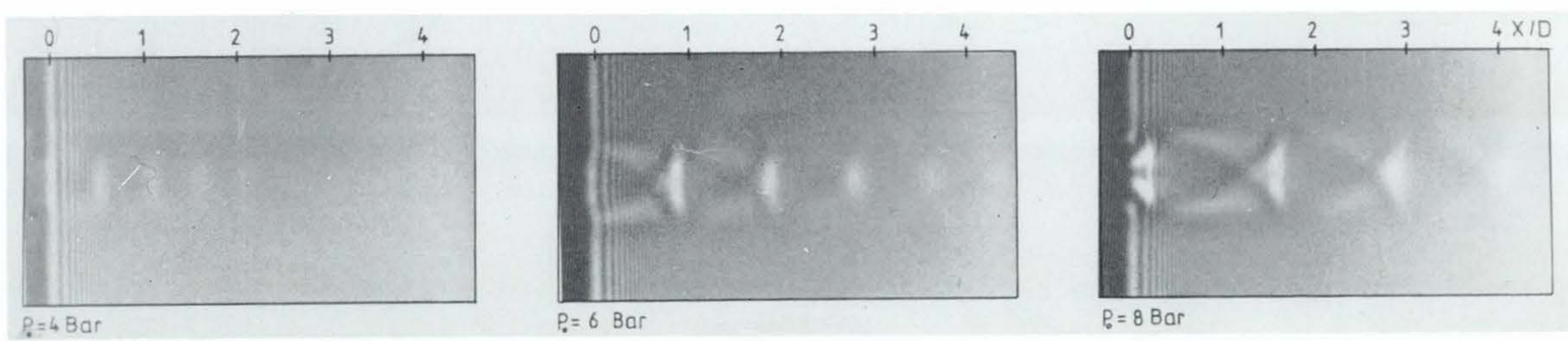

Figure 6.5 Centre-line velocities and shadowgraphs of the air jet from the modified Standard-core HemaJet at different input pressures

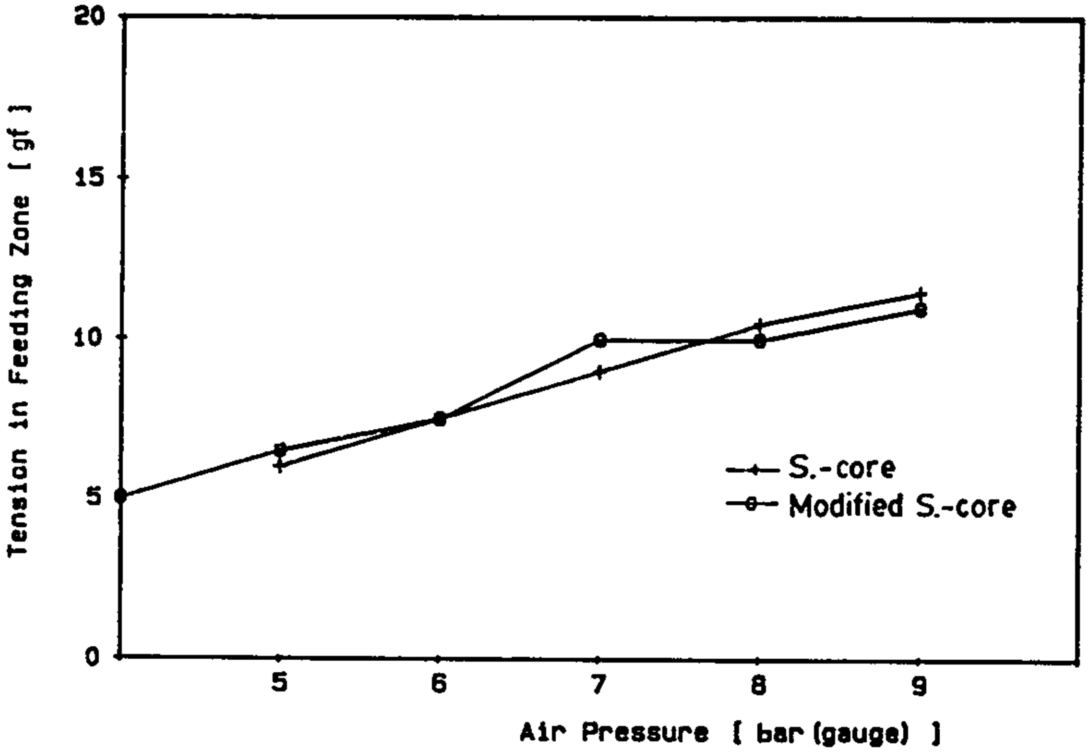

Figure 6.6a Comparison of the tension in feeding zone with the Standard-core HemaJet before and after the modification

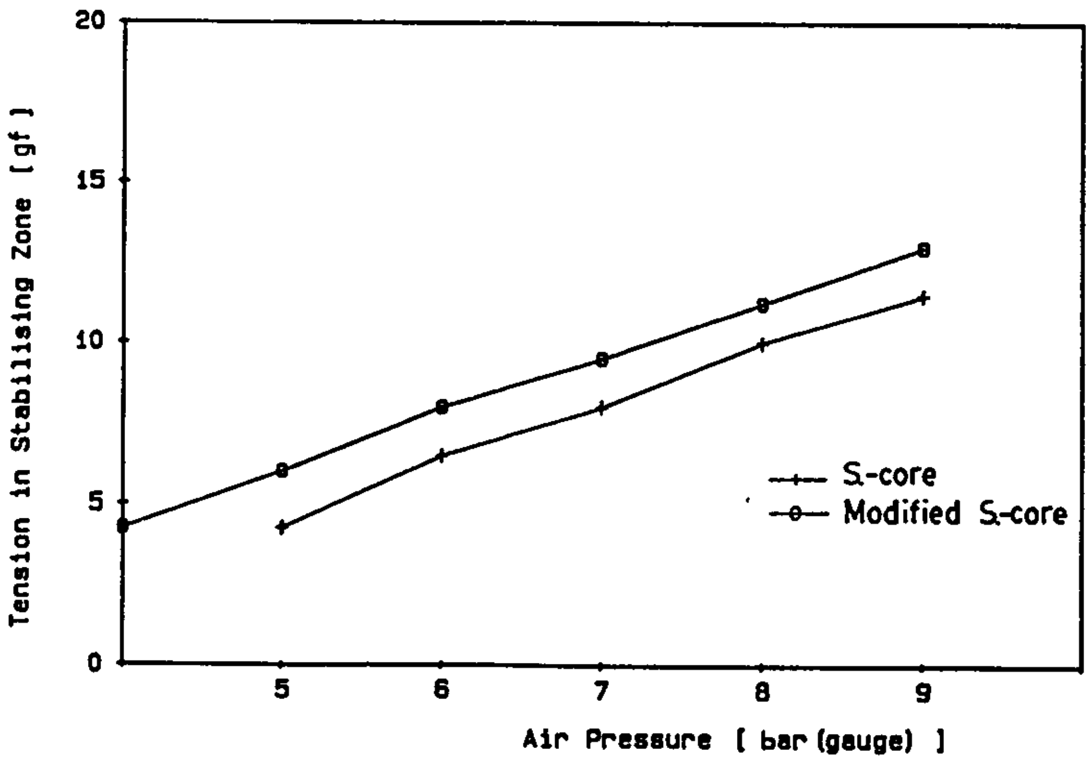

Figure 6.6b Comparison of the tension in stabilising zone with the Standard-core HemaJet before and after the modification

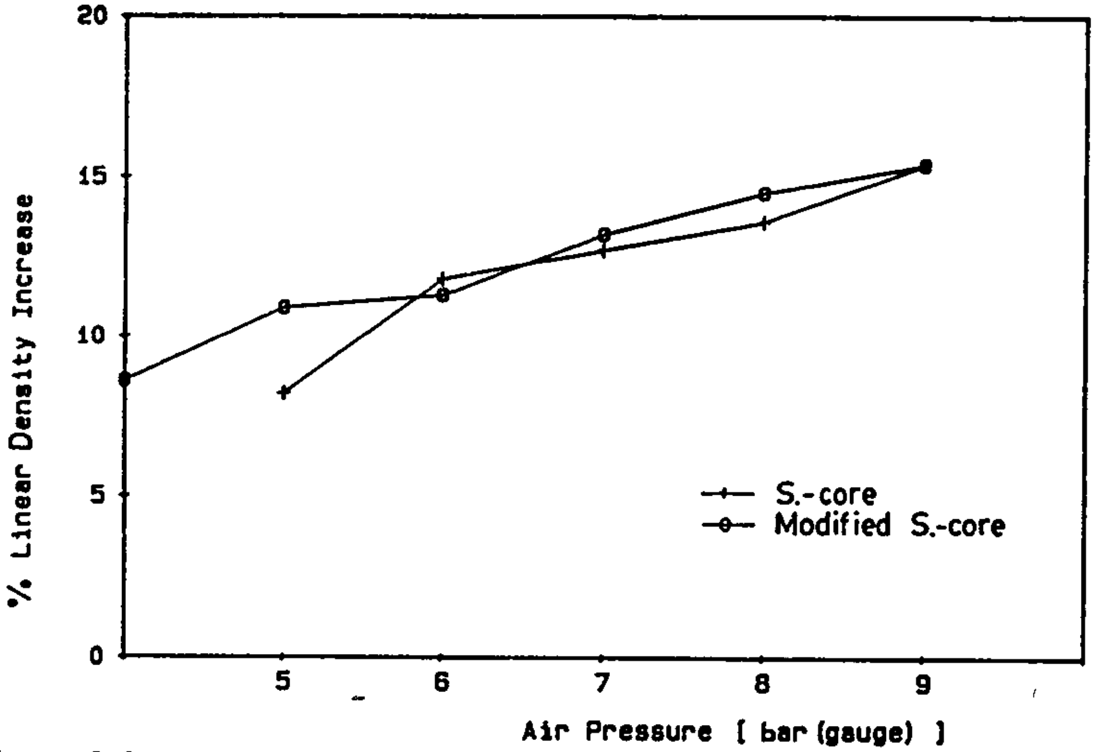

Figure 6.6c Comparison of the linear density increase of yarns produced with the Standard-core HemaJet before and after the modification

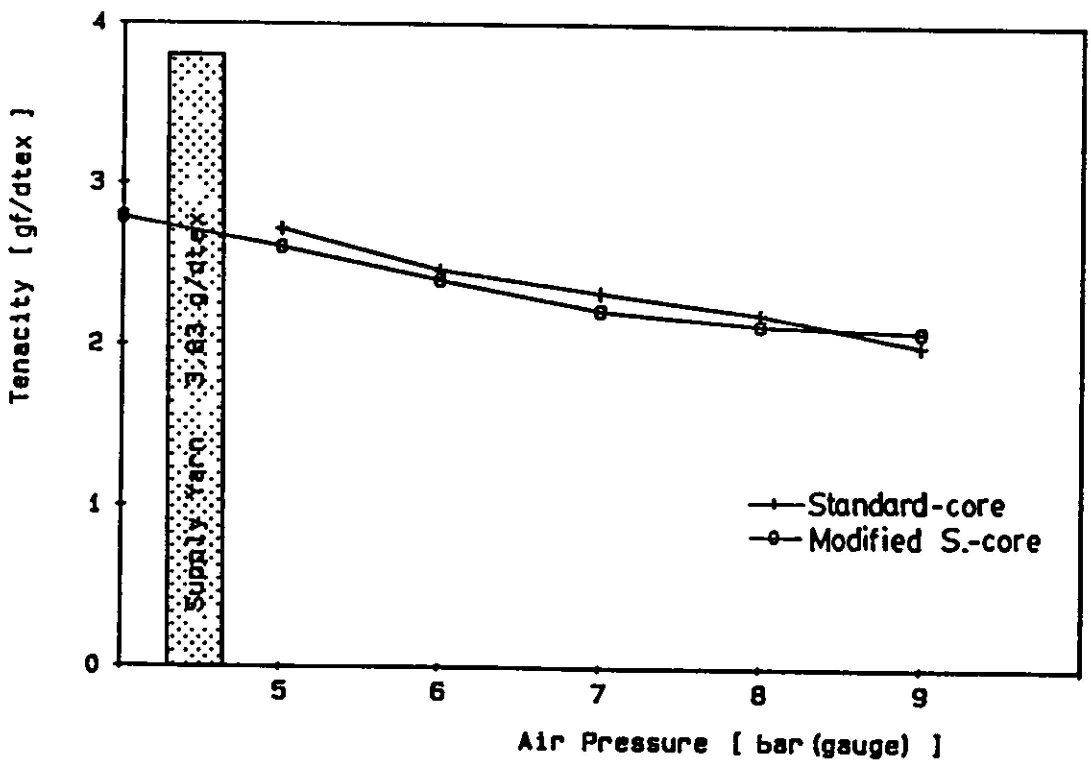

Figure 6.6d Comparison of the tenacity of yarns produced with the Standard-core HemaJet before and after the modification

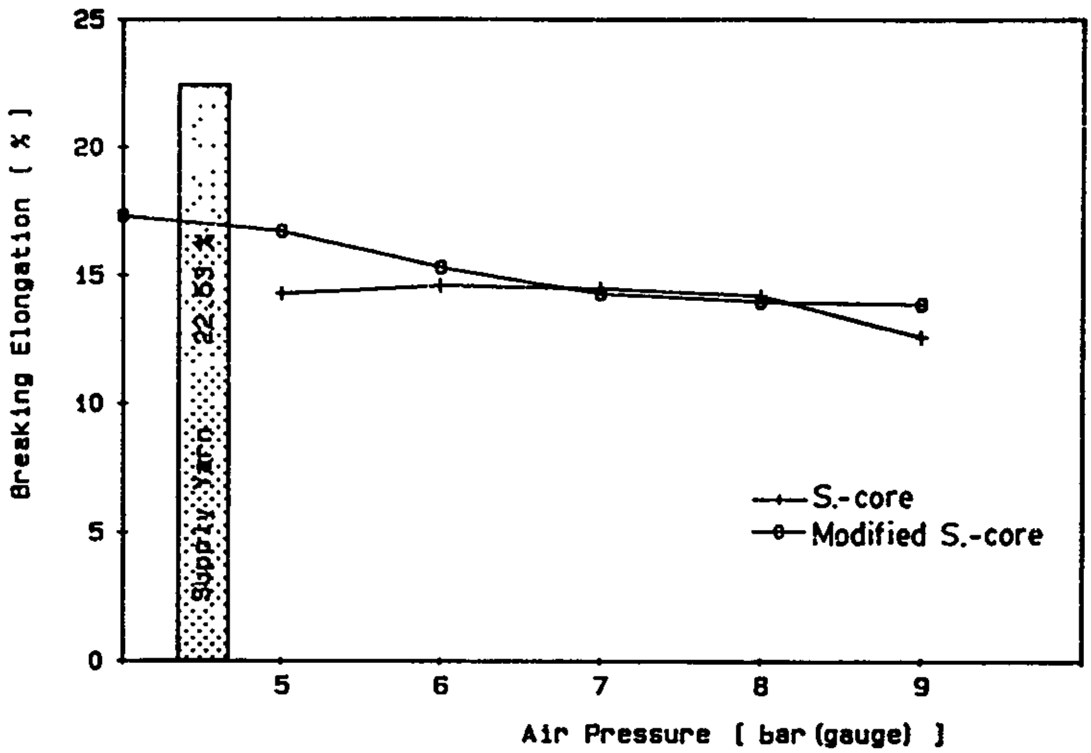

Figure 6.6e Comparison of the breaking elongation of yarns produced with the Standard-core HemaJet before and after the modification

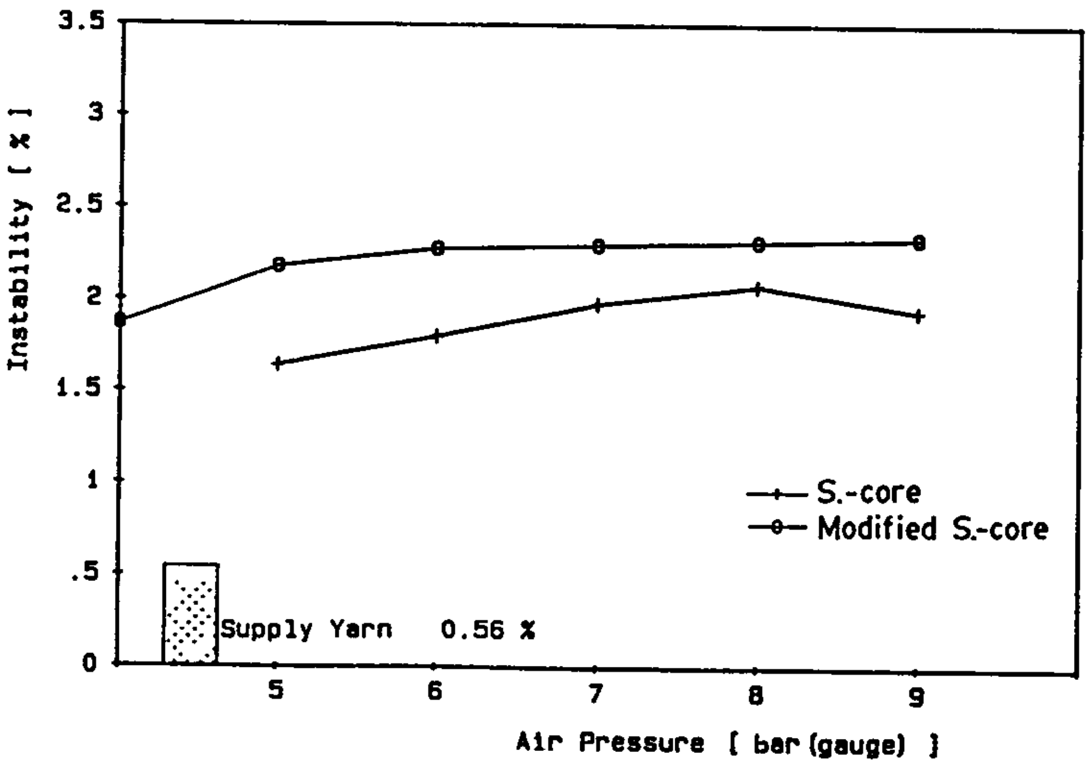

Figure 6.6f Comparison of the instability of yarns produced with the Standard-core HemaJet before and after the modification

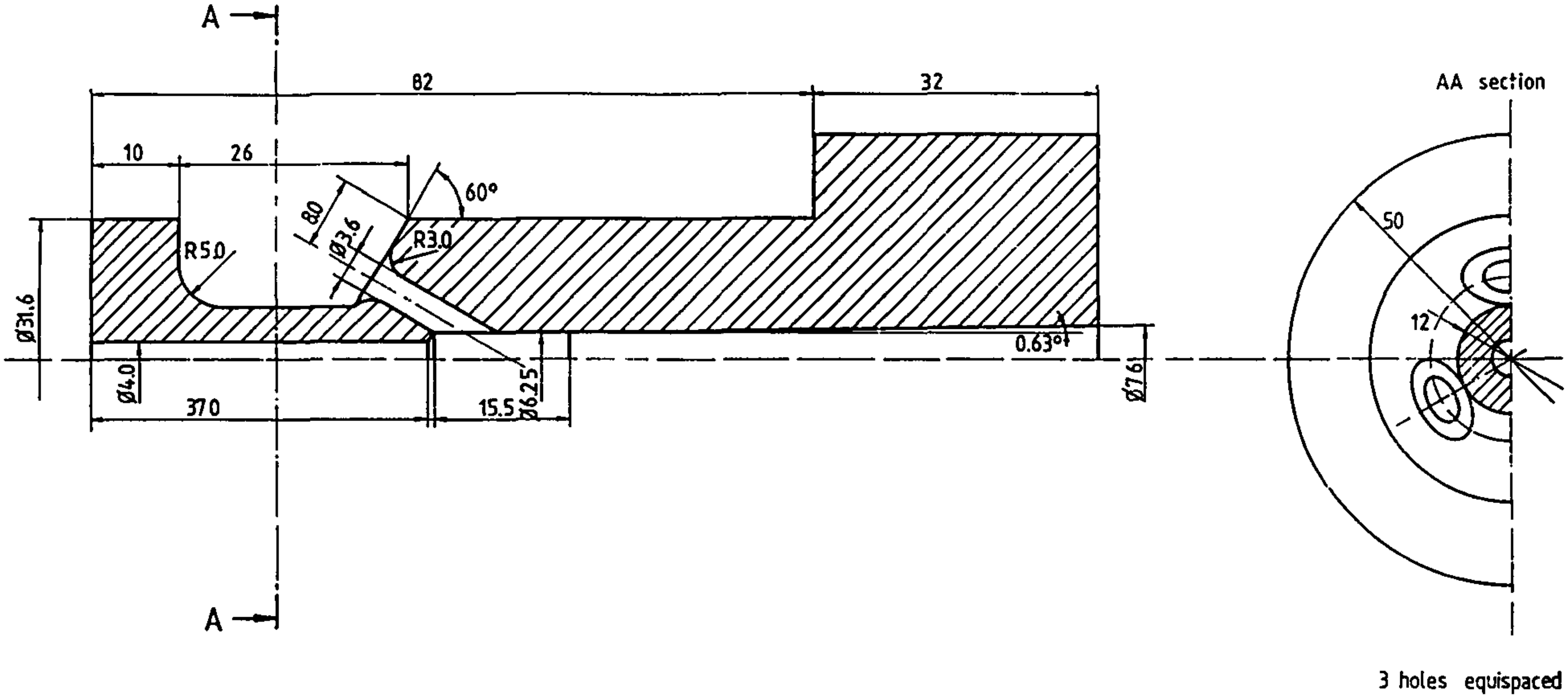

Figure 6.7a Technical drawing of the preliminary nozzle 1

A | AS DRAWN

ISSUE | DATE | MODIFICATION

THIS DRAWING IS THE PROPERTY OF LOUGHBOROUGH UNIVERSITY OF TECHNOLOGY
IT IS STRICTLY CONFIDENTIAL AND MUST NOT BE COPIED LOANED OR TRACED WITHOUT THEIR WRITTEN CONSENT.

1st ANGLE PROJECTION

ALL DIMENSIONS IN MILLIMETRES UNLESS OTHERWISE STATED

TOLERANCES
WHOLE NUMBERS ± 1 00
DECIMALS ± 0 10

SCALE 2:1

LOUGHBOROUGH UNIVERSITY OF TECHNOLOGY

DEPARTMENT OF MECHANICAL ENGINEERING

DRN A Devin | DATE 11.5.1986 | TITLE TEXTURING NOZZLE I

CHD | DATE

APP | DATE | DRAWING No ad p 1

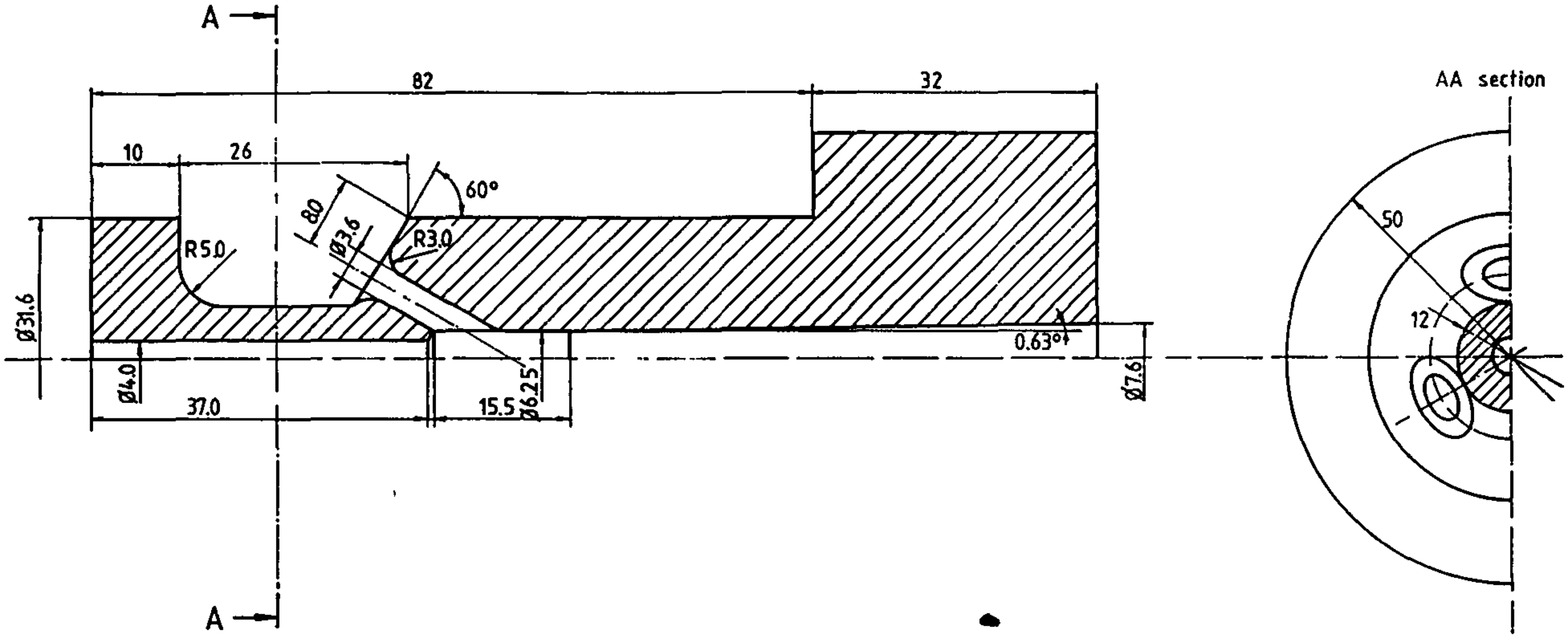

3 holes equispaced

ATTENTION: hole diameters 3.2, 3.6, 4.0 mm

Figure 6.7b Technical drawing of the preliminary nozzle 2

			THIS DRAWING IS THE PROPERTY OF LOUGHBOROUGH UNIVERSITY OF TECHNOLOGY IT IS STRICTLY CONFIDENTIAL AND MUST NOT BE COPIED LOANED OR TRACED WITHOUT THEIR WRITTEN CONSENT	ALL DIMENSIONS IN MILLIMETRES UNLESS OTHERWISE STATED	LOUGHBOROUGH UNIVERSITY OF TECHNOLOGY DEPARTMENT OF MECHANICAL ENGINEERING		
A		AS DRAWN		TOLERANCES WHOLE NUMBERS ± 1 00 DECIMALS ± 0 10	DRN A Devin CHD	DATE 11.5.1986 DATE	TITLE TEXTURING NOZZLE II
ISSUE	DATE	MODIFICATION	1st ANGLE PROJECTION	SCALE 2:1	APP	DATE -	DRAWING No ad p 2

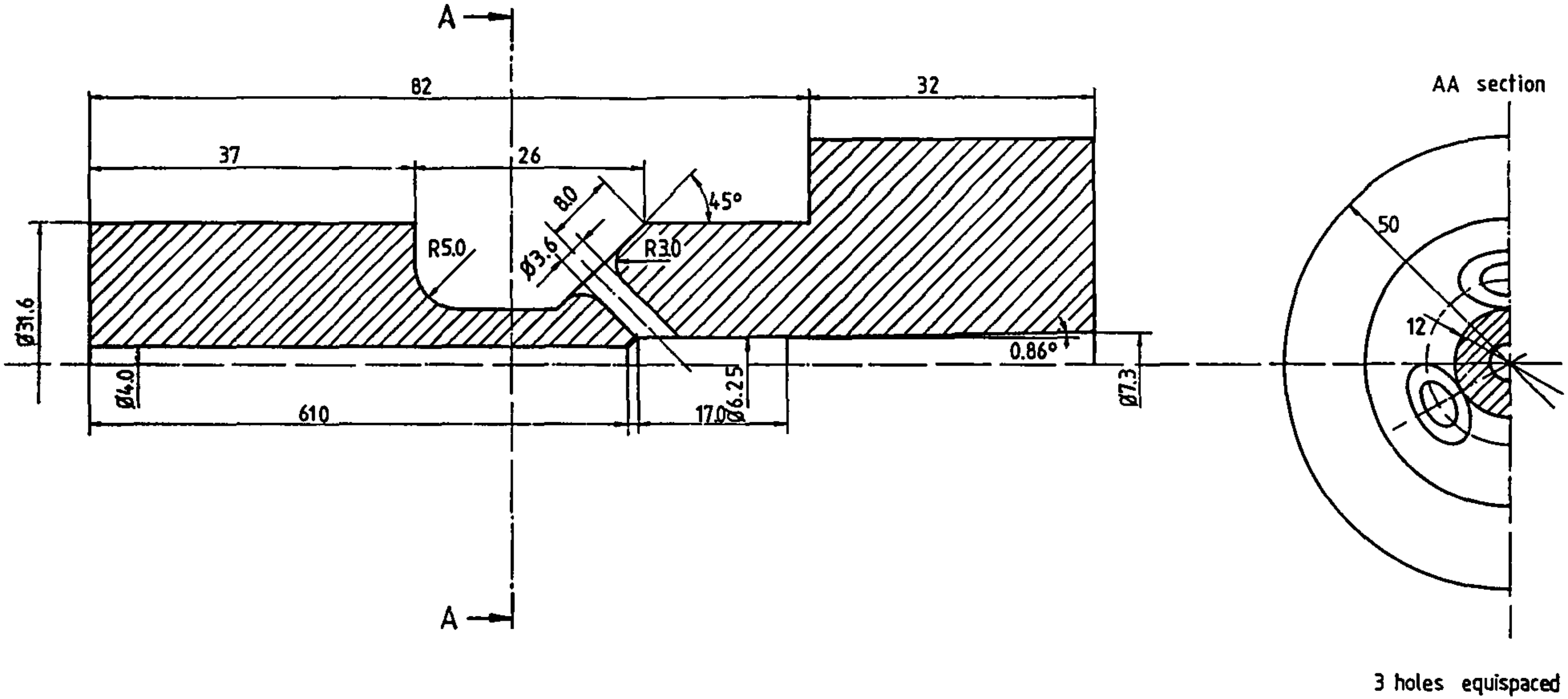

Figure 6.7c Technical drawing of the preliminary nozzle 3

ISSUE	DATE	MODIFICATION
A		AS DRAWN

THIS DRAWING IS THE PROPERTY OF LOUGHBOROUGH UNIVERSITY OF TECHNOLOGY
IT IS STRICTLY CONFIDENTIAL AND MUST NOT BE COPIED LOANED OR TRACED WITHOUT THEIR WRITTEN CONSENT.

1st ANGLE PROJECTION

ALL DIMENSIONS IN MILLIMETRES UNLESS OTHERWISE STATED

TOLERANCES
WHOLE NUMBERS ± 1 00
DECIMALS ± 0 10

SCALE 2:1

LOUGHBOROUGH UNIVERSITY OF TECHNOLOGY
DEPARTMENT OF MECHANICAL ENGINEERING

DRN A·Devin DATE 11 5.1986
CHD DATE
APP DATE

TITLE TEXTURING NOZZLE III

DRAWING No. ad.p 3

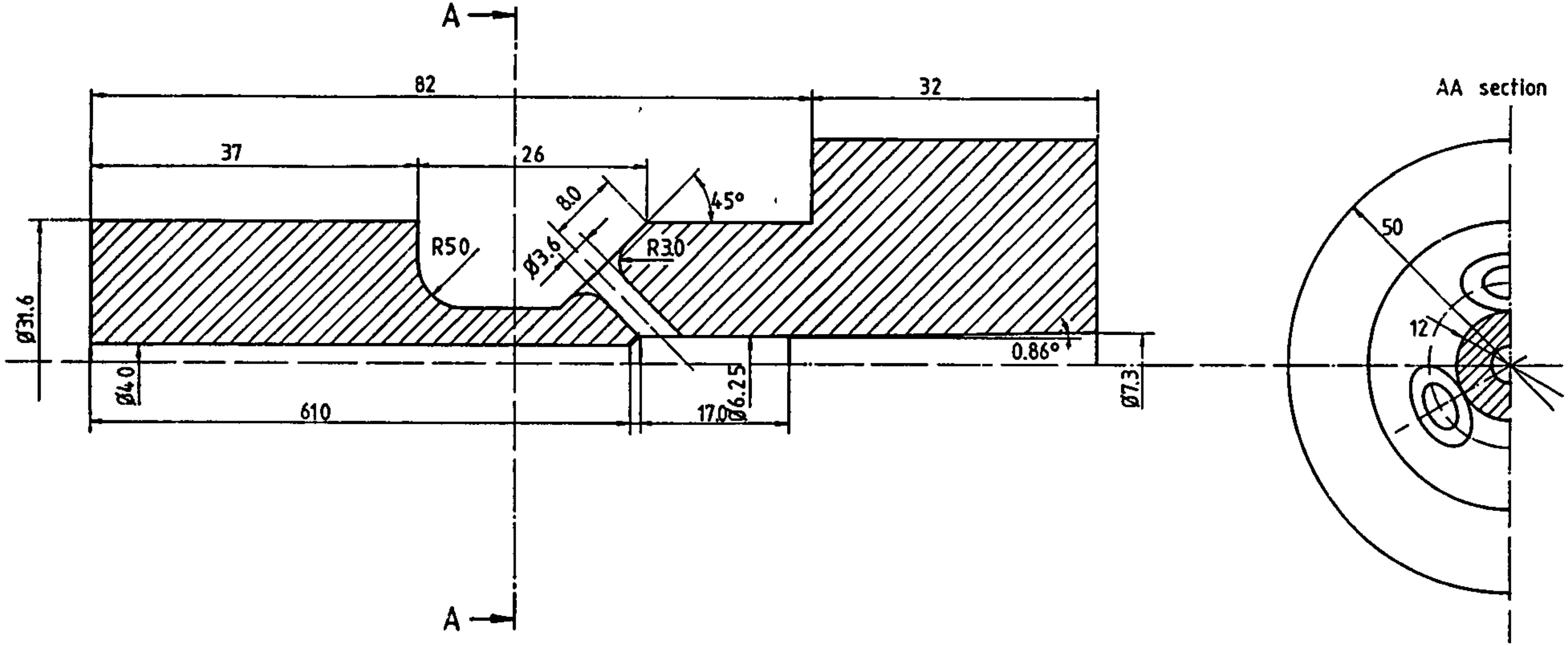

3 holes equispaced

ATTENTION: hole diameters 3.2, 3.6, 4.0 mm

Figure 6.7d Technical drawing of the preliminary nozzle 4

ISSUE	DATE	MODIFICATION					
A		AS DRAWN	THIS DRAWING IS THE PROPERTY OF LOUGHBOROUGH UNIVERSITY OF TECHNOLOGY IT IS STRICTLY CONFIDENTIAL AND MUST NOT BE COPIED LOANED OR TRACED WITHOUT THEIR WRITTEN CONSENT	ALL DIMENSIONS IN MILLIMETRES UNLESS OTHERWISE STATED	LOUGHBOROUGH UNIVERSITY OF TECHNOLOGY		
				TOLERANCES WHOLE NUMBERS ± 1.00 DECIMALS ± 0.10	DEPARTMENT OF MECHANICAL ENGINEERING		
					DRN A. Dewin	DATE 11.5.1986	TITLE TEXTURING NOZZLE IV
					CHD	DATE	
			1st ANGLE PROJECTION	SCALE 2:1	APP	DATE	DRAWING No ad p4

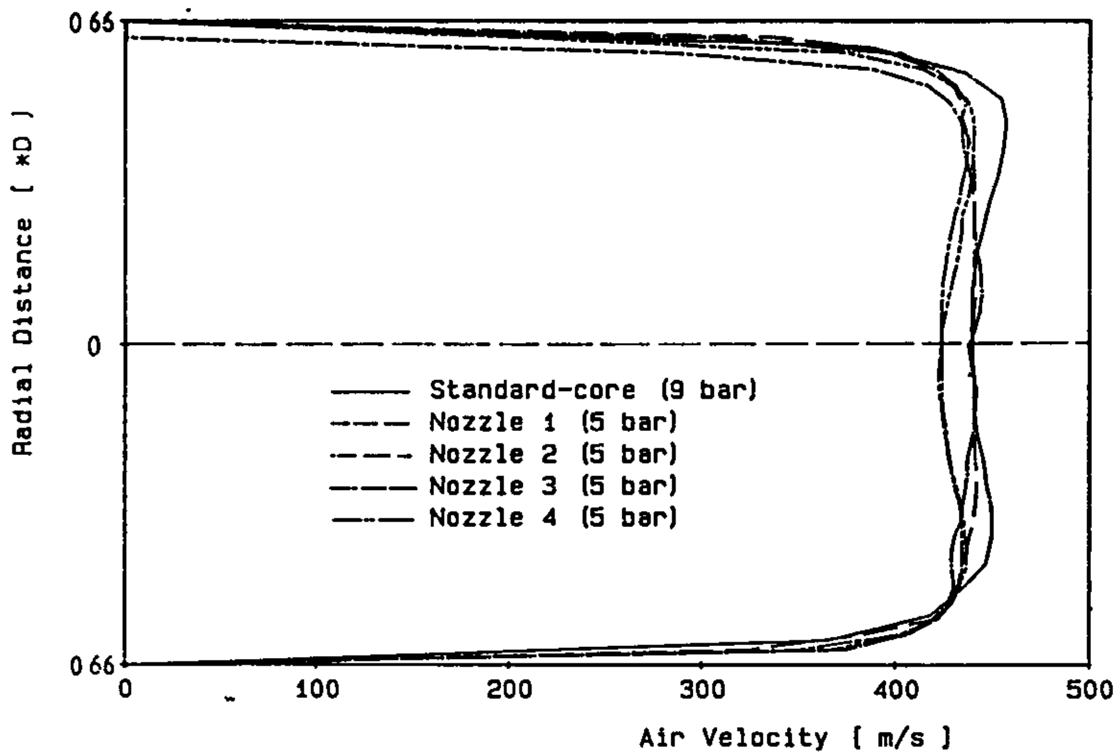

Figure 6.8a Traverse velocity distribution of the primary flows created by the preliminary nozzles 1 to 4

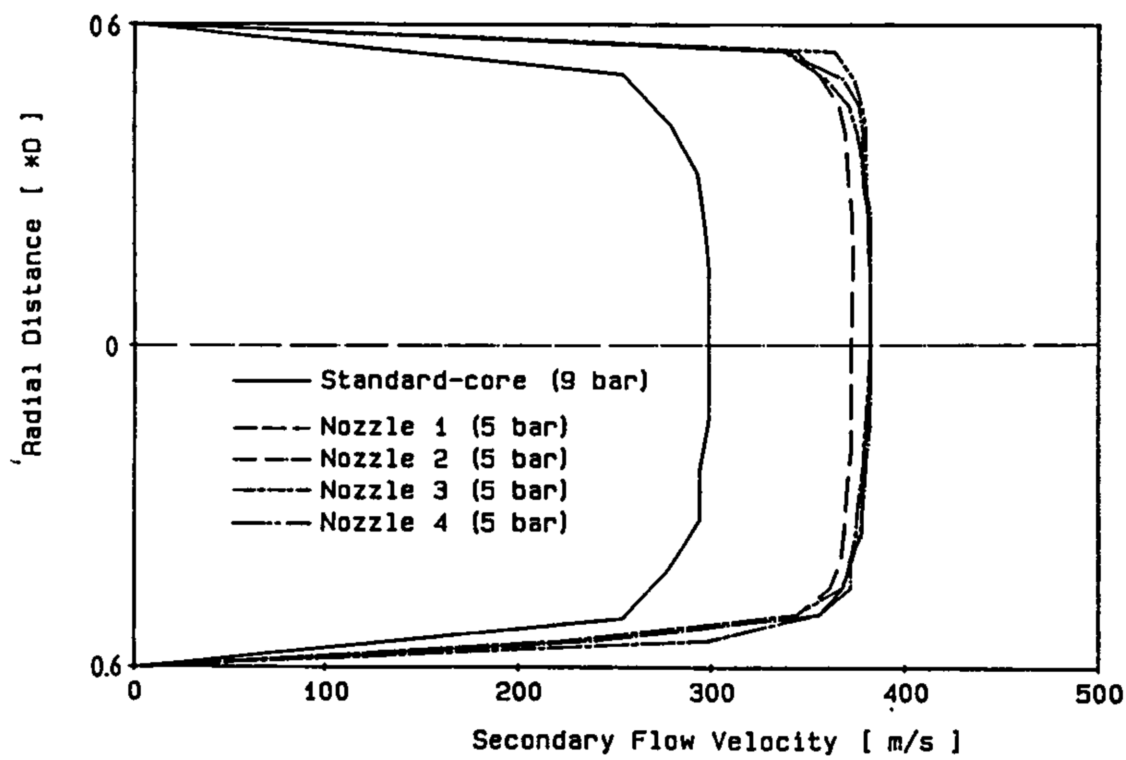

Figure 6.8b Secondary flow velocity distributions created by the preliminary nozzles 1 to 4

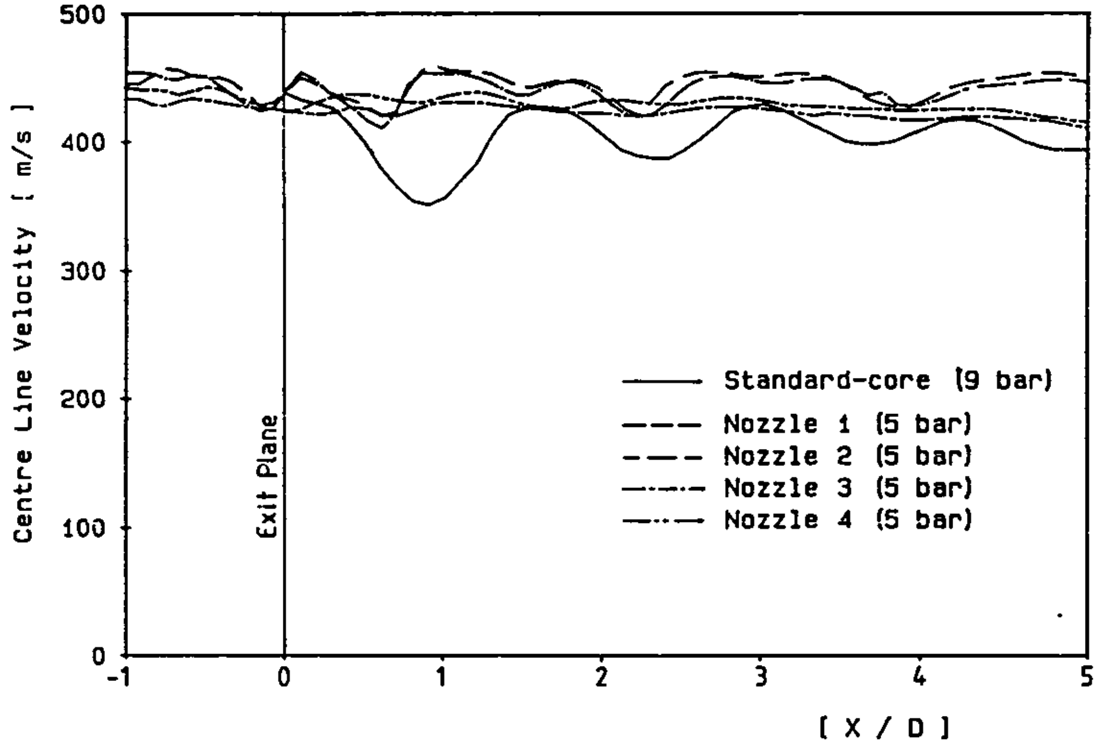

Figure 6.8c Centre line velocities created by the preliminary nozzles 1 to 4

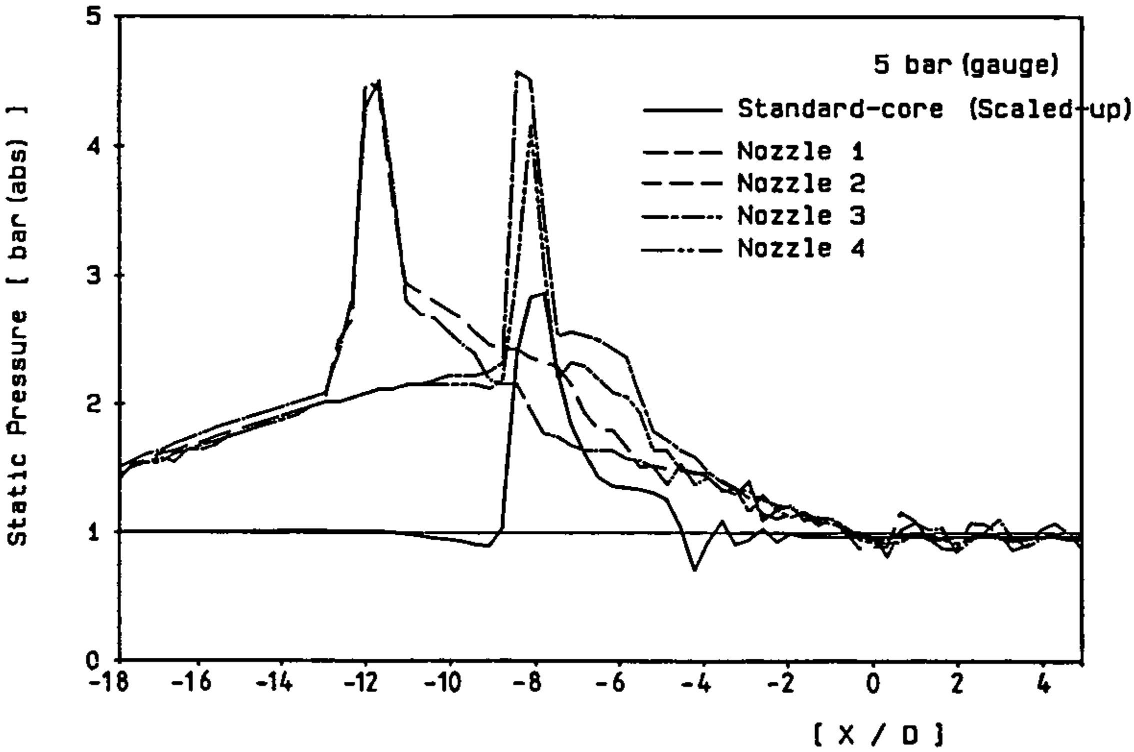

Figure 6.8d Static pressure distribution along the preliminary nozzles' centre-lines

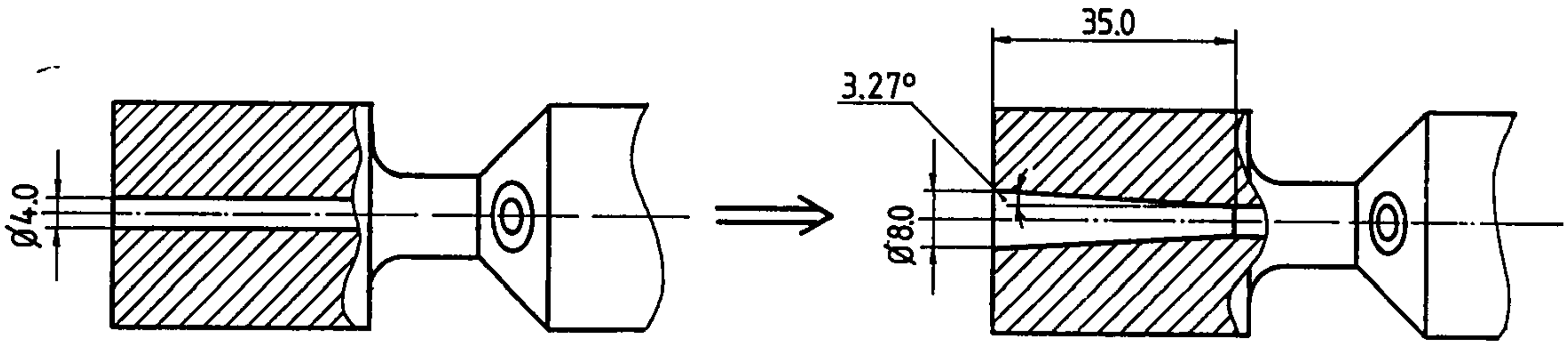

Figure 6.9 The modification of the secondary flow channel

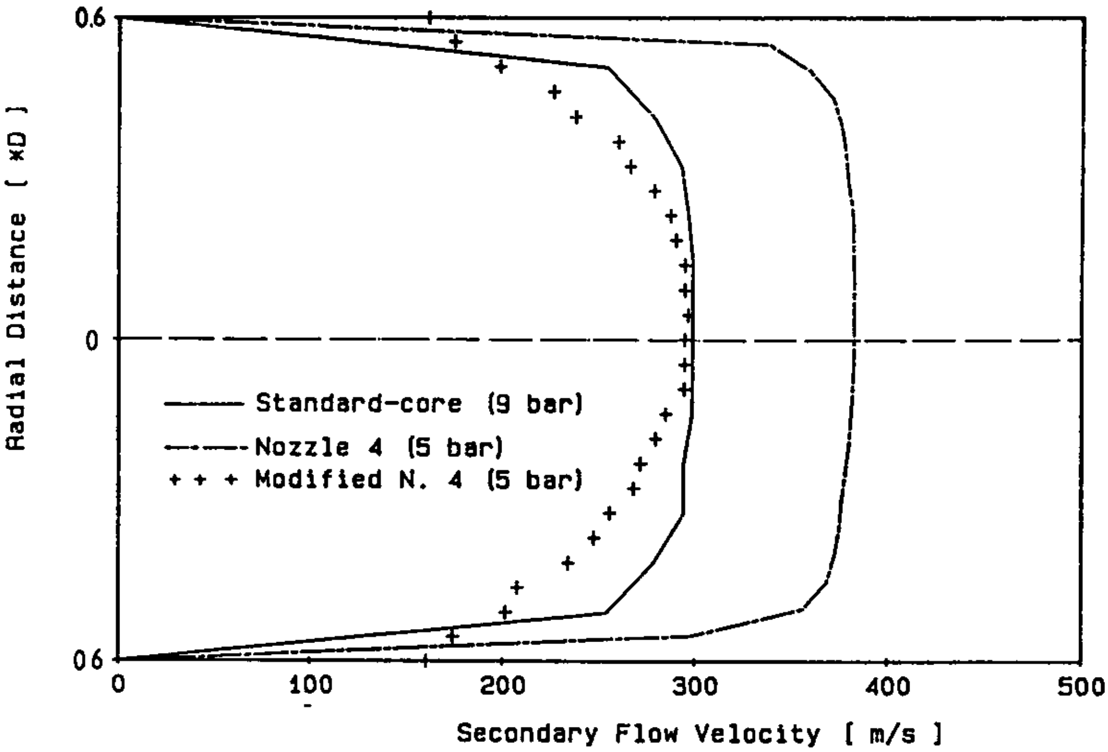

Figure 6.10a Traverse velocity distribution of the secondary flow of Nozzle 4 before and after modification

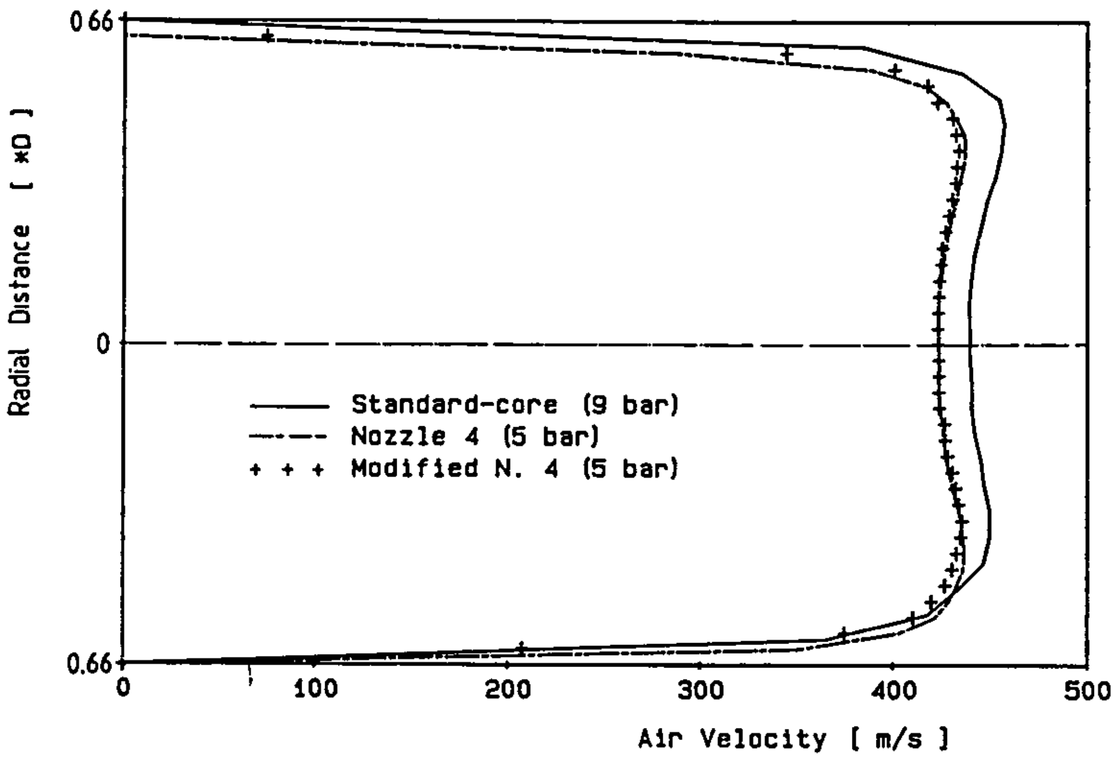

Figure 6.10b Traverse velocity distribution of the primary flow of Nozzle 4 before and after the modification

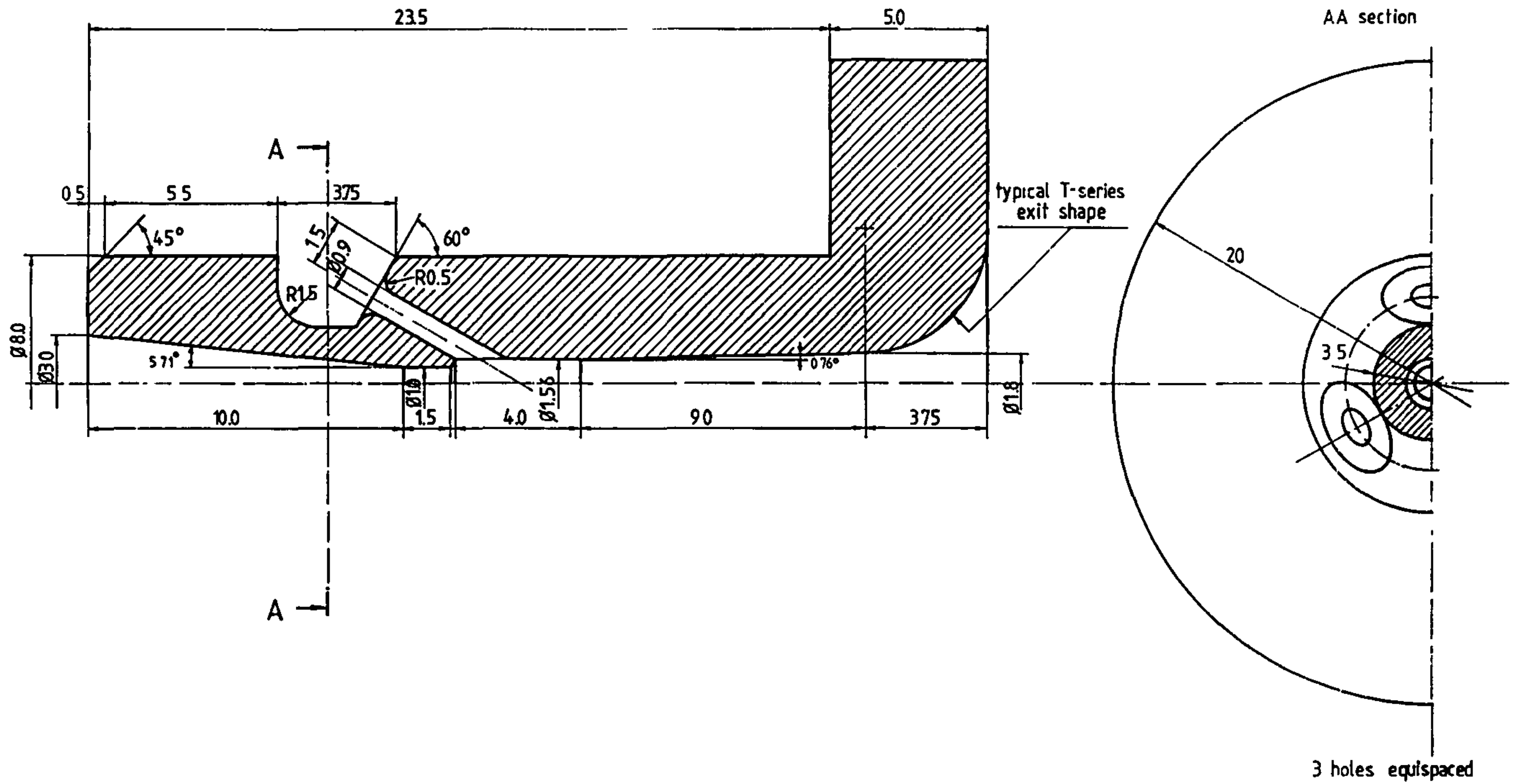

Figure 6.11a Technical drawing of prototype nozzle 1

ISSUE	DATE	MODIFICATION					
A		AS DRAWN	THIS DRAWING IS THE PROPERTY OF LOUGHBOROUGH UNIVERSITY OF TECHNOLOGY IT IS STRICTLY CONFIDENTIAL AND MUST NOT BE COPIED LOANED OR TRACED WITHOUT THEIR WRITTEN CONSENT.	ALL DIMENSIONS IN MILLIMETRES UNLESS OTHERWISE STATED.	LOUGHBOROUGH UNIVERSITY OF TECHNOLOGY		
				TOLERANCES WHOLE NUMBERS ± 1·00 DECIMALS ± 0 10	DEPARTMENT OF MECHANICAL ENGINEERING		
					DRN A. Dewin	DATE 21.7.86	TITLE TEXTURING JET I
					CHD	DATE	
			1ST ANGLE PROJECTION	SCALE 8:1	APP	DATE	DRAWING No. ad 1

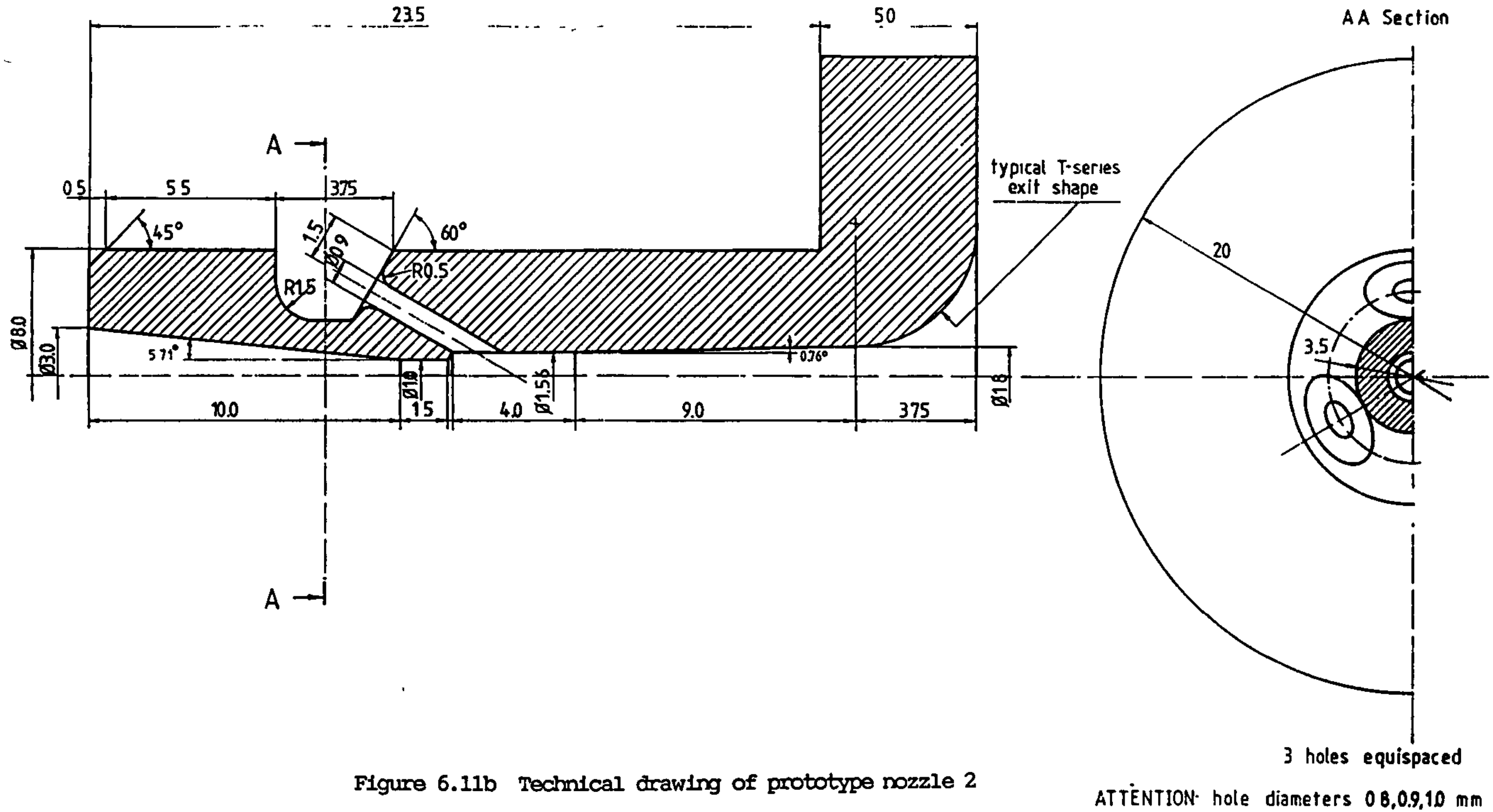

Figure 6.11b Technical drawing of prototype nozzle 2

ISSUE	DATE	MODIFICATION
A		AS DRAWN

THIS DRAWING IS THE PROPERTY OF LOUGHBOROUGH UNIVERSITY OF TECHNOLOGY IT IS STRICTLY CONFIDENTIAL AND MUST NOT BE COPIED LOANED OR TRACED WITHOUT THEIR WRITTEN CONSENT.

1st ANGLE PROJECTION

ALL DIMENSIONS IN MILLIMETRES UNLESS OTHERWISE STATED

TOLERANCES
WHOLE NUMBERS ± 1.00
DECIMALS ± 0.10

SCALE 8:1

LOUGHBOROUGH UNIVERSITY OF TECHNOLOGY
DEPARTMENT OF MECHANICAL ENGINEERING

DRN A. Demir	DATE 21.7.1986	TITLE TEXTURING JET II
CHD	DATE	
APP	DATE	DRAWING No. ad 2

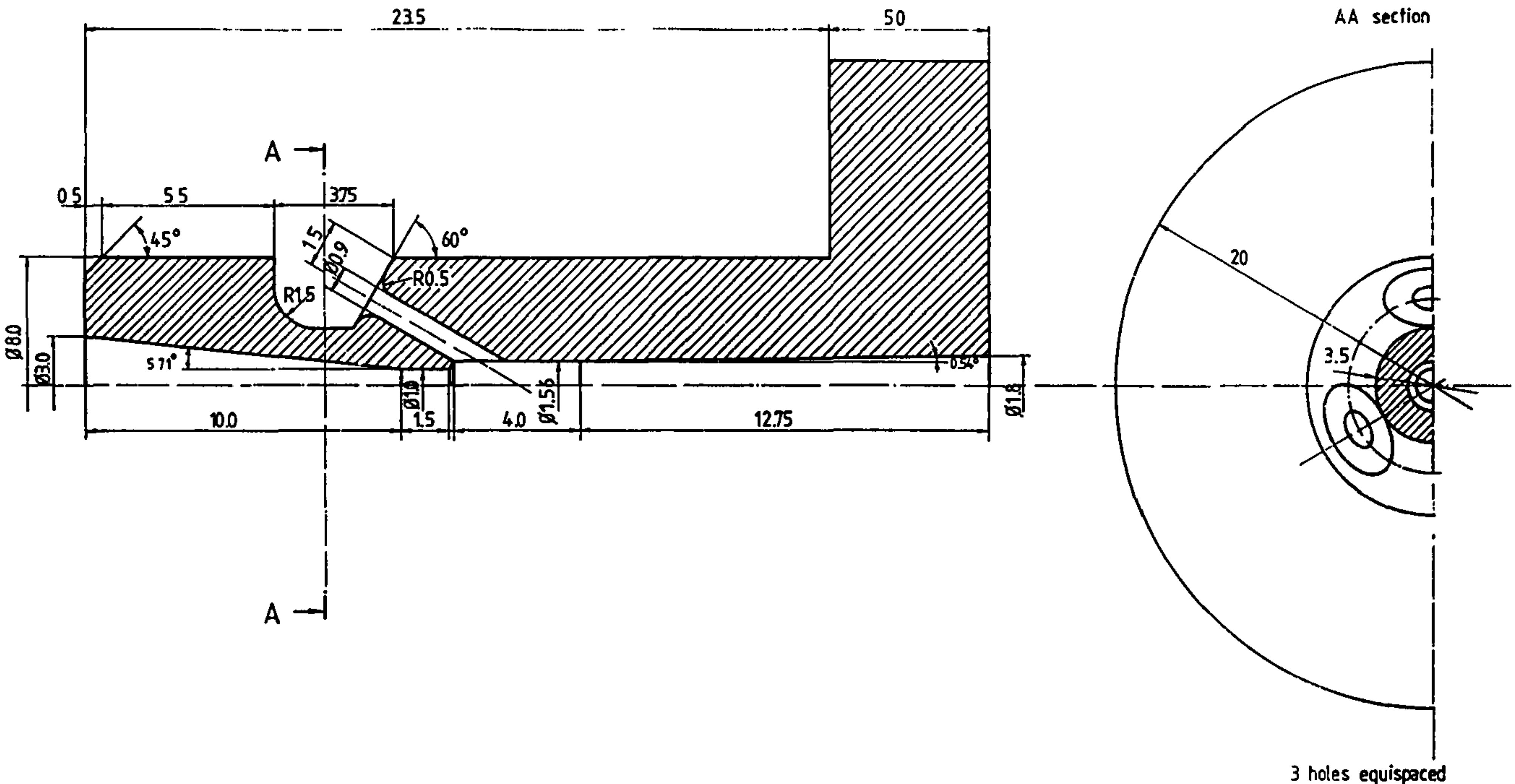

Figure 6.11c Technical drawing of prototype nozzle 3

ISSUE	DATE	MODIFICATION
A		AS DRAWN

THIS DRAWING IS THE PROPERTY OF LOUGHBOROUGH UNIVERSITY OF TECHNOLOGY IT IS STRICTLY CONFIDENTIAL AND MUST NOT BE COPIED LOANED OR TRACED WITHOUT THEIR WRITTEN CONSENT.

1st ANGLE PROJECTION

ALL DIMENSIONS IN MILLIMETRES UNLESS OTHERWISE STATED.

TOLERANCES
WHOLE NUMBERS ± 1.00
DECIMALS ± 0.10

SCALE 8:1

LOUGHBOROUGH UNIVERSITY OF TECHNOLOGY

DEPARTMENT OF MECHANICAL ENGINEERING

DRN A. Davis — DATE 21.7.1986
CHD — DATE
APP — DATE

TITLE TEXTURING JET III

DRAWING No. ad 3

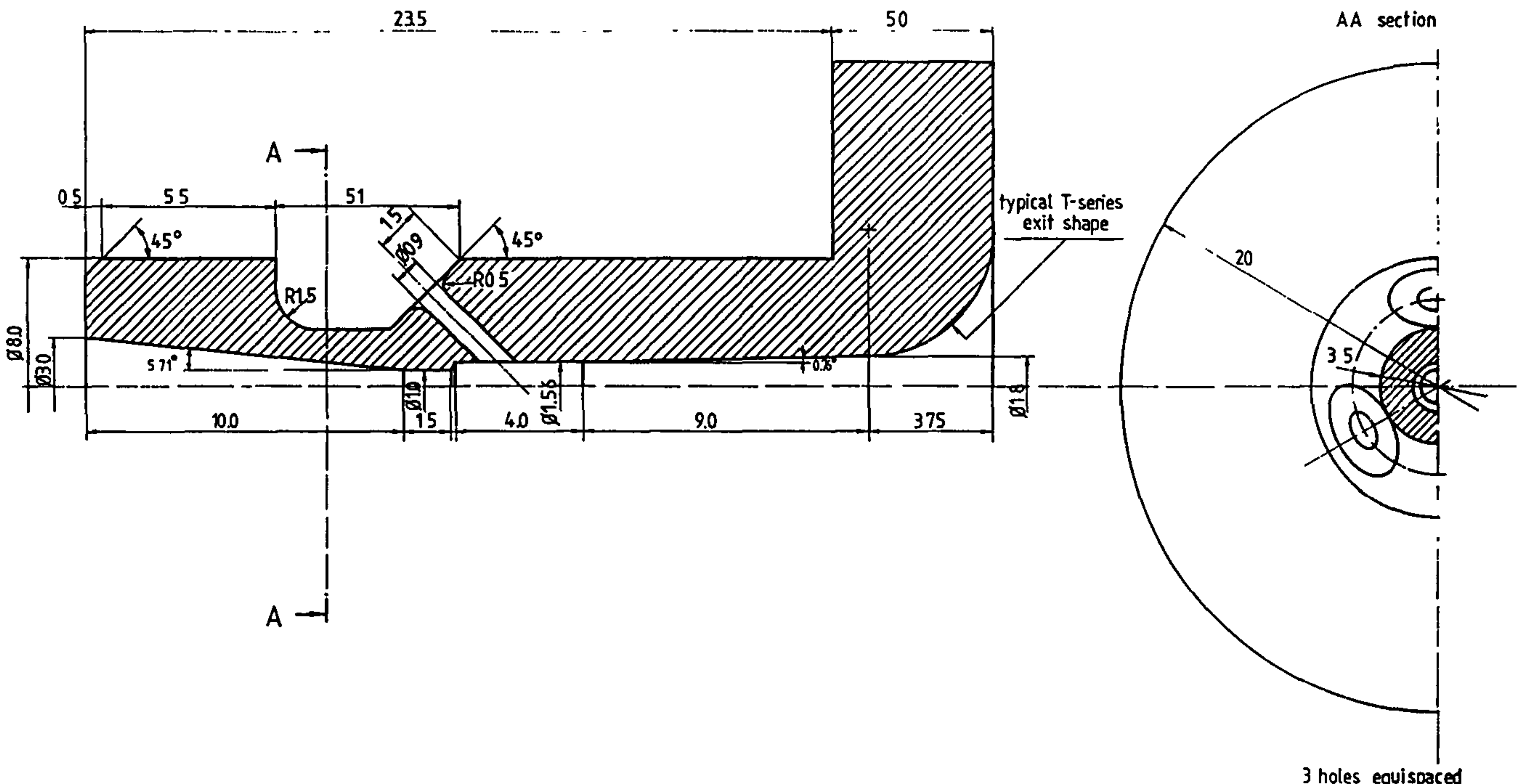

Figure 6.11d Technical drawing of prototype nozzle 4

A		AS DRAWN	THIS DRAWING IS THE PROPERTY OF LOUGHBOROUGH UNIVERSITY OF TECHNOLOGY IT IS STRICTLY CONFIDENTIAL AND MUST NOT BE COPIED LOANED OR TRACED WITHOUT THEIR WRITTEN CONSENT.	ALL DIMENSIONS IN MILLIMETRES UNLESS OTHERWISE STATED	LOUGHBOROUGH UNIVERSITY OF TECHNOLOGY		
				TOLERANCES WHOLE NUMBERS ± 1·00 DECIMALS ± 0 10	DEPARTMENT OF MECHANICAL ENGINEERING		
					DRN A·Demir	DATE 21·7·1986	TITLE TEXTURING JET IV
					CHD	DATE	
ISSUE	DATE	MODIFICATION	1st ANGLE PROJECTION	SCALE 8:1	APP	DATE	DRAWING No ad 4

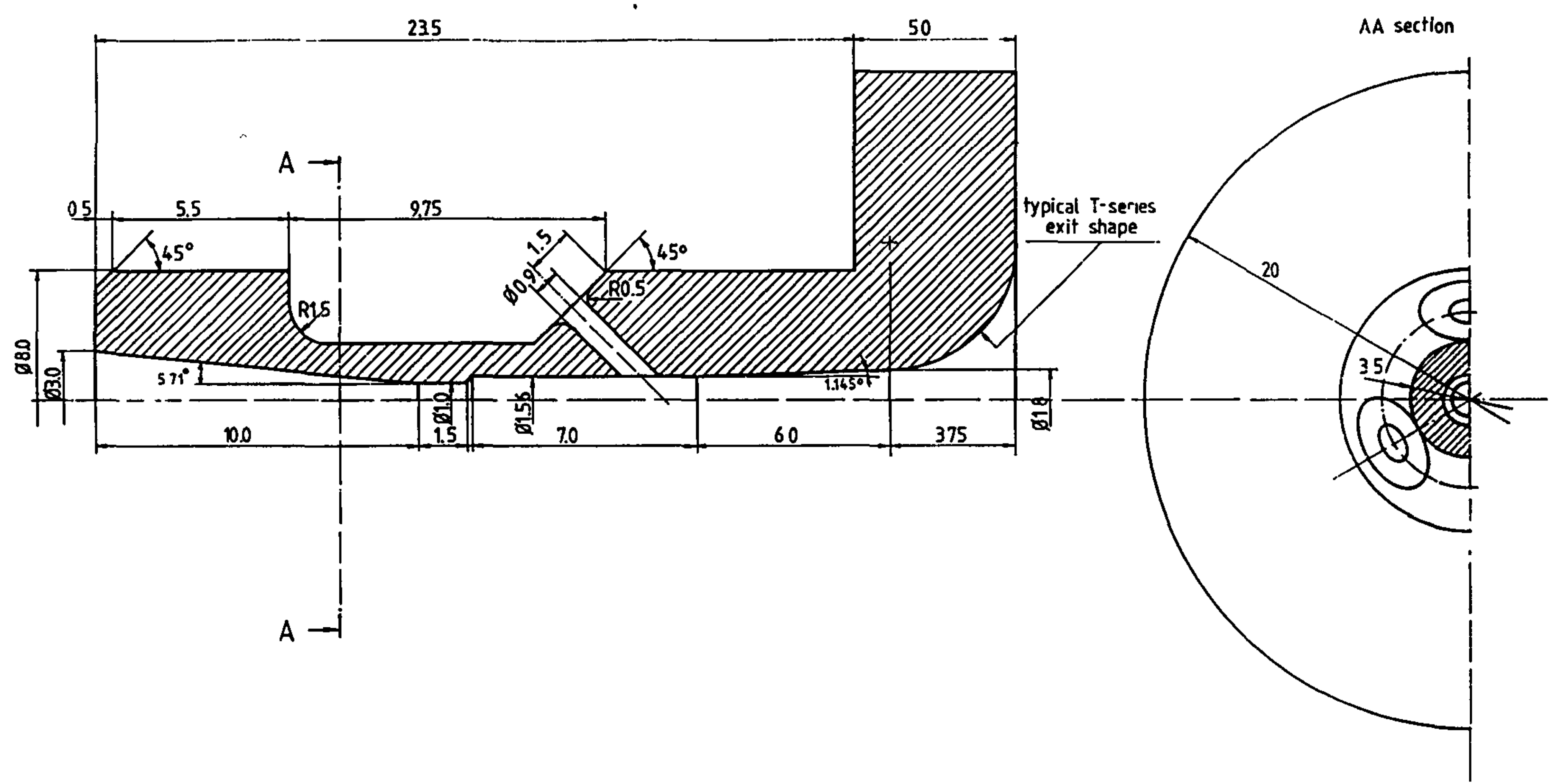

Figure 6.11e Technical drawing of prototype nozzle 5

ISSUE	DATE	MODIFICATION
A		AS DRAWN

THIS DRAWING IS THE PROPERTY OF LOUGHBOROUGH UNIVERSITY OF TECHNOLOGY
IT IS STRICTLY CONFIDENTIAL AND MUST NOT BE COPIED LOANED OR TRACED WITHOUT THEIR WRITTEN CONSENT.

1st ANGLE PROJECTION

ALL DIMENSIONS IN MILLIMETRES UNLESS OTHERWISE STATED.

TOLERANCES
WHOLE NUMBERS ± 1.00
DECIMALS ± 0.10

SCALE 8:1

LOUGHBOROUGH UNIVERSITY OF TECHNOLOGY
DEPARTMENT OF MECHANICAL ENGINEERING

DRN A. Dawin	DATE 21.7.1986	TITLE	TEXTURING JET V
CHD	DATE		
APP	DATE	DRAWING No	ad 5

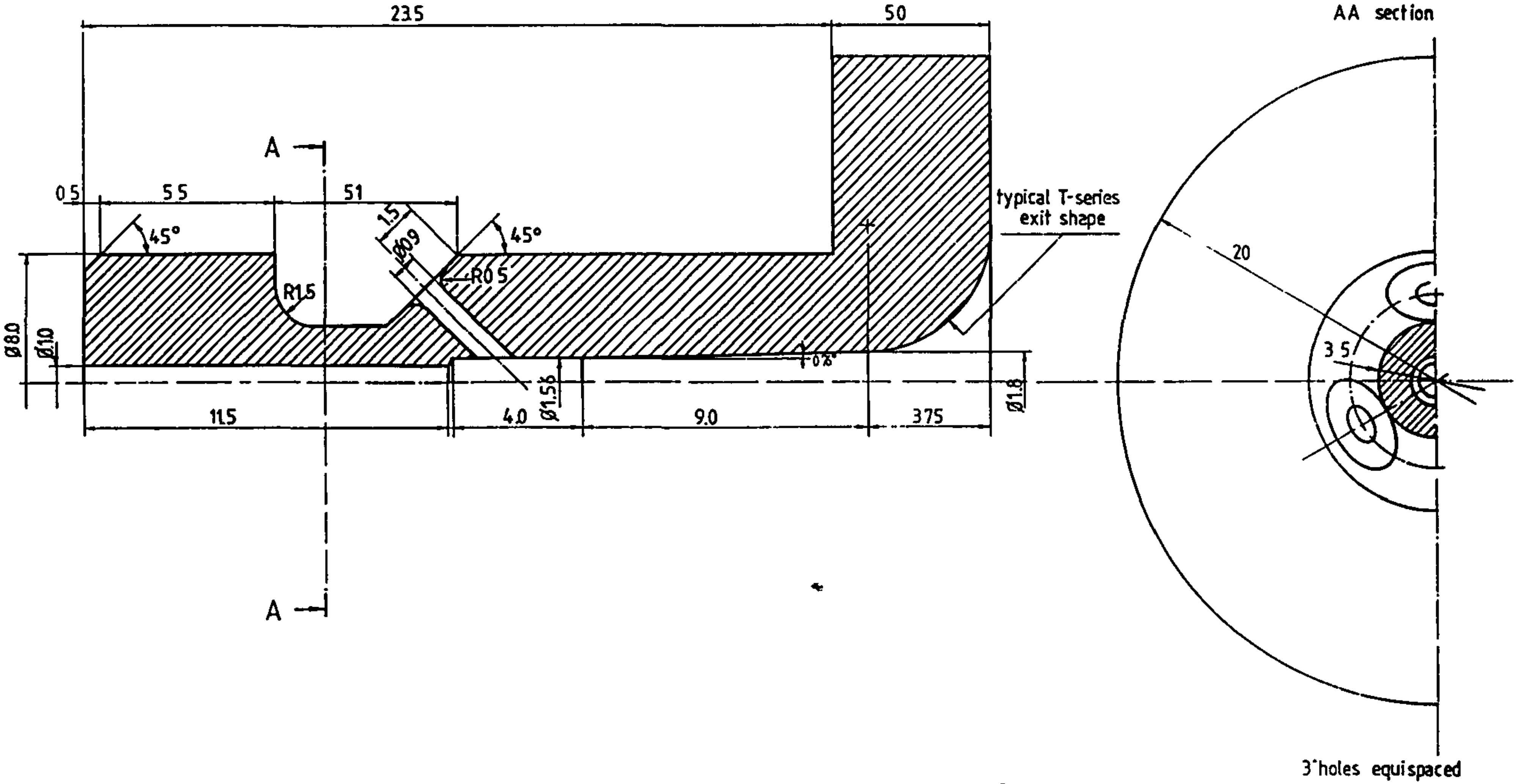

Figure 6.11f Technical drawing of prototype nozzle 6

ISSUE	DATE	MODIFICATION
A		AS DRAWN

THIS DRAWING IS THE PROPERTY OF LOUGHBOROUGH UNIVERSITY OF TECHNOLOGY
IT IS STRICTLY CONFIDENTIAL AND MUST NOT BE COPIED LOANED OR TRACED WITHOUT THEIR WRITTEN CONSENT.

1st ANGLE PROJECTION

ALL DIMENSIONS IN MILLIMETRES UNLESS OTHERWISE STATED

TOLERANCES
WHOLE NUMBERS ± 1 00
DECIMALS ± 0 10

SCALE 8 1

LOUGHBOROUGH UNIVERSITY OF TECHNOLOGY
DEPARTMENT OF MECHANICAL ENGINEERING

DRN A Demir DATE 21.7.1986
CHD DATE
APP DATE

TITLE TEXTURING JET VI

DRAWING No ad 6

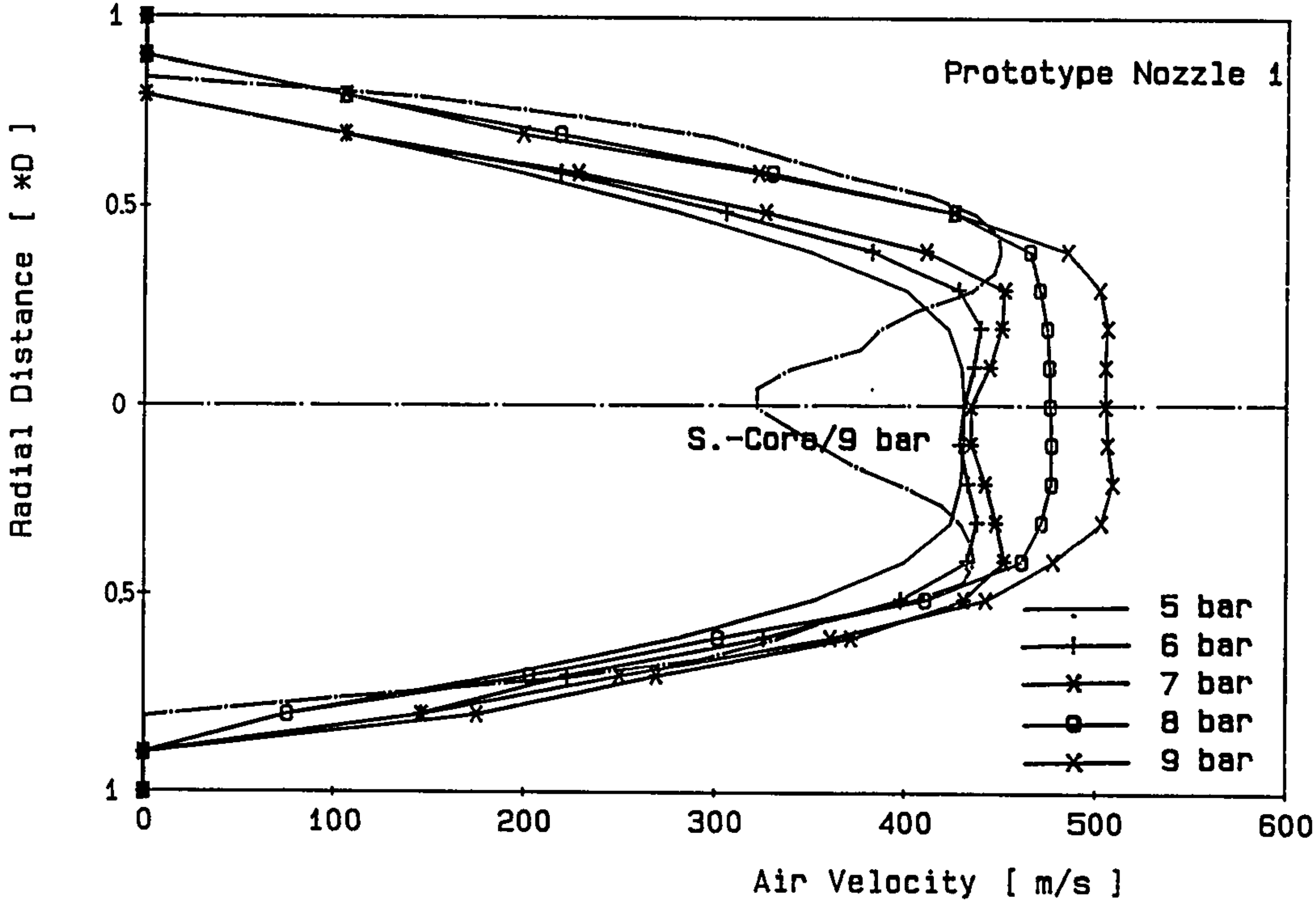

Figure 6.12a Axial air velocity distribution at the exit plane of the prototype nozzle 1

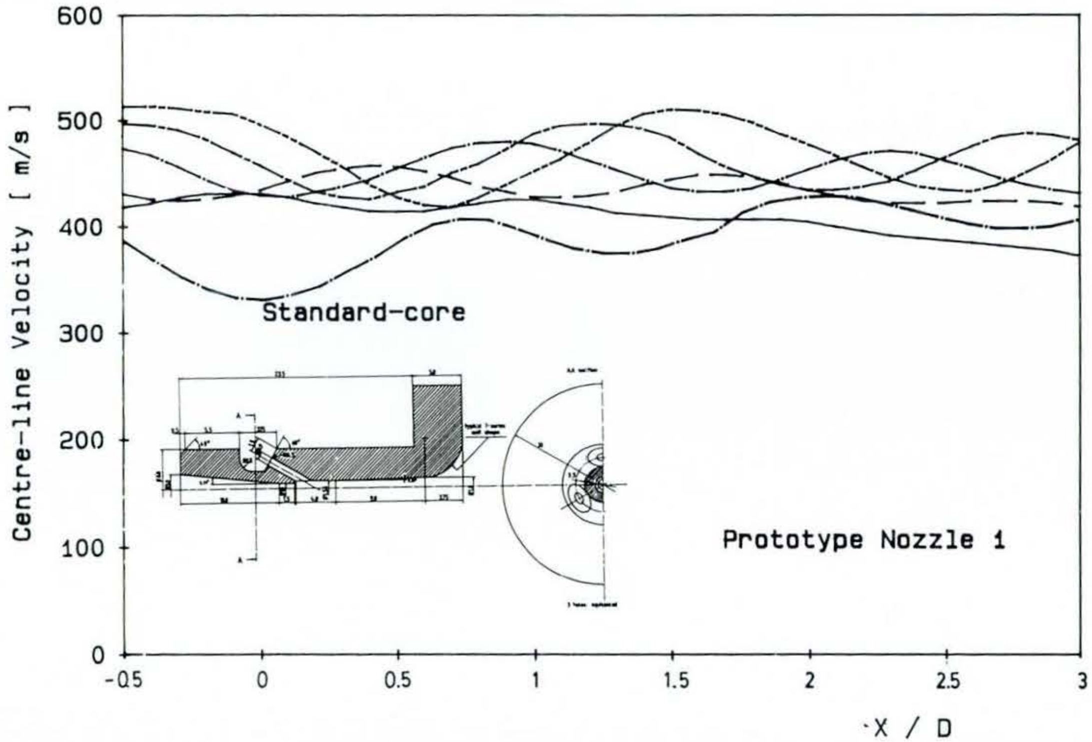

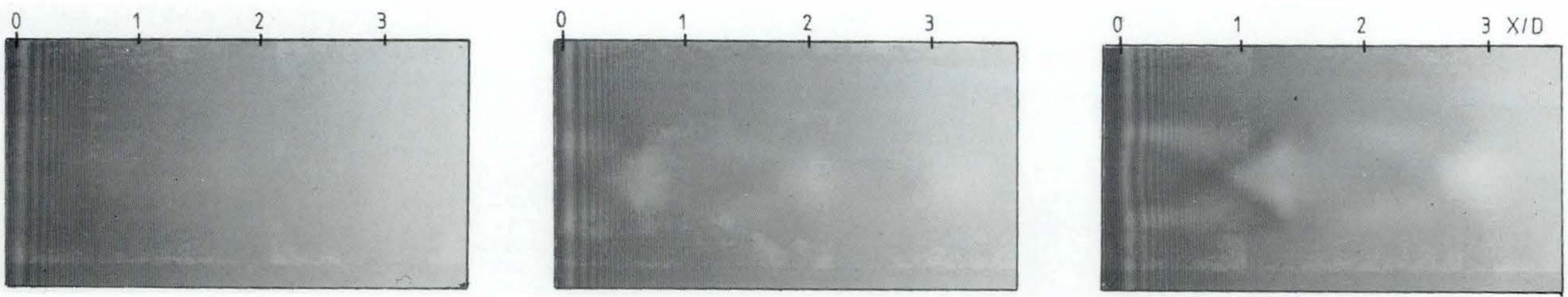

P_o= 5 bar

P_o= 7 bar

P_o= 9 bar

Figure 6.12b Centre-line velocity fluctuations and shadowgraphs of the air-jets created by the prototype nozzle 1

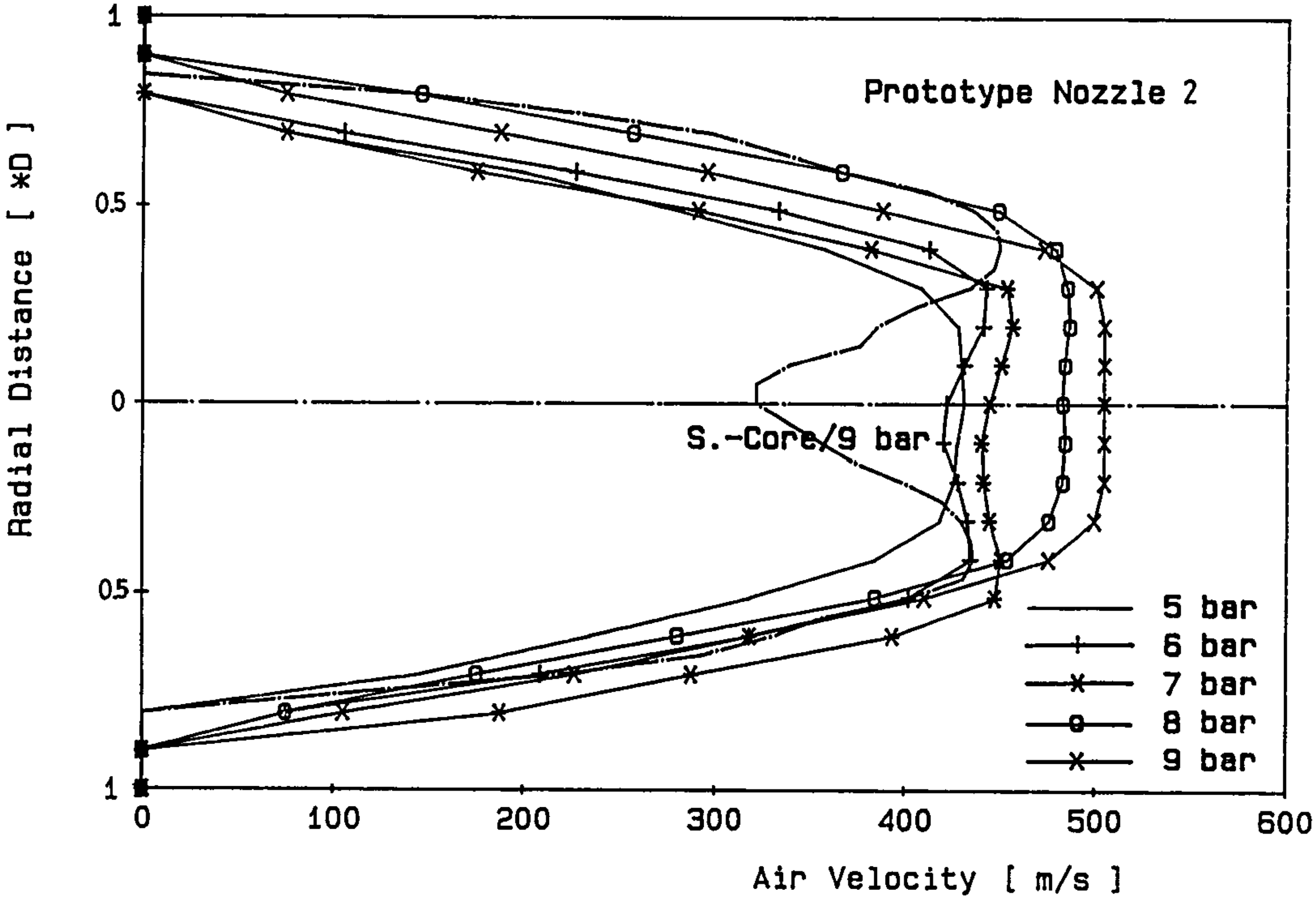

Figure 6.13a Axial air velocity distribution at the exit plane of the prototype nozzle 2

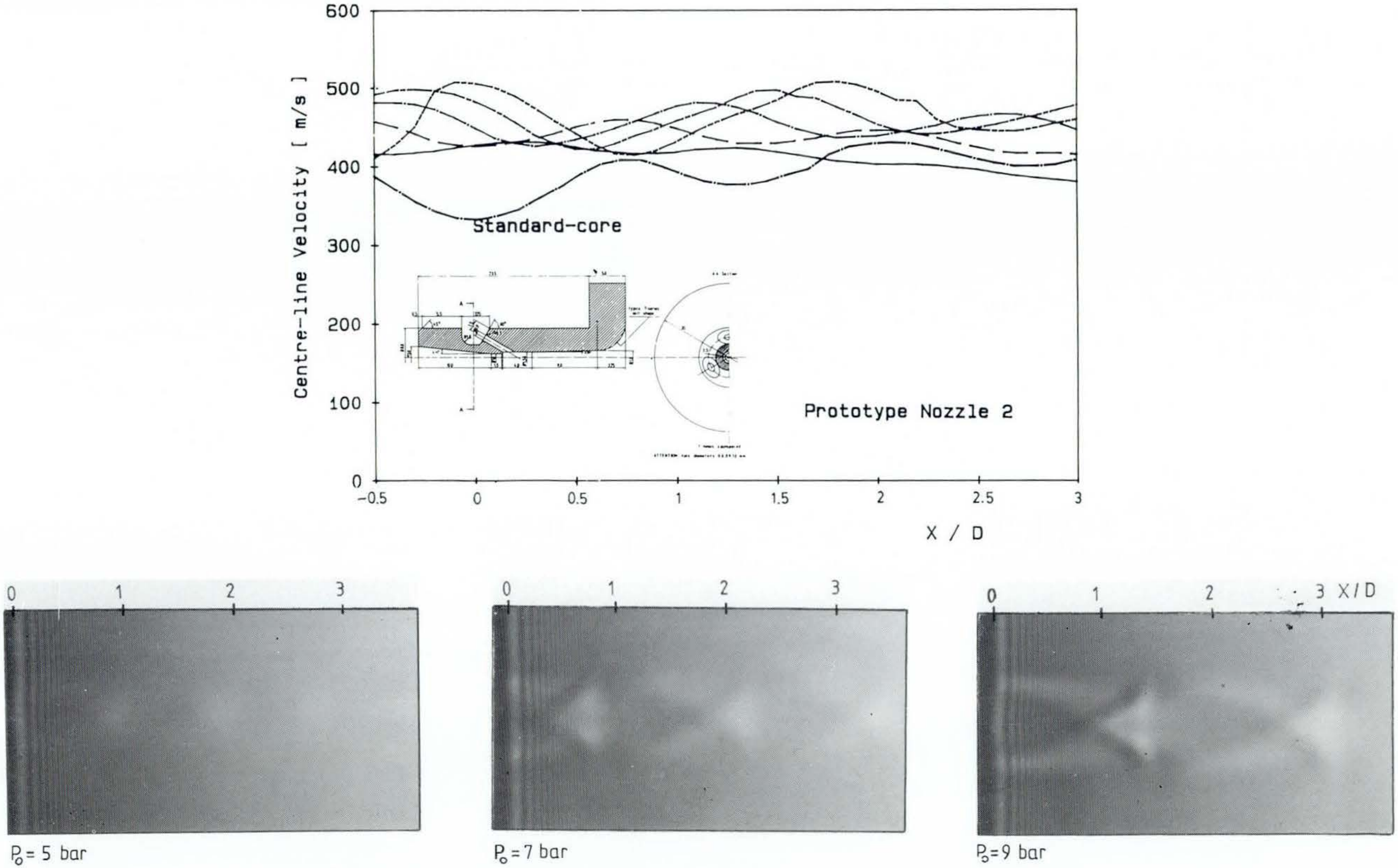

Figure 6.13b Centre-line velocity fluctuations and shadowgraphs of the air-jets created by the prototype nozzle 2

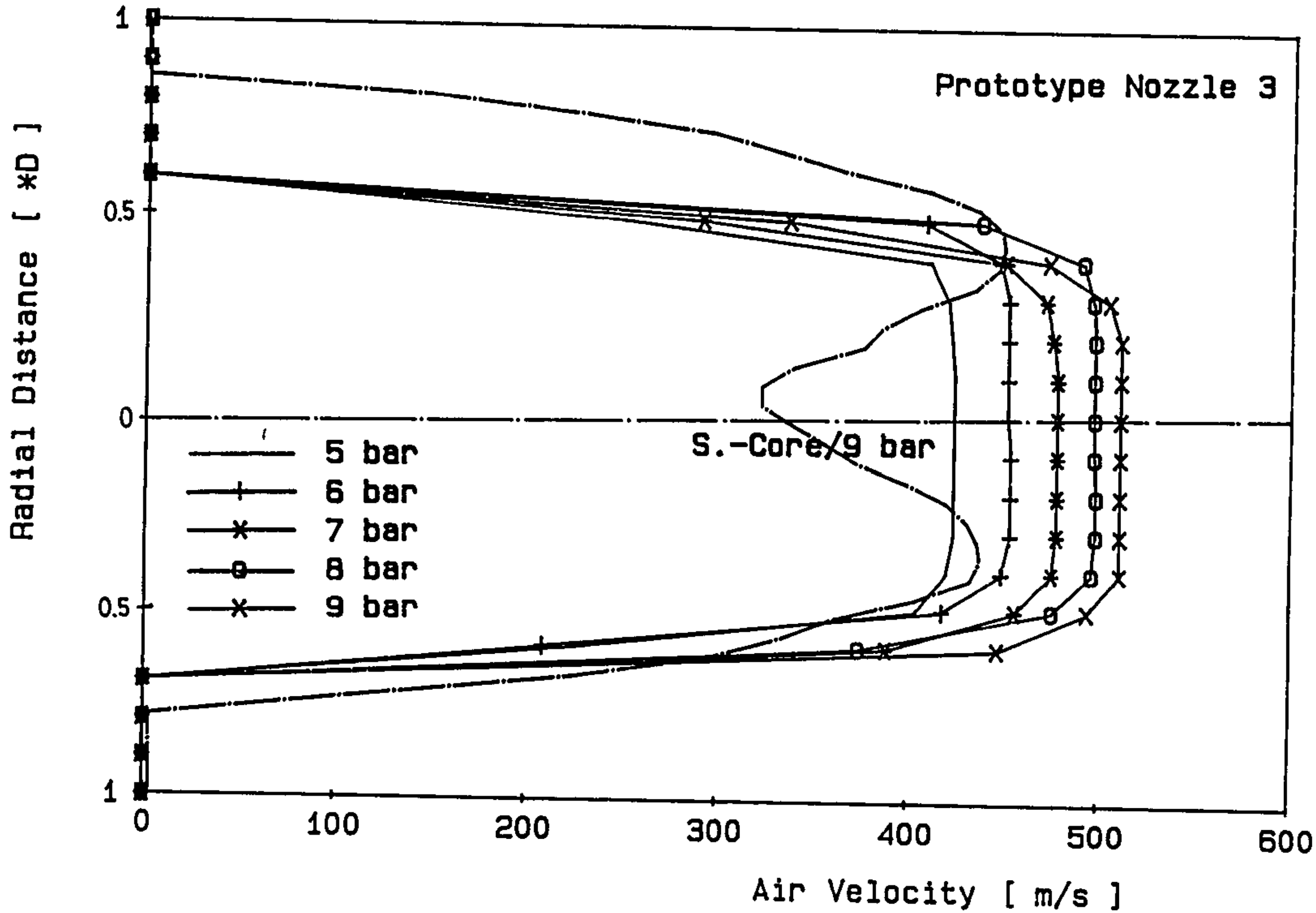

Figure 6.14a Axial air velocity distribution at the exit plane of the prototype nozzle 3

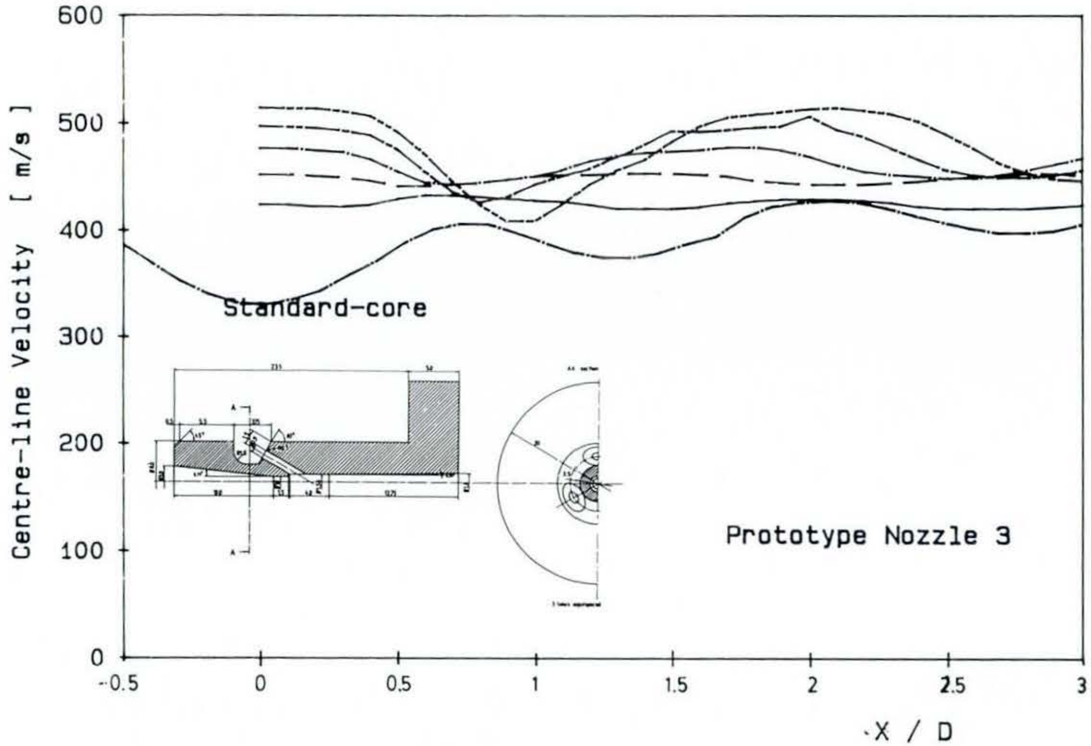

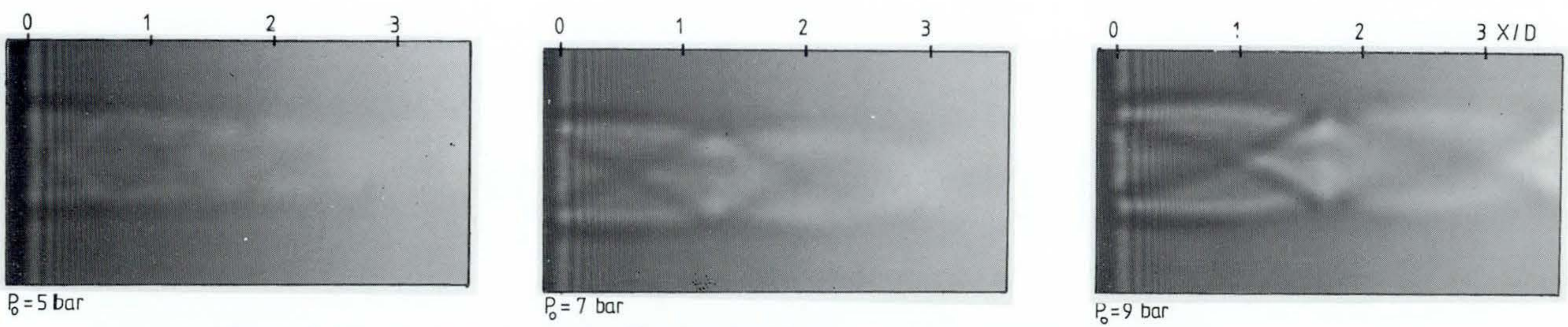

Figure 6.14b Centre-line velocity fluctuations and shadowgraphs of the air-jets created by the prototype nozzle 3

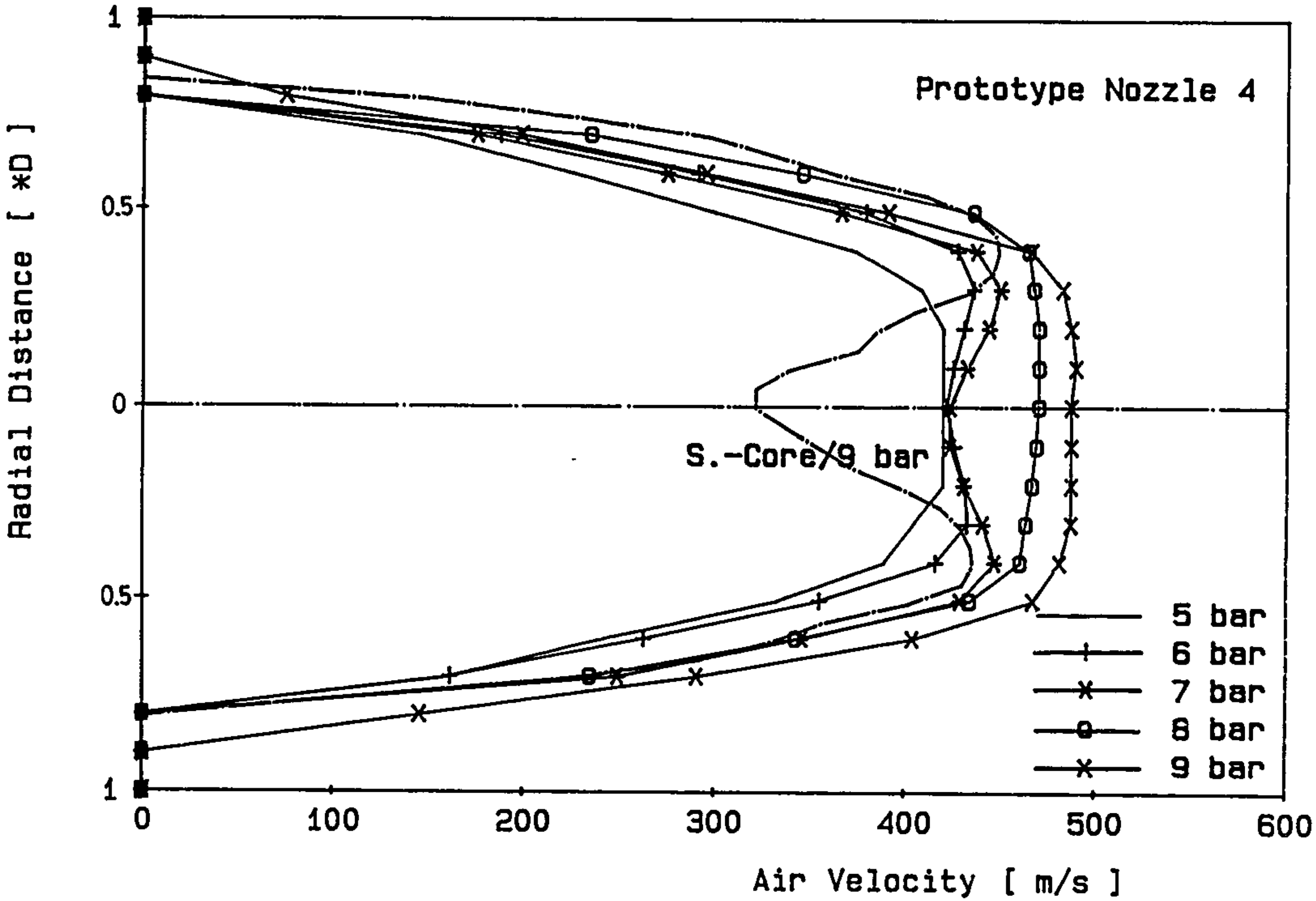

Figure 6.15a Axial air velocity distribution at the exit plane of the prototype nozzle 4

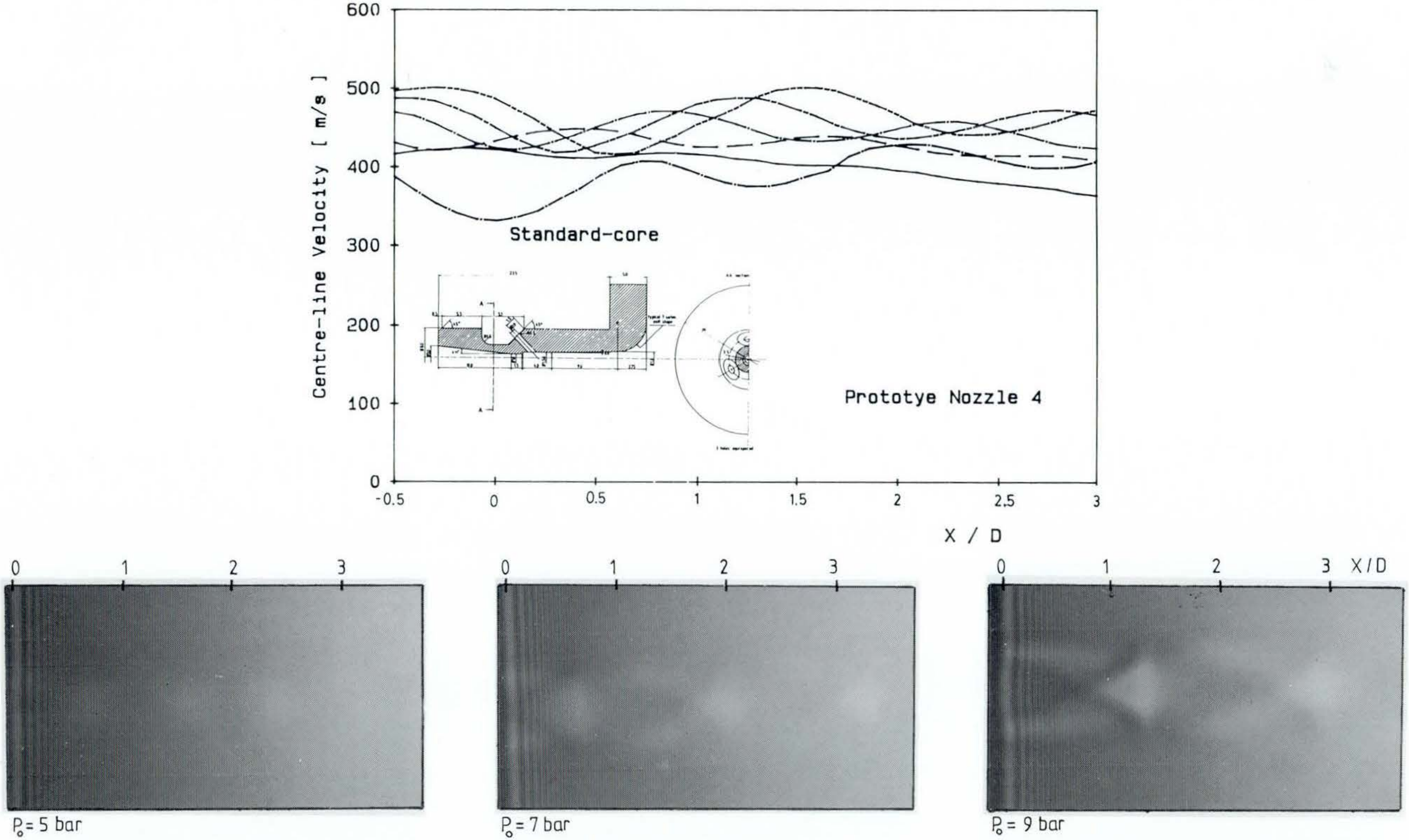

Figure 6.15b Centre-line velocity fluctuations and shadowgraphs of the air-jets created by the prototype nozzle 4

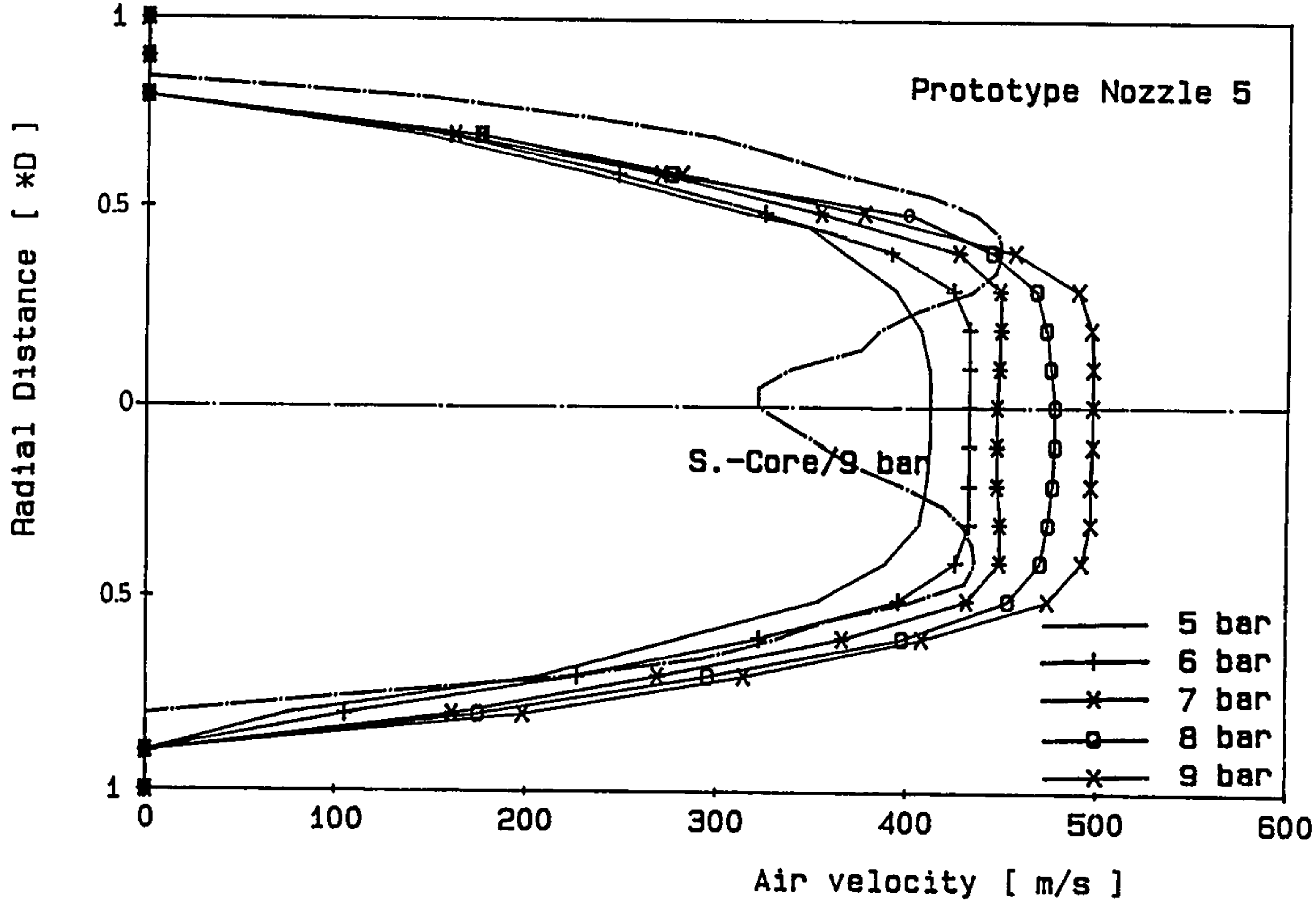

Figure 6.16a Axial air velocity distribution at the exit plane of the prototype nozzle 5

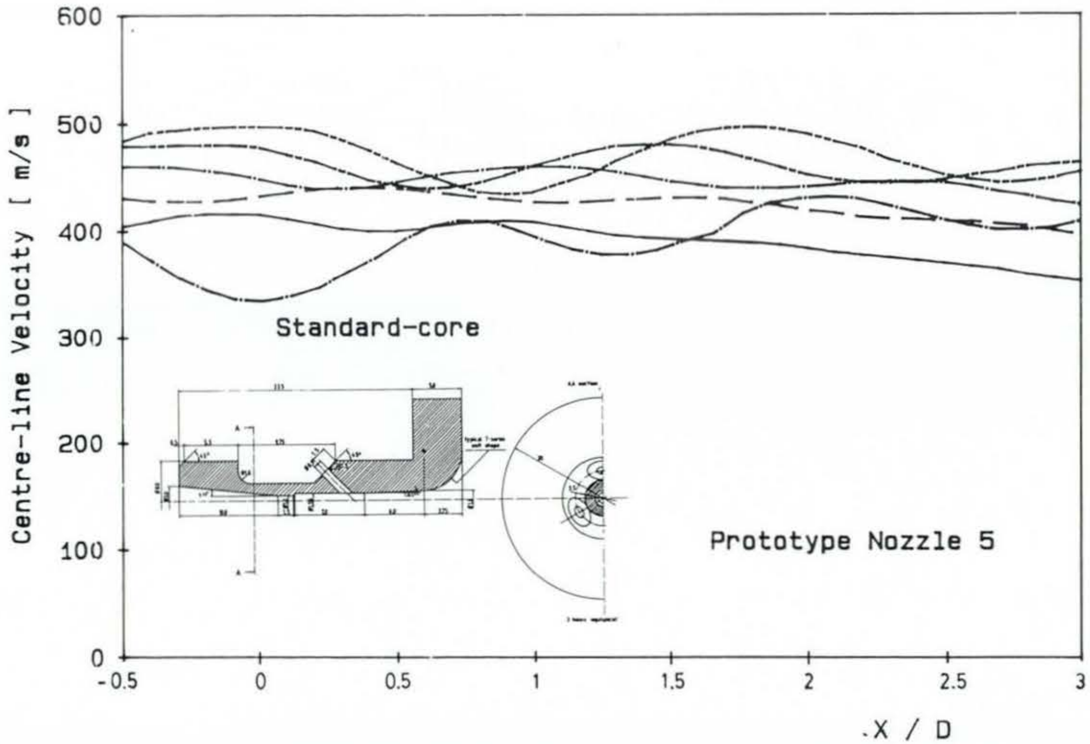

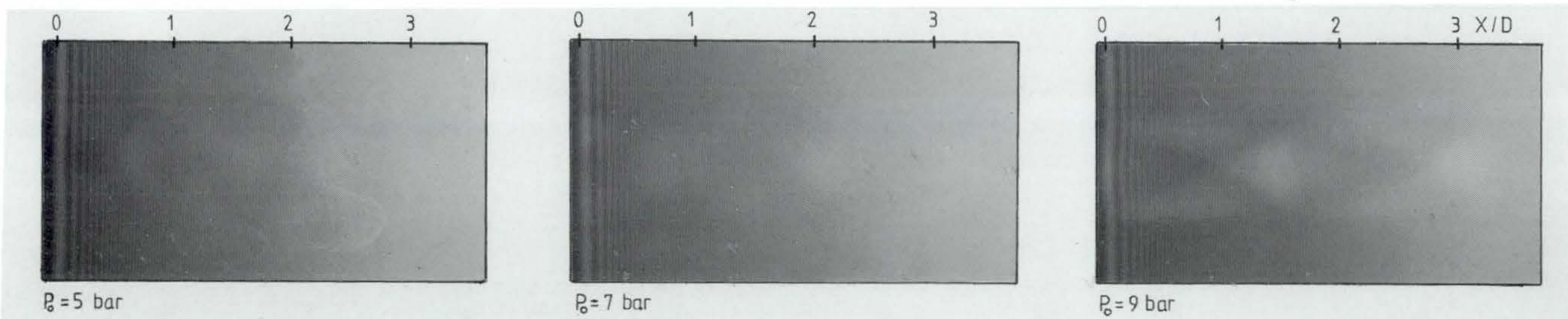

Figure 6.16b Centre-line velocity fluctuations and shadowgraphs of the air-jets created by the prototype nozzle 5

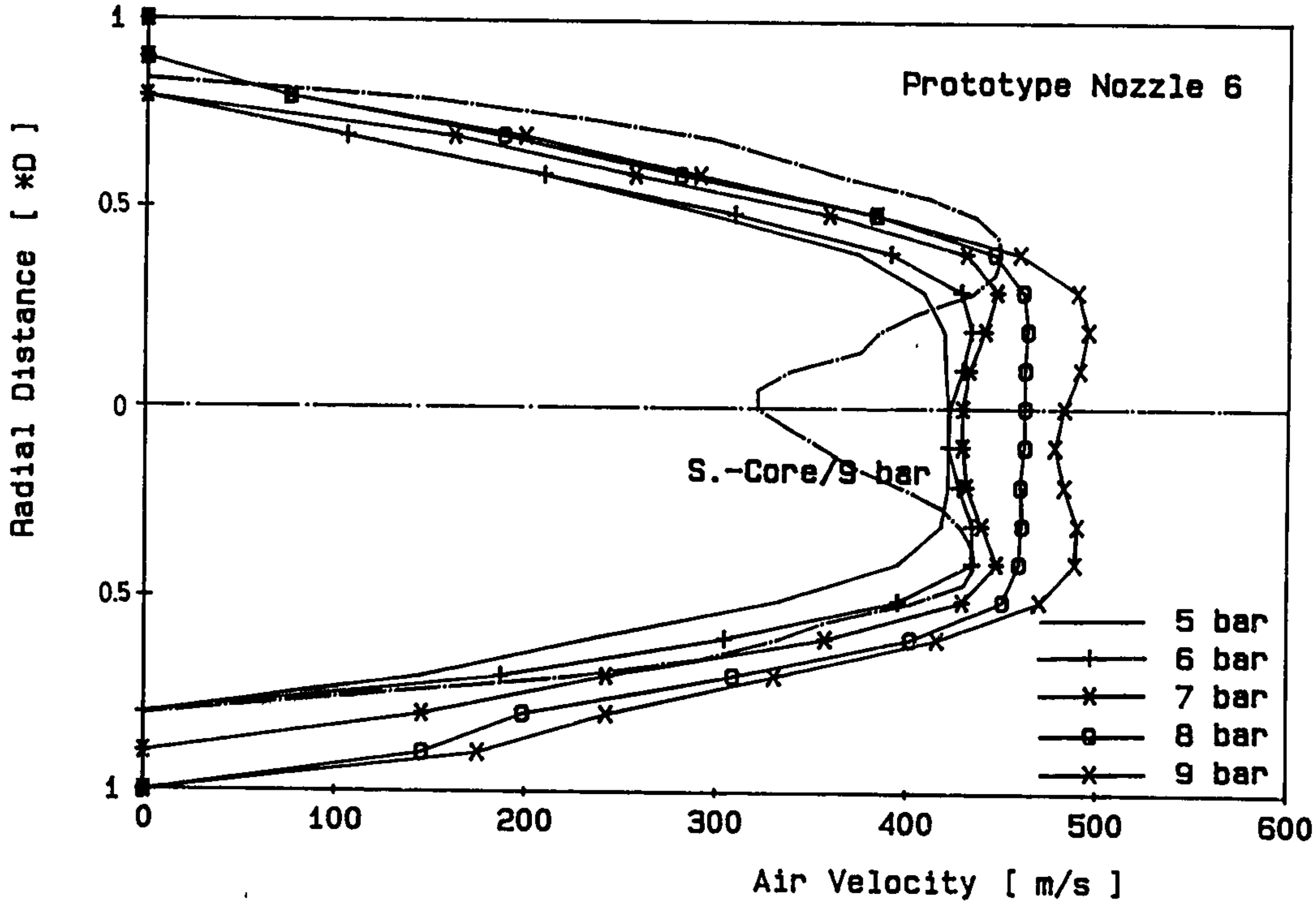

Figure 6.17a Axial air velocity distribution at the exit plane of the prototype nozzle 6

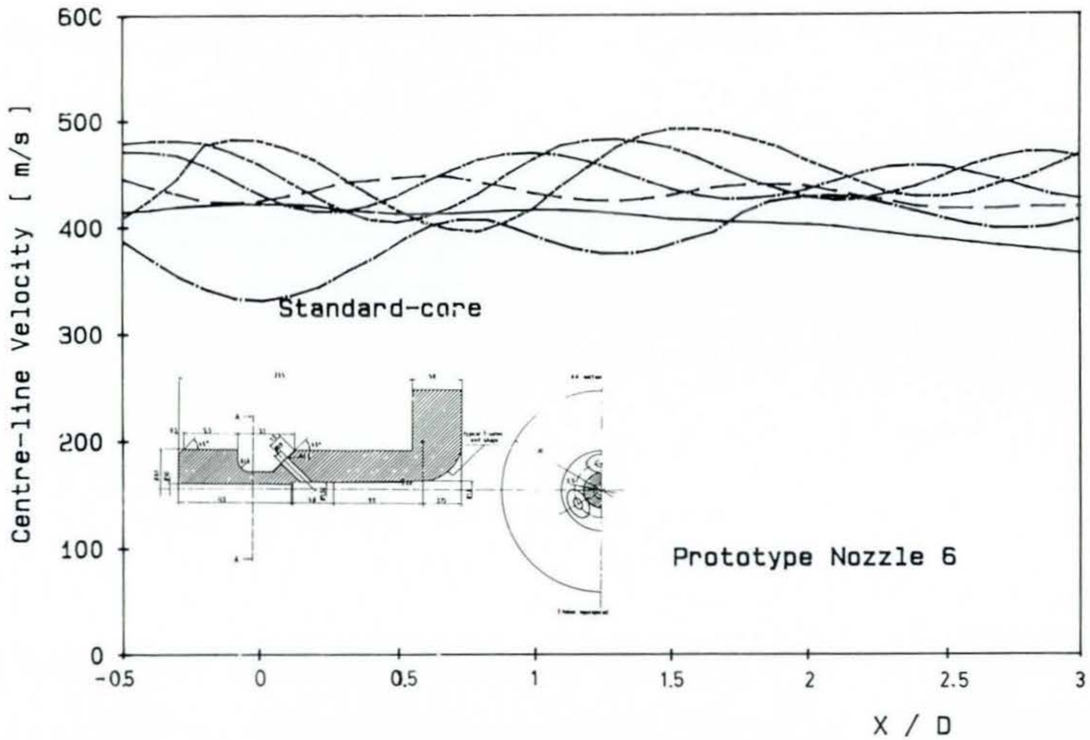

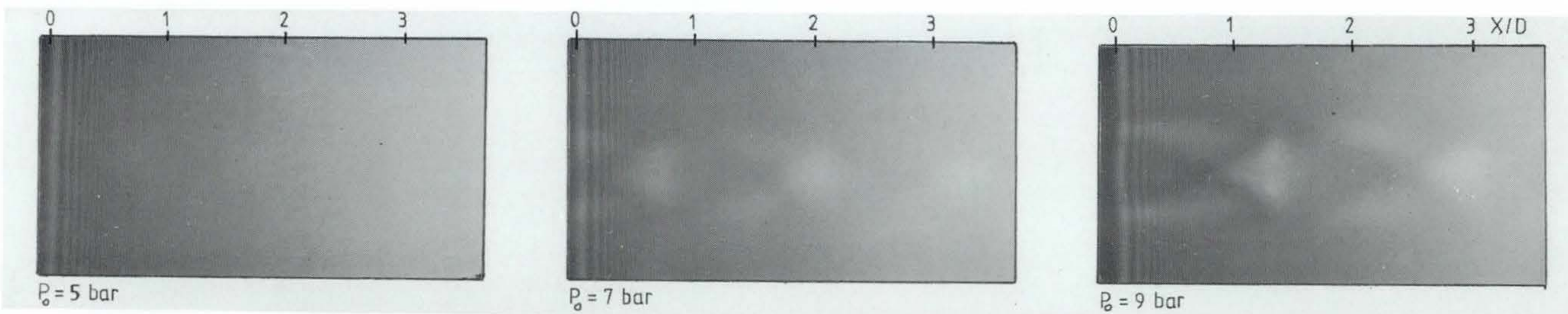

Figure 6.17b Centre-line velocity fluctuations and shadowgraphs of the air-jets created by the prototype nozzle 6

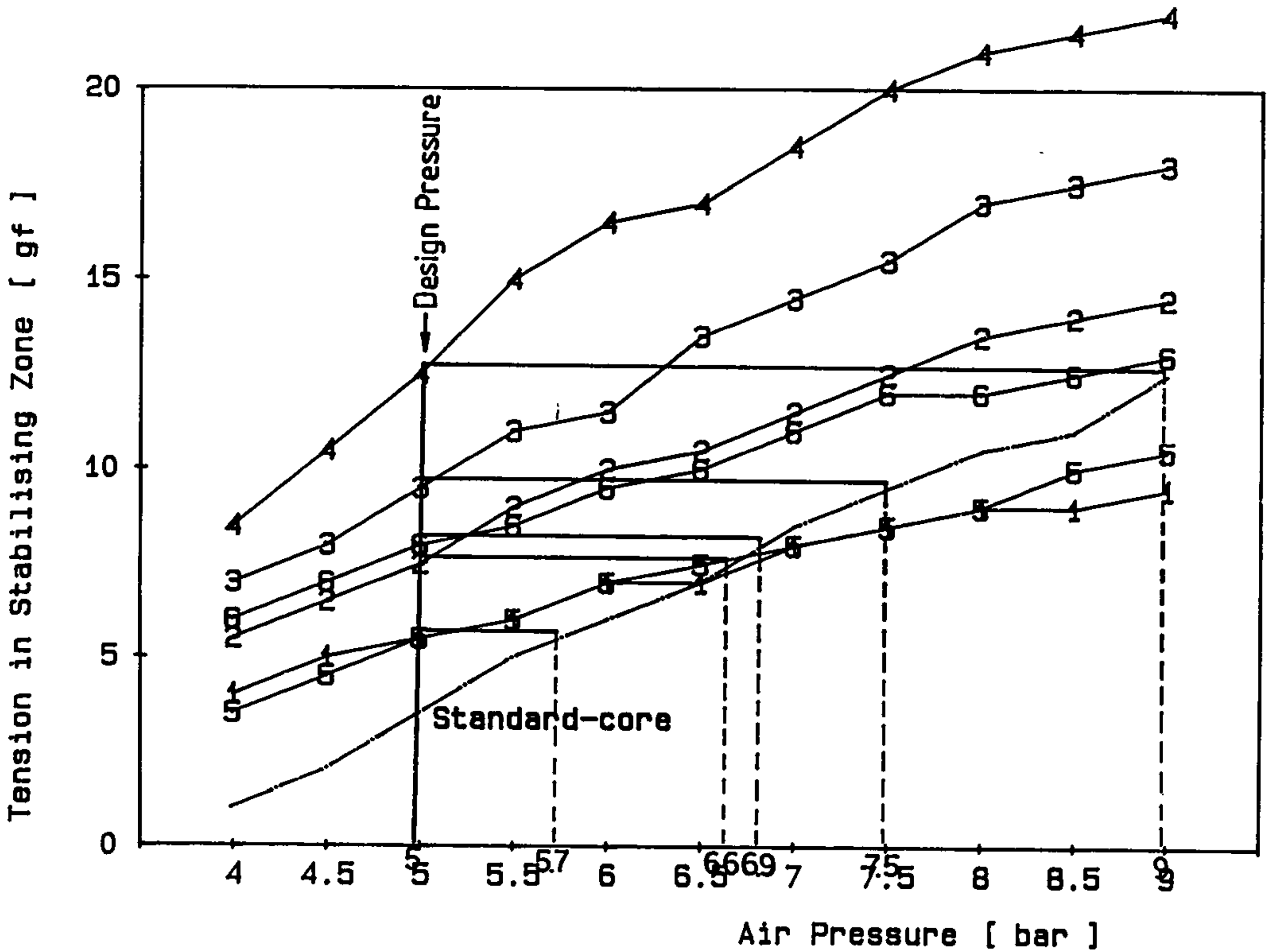

Figure 6.18 Variations in the tension in the stabilising zone with the prototype nozzles 1 to 6

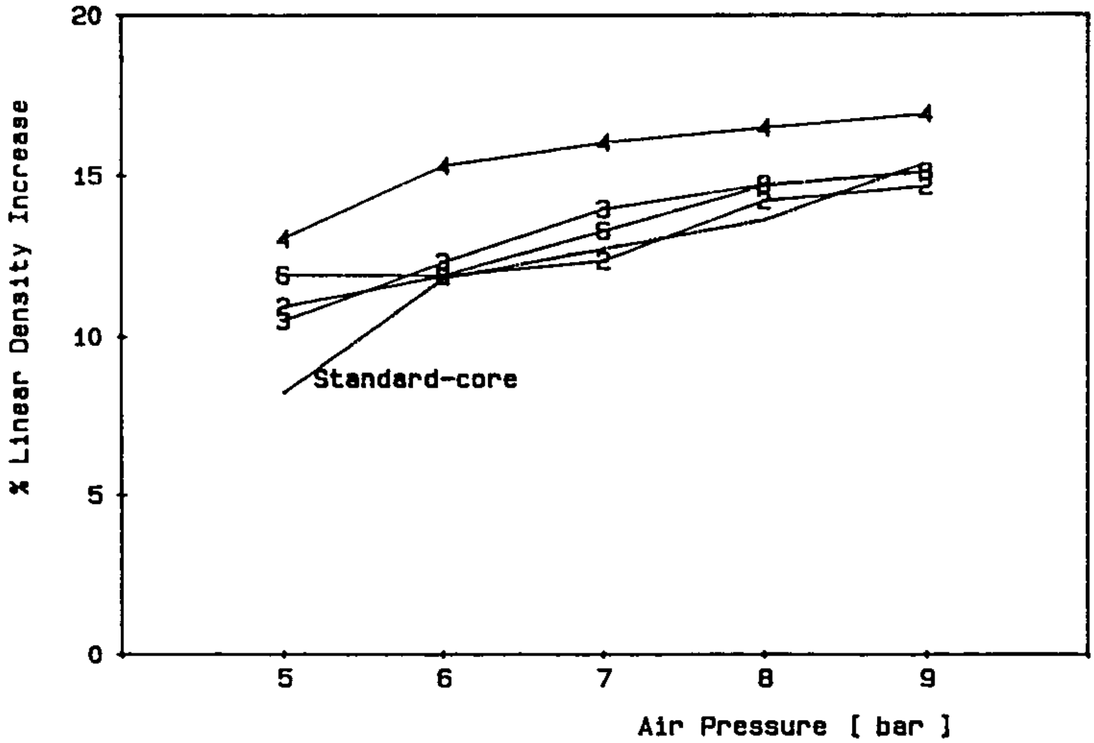

Figure 6.19a Percentage lineardensity increase of yarns textured with the prototype nozzles 2, 3, 4, and 6, compared with those from the Standard-core HemaJet

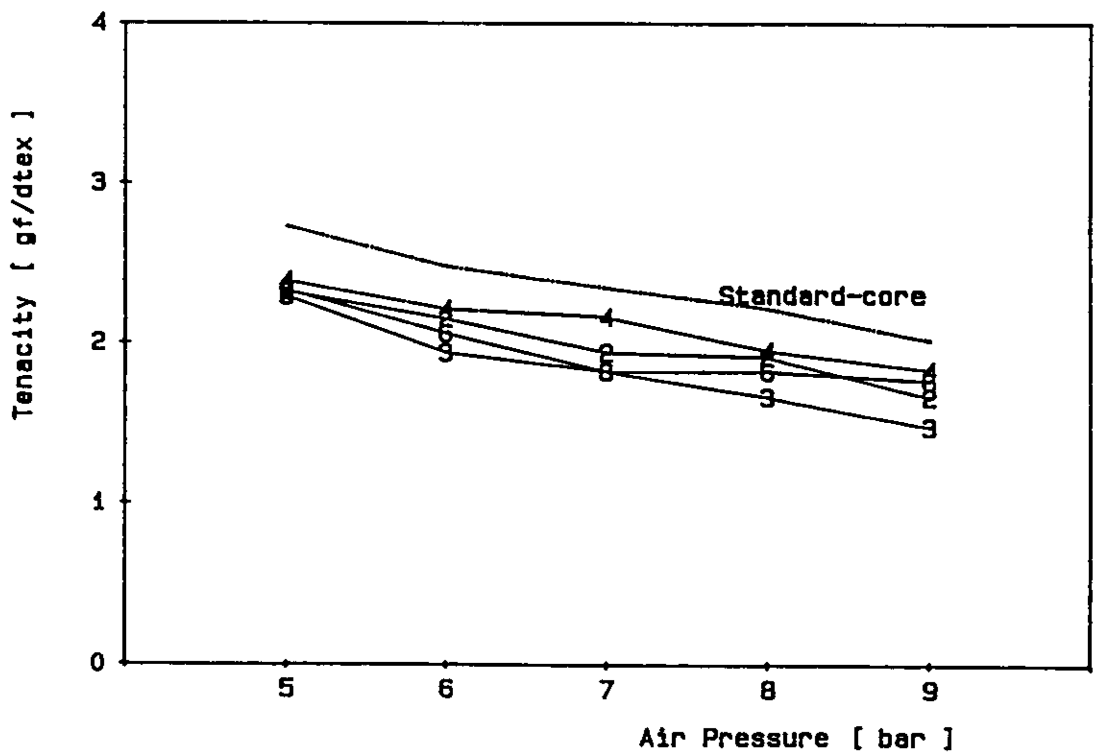

Figure 6.19b Tenacity of yarns textured with the prototype nozzles 2, 3, 4, and 6, compared with those from the Standard-core HemaJet

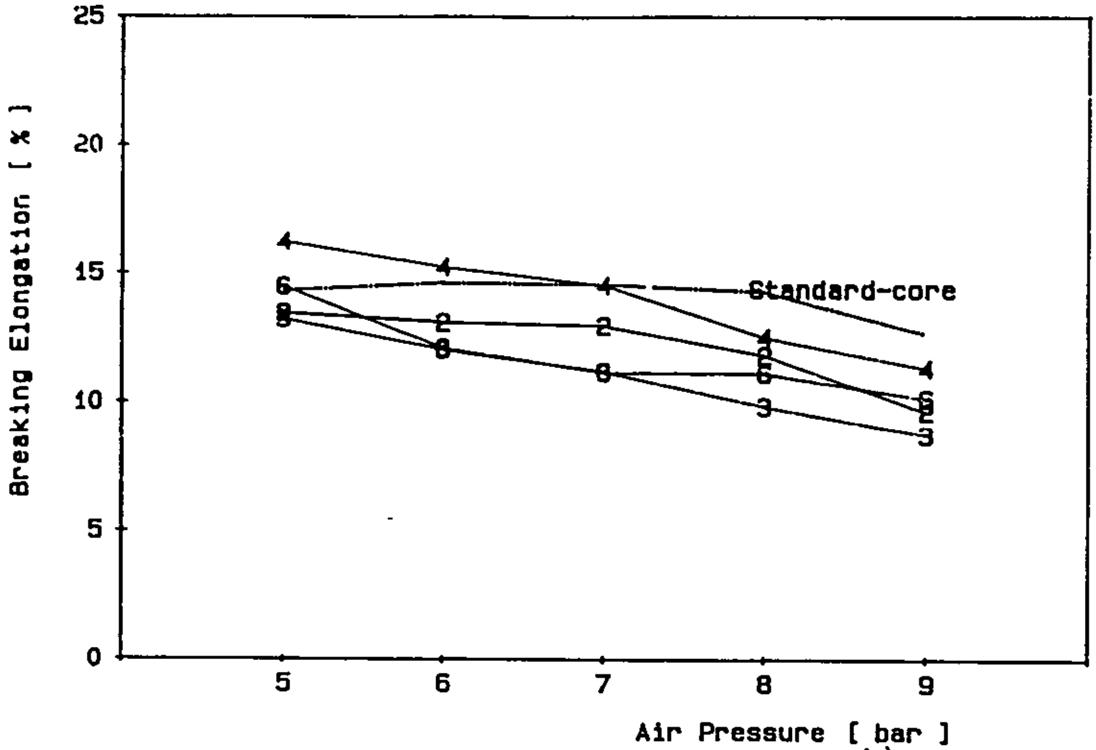

Figure 6.19c Breaking elongation of yarns textured with the prototype nozzles 2, 3, 4, and 6, compared with those from the Standard-core HemaJet

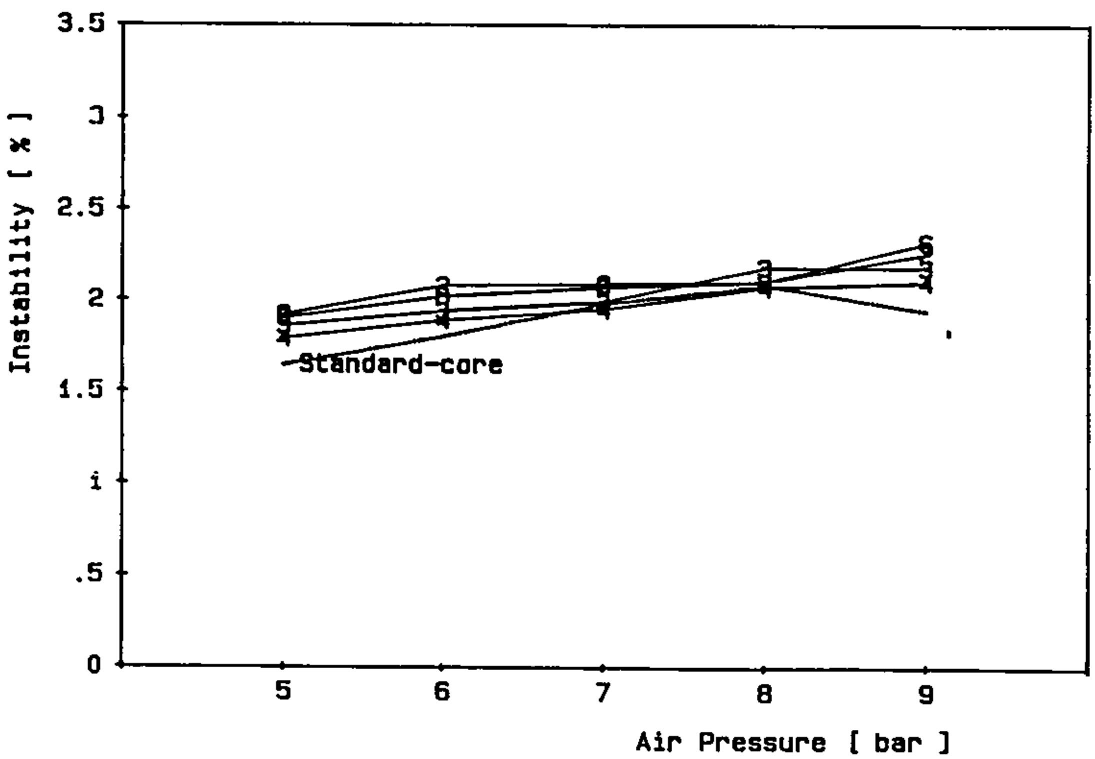

Figure 6.19d Instability of yarns textured with the prototype nozzles 2, 3, 4, and 6, compared with those from the Standard-core HemaJet

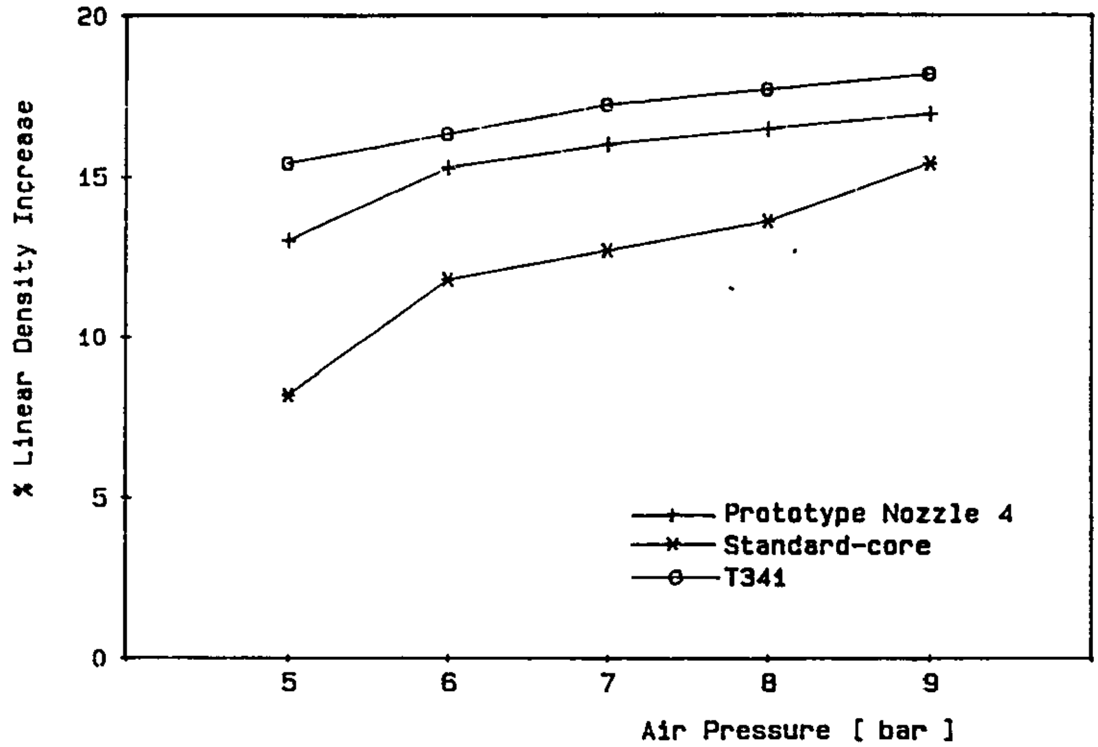

Figure 6.20a Comparison of the percentage linear density increase of yarns textured with the T341, prototype 4, and Standard-core nozzles

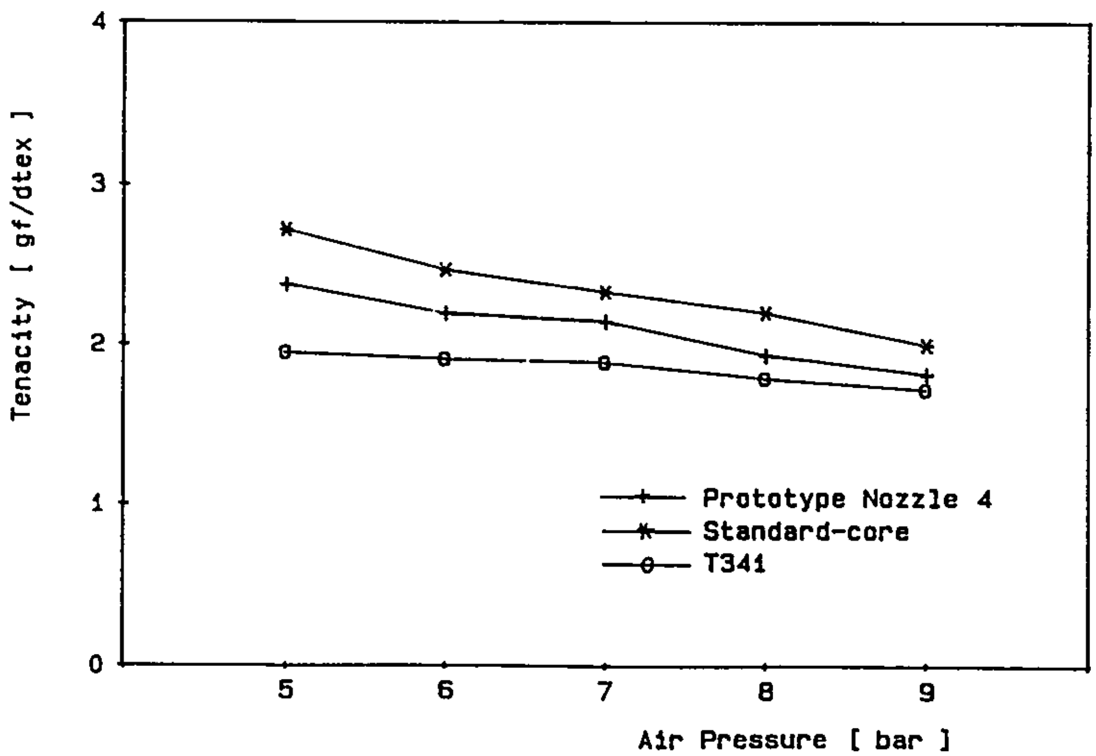

Figure 6.20b Comparison of the tenacity of yarns textured with the T341, prototype 4, and Standard-core nozzles

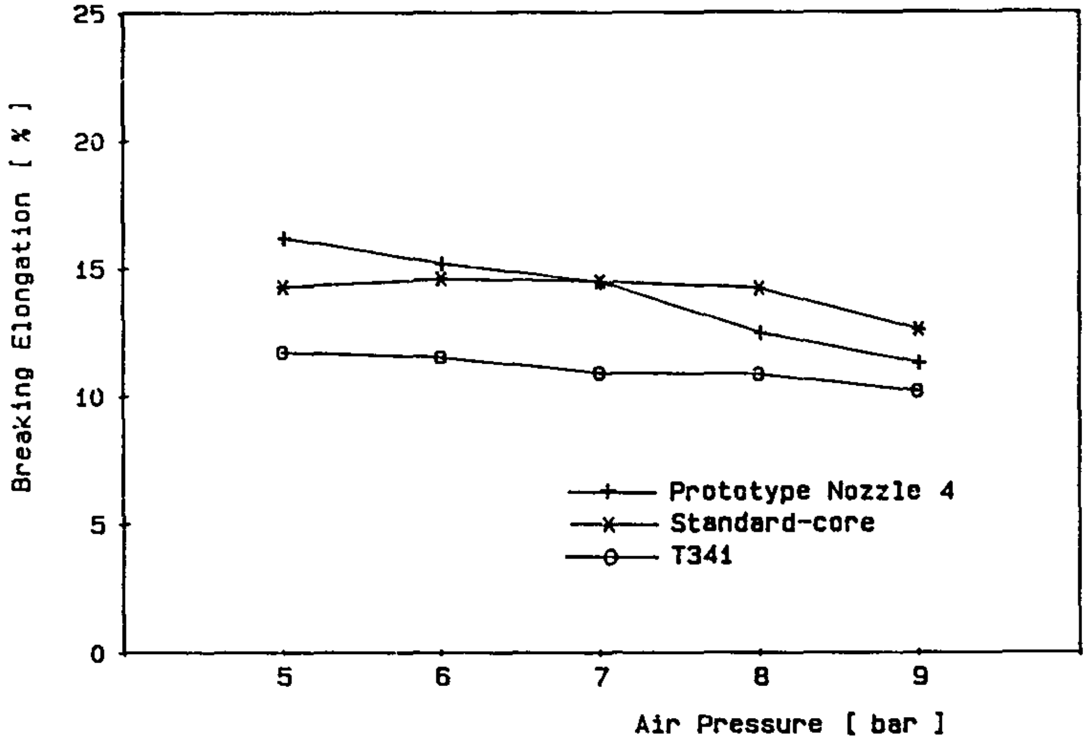

Figure 6.20c Comparison of the breaking elongation of yarns textured with the T341, prototype 4, and Standard-core nozzles

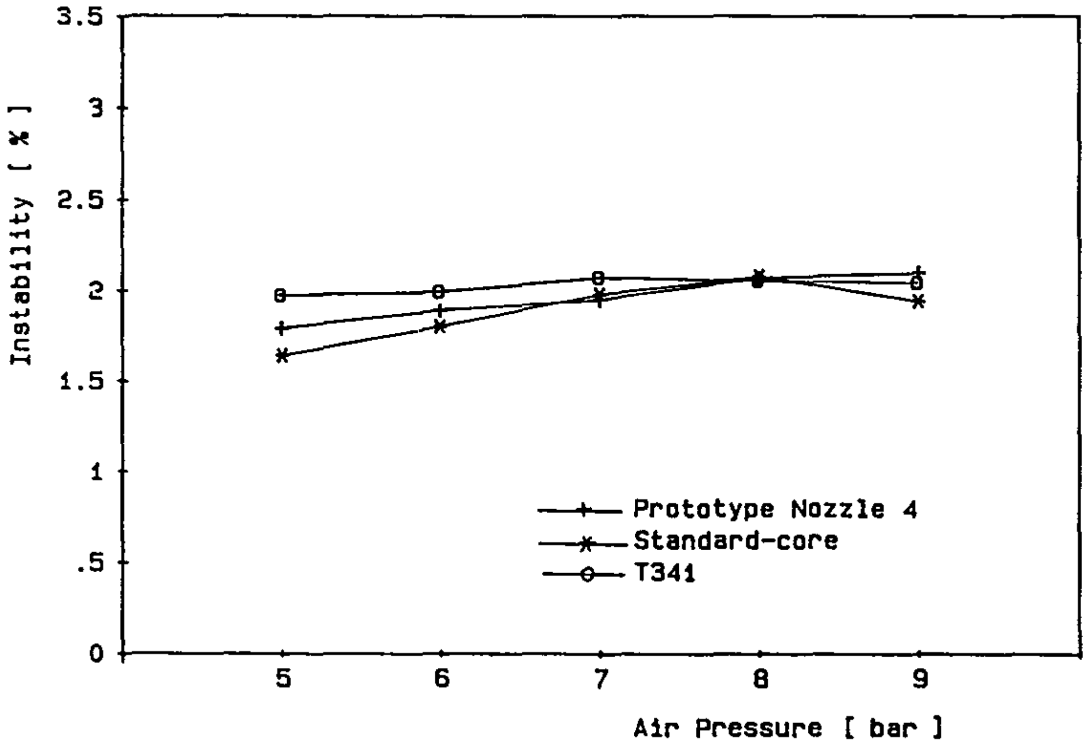

Figure 6.20d Comparison of the instability of yarns textured with the T341, prototype 4, and Standard-core nozzles

CHAPTER 7

EFFECTS OF WETTING ON THE AIR-JET TEXTURING PROCESS

In modern industry, dry air-jet texturing, i.e. texturing without the application of water, is rarely used because it does not produce successfully textured yarns with the desired qualities. The entanglement and surface loops of such yarns are easily removed by the effects of even slight tensions.

Several methods for water application have been developed alongside other developments in air-jet texturing. In the early days of the process, the conventional way of wetting the yarn was by threading it through a water bath as shown in Fig. 7.1a. Modern machines however make use of a simpler technique of wetting in the form of a wetting unit either integrated with or separate from the nozzle housing (Figs. 7.1b and c). Both of these methods have their advantages and disadvantages. It could be argued that more uniform wetting would be achieved by means of a water bath since the yarn is immersed into the water for a longer period. On the other hand, the water in the tub is contaminated by the spin-finish washed away from the yarn surface, and consequently this contamination reduces the wetting properties of the water, and results in a less effective application. However, the main superiority of the wetting unit over the wetting bath is that the former facilitates the precise control of the water applied and always provides fresh clean water.

Wet texturing, although it produces superior yarns, has its own drawbacks. First of all, since most of the spin-finish on the filaments is washed away by the water, as illustrated in Fig. 7.2 which shows the spin-finish content of the yarn before and after both wet and dry texturing; the wet textured yarn requires the application of oil in order to gain improved anti-static and reduced frictional properties. Secondly, the effluent water contaminated by the spin-finish materials needs to be cleaned if it is to be recycled and the texturing nozzles should also be cleaned frequently[103]. Idle machine time during this cleaning procedure obviously increases the cost of the textured yarn.

7.1 Previous Work

The consequences of water application are very well known. However, the mechanism of this improvement has not yet been fully explained. Apart from the recent publication by Acar et al[58], there is no other published information regarding the effects of water on the air-jet texturing process. Fischer[66], and Bock and Lünenschloss[47], made comments on the possible mechanism of the effects of the wetting, but did not support their claims by either experimental results or theoretical explanations. Bock and Lünenschloss have shown that only a small amount of water is necessary to impart the desired effects of wetting.

7.1.1 Condensation shocks

Fischer[66], having ruled out the possibility of reducing the friction by wetting, refers to publications[104,105] on the formation of condensation shock waves by humid air in the supersonic nozzles and concluded that such condensation shocks may be regarded as contributing to the improved interlacing of wetted filament yarns in the air jets.

Bock and Lünenschloss[47], although admitting their lack of knowledge of the mechanism of wetting that causes the known improvements, surmised that the water entrained into the air flow may change the flow characteristics and cause condensation within a de Laval nozzle, but they offered no experimental evidence to support this claim.

7.1.2 Lubricating effects of water

Using two-phase (gas-solid particles mixture) equilibrium flow theory, Acar et al[58] argued that the water droplets reduce the overall velocity of the flow, which in turn may cause an adverse effect on the texturing process. Furthermore, Acar et al sought for possiblities of reducing the filament/solid surface friction and redesigned the yarn path by realigning the feed rollers, wetting unit and the texturing nozzle. However, they came to the conclusion that this arrangement, without wetting the filaments, did not improve the process, because it did not reduce the filament/filament friction. Having focused the attentions on the amount of water which is necessary to impart the desired effects, Acar et al concluded that the water acts as a lubricant so as to reduce the filament/solid surface and filament/filament friction, thereby resulting in improved conditions for better loop and entanglement formation.

Acar et al[58], like Bock and Lünenschloss[47], came to the conclusion that a small amount of water is sufficient to impart the desired effects of wetting. Additionally, by modifying the conventional single chamber nozzle enclosure into two separate chambers, Acar et al showed that the amount of water mixed with the primary flow is negligible, since the secondary flow blows off nearly all of the water used to wet the filaments. Both of these research publications claim that the excessive application of water beyond the required minimum limit does not give any appreciable improvement to the processing conditions.

7.2 Quantity of Water Required

In this current work, in order to shed more light on the aspect of the water application, an experiment was devised in which the amount of water was increased in small increments from zero consumption, the average tension in the stabilising zone being recorded. The experiment was repeated for various air pressures. The variations in the tension in stabilising zone with varying amounts of water applications is given in Fig. 7.3. As seen in this figure, the maximum tension is obtained at about 0.06 litre/hour water application. Above this amount, the tension remains virtually unchanged irrespective of the amount of water applied. However, the peak tension value appears to shift towards slightly higher water quantities as the air pressure is increased from 5 to 9 bar. This may be due to the higher secondary flow fluxes, which blow more water off the filaments thereby letting lesser amounts of water into the nozzle.

In conclusion, this experiment shows that the amount of water which is necessary for an effective texturing is even less than those claimed by both Bock and Lünenschloss, and Acar et al. This minimum amount of required water varies with the secondary flow momentum flux as determined by the air pressure.

7.3 Frictional Effects

According to Olsen[106] the temperature and the viscosity of a lubricant are two important factors which affect the frictional behaviour of textile yarns and fibres in the hydrodynamic region, other factors being the yarn speed, lubricant viscosity, yarn and/or filament linear density, pre-tension, the roughness of the guides and/or yarn surfaces, and guide diameter. repeated

It is known that, for some textile applications, water has good lubricating qualities. The lubricational characteristics of both water alone and some water-wetting agent mixtures are discussed in this section and the effect of increasing the water temperature is also studied. In order to measure the friction between the filaments and solid surfaces, the following experiment has been devised and carried out.

As shown in Fig. 7.4, an almost tension free yarn is withdrawn from the package. A yarn tensioner is utilised to compensate for tension fluctuations during unwinding and to pretension the yarn up to a certain degree which is observed in the actual texturing process, because pre-tension is a known contributing factor to the filament/solid surface friction. The yarn, having passed through a wetting head is turned at right angles around a yarn guide identical to that used in the actual texturing process just prior to the nozzle. By varying the rotational speed of the roller W, the speed of the yarn can be altered from 100 to 600 m/min. Tensions before and after the yarn guide are monitored by means of the tensiometer so that the coefficient of friction can be calculated by the formula given in Fig. 7.4. The water application rate was kept constant at 0.2 litre/hour throughout the experiments.

The Figs. 7.5 and 7.6, the coefficient of friction is plotted against yarn speed. Fig. 7.5 clearly indicates that water reduces the filament/solid surface friction a great deal, whereas only slight variations in the friction have been observed by adding wetting agents into the water. On the other hand, Fig. 7.6 shows that the lubricating capability of water is slightly enhanced as its temperature is increased.

7.4 Water Temperature

It is known in practice that the texturing process is adversly affected when water at low temperatures (near to the freezing point) is used[107]. Therefore, it is thought that by changing the temperature of the water used in the texturing process, the frictional properties of the yarn could be affected, because water temperature affects both the yarn temperature and the guide temperature. The viscosity of the water, which is said to play a significant role in frictional properties in the hydrodynamic region[108], is also affected by the temperature.

Figs. 7.7a to f illustrate various properties of yarns textured with water temperatures of 15^{o}, 45^{o} and $65^{o}C$, the properties of dry textured yarns being also included for comparison purposes. Since cold water is known to yield poor texturing conditions, it was expected that increasing the water temperature would enhance the texturing quality. Nevertheless, the graphs show little improvement in the quality of yarns textured at higher water temperatures.

Therefore, it could be said that although the frictional properties of both the filament/solid surface and filament/filament interaction are altered by the temperature of the lubricant, the texturing could not be significantly improved.

7.5 Wetting Agents

It was thought that, by reducing the surface tension of the water, its wetting properties could be improved so as to penetrate the individual filament surfaces more effectively and thereby further reduce the friction. A number of wetting agents, properties of which are given in Table 7.1, were added to the water and their effects on the texturing were ascertained by producing yarns and testing them. Most manufacturers of wetting agent recommend a solution of 2 ml agent to each litre of water at specified temperatures for optimum results. At the pre-experimental stage, however, the amount of agent application was varied from 1 to 50 ml/l which seemed to make little effect. Therefore, the manufacturers' specified amounts of wetting agent were added into the water. The process was carried out in two steps, first being the measurement of tension in the stabilising zone. The results of the first step are given in Table 7.2. In the second step, those wetting agents which seemed to improve the process were re-used and the yarns produced. Finally, the yarn tests were carried out. Figs. 7.8a to f give the results of these tests as well as those dry textured yarns, and they indicate that any improvement in the process accomplished by adding the wetting agents into the water is too insubstantial for any positive conclusion to be drawn.

For the purpose of further investigation, therefore, it was decided to make use of two extreme frictional conditions and ascertain their possible consequences. One of these extreme conditions was to eliminate the filament/solid surface friction completely from the process; this corresponds to the realigned yarn path arrangement suggetede by Acar et al[58]. The other is to increase the filament/solid surface friction just before the nozzle by means of a very rough surfaced yarn guide.

7.6 Elimination of Filament/Solid Friction Before the Nozzle

By realigning the yarn path in a straight line prior to the nozzle, Acar et al[58] virtually eliminated the yarn-to-yarn guide friction. This alternative yarn path, however, without wetting the yarn made no improvement to the process and produced similar yarns to the conventional yarn path arrangement as indicated by the tension measurements in the stabilising zone (Fig. 7.9b). Therefore, no further attempt was made to test the yarns textured with a realigned yarn path under dry conditions, whereas the yarns textured under wet conditions with the realigned yarn path arrangement were tested.

Figs. 7.9a to f illustrate that the realigned yarn path arrangement with yarn wetting shows little improvement in the process, although no friction between the yarn and the guide occurs. Therefore, it could be concluded that the yarn/guide friction seems to play an insignificant role in texturing. Two further friction sources, however, still exist. These are the friction between the yarn and the nozzle walls, and interfilament friction.

7.7 Increasing the Filament/Solid Friction

Had there been a substantial effect of friction occuring between the supply yarn and the yarn guide prior to its entrance to the nozzle, it could have been expected that the high friction between these surfaces would have worsened the texturing. In order to prove this hypothetical prediction, the surface roughness of the yarn guide was increased by coating it with a highly rough-surfaced sheet whose surface roughness is compared, in Fig. 7.10, with that of a conventional yarn guide. These surface traces were obtained by using surface scanning equipment[109]. Before mounting it on the nozzle housing, the friction measurements were carried out as described earlier in Section 7.3. As can be seen in Fig. 7.11, a significant increase in friction is observed with this rough surfaced yarn guide. The figure depicts a rather unexpected result regarding the effect of wetting with these two yarn guides. Although, the wetting of the yarn reduces the friction between the yarn and the smooth yarn guide, it increases the friction between the yarn and the rough-surfaced yarn guide. This is of further benefit to the investigation planned here, because the wetting of the yarn will not reduce the friction; on the contrary it will increase the friction during the texturing process.

Having obtained the frictional properties of both smooth and rough surfaced yarn guides, under wet and dry conditions, these yarn guides were mounted on the nozzle housing and yarns textured at varying air pressures. Figs. 7.12a to f show the tension in the stabilising zone and other textile properties. As seen in Fig. 7.12b, both of the yarn guides resulted in similar inferior yarn texturing under dry conditions, although their frictional properties were rather different. Therefore the dry processing was omitted for further yarn production and testing procedures. Figs. 7.12c to f indicate that no worsening of the process occured with the rough surfaced yarn guide under wet conditions, although the yarn/yarn guide friction still persists.

In conclusion, it could be said that neither the complete elimination nor an increase of the friction occuring between the yarn and the yarn guide just before the nozzle, could eliminate the necessity for water application during the air-jet texturing.

7.8 Water Injection into the Air

By utilising a high pressure water pump, water was injected into the nozzle housing through a small tapping of 0.5 mm diameter to avoid any possible disturbance of the air pressure. During this experiment, the amount of water injected was carefully measured by means of a fine rotameter. Fig. 7.13 shows the tension variations in the stabilising zone with varying amounts of water injected. It is noted that there is an optimum amount of water required below and above which the texturing is less effective. This optimum amount was found to be about 0.06 l/h which is well below the conventionally applied amount as concluded in Section 7.2. As the amount of water was increased, the excess water completely destroyed the process and resulted in a breakdown. It was also observed that the great deal of water injected is entrained into the primary flow and only a small fraction of it mixed with the secondary flow. To visualise this event, a two chamber nozzle enclosure has been used and photographed before and after the water injection (Fig. 7.14). The effect of this water entrainment into the primary flow has also been monitored by texturing yarns at varying air pressures and testing them. The results are given in Figs. 7.15a to e. In conclusion, it could be suggested that a very small quantities of water droplets suspended in the flow play a significant role by reducing the interfilament friction as well as the filament-to-nozzle wall friction. Above this critical amount, the increase in water droplets not only appear to make no further difference in the frictional behaviour but also adversely affect the flow characteristics.

Since water is injected into the air when it is in the nozzle housing, the density of the mixture would be increased. As this heavy density air-water mixture hits the opposing wall of the nozzle duct, wearing of the nozzle duct is anticipated. On the other hand, with water injection, the required amount of water has been found to be very small and easily controllable. Therefore, the amount of spin-finish that washed away by the water injected into the air is likely to be less than that washed away by conventional wetting methods.

7.9 Effects of Water Droplets on the Air Flow

The flow of humid air through supersonic nozzles, and also formation of a condensed phase in high-velocity flows, have been widely investigated both experimentally and theoretically by various researchers[110-118]. Almost all of them have assumed the supply conditions to be air-water vapour (i.e. moist air) or steam and consequently concluded that the mixture flowing in the nozzle first becomes supersaturated and then condensation occurs. Provided that the relative humidity of the mixture is high enough, the flow in the nozzle will be affected by the latent heat released by the condensation and a condensation shock wave will eventually be formed in the supersonic section of the nozzle. The ultimate consequence of this condensation shock wave is observed as a sudden increase in the static pressure and in turn a decrease in the flow velocity (Figs. 7.16a and b) as reported by Pouring[111] and Matsuo et al[118].

In the case of texturing nozzles, although the supply air is dry, a small amount of water is carried along with the filaments and hence is mixed into the air flow. In the experiments mentioned in Section 7.8, water is also injected into the air as fine water droplets. These water droplets create a mistiness in the air at the exit of the nozzle. Acar et al[58] has shown theoretically that water droplets slow down the overall velocity of the flow. In order to verify this theoretical prediction, velocity measurements of a free jet from both a straight pipe and the Standard-core HemaJet nozzle were attempted when a small amount of water was injected into the compressed air when the air is still stagnant. Unfortunately, the pitot tube failed to record the total pressures of the air-water mixture due to ice formation at the tip of the probe. Nevertheless, the shadowgraph technique, used to visualise the flow of dry air and air-water mixture emerging from the straight pipe, showed no noticable difference between these two flows (Fig. 7.17). Fig. 7.18 has also revealed that water droplets do not interfere at all with the shock waves from the Heberlein Standard-core texturing nozzle. Thus, it can be concluded that small amounts of water droplets, as mixed into the air-jet in the texturing process, do not make any significant difference in the air flow.

7.10 Conclusions

The amount of water which is typically been used in practice is much beyond the required amount. Since the excess water creates additional problems, the amount of water should therefore be reduced. Even further improvements in yarn wetting could be achieved by injecting water into the nozzle housing, provided that the cost of supplying high pressure water is feasible and also that the wearing problem of nozzles is solved. In the case of water injection, the process becomes cleaner since all the water injected mixes with the air forming only a mist, and less spin-finish material is surmised to be washed away from the yarn surface.

The experimental work has shown that no additives, i.e. wetting agents, make any significant improvement either in the lubricating properties of water or in the texturing process. Some slight improvement in the process was achieved when the water is heated up to 65^{o}C.

It can be concluded that the filament/solid surface friction occuring between the yarn and the yarn guide just prior to the nozzle (for the conventional yarn path arrangement) is of no significance.

Although there is evidence that water enters the primary flow, no condensation has been observed due to the fact that the water particles are in the form of water droplets at both the entrance and exit of the nozzle. Consequently, no phase change occurs in the nozzle or in the downstream section of the air flow. Therefore, the mechanisms for water effects on the texturing, which are based on the formation of condensation shock waves, are indeed invalid.

The most important effects of water droplets are seen in the primary flow section of the nozzle. Having ruled out the possibilities for the formation of condensation shock waves, the only effect of water droplets would seem to reduce the interfilament friction, and the filament-to-nozzle wall friction. It could be suggested that water injection into the air reduces the friction further and in turn this could result in better texturing by facilitating the easy relative movements of the filaments.

TABLE 7.1 THE PROPERTIES OF WETTING AGENTS ADDED TO THE WATER BEFORE APPLICATION TO THE YARN

	WA1	WA2	WA3	WA4	WA5	WA6	WA7	WA8	WA9	WA10	WA11	WA12
TRADE NAME	Sandopan LF	Savotex WA/60	Fwidol WA/60	Defindol Conc.	Sandozin NE Liquid	Sandopan DTCL Liquid	Sandopan NI Liquid	Sandopan CEN Liquid	Sandozin N Liquid	Sandozin C Liquid	Electol	Fairy Liquid
PRODUCER	Sandoz	Standard chemicals	Henkel	Henkel	Sandoz	Sandoz	Sandoz	Sandoz	Sandoz	Sandoz	Vickers	-
TYPE	Polyalty-lene Oxide	Di-alkyl sulpho-succinate sodium salt	Alkylacyl Polyglycol Ether	Alkyl Polyglycol Ether	Sulphona-ted Fatty Acid deri-vative	Modified Polyglycol Ether	Alkyl Phenyl Polyglycol Ether	Phosphoric Acid Ester	Sulpho-Succinate	Alkyl aryl Sulpha-mate	Anti-static Agent	Washing-up Liquid
IONIC NATURE	Non-Ionic	Anionic	Non-Ionic	Non-Ionic	Anionic	Anionic/ Non-Ionic	Non-Ionic	Anionic	Anionic	Anionic		
APPLICA-TION ml/l	2	2	2	2	2	2	2	2	2	2	2	2

Table 7.2 Effects of wetting agents on the tension in stabilising zone with varying air pressures

		TENSION IN STABILISING ZONE [gf]												
	Wetting Agent	Water	WA1	WA2	WA3	WA4	WA5	WA6	WA7	WA8	WA9	WA10	WA11	WA12
AIR PRESSURE [bar]	5	4.5	4.0	4.5	4.0	4.5	5.0	5.0	4.5	4.5	5.5	5.0	4.75	5.5
	6	6.5	5.5	6.5	5.5	6.5	7.0	7.0	6.5	7.0	8.5	7.0	6.5	8.25
	7	7.5	6.5	8.0	7.25	8.5	9.0	9.0	8.0	8.0	10.0	9.0	8.0	10.0
	8	9.0	7.0	9.0	8.5	9.0	10.5	10.0	9.0	10.0	12.0	9.5	9.5	11.5
	9	10.0	8.0	9.75	9.0	9.5	11.25	10.5	10.0	10.5	13.0	10.5	10.0	12.5

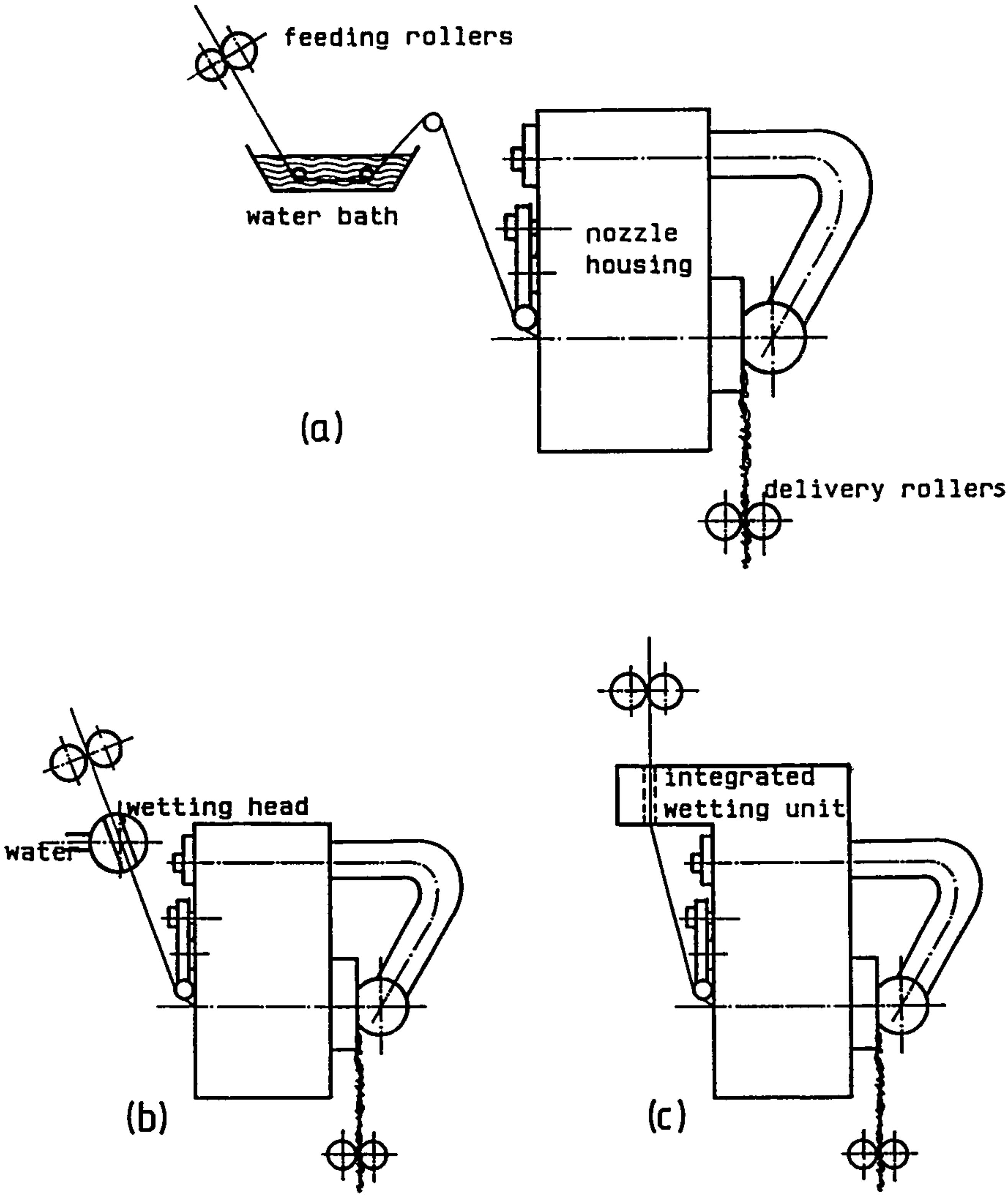

Figure 7.1 The methods for water application to the supply yarn: (a) by means of a water bath; (b) by means of a wetting unit separated from the nozzle housing; and (c) by means of a wetting unit integrated with the nozzle housing

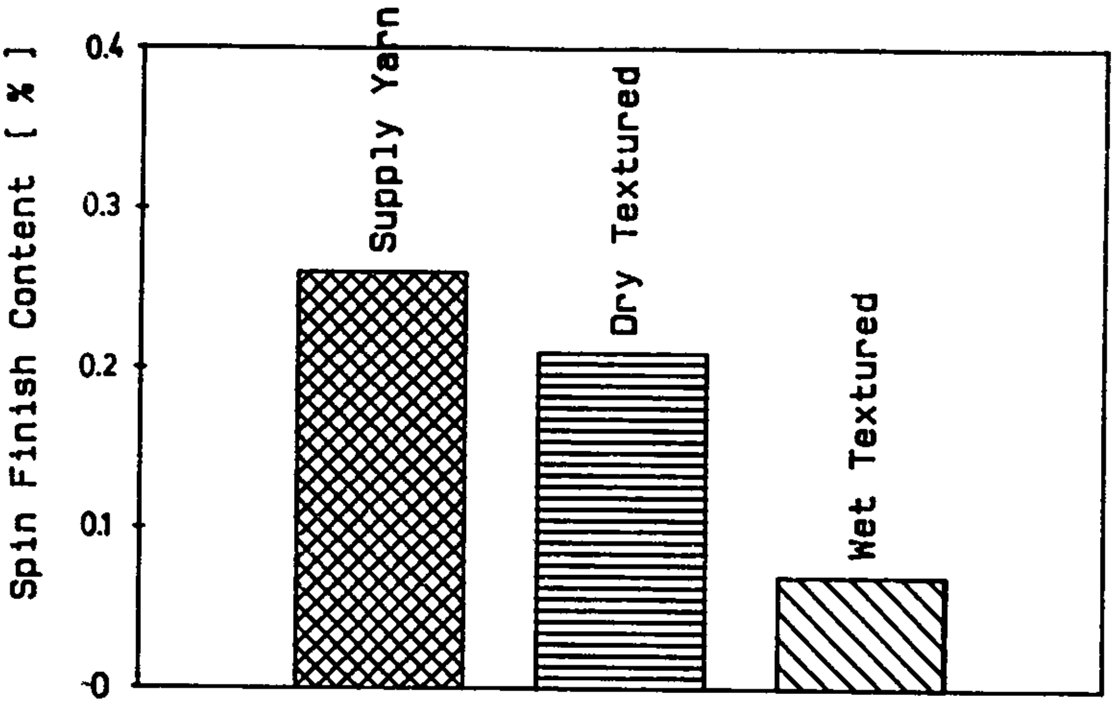

Figure 7.2 Comparison of the amount of spin-finish material left on the yarn surface after dry and wet texturing

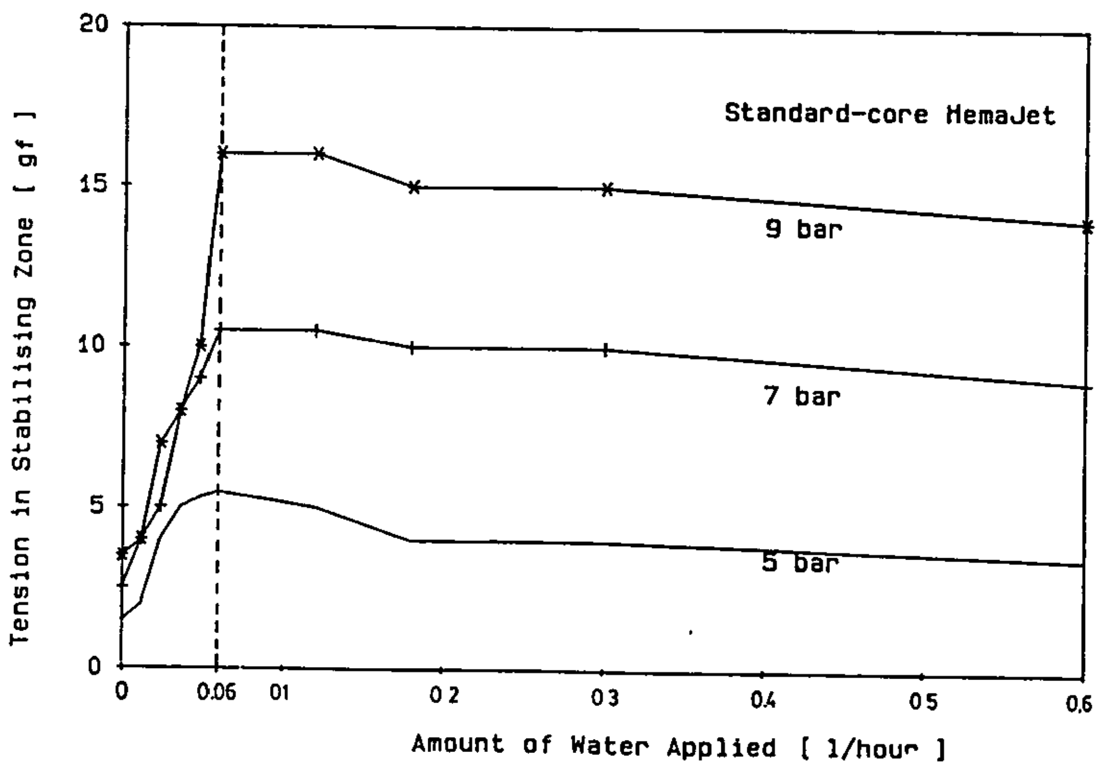

Figure 7.3 Variations in the tension in the stabilising zone with different amount of water application

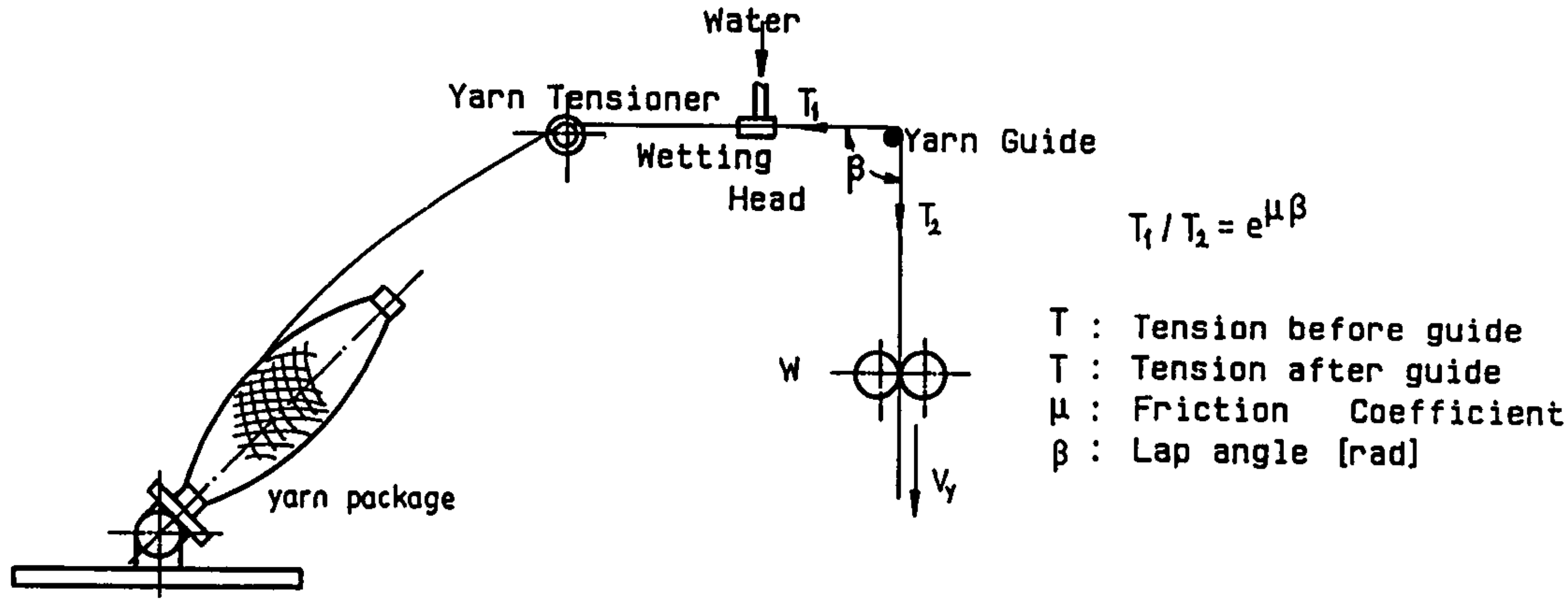

Figure 7.4 Yarn/solid surface friction measurement rig

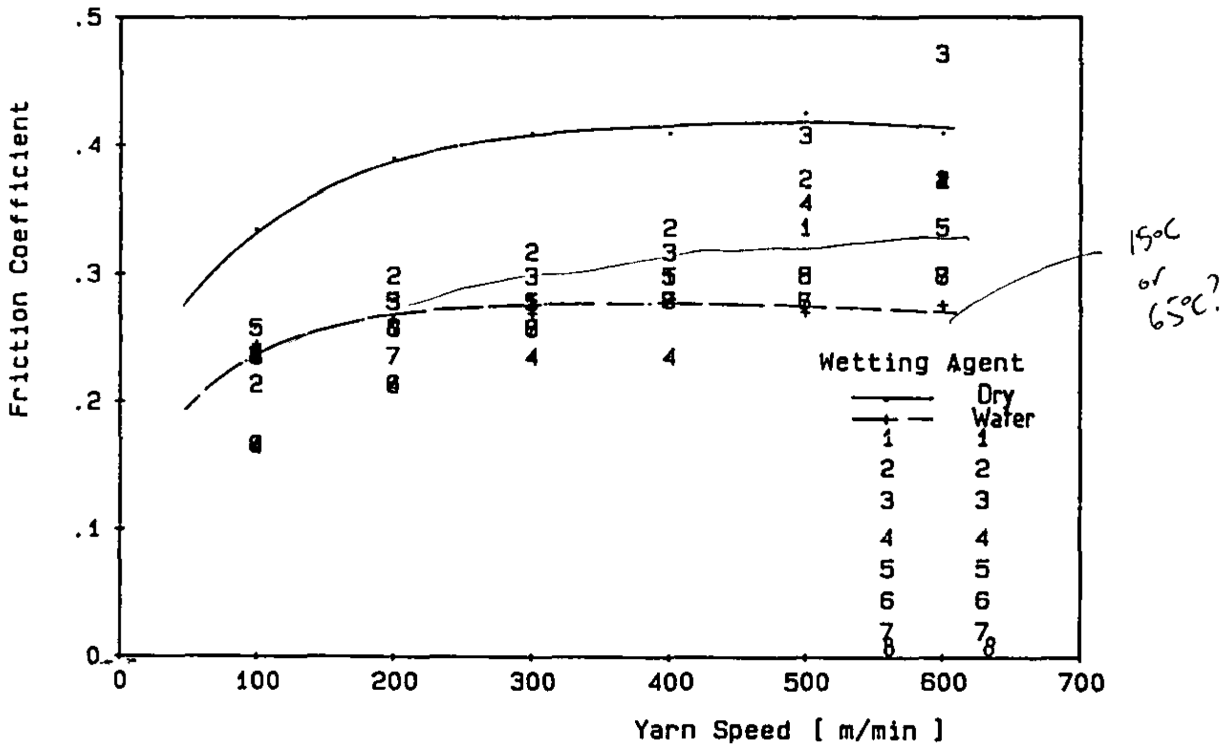

Figure 7.5 Effects of wetting agents added into the water on the filament/solid surface friction

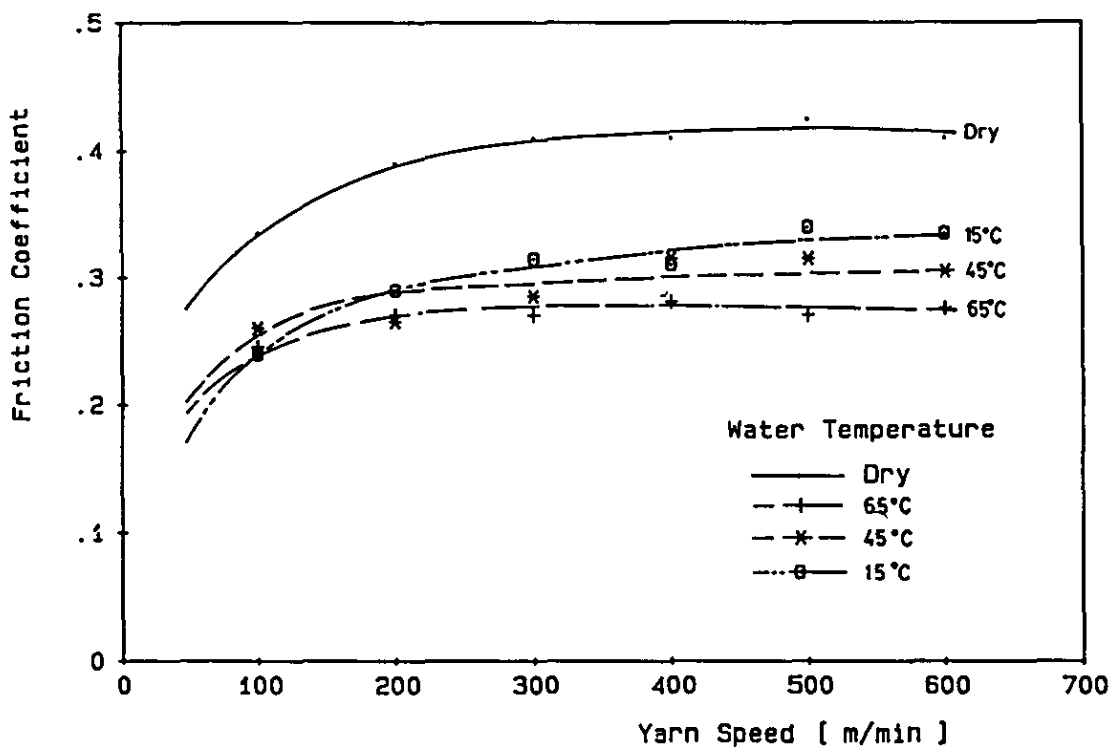

Figure 7.6 Effects of water temperature on the filament/solid surface friction

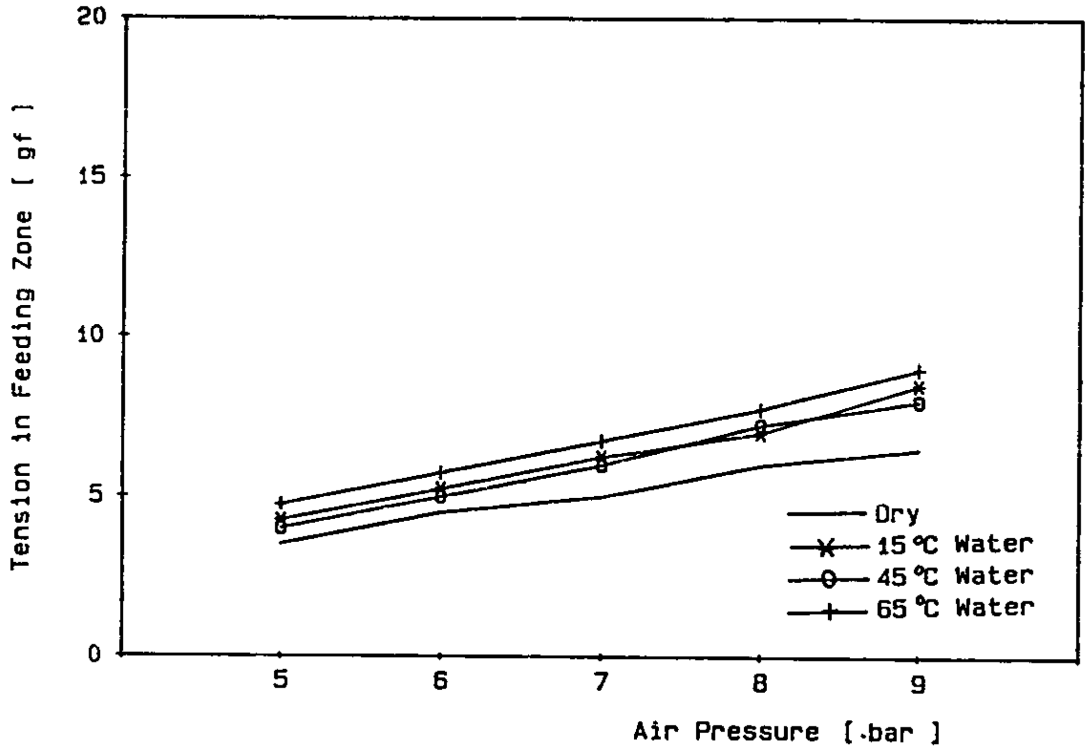

Figure 7.7a The tension in feeding zone at different water temperatures

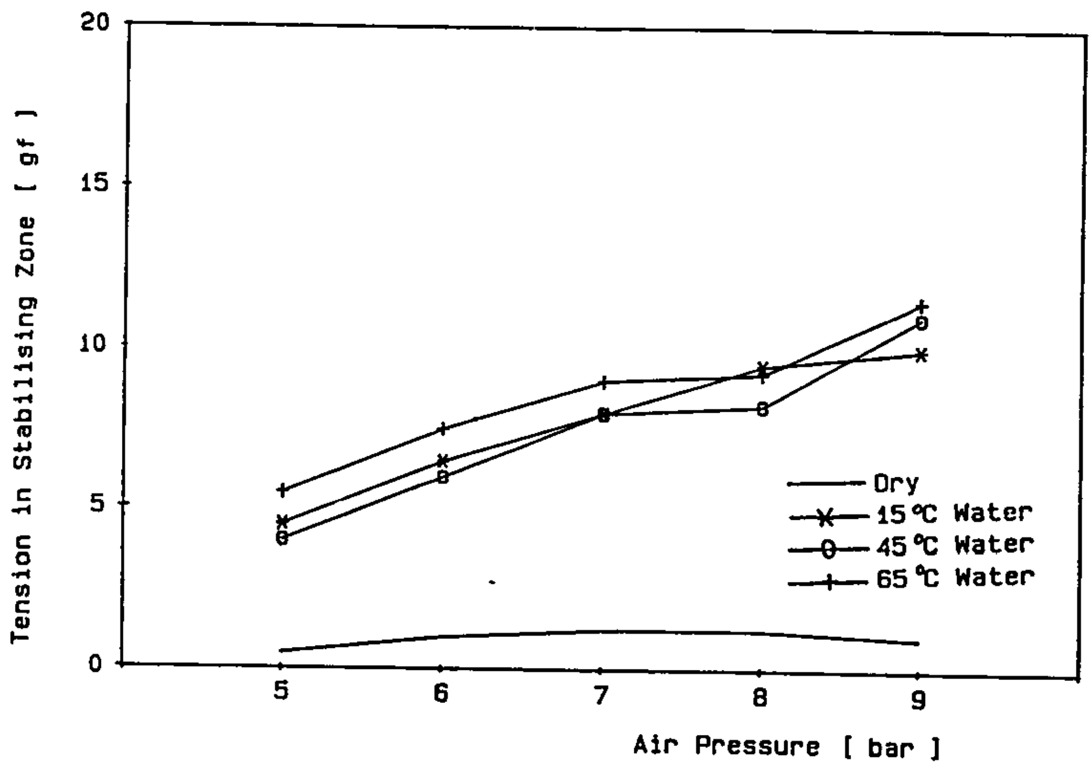

Figure 7.7b The tension in stabilising zone at different water temperatures

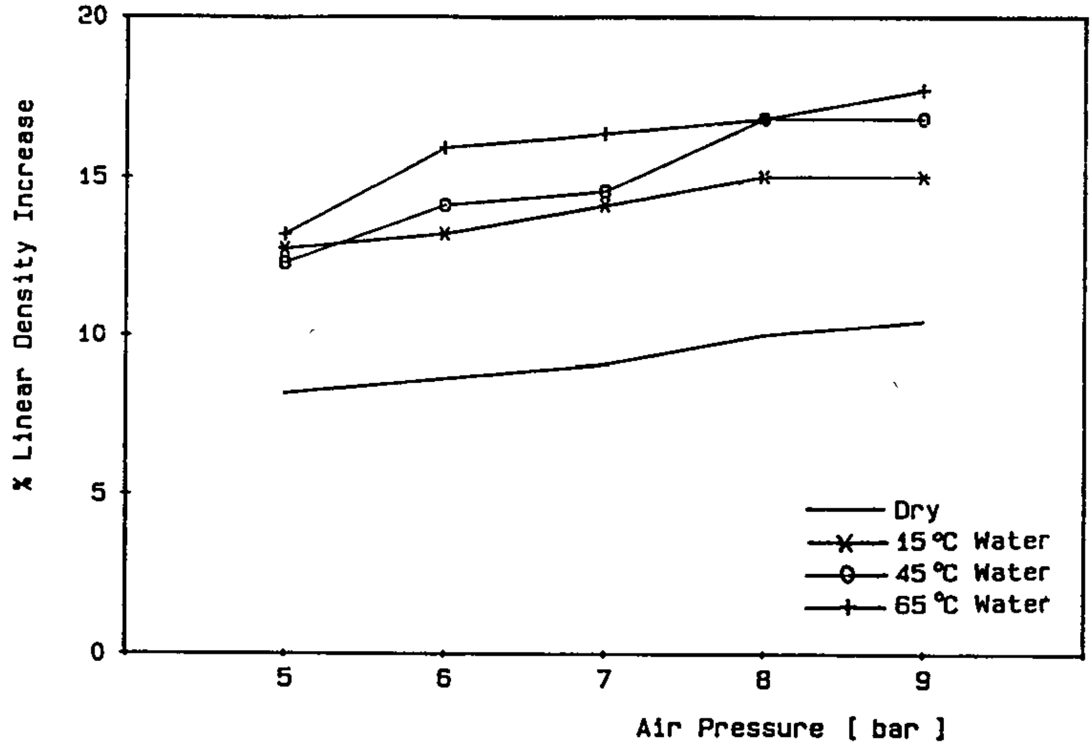

Figure 7.7c The linear density increase of yarns textured at different water temperatures

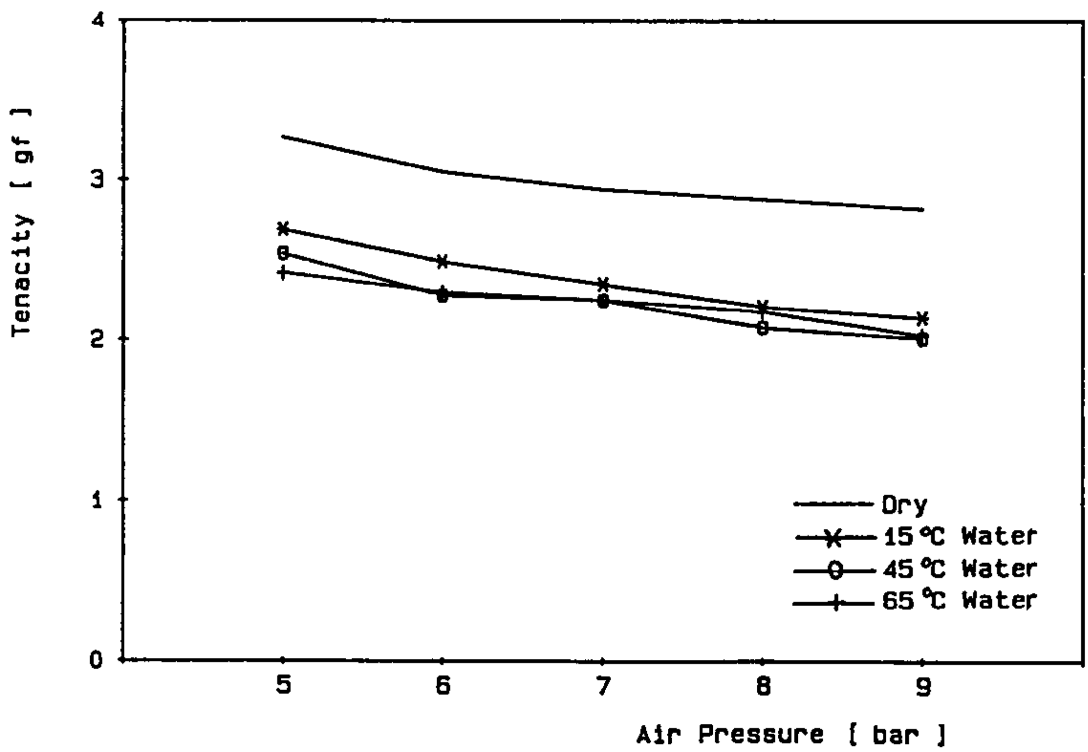

Figure 7.7d The tenacity of yarns textured at different water temperatures

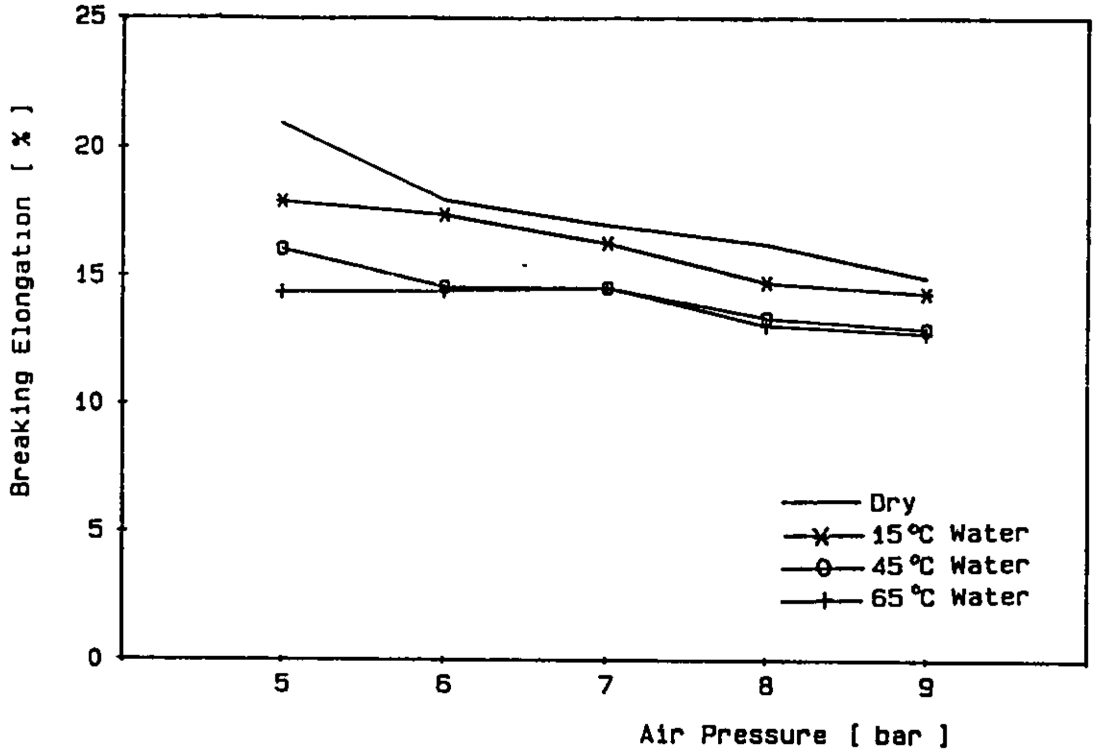

Figure 7.7e The breaking elongation of yarns textured at different water temperatures

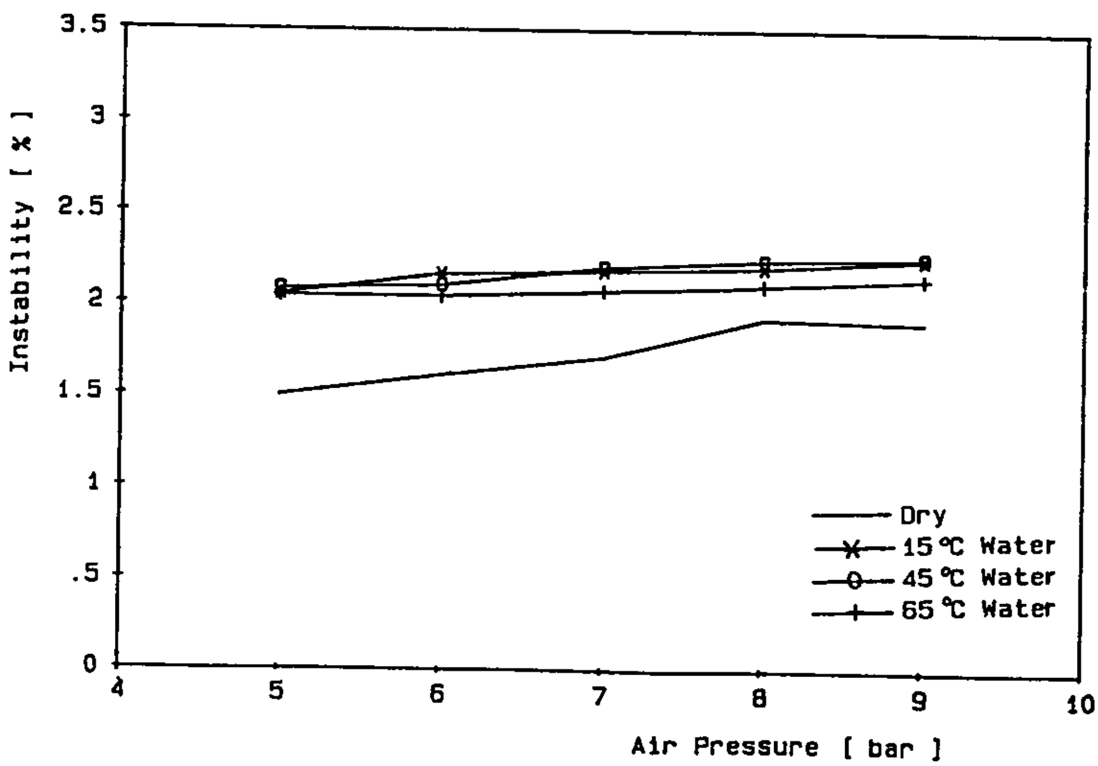

Figure 7.7f The instability of yarns textured at different water temperatures

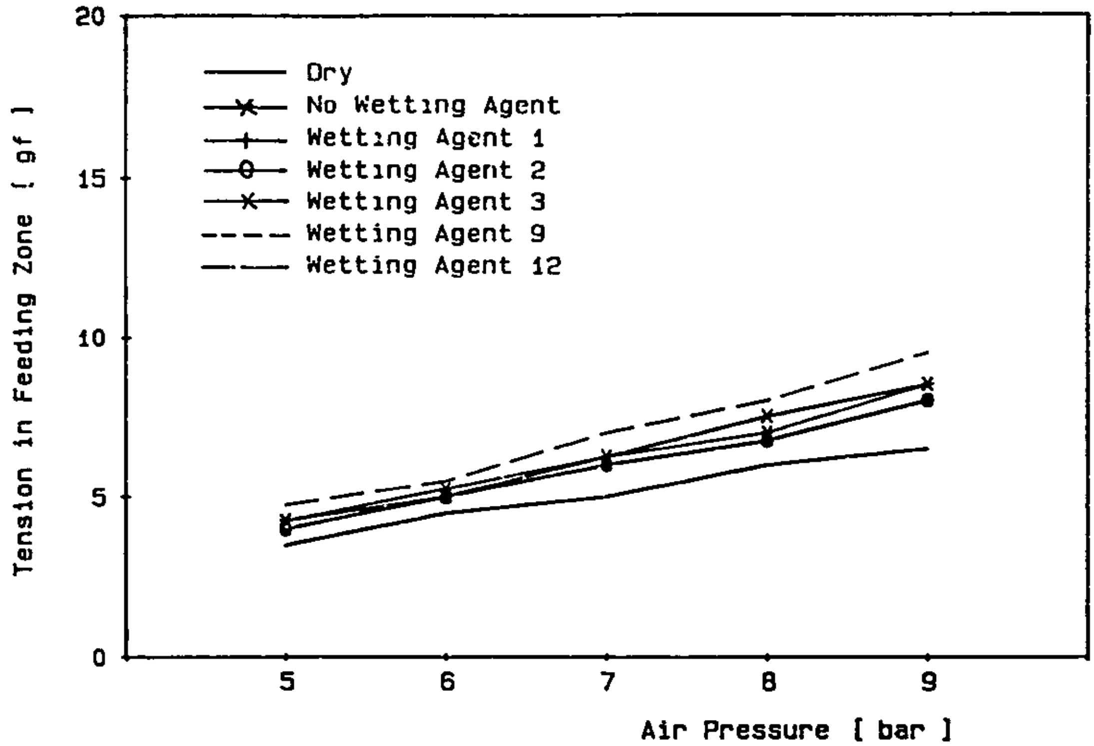

Figure 7.8a The effects of wetting agents added into the water on the tension in feeding zone

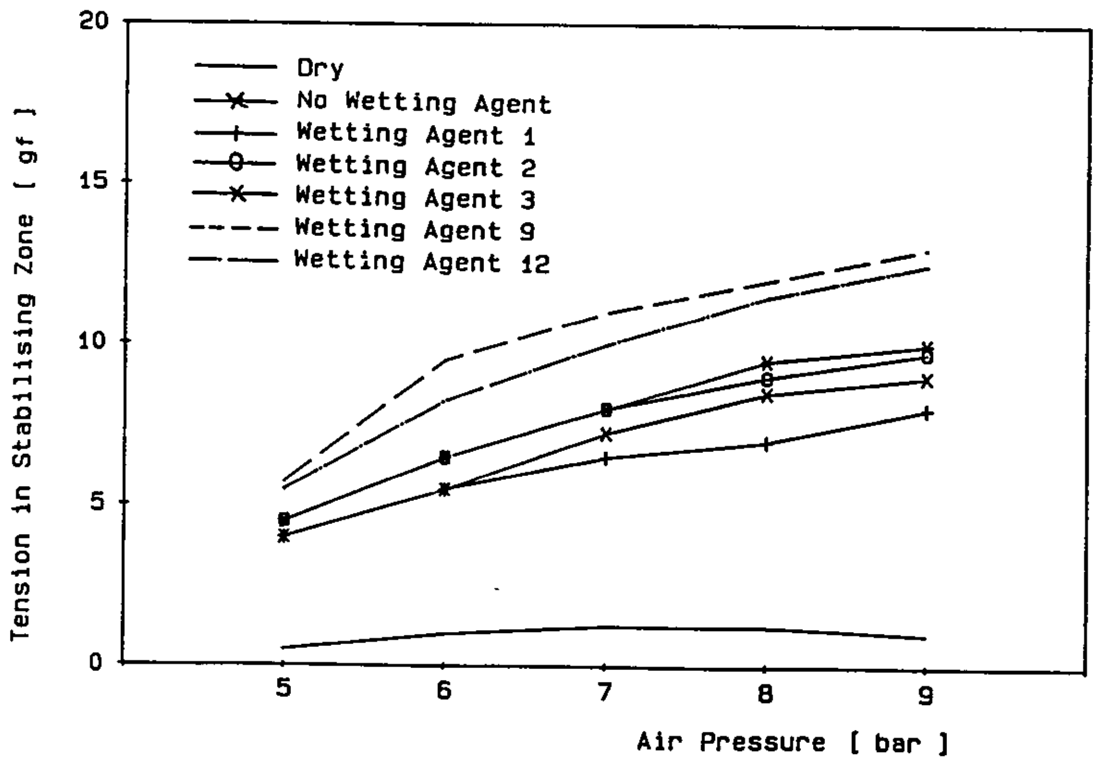

Figure 7.8b The effects of wetting agents added into the water on the tension in stabilising zone

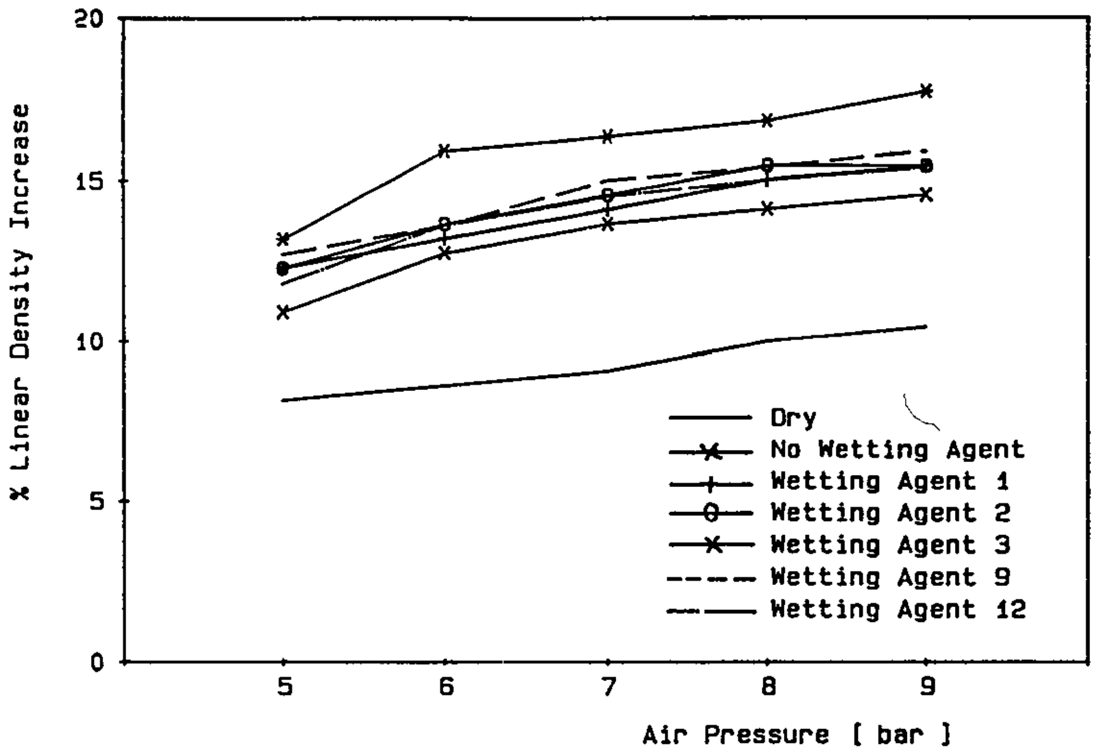

Figure 7.8c The effects of wetting agents added into the water on the linear density increase of yarns textured

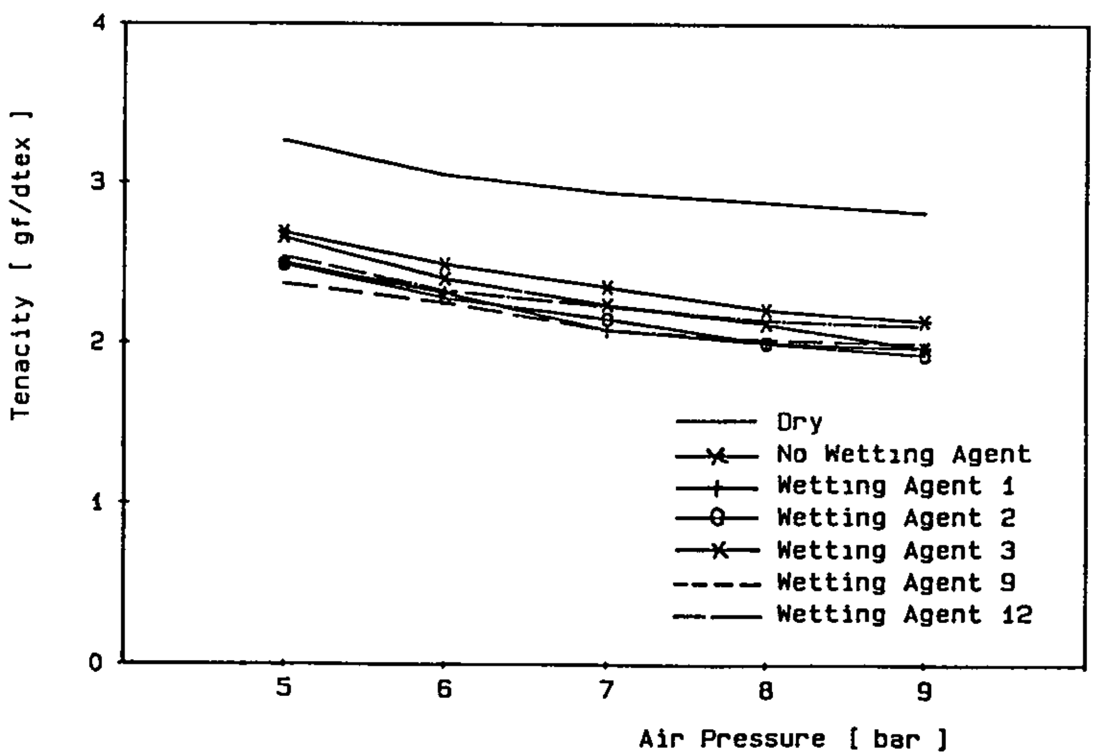

Figure 7.8d The effects of wetting agents added into the water on the tenacity of yarns textured

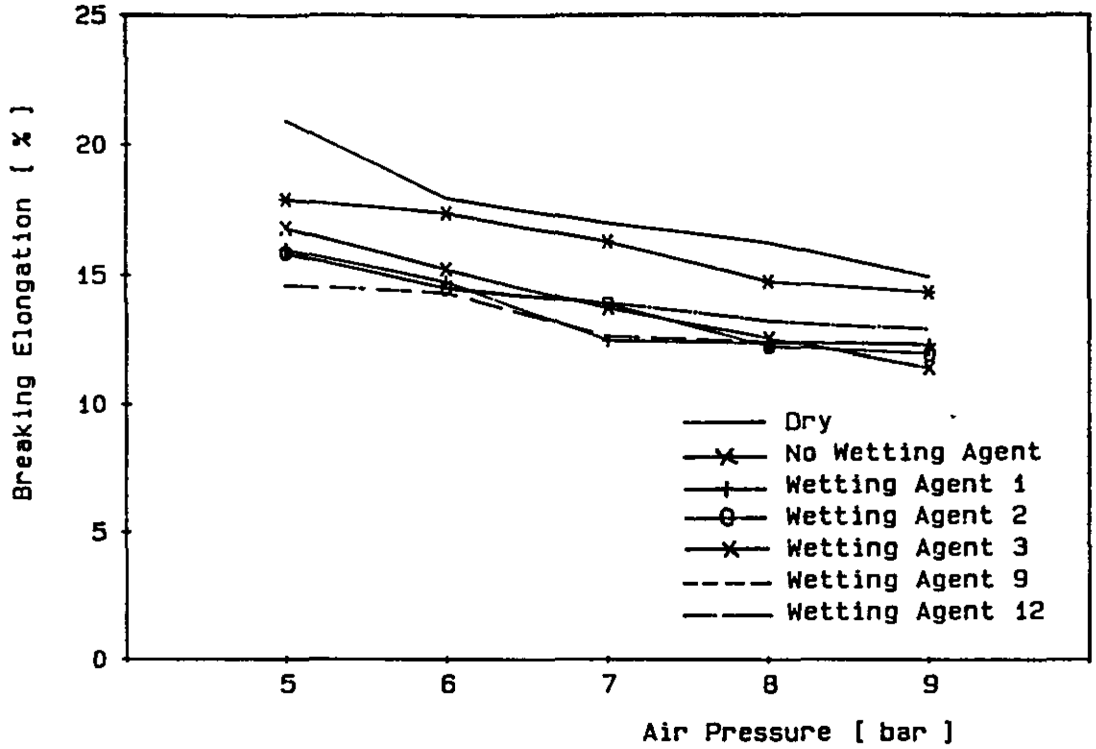

Figure 7.8e The effects of wetting agents added into the water on the breaking elongation of yarns textured

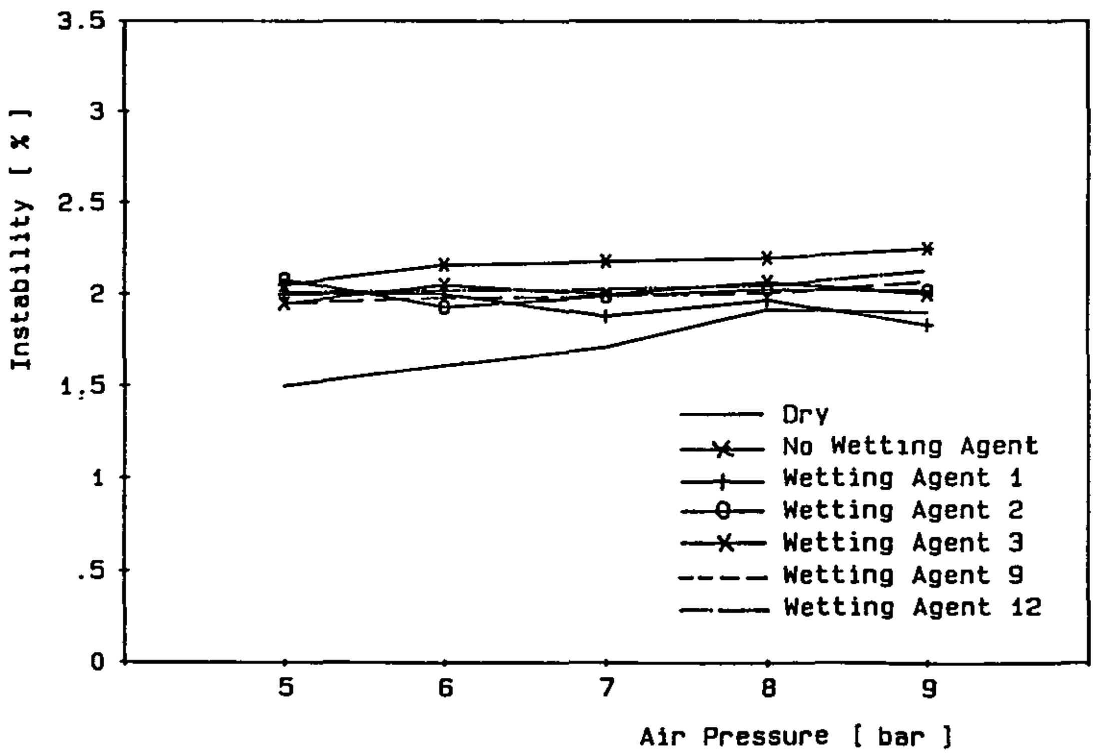

Figure 7.8f The effects of wetting agents added into the water on the instability of yarns textured

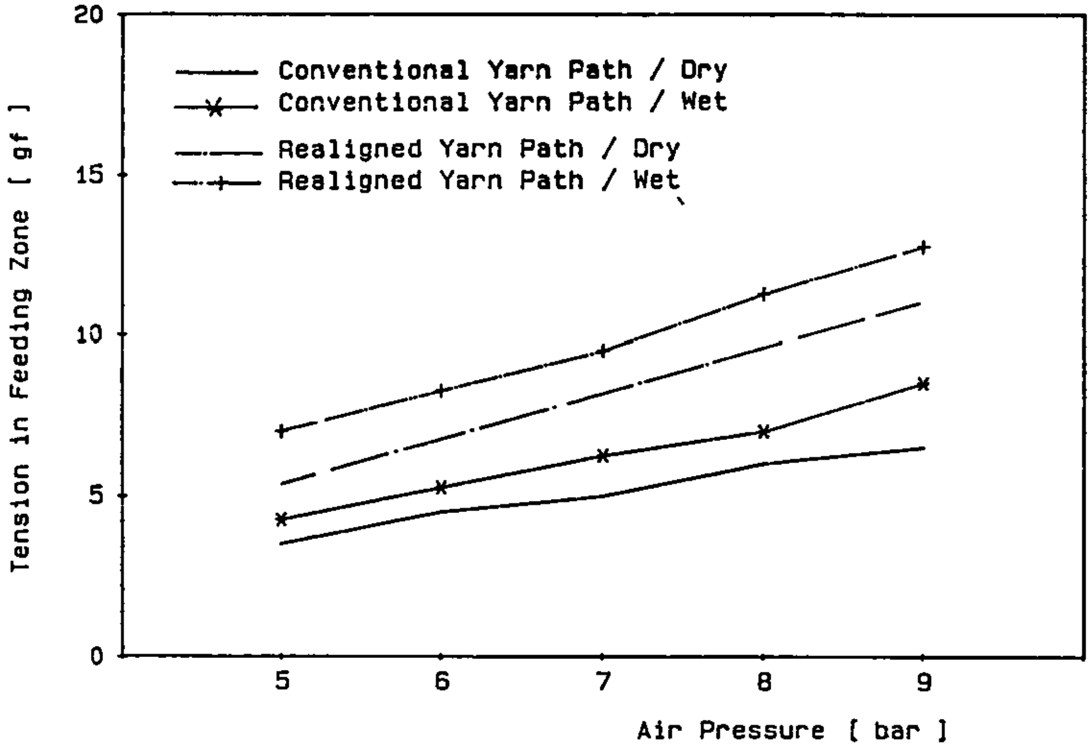

Figure 7.9a The tension in feeding zone with realigned yarn path arrangement

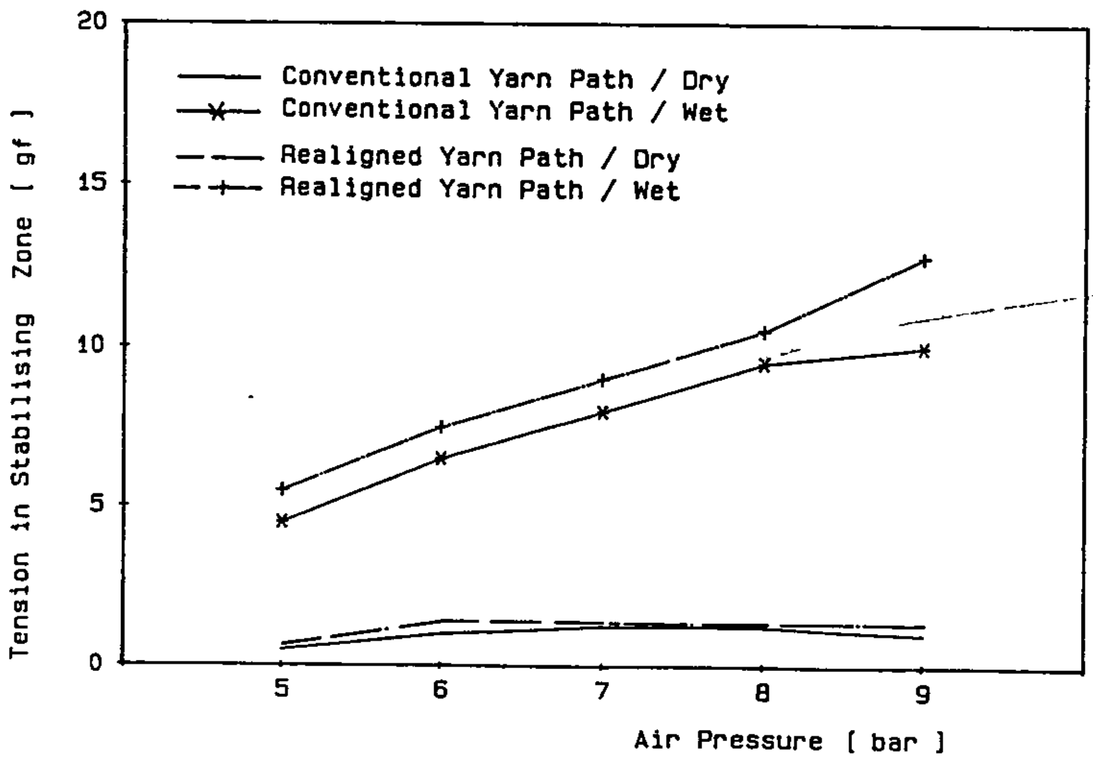

Figure 7.9b The tension in stabilising zone with realigned yarn path arrangement

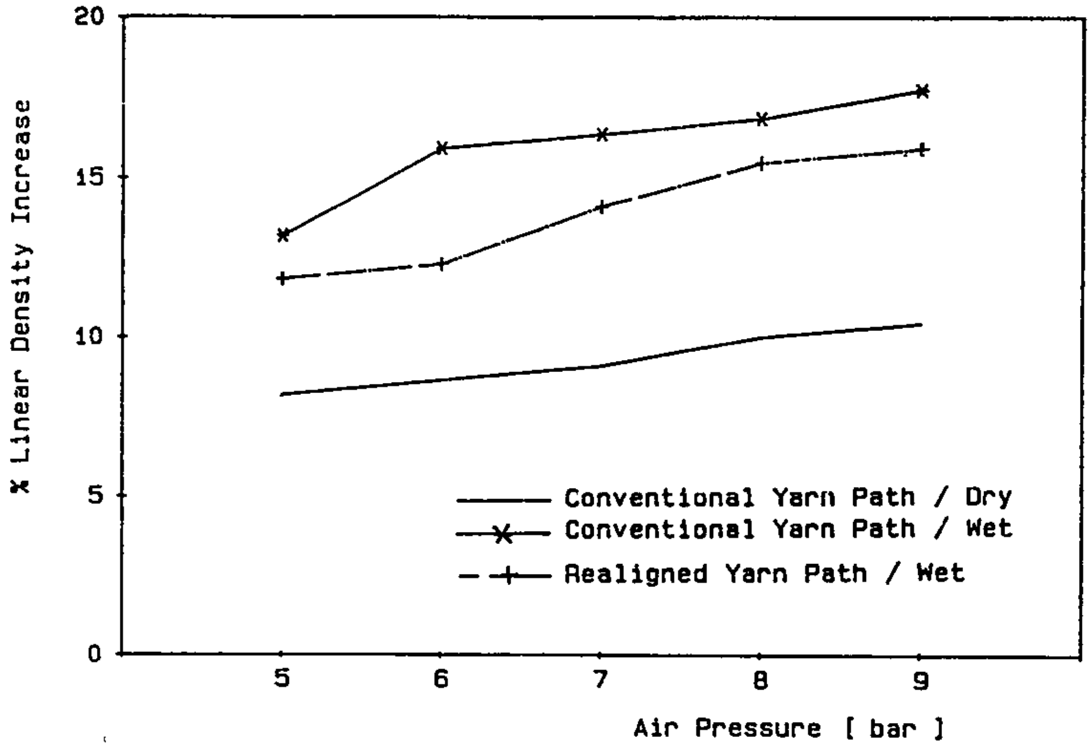

Figure 7.9c Linear density increase of yarns textured with realigned yarn path arrangement

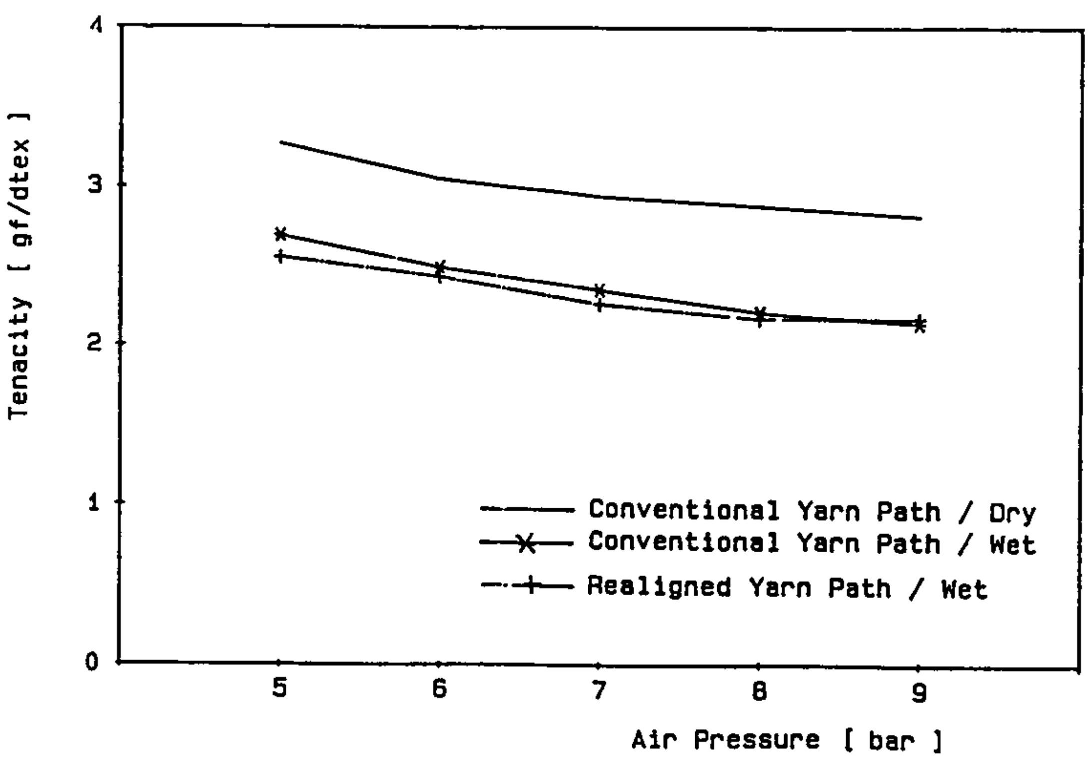

Figure 7.9d Tenacity of yarns textured with realigned yarn path arrangement

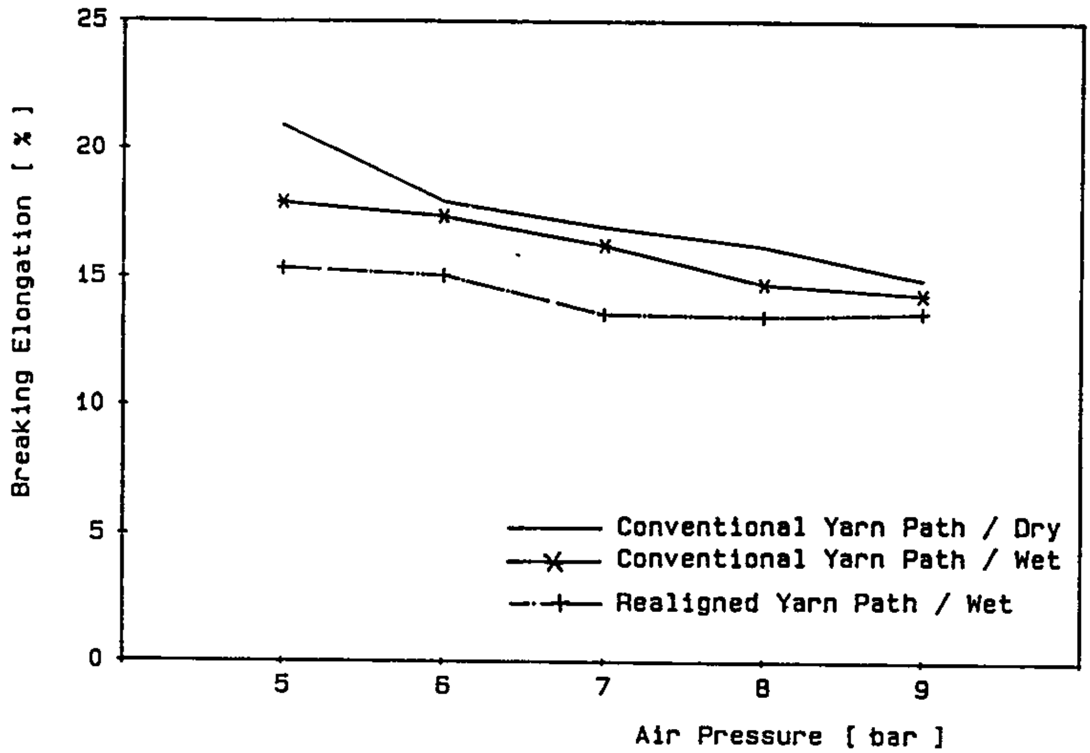

Figure 7.9e Breaking elongation of yarns textured with realigned yarn path arrangement

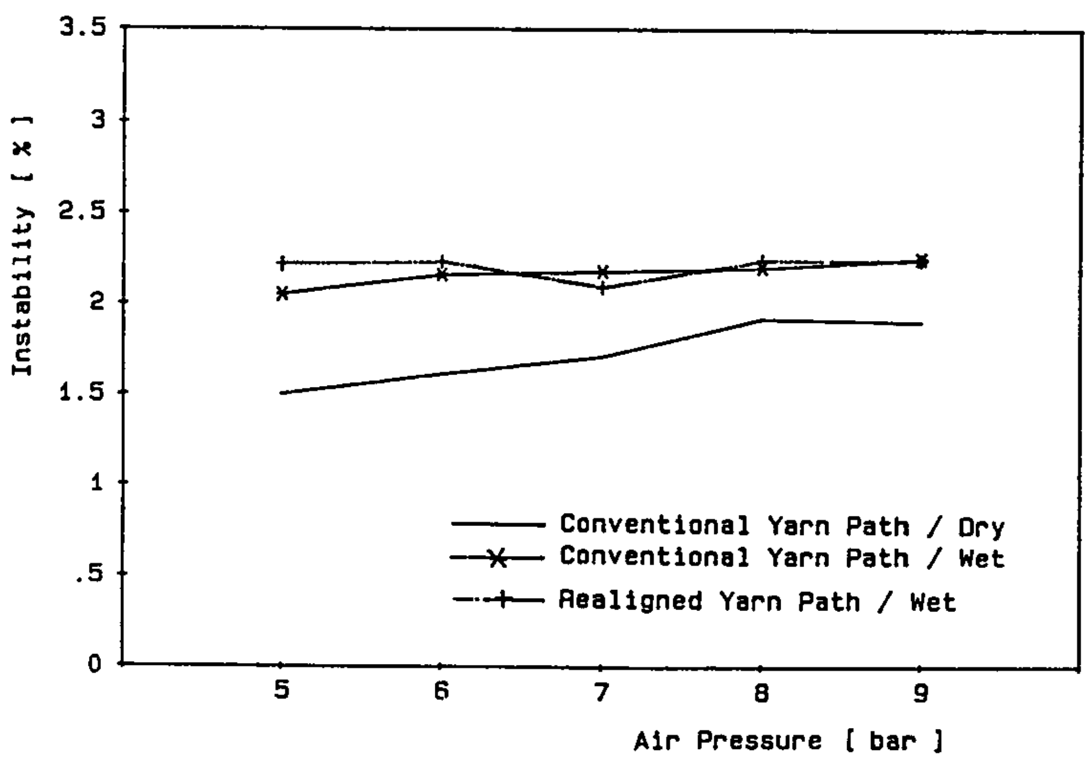

Figure 7.9f Instability of yarns textured with realigned yarn path arrangement

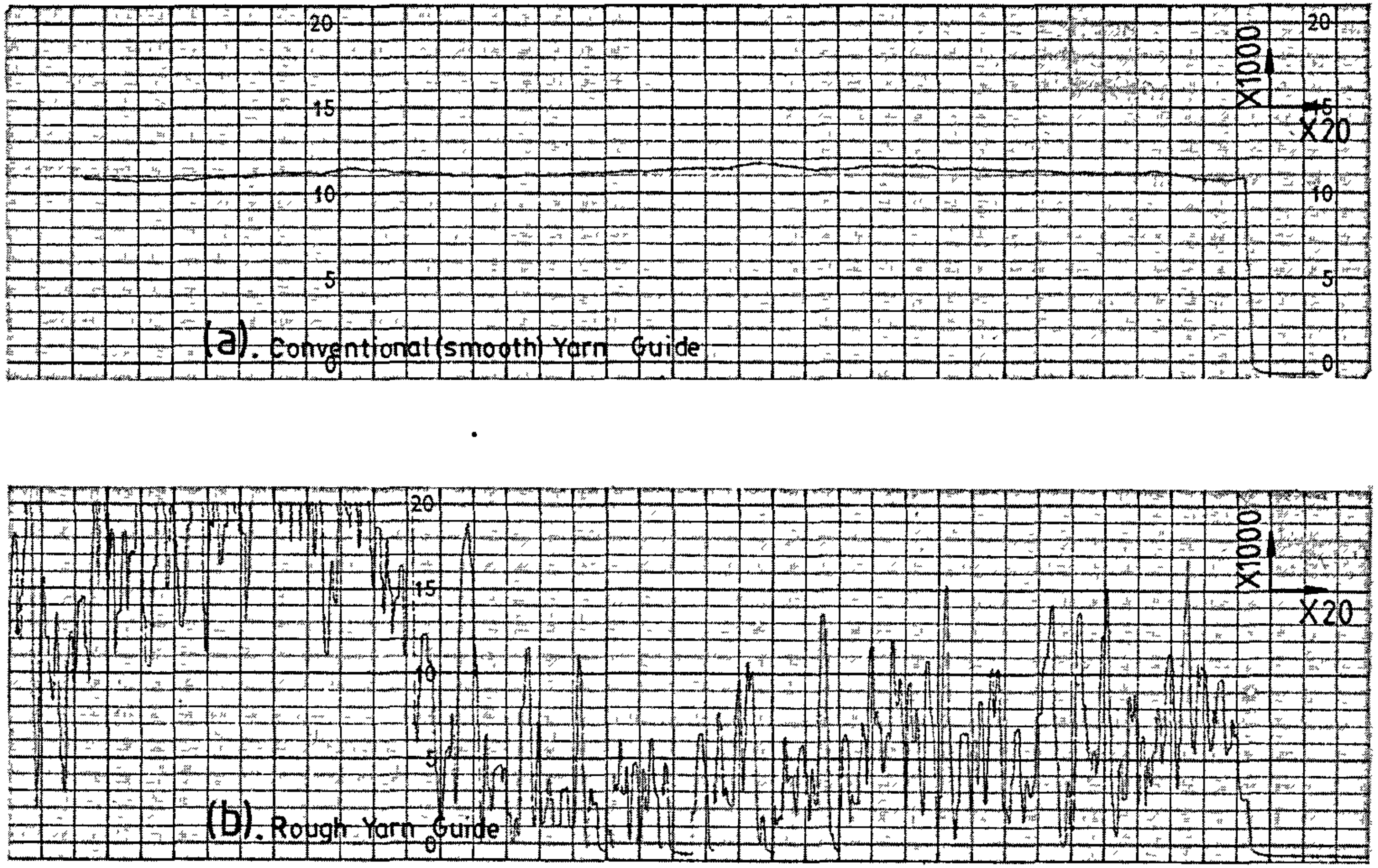

Figure 7.10 Comparison of the surface traces of two different yarn guides

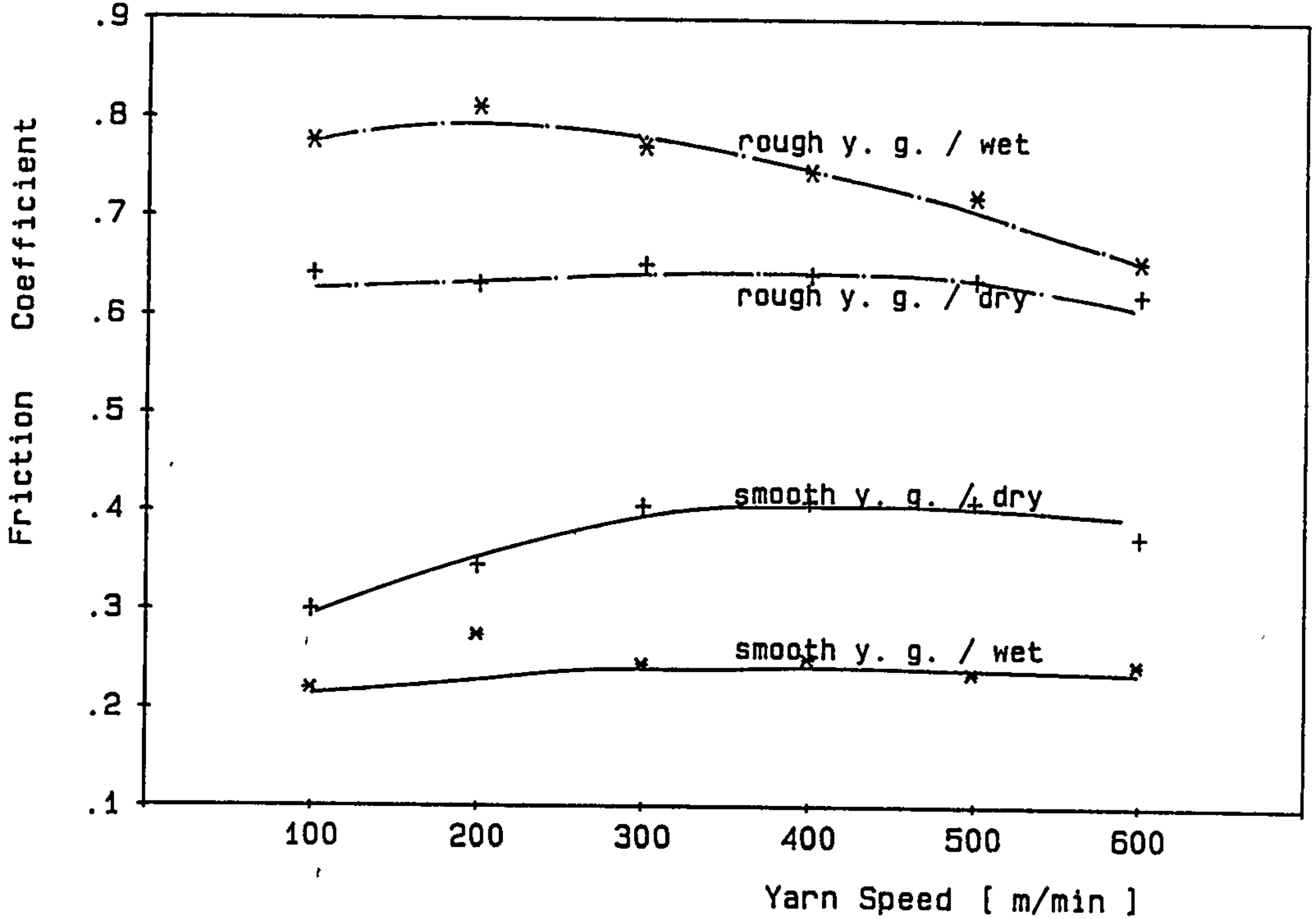

Figure 7.11 The effects of yarn surface roughness on the filament/solid surface friction

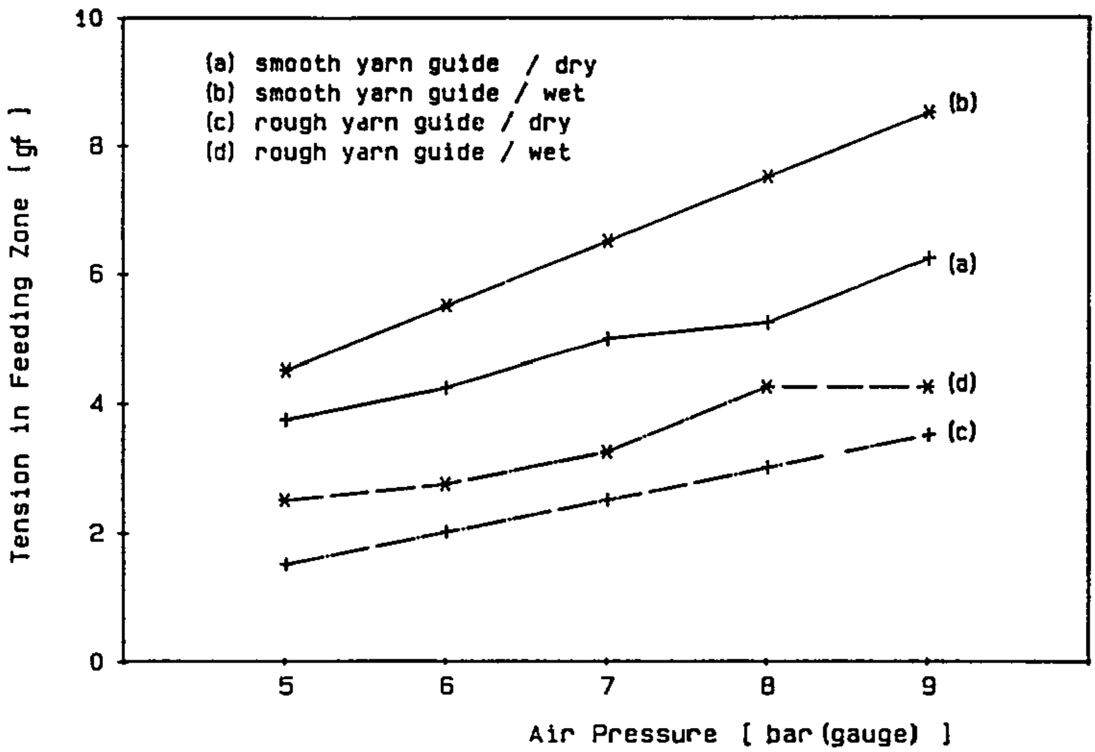

Figure 7.12a The tension in feeding zone with smooth and rough surfaced yarn guides

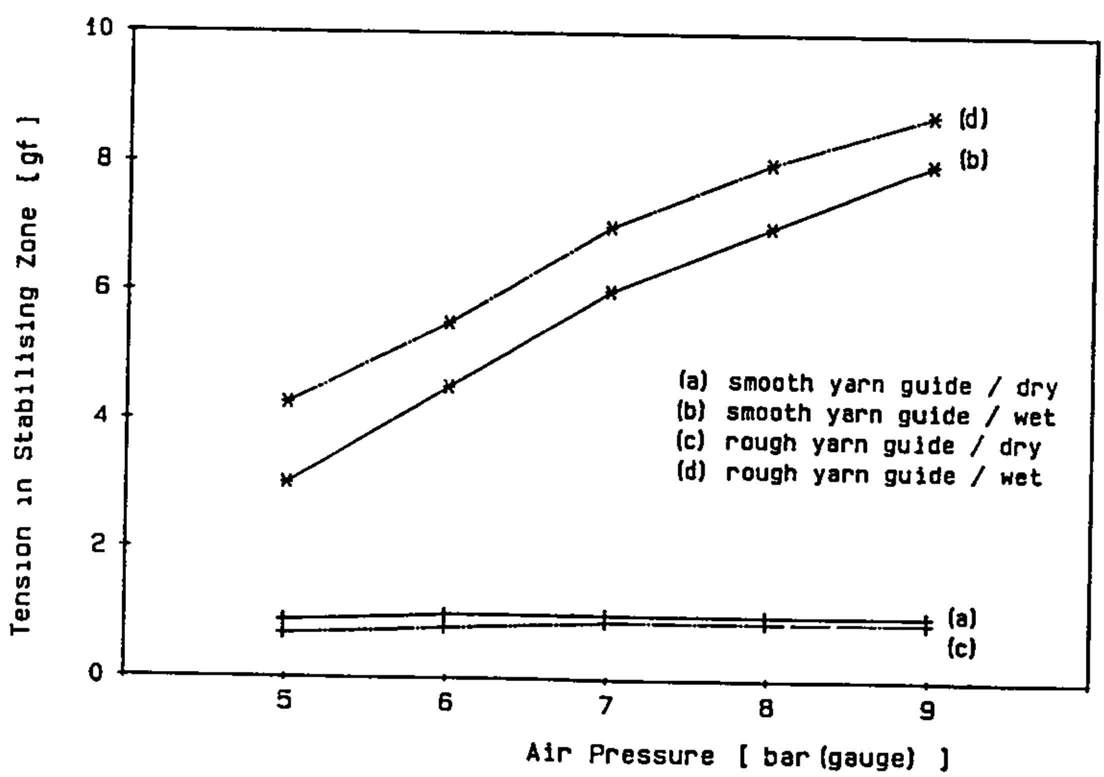

Figure 7.12b The tension in stabilising zone with smooth and rough surfaced yarn guides

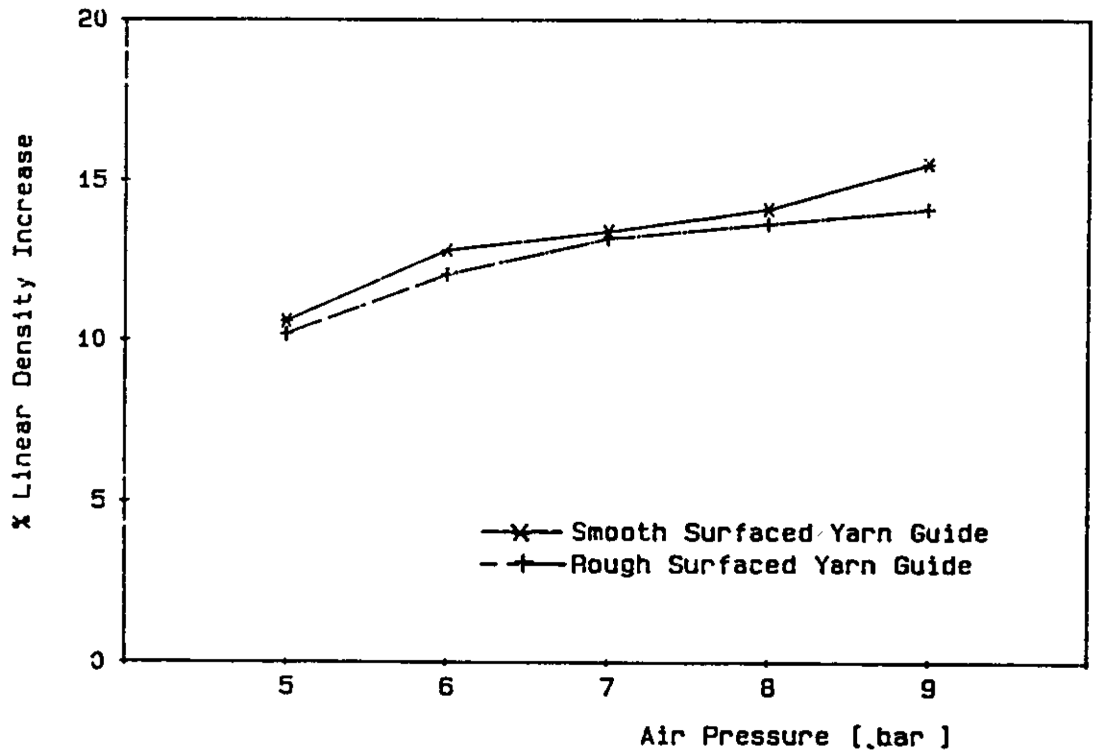

Figure 7.12c Linear density increase of yarns textured with smooth and rough surfaced yarn guides

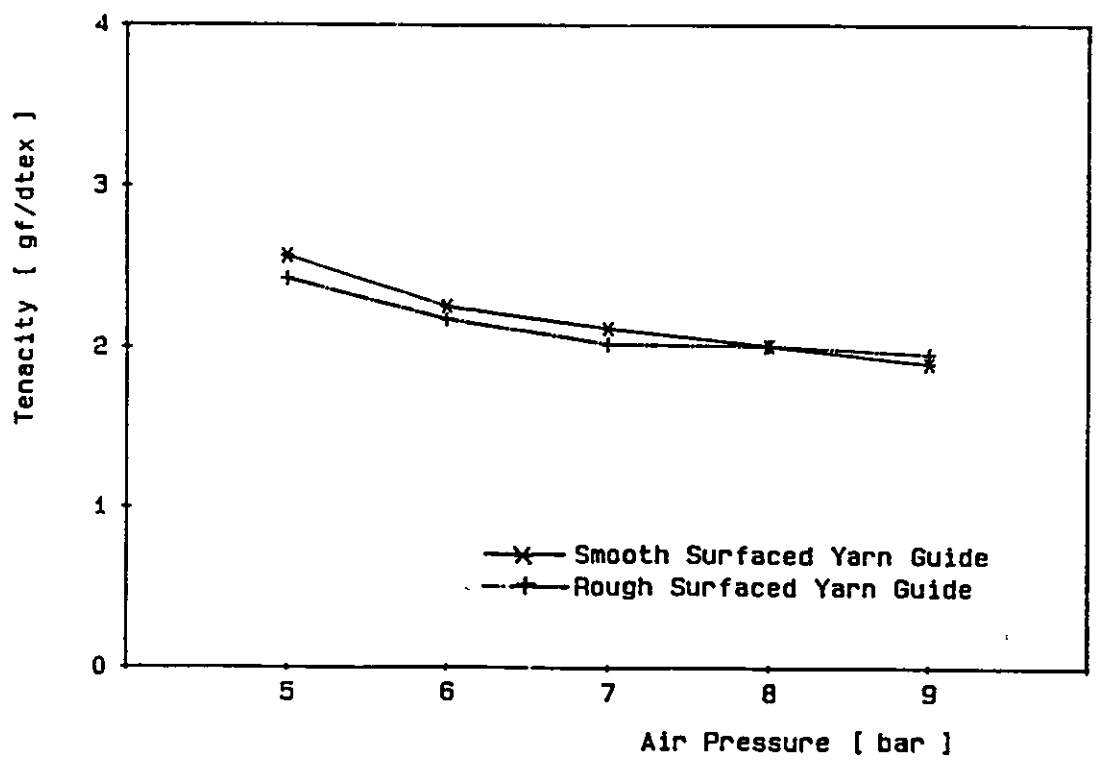

Figure 7.12d Tenacity of yarns textured with smooth and rough surfaced yarn guides

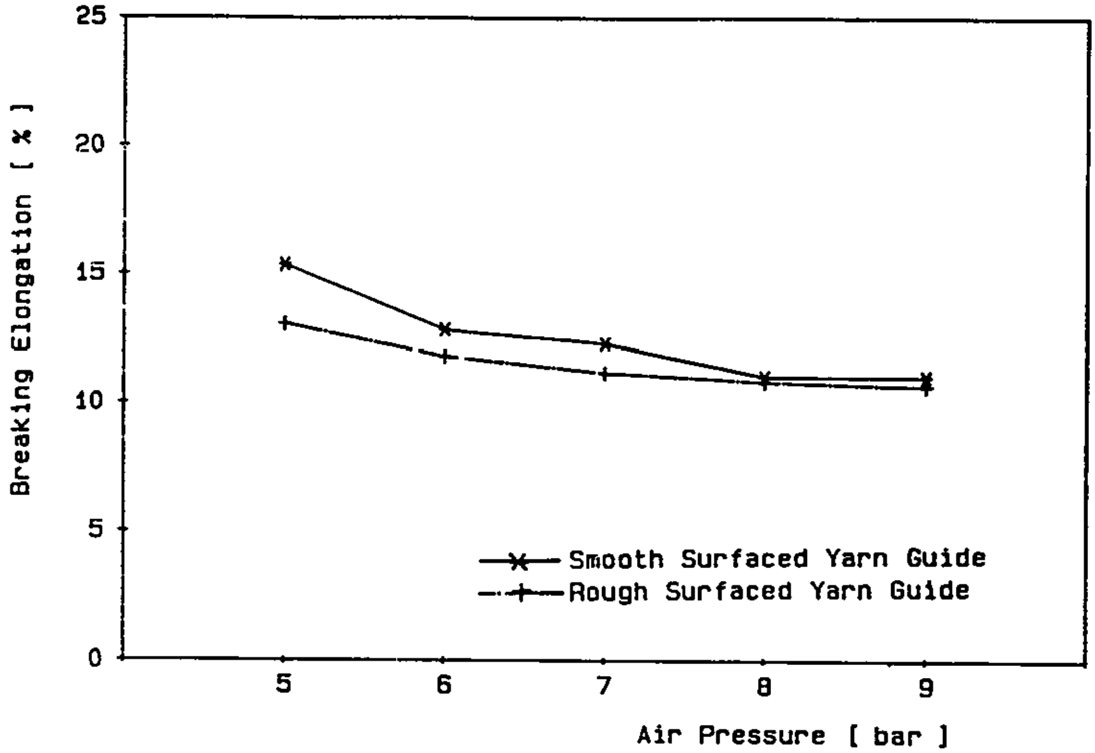

Figure 7.12e Breaking elongation of yarns textured with smooth and rough surfaced yarn guides

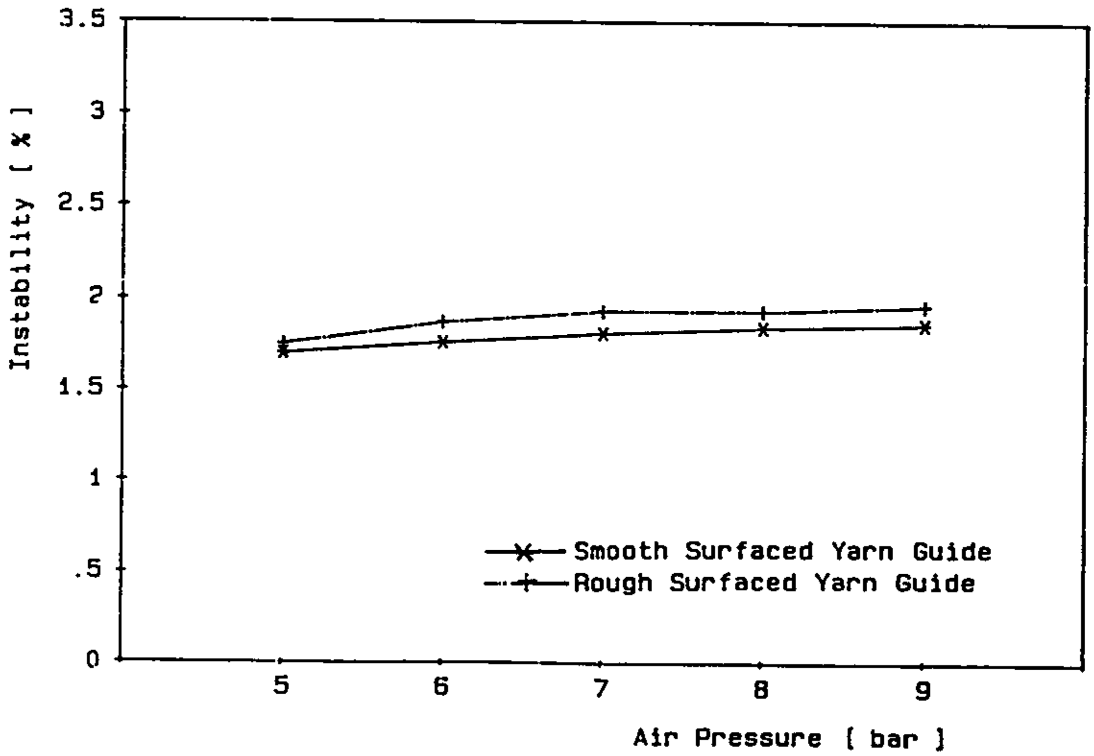

Figure 7.12f Instability of yarns textured with smooth and rough surfaced yarn guides

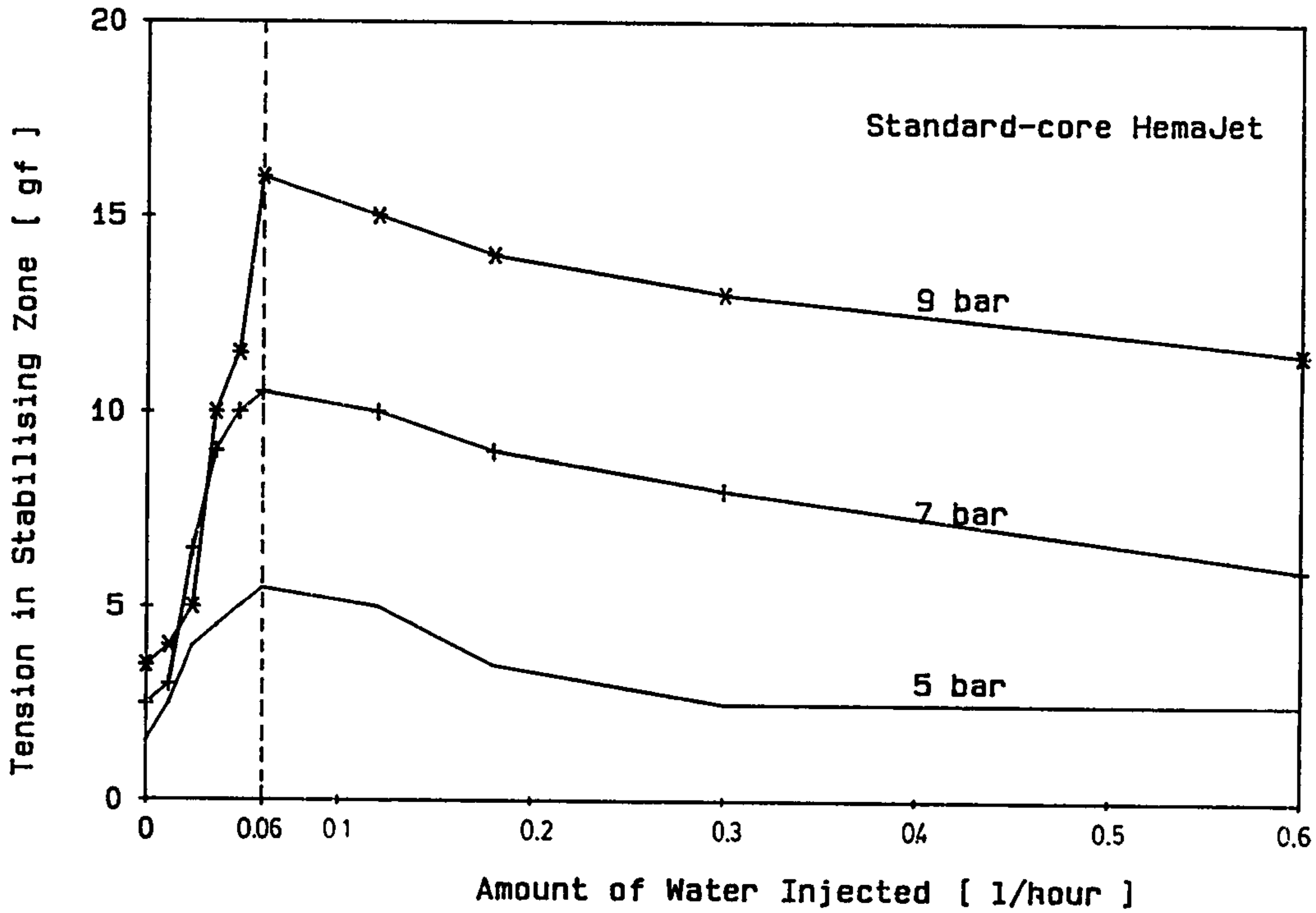

Figure 7.13 The effects of amount of water injected into the air on the tensions in the stabilising zone

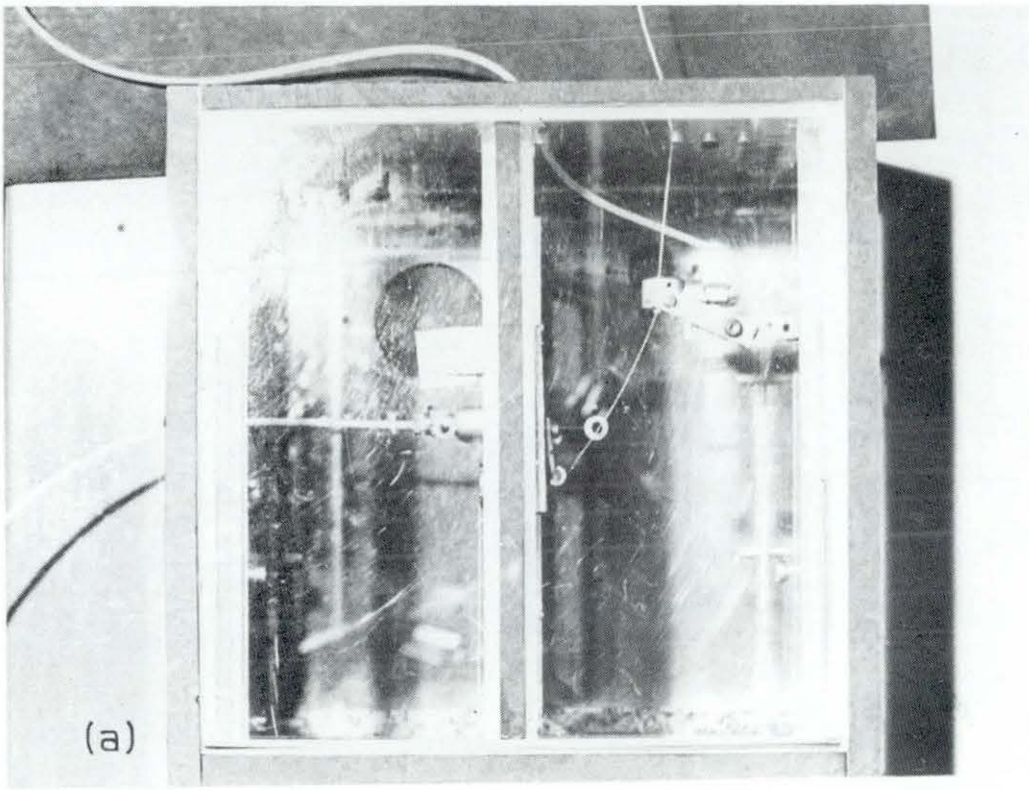

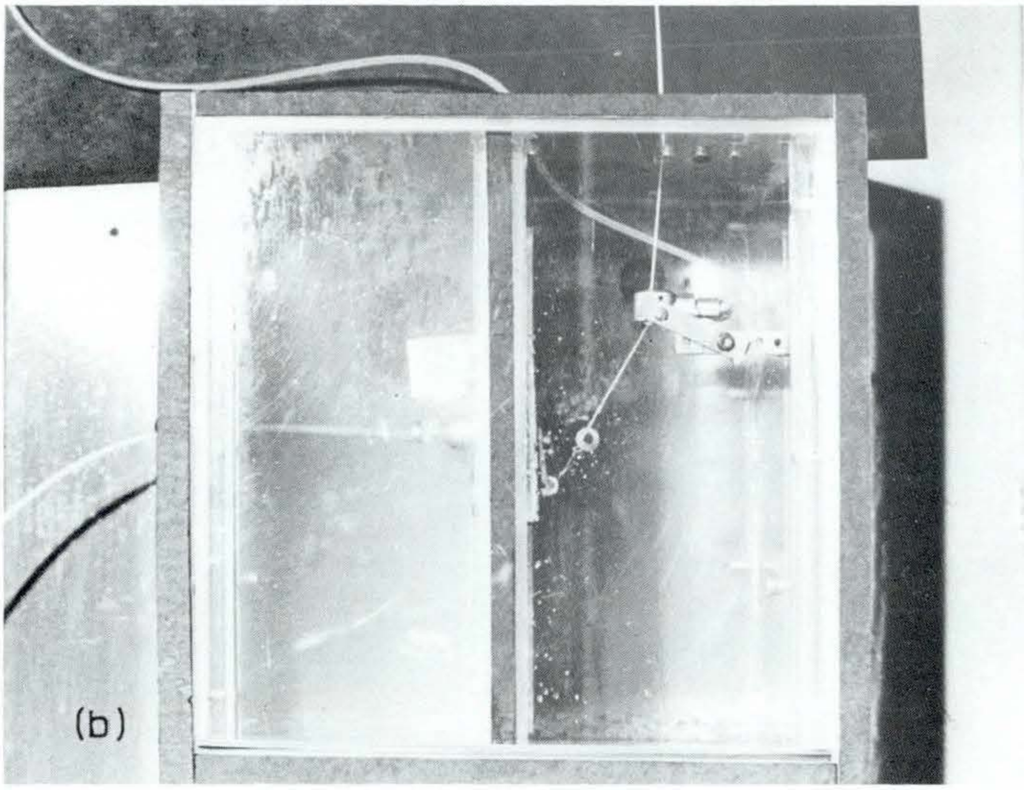

Figure 7.14 The photographs of two chamber nozzle enclosure during the texturing: (a) no water is applied; and (b) water is injected into the air

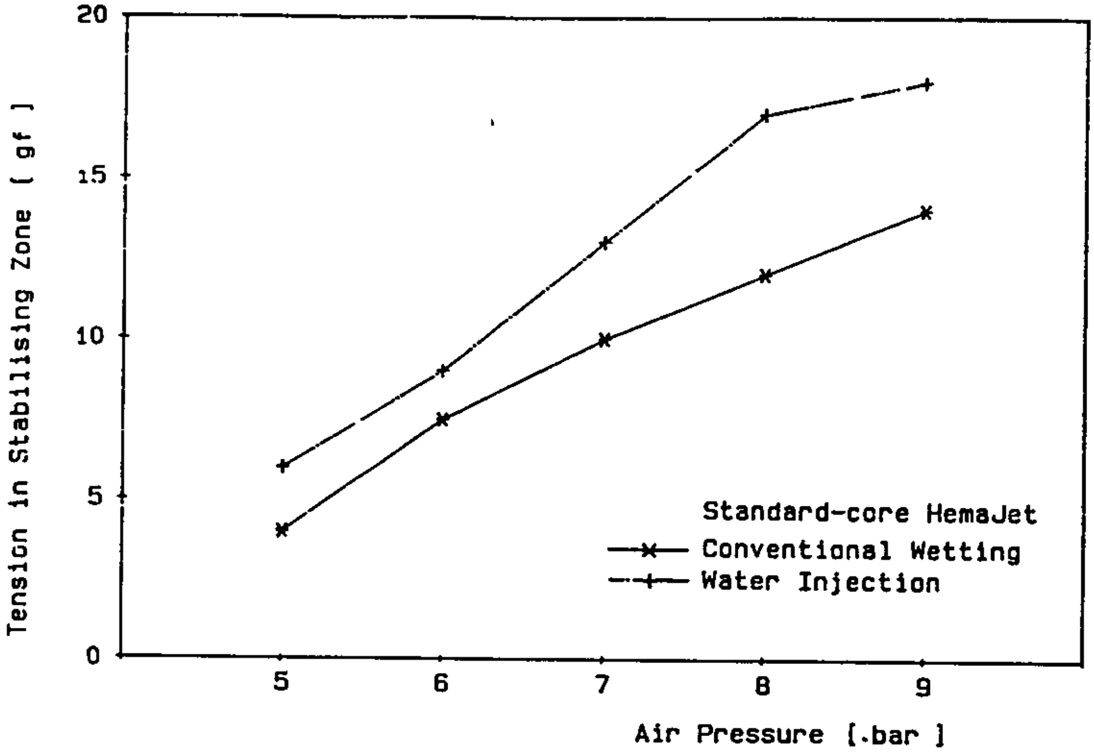

Figure 7.15a Comparison of tension in stabilising zone with water injection and conventional wetting

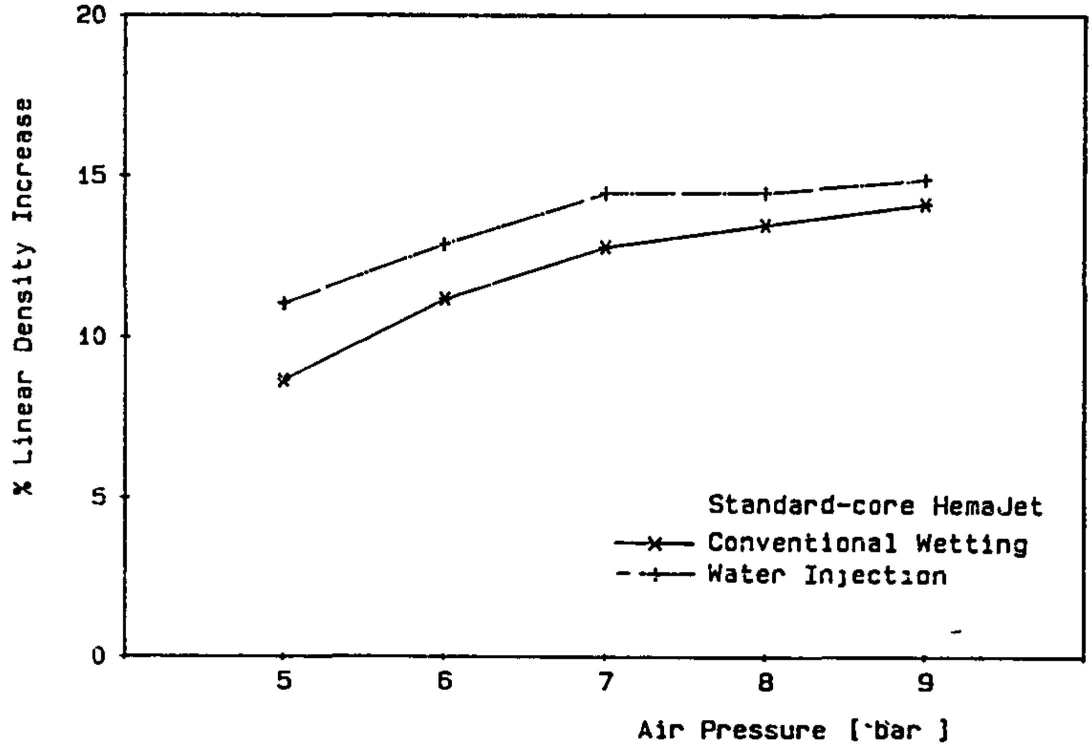

Figure 7.15b Comparison of linear density increase of yarns textured with water injection and conventional wetting

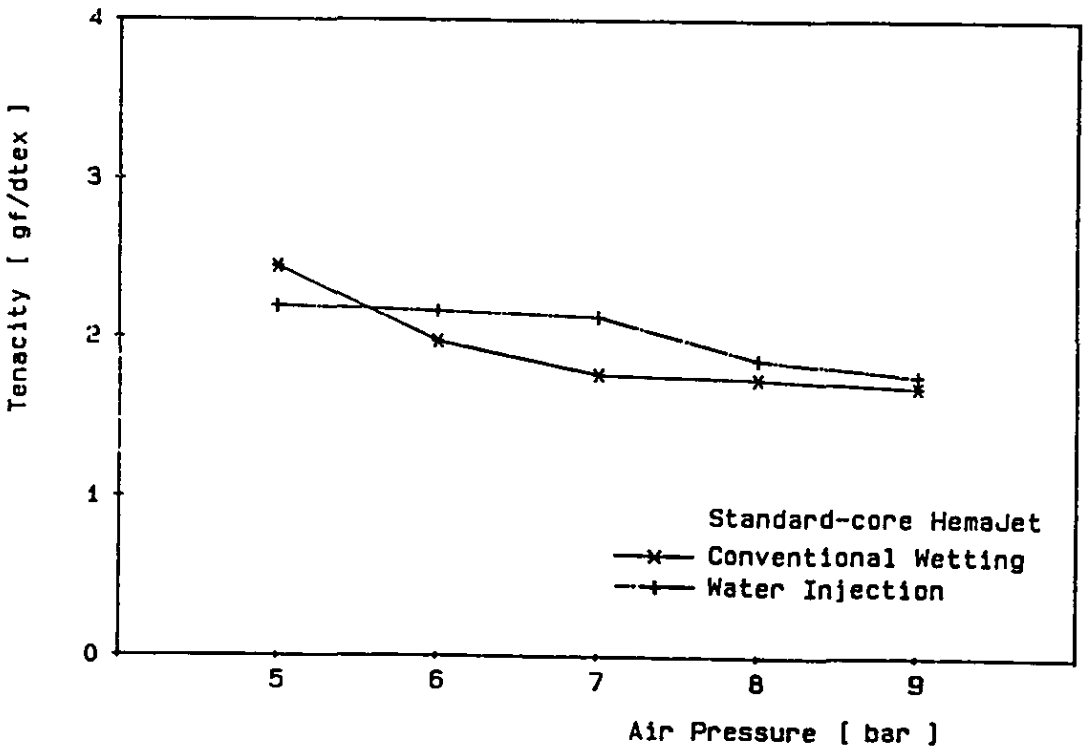

Figure 7.15c Comparison of tenacity of yarns textured with water injection and conventional wetting

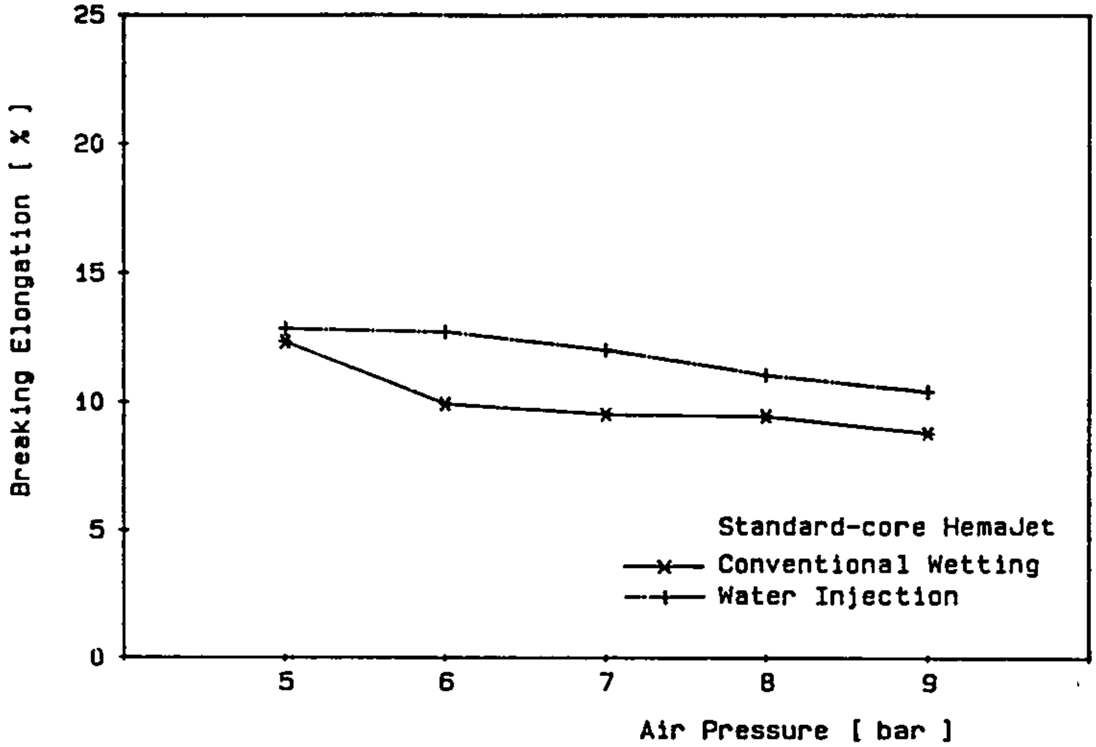

Figure 7.15d Comparison of breaking elongation of yarns textured with water injection and conventional wetting

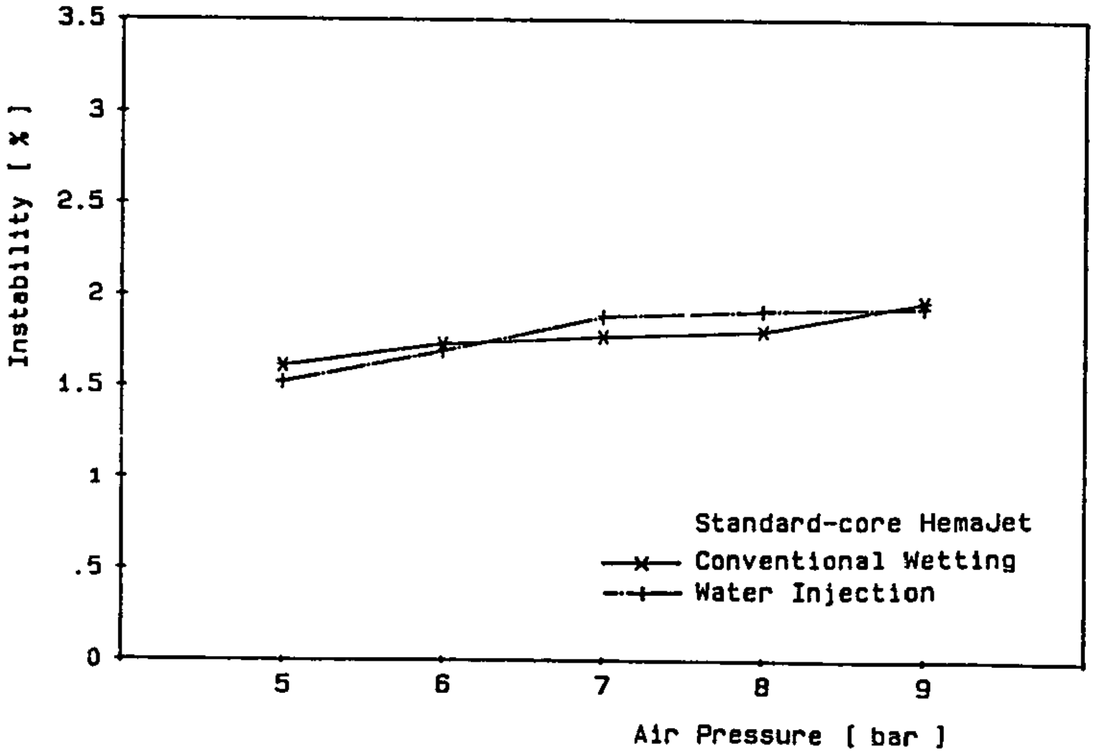

Figure 7.15e Comparison of instability of yarns textured with water injection and conventional wetting

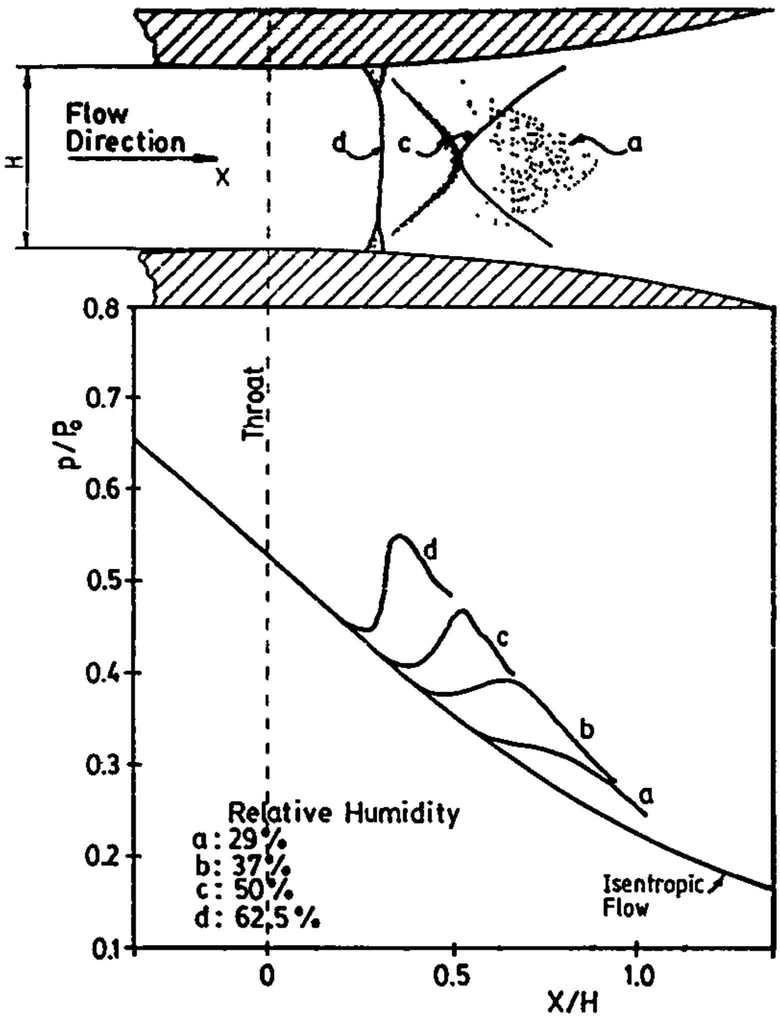

Figure 7.16a The effects of condensation shock waves on the static pressure distribution along the centre-line of the nozzle (after Pouring[111])

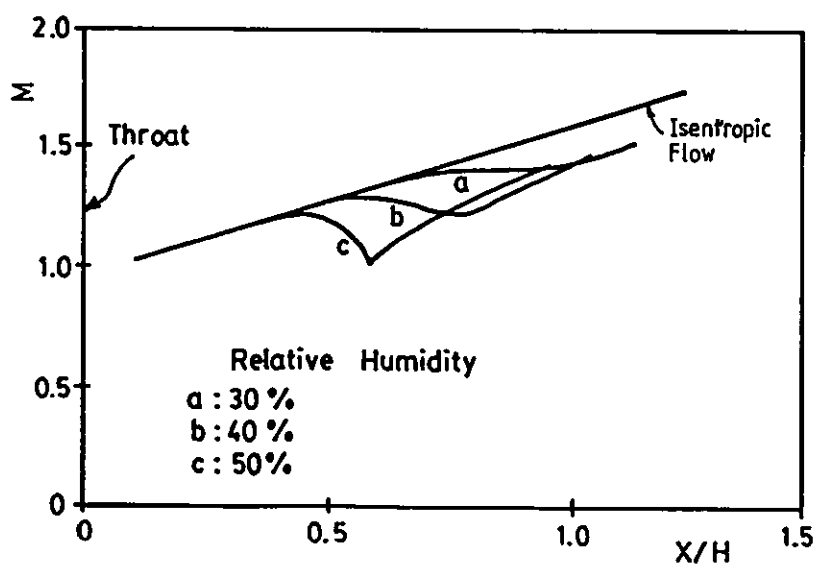

Figure 7.16b The effects of condensation shock waves on the flow velocities along the centre-line of the nozzle (after Motsuo et al[118])

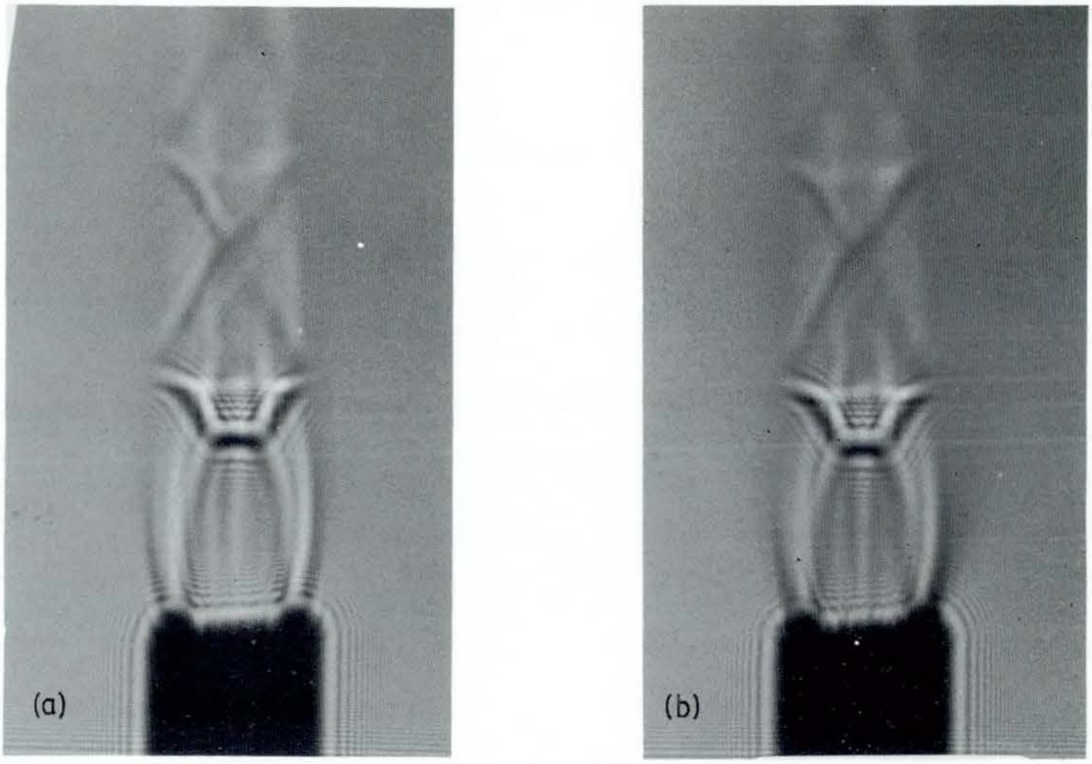

Figure 7.17 Shadowgraphs of a jet from a pipe at 7 bar: (a) before; and (b) after the water injection

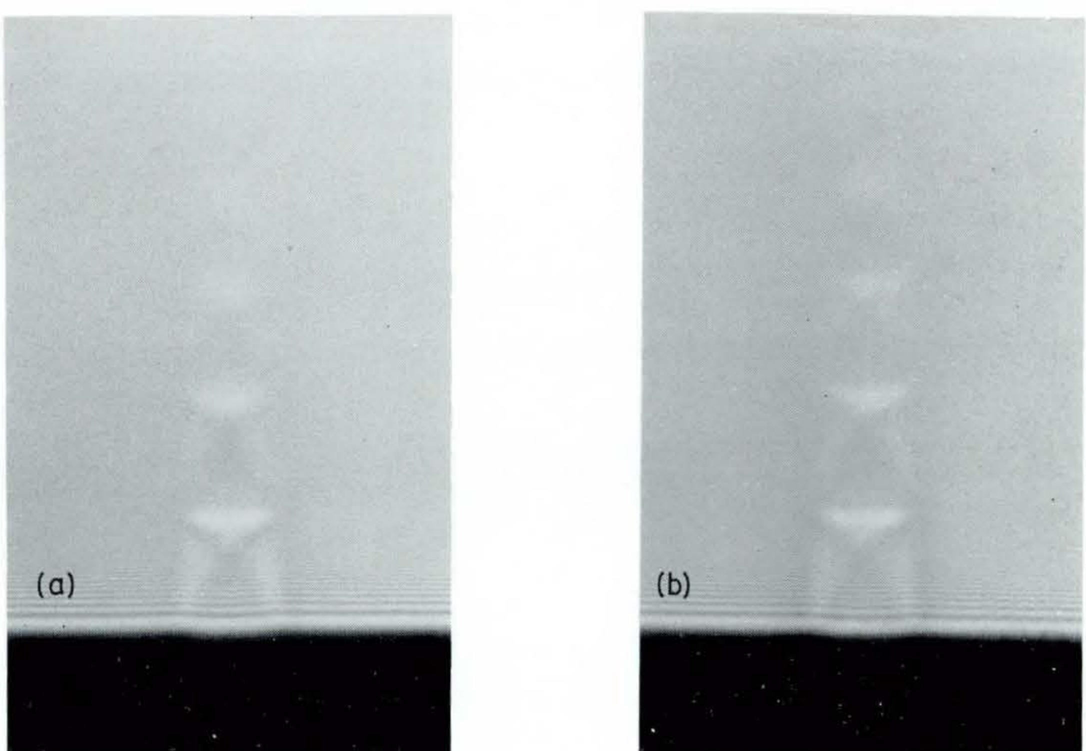

Figure 7.18 Shadowgraphs of a jet from the Standard-core HemaJet at 7 bar: (a) before; and (b) after the water injection

CHAPTER 8

INSTABILITY TESTS FOR AIR-JET TEXTURED YARNS

8.1 Instability

A close examination of a typical sample of air-jet textured yarn reveals that some of the loops which characterise such yarns can be pulled out by applying tension. This is illustrated in Figs. 8.1a to e by the photographs of a typical portion of air-jet textured yarn under progressively applied loads of 50, 100, 200, 300, and 400 gf respectively. Figs. 8.2a to e show the same yarn portion when the load is released in reverse order to the loading. It illustrates that the loops do not recover their original shapes and positions, i.e. some loops are at least partially pulled out, and thus it is likely that the yarn will be permanently extended. If the tension is further increased so as to break the yarn, examination of the broken yarn reveals that some of the loops are still intact on the yarn as shown in Fig. 8.3. The number of loops remaining intact depends on the 'stability' of the loops. This is determined not only by the supply yarn properties, such as material, linear density per filament, number of filaments, and shape of the filament cross-section, but also by the process parameters such as type of nozzle, air pressure, texturing speed, overfeed, and whether wet or dry processing is involved (See Chapter 10).

The easy pulling out of loops under working tensions would be a disadvantage in fabric forming processes, since the bulk of the yarn would be reduced and the possibility of fabric irregularity increased. Therefore, a quality control test is required to determine the stability of the yarn. Unfortunately there is no widely accepted standard method. In this chapter, available methods are discussed and compared.

8.2 Instability Tests

Two test methods have apparently been used in industry. They both depend on hanging weights, either at one end of a single yarn or a hank of yarn, but they have basic differences in their method of calculation as a consequence of the different stability concepts involved. Methods based on other techniques for measuring the yarn stability have also been described and used in various research works, these being mainly based on load-elongation curves obtained by tensile tests or on stress-strain curves obtained by a strainometer.

In order to carry out yarn tests using the various methods, a series of yarns were textured over a range of processing conditions. A two-fold 110 dtex/f66 polyester yarn (i.e. 220 dtex/f132) was used as a supply yarn. Heberlein's T100 HemaJet was employed. 400 m/min texturing speed, 20% overfeed, 7 bar air pressure with water applied at a rate of 1 litre/hour were taken as standard texturing conditions. When any one of these process parameters was altered all the other parameters were kept constant at the standard conditions. Tests were made of other yarn properties, namely linear density, tenacity and breaking elongation, in order that they could be related to the measures of stability.

8.2.1 Weight hanging methods

8.2.1.1 Du Pont method

The Du Pont Company defined a stability test for Taslan yarns[63]. Its purpose is to determine the permanent increase in length of a textured yarn after applying a load and removing it after a certain time is elapsed, this being an indication of the stability of the texturing effect. For this purpose, a simple stability tester is described comprising a vertical board with a toggle clamp at the top on which to hang the textured yarn. At a distance of 100 cm below is a marking notch and beneath this is a centimetre scale. Provision is made for hanging weights on the specimen yarn by means of a weight hanger.

The procedure is illustrated in Fig. 8.4 and can be described as follows: A weight of approximately 0.01 gf/denier (0.009 gf/dtex), W_1 is hung at the end of the yarn and this weight is left on the specimen throughout the test. A 100 cm section on thus tensioned specimen is marked. The specimen is then subjected to a further load of 0.33 gf/denier (0.297 gf/dtex), W_2, (based on the textured yarn linear density) for 30 seconds. Using the 100 cm mark as datum, the permanent elongation in the length of the specimen is measured 30 seconds after the load W_2 has been removed. This percentage elongation is taken as the direct reading of the 'stability'. Du Pont suggest that a satisfactory textured yarn must have a stability of less than 5%[63].

As can be seen from the test procedure, a 100 cm long single yarn specimen is used to measure the permanent elongation in the yarn. The applied load, W_2, is 0.297 gf/dtex and it is applied for 30 seconds. Although it is not explained why a load of 0.297 gf/dtex is applied and why it is applied for 30 seconds it appears reasonable to use a 100 cm specimen length to facilitate a direct percentage reading.

8.2.1.2 Heberlein method

In another weight hanging test method[70], suggested by the Heberlein Company, a hank of textured yarn is used instead of a single yarn specimen. The yarn is wrapped on a reel of a 100 cm circumference in order to form a small hank of approximately 2500 dtex, the number of wraps being

$$\text{No. of wraps} = \frac{2500 \text{ (dtex)}}{2 \times \text{supply yarn linear density (dtex)}} \qquad 8.1$$

(to the nearest whole number)

As indicated in Fig. 8.5, the hank is first tensioned for 60 seconds with approximately 25 cN load (corresponding to 0.01 cN/dtex (=0.01 gf/dtex)), based upon the linear density of the untextured yarn, and length 'a' is measured. A load of 1250 cN (corresponding to 0.5 cN/dtex (=0.5 gf/dtex)) is then substituted for this load and applied for 60 seconds and the length 'b' is recorded. 60 seconds after removing this load, the 25 cN (25.48 gf) load is reapplied to the hank and, after a further 60 seconds, the length 'c' is measured. Two values are then calculated for instability:

$$\text{Instability I } (\%) = [(b-a)/a] \times 100 \qquad 8.2$$

$$\text{Instability II } (\%) = [(c-a)/a] \times 100 \qquad 8.3$$

Instability I measures the percentage elongation of the yarn whilst under a certain applied load, which is a different concept to the Du Pont measurement of permanent elongation after the load has been removed. It appears that Heberlein was somewhat unsure about the concept of instability and therefore suggested a second way to measure it; hence Instability II measures the permanent elongation in the yarn after the applied load has been removed, similarl to the Du Pont method.

It should be noted that, in contrast to the Du Pont method, the term 'instability' is used by Heberlein, instead of 'stability' following Wray's earlier suggestion. Wray[64] had stated in 1969 that:

> "The use of the word 'stability' for the values obtained by the Du Pont test is unfortunate since the lower the percentage value the more stable is the yarn. A more correct term for this measurement would have been 'instability'." (Wray[64], p.117)

The term 'instability' will therefore also be used throughout the rest of this study.

8.2.2 Other instability methods

8.2.2.1 Wray's methods

In 1965, during the early days of air-jet texturing when pretwisted yarns were used as supply material, Wray[64] observed that the textured yarn untwisted under the applied loads; he therefore claimed that the value of instability measured by any method which did not prevent untwisting included additional elongation due to removal of twist. Hence he devised an alternative method in which he made use of an 'Instron' constant rate-of-elongation tensile tester, which did not suffer from losing yarn twist during testing. From the load elongation curve, as illustrated in Fig. 8.6, he defined the instability of the yarn as follows:

$$\text{Instability (\%)} = e_t - e_p \qquad 8.4$$

Where e_p and e_t are the percentage elongation of the supply and textured yarns respectively at a constant load of W = 0.297 gf/dtex (See Fig. 8.6), this corresponding to the load used in the Du Pont tests.

This method of instability measurement was an attempt to eliminate the effect of the elastic deformation of straight, load carrying filaments of the textured yarn. Wray claimed that the percentage permanent elongation in the textured yarn was obtained by this method, by subtracting the percentage elongation of the supply yarn (e_p) from the percentage elongation of textured yarn (e_t). It was implied that the elongation of textured yarn under an applied load also included the elastic deformation of the constituent filaments, i.e. elongations of the individual filaments also contributed to the instability of the textured yarn.

Although it is true that the load bearing filaments will elongate under the applied loads (whereas loop forming filaments will not), it is not known what amount of elongation is caused by the pulling out of loops and what amount is caused by the elastic deformation of the individual filaments. Therefore it is debatable whether the measurements obtained by this method reflect the permanent elongation of the textured yarn.

Wray[64] also devised a quicker method of measuring yarn instability based on principles similar to the Instron tensile tester method. This technique incorporated the use of a strainometer, which imposed a 5% constant strain on the yarn as it passed continuously over rollers. A third roller between these two rollers acted as a sensor to measure the tensions in the yarn, which enabled a calculation of the yarn instability to be made. Unfortunately, this method suffers from the same shortcomings as those described above.

8.2.2.2 Acar's method

A recent suggestion for instability measurements of air-jet textured yarns was made by Acar[55]. This was also based on the load-elongation curves from a tensile testing machine of the Instron type. He measured the percentage elongation corresponding to loads of 0.01 gf/dtex and 0.5 gf/dtex, corresponding to the loads used in the Heberlein tests, as a measure of the yarn instability, see Fig. 8.7 Hence,

$$\text{Instability (\%)} = \Delta l \;/\; \text{Specimen Length} \qquad 8.5$$

Acar's method suggests that the elongation of textured yarn under applied loads should be taken as the measure of yarn instability, rather than the difference of elongations of the textured and supply yarns, as suggested by Wray, because the contribution of the extension of load-bearing parallel filaments of the textured yarn to the overall elongation is difficult to account for.

8.3 Two Contrasting Yarn Instability Concepts

As seen in the preceeding section, the instability methods used both in industry and by research workers vary considerably not only regarding detail but also regarding basic agreement as to what actually needs to be measured. Nevertheless it is suggested that they can be grouped in the following two contrasting categories from the viewpoint of the concept of instability:

i) The concept of instability as a measure of the tendency of the textured yarn to elongate under maintained applied loads, thereby corresponding to the loads applied during later processes such as weaving, knitting, etc. Therefore, no attempt is made to account for the separate contributions of loop removal and elastic (recoverable) deformation to yarn elongation, because the percentage elongation under a maintained applied load is taken as a measure of instability, e.g. the Heberlein Instability Method I and Acar's method which use an Instron tensile testing machine.

ii) The concept of instability as a measure of the lack of permanence of loops formed by the texturing process whereby the elastic (recoverable) deformation of the yarn under the applied load does not contribute to the yarn instability because the load is removed to allow the yarn to recover from such elongations before measurement occurs. Therefore the percentage permanent elongation is taken as the measure of instability, e.g. Du Pont Method, and the Heberlein Instability II method.

It is clear that no consensus of agreement exists regarding the basis for a standard method for instability measurement and inevitably the results reported in various research works do not agree with each other. Therefore there is a need for a standard instability test for air-jet textured yarns. In the following sections the known instability methods will be critically analysed and, in order to initiate discussion to the subject, a method based on one of the above two contrasting concepts will be suggested as a standard method.

8.4 Simulation of Weight Hanging Methods on a Tensile Tester

The procedure used in weight hanging methods is rather tedious and the load is applied for rather arbitrarily chosen periods. For instance, Du Pont suggests that the measurement of permanent elongation should be taken after a 30 second application of 0.297 gf/dtex weight and a 30 second relaxation following the removal of this load, where a weight of 0.009 gf/dtex is constantly applied throughout the test. On the other hand, Heberlein suggests a 60 second application of a 0.5 gf/dtex weight, a 60 second relaxation without any weight, followed by a 60 second application of a 0.01 gf/dtex load before reading the permanent elongation.

Test results for yarns textured at varying air pressure are shown in Fig. 8.8 for the Du Pont and Heberlein Instability II methods, both of which measure the permanent elongations after the applied loads have been removed. Both tests give similar results but the accuracy of the test results is rather low, because the elongation can not be read as acurately as with an Instron tensile tester and human errors are inevitable.

Alternatively the weight hanging methods can easily be simulated by using a tensile testing machine of the Instron type. The required load can be applied to the specimen yarn, and a certain time can be allowed to ellapse, before the load is released. Hence the permanent extension of the yarn after the load is removed can be calculated more accurately from the load-elongation curves so as to simulate instability concept (ii) in the preceeding section. Since, as will be shown in Section 8.5, relaxing the yarn under an applied load for a certain period has an insignificant contribution to the elongation of the yarn, the tensile testing machine can be set to extend the yarn until it reaches the required load, the action being immediately reversed when this load is reached, so that the conditions revert to zero loading. Hence the permanent elongation of the yarn can be measured as illustrated in Fig. 8.9 which was obtained from an Instron tensile tester. Results from such a test by using the loads specified in the Heberlein tests are also plotted in Fig. 8.8, which demonstrates reasonable agreement with the test results of the Du Pont and Heberlein II methods. The advantage of the simulation using the tensile testing machine is that it is accurate, faster, and relatively easier to perform than these weight-hanging methods.

8.5 Effects of Test Load and Duration of Applications

The different loads used for the Heberlein and Du Pont stability tests cannot both be representative of the applied tensions during further processing into fabrics. Therefore a representative standard load should be decided on based on practical fabric forming process conditions and only this load should be used in the instability tests. This will require further investigation but the loads suggested by Heberlein have been used in the tests reported in this work.

Is the duration of application of load important? To answer this question an experiment was designed and carried out by using an Instron tensile tester which can provide very accurate readings. A constant test load of 110 cN (112 gf), equivalent to loads used in Heberlein instability tests (i.e. 0.5 gf/dtex), was applied to a specimen of the 'standard' yarn for 15 minutes.

The test procedure was as follows: The Instron machine was set to 112 gf and the elongation of the yarn started. When this load was reached, the elongation of the yarn was stopped automatically. As the time elapsed the load applied to the yarn reduced gradually below the preset value of 112 gf due to the relaxation in the yarn. Then the machine automatically restarted the elongation process which was again stopped automatically when the load reached the preset value of 112 gf. This cycle repeated itself several times within the 15 minute test period.

Fig. 8.10 is a reproduction of the chart recording from such a test, illustrating that the application of a constantly maintained load for a certain period can have a slight effect on the extension of the yarn, especially during the early stages of the load application period. Nevertheless, the overall effect within the 15 min test duration was insignificant, as illustrated in Fig. 8.11a and b. The initial elongation of the yarn under the applied test load was 1.868%. The additional effects of applying a constantly maintained load for 30 s and 60 s durations were only to increase the elongations to 1.881 and 1.885% respectively and indeed total elongation for a 15 min application of this load was only 1.897%. It can be concluded that the constantly maintained application of the test load has a negligible effect on the elongation of the yarn and hence on the instability test results. Consequently the application of constant loads for any specified time periods can be eliminated.

8.6 Effects of the Specimen Type and Length

Heberlein suggests the use of a hank of yarn in the tests, whilst Du Pont uses a 100 cm long single yarn. Does using the hank instead of a single yarn affect the test results? Does the specimen length have a significant effect? Some answers to these questions will be sought in this section.

First the effect of using a hank and a bundle of yarn instead of a single yarn is examined. By using the Instron machine and Acar's test method the following tests were performed:

a) with a single end of yarn fixed in the pneumatic jaws (Acar method). Test results are shown in Table 8.1

b) with a hank of yarn hung over hooks fixed in the pneumatic jaws. Since the hank opened out under the applied load, it was not possible to carry out the test, when the two ends of the yarn in the hank were left free. Therefore, although this adverse effect is not made clear by Heberlein, two ends of the yarn had to be tied to make a closed loop hank for the tests to be undertaken and thus cause an equal distribution of the load to each constituent loop in the hank to be achieved. The test results (Table 8.1) show that this closed loop hank method (Heberlein I on Instron) gives slightly higher instability readings than those obtained by using a single yarn specimen (Method (a)).

c) with a bundle of yarns fixed in the pneumatic jaws. This creates a positive grip of each yarn within the bundle. As shown in Table 8.1 this test showed slightly higher instability than the other two methods (a) and (b) which can be attributed to the nonuniform distribution of load to every yarn in the bundle. Therefore it was concluded that this is not a suitable method for yarn instability tests.

It can be argued that a single yarn specimen, such as method (a), is the most suitable basis for yarn instability tests because a single yarn is easier to handle and the question of non-uniformly distributed load through the bundle does not arise. The only alternative to this could be a hank of yarn with a closed loop (ends tied) hung on low friction hooks as in method (b) and it might be argued that the longer specimen length might give a better overall representation of the yarn characteristics. But does the longer specimen length provided by a hank result in a better representation of the yarn characteristics? To answer this question the effect of specimen length was examined by using a single yarn of various specimen lengths and Fig. 8.12 shows that the specimen length has an insignificant effect on the test results. Therefore it can be concluded that a single yarn should be used in the instability tests for its convenience in handling, the specimen length being chosen to suit the apparatus used and the testing conditions. Consequently, in the tests reported in this report a single end yarn with a 30 cm specimen length was used.

8.7 Summary of Conclusions

The above-mentioned findings can be summarised as follows:

a) A consensus should be reached regarding the yarn stability concept (See Section 8.3). Whilst some industrialists and researchers have assumed it to be (i) a measure of the elongation of the air-jet textured yarn under an applied load, others have taken it to be (ii) a measure of the permanent elongation after such an applied load has been removed.Since, on the one hand, air-jet textured yarns are not stretch yarns and, on the other, they are under maintained tensions during most of the further fabric forming processes, i.e. whilst undergoing weaving or knitting, it would be more reasonable to take the elongation of the yarn under a maintained tension as a measure of yarn instability. Therefore concept (i) more closely simulates real conditions.

b) Whichever concept is finally accepted as a basis for a standard test method of yarn instability, the tensile testing machines can be used for improved instability tests. As discussed in Section 8.2.2, an instrument such as the Instron machine gives more accurate readings of the yarn elongation, even under very small loads, than the crude weight hanging methods described in Section 8.2.1 and therefore it is more reliable than these.

c) A single yarn specimen is much easier to handle and therefore it is more practical in use than a yarn hank or bundle. (See Section 8.6)

d) The specimen length has no significant effect on the tests, and hence any convenient length of yarn can be used. (See Section 8.6)

e) The effect of the duration of the application of load on the test results is not significant,and therefore the application of loads for relatively long periods are unnecessary. (See Section 8.5)

f) The amount of load that should be applied to the yarn during the tests is far from being agreed (See Section 8.5), but it should be representative of the tensions imparted during further processing stages such as weaving, knitting, etc.

8.8 A recommended Test Method

In the light of the work described and conclusions derived from it, the following basis for an improved test method is recommended.

i) A tensile tester of the Instron type should be used to measure the yarn elongation;
ii) Single yarn specimens are adequate;
iii) The specimen length should be sufficiently small to permit ease of handling; a 30 cm length is convenient for most machines and is therefore recommended.
iv) Until an agreement is reached regarding the loads that should be applied, the Heberlein suggestion (Section 8.2.1.2) of a 0.5 gf/dtex test load should be used and a load of 0.01 gf/dtex should also be adequate to pretension the yarn;
v) The elongation under this test load should be taken as a measure of the instability (concept (i) in Section 8.3) rather than the permanent elongation measured after the load is removed (concept (ii)) because it represents the actual case that loads are constantly applied during other textile processes.

The procedure for this improved test would read as follows:

a) Prepare the tensile testing machine for the test. Recommended test conditions are as follows:
i) Distance between pneumatic jaws i.e. specimen length, 30 cm;
ii) Cross-head speed, 2 cm/min;
iii) Chart speed, 10 cm/min.

b) Take approximately 50 cm length of textured yarn from a representative package. Use care not to damage the yarn during removal from the package.

c) Clamp both ends of the yarn in the pneumatic jaws. Use care not to over-tension the specimen during clamping.

d) Operate the machine and record the elongation up to a value slightly greater than the load corresponding to 0.5 gf/dtex, based on the untextured yarn linear density.

e) From the recorded load-elongation chart calculate the percentage elongation between the loads 0.01 gf/dtex and 0.5 gf/dtex.

This percentage elongation gives the instability of the yarn. This procedure should be repeated for a reasonable number of randomly selected specimens, preferable from different packages of yarn and from different places of one package, to obtain reliable test results.

Test results using this specified method are shown in Fig. 8.13 and they are compared with the results of all the other methods described in Section 8.2. Although they each yield different results, due to differences in the concepts and assumed parameters on which they are based, they all show the same basic trend, i.e. an increase of instability with increasing values of the air pressure used for texturing.

8.9 General Conclusions

Instability tests alone are inadequate for judging the quality of air-jet textured yarns. For example yarns textured at very low overfeeds, low air pressures, and high texturing speeds will exhibit a very smal number of loops. Test results of such yarns show low instability, and yet they would be suitable for many end-uses. On the other hand yarns textured at high overfeeds, high air pressures, and low texturing speeds will exhibit increased number of loops and have desirable qualities for many end uses, but they will be accompanied by higher instability values (See Chapter 10).

Therefore, if judging from the instability viewpoint alone, the former yarn would appear to be preferable to the latter yarn but obviously this would be misleading from the viewpoint of quality and consumer acceptability. Therefore the producer of air-jet yarns need to measure other yarn properties, such as percentage linear density increase, tenacity, percentage breaking elongation, and the number and frequency of loops as well as instability in order to obtain a total assessment of yarn quality.

To illustrate this point, Figs. 8.14a, b, c and d show the instability, percentage linear density increase, tenacity, and percentage breaking elongation of typical textured yarns produced with varying working air pressures. Instability, as discussed in Section 10.3.1, shows an increase with increasing air pressure (Fig. 8.14a), indicating a deterioration of the yarn quality. This can be attributed to the higher number of loops at increased air pressure (See Chapter 10) which also increases the probability that many of these loops will be removed under the loads applied. An increased number of loops also cause the load to be shared by a reduced number of parallel filaments in the yarn, which in turn contributes to increased yarn instability.

On the other hand, the yarn linear density increases with increasing working pressures (Fig. 8.14b), thus indicating a better texturing effect due to a greater number of loops. The tenacity (Fig. 8.14c) and breaking elongation (Fig. 8.14d) both decrease with increasing working pressure, this also indicating a better texturing effect and greater number of loops. The SEM photographs shown in Fig. 8.15 also show that the textured yarn structure of these yarns improves for the greater air pressures. Therefore it can be concluded that, despite increasing yarn instability the overall yarn properties are improved.

Consequently, it is recomended that the structure and physical properties of the air-jet textured yarns should be analysed before deciding on the suitability for particular end-uses. The instability tests should only be viewed as a precautionary assessment to warn the producer of any likely deterioration of the textured yarn structure during the further processing, it will have to undergo. The amount of instability that can be permitted is therefore a matter of judgement for the producer in order that the total desirable yarn properties are transmitted to the final fabrics.

TABLE 8.1

Comparison of instability test results*

Method of Test	Instability [%]
Du Pont	0.345
Du Pont on Instron	0.290
Heberlein I	2.134
Heberlein I on Instron	2.018
Heberlein II	0.450
Heberlein II on Instron	0.410
Hank with Pneumatic Clamps	2.151
Wray	1.458
Acar	1.868

*Texturing conditions deployed to produce the standard yarn used in these tests were 7 bar air pressure, 20% overfeed, 400 m/min texturing speed, and 1 litre/hour water application.

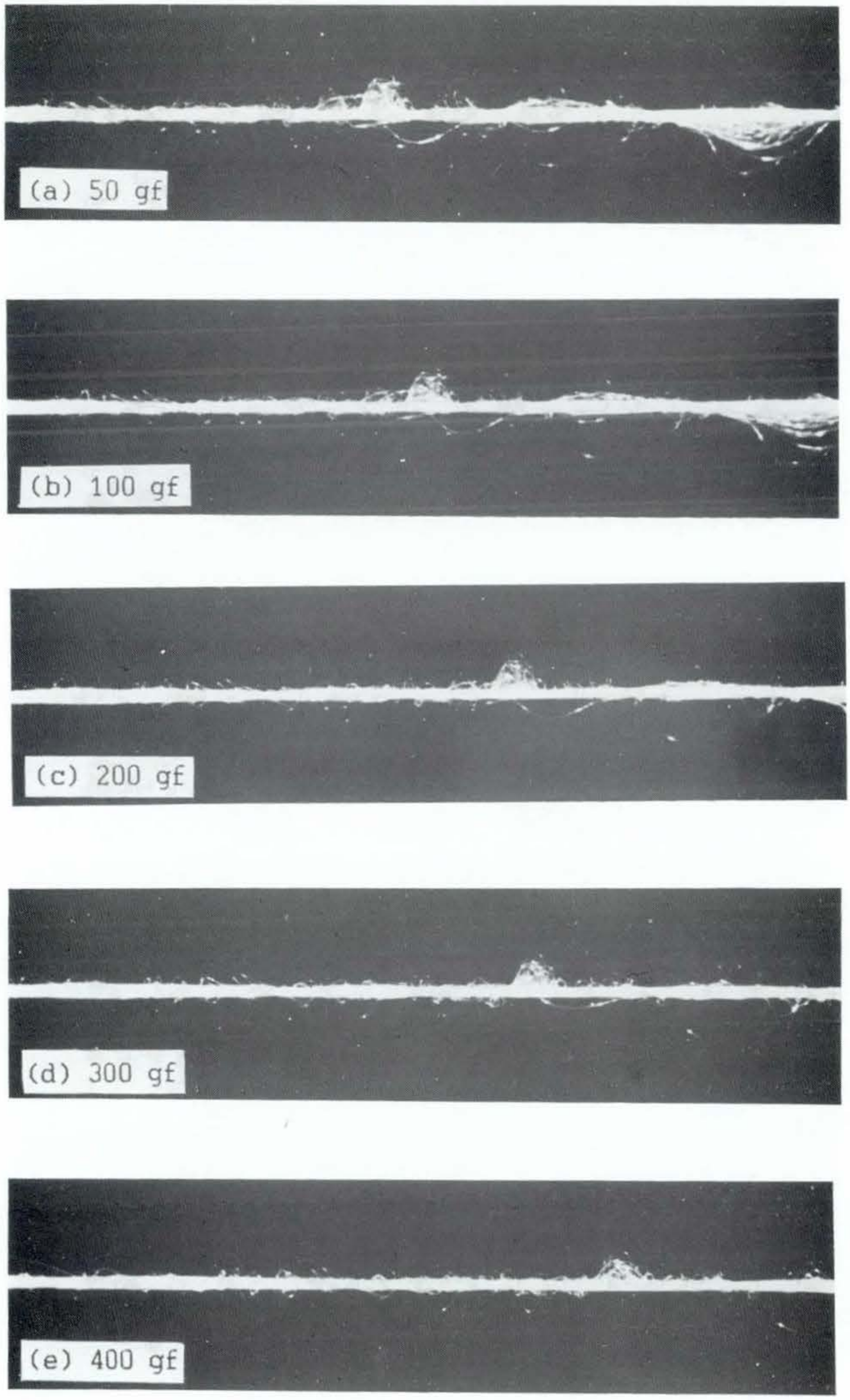

Figure 8.1 Air-jet textured yarns under increasing tension

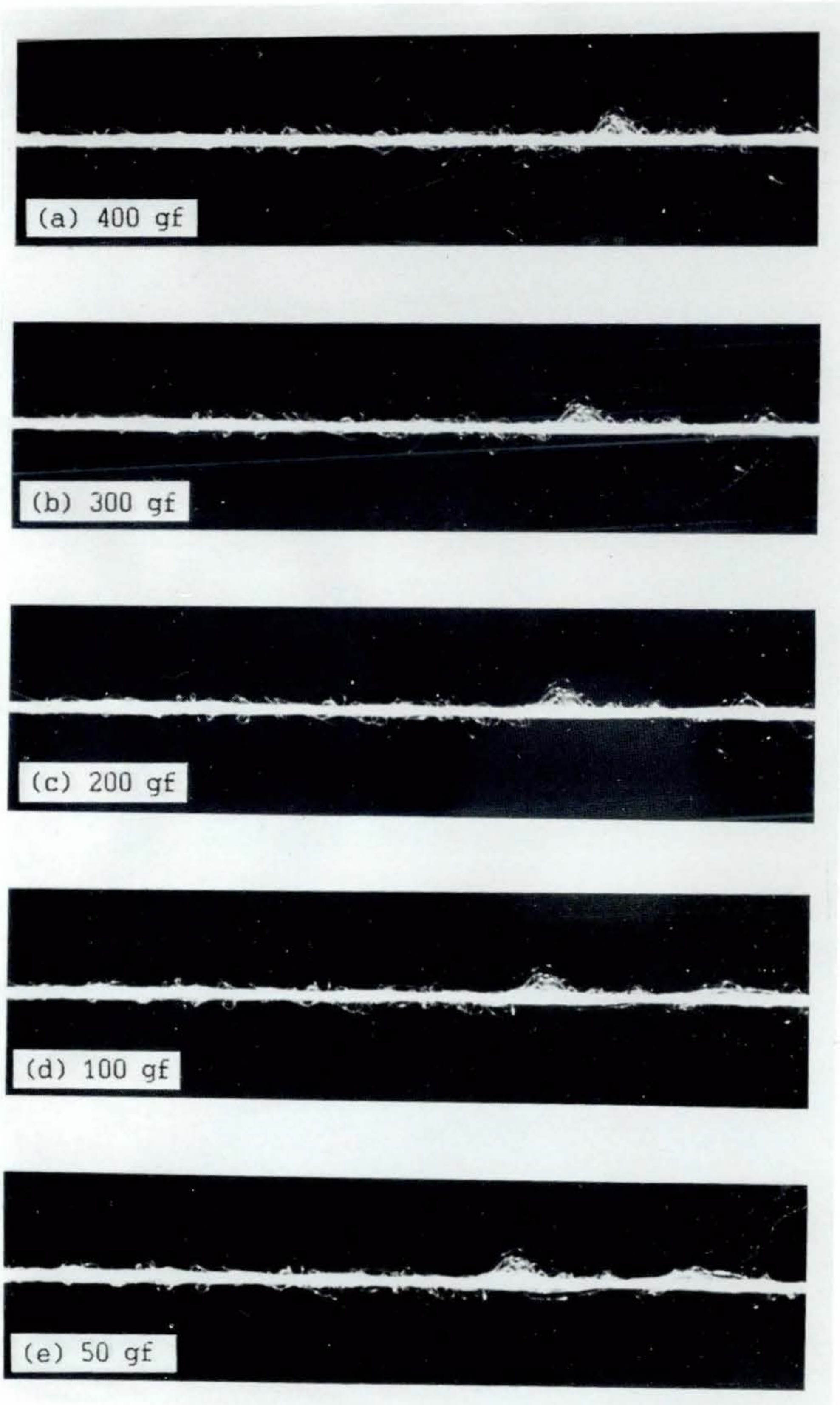

Figure 8.2 Air-jet textured yarns under decreasing tension

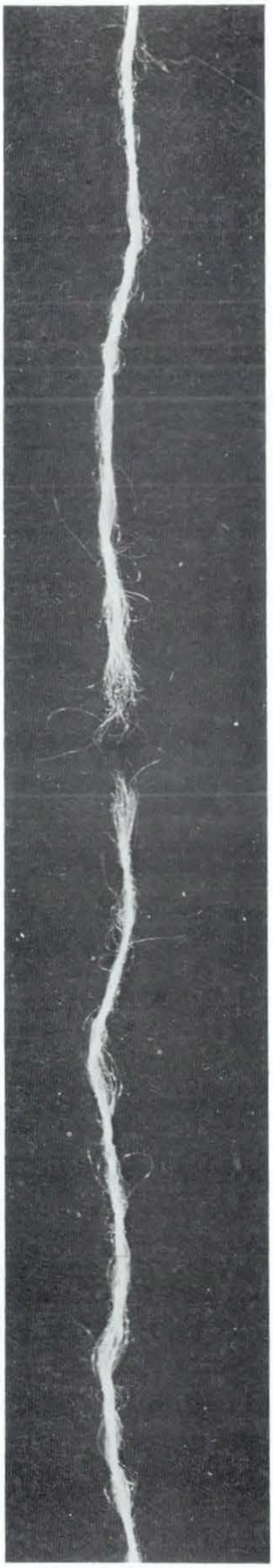

Figure 8.3

A broken air-jet textured yarn illustrating that not all the loops have been pulled out

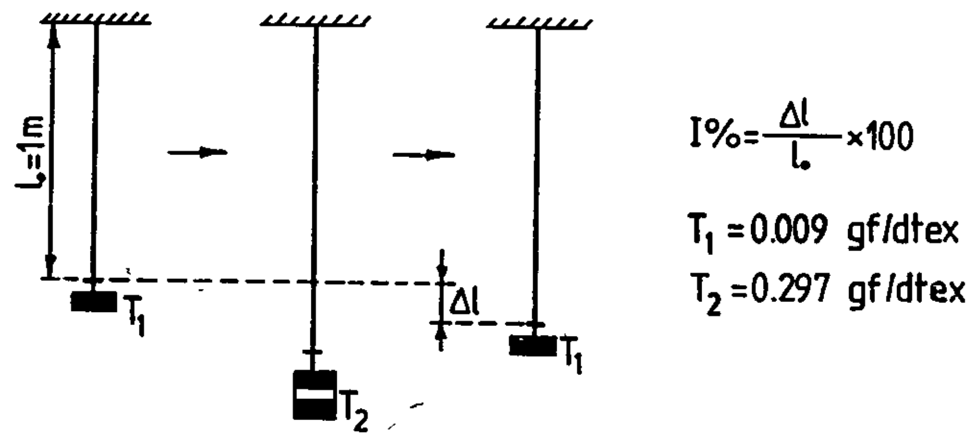

Figure 8.4 Du Pont's stability test method

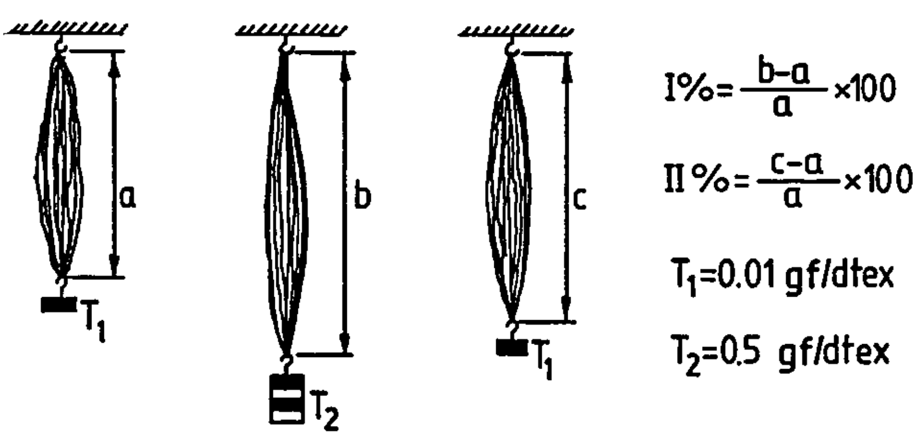

Figure 8.5 Heberlein's instability test method

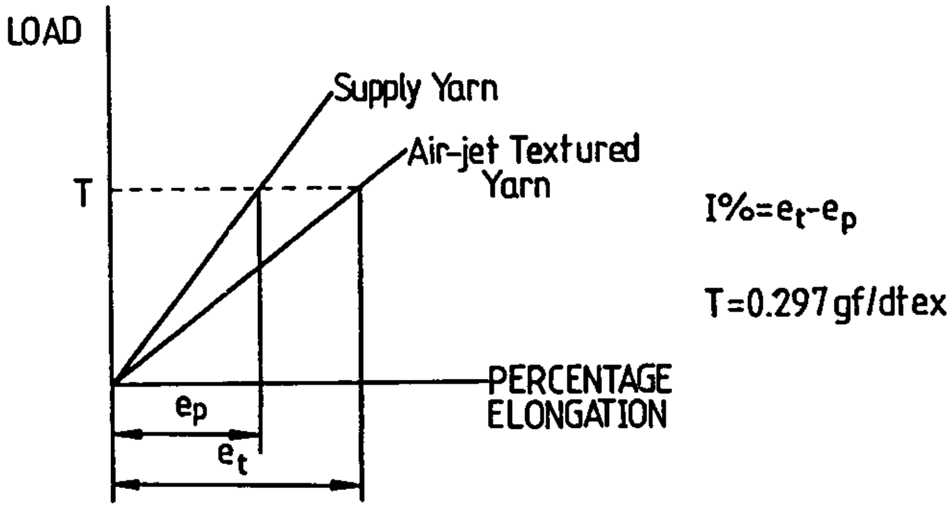

Figure 8.6 Wray's instability concept

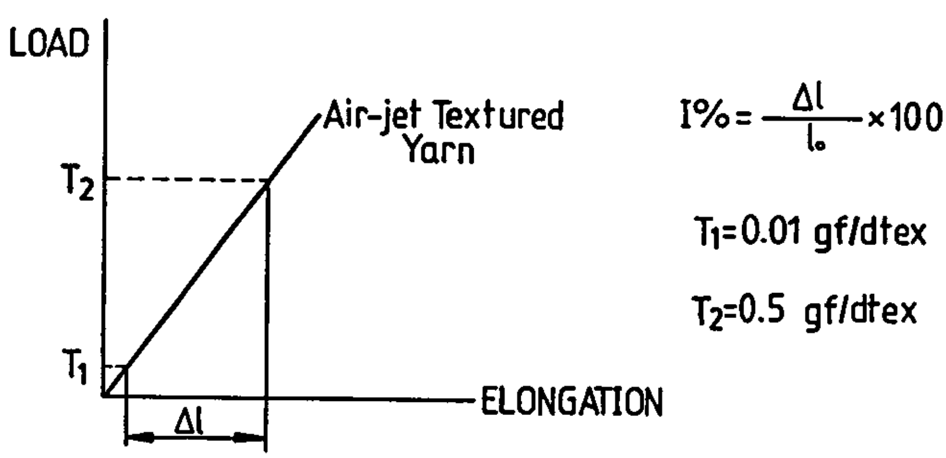

Figure 8.7 Acar's instability concept

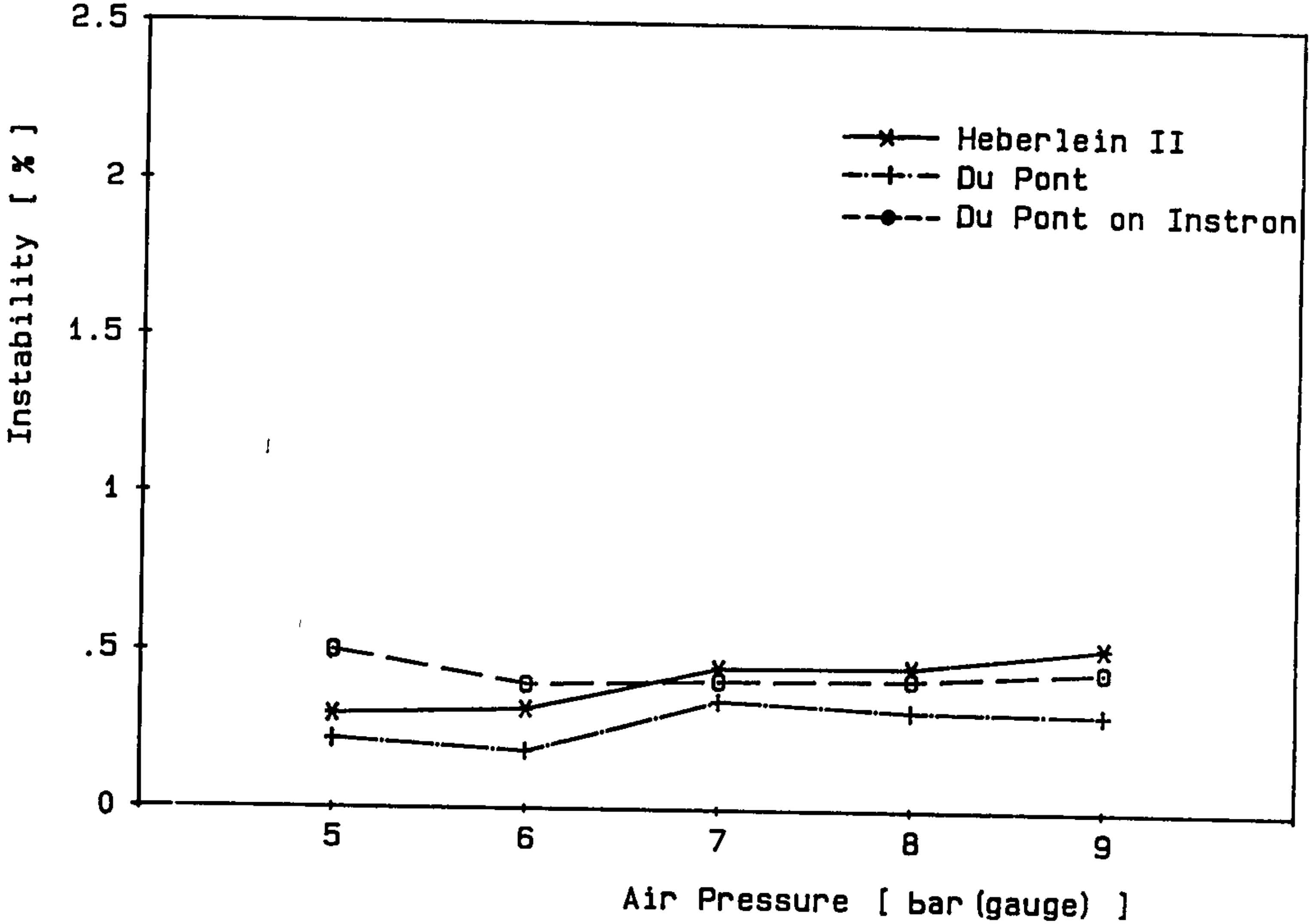

Figure 8.8 Comparison of instability test methods based on permanent elongation

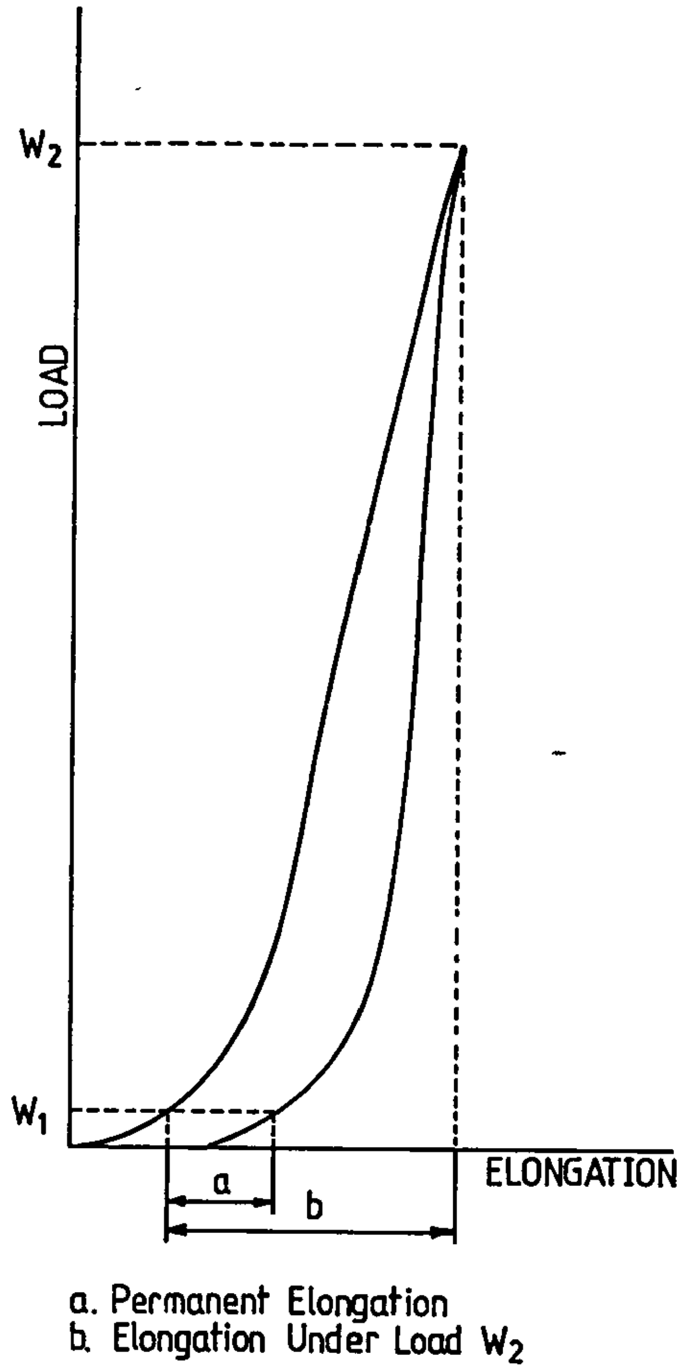

Figure 8.9 Simulation of a weight-hanging instability test method by using a tensile testing machine

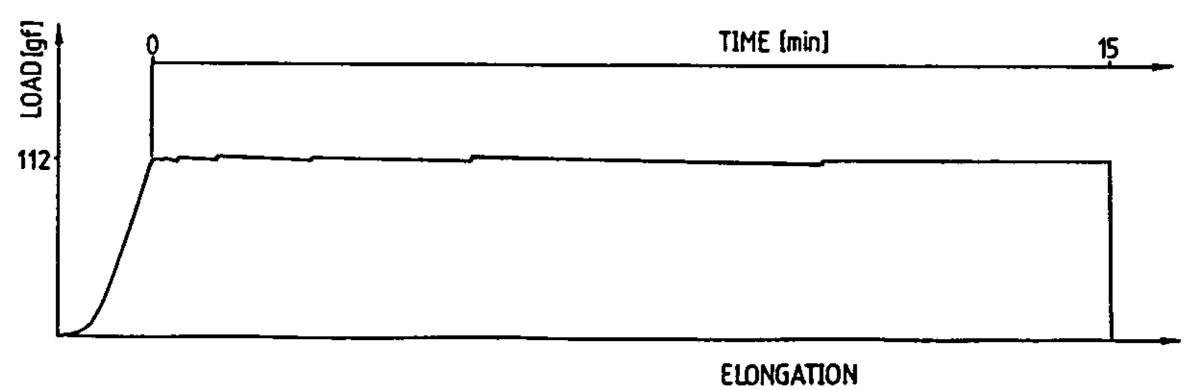

Figure 8.10 Load-elongation diagram for an air-jet textured yarn with a constant load applied over 15 minutes

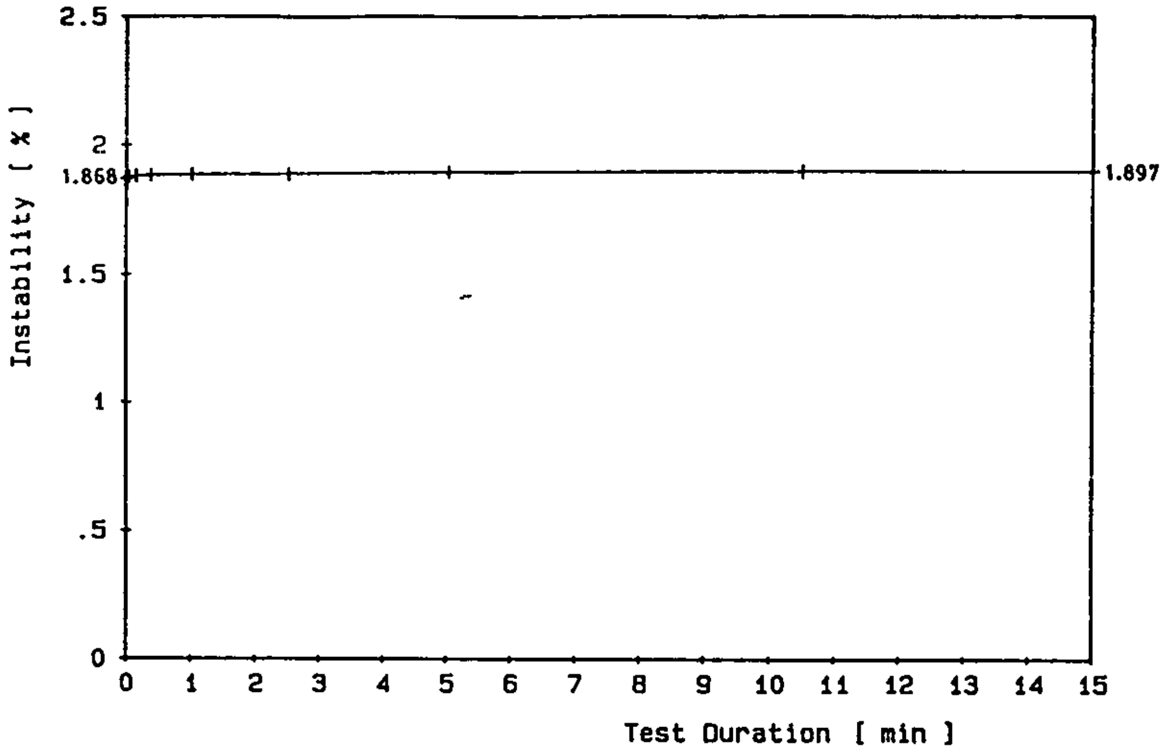

Figure 8.11a Effect of test duration on yarn instability

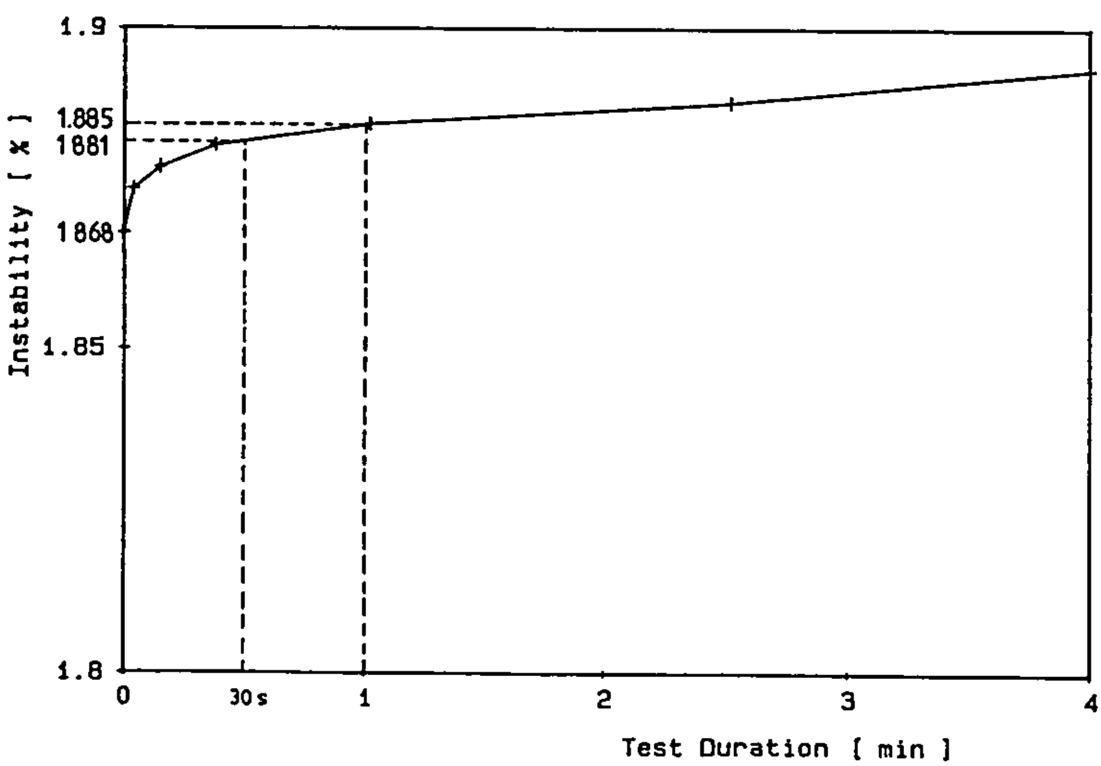

Figure 8.11b Magnification of Fig. 8.11a to show the effect of the first 4 minutes of load application

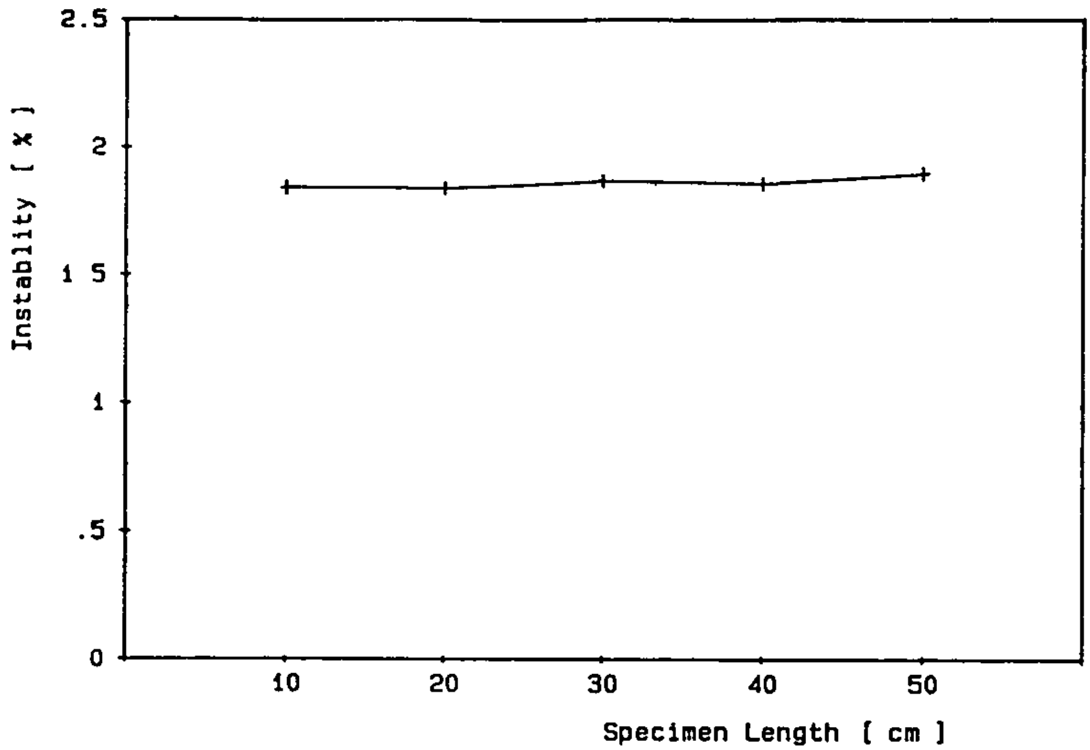

Figure 8.12 Effect of varying specimen length on the instability

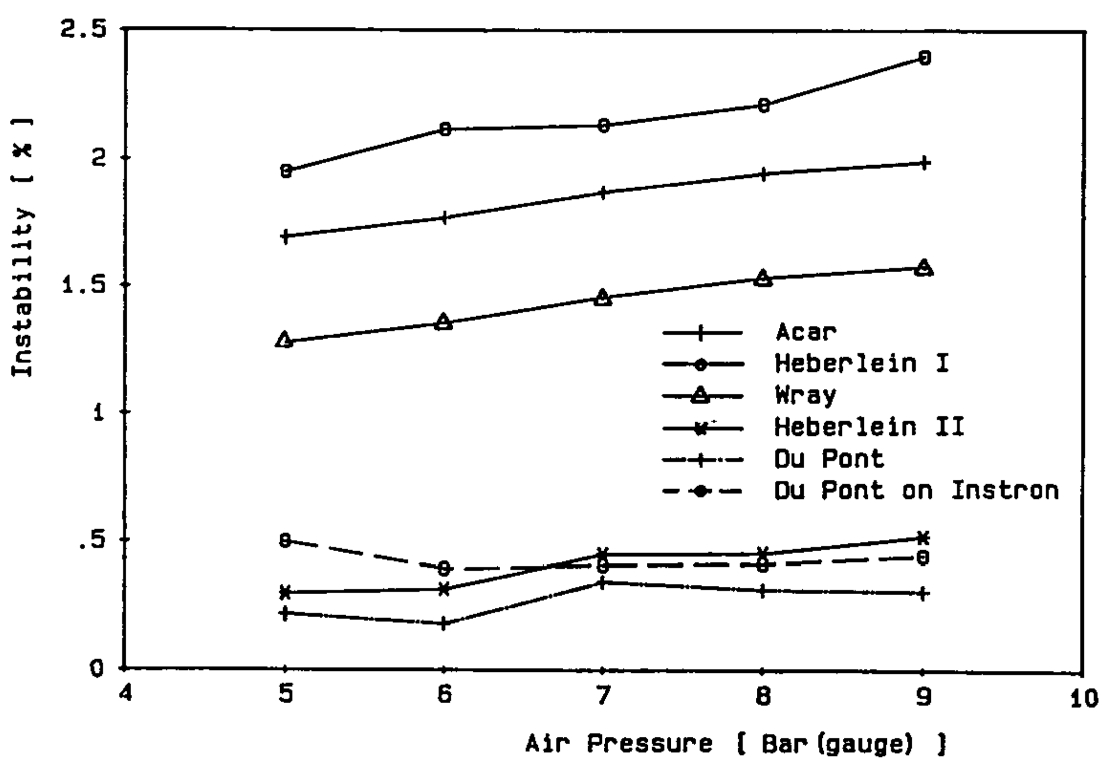

Figure 8.13 Comparison of different instability test methods for yarns textured with varying air pressures

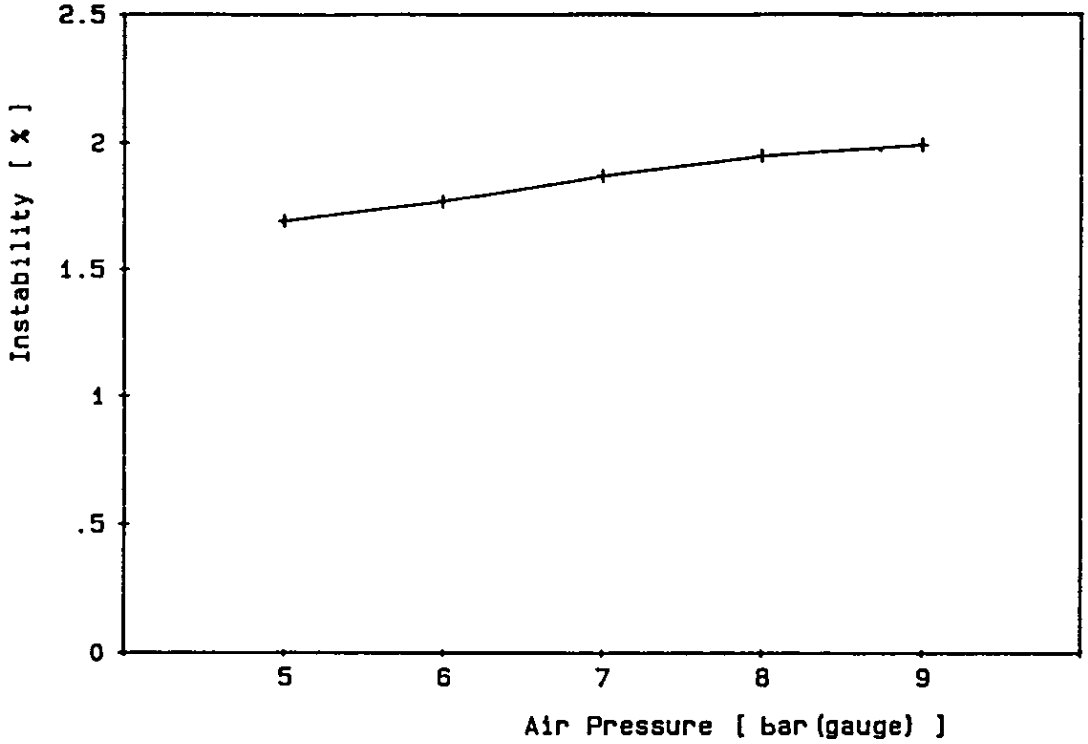

Figure 8.14a Instability of yarns textured with varying air pressures

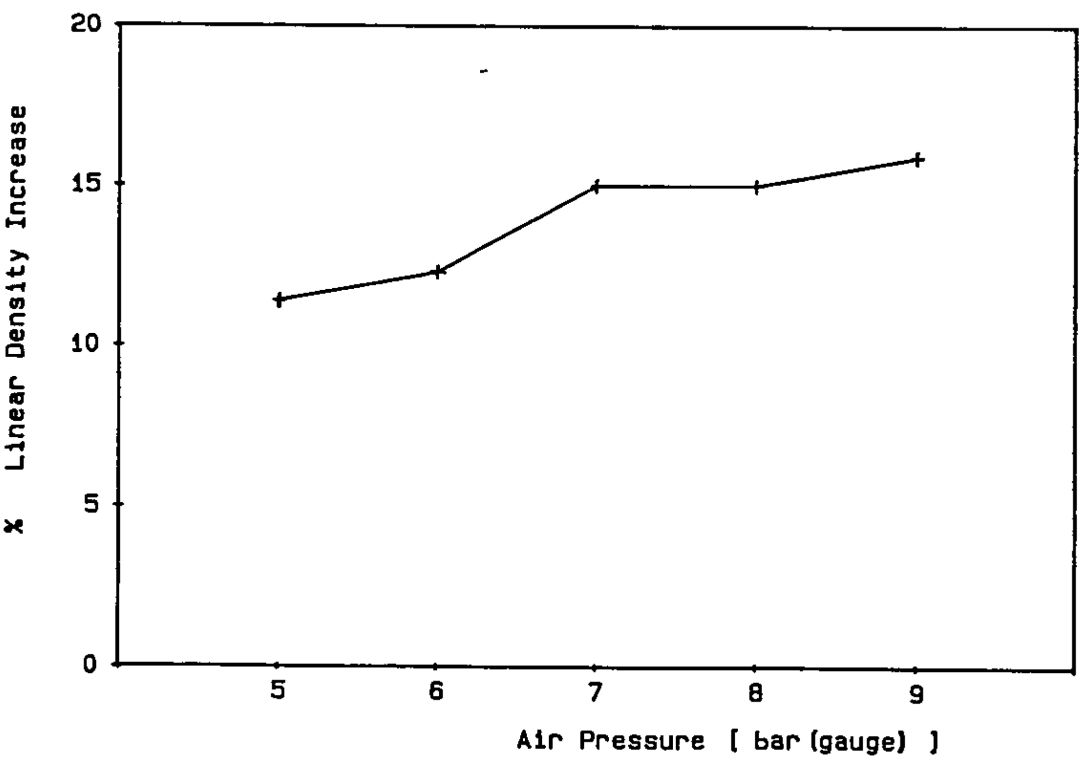

Figure 8.14b Percentage linear density increase of yarns textured with varying air pressures

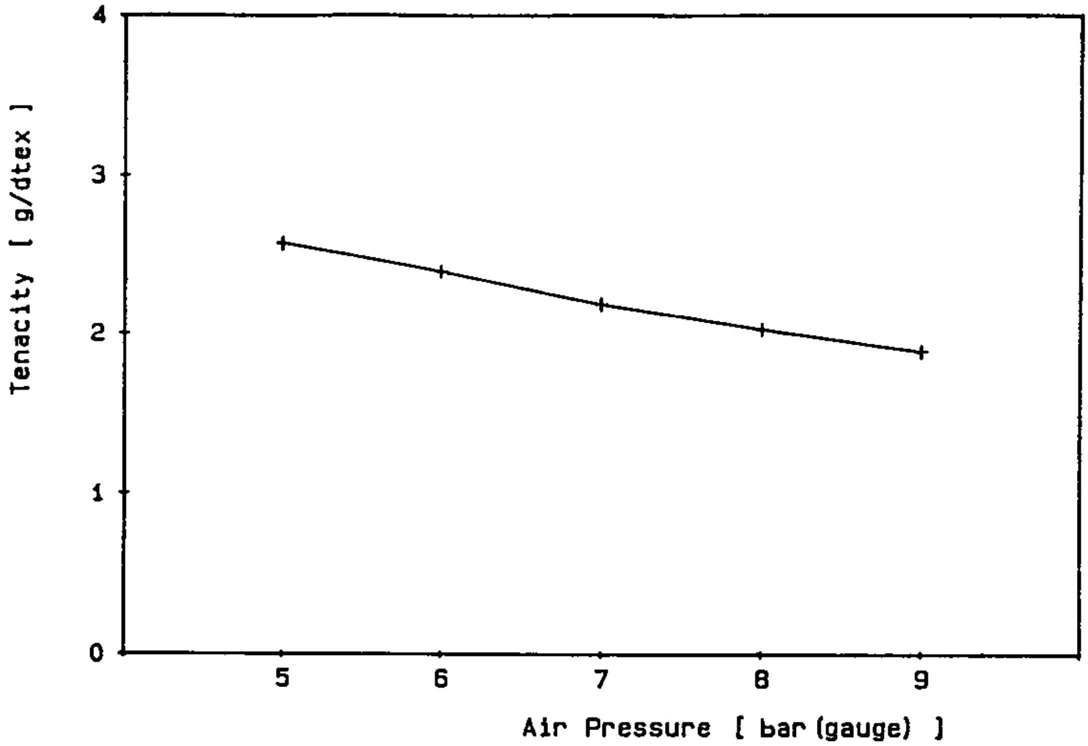

Figure 8.14c Tenacity of yarns textured with varying air pressures

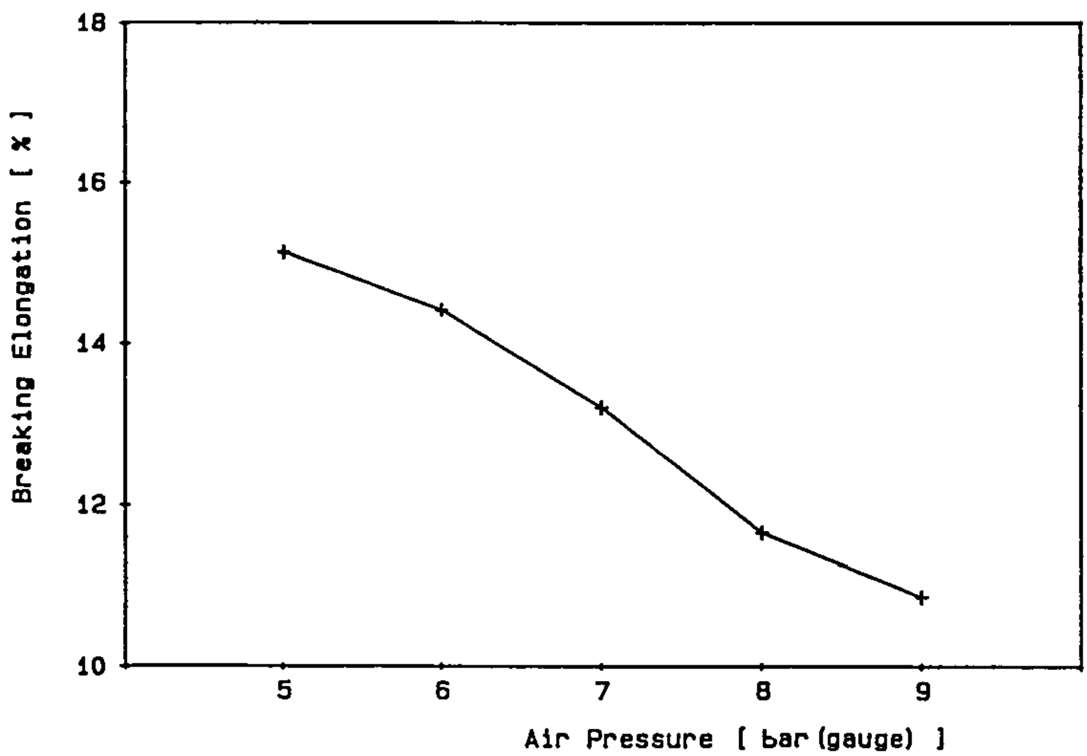

Figure 8.14d Percentage breaking elongation of yarns textured with varying air pressures

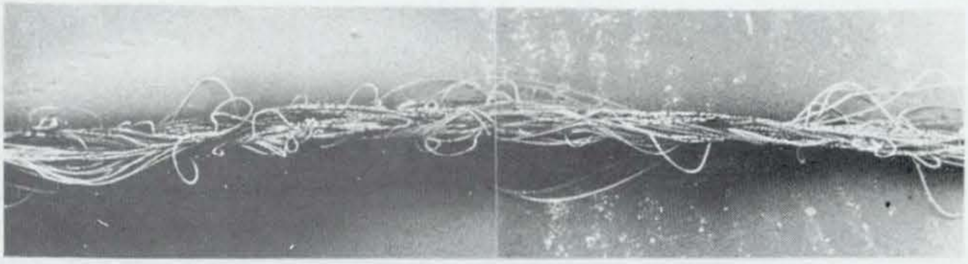

(a) 5 Bar(gauge)

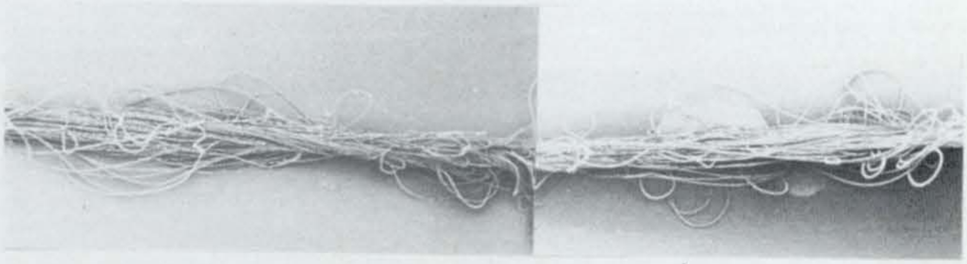

(b) 6 Bar(gauge)

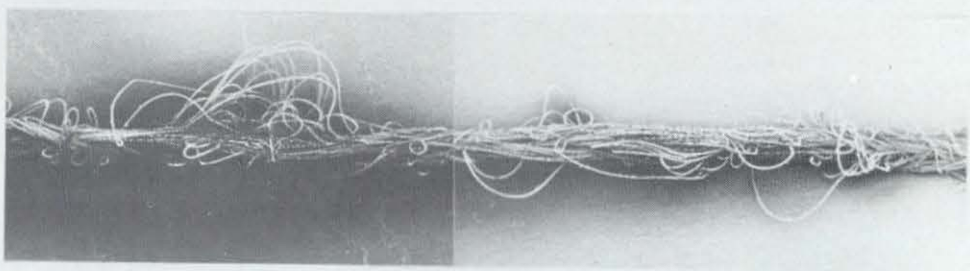

(c) 7 Bar(gauge)

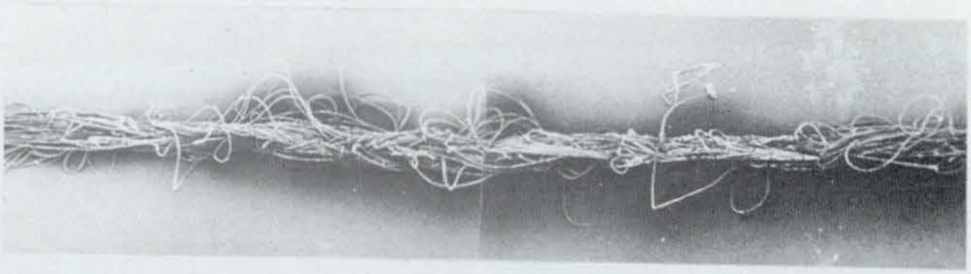

(d) 8 Bar(gauge)

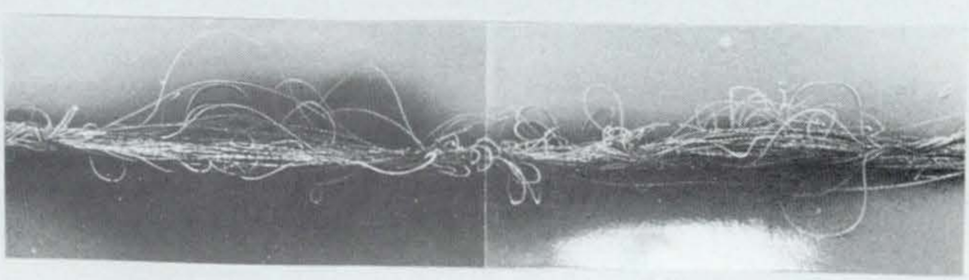

(e) 9 Bar(gauge)

Figure 8.15 SEM photographs of yarns textured with different air pressures

CHAPTER 9

ON-LINE QUALITY CONTROL OF AIR-JET TEXTURED YARNS

9.1 Introduction

Provided that certain precautions are taken into consideration, the instability of air-jet textured yarns yields valuable information, as was discussed in Section 8.9. But these 'off-line' techniques are either too primitive, thereby giving unreliable, inconsistent results, or they are too sophisticated, thereby requiring expensive equipment, such as an Instron Tensile Testing machine. They are also tedious and time-consuming.

Using the fundamental principles of the suggested improved instability measurement technique, based on the use of an Instron machine, as was explained in Section 8.8, simple, and easy to manufacture 'off-line' test device have been developed, as will be discussed in Sections 9.2 and 9.3.

Like all other 'off-line' instability measuring techniques the improved test is carried out after the texturing is completed, no direct feed-back to the texturiser being provided to modify the processing conditions to give any desired texturing effect. Therefore, same instability measuring concept has been utilised to develop an 'on-line' instability measuring system which offers the potential of providing the necessary feed-back to the texturing machine as will be discussed in Section 9.4.

9.2 An 'Off-line' Instability Measuring Device

The fundamental concept of the suggested instability measuring technique, described in Section 8.8, consists of applying a certain load to the yarn and measuring the elongation of the yarn under this load. This basic requirement can simply be achieved by stretching the yarn between two clamps up to the specified tension and measuring the elongation of the yarn. In order to provide for this, a simple device was designed and built. This device, as shown in Fig. 9.1, consists of two movable clamps with a tension sensing head situated between them. It is referred as the 'off-line' instability measuring device.

The yarn fed through the tension head is secured between the clamps. The required pre-tension T_1 (See Fig. 8.7) is created by moving the clamp which is seen on the left-hand side of the device. Then using the micrometer head of the right-hand clamp, the pillar is moved outwards to create the predetermined higher tension T_2. As soon as the tension in the yarn reaches this T_2 value, the elongation of the yarn is recorded from the micrometer head reading. The measurement is repeated several times with different yarn specimens and using the average elongation and the distance between the clamps as the specimen length, the instability is calculated as was described in Section 8.8.

Figs. 9.2a, b and c show the test results obtained from three different sets of yarns textured with varying amounts of air pressure, overfeed and texturing speed. All the yarns were tested using both the Instron tensile testing machine and the 'off-line' device and the overall comparison of these two measurements shows a close matching.

It is suggested that this simple device is suitable for those texturing mills which do not possess a tensile testing machine and for those which require an easy and quick assessment of the yarn quality to provide feed-back for the texturing machine operator to make any necessary process corrections.

9.3 Microcomputer Controlled 'Off-line' Instability Tester

The inherent drawbacks of all conventional instability measuring methods, such as those using weight hanging techniques, also partly exist in the above described 'off-line' instability tester. These are mainly reading and handling errors which can be reduced through a microcomputer controlled system. Therefore, a device with two yarn clamps, one of which is mounted on a slide, the other attached to a load cell, was designed and built (Fig. 9.3). The precision lead screw of the slide is driven by a stepping motor which is controlled by a BBC-Master microcomputer. The load cell, on the other hand, consists of a vertical cantilever with two strain gauges on both sides these being arranged in an electrical circuit so as to form a Wheatstone Bridge. When a deflection is created by the contact of the yarn clamp, the balance of the Wheatstone Bridge is destroyed. The amount of un-balance is then measured, amplified and outputted as a voltage by the anciliary electronic circuitry. The voltage output is fed to the A/D (Analog to Digital) converter of the microcomputer.

The software, given in Appendix F, having obtained the supply yarn linear density to determine the required T_2 tension and the number of tests to be carried out, prompts the user to fix the yarn between the clamps and hit a key on the keyboard to commence the measurement process. By moving the clamp mounted on the slide, a tension is created in the yarn such that, if this tension is less than the required tension T_1, the computer stretches the yarn further by sending more steps to the motor. As soon as the tension T_2 is reached, the action is stopped and from the number of steps sent to the motor, which are counted during the process, the elongation of the yarn is computed. Finally from the tension and elongation, the instability is automatically calculated and displayed. To repeat the test with another specimen, the user is again prompted to fix another sample. At the end, the average instability value is calculated by the software and displayed on the screen (See Fig. 9.4).

Since both the elongation and tension are measured by the computer, errors are expected to be negligible, although the human yarn handling errors can still exist. The system is less tedious than the previous hand-driven device and hence more tests could be carried out in any given time.

The results of instability measurements carried out by this microcomputer controlled instability tester are also included in Fig. 9.2 which shows good agreement with the results of the other two test methods, i.e. the Instron method and hand controlled 'off-line' device.

9.4 'On-line' Instability Measuring System

It was considered that the instability measuring method described in Sections 9.2 and 9.3, would perhaps be implemented in a system which, for the first time, would provide for instability measurements on running textured yarns. This 'on-line' instability measuring technique was in fact, achieved by stretching the yarn between two rotating rollers and recording the speeds of these rollers. Similar to the 'off-line' instability measuring device, a tension sensor is required to monitor the tension in the yarn. Since the required tension in the yarn T_2 can only be created by increasing the speed of second roller with respect to the first, the roller speeds need to be adjustable. Due to variations in the yarn quality, the system requires continuous monitoring and feed back to the roller speed control, which will maintain a constant tension of T_2. This can only be achieved by a dedicated microcomputer, or a microprocessor control, together with the necessary hardware and software.

In order to meet all these requirements, a system which comprises a pair of mechanical variators and yarn feed rollers, an interface circuit to BBC-Master microcomputer, and a Rothschild R1092 tensiometer, has been developed and set-up. The system, as seen in Fig. 9.5, has been fitted to the purpose built texturing machine to provide an 'on-line' measurement.

9.4.1 The mechanical drive system

Fig. 9.6 shows the mechanical drive used for the on-line measuring system in which two cone-drum type, purpose-built variators are fixed on a steel frame. The variators are driven by a 2 HP electric motor in association with an electronic speed controller, (Allspeeds 2000) using vee and timing belts.

The speed adjustment of both rollers is made by changing the speed ratio of the cone-drum variators by using stepping motors driven by the BBC-Master microcomputer. The roller speeds are measured by slotted discs and suitable opto-sensors which have been fixed to the other end of the roller shafts.

9.4.2 Interfacing to BBC-Master microcomputer

Using the BBC-Master microcomputer's 6522 VIA (Versatile Interface Adaptor), the stepping motors' driving circuit is controlled, and the pulses created by the slotted discs-opto sensor couple is counted to measure the roller speeds. The analogue outputs of the tensiometers are also recorded by the A/D (Analogue to Digital) converter of the microcomputer.

The stepper motor driving circuit shown in Fig. 9.7 comprises a stepper motor driving chip, SAA1027, and a buffer chip, 7407. The direction in which the stepper motor is required to rotate is provided from the BBC's user port in the form of 1 (logic high) or 0 (logic low). The number of steps is also given through a user port as a series of pulses. These pulses are then transferred to the driver chip where they are converted into a train of pulses which feed the coils of the stepper motor in the given direction.

In the pulse counting circuit to measure the shaft speeds, the ultraviolet light emitted from the emittor of the opto-switch is received by the collector which acts as a kind of phototransistor only when the slotted disc does not obstruct the path and a pulse is created. If the slotted disc is rotated, the opto-sensor will send a series of pulses to the interface circuit. Since the opto-switch used, is not compatible with the TTL (Transistor to Transistor Logic) interfacing circuit, the necessary additions to the opto-switch have been made as shown in Fig. 9.8. The purpose of the NPN (Negative-

Positive-Negative) type transistors in the circuit is to pull the signal to 0 (logic low) when the switch is off.

Since on the one hand, the speeds of two rollers are required to be measured, and on the other hand the microcomputer is only able to process one set of pulses at a time, the logic circuit given in Fig. 9.9 has been designed to admit only one pulse train at a time. In order to select the pulses sent from the opto-switch 1, the PB4 pin of the user port should be made logic high and, a logic low voltage should be applied to the PB5. Then the pulses will be allowed to enter to the PB6 pin of the user port. Similarly, to select opto switch 2, PB4, again, should be made 1, as well as PB5. The pin PB4 enables the pulses to flow to PB6. While PB4 is logic 0, there will be no pulses coming into the pin PB6. The pins of the user port are assigned as in Table 9.1.

Lastly, the analogue signal from the tensiometer is reduced by means of a two resistor potential divider due to the voltage limitation of the microcomputer, and fed to the built-in A/D converter of the BBC-Master microcomputer.

9.4.3 Software

Once communication between the external system and the microcomputer has been achieved through the interface circuit, the microcomputer is then able to drive, control and perform the desired function by using suitable software. This necessary software has been written in Basic programming language with machine-code embedded in it to speed up the computation when required. Listing of the program is given in Appendix G.

When the program is executed, the first task the computer performs is to define the VIA's port pins as output/input so that the user port is assigned according to the pin mapping shown in Table 9.1. Then the internal counter in VIA is initialised to count pulses coming from the external sources selected by PB4, PB5. From then onwards, the routine is so designed that it facilitates interactive working with the user. Initially, the speed of the first roller is set according to the upstream yarn tension to implement the winding-up tension during the process; then the tension between the two rollers of the system is adjusted by increasing or decreasing the speed of the second roller. As soon as the required yarn tension T_2 is reached, the second phase of the test procedure is performed for 60 seconds. During this period, the yarn tension is kept constant, the speeds of the rollers are measured, and the speed ratio is kept in an array for further processing. When the time elapses, an average of the recorded tensions is calculated and displayed. Finally, the user is prompted if the measurement is to be repeated, analysed, the graphs on the screen are to be dumped, or if they are to be stored on a floppy disk.

When the data is to be analysed, the program calculates the the minimum value, maximum value, arithmetic mean, standard deviation, and the coefficient of variation. The frequency histogram together with another presentation of the obtained data is also plotted on the screen (Fig. 9.10).

9.5 Results and Discussion

The system described in Section 9.4 has been tested with various types of yarns textured under differing process conditions. Fig. 9.10 shows a typical computer print out of test carried out. As the figure depicts, 194 readings are taken in 60 seconds and the average instability is printed at the top of the graphs. The top half of the graphs I show the tension fluctuations during the test, together with the instability fluctuations. The graph II depicts the results of a statistical analysis of the data obtained.

The results obtained from the 'on-line' instability measuring system are compared with the results obtained from the Instron tensile testing machine. A good qualitative agreement, as seen in Figs. 9.11a, b, and c for varying process conditions, has been observed showing the viability of the system.

When instability is measured during the process, questions such as "Is the structure of the individual filaments in the yarn affected?" or "Is the 'on-line' test method a destructive measuring technique?" inevitably arise.

Piller[71], measuring the loop frequency before and after instability tests, showed that the loop frequency is not reduced. He therefore concluded that during the instability tests the elementary filaments are only extended, without removal of the loops. The yarn tests, i.e. instability, linear density and tenacity (Fig. 9.12), carried out on yarns before and after the 'on-line' instability measurement process also confirmed Piller's conclusion in that the effects of an 'on-line' instability test on the yarn quality is negligible. Therefore this 'on-line' test can be used safely without altering the properties of the textured yarn.

9.6 Conclusions

A simple 'off-line' instability measuring device (Section 9.2) which will be of help to most the texturing mills, facilitates an easy and quick instability measurement. The accuracy and reliability of the device can be improved by a dedicated microcomputer or a microprocessor control (Section 9.3). The microcomputer controlled system makes the measurements even easier and quicker.

An 'on-line' instability measuring instrument (Section 9.4) is shown to be feasible and a provisional patent protection is currently being negotiated. The same system could be further adopted by feeding the information acquired to the texturing machine and the process parameters could be adjusted to obtain a desired yarn quality. Alternatively, the operator could be warned and informed immediately after a fault in yarn quality is detected.

A more compact version of the 'on-line' instability tester, together with its microcomputer and electronic hardware, could be fixed on a trolley so that it can be transported from one texturing position to another to set-up and check the quality of the yarn textured in that particular position.

TABLE 9.1

User port setting of BBC-Master microcomputer

PORT B	INPUT/OUTPUT
PB0.....Step 1	Output
PB1.....Direction 1	Output
PB2.....Step 2	Output
PB3.....Direction 2	Output
PB4.....Pulse Enable	Output
PB5.....Pulse Gate Select	Output
PB6.....Pulse Input	Input

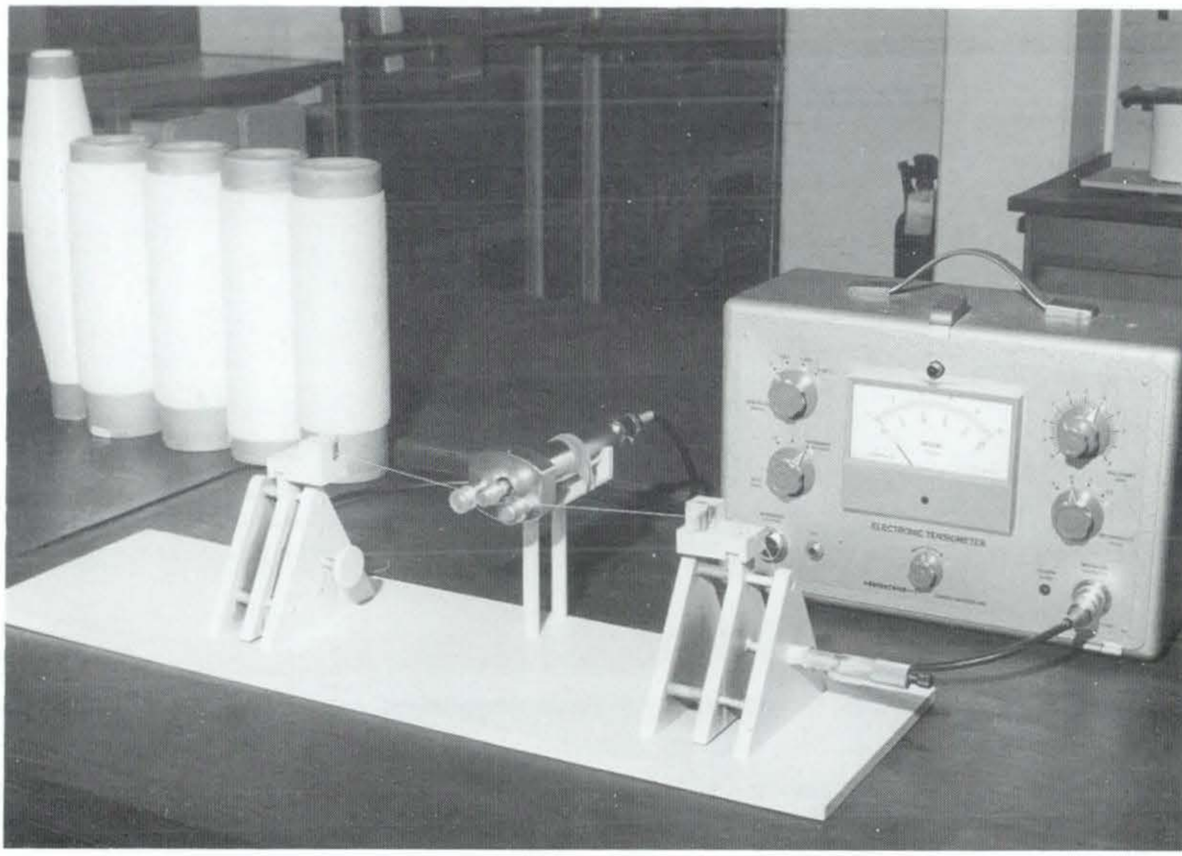

Figure 9.1 Manual control 'off-line' instability tester

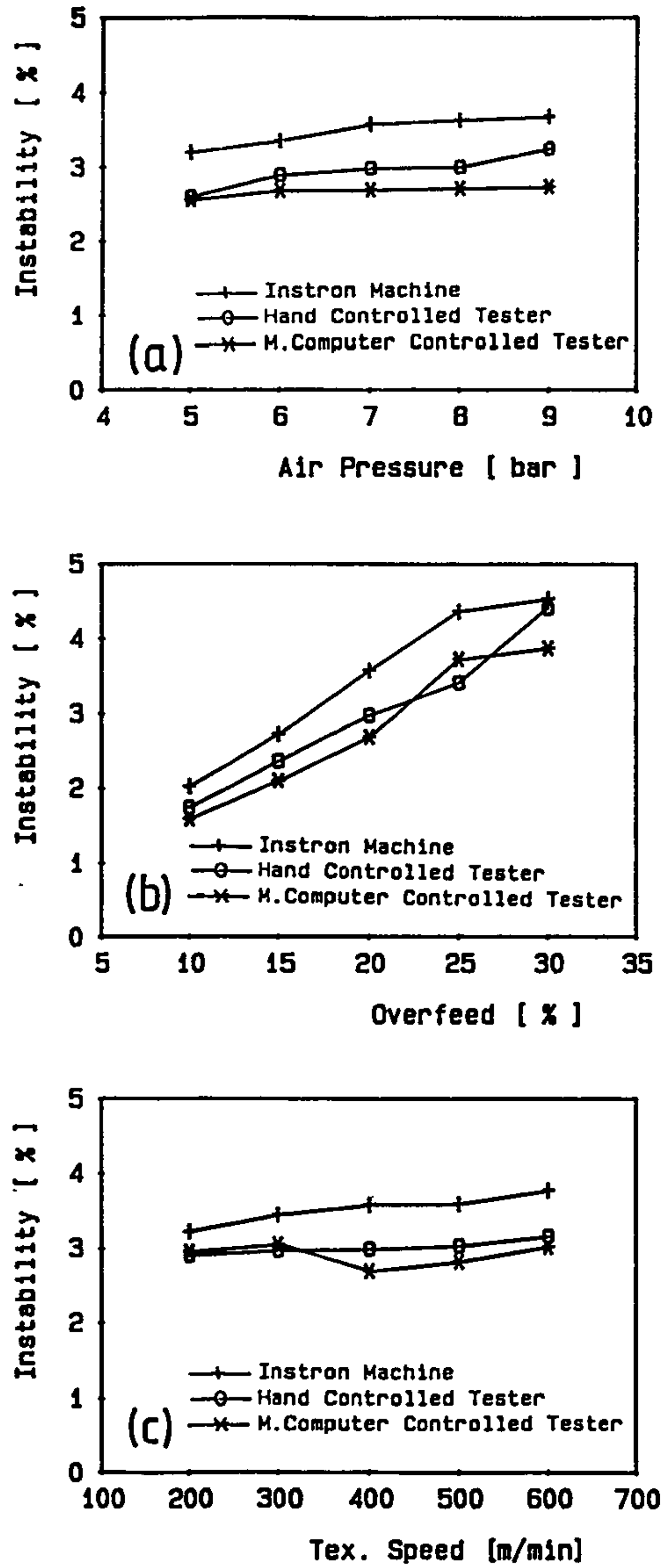

Figure 9.2 Comparison of the instability results measured by: Instron tensile testing machine; manual control instability tester; and microcomputer controlled instability tester

Figure 9.3 Microcomputer controlled instability tester

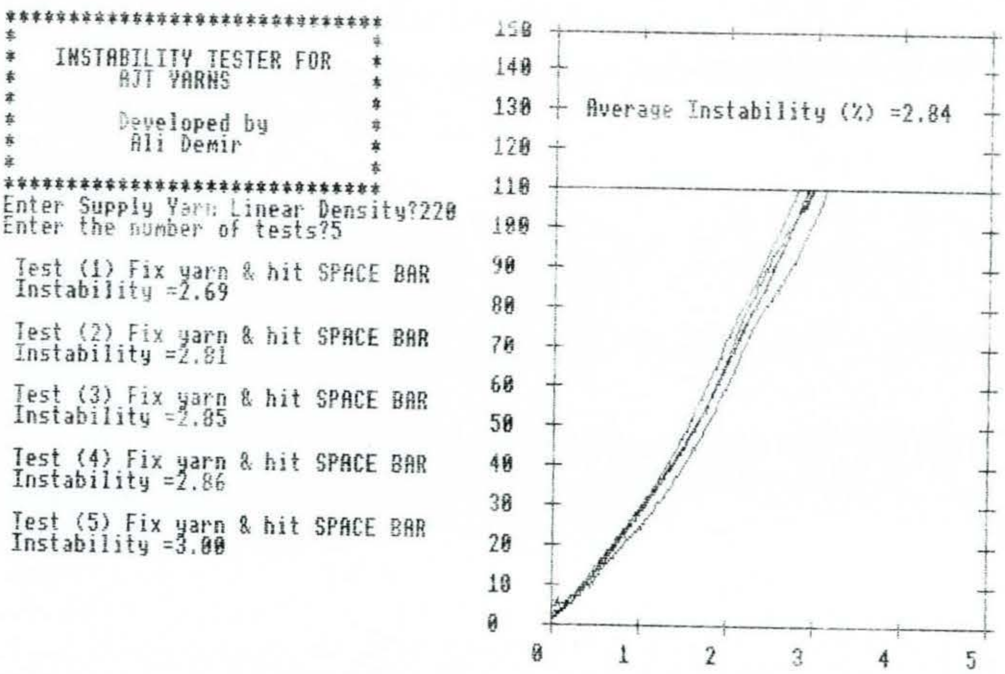

Figure 9.4 A typical screen display of microcomputer controlled instability tester

Figure 9.5 'On-line' instability measuring system fitted to the texturing machine

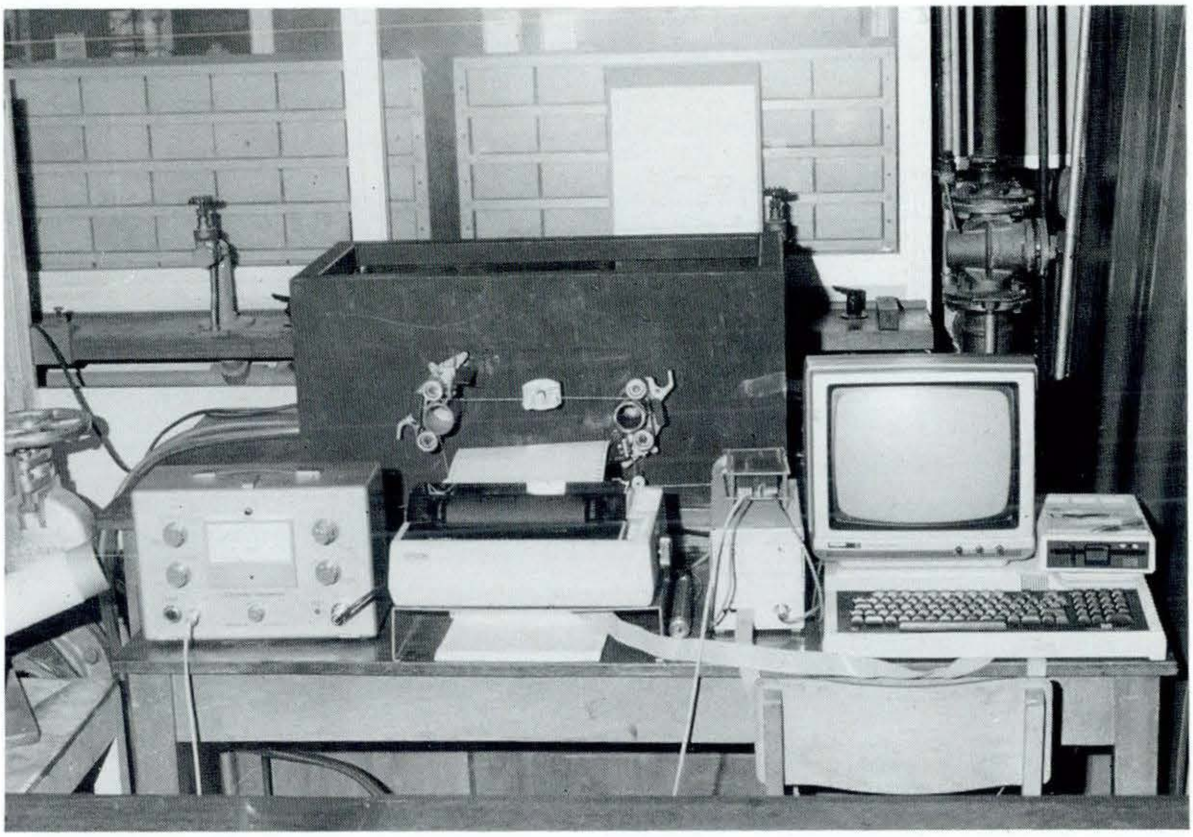

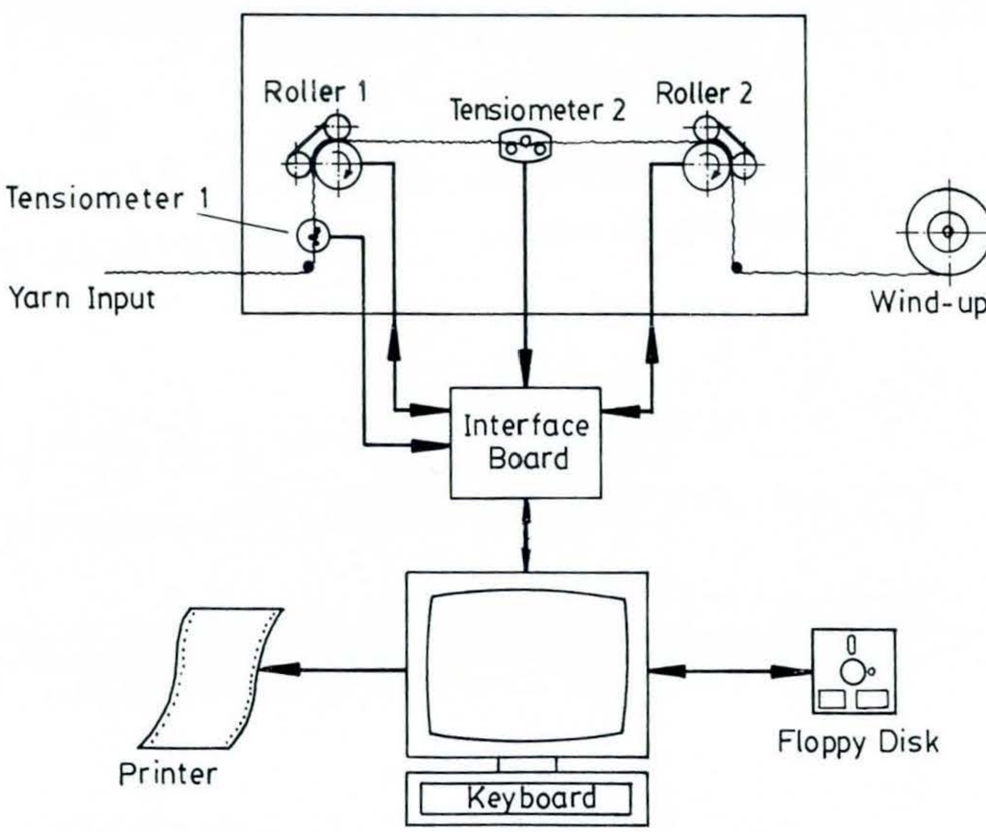

Figure 9.6 Principles of 'on-line' instability measuring system

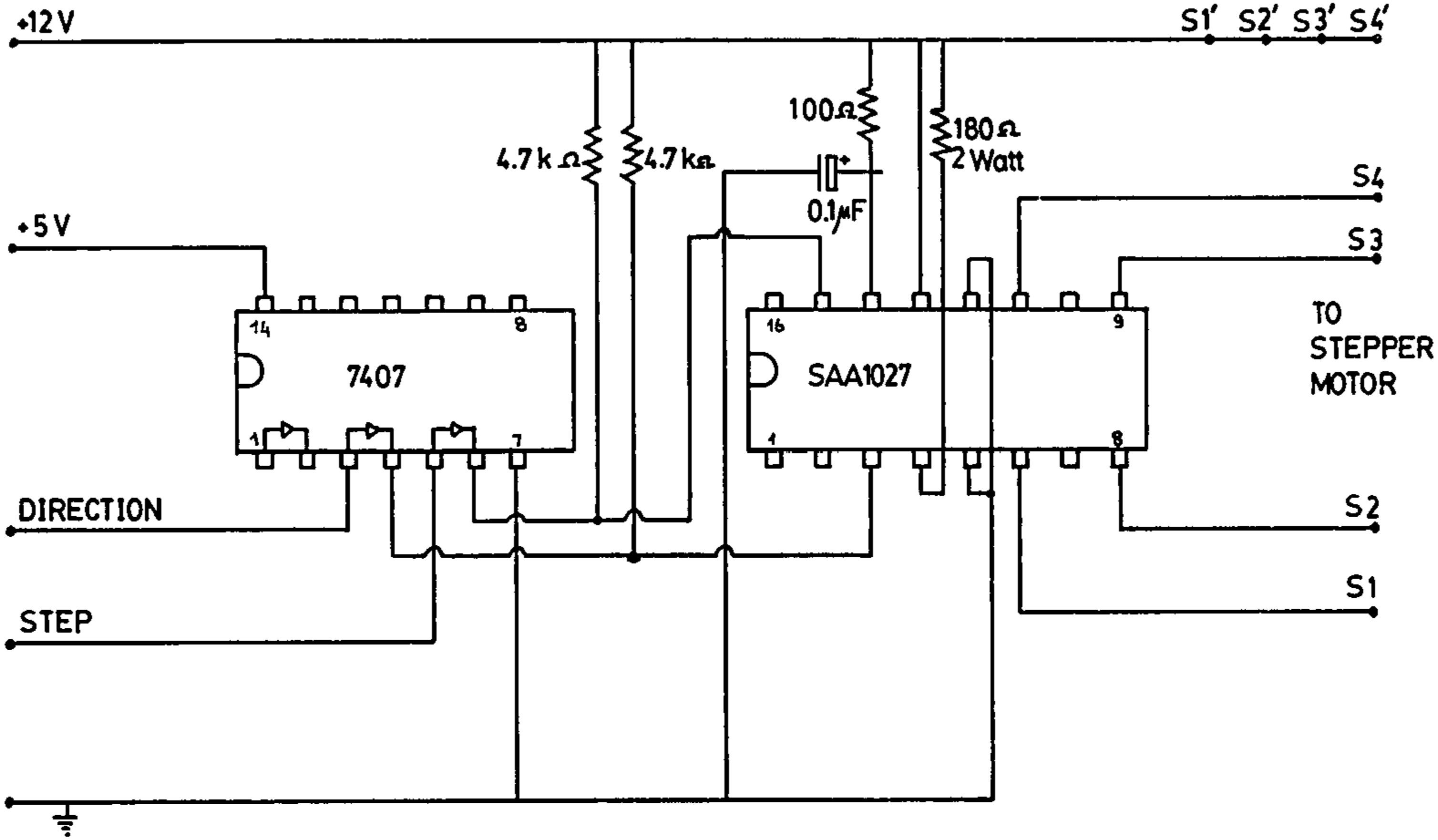

Figure 9.7 Circuit diagram of the stepper motor driving board

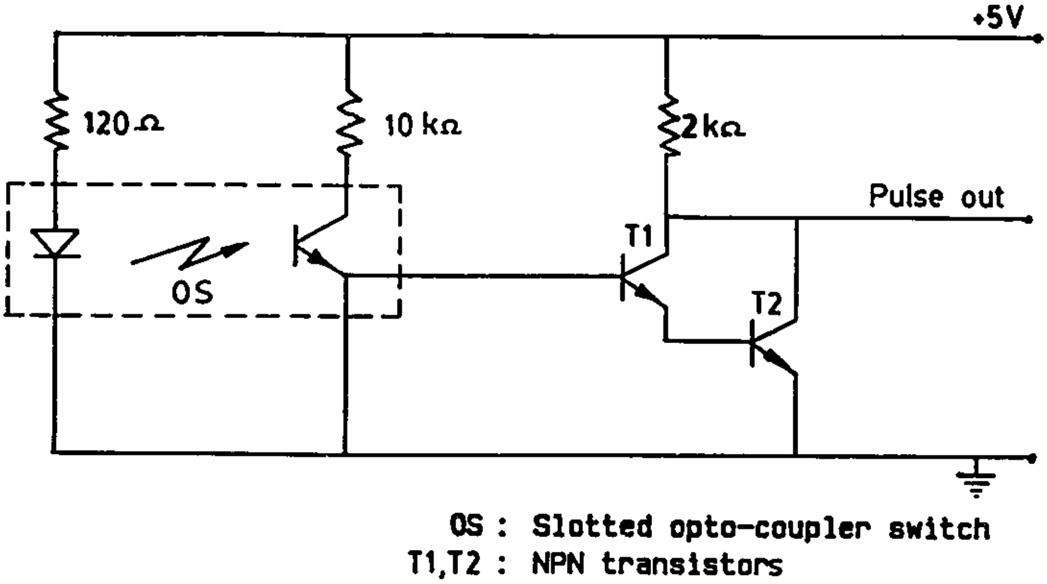

Figure 9.8 Circuit diagram of opto-switch used for measuring the roller speeds

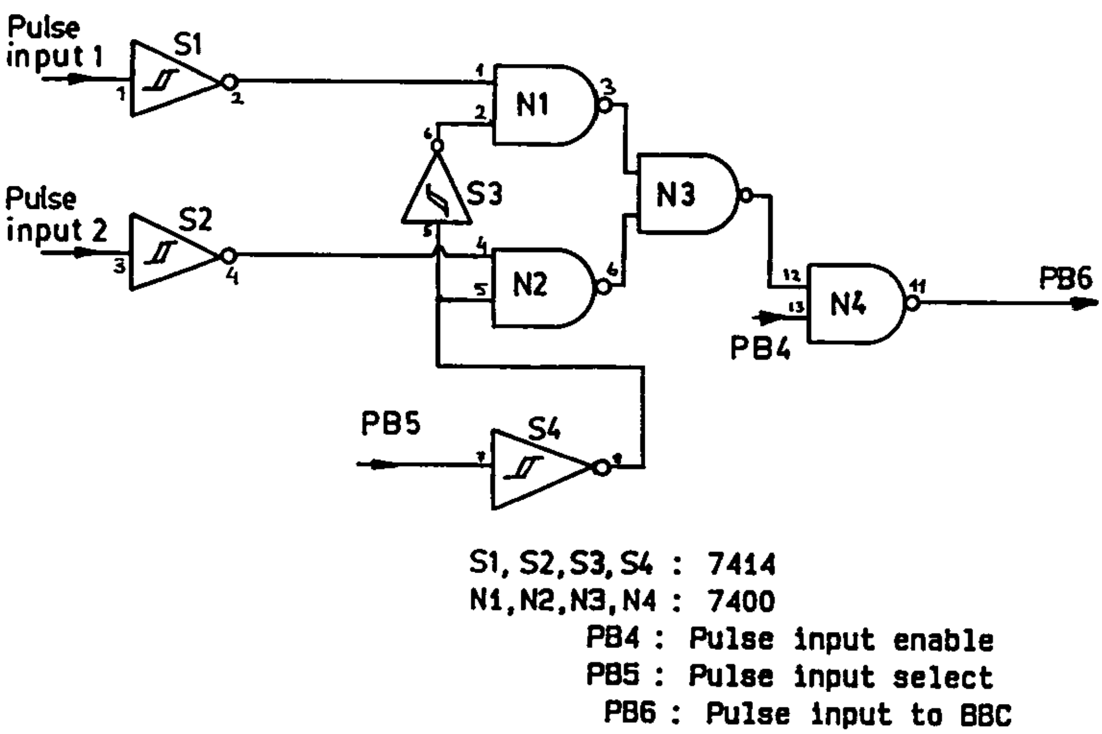

Figure 9.9 Interface logic circuit

I.

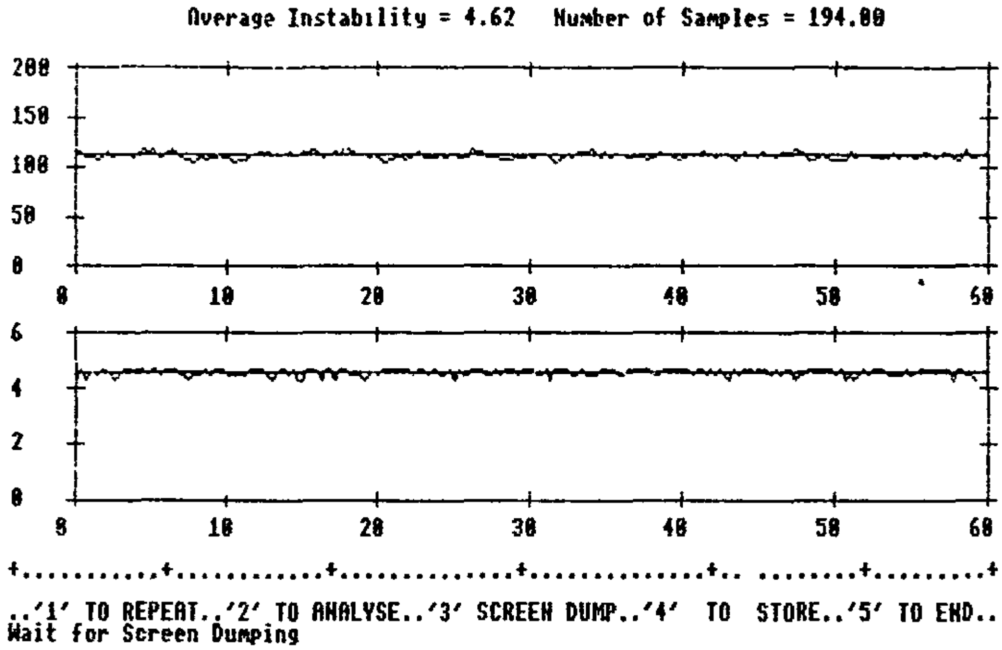

II.

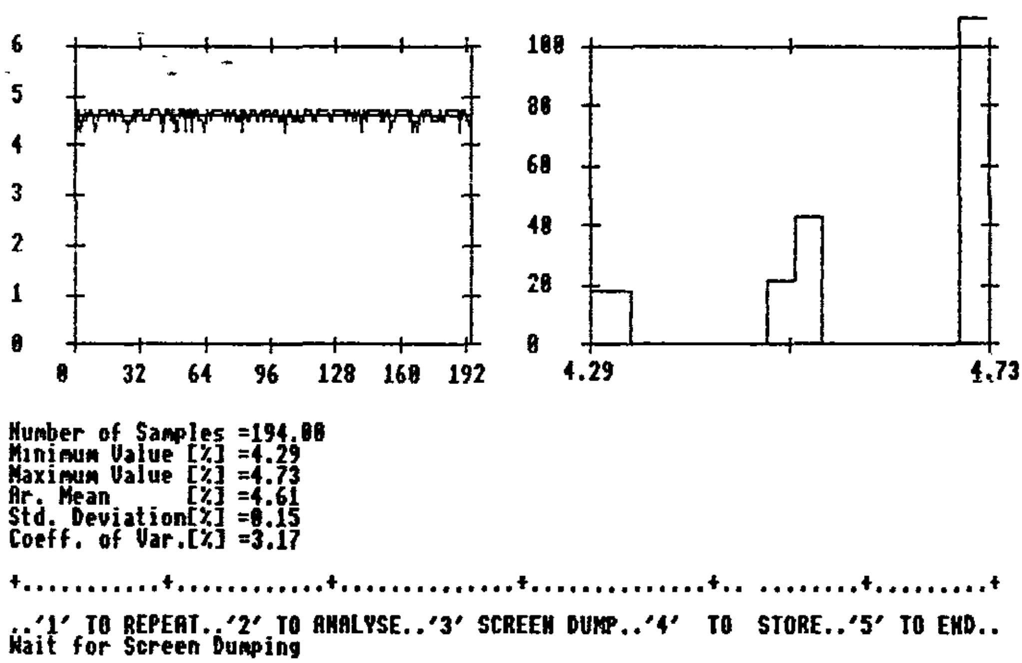

Figure 9.10 Typical screen displays of 'on-line' instability measuring system: I. Tension and instability fluctuations during the test; and II. Statistical analysis of data obtained

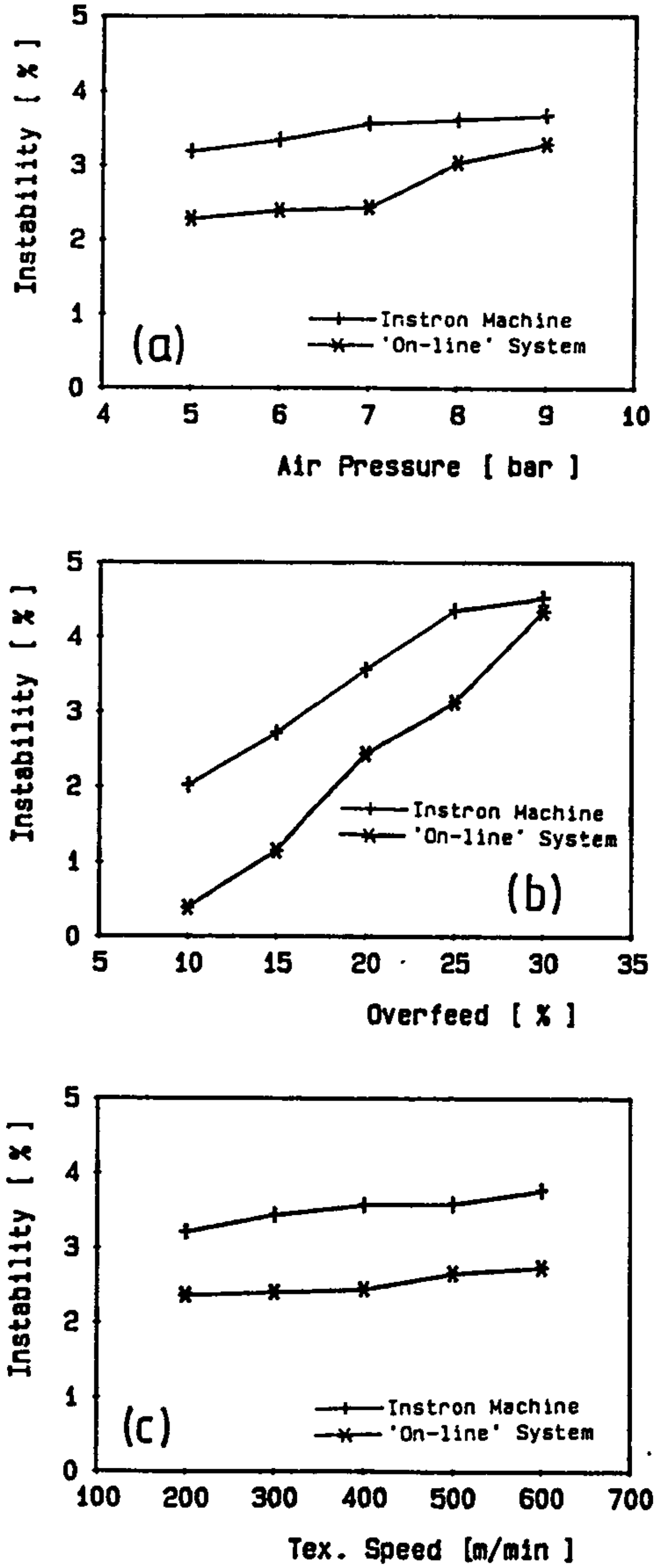

Figure 9.11 Comparison of instability results measured by: Instron tensile testing machine; and 'on-line' instability measuring system

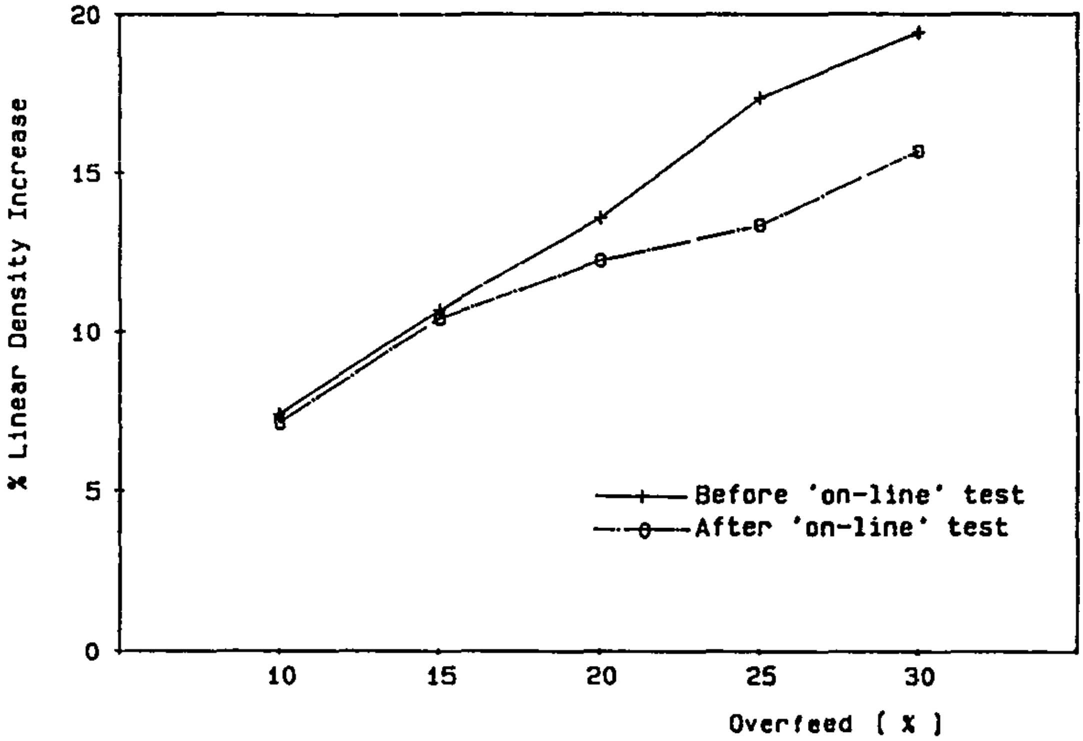

Figure 9.12a Effects of 'on-line' instability measurement on the linear density of yarns

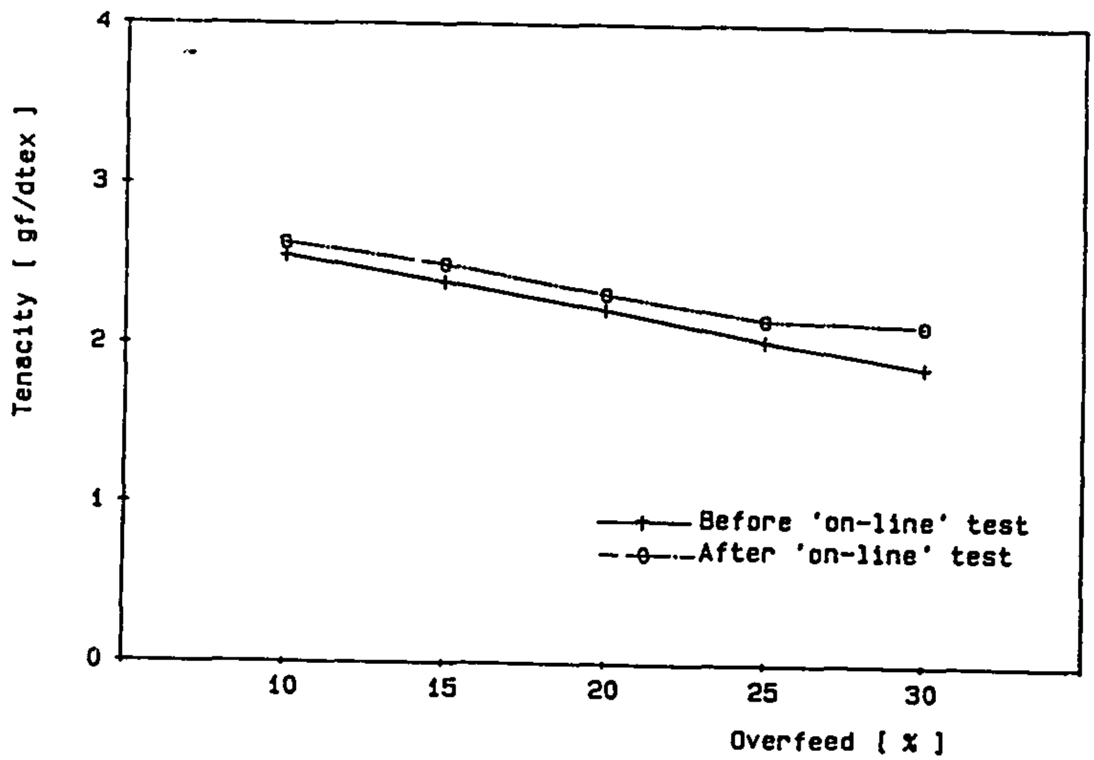

Figure 9.12b Effects of 'on-line' instability measurement on the tenacity of yarns

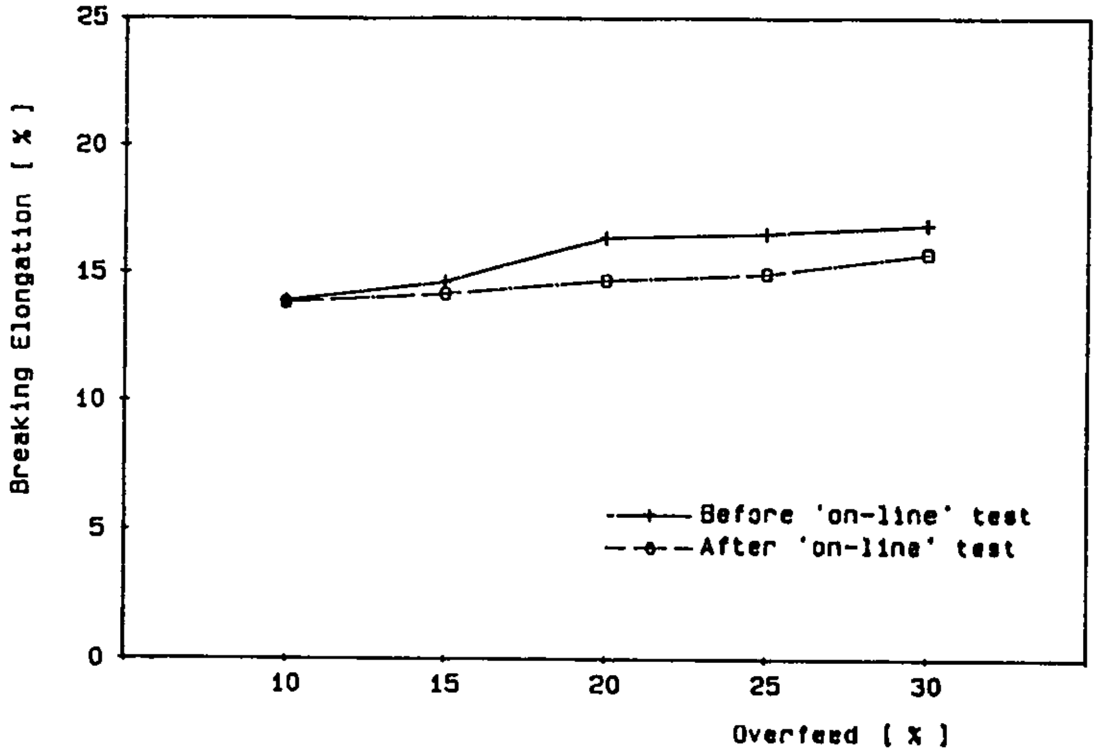

Figure 9.12c Effects of 'on-line' instability measurement on the breaking elongation of yarns

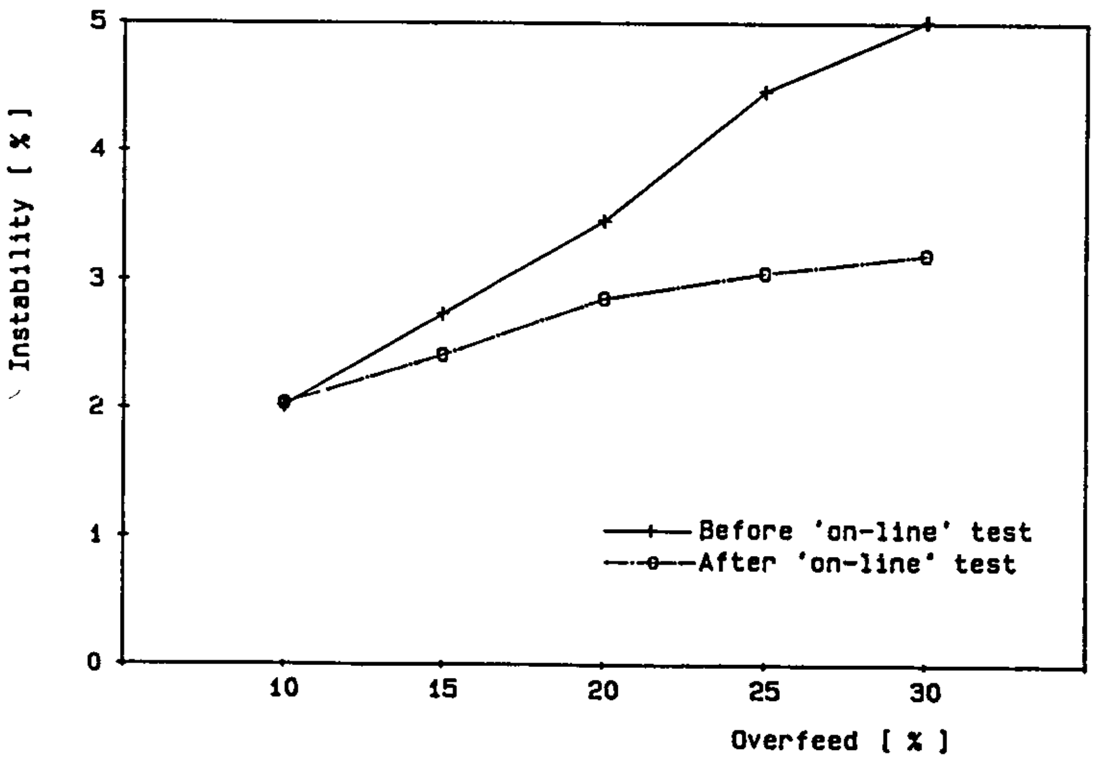

Figure 9.12d Effects of 'on-line' instability measurement on the instability of yarns

CHAPTER 10

EFFECTS OF PROCESS AND SUPPLY YARN PARAMETERS ON THE PROPERTIES OF AIR-JET TEXTURED YARNS

10.1 Properties of Air-jet Textured Yarns

10.1.1 Instability

The concept of instability and several existing instability test methods have been critically studied in Chapter 8 in which a standard instability test method has also been recommended (section 8.8). It was concluded that instability tests alone would yield misleading information regarding the yarn quality and its suitability for intended end-use, and that such tests should be supported by further tests and visual assessment of the yarn structure (See Section 8.9). Therefore, the instability test results reported in this chapter will be supported by linear density and strength tests together with microscopic visual assesement of yarn structure.

10.1.2 Increase in linear density

Air-jet texturing causes longer lengths of synthetic filaments to be compacted into shorter lengths with an entangled structure. The resultant yarn is stable, does not stretch and does not lose its interlaced and intermingled structure even under relatively higher loads. Therefore, a considerable linear density increase is expected from an air-jet textured yarn. An increase in the yarn linear density at varying process conditions but at a given overfeed can be interpreted as an increase in the effectiveness of the texturing process.

Theoretically, it is expected that the increase in linear density will be equal to the amount of overfeed irrespective of the process and the supply yarn parameters. Nevertheless, this theoretical expectation is never met in practice due to both the on-line stabilising process and the winding up tension. Since a well textured yarn will resist the stabilising and winding up tensions, the loops will stay intact within the well entangled core and consequently its linear density will be higher than that of a poorly textured yarn. This therefore implies that the amount of increase in linear density is influenced both by the process itself and by those supply yarn parameters which affect the degree of entanglement and loop formation.

10.1.3 Strength

Rozmarynowska and Godek[68] in 1966 and also very recently Kollu[13] have disclosed their research findings on the effects of the air-jet texturing process on the individual filaments. The former researchers used physico-mechanical tests such as SEM (Scanning Electron Microscopy) scanning, strength measurement, birefringence and criystallite orientation tests. The latter has only deployed SEM scanning and strength measurement on individual filaments before and after texturing. However, both have come to the same conclusion that the air-jet texturing process, however severe it may be (up to 5 bar air pressures in the former and up to 11 bar pressures in the latter), caused no damage on the individual filaments in the form of crack, local cross-sectional shrink (thinning) or even chip formation on the filament surface. Consequently, it is concluded that any decrease in strength after texturing results solely from the entanglement of the originally parallel arrangement of the constituent filaments of the supply yarn.

Comparisons of the load elongation curves (Fig. 10.1) of untextured and textured yarns reveal striking differences. All of the filaments in an untextured yarn simultaneously share the applied load to the yarn and firstly deform elastically. When the load is increased beyond the elastic limit, all of the filaments are then plastically deformed, the filaments exhibiting an increasing strength under this increasing load (i.e. hardening) up to the yield point where they start to elongate rapidly (Fig. 10.1a). When the stress in an individual filament exceeds its breaking stress, it will break irrespective of the other filaments' conditions. Therefore, in a supply yarn the filaments break singly at different times, probably due to slight variations in their diameter, and some of the filaments appear to elongate more than others. Nevertheless, for the purpose of the strength tests, the load which causes most of the filaments to break is taken as the breaking load for the yarn and the corresponding elongation is regarded as the breaking elongation.

Textured yarns, however, exhibit totally different load elongation characteristics (Fig.10.1b) . Since the filaments are randomly entangled and some of these local entanglements and loops are removed under the applied load, the deformation of a textured yarn starts with permanent elongation. No hardening of the textured yarns is observed as the loading is increased, due to the fact that none of the individual filaments are continuously subjected to the applied load during the entire test period. All filaments exhibit loops and entangled sections intermittently along their lengths but these are separated by straight portions of filaments. At any section of the yarn, at any particular instance, only these straight portions will resist the applied load. However, when the loops associated with these particular filaments have been pulled out under the applied load, their effective lengths are increased; consequently some other less straight slack filaments in the same region may become subject to the applied load and in turn contribute to carrying it.

It is most likely that within the length of yarn tested, a particular section will be more effectively entangled than the rest and will have fewer load carrying filaments; these will be surrounded by filaments which exert lateral forces that increase the interfilament friction at this section. These load bearing, firmly entangled filaments will rapidly reach the breaking point simultaneously within a very short time and consequently an almost instantaneous breakage of the yarn will occur at this section. The load-elongation curves of an air-jet textured yarn and a spun staple cotton yarn are very similar as shown in Fig. 10.1, suggesting that other physical characteristics of these yarns may also be similar.

In general, synthetic untextured filament yarns have higher tenacities* than air-jet textured yarns. This is because all the individual filaments share the applied load and virtually there is no lateral force on the filaments. However, an air-jet textured yarn has a reduced strength because the applied load is borne only by a small fraction of the individual filaments.

Therefore, the effectiveness of the nozzle and thus the texturing process could be observed as a reduction in tenacity i.e. a better textured yarn (one with many small compact and entangled loops) will exhibit a greater decrease in tenacity when compared with the supply filament yarn from which it is produced.

10.2 Test Plan

Process parameters, (e.g. air pressure, texturing speed, overfeed, stabilising extension, wet or dry processing and the use of impact element) together with supply yarn parameters (e.g. the material, linear density per filament, number of filaments, filament cross-sectional shape and applied spin-finish) all play an important role in determining the final properties of air-jet textured yarns, (e.g. instability, linear density, strength, bulk, and the size and frequency of loops). The effects of these parameters on the instability, linear density and strength of the textured yarns are ascertained in Sections 10.3 and 10.4 where SEM photographs of typical yarns are used to illustrate the visual surface characteristics of these textured yarns.

---

*"The maximum specific stress that is developed in a tensile test taken to rupture" is termed as 'tenacity' by the Textile Institute's 'Textile Terms and Definitions[119]'.

A purpose-built single-head texturing machine designed and built by Acar[42] was used to investigate the process parameters, mainly with a Heberlein T100 HemaJet texturing nozzle. Heberlein Standard-core and T341 HemaJets together with Taslan Type XIV nozzles were also used. The process parameters were: 10% to 30% overfeed by increments of 5%; texturing speed varying from 200 m/min to 600 m/min by increments of 100 m/min; varying air pressure from 5 bar to 9 bar by increments of 1 bar; and stabilising extension in the range of 0-10% with increments of 2%. A processing condition of 20% overfeed, 400 m/min texturing speed, and 7 bar air pressure, with 1 l/hr water application to the supply yarn together with 4% stabilising extension was chosen as reference conditions. The T100 HemaJet texturing nozzle was used at these reference conditions without using the impact element. Whenever one of the processing parameters was varied to investigate its effect on the yarn properties, the other parameters were kept at the reference conditions.

Polyamide and polyester were the only two yarn materials used. The filament linear density ranged from 1.67 dtex to 6.8 dtex whilst the number of filaments was kept approximately constant. In order to ascertain the effects of total yarn linear density (i.e. number of filaments), a 110 dtex 66 filament polyester yarn was folded to form 220, 330, and 440 dtex yarns. The properties of the supply yarns used are given in Table 10.1.

Having conditioned the textured yarns in the laboratory atmosphere for over 24 hours, the instability was measured on the Instron tensile testing machine in compliance with the test method recommended in Section 8.8, ten specimens for each type of yarn, taken from randomly chosen sections of yarn packages, being tested. Strength tests were also made on the Instron tensile testing machine, again by using ten random specimens, to obtain the average breaking load, elongation and tenacity. Linear density calculation involved weighing 200 meters of yarn which had been measured under a slight tension which did not remove any entanglements.

Different supply yarns have different tenacities and breaking elongations (Table 10.1) thereby giving absolute tenacity values which would not be informative for comparison purposes. Therefore, percentage decrease in tenacities have been calculated from the experimental results and these are presented in graphical format.

10.3 Effects of Process Parameters

10.3.1 Air pressure

As the air pressure is increased, the flow velocity which is the main driving force that opens up the filaments to enable them to entangle and texture, also increases. The non-uniformity and turbulence of the air flow are also enhanced by increasing air pressures (See Section 4.3). An improved texturing of the yarn is therefore expected at higher pressures. One might also anticipate a more stable entanglement, i.e. less instability for yarns textured at high pressures but Fig. 10.2a depicts a very slight increase in the instability of air-jet textured yarns as the pressure increases. From a comparison of the SEM photographs of two yarns textured at the two extremes of pressure, it is observed that yarn textured at 5 bar contains larger but fewer loops whereas yarn textured at 9 bar shows a compact yarn core and a greater number of loops due to the improved texturing conditions. The slightly increased instability at higher pressures probably arises from the greater number of loops which increase the likelihood of loop removal but in no way can this increased instability be interpreted as a deterioration of the texturing quality. The ensuing considerations of other properties such as the linear density increase and the decrease in tenacity substantiate this argument.

Since the amount of overfeed is kept constant at 20%, any variation in the linear density of the yarn must be caused by better entanglement and loop formation at higher air pressures. Fig. 10.2b indicates that the linear density increase of the textured yarn increases from 12% at 5 bar to 14.5% at 7 bar with a very small increase when the pressure is increased beyond this value. These results are typical for the supply yarn and for the texturing nozzle used, viz. the Heberlein T100 HemaJet, and cannot be generalised for other nozzles. For example, the T341 HemaJet and Taslan XIV nozzles produce textured yarns with linear densities almost linearly increasing with increasing air pressures.

Fig. 10.2c shows that the yarns textured at 5 bar exhibit approximately 60% of the supply yarn tenacity. When the air pressure is increased further upto 9 bar, the reduction in tenacity would reach approximately 50%. This reduction in yarn strength follows from the increased numbers of loops, as depicted by the SEM photographs, which in turn reduces the number of load bearing filaments thereby causing a reduced strength as was argued in Section 10.1.3.

10.3.2 Overfeed

When the overfeed is as low as 10%, the excess lengths of filament available to form loops and arcs are indeed small. Consequently, the texturing is poor with very few loops on the surface and a slight reorientation in the core of this yarn as seen in the SEM photograph in Fig. 10.3. It exhibits a low level of instability, due to the presence of more straight unlooped load-bearing filament portions but it would be unacceptable for many end-uses.

As the overfeed is increased more excess lengths of filament are available to form loops which tend to cover the yarn surface. This increases the instability of the yarn (Fig. 10.3a) without discrediting its acceptability as was argued in Section 10.3.1. High-speed shadowgraphs of the emerging air-jet during texturing process have revealed that the flow becomes more disturbed as the overfeed is increased. Consequently the texturing power of the jet decreases at higher overfeeds and as seen in the SEM photographs of a 30% overfeed textured yarn (Fig. 10.3), its surface is covered with many slack and large loops. For the given supply yarn and reference process conditions, the overfeed which yields suitable texturing from the loop appearance viewpoint varies between 15% and 25%. However higher overfeeds may as well be deployed for special purposes such as core-and-effect, fancy and slub yarns.

At low overfeeds, the excess lengths of filaments are insufficiently long to form stable loops and arcs. On the other hand, as the overfeed is increased beyond the capability of a particular nozzle, effective entanglement of the filaments is unattainable. Therefore, for any particular nozzle, there is a range of overfeed over which effective texturing can be achieved. Fig. 10.3b, shows that the overfeed has paramount influence on the linear density of the textured yarn. Provided that the other supply yarn and process parameters are acceptable, a desired linear density can be obtained by varying the amount of overfed filaments introduced to the nozzle.

Fig. 10.3c shows that, at 10% overfeed, only a 29% decrease in tenacity occurs due to the poor entanglement and loop formation. In the resultant yarn, the majority of the filaments are approximately straight and hence can carry more load. As the overfeed is increased up to 20% the effectiveness of texturing is rapidly enhanced and due to better filament entanglement the tenacity of the yarn is correspondingly decreased by 45%. Above 20% overfeed, the rate of tenacity decrease is not as high because of the less effective texturing referred to above.

10.3.3 Texturing speed

Fig. 10.4a reveals only a very slight increase in yarn instability with increasing texturing speeds. Since the resultant forces and torques on the filaments are mainly generated by the relative velocity between the filaments and the surrounding air flow[82], higher forces and torques are exerted on the individual filaments at lower texturing speeds. These greater fluid forces cause a better entanglement and a more firmly fixed loop formation. As the texturing speed is increased, the filament speed is also increased, hence the resultant forces decrease. Consequently the texturing becomes less effective thereby resulting in large and unstable loop formation as depicted by the SEM photograph of yarn textured at 600 m/min.

For the particular nozzle used, the texturing at 400 m/min is almost as effective as at 200 m/min (Fig. 10.4b and 4c) although at speeds greater than 400 m/min the texturing quality is markedly reduced due to large and unstable loop formation. Only approximately 1/3 of the overfed lengths of filaments supplied could be retained in the yarn at 600 m/min texturing speed, whereas at 200 m/min texturing speed, approximately 3/4 of overfed lengths appear to be fixed in the yarn which exhibits stable loops and a highly entangled core structure.

10.3.4 Stabilising extension

The purpose of the stabilising extension, which is performed 'on-line' on the machine subsequent to the texturing zone, is to pull out those loops which are not firmly fixed to the core of the yarn. The level of this extension usually varies from 2% to 6%, because at higher levels permanent yarn damage or even breakage could occur. For the purpose of investigation however, the stabilising extension is here varied from 0 to 10%.

Fig. 10.5a illustrates a steady decrease in instability with increasing stabilising extension. This is obviously due to the removal of large and loose loops on the yarn prior by the application of increasing stabilising extensions. At 10% stabilising extension, very few loose loops stay intact to the core of the yarn as illustrated on the SEM photograph of this yarn (Fig. 10.5) where it can be seen that some of the loops were broken up to form free fibre ends due to the high tension build up in the yarn. Further evidence for this was the accumulation of fluff around the take-up rollers. It is therefore recommended that the stabilising extension should not be so high as to cause broken filament ends, and a range of about 2%-4% seemed reasonable for the particular supply yarn and process conditions used.

Fig. 10.5b shows the experimental linear density increase with increasing stabilising extensions together with the theoretically predicted linear density increase which is the overfeed (20% in this case) minus the amount of stabilising extension. Since all linear density measurements have inevitably been carried out under a slight tension, some of the loops and entanglement of air-jet textured yarns may have been removed by the effect of this tension particularly for low stabilising extensions (less than 2.5% for the conditions considered). At higher stabilising extensions, the loops and filament entanglement resist the applied tension and the yarn extends partially elastically so that when the load is removed it recovers some of the extension and therefore possesses a higher linear density than theoreticaly predicted.

Fig. 10.5c indicates that the amount of stabilising extension applied during the process has little effect on the resultant yarn tenacity.

10.3.5 Wet and dry processing and the use of an impact element

Water application to the filaments prior to their entry to the nozzle is now a well recognised requirement for better texturing (See Chapter 7). However, the use of impact elements in the form of a cylindrical bar, spherical element or flat plate, placed at the exit of the nozzle, are only recommended for particular applications such as low linear density yarns or high speed operations. Fig. 10.6a shows that the instability increases both with wet processing and with the use of an impact element of spherical shape. Such increases, provided that they are within acceptable limits, are indicative of improved yarn quality. The SEM photographs also support this argument in that dry textured yarns exhibit larger and fewer loops than wet textured yarns, as do wet textured yarns with respect to yarns textured with the impact element.

Although the use of an impact element is not essential, wetting of the supply yarn prior to the nozzle is a well accepted requirement of the air-jet texturing process (See Chapter 7).

Texturing is enhanced by the water application, because the overfed filaments are better entangled and surface loops are firmly fixed to the compact core of the yarn. This better entanglement causes only a small fraction of the linear density increase in the yarn to be lost under both the stabilising and winding up tensions (Fig. 10.6b). Dry texturing however yields poor texturing in that most of the loops and entanglements are removed under such tensions.

As seen in Fig. 10.6c, when the yarn is dry textured at 9 bar air pressure, the texturing is so poor that only about 26% decrease in tenacity is observed thus indicating little change from the basic straight filament supply yarn. However, when it is wet textured at the same pressure, the decrease in tenacity, indicative of better texturing, goes up to about 48%. The same trends can be observed at other air pressures and this improved effectiveness of texturing is due to reduced interfilament friction as concluded in Section 7.10.

The deployment of an impact element does not seem to make any further significant improvement of wet textured yarns. When the linear densities of such textured yarns are compared, it is concluded that the impact element contributes little to the process and the lack of a further significant reduction in the tenacity due to the use of impact element adds further evidence to support this conclusion.

10.3.6 Nozzle type

As far as the instabilities of the textured yarns are concerned, the T100 and T341 HemaJets produce similar yarns. The Standard-core HemaJet, produces yarns with reduced instability whereas the yarns textured by the Taslan Type XIV nozzle possess the highest instability (Fig. 10.7a). Nevertheless, the instabilities of the yarns produced by the four nozzles considered are in the same close range, particularly at high pressures (Fig. 10.7a). Fig. 10.7 also includes the typical SEM photographs of two yarns textured by T341 HemaJet and Taslan Type XIV nozzles. The distinctive nature of the yarn textured by the Taslan XIV is that the large loops and arcs are dominant on the surface of the yarn, whilst the yarns textured by the HemaJets appear to possess greater numbers of smaller sized loops.

Fig. 10.7a depicting similar instabilities for the yarns textured by the T100 and T341 HemaJets, suggests that these two yarns are of the similar quality. However when their linear densities and tenacities are compared, it will be appreciated that the two yarns produced by two different nozzles have different characteristics.

Fig. 10.7b illustrates that the yarns textured by the T341 HemaJet attain the highest linear density corresponding to an increase of about 17%. This clearly indicates that the overfed filaments are so effectively entangled that even a stabilising extension of 4% had little adverse effect and this satisfactory texturing could be attributed to the higher air velocities achievable by this nozzle (See Section 4.3) at the cost of a greater compressed air consumption than the other nozzles considered. This argument is also supported by the result for the Taslan XIV nozzle which possesses the second highest flow velocities.

The strength test results indicate that the T341 HemaJet, which produces the highest air velocity, displays the greatest decrease in tenacity, approximately 50% as seen in Fig. 10.7c. From Fig. 10.7c and Fig. 10.7b it will be noticed that the nozzles considered show similar trends as far as the linear densities and strengths of the yarns are concerned and their relative texturing effectiveness could be ranked in the following order: the T341 HemaJet, Taslan XIV, T100 and Standard-core HemaJet. The T100 HemaJet is more effective than the standard-core HemaJet, despite its reduced air consumption and lower air velocities (Section 4.1). This can be attributed to its improved design which accounts for why the Standard-core HemaJets are regarded as obsolete by todays textile industry and are no longer produced.

10.4 Effects of Supply Yarn Parameters

10.4.1 Material

Two different polymer yarns, i.e. polyester and polyamide were used. The filament linear density and the number of filaments, and hence the total linear density of these yarns were kept as close as possible although there was no control over their cross-sectional shapes and the applied spin-finishes. They were textured under reference conditions but at varying air pressures.

Fig. 10.8 indicates that the polyamide yarn exhibits lower instability, slightly lower linear density increase, and lower percentage tenacity decrease indicating that the polyester filament yarn is more suitable for air-jet texturing, although both can be textured effectively. This is also manifested in the presence of more undesired parallel filaments in the core of the polyamide yarn as seen from the SEM photographs. However, it could be argued that the difference in texturing quality is caused by differences in spin finish and filament cross-section.

10.4.2 Filament linear density

Supply yarns with approximately same number of filaments but with varying filament linear densities were tested to analyse how this affected the textured yarn properties.

Acar et al[82] have shown that the total drag force on the filaments is dependent on the surface and projected areas of the filaments in the air flow and greater drag force acts on filaments with increased areas. It is also known that bending and torsional stiffnesses are directly proportional to the second moment of area about a diameter and to the polar second moment of area, respectively. Therefore, it was concluded that the smaller the second moments of areas, the smaller the forces and torques required to bend and twist the filament, respectively.

The findings and conclusions of Acar et al showed that, for an equal total yarn linear density, yarns consisting of finer filaments require smaller fluid forces to displace and entangle them than those consisting of coarser filaments. This is due to the reduced bending and twisting rigidities, and increased surface and projected areas of finer filaments. Therefore it could be anticipated that finer filaments will be better textured.

This point is verified by Figs. 10.9b and c which show reductions in textured yarn linear density and in tenacity decrease with increasing filament linear density, thereby indicating that finer filaments produce better textured yarns.

On the other hand, the instability curve (Fig. 10.9a) indicates an increase with the increasing linear density up to approximately 2 dtex and then displays a reduction. The low instability at the fine filament end of the range may be because of the enhanced texturing effect which may give rise to the interfilament friction that holds the entangled filaments and loops together under the applied loads. As the filaments get coarser the entanglement and loop formation deteriorate producing yarn with fewer loops and a poorly entangled core, resulting in a reduction in the yarn instability. This indicates that improved yarn stability can be obtained together with improved loop and entanglement formation, if the individual filament linear density is kept below a certain value. For the particular conditions considered, the most suitable supply yarns for air-jet texturing should comprise filaments finer than 2 dtex linear density but this could, of course, be different with other process and supply yarn parameters and with other texturing nozzles.

The better texturing obtained with finer filaments is also evidenced by the SEM photographs (Fig. 10.9), where 1.67 dtex per filament yarn displays better entangled core and surface loops, whereas 6.8 dtex per filament yarn has only mingled and disorientated filaments with virtually no loops present.

10.4.3 Number of filaments (total yarn linear density)

As the number of filaments increases, an enhancement in yarn quality is rightly expected because potential for filament entanglement is increased. However, the experiments with different types of nozzles have revealed that the above statement holds only for the number of filaments which a particular design of nozzle can texture effectively at given process conditions. When this optimum number of filaments is exceeded a detorioration in yarn quality is observed for two reasons: firstly that the air-flow is progressively more disturbed by the presence of increasing numbers of filaments, as is also observed in the case of high overfeeds; and secondly because the increased number of loops, arising from the presence of more filaments, increases the likelihood of the loops to be pulled out under applied tension.

Fig. 10.10 illustrates that, for the T100 HemaJet at reference conditions, the optimum number of filaments is less than 66, for the particular 1.67 dtex per filament yarn (110 dtex/66 filaments) used. However this optimum number is in the region of 198 filaments when the T341 HemaJet nozzle is used at the same texturing conditions thereby verifying that some nozzles are more suitable than others for particular yarn and process conditions. The measured yarn properties all show reduced values of instability, percentage linear density increase, and percentage tenacity decrease, as the total yarn linear density is increased from 110 dtex to 440 dtex. Also a deterioration in loop and entanglement formation is observed in the SEM photographs of the yarn with increased number of filaments although this yarn would probably be acceptable for many end-uses.

In conclusion, the number of filaments of the yarn to be textured should always be borne in mind, together with other process and supply yarn parameters, before a suitable nozzle is chosen from the range available.

10.5 Conclusions

The properties, and in particular the instability, of air-jet textured yarns have been shown to be greatly influenced by altering the processing parameters. The supply yarn properties also affect the final yarn properties. The optimization of any given textured yarn property almost always affects other yarn characteristics, and therefore this must be borne in mind in selecting process and supply yarn parameters for specific end-uses.

The experimental results have revealed that the main process parameter which has significant effect on the instability of the textured yarn is the overfeed. The linear density of a particular yarn can be increased by increasing the overfeed; by increasing the air pressure; by decreasing the process speed; by wetting the filament yarn; and by deploying an impact element. Different nozzles produce textured yarns with different properties from the same supply yarns. As the stabilising extension is increased beyond 4%, the loops and bows are destroyed and thence the instability of the yarn is reduced. For the particular processing conditions used, polyester yarns were shown to texture better than polyamide yarns.

The research reported has also suggested that a yarn suitable for air-jet texturing should have a filament linear density less than 2 dtex. The possibility of air-jet texturing of supply yarns with filament linear densities much higher than 2 dtex is indeed poor because, whilst they may exhibit slight increases in their yarn linear densities after texturing, this only arises from the reorientation of the filaments in the yarn core and the formation of large and unstable loops. Furthermore, it has been shown that, for a given texturing nozzle, there is an optimum number of filaments which can be textured most effectively. Therefore the nozzle type should be carefully chosen when a particular yarn is to be textured.

TABLE 10.1

The properties of supply yarns used

Material	Source	Yarn Lin. Density [dtex]	No. of filaments	Filament lin. den. [dtex]	Tenacity [g/dtex]	Elongation at T^* [%]
Polyester	ICI	110	66	1.67	3.64	0.52
Polyester	Du Pont	156	68	2.30	4.94	1.8
Polyamide	Du Pont	167	68	2.45	4.25	0.54
Polyester	ICI	175	66	2.65	3.96	0.59
Polyester	ICI	220	132	1.67	3.83	0.56
Polyester	ICI	234	60	3.90	4.40	1.34
Polyester	ICI	330	198	1.67	3.55	0.56
Polyester	ICI	440	264	1.67	3.58	0.55
Polyester	Du Pont	470	68	6.80	7.42	1.16

(*) Tension which corresponds to the value of tension used in measuring the instability of textured yarns.

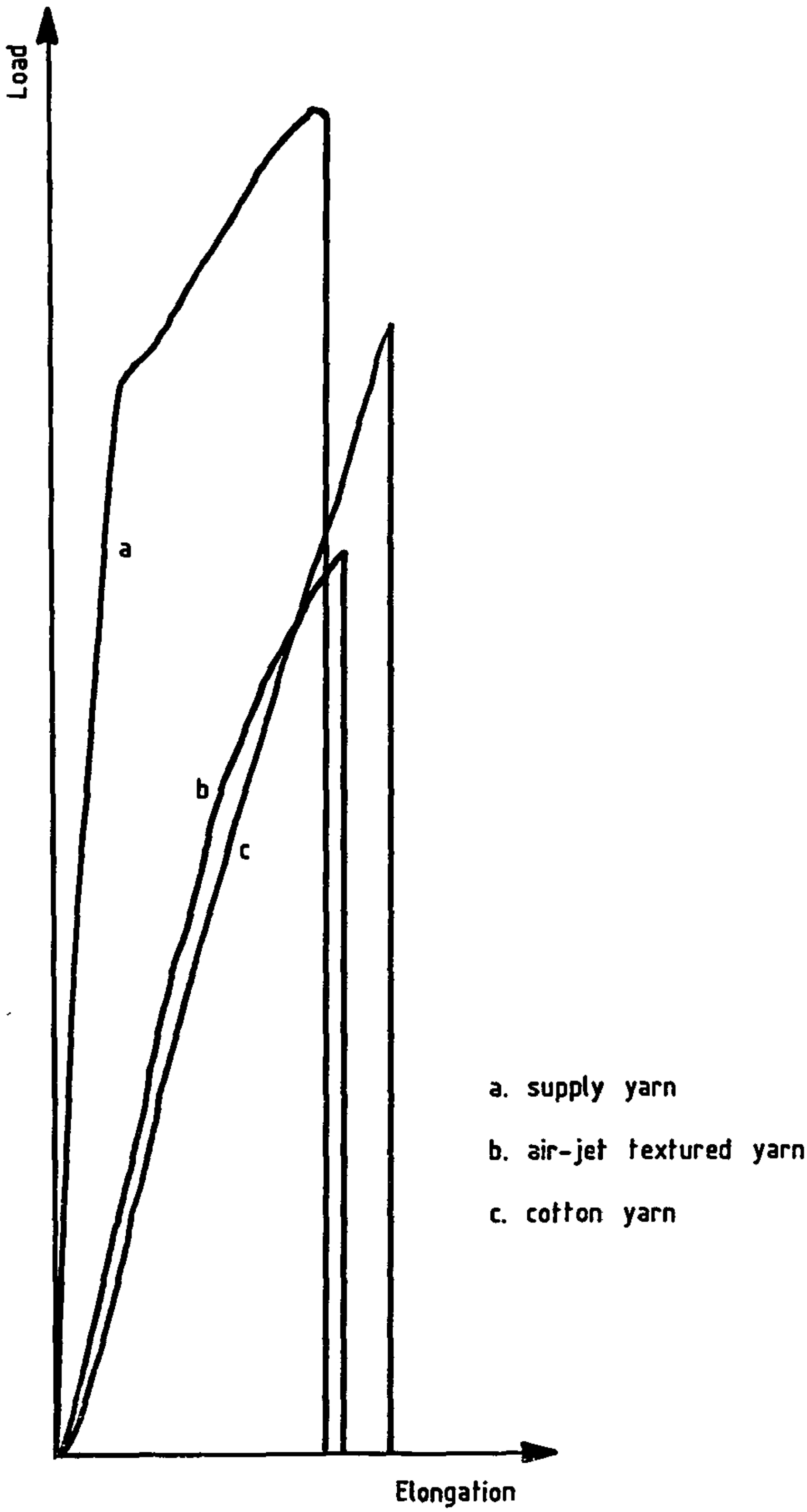

Figure 10.1 Comparison of stress-strain curves of: (a) untextured; (b) air-jet textured; and (c) cotton yarns

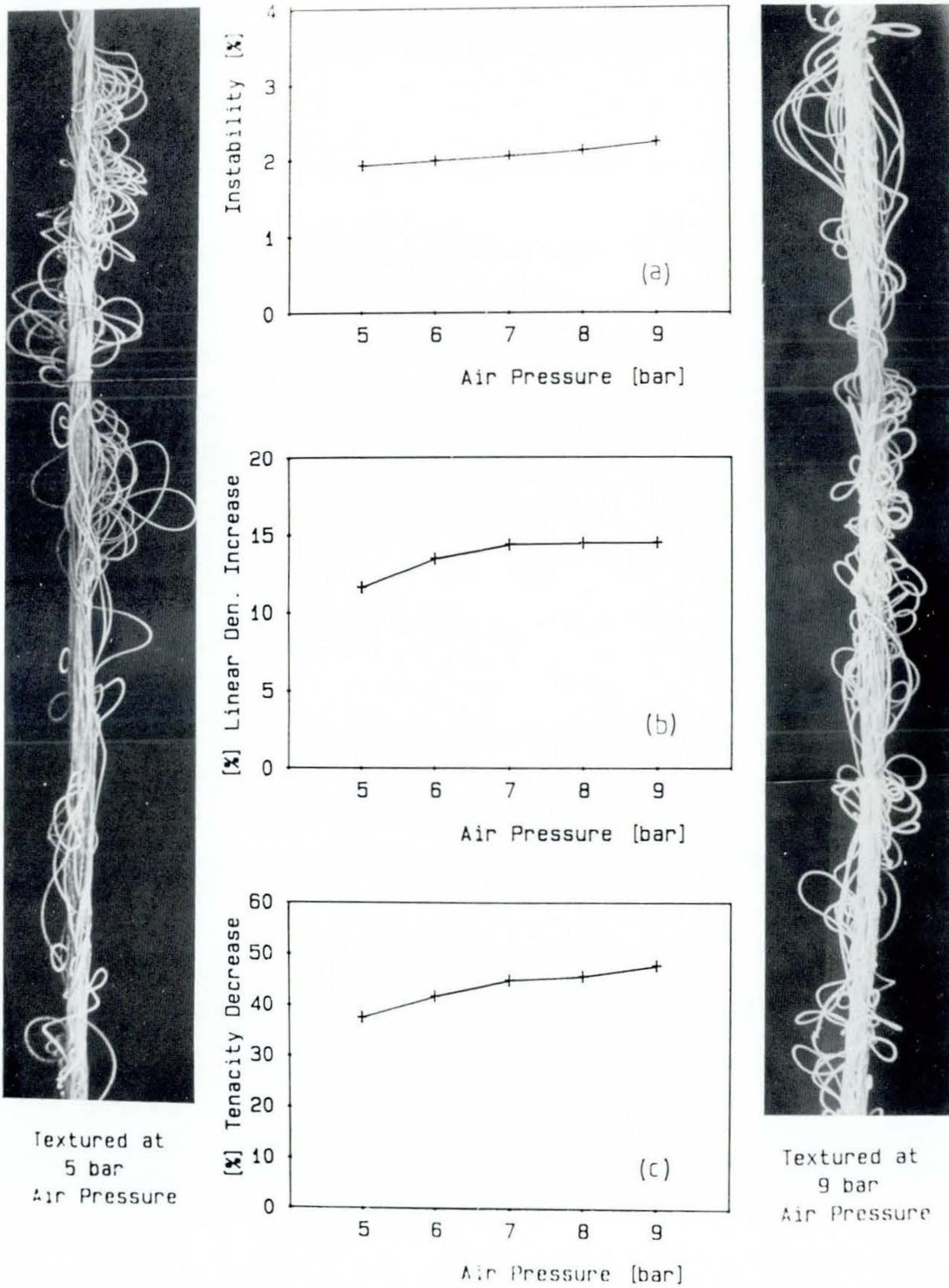

Figure 10.2 Effects of air pressure on the properties of air-jet

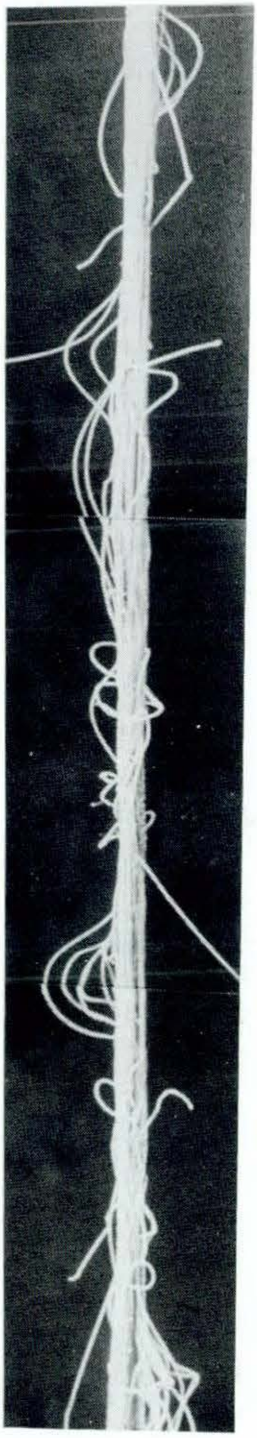

Textured at
10%
Overfeed

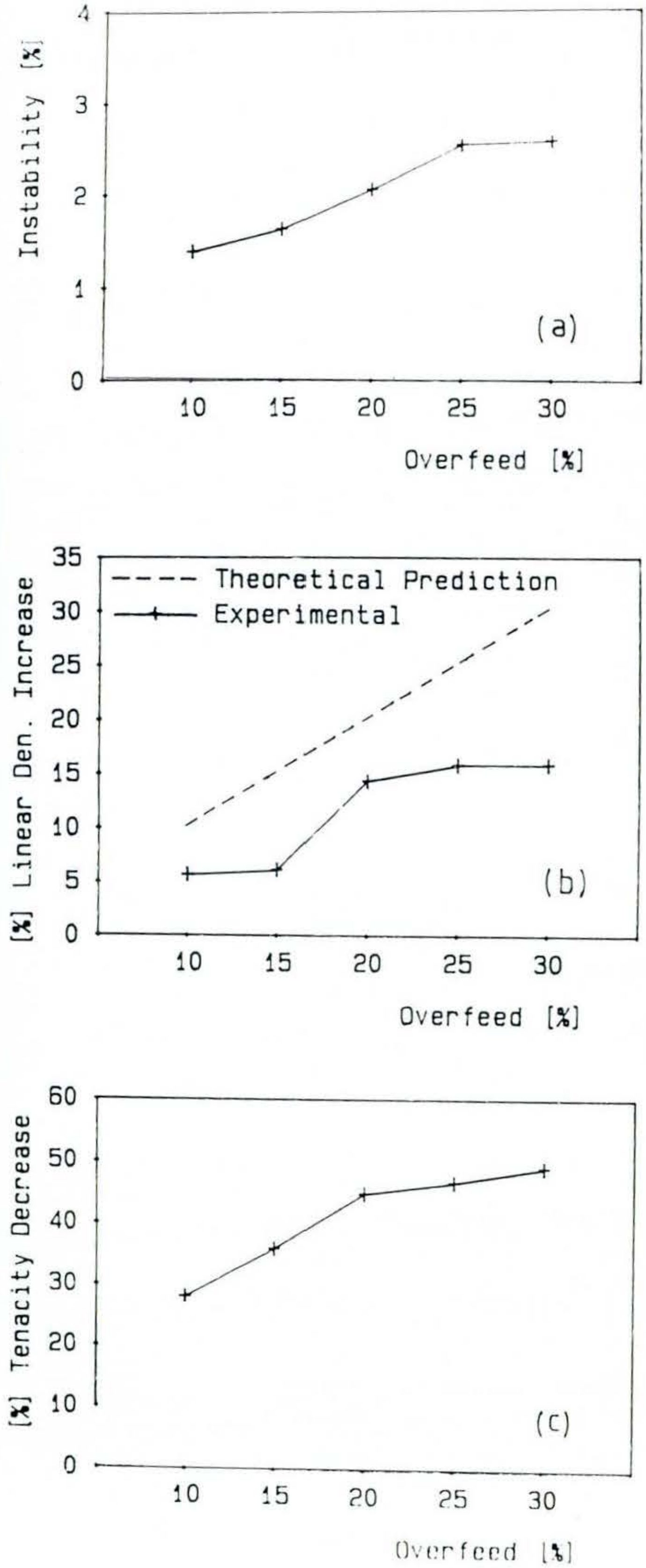

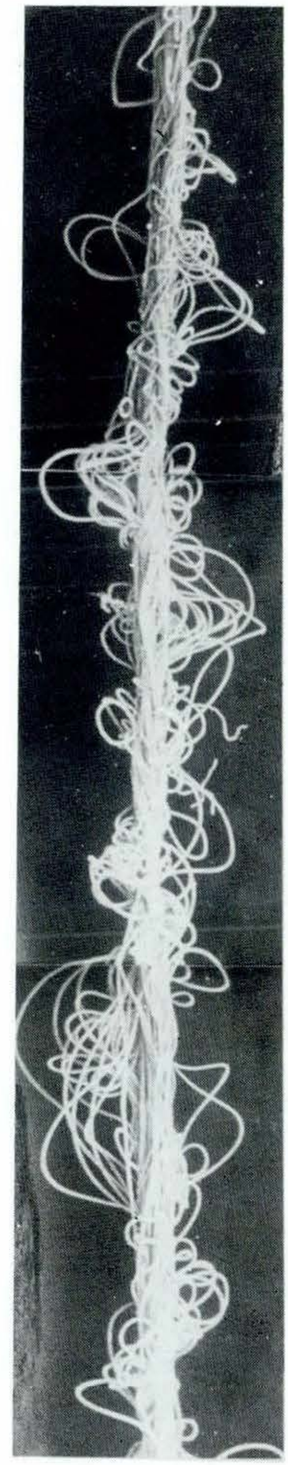

Textured at
30%
Overfeed

Figure 10.3 Effects of overfeed on the properties of air-jet textured yarns

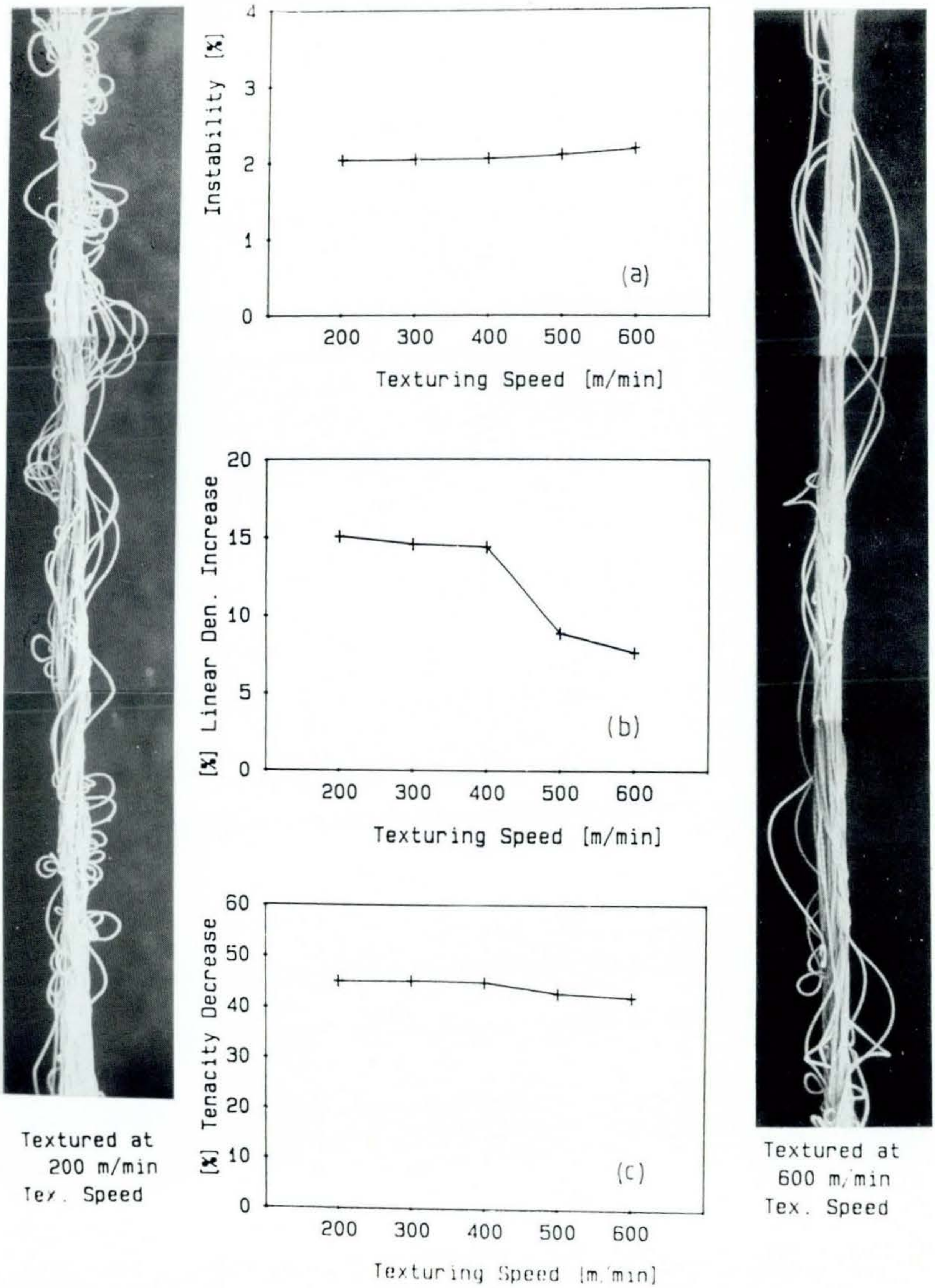

Figure 10.4 Effects of texturing speed on the properties of air-jet textured yarns

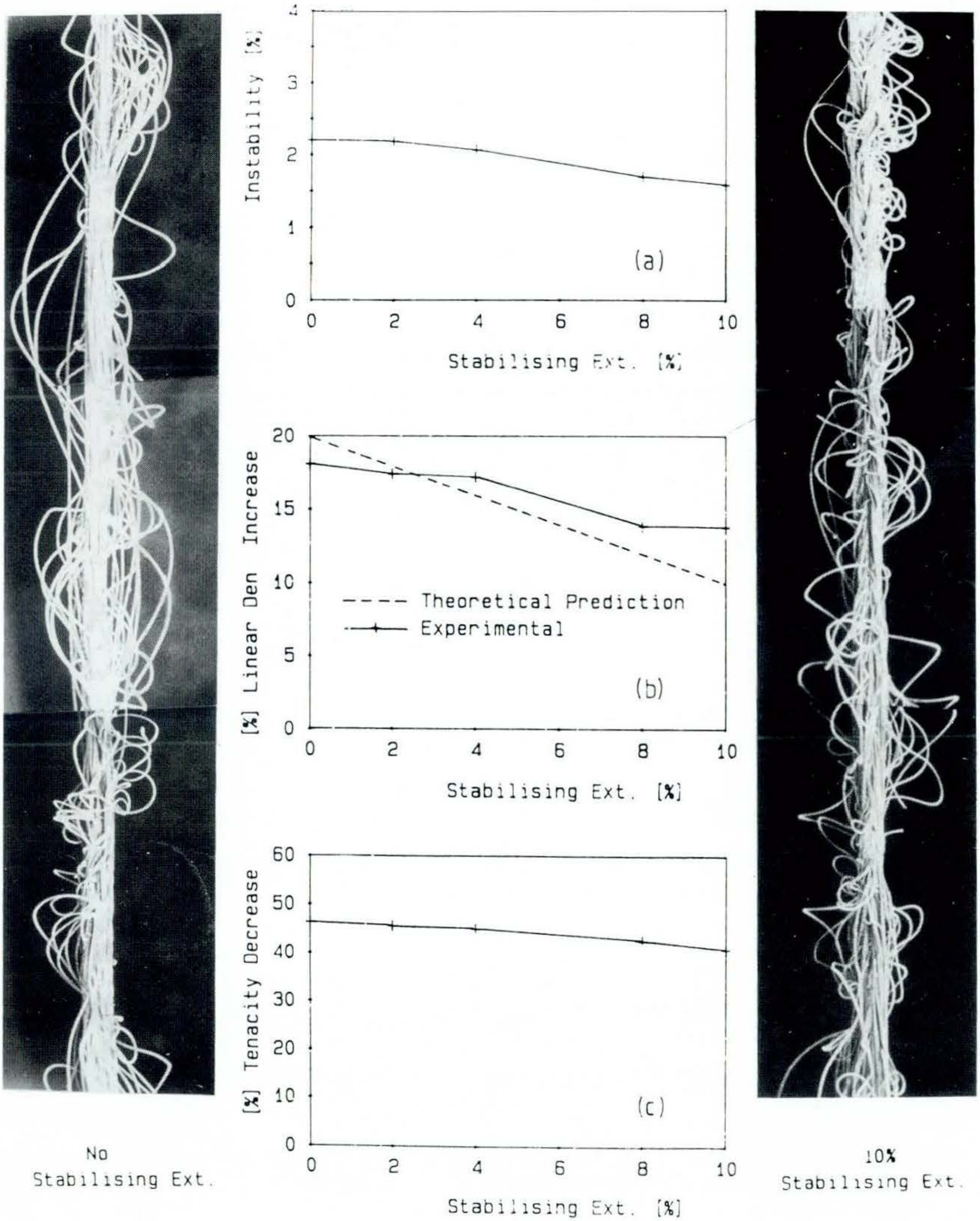

Figure 10.5 Effects of stabilising extension on the properties of air-jet textured yarns

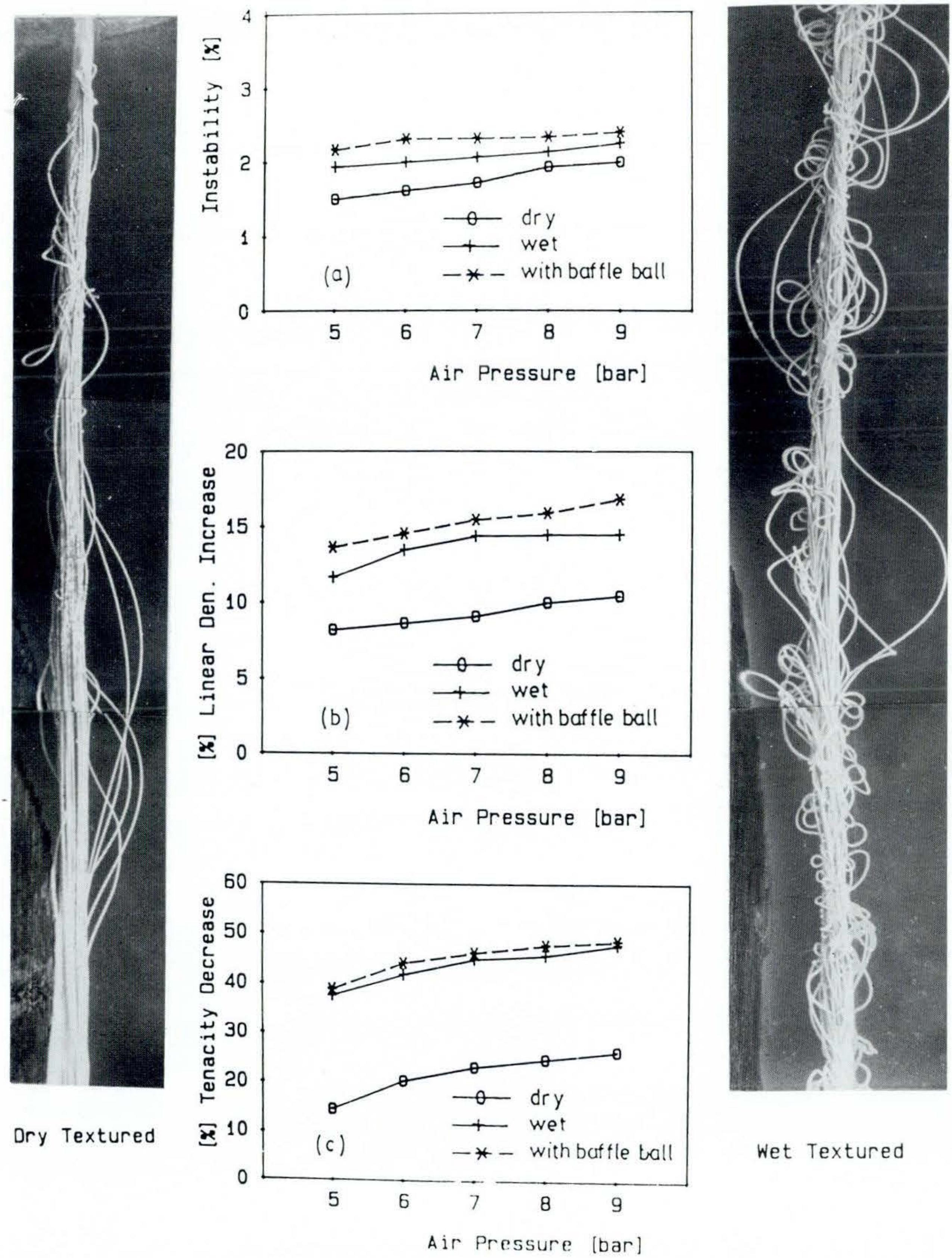

Figure 10.6 Effects of wet texturing and use of an impact element on the properties of air-jet textured yarns

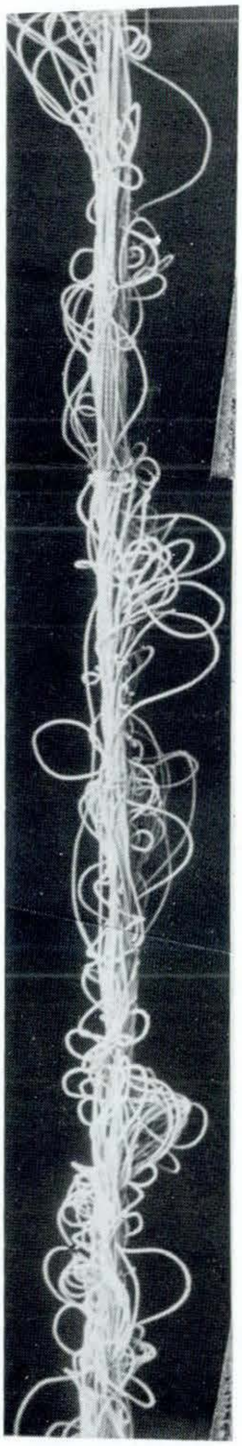

Textured with
T341
HemaJet

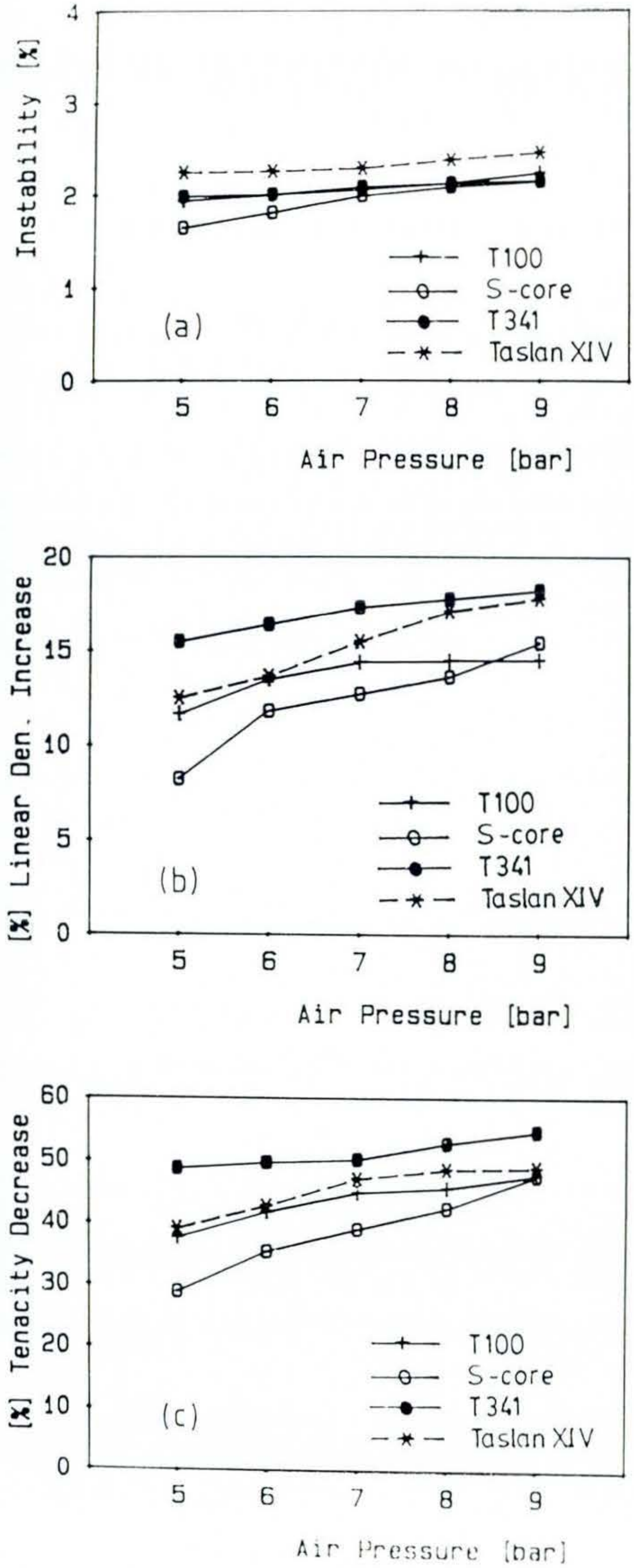

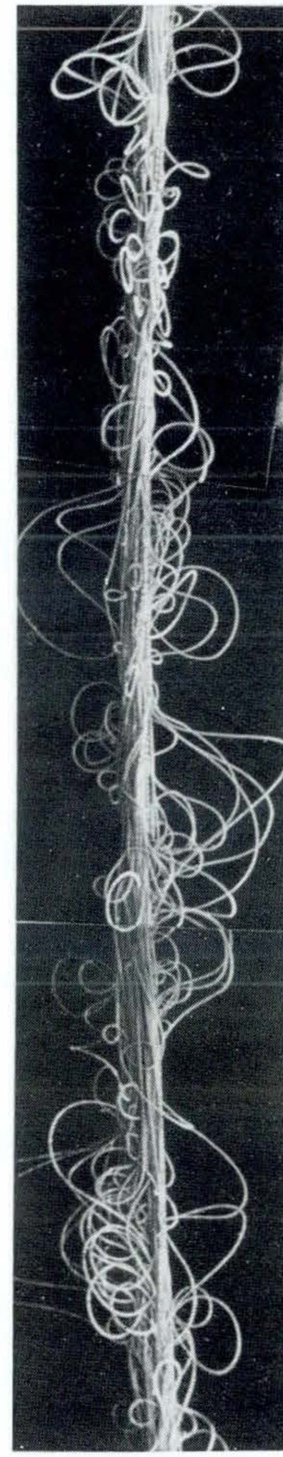

Textured with
Taslan XIV
Nozzle

Figure 10.7 Effects of nozzle type on the properties of air-jet textured yarns

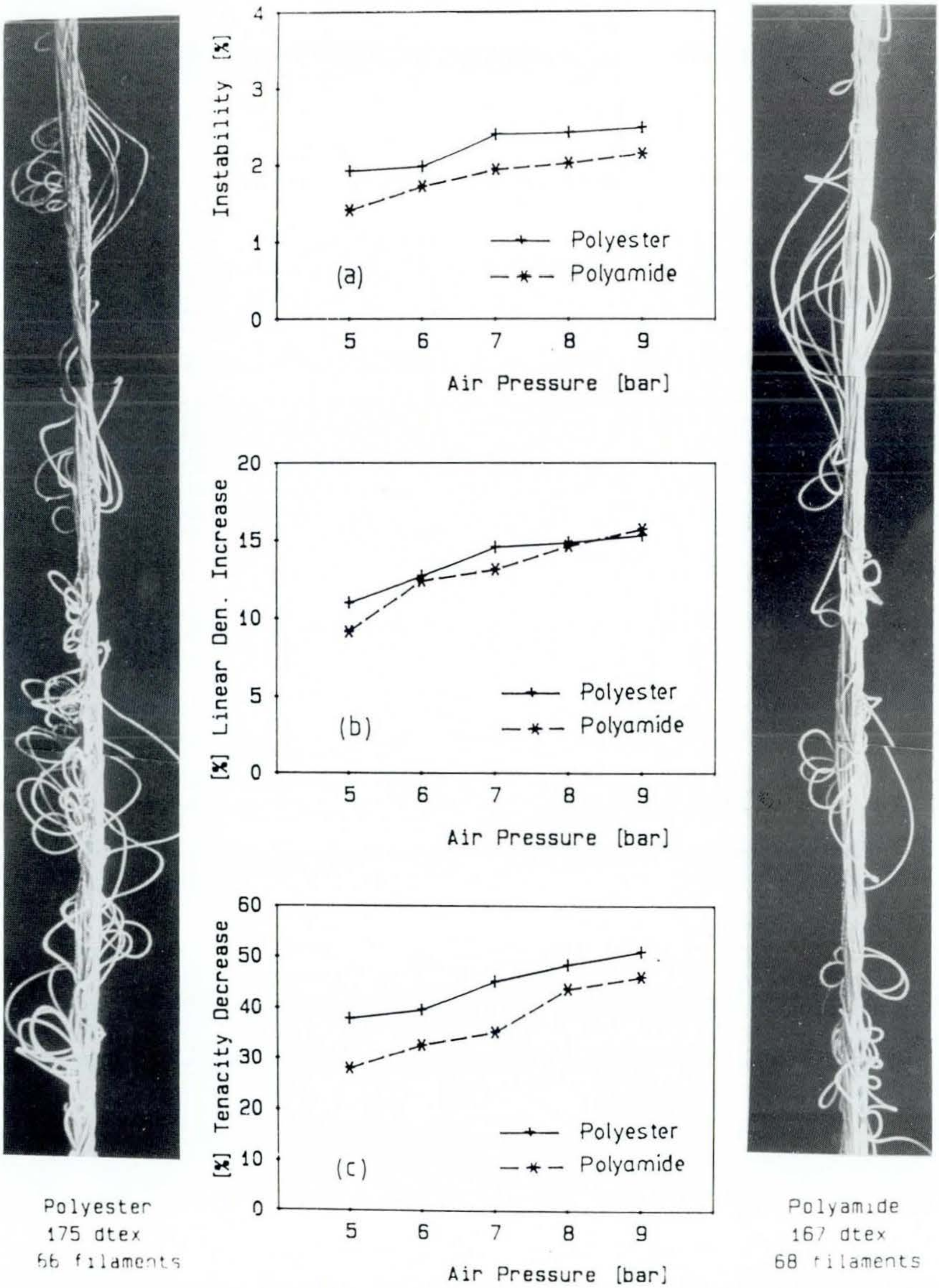

Figure 10.8 Effects of supply yarn material on the properties of air-jet textured yarns

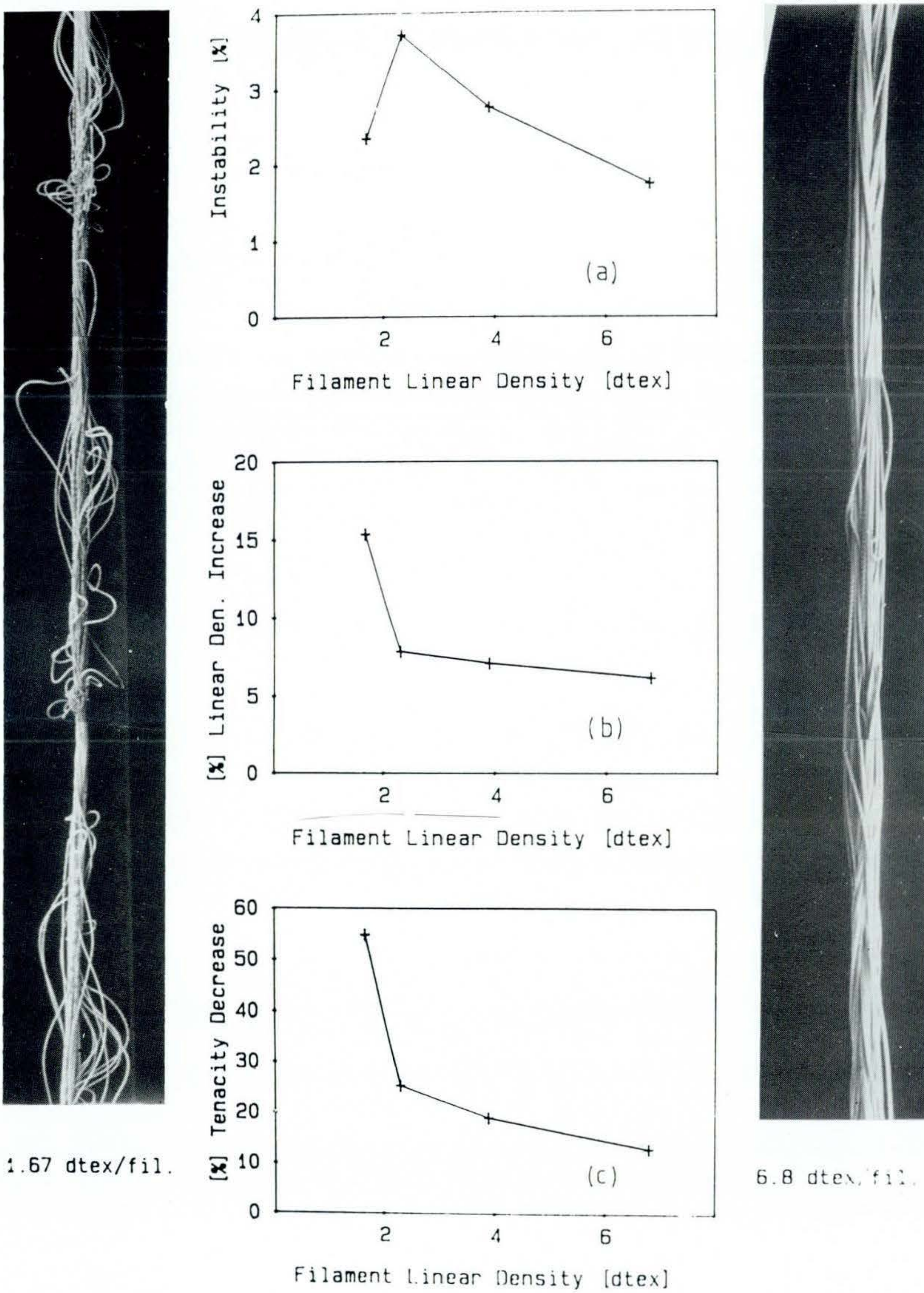

Figure 10.9 Effects of linear density per filament on the properties of air-jet textured yarns

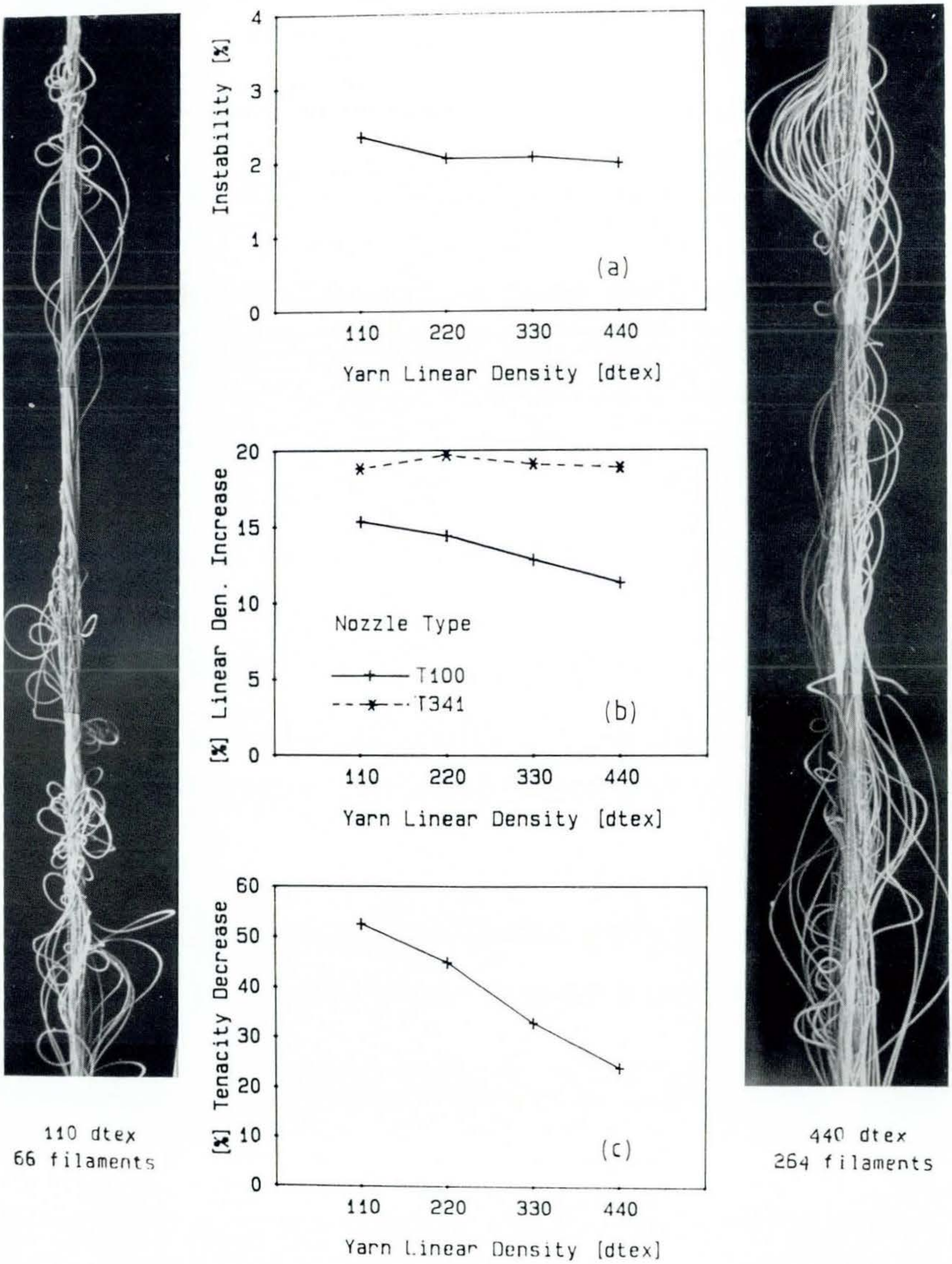

Figure 10.10 Effects of total supply yarn linear density on the properties of air-jet textured yarns

CHAPTER 11

GENERAL CONCLUSIONS AND SUGGESTIONS FOR FURTHER WORK

11.1 General Conclusions

The results of the research reported in this thesis has advanced knowledge in the following aspects of the air-jet texturing process:

(i) Aerodynamics of the texturing nozzles;

(ii) The effects of filament yarn wetting;

(iii) Instability of air-jet textured yarns; and

(iv) The effects of process and supply yarn parameters on the properties of air-jet textured yarns.

Investigations into the air flow within the current cylindrical industrial nozzles not only caused a thorough understanding of the air flow but also led to the design of more effective nozzles.

The investigation into the effects of wetting the supply yarn has shown that the prime effect of wetting is to reduce the interfilament friction and consequently to facilitate the longitudinal displacement of the filaments which is known to improve their entanglement possibilities.

The investigation into the air flow, texturing process, and effects of wetting, substantiated the loop and entanglement formation mechanism proposed by Acar et al[56,57]. Therefore, it can be said that the loop and entanglement formation is caused by the non-uniform fluid forces exerted on the scattered individual filaments which cause them to travel at different speeds creating relative longitudinal displacements. The right-angled delivery of the filament bundle with respect to the nozzle axis further enhances the fluid force difference due to the fact that no fluid forces exist outside the free air-jet. This in turn creates the loops and arcs in such a way that an instantaneously faster moving filament is blown out further than a slower moving filament. At the same time the whole bundle of the filaments moves and changes position within the jet, and the fluid forces acting on the filaments also change and in turn it is more likely that a once faster moving filament becomes a slower moving filament and consequently the trailing end of it is fixed into the core of the yarn thereby creating a loop or arc. Since this process occurs instantaneously, and repeats itself at random intervals for different filaments, the loops and arcs are thus randomly created.

The effectiveness of the filament entanglement is best assessed by instability measurements provided that other yarn properties, such as percentage linear density increase, tenacity, percentage breaking elongation, and the number and frequency of the loops, are also taken into consideration. However, the instability measurements should be carried out either on an Instron type tensile testing machine or on specially designed instability testers with a single yarn specimen. The elongation of the specimen under a load of 0.5 cN/dtex should be taken as the measure of instability. An 'on-line' instability measurement further facilitates quick assessment of the yarn quality and could eventually be developed to even give feed back either directly to the machine or at least to the machine operator.

The most influential process parameter determining the final yarn properties, especially that of instability, is found to be the overfeed; however other process parameters also investigated all play important roles; air pressure, texturing speed, stabilising extension, wet or dry processing, and the use of an impact element.

Supply yarn properties, such as the material, filament linear density and the number of filaments, the linear density of individual filaments are found to be the most crucial factor. The research concluded that a filament yarn suitable for air-jet texturing should compose of filaments of less than 2 dtex linear density.

11.2 Suggestions for Further Work

11.2.1 Nozzle development

The prototype nozzles designed and developed by the author, and reported in Section 6.5 showed potential for reducing the compressed air consumption up to 60% of that of the original commercial design. Therefore, the commercial utilisation of these nozzles could contribute to the air-jet texturing industry. Furthermore, the knowledge and experience gained from the nozzle investigations, which are reported in this thesis, could assist the designs of new nozzles for special purposes. For such nozzle developments, the collaboration of research institutions and industry would be desirable due to the presence of machining expertise and facilities in industry, and knowledge and understanding in research institutions.

With the collaboration of industrial companies, purpose-designed texturing nozzles could be developed for the texturing of industrial yarns from, for example, glass and carbon filaments, which cannot be textured by any other known method.

11.2.2 Process investigation

High speed still-shadowgraphs and still-photography techniques used in this work yielded useful information regarding air flow and filament interaction. However monitoring of the consecutive interactions by means of high speed cine-filming techniques could produce even further useful information. Such techniques, when used with precision made flat (two dimensional, transparent walled) nozzles, could shed more light on the filament behaviour within the nozzle.

Since the loop formation occurs at a very high speed, and causes yarn tension fluctuations in the delivery zone, a high-speed tension monitoring in the feed and delivery zones, and the possible correlation of these two, could produce invaluable information regarding the texturing formation and its rate.

11.2.3 On-line quality control and feed back systems

Section 9.4 showed the possibility of an on-line instability measurement. The results of such a measurement, together with a data base on desired and undesired yarn properties developed through experience, could be used to feed back to the texturing machine to obtain the optimum yarn quality. Such a system could be used on one of the many positions of a texturing machine to establish the desired machine settings and the result could then be applied to the other positions.

A yarn characterisation technique as reported Acar et al[67], with increased throughput speeds could further improve the setting-up procedure for a desired yarn. An investigation into the feasibility and economic aspects of such a system would be of value.

11.2.4 Miscellaneous other suggestions

The effects of supply yarn properties on the properties of air-jet textured yarns have been reported in Section 10.4. However this investigation was limited to the particular supply yarn material, filament linear density and the number of filaments. Other supply yarn properties, such as cross-sectional shape of the filaments and the spin-finish applied, should also be investigated.

The existing stabilising extension removes many of loops which are desirable for air-jet textured yarns. However, an 'on-line down twisting process' (instead of the stabilising extension process) could possibly bind many of those loops and also create small loops from larger ones. For this purpose, a high-speed twisting device needs to be developed, but the possible consequences of such an arrangement would also need to be investigated.

It is known that the air-jet texturing process can effectively blend continuous multifilament yarns. However, the blending of continuous filament yarns with staple fibres is still a virtually unknown prospect for air-jet texturing. Possible ways of staple fibre injection into the nozzle, where the filaments are opened and entangled, could be usefully investigated. Such a process might further improve the natural feel and appearance of air-jet textured yarns; down-twisting, as suggested above, and continuous heat-setting could help to maintain the staple fibres intact in the yarn core.

APPENDIX A

CALCULATION OF THE FLOW VELOCITY BY USING PITOT TUBE IN SUBSONIC AND SUPERSONIC FLOWS

Total pressure as measured by pitot tubes in subsonic and supersonic flows can be used to calculate flow velocities in the axial direction. The process by which the fluid is brought to rest at the nose of a pitot tube is assumed to be frictionless and adiabatic. For subsonic flows (Fig. A.1) then:

$$V^2/2=C_p(T_o-T)=C_pT_o[1-(P/P_o)^{(\gamma-1)/\gamma} \qquad \text{A.1}$$

where the suffix 'o' refers to total conditions.

If T_o and ratio (P/P_o) of static to total pressures are both known, then the velocity of the stream may be determined.

For supersonic flows, a shock wave forms ahead of the pitot tube (Fig. A.2). If the axis of the pitot tube is parallel to the oncoming flow, the shock wave may be assumed mormal to the stream line leading to the stagnation point, then the pressure rise across the shock is given by:

$$(P_o)_2/P_1=\{[(\gamma+1)^{\gamma+1}]/(2\ M_1{}^2-\gamma+1)\}(M_1{}^2)^{1/\gamma-1} \qquad \text{A.2}$$

This equation enables the upstream Mach number, M_1, to be calculated from the ratio of downstream total pressure $(P_o)_2$ to the upstream static pressure (P_1). Since the stagnation temperature does not change across the shock wave, then:

$$C_pT_o=C_pT_1+V_1{}^2/2=C_p(V_1{}^2/\gamma RM_1{}^2)+V_1{}^2/2 \qquad \text{A.3}$$

Thus V_1 may also be calculated if T_o is known. Therefore the downstream stagnation pressure, $(P_o)_2$, stagnation temperature, T_o, and upstream static pressure, P_1, are required to be measured.

In the application of this method to a free jet, when it is not practicable to measure the static pressure, it can be assumed that the static pressure is atmospheric.

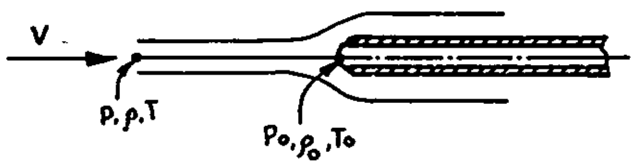

Figure A.1 Pitot tube in a subsonic flow

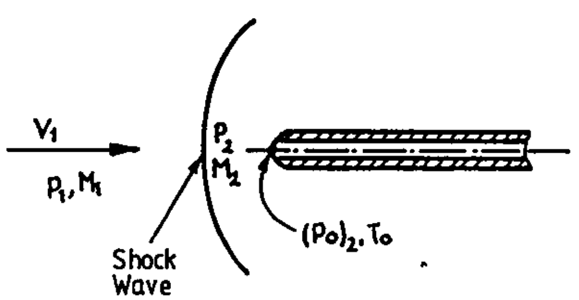

Figure A.2 Pitot tube in a supersonic flow

APPENDIX B

ISENTROPIC FLOW THROUGH CONVERGING NOZZLES

Fig. B.1 shows the converging section of the inlet hole of the texturing nozzles. Since the nozzle housing is sufficiently large the flow conditions in it are assumed to be the stagnation conditions P_o, ρ_o and T_o where $V_o=0$. Assuming that the flow takes place isentropically, the velocity of air crossing the plane of the throat A_t, defined as the 'isentropic throat speed' $V_t^{\prime}$ is given by

$$V_t^{\prime}=a_o\{[2/(\gamma-1)][1-(P_t^{\prime}/P_o)^{(\gamma-1)/\gamma}]\}^{1/2} \qquad \text{B.1}$$

where a_o is the stagnation speed of sound. The Mach number for the flow in the throat section A_t is

$$M_t=\{[2/(\gamma-1)][(P_o/P_t^{\prime})^{(\gamma-1)/\gamma}-1]\}^{1/2} \qquad \text{B.2}$$

It is obvious that when the pressure difference between the nozzle housing pressure and the ambient pressure is zero (i.e. $P_o=P_a$), no flow takes place through the nozzle. However, if the pressure in the nozzle housing is gradually increased, air will start flowing and until a certain pressure ratio $P_t^{\prime}/P_o=p^*/P_o$ is reached the flow will accelerate. When 'the critical pressure ratio' is attained, the isentropic throat speed $V_t^{\prime}$ is equal to a^*, the critical speed of sound, and the mass flow rate reaches the maximum for a given pressure (i.e. critical mass flow rate). If the pressure is further increased, P^* also increases, but the ratio p^*/P_o remains constant. The Mach number in the throat remains constant at the value of unity, and mass flow rate remains at the critical value $\dot{m}^*$ corresponding to the stagnation pressure P_o and stagnation temperature T_o.

Under the critical conditions where the speed of the flow is equal to the speed of sound, the critical pressure ratio is given by

$$P^*/P_o=(2/\gamma+1)^{\gamma/\gamma-1} \qquad \text{B.3}$$

By using this, the maximum throat speed i.e. critical speed of sound a^* and the corresponding critical mass rate of flow $\dot{m}^*$ could be expressed as follows:

$$(V_t')_{max}=a^*=[2\gamma RT/(\gamma+1)]^{1/2} \qquad \text{B.4}$$

and

$$\dot{m}^*=\psi^* P_o A_t/(\gamma RT)^{1/2}, \qquad \text{B.5}$$

where

$$\psi^*=\gamma[2/(\gamma+1)]^{(\gamma+1)/2(\gamma-1)} \qquad \text{B.6}$$

When any form of nozzle operates with the critical speed of sound a in its throat, the flow is said to be 'choked' and the corresponding mass flow rate is also called the 'choking mass flow rate'.

In an actual converging nozzle of circular cross-section, however, the assumption of one dimensional flow may not be valid especially when the converging angle is steep as in the case of the inlet hole. Furthermore, the formation of a 'vena contracta', which is created by the inward radial momentum of the air, causes the actual throat area to be smaller than the geometrical diameter. The combination of these two reduces the mass flow rate to a value smaller than that for a one dimensional flow. Therefore the theoretical predictions need to be corrected by a 'Discharge Coefficient' which is the ratio of the actual flow rate to the one-dimensional isentropic flow rate.

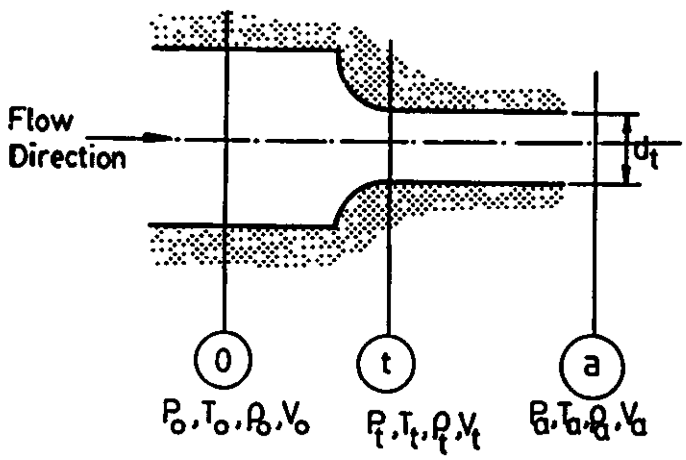

Figure B.1 Converging nozzle model

APPENDIX C

COMPRESSIBLE FLOW ACROSS AN ABRUPT ENLARGEMENT

Benedict et al[94] have studied the flow across an abrupt enlargement including incompressible and compressible flows. They also extended their work into two different compressible flow cases as subsonic and supercritical flow. Here in this appendix, however, only the compressible supercritical flow case will be given due to its relevance to the air-jet texturing nozzles.

Fig. C.1 illustrates the flow across an abrupt enlargement. The three basic conservative relations of the system are applied as follows:

Conservation of mass (presumes one-dimensional velocity distribution):

$$\dot{m}=\rho_1 A_1 V_1=\rho_2 A_2 V_2 \qquad \text{C.1}$$

Consrvation of Momentum (presumes frictionless flow from 1 to 2):

$$P_1 A_1+P_1'(A_2-A_1)-P_2 A_2=\dot{m}(V_1-V_2) \qquad \text{C.2}$$

Conservation of Energy (presumes adiabatic flow):

$$T_1/T_2=[2+(\gamma-1)M_2^2]/[2+(\gamma-1)M_1^2] \qquad \text{C.3}$$

When equations C.1, C.2 and C.3 are combined, in terms of the perfect gas equation of state (pv=RT), there results:

$$\{M_2[2+(\gamma-1)M_2^2]^{1/2}\}/(1+\gamma M_2^2) = \{m_1[2+(\gamma-1)M_1^2]^{1/2}\}/[1+ M_1^2+(P_1'/P_1)(1-\psi/\psi)] \qquad \text{C.4}$$

where $\psi=A_1/A_2$, the area ratio.

In the case of supercritical flow, i.e. when $M_1=1$, equation C.4 yields p_1'/p_1 for every value of M_2. This equation rearranges to:

$$(P_1'/P_1)_{supercritical}=(\gamma/1-\gamma)(1+\gamma)^{1/2} * \{\{(1+\gamma M_2^2)/M_2[2+(\gamma-1)M_2^2]^{1/2}\} -(1+\gamma)^{1/2}\} \qquad C.5$$

Also, by applying continuity, equation C.1, in its more general form becomes:

$$(P_{t1}/P_{t2})(A_1/A_2)\Gamma_1=\Gamma_2 \qquad C.6$$

where:

$$\Gamma=M/\{[2+(\gamma-1)M^2]/(\gamma+1)\}^{(\gamma+1)/2(\gamma-1)} \qquad C.7$$

Therefore, the pertinent total pressure across the abrupt enlargement is obtained as:

$$P_{t2}/P_{t1}=\psi\Gamma_1/\Gamma_2 \qquad C.8$$

Similarly, the static pressure ratio is given by:

$$P_1/P_2=\Gamma_2 R_1/\psi\Gamma_1 R_2 \qquad C.9$$

where:

$$R=(1+((\gamma-1)/2)M^2)^{-\gamma/\gamma-1} \qquad C.10$$

Equations C.5, C.8 and C.9 completely describe compressible flow across an abrupt enlargement. The equation C.9 is numerically solved for the pressure ratio ranging from 2 to 6 and for the area ratios 0.5, 0.6, 0.8 and 1.0. The results are given in Figs. C.2 and C.3 depicting the Mach number and the total pressure ratios respectively. The total pressure ratio is the indicative of the step loss across abrupt enlargement. Fig. C.3 illustrates that the flow losses increase as the area ratio decreases, i.e. more restriction to the flow.

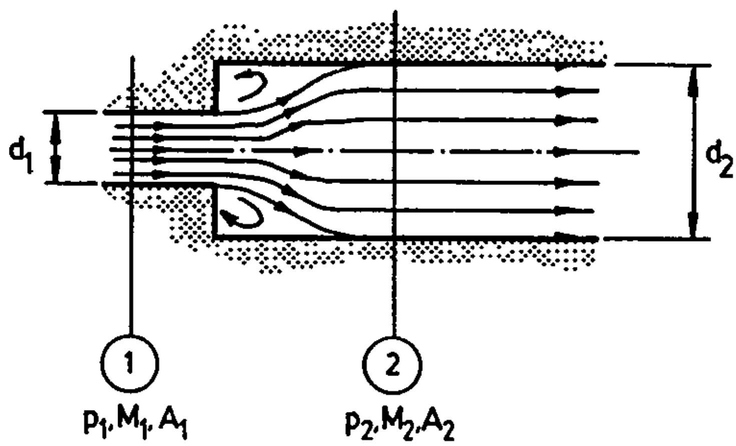

Figure C.1 Abrupt enlargement of a flow

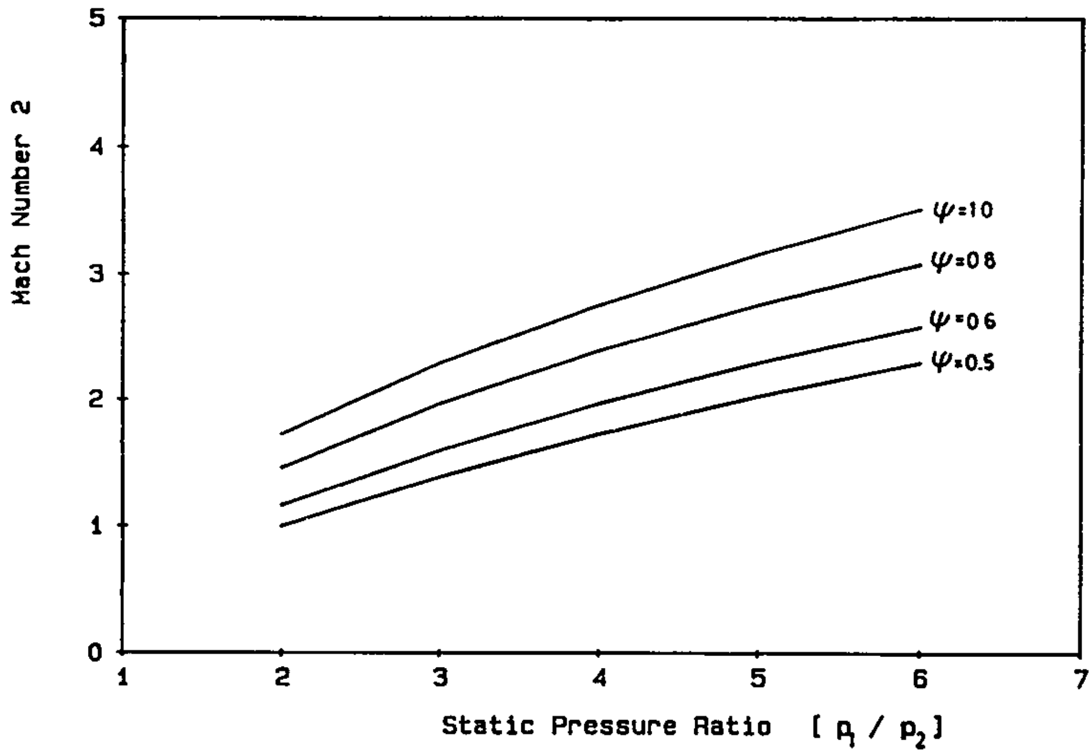

Figure C.2 Variation of the Mach Number 2 with the pressure ratio

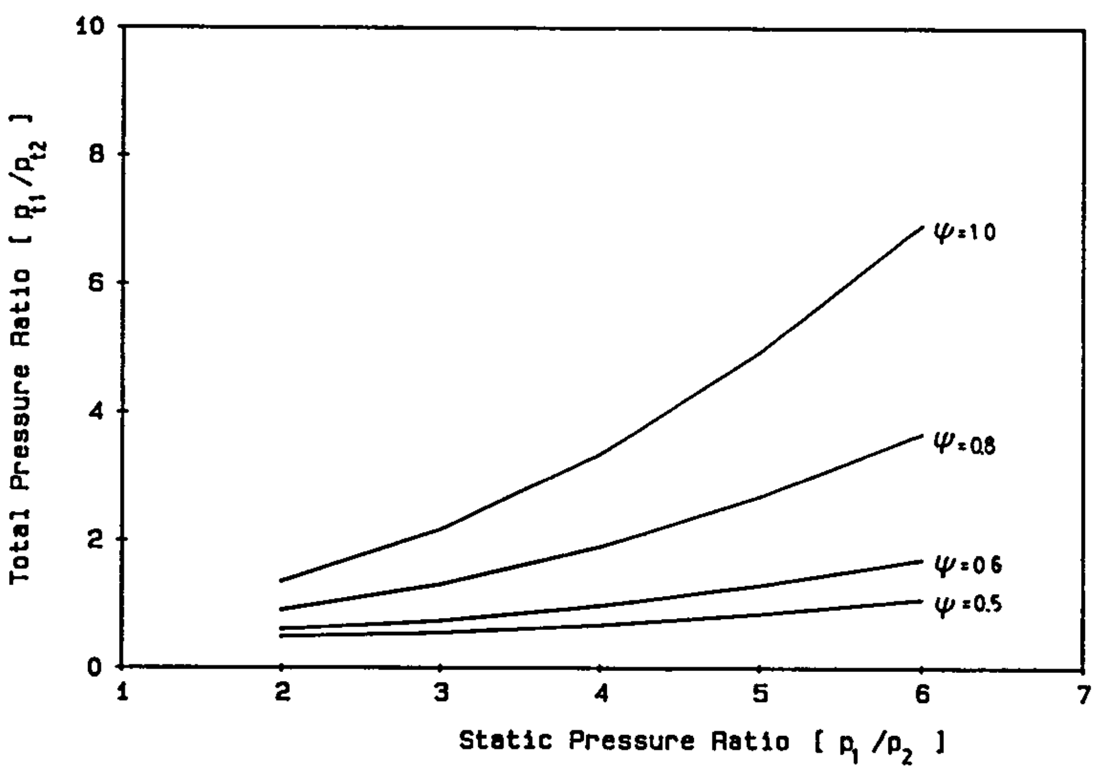

Figure C.3 Variation of the pressure loss with the pressure ratio

APPENDIX D

UNDEREXPANDED SUPERSONIC JETS

When the flow Mach number is equal to unity at the exit of a nozzle, Fig. D.1 illustrates the conditions that may occur. Since the flow in the nozzle is sonic, the exit boundary conditions are different from those of the subsonic flow, because the flow velocity exceeds the propagation speed of small pressure waves and the fluid arriving at the exit plane is unaware of the ambient pressure. Consequently, if p_e is smaller than p_{atm}, the sudden compression of the fluid flowing out of the nozzle results in a discontinuous pressure increase known as a shock wave. In the case of only a slight difference between p_e and p_{atm} as illustrated in Fig. D.1a the shock waves are attached to the rim of the nozzle in the vicinity of the exit plane. If p_{atm} is much larger than p_e , then the shock wave system moves upstream into the flow nozzle, and may eventually become a 'normal shock wave'. However, if p_e is greater than p_{atm}, the expansion from p_e to p_{atm} occurs outside the flow passage through a series of expansion waves (fans) or so called rarefaction waves as illustrated in Fig. D.1c. There may be another case in which the exit pressure p_e is equal to the ambient pressure p_{atm}, although the flow speed is still supersonic. In this case no standing wave occurs and a supersonic flow parallel to the nozzle axis,emerges from the nozzle as illustrated in Fig. D.1b.

To summarize, we can say that three cases of supersonic nozzle operation are possible. When the flow is so accelerated that the flow pressure becomes less than the ambient pressure, a case of inequilibrium is present and therefore the equilibrium is maintained through shock waves. This condition of the nozzle operation is called as 'overexpansion'. On the other hand, when the flow is not sufficiently expanded to equilize the flow pressure at the exit to the ambient pressure, the equilibrium is sought through a series of expansion waves. Since there is an excess pressure at the exit, this case is called as 'underexpansion'. Finally, if the flow possesses a pressure at the exit which is the same as the ambient pressure, then equilibrium is already attained, therefore no further expansion or compression takes place and no pressure waves are observed. This case is called 'ideal' or 'the design condition'.

Consider a slightly underexpanded supersonic nozzle as sketched in Fig. D.2. The pressure in region 1 is slightly higher than the external pressure p_{atm}. In region 2, the pressure however must be equal to p_{atm}, because no pressure discontinuities are possible across a free boundary. Thus, an expansion wave separates the regions 1 and 2. To be strictly accurate, an expansion, or Prandtl-Meyer fan occurs at points a and b. If the pressure difference across the fan is small, however, it may be approximated by a single expansion wave. All flow properties through an expansion wave change smoothly and continuously, with the exception of the wall streamline at the corners a and b which changes discontinuously at point A[95]. Across the expansion wave, the Mach number increases and the pressure, temperature, and density all decrease. When two expansion waves originating from a and b intersect on the centre line, they are sligtly bent outwards and continue their way until the free boundary where they are reflected as shock waves.

Flow in region 1 is axial, whereas in region 2 it also possesses a radial component. In region 3, however, the flow must be parallel to the axis due to the symmetry of the flow. This change in the direction of the flow occurs through the bent expansion waves, and the flow loses its pressure. Hence the pressure in region 3 becomes less than the ambient and causes another inequilibrium. It is a fact that the natural balance must be maintained. This takes place through the reflected shock waves and the flow is somehow compressed to the atmospheric pressure in region 4. Across the shock wave, the Mach number decreases, and the pressure, temperature, and density all increase. The shock waves intersect on the centre line and are bent inwards so that the flow in region 5 could be parallel to the flow axis and the flow is further compressed, the pressure in region 5 is thus higher than the atmospheric pressure. When the shock waves reach to the free pressure boundary, they are reflected as expansion waves. The process of expansion following a compression continues semi-periodically until the excess pressure of the jet is dissipated by the action of viscous losses at the jet boundary.

In the case of an overexpanded jet where the exit pressure is less than the ambient pressure (Fig. D.1a), the phenomenon described above takes place in an alternative form, i.e. first compression, then expansion, etc.

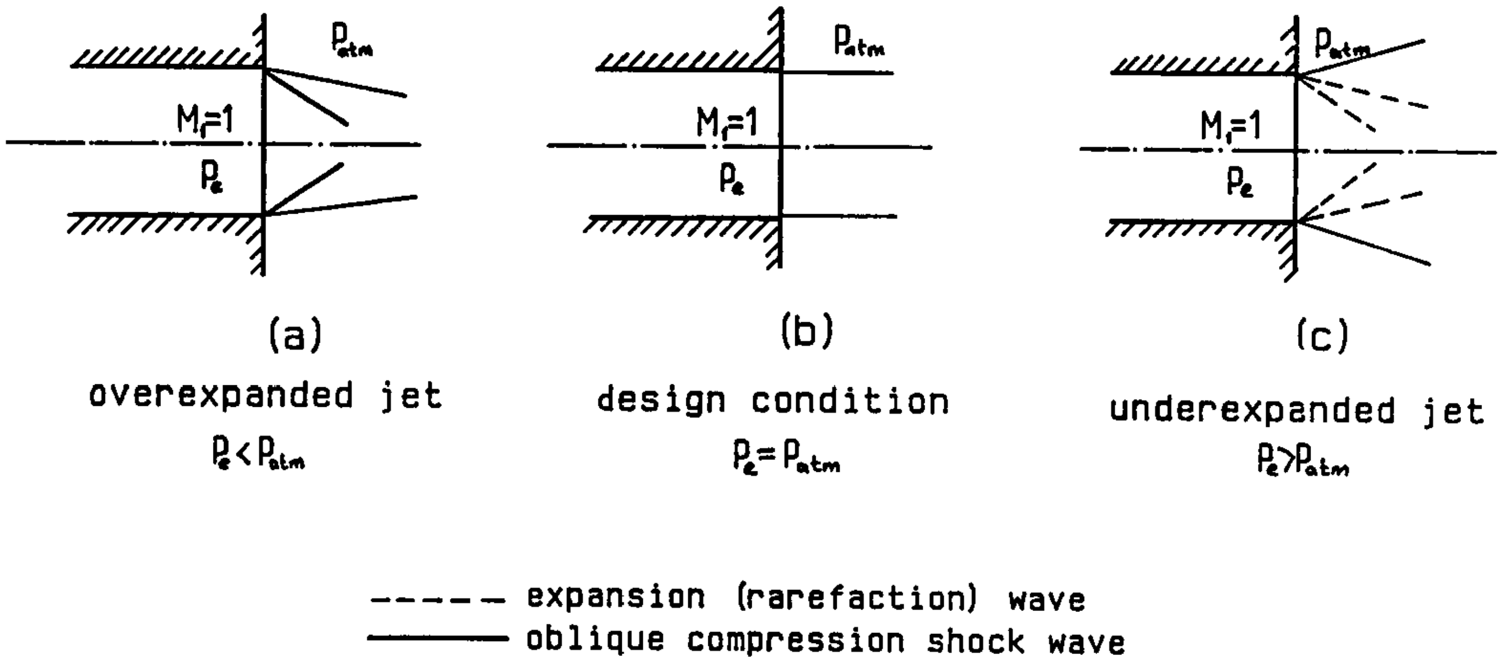

Figure D.1 Three types of supersonic nozzle operation: (a) overexpansion; (b) design condition; and (c) underexpansion

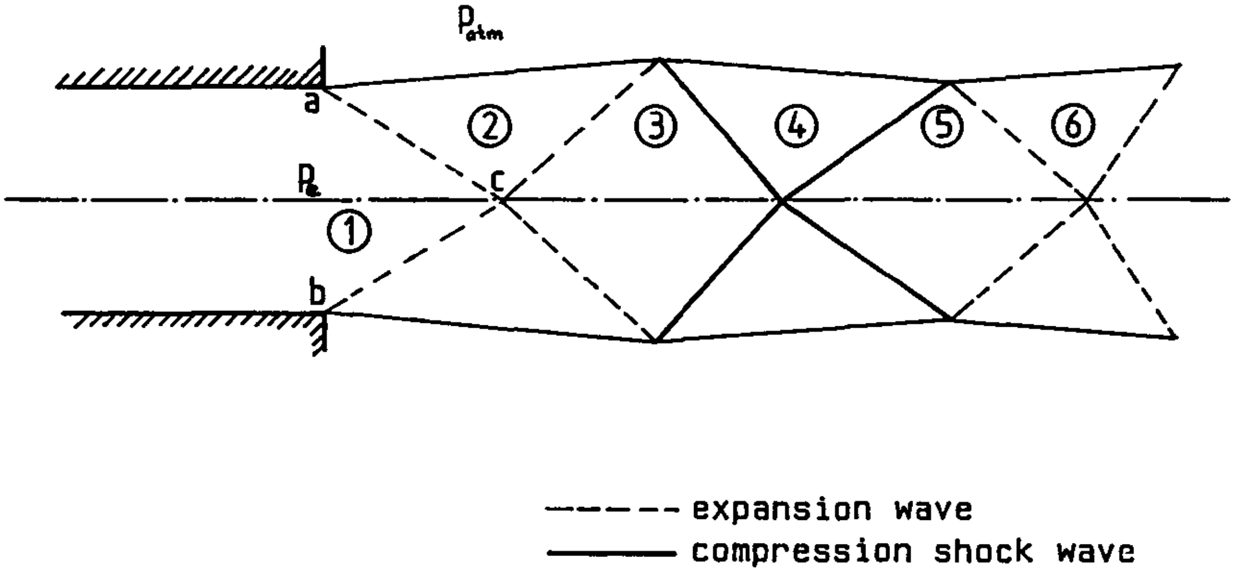

Figure D.2 Reconstruction of a jet from an sonic underexpanded nozzle

APPENDIX E

MATHEMATICAL MODEL FOR THE AIR FLOW IN CYLINDRICAL NOZZLES

For the purpose of theoretical analysis, Acar et al[51] have defined the whole flow system by dividing the nozzle into three parts (or control volumes), as illustrated in Fig. E.1. To simplify the mathematical treatment of the flow undisturbed by the filaments, it was assumed that the flow was isentropic and one-dimensional in each control volume, the velocity profiles across both primary and secondary flow exit planes were uniform, and the exit pressures of both primary and secondary flows were atmospheric.

Control volume 1 applies to the air inlet bores, which usually have the form of converging nozzles. Since the conventional operating pressures are much higher than the critical pressures, it is possible to apply the clasical steady one-dimensional gas dynamic equations to calculate the critical flow conditions at the throat of these converging inlet bores as follows;

$$P_t' = P^* = [2/(\gamma+1)]^{/(\gamma-1)} P_o \qquad \text{E.1}$$

$$T_t' = T^* = [2/(\gamma+1)] T_o \qquad \text{E.2}$$

and:

$$\rho_t' = \rho^* = [2/(\gamma+1)]^{\gamma/(\gamma-1)} \rho_o \qquad \text{E.3}$$

In control volume 2, the flows from the inlet bores mix together, and outgoing flows occur in the primary and secondary directions as shown in Fig. E.1. The flow properties in the core of a free jet is known to be unchanged up to approximately 6 diameters away from the throat, for example as shown by Gaunter et al[97]. Therefore the critical conditions achieved at the throat of the converging nozzles (control volume 1) can be considered to be unchanged at the inlet boundary of the control volume 2, which is adjacent to the outlet boundary of the control volume 1. Hence the input data to the control volume 2 is that corresponding to the critical conditions (i.e. M=1), achieved at the throat (exit) of control volume 1.

One of the constructional constraints of the cylindrical nozzles is that the throat area of the inlet bores is smaller than the cross-sectional area of the duct. This implies that, for an incompressible flow, the cross-sectional areas of the primary and secondary flows, after collision and mixing in control volume 2, are also smaller than the main duct cross-sectional area. Since the flow in question is compressible, both primary and secondary flows will immediately expand to the wider boundary of the main duct of the texturing nozzle. Since this expansion is taken into account when considering flow in control volume 3, it is assumed that no expansion takes place within control volume 2 and that the properties of the outgoing flows are the same as those of the incoming flows. This assumption facilitates to apply the theory for the incompressible collision and mixing of the jets, as described by Gurevich[98] for two mixing jets can be applied to control volume 2 to calculate the mass flow division into primary and secondary flows. The areas of both primary and secondary flows, and hence the mass flow rates, can thus be calculated by extending the theory of collision of two jets to any number of jets colliding at the same point on the axis of the texturing nozzle.

The concept of continuity states that the total mass flow of the incoming jets is equal to the sum of the primary and secondary mass flows. Thus, if n incoming jets are used:

$$\sum_{i=1}^{n} (\rho AV)_i = (\rho AV)_p + (\rho AV)_s \qquad \text{E.4}$$

Since the density and velocity of the incoming and outgoing flows were assumed to be the same, equation E.4 becomes:

$$\sum_{i=1}^{n} A_i = A_p + A_s \qquad \text{E.5}$$

Similary applying the concept of momentum change in the x direction:

$$\sum_{i=1}^{n}(\rho AV^2 \cos\alpha)_i-(\rho AV^2)_p-(\rho AV^2)_s=0 \qquad \text{E.6}$$

Equation E.6 can be similarly simplified to:

$$\sum_{i=1}^{n}A_i \cos\alpha_i-A_p-A_s=0 \qquad \text{E.7}$$

In this equation α_i is the angle made by the i_{th} inlet jet with the x axis. When all jets are at the same angle α, then:

$$A_p=1/2 \sum_{i=1}^{n} A_i(1+\cos\alpha) \qquad \text{E.8}$$

and:

$$A_s=1/2 \sum_{i=1}^{n} A_i(1-\cos\alpha) \qquad \text{E.9}$$

Thus the primary and secondary flow rates, applying the concept of continuity, are:

$$\dot{m}_p=(\rho AV)_p \qquad \text{E.10}$$

and:

$$m_s=(\rho AV)_s \qquad \text{E.11}$$

where:

$$\rho_s=\rho_p=\rho_t$$

and:

$$V_p=V_s=(V_t')_{max}$$

The expansion of the outgoing flows from the control volume 2 to the nozzle boundary in control volume 3 (Fig. E.1), can be treated as a sudden enlargement, as is, for example, discussed by Benedict et al[96]. This occurs when A_p and A_s are being expanded to A_n in control volume 3, where A_n is the cross-sectional area of the main duct. For such abrupt enlargements the static pressure ratio is given by:

$$P_1/P_2=(M_2/\psi M_1)[(2+(\gamma-1)M_2^2)/(2+(\gamma-1)M_1^2)]^{1/2} \qquad \text{E.12}$$

where: $\psi=A_1/A_2$ and the suffixes 1 and 2 apply to the situations before and after expansion through an abrupt enlargement, as studied in Appendix C.

It was assumed that the static pressure at the exit of both the primary and secondary flows were atmospheric and therefore M_2 can be calculated by using equation E.12. Once M_2 is calculated the other properties of the flow can also be calculated by using the theory of a steady one-dimensional flow of a perfect gas. Thus:

$$V_2=M_2a_2=M_2(\gamma RT_2)^{1/2} \qquad \text{E.13}$$

$$T_2=[(2+(\gamma-1)M_1^2)/(2+(\gamma-1)M_2^2)]T_1 \qquad \text{E.14}$$

and:

$$\rho_2=(P_2/P_1)(T_1/T_2)\rho_1 \qquad \text{E.15}$$

Equations (E.12-E.15) are applicable to both primary and secondary flows.

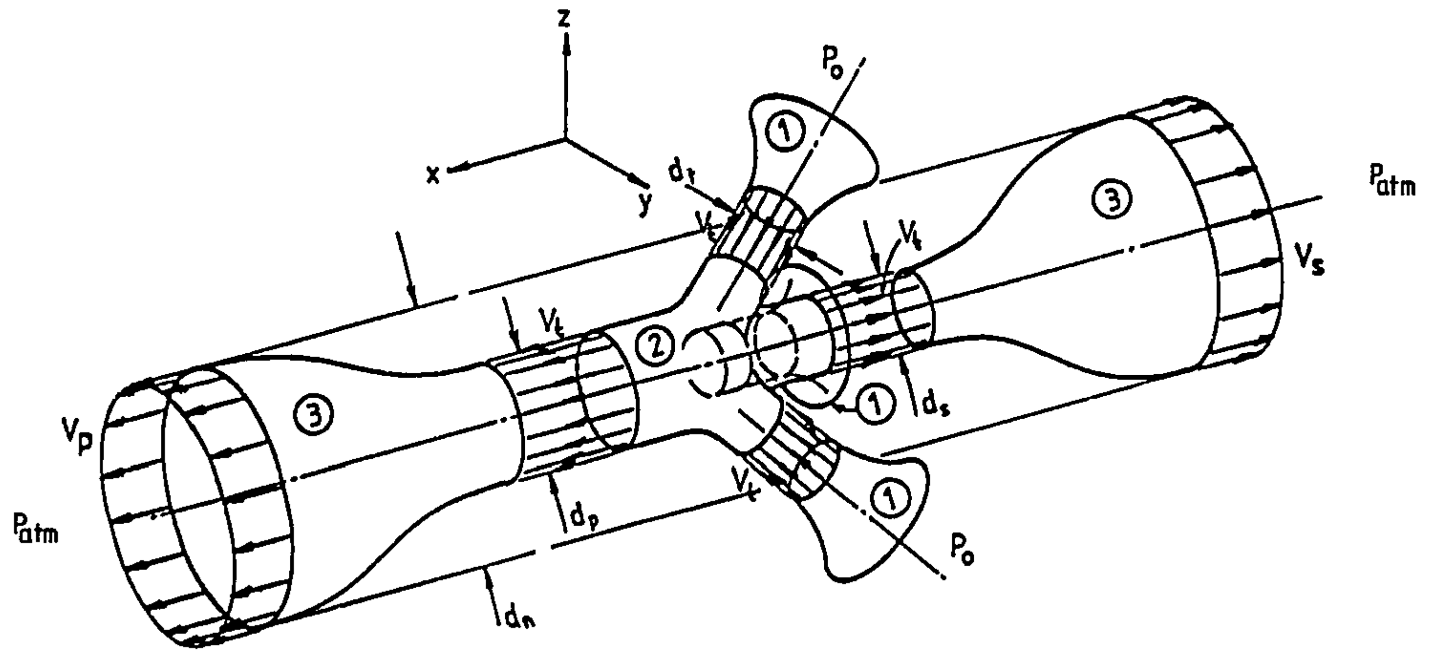

Figure E.1 Control volumes for the air flow through the Standard-core HemaJet (After Acar et al[51])

APPENDIX F

COMPUTER SOFTWARE FOR MANUAL CONTROL INSTABILITY TESTER

```
 10 CLS
 20 PRINT "******************************"
 30 PRINT "*                            *"
 40 PRINT "*   INSTABILITY TESTER FOR   *"
 50 PRINT "*         AJT YARNS          *"
 60 PRINT "*                            *"
 70 PRINT "*         Developed by       *"
 80 PRINT "*          Ali Demir         *"
 90 PRINT "*                            *"
100 PRINT "******************************"
110 DIM INS(20)
120 INPUT"Enter Supply Yarn Linear Density";LD%
130 INPUT"Enter the number of tests";N%
140 CRV%=(LD%*0.5)*900/150+100
150 OX=700 :LX=550 :OY=100 :LY=900 :XI=0 :XM=5 :YI=0 :YM=150
160 PROCDrax (1,10)
170 OSCLI"*FX16,2" :OSCLI"*FX190,8"   :OSCLI"FX17,1"
180 K=12
190 FOR J% = 1 TO N%
200 SOUND 1,-10,J%*10,6
210 @%=&10
220 PRINT TAB(1,K) "Test (";J%;") Fix yarn & hit SPACE BAR"
230 IF (INKEY$(100) <> " ") THEN 230
240 SOUND 1,-8,10,4
250 REM Pre-tensioning"
260 P%=0
270 PRINT TAB(1,K+1)"Pre-tensioning"
280 Y%=(ADVAL(1)/93)*1.75+100
290 IF Y% < 110 THEN PROCStep (5,"B")  ELSE GOTO 320
300 P%=P%+1
310 GOTO 280
320 I%=1 :X% = 700
330 PRINT TAB(1,K+1)"Testing          "
340 Y%=(ADVAL(1)/93)*1.75+100
350 IF Y% < CRV% THEN PROCStep (5,"B")  ELSE GOTO 410
360 DRAW X%,Y%
370 SOUND 1,-3,200-I%,3
380 X%=X%+2
390 I%=I%+1
400 GOTO 340
410 ST%=(I%+P%)*5 :INS(J%)=((I%*5)/96)/3
420 @%=&2020A :PRINT TAB(1,K+1) "Instability =";INS(J%)
430 K=K+3
440 PRINT TAB(1,K)"Reversing" :PROCStep (ST%,"F")  :MOVE 700,100 :NEXT J%
450 TINS=0.0
460 FOR J%=1 TO N% :TINS=TINS+INS(J%) :NEXT J%
470 AVE=TINS/N% :SOUND 1,-11,30,20
480 PRINT TAB(46,4) "Average Instability (%) =";AVE
490 PRINT TAB(1,K)"Complete     "
500 END
510 :
520 REM Subroutines
530 DEF PROCDrax (XS,YS)
540 @%=&10
550 MOVE FNX(0),FNY(0)
560 FOR YA=0 TO YM STEP YS :DRAW FNX(0),FNY(YA) :PROCYTICK (X,Y)
570 PLOT 0,-80,15 :VDU5 :PRINT;YA :VDU4 :MOVE FNX(0),FNY(0) :NEXT YA
580 FOR XA=0 TO XM STEP XS :DRAW FNX(XA),FNY(YM) :PROCXTICK (X,Y) :NEXT XA
590 XP=(LX+OX) :MOVE OX,CRV% :DRAW XP,CRV%
600 MOVE FNX(0),FNY(0)
610 FOR XA=0 TO XM STEP XS :DRAW FNX(XA),FNY(0) :PROCXTICK (X,Y)
620 PLOT 0,-23,-30 :VDU5 :PRINT;XA :VDU4 :MOVE FNX(0),FNY(0) :NEXT XA
```

```
630 FOR YA=0 TO YM STEP YS :DRAW FNX(XM),FNY(YA) :PROCYTICK (X,Y) :NEXT YA
640 MOVE FNX(0),FNY(0)
650 ENDPROC
660 DEF FNX(XX) :X=(XX-XI)/(XM-XI)*LX+OX :=X
670 DEF FNX2(XX) :X=(XX-XI)/(XM-XI)*LX*.96+OX :=X
680 DEF FNY(YY) :Y=(YY-YI)/(YM-YI)*LY+OY :=Y
690 DEF PROCYTICK (X,Y) :N=10 :DRAW X+N,Y :DRAW X-N,Y :MOVE X,Y :ENDPROC
700 DEF PROCXTICK (X,Y) :N=10 :DRAW X,Y+N :DRAW X,Y-N :MOVE X,Y :ENDPROC
710 DEF PROCStep (S%,D$)
720 OSCLI"*FX151,98,127"
730 IF D$="F" THEN A$="*FX151,96,0":B$="*FX151,96,4" :GOTO 760
740 IF D$="B" THEN A$="*FX151,96,8":B$="*FX151,96,4"
750 FOR K%=1 TO S% :OSCLI A$ :FOR L=1 TO 35:NEXT L:OSCLI B$ :NEXT K%:GOTO
760 FOR K%=1 TO S% :OSCLI A$ :FOR L=1 TO 35 :NEXT L :OSCLI B$ :NEXT K%
770 ENDPROC
```

APPENDIX G

COMPUTER SOFTWARE FOR 'ON-LINE' INSTABILITY MEASURING SYSTEM

```
 10 REM ******************************************************
 20 REM *                                                    *
 30 REM *          ON-LINE INSTABILITY MEASUREMENT OF        *
 40 REM *               AIR-JET TEXTURED YARNS               *
 50 REM *                                                    *
 60 REM *                    Ali Demir                       *
 70 REM *                                                    *
 80 REM *                  January 1987                      *
 90 REM *                                                    *
100 REM ******************************************************
110 REM Define VIA Port Addresses
120 PB = &FE60
130 PBDR = PB + 2
140 T1CL = PB + 6
150 T1CH = PB + 7
160 T2CL = PB + 8
170 T2CH = PB + 9
180 ACR  = PB + 11
190 RFI = PB + 13
200 IER = PB + 14
210 REM Define Subroutine Addresses
220 OSBYTE = &FFF4
230 DIM Q% 200
240 FOR C%=0 TO 2 STEP 2
250 P% = Q%
260 [
270 OPT  C%
280 .setall LDA £&BF      \set the ports IO channels
290 STA PBDR
300 LDA £&20              \initialise the counter to count pulses
310 STA ACR
320 LDA £0                \disable port intrrupts
330 STA IER
340 RTS
350  readval SEI
360 LDA £0                \select first input
370 STA stapb
380  JSR initco
390 LDA T2CH
400 STA speed1
410 LDA T2CL
420 STA speed1 + 1
430 LDA £&20              \select second input
440 STA stapb
450  JSR initco
460 LDA T2CH
470 STA speed2
480 LDA T2CL
490 STA speed2 + 1
500 CLI
510 RTS
520 .initco LDA £&10      \enable the pulses to enter
530 ORA stapb             \get pulse gate from a copy register
540 STA PB
550 LDA £0                \initialise the counter to 0
560 STA T2CL
570 STA T2CH
580 .delay LDY £&0        \delay for pulse counting
590 .loop1 LDX £0
600 .loop2 DEX
610 BNE loop2
620 DEY
```

```
 630 BNE loop1
 640 LDA £0                 \stop entering the pulses
 650 STA PB
 660 RTS
 670 .step1 LDA gofor        \ to drive stepper 1
 680 .repeat1 STA PB
 690 JSR stepdly
 700 LDA gofor
 710 EOR £1
 720 STA gofor
 730 DEC stepnum
 740 BNE repeat1
 750 RTS
 760 .step2 LDA gofor        \ to drive stepper 2
 770 .repeat2 STA PB
 780 JSR stepdly
 790  LDA gofor
 800 EOR £4
 810 STA gofor
 820 DEC stepnum
 830 BNE repeat2
 840 RTS
 850 .stepdly LDY £&28        \ delay for 0.1 second for s.m.
 860 .loop3 LDX £0
 870 .loop4 DEX
 880 BNE loop4
 890 DEY
 900 BNE loop3
 910 RTS
 920 .gofor EQUB 0           \select step direction
 930 .stepnum EQUB 0         \select step amount
 940 .stapb EQUB 0           \temporary storage
 950 .speed1 EQUW 0          \speed value storage
 960 .speed2 EQUW 0
 970 ]
 980 NEXT
 990 :
1000 REM Main Program
1010 DIM Y%(500),X(500),Y(500),J%(500)
1020 CALL setall
1030 OSCLI"*FX16,2"
1040 OSCLI"*FX190,8"
1050 MODE 129
1060 @% = &20304
1070 PROCSetspd
1080 MODE 128
1090 PROCSetpretens
1100 PROCSettens
1110 PROCOpr
1120 :
1130 REM Subroutines
1140 DEF PROCOpr
1150 OX=100 :LX=1150 :OY=250 :LY=250 :XI=0 :XM=60 :YI=0 :YM=6 :CRV=250
1160 CLS :PROCDrax (10,2)
1170 OX=100 :LX=1150 :OY=600 :LY=300 :XI=0 :XM=60 :YI=0 :YM=200 :CRV=770
1180 PROCDrax (10,50)
1190 X% = TIME
1200 OLDY1% = 250 :OLDY2% = 600 :OLDX1% = 100
1210 SUM = 0
1220 OSCLI"*FX17,1"
1230 I%=1
1240 REPEAT
1250 X1% = (TIME -X% )*0.57 + 100 : PROCFindrt
1260 SUM = SUM+RATIO
1270 INSA =(RATIO-1)*100
1280 Y%(I%)=INSA*100
1290 Y1% = INT(INSA*(250/6)) + 250
```

```
1300 Y2% = (ADVAL(1)/155)*1.1+600
1310 IF ( Y2% < 760 ) THEN  PROCstpm (2,"F",2)
1320 IF ( Y2% > 780 ) THEN  PROCstpm (2,"B",2)
1330 TENS = (Y2% - 600)/1.5 .@%=&00020200
1340 PRINT TAB(20,1);"N = "I%;"    Ins [%] = ";INSA;"    Tens [g] = ";TENS
1350 MOVE OLDX1%,OLDY1%
1360 DRAW  X1%,Y1%
1370 OLDY1% = Y1%
1380 MOVE OLDX1%,OLDY2%
1390 DRAW  X1%,Y2%
1400 OLDY2% = Y2%
1410 OLDX1% = X1%
1420 I%=I%+1
1430 UNTIL (TIME -X%)>2000
1440 N%=I%-1
1450 AVE = ((SUM / N%)-1)*100
1460 PRINT TAB(15,1)"Average Instability = "AVE ;"   Number of Samples = "N%
1470 Y% = (AVE*(250/6))+250 :MOVE 100,Y% :DRAW 1250, Y%
1480 PROCQuest
1490 ENDPROC
1500 :
1510 DEF PROCSetspd
1520 PROCFindrt
1530 PRINT TAB(1,10)"SPEED 1 =";SPD1
1540 PRINT TAB(23,10)"SPEED 2 =";SPD2
1550 INS=(RATIO-1)*100
1560 PRINT TAB(18,12)"RATIO =";RATIO
1570 PRINT TAB(2,15)"SET THE SPEED 1 AND PRESS 'C' TO CONT."
1580 IF (INKEY$(100) <> "C") THEN 1520
1590 ENDPROC
1600 :
1610 DEF PROCSetpretens
1620 OSCLI"*FX17,2" :CRV=700
1630 OX=100 :LX=500 :OY=500 :LY=400 :XI=0 :XM=10 :YI=0 :YM=20
1640 CLS :PROCDrax(2,5)
1650 PRINT TAB(10,20)"Pretensioning Procedure"
1660 PRINT TAB(10,21)"Tension [g] VS Time [s]"
1670 X%=TIME
1680 IF (ADVAL(0) DIV 256 <> 1) THEN 1680
1690 X1%=(TIME-X%)*0.26+100 :Y1%=(ADVAL(2)/80)*2.8+500
1700 PLOT5, X1%,Y1%
1710 DIF=(Y1%-CRV) :S%=ABS(DIF)/10
1720 IF ABS(DIF) < 10 THEN ENDPROC
1730 IF DIF > 0 THEN 1740 ELSE 1750
1740 PROCstpm (1,"B",S%) :PROCstpm (2,"B",S%) :GOTO 1760
1750 PROCstpm (1,"F",S%) :PROCstpm (2,"F",S%)
1760 IF X1% > 600 THEN 1600 ELSE GOTO 1680
1770 :
1780 DEF PROCSettens
1790 OSCLI"*FX17,1" :CRV=720
1800 OX=750 :LX=500 :OY=500 :LY=400 :XI=0 :XM=10 :YI=0 :YM=200
1810 PROCDrax(2,20)
1820 PRINT TAB(48,20)"Tensioning Between the Rollers"
1830 PRINT TAB(50,21)"Tension [g] VS Time [s]"
1840 X%=TIME
1850 IF ADVAL(0) DIV 256 <> 1 THEN 1850
1860 X1%=(TIME-X%)*0.26+750 :Y1%=(ADVAL(1)/106.505)+500
1870 PLOT5, X1%,Y1%
1880 DIF=(Y1%-CRV) :S%=ABS(DIF)/10
1890 IF ABS(DIF) < 10 THEN ENDPROC
1900 IF DIF > 0 THEN PROCstpm (2,"B",S%) ELSE PROCstpm (2,"F",S%)
1910 IF X1% > 1250 THEN 1780 ELSE GOTO 1850
1920 .
1930 DEF PROCFindrt
1940 REM Reads Speeds and Their Ratios
1950 CALL readval
1960 SPD1 =(((255 - ?speed2)*256 + 255 - ?(speed2 + 1))*6 1)
1970 SPD2 =(((255 - ?speed1)*256 + 255 - ?(speed1 + 1))*6.1)
1980 RATIO =(SPD2/SPD1)
1990 ENDPROC
```

```
2000 :
2010 DEF PROCstpm (M,D$,step)
2020 IF D$="F" THEN DIR=0
2030 IF M=1 AND D$="B" THEN DIR=2
2040 IF M=2 AND D$="B" THEN DIR=8
2050 IF M=1 THEN SM=step1 ELSE SM=step2
2060 ?stepnum=step
2070 ?gofor=DIR
2080 CALL SM
2090 ENDPROC
2100 .
2110 DEF PROCAnalys
2120 REM Arithmetic Mean
2130 SUM=0
2140 FOR I%= 1 TO N% :Y(I%)=Y%(I%)/100 :SUM=SUM+Y(I%) : NEXT I%
2150 AVE=SUM/N%
2160 FOR I=1 TO N% :X(I)=I :NEXT I
2170 REM Standard Deviation & Coef. of Variation
2180 SUMSD=0
2190 FOR I% = 1 TO N%
2200 T=(Y(I%)-AVE)^2
2210 SUMSD=SUMSD+T
2220 NEXT I%
2230 SD=SQR(SUMSD/(N%-1))
2240 CV=(SD/AVE)*100
2250 REM Frequency Distribution
2260 PROCMaxmin
2270 BIN%=30
2280 K%=0
2290 M%=(YM%-YI%)
2300 FOR I%=1 TO N%
2310 Z%=INT((Y%(I%)-YI%)/M%*BIN%)+1
2320 IF Z% < 1 THEN J%(1)=J%(1)+1 :GOTO 2350
2330 IF Z% > BIN% THEN J%(BIN%)=J%(BIN%)+1 :GOTO 2350
2340 J%(Z%)=J%(Z%)+1
2350 NEXT I%
2360 REM Distribution Plotting
2370 OX=100 :LX=500 :OY=500 :LY=450 :XM=N% :YM=6 :XI=0 :YI=0 :CRV=500
2380 CLS :XS%=N%/6 :PROCDrax (XS%,1)
2390 PROCLine (N%)
2400 REM Frequency Plotting
2410 MOVE FNX(X(1)),FNY(AVE) :DRAW FNX(X(N%)),FNY(AVE)
2420 FOR I%=0 TO N% : X(I%)=I% :NEXT I%
2430 OX=750 :LX=500 :OY=500 :LY=450 :YM=N% :YI=0 :XM=BIN% :XI=0 :CRV=500
2440 XS%=BIN%/3 :YS%=N%/6 :PROCDrax (XS%,YS%)
2450 PROCBarcht (BIN%)
2460 PROCWrite
2470 PROCQuest
2480 ENDPROC
2490 :
2500 DEF PROCDrax (XS,YS)
2510 @%=&10
2520 MOVE FNX(0),FNY(0)
2530 FOR YA=0 TO YM STEP YS :DRAW FNX(0),FNY(YA) :PROCYTICK (X,Y)
2540 PLOT 0,-80,15 :VDU5 :PRINT;YA :VDU4 :MOVE FNX(0),FNY(0) :NEXT YA
2550 FOR XA=0 TO XM STEP XS :DRAW FNX(XA),FNY(YM) :PROCXTICK (X,Y) :NEXT XA
2560 XP=(LX+OX) :MOVE OX,CRV :DRAW XP,CRV
2570 MOVE FNX(0),FNY(0)
2580 :
2590 FOR XA=0 TO XM STEP XS :DRAW FNX(XA),FNY(0) :PROCXTICK (X,Y)
2600 PLOT 0,-23,-30 :VDU5 :PRINT;XA :VDU4 :MOVE FNX(0),FNY(0) :NEXT XA
2610 FOR YA=0 TO YM STEP YS :DRAW FNX(XM),FNY(YA) :PROCYTICK (X,Y) :NEXT YA
2620 MOVE FNX(0),FNY(0)
2630 ENDPROC
2640 :
```

```
2650 DEF PROCWrite
2660 @%=&00020200
2670 PRINT TAB(1,20)"Number of Samples =";N%
2680 PRINT TAB(1,21)"Minimum Value [%] =";YI%/100
2690 PRINT TAB(1,22)"Maximum Value [%] =";YM%/100
2700 PRINT TAB(1,23)"Ar  Mean      [%] =";AVE
2710 PRINT TAB(1,24)"Std. Deviation[%] =";SD
2720 PRINT TAB(1,25)"Coeff. of Var.[%] =";CV
2730 ENDPROC
2740 :
2750 DEF PROCLine (N%) :MOVE FNX(X(1)),FNY(Y(1))
2760 FOR I%=1 TO N% :DRAW FNX(X(I%)),FNY(Y(I%)) :NEXT I%
2770 ENDPROC
2780 :
2790 DEF PROCBarcht (N%) :MOVE FNX(0),FNY(J%(1)) :F=(FNX2(X(2))-FNX2(X(1)))/2
2800 FOR I=1 TO N% :X= FNX2(X(I)) :Y=FNY(J%(I)) :DRAW X-F,Y :DRAW X+F,Y
2810 NEXT I
2820 ENDPROC
2830 :
2840 DEF FNX(XX) :X=(XX-XI)/(XM-XI)*LX+OX :=X
2850 DEF FNX2(XX) :X=(XX-XI)/(XM-XI)*LX*.96+OX :=X
2860 DEF FNY(YY) :Y=(YY-YI)/(YM-YI)*LY+OY :=Y
2870 DEF PROCYTICK (X,Y) :N=10 :DRAW X+N,Y :DRAW X-N,Y :MOVE X,Y :ENDPROC
2880 DEF PROCXTICK (X,Y) :N=10 :DRAW X,Y+N :DRAW X,Y-N :MOVE X,Y :ENDPROC
2890 :
2900 DEF PROCMaxmin
2910 XM=0 :XI=0 :YM%=0 :YI%=600
2920 FOR I%=1 TO N%
2930 IF X(I%)>XM THEN XM=X(I%)
2940 IF X(I%)<XI THEN XI=X(I%)
2950 IF Y%(I%)>YM% THEN YM%=Y%(I%)
2960 IF Y%(I%)<YI% THEN YI%=Y%(I%)
2970 NEXT I%
2980 ENDPROC
2990 :
3000 DEF PROCRead
3010 REM Read data files
3020 INPUT"Enter Filename  ";FL$ :FL$=":0.D."+FL$
3030 J=OPENIN FL$ :INPUT £J,N% :PRINT"Reading "FL$
3040 FOR I%=1 TO N% :INPUT £J,Y%(I%) :NEXT I% :CLOSE £J
3050 FOR I%=1 TO N% :X(I%)=I%
3060 ENDPROC
3070 :
3080 DEF PROCQuest
3090 PRINT TAB(1,27)"+.......  ...+...........+.............+..............+.
........+.........+"
3100 PRINT TAB(1,29)"..'1' TO REPEAT..'2' TO ANALYSE..'3' SCREEN DUMP..'4'  TC
STORE..'5' TO END.."
3110 INPUT" ENTER OPTION.... .. .."O%
3120 IF O%=1 THEN GOTO 1090
3130 IF O%=2 THEN PROCAnalys
3140 IF O%=3 THEN PROCDump
3150 IF O%=4 THEN PROCLog
3160 IF O%=5 THEN END
3170 IF O% > 5 THEN 3090
3180 ENDPROC
3190 :
3200 DEF PROCDump
3210 PRINT TAB(1,30)"Wait for Screen Dumping  "
3220 *SDUMP
3230 PROCQuest
3240 ENDPROC
3250 :
3260 DEF PROCLog
3270 REM Stores Data in Y%(I%)
3280 INPUT"   Filename ";FL$
3290 FL$=":0.D."+FL$
3300 J=OPENOUT FL$
3310 PRINT £J,N% :FOR I%=1 TO N% :PRINT £J, Y%(I%) :NEXT I%
3320 CLOSE £J
3330 PROCQuest
3340 ENDPROC
```

REFERENCES

1. FISCHER K E and WILSON D K, Air-jet Texturing: An Alternative to Spun Yarn Production, In: Textile Machinery: Investing for the Future, The Textile Institute, Manchester, 1982.

2. EVANS M, Dunlop Aerospace, Private Communication, April 1987.

3. STEINMAN A J, Air Jet Texturing, Air Jet Texturing Conference, Clemson University, Greenville, S.C., 18-19 Sept. 1985.

4. WRAY G R, The Construction and Resultant Properties of Air-textured Filament Yarns, PhD Thesis, University of Manchester, 1965.

5. MONSANTO Co. Textured Yarn Technology, Vol. 1, 1967, 494 pages.

6. PILLER B, Bulked Yarns, The Textile Trade Press, Manchester, 1973, 571 pages.

7. SIVAKUMAR V R, The Mechanism of Bulking of Air Textured Yarns, PhD Thesis, UMIST, Manchester, 1975.

8. HOLDEN G A, Advances in Air Texturing, Bulked Yarn Conference, UMIST, Manchester, 1975.

9. WILSON D K, The Production of Textured Yarns by Methods other than the False-twist Technique, Textile Progress, 1977, Vol. 9, (3), 63 pages.

10. WRAY G R and ACAR M, The Production and the Properties of Air-jet Textured Continuous Filament Yarns, International Textile Symposium, Izmir, Turkey, 2-4 Nov. 1981, (Proceedings published by Ege University Press, Izmir, 1984).

11. KOLLU T, Structure and Properties of Air-jet Textured Yarns, MSc. Thesis, UMIST, Manchester, 1982.

12. GÜLAL B, Blending Synthetic Yarns by Air-texturing, MPhil. Thesis, Leeds University, 1983.

13. KOLLU T, Air-jet Textured Yarns, PhD Thesis, UMIST, Manchester, 1985.

14. ACAR M and WRAY G R, An Analysis of the Air-jet Yarn Texturing Process, Part I: A Brief History of developments in the Process, Journal of Textile Institute, 1986, Vol. 77, (1), 19-27.

15. BREHM G, Texturing of Polyester and Other Filament Yarns, Chemiefasern/Textil-industrie, August 1979, Vol. 28/80, 706-708.

16. GLEN J M, Texturing: The Future is Now, Fiber producer,1979, Vol. 7, (4/2), 45,46,67 (3 pages).

17. WILSON D K, Apparel Fabrics-What Chances Have Air-Jet Textured Yarns?, Textile Institute and Industry, 1979, Vol. 17, (5), 170-174.

18. WILSON D K, Lighter Fabrics from Air-textured Yarns, Textile Institute and Industry, 1979, Vol. 17, (10), 360-362.

19. PILLER B and LESYKOVA E, Structure and Economical Aspects of Air-jet Textured Filament Yarns, Melliand Textilberichte (Eng. Edition), 1982, Vol. 63/11, (7), 485-493.

20. FISCHER K and KESSLER J, Air Texturing - Spunlike Yarns Made of Filament, Melliand Textilberichte (Eng. Ed.), June 1986, Vol. 12, (6), 383-387.

21. WILSON D K, Economic Aspects of Air-jet Texturing, Air-jet Texturing Process, One Day Symposium, Loughborough Univiversity of Technology, 11 July 1984.

22. LONGNECKER F R, Air Jet Texturing Conference, Clemson University, Greenville, S.C., September 1984.

23. WILSON D K, Air Jet Texturing - The Latest Technological Developments, Air Jet Texturing Conference, Clemson University, Greenville, S.C., September 1984.

24. KOLLU T, UMIST, Private Communication, May 1985.

25. WILSON D K, Breakthrough of Air Textured Yarns, Fiber Producer, August 1982, Vol. 10, (4), 86-88.

26. WRAY G R and ACAR M, Past, Present and Future of the Air-jet Texturing, Air Jet Texturing Conference, Clemson University, Greenville, S.C., 18-19 September 1985.

27. HOFFSOMMER K P, Air Texturing for the 1980's: A Look Backward and Forward, Fiber Producer, 1980, Vol. 8, (6), 22-77 (6 pages).

28. B.P. 732 929. Du Pont de Nemours, Dec. 15, 1952.

29. PRICE S T, Air Texturing, Modern Textiles, 1976, Vol. 57, (7), 28-31.

30. PHILLIPS M, Air Texturing: Where Are the Fabrics?, America's Textiles, 1983, Vol. 12, (5), 17-20.

31. ISAACS III A, Air Texturing Prepares for Lift-off Again, Textile World, 1984, (10), 48-55.

32. B.P. 762 630. Du Pont de Nemours, July 19, 1954.

33. B.P. 893 020. Du Pont de Nemours, May 20, 1960.

34. WRAY G R and ENTWISTLE J H, The Modification of a Taslan Jet to Operate Low Air Pressures, Journal of Textile Institute, 1969, Vol. 60, (10), 411-419.

35. B.P. 1 282 148. Du Pont de Nemours, June 27, 1969.

36. B.P. 1 279 908. Du Pont de Nemours, Nov. 9, 1970.

37. B.P. 1 448 100. Du Pont de Nemours, Dec. 14, 1973.

38. Taslan Jet Information Sheet Type XIV and Type XV.

39. U.S.P. 4 574 436. Du Pont de Nemours, Apr. 29, 1985.

40. ACAR M, Current State of Technology in Air-jet Texturing, 4th International Textile Symposium, Izmir, Turkey, 15-17 October 1986.

41. U.S.P. 4 097 975. Heberlein Maschinenfabrik, Jul. 19, 1977.

42. ACAR M, Analysis of the Air-jet Texturing Process and Development of Improved Nozzles, PhD Thesis, Loughborough Univiversity of Technology, 1984.

43. WRAY G R and ENTWISTLE J H, An Investigation of the Air-jet Bulking Process, Journal of Textile Institute, 1968, Vol. 59, (11), 122-136.

44. ŞEN H, A Study of the Air-jet type Bulked Filament Yarn Process, PhD Thesis, Loughborough Univiversity of Technology, 1970.

45. BOCK G, Texturing Filament Yarns in an Air Flow Tangling Mechanism, International Textile Bulletin/Spinning, 1981, (4), 359-389.

46. BOCK G and LÜNENSCHLOSS J, Air Flow and Loop Formation during Aerodynamic Texturing, Chemiefasern/Textil-Industrie, 1981, Vol. 31/83, (3), 202-204 and (5), 380-384+E41.

47. BOCK G and LÜNENSCHLOSS J, An Analysis of the Mechanism of Air-jet Texturing, Textile Machinery: Investing for the Future, The Textile Institute, Manchester, 1982.

48. BOCK G and LÜNENSCHLOSS J, Der Verwirbelungsprozess beim Luftblastexturieren, Textile Praxis International, 1984, Vol. 39, (6), 551-558.

49. BOCK G, and LÜNENSCHLOSS J, Einfluss von Druck und Dusenenstellung beim Luftblastexturieren, Chemiefasern/Textilindustrie, Vol. 34/86, (7-8), 492-496.

50. ACAR M, TURTON R K and WRAY G R, An Analysis of the Air-jet Yarn Texturing Process, Part II: Experimental Investigation of the Air-flow, Journal of Textile Institute, 1986, Vol. 77, (1), 28-43.

51. ACAR M, TURTON R K and WRAY G R, Air Flow in Yarn Texturing Nozzles, Trans. of ASME: Journal of Engineering for Industry, August 1987, Vol. 109, 197-202.

52. ZUCROW J M and HOFFMAN J D, Gas Dynamics (2 Vols.), John Wiley and Sons, Inc., New York, 1976, 772 and 480 pages.

53. SHAPIRO B, The Dynamics and Thermodynamics of Compressible Fluid Flow (2 Vols.), The Ronald Press Company, New York, 1963, 1185 pages.

54. WRAY G R, The Construction of Air-textured Filament Yarns, In: Bulk, Stretch, and Texture, The Textile Institute, Manchester, 1966, 18-28.

55. ACAR M, ALEXANDER A J, TURTON R K and WRAY G R, The Mechanism of the Air-jet Texturing Process, In: Texturing Today, Shirley Institute Publications S.46, Manchester, 1983, 207-230.

56. ACAR M, ALEXANDER A J, TURTON R K and WRAY G R, Loop Formation Mechanism in the Air-Jet Texturing Process, International Textile Bulletin, (3), 1983.

57. ACAR M, TURTON R K and WRAY G R, An Analysis of the Air-jet Yarn Texturing Process, Part VI: The Mechanism of Loop Formation, Journal of Textile Institute, 1986, Vol. 77, (6), 371-376.

58. ACAR M, TURTON R K and WRAY G R, An Analysis of the Air-jet Yarn Texturing Process, Part V: The Effects of Wetting the Yarn, Journal of Textile Institute, 1986, Vol. 77,

59. SCHULTZ K, New Machinery for Air-jet Texturing, Chemiefasern/Textil-Industrie, October 1975, Vol. 25/77, (10), 929-932.

60. SCHWEIZER U, FK6T Air Texturing Machine, Textured Yarn Association of America, Inc. Convention, Myrtle Beach, S.C., 3-5 August 1978.

61. U.K. Patent Application, G.B. 2 079 189 A Heberlein Maschinenfabrik AG, June 25, 1981.

62. ARTUNC H, The Air Texturing of Drawn and of High-speed Polyester Yarns, Chemiefasern/Textilindustrie, 1981, Vol. 31/83, 289-297 and E29.

63. Du Pont, Technical Information Bulletin, X-154, "Characteristics of Taslan Textured Yarns", October 1961.

64. WRAY G R, The Properties of Air-textured Continues Filament Yarns, Journal of Textile Institute, 1969, Vol. 60, (3), 102-126.

65. WRAY G R, A Rapid Method of Measuring Yarn Diameters, Journal of Textile Institute, 1970, Vol. 57, T134-T136.

66. FISCHER K, Aerodynamic Processes in Filament Yarn Production, International Textile Bulletin, 1979, (1), 17-38 (8 pages).

67. ACAR M, KING T G and WRAY G R, Textured Yarn Quality, Textile Asia, November 1986, Vol. 17, (11), 62-66.

68. ROZMARYNOWSKA K, and GODEK J, Effects of Processing on the Properties of Air Bulked Yarns, Bulk, Stretch and Texture, The Textile Institute, 1966, 29-41.

69. ŞEN H and WRAY G R, A Water-absorption Test for Assessing the Physical Bulk of Air-jet-type Bulked Yarns, Journal of Textile Institute, 1970, Vol. 61, 237-240.

70. Heberlein Yarn Technical Centre, "Description of Test Methods for Air-jet Textured Filament Yarns", August 1980, 6110, 13/8/80.

71. PILLER B, Development Trends in the Production of Air-jet Texturised Filament Yarn with Spun yarn Characteristics, Melliand Textilberichte (Eng. Ed.), 1979, Vol. 60/8, (2), 128-136.

72. KOLLU T, Mechanics of Air-jet Textured Yarns, 4th International Textile Symposium, Izmir, Turkey, 15-17 October 1986.

73. HOLDEN G A, Air Jet Textured Yarns for Woven Apparel Fabrics, In: Alternatives to Spun Yarns in Apparel Fabrics Conference, Shirley Institute Publication, S34, Manchester, 15 February 1979,

74. WILSON D K, On-line Control is Coming, Textile Horizons, 1981, (9), 26,27.

75. PRICE S T, Bulked Yarns Produced by Air Texturing, In: Modern Yarn Production, (Ed. by G R Wray), Columbia Press, Manchester, 1960, 139-151.

76. LÜNENSCHLOSS J and HELLI J G, Die Texturierung von Chemiefaden in Luftstrom, Part I-IV, Textile Praxis, 1969, Vol. 24, (8-11), 515-725 (21 pages).

77. DATYE K V and BOSE C, Air-Texturing, Man-Made Textiles in India, March 1982, Vol. 25, (3), 158-163.

78. HES L and PILLER B, Heat Transmission in Air-jet Textured Filament Yarns, Melliand Textilberichte (Eng. Ed.), 1982, Vol.11, (10), 678-682.

79. BOSE C and GOVINDARAJULU R, Effect of Denier on Air Textured Yarn, The Indian Textile Journal, 1982, Vol. 93, (9), 97,98.

80. BOCK G, and LÜNENSCHLOSS J, Heat Treatment of Air-jet Textured Polyester Filament Yarns, Chemiefasern/Textilindustrie, 1983, Vol. 33/85, (2), 103-106 and E12.

81. SENGUPTA A K, KOTHARI V K and ROY A K, Stability of Air Textured Yarns, Textile Research Journal, 1984, Vol. 54, (2), 125,126.

82. ACAR M, TURTON R K and WRAY G R, An Analysis of the Air-jet Yarn Texturing Process, Part IV: Fluid Forces Acting on the Filaments and the Effects of Filament Cross-sectional Area and Shape, Journal of Textile Institute, 1986, Vol. 77, (4), 247-254.

83. WILSON D K, Texturing by Air and other Methods, Process and Products, Unpublished Paper, 1986.

84. PRITTS M A, How to Assure Economical Air-jet Texturing, Textile World, 1983, (11), 47-50 (2 pages).

85. ŞEN H and WRAY G R, Apparatus for Manufacturing Yarns of the Air-jet-bulked Type Without the Use of Air, Journal of Textile Institute, 1970, Vol. 61, 77-87.

86. ŞEN H and WRAY G R, The Properties of Yarns of the Air-jet-bulked Type Produced Without Use of Air, Journal of Textile Institute, 1971, Vol. 62, 335-349.

87. Enterprise Machine and Development Corp., Sidewinder Air-Texturing Machine Catalogue.

88. Eltex Reutlingen, Air Texturing Machine Catalogue.

89. TANI M and SASAKI Y, Spunlike Texturing as a Substitution of Spinning of Staple Fibres, 24th International Man-made Fibres Congress, Dornbirn, Austria, 25-27 September 1985.

90. Ingersol-Rand Co. Air Compressors are Key to Texturing of Synthetic Fibres, Fiber Producer, June 1980, Vol. 8, (6), 48-51 (2 pages).

91. RILLING R, Further Developments in the Field of Air Texturing, Chemiefasern/Textil-Industrie, 1981, Vol. 31/83, (4), 298-301 +E30-E31.

92. DENTON M J, EATON D C and BAKER A H, Noise in False-twist Texturing Plant, In: Texturing Today, Shirley Institute Publication S.46, Manchester, 1983, 65-107.

93. HOLDER D W, and NORTH R J, Schlieren Methods, Her Majesty's Stationery Office, London, 1963, 106 pages.

94. BENEDICT R P, WYLER J S, DUDEK J A, and GLEED A R, Generalised Flow Across an Abrupt Enlargement, Trans. Of the ASME: Journal of Engineering for Power, July 1976, 327-334.

95. ANDERSON J D, Modern Compressible Flow, with Historical Perspective, McGraw-Hill, New York, 1982, 466 pages.

96. CHE-HAING C, Axially Symmetric Supersonic Turbulent Jets Discharged from a Nozzle with Underexpansion, In: Turbulent Jets of Air, Plasma and Real Gas, Edited By: Abramovich GN, Translated from Russian, Consultants Bureau, New York, 1969.

97. GAUNTER J W, LIVINGOOD N B, and HRYCAK P, Survey of Literature on Flow Characteristics of a Single Turbulent Jet Impinging on a Flat Plate, NASA Technical Note, February 1970, NASA TN D-5652.

98. GUREVICH M, Theory of Jets in Ideal Fluids, London, Academic Press, 1965, 353-366.

99. SOO S L, Gas Dynamic Processes Involving Suspended Solids, A.I.Ch.E. Journal, September 1961, Vol. 7/3, 384-391.

100. ABRAHAM O, BINN J H, DEBOER B G, and STEIN G D, Gas Dynamics of Very Small Laval Nozzles, Physics of Fluids, June 1981, Vol 24/6, 1017-1031.

101. MARKS M R, ICI Fibers Co., Gloucestershire, UK, Private Communication, 1985.

102. SIMMEN C, Heberlein Maschinenfabrik A.G., Switzerland, Private Communication, March 1986.

103. WHITEHEAD B, Milliken Ltd., Manchester, Private Communication, November 1984.

104. HERRMANN R, Der Kondensationsstoss in Ueberschall-Windkanal-dusen, Info 19 201, 1942

105. OSWATITSCH K, Kondensationserscheinungen in Ueberschalldusen, Z A M M 22 H1, 1942.

106. OLSEN J S, Frictional Behaviour of Textile Yarns, Textile Research Journal, January 1969, Vol. 39, 31-37.

107. Air-jet Texturing, One Day Symposium, Loughborough University of Technology, 11 July 1984.

108. SCHICK M J, Friction and Lubrication of Synthetic Fibres, in Surface Characteristics of Fibres and Textiles, (Ed. by M J Schick), Marcel Dekker Inc., 1-65, 1977.

109. Rank Taylor and Hobsons Surface Scanning Equipment Manual.

110. WEGENER P P, POURING A A, Experiments on Condansation of Water Vapor by Homogeneous Nucleation in Nozzles, The Physics of Fluids, March 1964, Vol 7/3, 352-361.

111. POURING A A, Thermal Choking and Condensation in Nozles, The Physics of Fluids, October 1965, Vol. 8/10, 1802-1810.

112. KANG S W, Analysis of Condensation Droplet Growth in Rarefied and Continium Environments, AIAA Journal, July 1967, Vol. 5/7, 1288-1295.

113. SALTANOV G A, SELEZNEV L I, and TSIKLAURI G V, Generation and Growth of Condensed Phase in High-velocity Flows, Int. J. Heat and Mass Transfer, 1973, Vol. 16, 1577-1587.

114. SISLIAN J P, and GLASS I I, Condensation of Water Vapor in Rarefaction Waves: I. Homogeneous Nucleation, AIAA Journal, December 1976, Vol. 14/12, 1731-1737.

115. KOTAKE S, and GLASS I I, Condensation of Water Vapor in Rarefaction Waves: II. Heteregeneous Nucleation, AIAA Journal, February 1977, Vol. 15/2, 215-221.

116. GLASS I I, KAIRA S P, and SISLIAN J P, Condensation of Water Vapor in Rarefaction Waves: III. Experimental Results, AIAA Journal, May 1977, Vol. 15/5, 686-693.

117. MATSUO K, KAWAGOE S, SONODA K and SETOGUCHI T, Oscillations of Laval Nozzle Flow with Condensation, Bulletin of JSME, September 1983, Vol. 26/219, 1556-1562.

118. MATSUO K, KAWAGOE S, SONODA K, and SAKAO K, Studies of Cendensation Shock Waves, Bulletin of JSME, July 1985, Vol. 28/241, 1416-1422.

119. Textile Terms and Definitions, (Ed. by C A Farnfield), The Textile Institute, Manchester, 1975, 228 pages.